

ADVANCES in DEEP FOUNDATIONS

**YOSHIAKI KIKUCHI, MAKOTO KIMURA,
JUN OTANI & YOSHIYUKI MORIKAWA
EDITORS**

ADVANCES IN DEEP FOUNDATIONS



BALKEMA – Proceedings and Monographs
in Engineering, Water and Earth Sciences

PROCEEDINGS OF THE INTERNATIONAL WORKSHOP ON RECENT ADVANCES OF DEEP FOUNDATIONS (IWDPF07), PORT AND AIRPORT RESEARCH INSTITUTE, YOKOSUKA, JAPAN, 1–2 FEBRUARY, 2007

Advances in Deep Foundations

Editors

Yoshiaki Kikuchi

Port & Airport Research Institute, Yokosuka, Japan

Jun Otani

Kumamoto University, Kumamoto, Japan

Makoto Kimura

Kyoto University, Kyoto, Japan

Yoshiyuki Morikawa

Port & Airport Research Institute, Yokosuka, Japan



Taylor & Francis

Taylor & Francis Group

LONDON / LEIDEN / NEW YORK / PHILADELPHIA / SINGAPORE

This edition published in the Taylor & Francis e-Library, 2007.

“To purchase your own copy of this or any of Taylor & Francis or Routledge’s collection of thousands of eBooks please go to www.eBookstore.tandf.co.uk.”

Taylor & Francis is an imprint of the Taylor & Francis Group, an informa business

© 2007 Taylor & Francis Group, London, UK

All rights reserved. No part of this publication or the information contained herein may be reproduced, stored in a retrieval system, or transmitted in any form or by any means, electronic, mechanical, by photocopying, recording or otherwise, without written prior permission from the publishers.

Although all care is taken to ensure integrity and the quality of this publication and the information herein, no responsibility is assumed by the publishers nor the author for any damage to the property or persons as a result of operation or use of this publication and/or the information contained herein.

Published by: Taylor & Francis/Balkema
P.O. Box 447, 2300 AK Leiden, The Netherlands
e-mail: Pub.NL@tandf.co.uk
www.balkema.nl, www.taylorandfrancis.co.uk, www.crcpress.com

ISBN 0-203-93841-0 Master e-book ISBN

ISBN 13: 978-0-415-43629-8 (hbk)

Table of contents

Preface	IX
Organizing Committee & Research Committee	XI
<i>Keynote lectures</i>	
Recent research into the behaviour of jacked foundation piles <i>D.J. White & A.D. Deeks</i>	3
Centrifuge modelling of pile foundation <i>C.F. Leung</i>	27
Advanced modeling tools for the analysis of axially loaded piles <i>R. Salgado, M. Prezzi & H. Seo</i>	49
CPT-based design of displacement piles in siliceous sands <i>B.M. Lehane, J.A. Schneider & X. Xu</i>	69
Recent advances in designing, monitoring, modeling and testing deep foundations in North America <i>C. Vipulanandan</i>	87
Current design practice for axially loaded piles and piled rafts in Germany <i>C. Vrettos</i>	101
Recent advances in the analysis of pile foundation in China <i>M. Huang, F. Liang & Z. Li</i>	115
Current status of deep and pile foundations in Korea <i>S. Jeong, C. Cho, D. Seo, J. Lee, H. Seol, Y. Kim & J. Lee</i>	125
Trend of research and practice of pile foundations in Japan <i>T. Matsumoto, P. Kitiyodom & T. Shintani</i>	143
<i>Technical papers</i>	
<i>Axial and lateral bearing capacity of piles</i>	
Vertical bearing capacity of large diameter steel pipe piles <i>Y. Kikuchi, M. Mizutani & H. Yamashita</i>	177
Back analysis of Tokyo port bay bridge pipe pile load tests using piezocone data <i>J.A. Schneider, D.J. White & Y. Kikuchi</i>	183
Pile foundation design of the connecting bridge for New-Kitakyushu airport <i>H. Ochiai, N. Yasufuku, Y. Maeda & S. Yasuda</i>	195
Numerical prediction of long-term displacements of pile foundation <i>K. Danno, K. Isobe & M. Kimura</i>	203
Side resistance of piles considering strain levels <i>M. Suzuki, M. Shirato, S. Nakatani & K. Matsui</i>	211

Evaluation of vertical and lateral bearing capacity mechanisms of pile foundations using X-ray CT <i>K. Morita, J. Otani, T. Mukunoki, J. Hironaka & K.D. Pham</i>	217
Dynamic and static horizontal load tests on steel pipe piles and their analyses <i>P. Kitiyodom, T. Matsumoto, K. Tomisawa, E. Kojima & H. Kumagai</i>	225
<i>New types of pile construction methods</i>	
Press-in piling technology: Development and current practice <i>M. Motoyama & T.L. Goh</i>	233
Centrifuge modelling of the base response of closed-ended jacked piles <i>A.D. Deeks & D.J. White</i>	241
Development on battered pile with screw pile method (NS-ECO pile) <i>A. Komatsu</i>	253
BCH method applicable to the construction under overhead restrictions <i>S. Tajima, T. Yoshikawa, S. Saito, H. Kotaki & M. Koda</i>	259
Mechanical joint “KASHEEN” for large-diameter steel pipe piles <i>G. Mori & H. Tajika</i>	267
<i>New types of deep foundations</i>	
Vertical bearing capacity of bored pre-cast pile with enlarged base considering diameter of the enlarged excavation around pile toe <i>K. Kobayashi & H. Ogura</i>	277
Seismic performance of a group-pile foundation with inclined steel piles <i>K. Okawa, H. Kamei, F. Zhang & M. Kimura</i>	285
Development of design method for a soft landing breakwater with piles <i>Y. Kikuchi</i>	291
Settlement and load-sharing of a piled raft foundation combined with grid-form soil-cement walls on soft ground <i>K. Yamashita & T. Yamada</i>	299
Earthquake resistant reinforcement method for pile foundations using effect of confinement of ground solidification body <i>Y. Adachi, K. Urano, T. Takenoshita, N. Tanzawa & M. Kawamura</i>	307
A design approach for composite ground pile and its verification <i>K. Tomisawa & S. Miura</i>	313
A study of reinforcing methods for existing bridges on soft ground with a solidification improvement <i>H. Fukada, K. Kato, N. Segawa, T. Ooya & Y. Shioi</i>	321
Development of sheet-pile foundation combining footing with sheet-piles <i>H. Nishioka, M. Koda, J. Hirao & S. Higuchi</i>	327
Recent technology development of steel pipe sheet pile foundation in Japan <i>T. Katayama</i>	335
Development of three-dimensional frame analysis method for H-joint Steel Pipe Sheet Pile foundation system <i>M. Kimura, K. Isobe & Y. Nishiyama</i>	341
Development of a composite pile system consisting of soil cement columns and H-beams <i>O. Kaneko</i>	349

Application of highcapacity micropiles for seismic retrofitting in Japan <i>Y. Otani & M. Hoshiya</i>	355
Field experiment on installation of suction foundation <i>H. Yamazaki, H. Yoshinaga & K. Kaneda</i>	361
Sample of proposal in consulting services using new technology/methods <i>M. Komatsu</i>	367
<i>Ground improvement</i>	
Bearing capacity and settlement behavior of the spread foundation building on improved ground by non-vibratory sand compaction pile method <i>H. Yoshitomi, T. Ohnishi, Y. Yoshinari & T. Umeno</i>	373
Centrifuge model tests on deep mixing column failure under embankment loading <i>M. Kitazume & K. Maruyama</i>	379
Load transfer and failure mechanisms in the reinforced ground beyond vertically loaded pile <i>J. Hironaka, T. Hirai, Y. Watanabe & J. Otani</i>	385
Ground improvement for the second phase construction of Kansai International Airport <i>Y. Morikawa, T. Tabata & T. Emura</i>	389
<i>Seismic design and seismic problems</i>	
Seismic design specifications for Japanese highway bridge deep foundations against large earthquakes <i>M. Shirato & S. Nakatani</i>	397
New seismic design concept for port facilities <i>T. Sugano & T. Tanaka</i>	403
Centrifuge tests on pile foundation-structure systems affected by liquefaction-induced soil flow after quay wall failure <i>T. Tazoh, M. Sato, G. Gazetas & J. Jang</i>	409
Mechanical behaviors of sandy ground during or after liquefaction <i>B. Ye, A. Yashima, G.L. Ye & F. Zhang</i>	417
Author index	425

Preface

The emerging design methodology Reliability-Based Design has become today's norm in Japanese structural design codes and will soon be included in the international standard codes. To meet this trend, methods for the design and construction of deep foundations have made large advances. As deep foundation construction is one of the most important and applied executions in geotechnical engineering worldwide, both research work by academics and the experience and ideas of practitioners are required to develop this field and meet future standards.

The International Workshop on Recent Advances in Deep Foundations (IWDPF07, Yokosuka, Japan, 1–2 February 2007) was held to transmit the information on recent advances in deep foundations to an international audience and to provide academics and practitioners the opportunity to discuss the latest developments.

Every year more than thousand technical papers are presented at the Japanese National Conference on Geotechnical Engineering, but most of these articles are unfortunately not transmitted to other countries. As structural design codes are nowadays written with international standards, a significant amount of useful information would get lost if this information would not be published in a medium that is accessible to an international audience. For this reason, the IWDPF07 workshop has been focused on collecting the contributions that present Japanese technologies and experiences which are of interest to a broad, international audience. The result of this effort, this proceedings volume, comprises nine keynote lectures, prepared by outstanding international experts and 34 technical papers. In addition to papers on recent research achievements and on case histories, a significant number of the technical papers is dealing with the practical development of deep foundations, seismic design methods, liquefaction problems, and ground improvements.

This workshop was held with the support of the Port and Airport Research Institute (PARI) and the Japanese Geotechnical Society (JGS). The research committee of JGS – “On the concept for evaluation of new technology on foundation structure design” – is the mother body of this workshop. We would like to express sincere gratitude to both organizations and the committee for their strong support of this workshop.

The editors hope that these proceedings will be interesting and fruitful to researchers and practitioners who are active in the development of deep foundation design methods and construction methods.

Yoshiaki Kikuchi
Co-chairman of IWDPF07

Organizing Committee

Co-Chairmen

Dr. Yoshiaki Kikuchi, Port & Airport Research Institute
Prof. Makoto Kimura, Kyoto University

Secretary

Dr. Yoshiyuki Morikawa, Port & Airport Research Institute

Members

Prof. Jun Otani, Kumamoto University
Dr. Masahiro Shirato, Public Works Research Institute
Dr. Kouichi Tomisawa, Civil Engineering Research Institute for Cold Region
Dr. Hisashi Fukada, Fudo Tetra Corporation
Dr. Ken-ichi Horikoshi, Taisei Corporation
Mr. Masataka Tatsuta, Nippon Steel Corporation

Research Committee on the Concept for Evaluation of New Technology on Foundation Structure Design (JGS)

Chairman

Prof. Makoto Kimura, Kyoto University

Secretary

Dr. Hisashi Fukada, Fudo Tetra Corporation

Members

Mr. Jiro Fukui, Public Works Research Institute
Dr. Yozo Goto, National Research Institute for Earth Science and Disaster Prevention
Mr. Motohisa Hara, Penta-Ocean Construction
Dr. Ken-ichi Horikoshi, Taisei Corporation
Mr. Akio Inoue, Obayashi Corporation
Dr. Yoshiaki Kikuchi, Port & Airport Research Institute
Dr. Masayuki Koda, Railway Technical Research Institute
Mr. Masataka Komatsu, Japan Bridge & Structure Institute, Inc
Mr. Yoshinobu Miura, Kyushukensetsu Consultant
Dr. Katsunori Okawa, Mitsubishi Heavy Industries, Ltd.
Prof. Satoru Ohtsuka, Nagaoka University of Technology
Prof. Jun Otani, Kumamoto University
Dr. Masahiro Shirato, Public Works Research Institute
Mr. Shinichi Tajima, Kajima Corporation
Mr. Masataka Tatsuta, Nippon Steel Corporation
Dr. Takashi Tazoh, Shimizu Corporation
Mr. Kouichi Tomisawa, Civil Engineering Research Institute for Cold Region
Mr. Kiyoshi Yamashita, Takenaka Corporation
Prof. Feng Zhang, Nagoya Institute of Technology

Keynote lectures

Recent research into the behaviour of jacked foundation piles

D.J. White

*Centre for Offshore Foundation Systems, University of Western Australia, Perth, Australia
Cambridge University Engineering Department, UK*

A.D. Deeks

Cambridge University Engineering Department, UK

ABSTRACT: Pile jacking technology uses static jacking force to install large pre-formed displacement piles without the noise and vibration associated with dynamic piling methods. Recent research into the mechanisms governing the shaft and base resistance of displacement piles is reviewed, and the differences between jacked and driven piles are highlighted. Methods for predicting the resulting pile stiffness and capacity are described, within the framework of recently-developed CPT-based prediction methods. Compared to driven piles, jacked installation leads to enhanced plugging and residual base load, and reduced friction fatigue. The resulting axial response is stiffer and can be stronger than an equivalent driven or bored pile. Recent applications of jacked H-piles to support axial load are reported, and a novel technique for optimising the ratio of axial capacity to installation force via plugging is described.

1 INTRODUCTION

1.1 Motivation for pile jacking technology

The expansion of urban development into increasingly marginal sites, and the invention of new pile construction techniques, make the economics of deep foundations increasingly attractive. Recent technological improvements have led to a proliferation of pile types and installation methods. Displacement piles, driven into the ground by hammering or vibration, remain widely used for offshore and nearshore foundations. For onshore foundations, non-displacement piles have increased in popularity during the past 50 years since these can be installed without the noise and vibration associated with conventional methods of pile driving.

Increasingly stringent environmental legislation now precludes the use of pile hammers in urban areas, and restricts the disposal of spoil created by the construction of conventional bored piles. In response, alternative construction methods for pile foundations have evolved. These developments have been driven by a desire either to improve the performance of the foundation or to reduce the environmental impact of its construction. Performance is quantified by the strength and stiffness of the foundation. Noise, ground vibrations and spoil material (particularly from urban brownfield sites) all have negative environmental impacts.

One such new construction technique is pile jacking, which is the subject of this review paper. Pile jacking has historically been used for the construction of small foundation piles, as are used for minor underpinning works. More recently, high-capacity jacking machines have been developed, which offer the opportunity for the foundations of large buildings or heavy structures to be installed without the noise and vibration associated with conventional methods of displacement piling. Some pile jacking systems can be supported on the pile wall under construction, rather than a piling mat, which reduces the need for temporary works leading to shorter construction schedules and reduced material use.

For displacement piles, the installation method – jacking, or dynamic driving – has an effect on the deformation of the soil during installation, and the resulting stress field around the pile. In turn, these factors affect the pile behaviour during subsequent loading. In design practice, the effect of installation method is rarely considered when assessing the response of a pile foundation. In some cases, design codes and research papers recommend empirical factors to differentiate between the capacity of bored and driven piles (e.g. Bustamante & Gianselli 1982, De Beer 1988, Ghionna et al. 1993) but as pile jacking is a relatively new technology little advice exists for predicting the behaviour of jacked piles.

In addition to the short-term impact of noise and vibration during the construction process, the

environmental impact of foundation construction extends to the energy and resource use prior to installation, and subsequent to the initial working life of the foundation. If dynamic installation is discounted in urban areas due to the unacceptable ground vibrations, the choice between jacked or bored installation methods is linked to the choice between steel or concrete piles. The extraction and re-use of steel piles, which is made possible by pile jacking rigs, reduces the whole life cost of this type of foundation (Dawson, 2001, Chau et al. 2006).

If the environmental benefits of pile jacking are to become more widely exploited, research into the influence of installation method on pile behaviour must be disseminated amongst practitioners to establish this knowledge in engineering practice.

This paper reviews recent research into the behaviour of piles installed by jacking. The following topics are covered:

1. Pile jacking technology and the environmental impact of pile jacking compared to alternative pile construction techniques;
2. Recent research into the fundamental mechanisms underlying the installation and loading of displacement piles;
3. Recent guidance for predicting the axial capacity and load-settlement response of piles, with emphasis on the differences between driven and jacked piles;
4. Recent research into the use of H-piles, focussing on differences in behaviour of jacked and driven piles due to plugging.

A significant proportion of the research reported in this paper is related to the ‘press-in’ method of pile jacking, reflecting the authors’ experiences in a long-term research programme at the University of Cambridge supported by Giken Seisakusho Co. Ltd. However, key outcomes from other major research projects into jacked piles are also reported.

1.2 Machine development

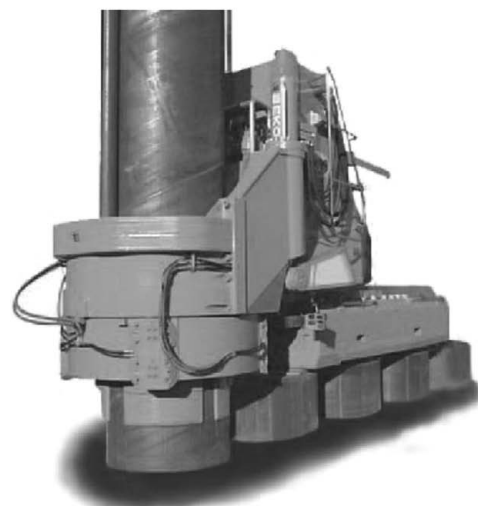
Pre-formed displacement piles can be installed by static jacking force alone if sufficient reaction force is available. Small rigs capable of pushing micro-piles into the ground for underpinning are in wide use. Reaction force is usually provided by the weight of the structure being underpinned.

Modern pile jacking machines operate by pushing the pre-formed pile – made from steel or precast concrete – into the ground with hydraulic rams, using static force alone. Reaction is provided either by kentledge (deadweight) or by gripping the heads of adjacent piles that have already been installed.

The first large pile jacking machine was the Taylow Woodrow ‘Pilemaster’, which was developed



(a) Sheet pile installation



(b) Tubular pile installation

Figure 1. ‘Silent piler’ jacking machines.

in the UK in 1960 for the installation of sheet piles. This machine stood on top of a row of sheet piles, and gained reaction from a pair of piles on either side of the pile currently being jacked downwards.

The first machine of the type now referred to as a ‘Silent Piler’ was produced by Giken Seisakusho Co. Ltd. in 1975. This type of machine ‘walks’ along the row of piles under construction, gaining reaction by gripping the previously-installed piles – an approach which has been termed the ‘press-in’ method’. Different types of Silent Piler are capable of installing sheet piles (Fig. 1a), tubular piles (Fig. 1b) or precast concrete piles.

An alternative to the ‘self-walking’ approach is to hang the hydraulic unit from the leader of a

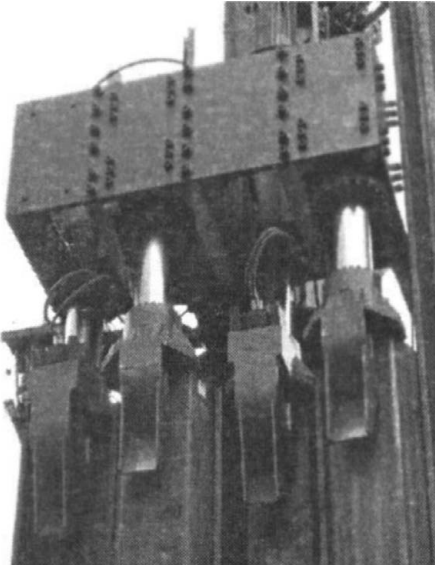


Figure 2. ‘Push-pull’ rig-mounted pile jacking unit (Filip 2006).

conventional piling rig, as used by the 2 MN capacity ‘Push-pull’ system produced by Dawson Construction Plant Ltd, UK (Fig. 2). This system has been used for the installation of small groups of piles which act in unison as a single larger pile after construction (Filip 2006).

Since the Pilemaster, the Silent Piler and the Push-pull systems gain reaction from previously-installed piles, only closely-spaced groups of piles or continuous walls can be installed by these methods. An alternative approach is to gain reaction force from either the deadweight of the machine, additional ballast or temporary ground anchors.

The use of a deadweight-reaction pile jacking machine was reported in Russia by Goncharov et al. (1964) (Fig. 3). The 350 kN weight of the tractor units of this machine was used as reaction force to drive precast concrete piles into clayey soils. More modern pile jacking machines that rely on kentledge for reaction are manufactured by Tianhe Machinery Ltd, China, and have been exported to Malaysia and Australia, where they are known as the ‘G-pile’ system (Fig. 4). The jacking unit of this machine can move horizontally within the footprint of the ballast, so multiple piles can be installed without unloading the deadweight.

The largest pile jacking machines of the Silent Piler type have a jack capacity of ~4 MN but weigh only ~400 kN. The largest Silent Pilers can install tubular piles of up to ~1.5 m diameter in strokes of length ~1 m. The largest G-pile machine has a jacking capacity (and a deadweight) of ~9 MN and can install

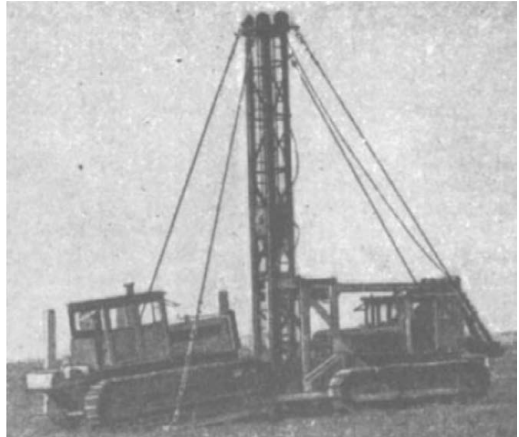


Figure 3. Early Russian jacking unit (Goncharov et al. 1964).



Figure 4. Deadweight-based pile jacking system (GEO 2006).

400 mm square precast concrete piles in 1.8 m jack strokes. When comparing these systems, the additional jacking capacity of the G-pile machine is offset by the operational complexity of moving 900 tonnes of deadweight around a site. A substantial piling mat is needed for soft ground sites. The mean bearing pressure exerted by the fully loaded 9 MN G-pile machine during movement of the jacking unit is ~300 kPa. In contrast, the ‘self-walking’ feature of the Silent Piler system extends to specially-designed pitching cranes and power packs. The resulting system requires no temporary works since all equipment is supported on the pile wall under construction (Fig. 5).

1.3 Applications of pile jacking

Most current design guidance for the axial and lateral response of piles has been derived from experience with dynamically driven or bored piles. As new installation



Figure 5. ‘Self-walking’ system without temporary works.

techniques have been developed, such as pile jacking, designers are required to assess whether current guidance is applicable, or whether modified methods are appropriate to reduce risk or exploit improved performance.

The installation method of a pile determines the stress state and level of disturbance of the soil immediately surrounding the pile, as described in Section 3 of this paper. These stresses and disturbance have a significantly influence on the axial response of the pile under working conditions. In contrast, the installation method has less effect on the lateral response of the pile. During lateral loading, the strength of more distant soil is mobilised, which is unaffected by the installation method.

Therefore, jacked piles have been widely adopted for laterally-loaded applications such as retaining walls supporting river banks and excavations, designed by conventional methods. Long linear projects, such as riverbank reinforcement, are particularly suited to ‘self-walking’ pile jacking systems due to the elimination of temporary works. Case studies describing recent applications of pile jacking systems for applications involving lateral loading are reported by Dubbeling et al. (2006).

In contrast, for axially-loaded applications, such as building or bridge foundations, designers have been cautious in adopting pile jacking technology, due to concerns that the installation procedure may not lead to the same capacity as conventional dynamic installation methods. This uncertainty has been reduced by recent research programmes involving axial load testing of jacked piles.

Recent case studies in which jacked piles have been used to support axial loads are reported by Li et al. (2003), Mitchell & Mander-Jones (2004), White et al. (2003), Filip (2006) and Lehane et al. (2003).

A beneficial feature of pile jacking is that the installation force provides an indication of the static bearing capacity during subsequent loading. As discussed later, it is important to recognise that consolidation and ‘set-up’ can cause changes in capacity after installation. Usually these effects lead to an increase in capacity, but in certain circumstances a loss of strength has been observed. Most pile jacking systems include direct measurement of the applied jack load during installation, and some systems have specific features to allow static maintained load tests to be conducted after installation, providing verification of the pile performance.

An additional requirement in order for jacked piles to be adopted for axially-loaded applications is the need for new acceptance or termination criteria in regions where the capacity of a pile must be confirmed at the completion of driving. Hammer-driven piles are conventionally installed to a specified set per blow as confirmation – based on a dynamic pile driving analysis – that the design capacity and stiffness requirements have been met.

2 ENVIRONMENTAL IMPACT

2.1 Noise emissions

Noise emissions on construction sites present a health hazard to site operatives and cause annoyance to neighbours. Noise levels are expressed in decibels, which are related to the fluctuating air pressure, p (Equation 1).

$$p (\mu\text{Pa}) = 20 \times 10^{\text{dB}/20} \quad (1)$$

Noise levels typically decrease with the logarithm of radius, r , from their source, due to spherical geometric spreading. The noise level of a source, N_{source} , can be attenuated using Equation 2 to deduce the noise level, N , at a remote point (Sarsby 2000).

$$N = N_{\text{source}} - 20 \log(r) - 8 \quad (2)$$

Guidance on acceptable noise levels during construction is given by British Standard BS5228 (1992). In urban areas N should not exceed 75 dB at the outside of a noise sensitive building such a residential or office building. In rural areas a lower limit of 70 dB applies.

Noise emissions from traditional dynamic or vibratory piling rigs have been reduced in recent years through the development of improved cushioning and

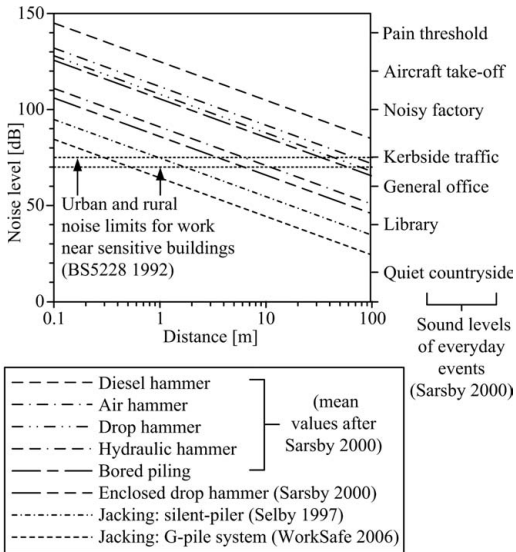


Figure 6. Noise limits and emissions from piling operations.

isolation systems. In Figure 6, various environmental noise levels are compared with the source noise levels, N_{source} , of typical piling equipment, including recent ‘quiet’ hammers and pile jacking machines. The human ear perceives a 10 dB increase in noise level as a doubling in loudness so the logarithmic scale obscures the true variation.

By plotting the theoretical attenuation of noise with distance (Equation 2), an indication of the minimum acceptable separation is found. Modern ‘quiet’ hammers are rarely acceptable in congested urban areas, but are increasingly used for new-build developments, where the minimum separation limits can be satisfied. The noise emissions from pile jacking machines do not exceed ambient urban noise.

2.2 Ground vibration

Design codes specify limits on the permissible ground vibrations from construction operations. These limits are intended to prevent disturbance to people and damage to nearby structures. The limits preclude the use of conventional dynamic piling methods in certain locations, particularly urban areas.

Ground vibrations are usually quantified by the peak velocity of particles in the ground as they are disturbed by the passing wave. The instantaneous particle velocity consists of three orthogonal components which are usually measured independently using a triaxial geophone. The most commonly used definition of peak particle velocity is the simulated resultant ppv. This is the vector sum of the maximum of each component regardless of

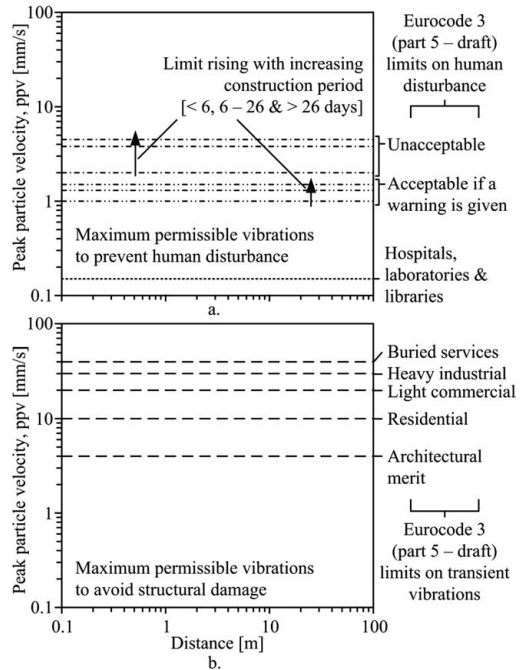


Figure 7. Maximum acceptable transient ground vibrations.

whether these component maxima occur simultaneously (Hiller & Hope, 1998).

Eurocode 3 (1992) provides guidelines for acceptable human exposure to ground vibrations depending on the length of the construction period (Fig. 7a). Structural damage thresholds are also specified, ranging from a ppv of 2 mm/s for buildings of architectural merit, to 15 mm/s for industrial buildings (Fig. 7b).

Ground vibration measurements near to pile jacking operations have been reported by Li et al. (2003), Rockhill et al. (2003) and White et al. (2002) (Fig. 8). The primary source of these vibrations is the elastic rebound of the pile head when the jacking load is released at the end of each stroke. If the pile is deviating during installation, lateral vibration can result in addition to upwards movement.

Good operational practices can reduce these sources of ground vibration. For example, the Silent Piler system allows the jacking force to be reduced in a controlled manner at the end of a downstroke, and a skilled operator can correct for any deviation before releasing the pile head. Figure 9 shows the time record of ground vibrations during installation of a sheet pile using a Silent Piler jacking machine. Negligible vibrations are recorded whilst the pile is moving but four transient pulses are evident between jacking strokes. The largest of these events correspond to the opening and closing of the chuck that grips the pile, and from

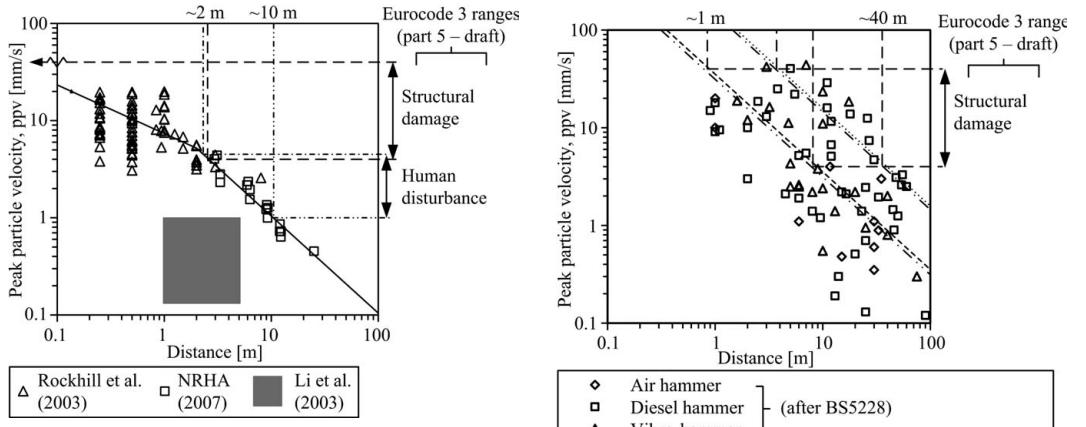


Figure 8. Ground vibrations near pile jacking operations.

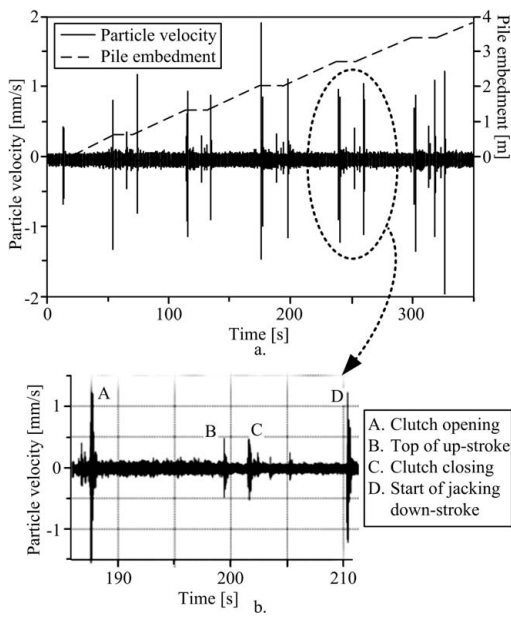


Figure 9. Ground vibration measurements during sheet pile installation using a Silent Piler jacking machine.

the impulse of hydraulic force at the start of the jacking stroke.

For comparison, a database of previously published measurements of ground vibrations during dynamic piling is shown in Figure 10 (Head & Jardine, 1992). Figures 7–8 and 10 are plotted on identical axes. The measured ground vibrations reduce in an approximately linear fashion with log radius. A number of empirical methods for predicting ground vibrations follow this trend, taking the general form of

◆ Air hammer □ Diesel hammer △ Vibro-hammer ····· Stiff ground 25 kJ impact hammer ---- Soft ground 5 kJ impact hammer - - - 2 kJ vibratory hammer - - - - 10 kJ vibratory hammer	(after BS5228) (after Eurocode 3: part 5 – draft)
------------------------------------------------------------------------------------------------------------------------------------------------------------------------------------------------------------------------------------------------------------------------------------------------------------------------------------------------------------------------------------------------------------------------------------------------------------------------	------------------------------------------------------------------------------------------------------------------------------------

Figure 10. Ground vibrations near pile driving operations.

Equation 3 (Attewell & Farmer (1973), BS5228 (1992), Eurocode 3 (1992)).

$$\text{ppv (mm/s)} = \frac{A}{r^n} \quad (\text{r in metres}) \quad (3)$$

The constant A in Equation 3 depends on the properties of the medium and the initial energy of the wave. If the medium is non-dissipative, the index n refers to the geometry of the wavefront. Geometric spreading of a cylindrical wavefront leads to $n = 0.5$, whilst for geometric spreading from a point source $n = 1$. Empirical guidance for the selection of A for dynamic pile driving methods is given by Eurocode 3 (1992), based on hammer energy and soil type. A value of $n = 1$ is recommended, reflecting that at relevant distances from the pile, the upper portion from which the vibrations radiate is best idealised as a point source.

For the jacked pile data shown in Figure 8, Rockhill et al. (2003) proposed a bilinear fit as a simple predictor for ground vibrations induced by pile jacking, linking ppv to the log of separation, r (Equation 4). Close to the pile, the bilinear fit uses an index of $n = 0.5$, reflecting that the pile is better represented as a line source at this close proximity. Further away, the index reverts to $n = 1$, indicative of spherical geometric spreading.

$$\text{ppv (mm/s)} = \min \left[\frac{7.7}{\sqrt{r}}, \frac{10.4}{r} \right] \quad (\text{r in metres}) \quad (4)$$

By combining Equation 4 with the Eurocode 3 limits, an indication of the minimum separation between pile jacking and sensitive structures can be assessed. For residential structures this intersection corresponds to

a nominal separation of around 0.5 metres. However, for practical purposes, the minimum separation is more likely to be limited by logistical constraints than the transmission of ground vibrations. For a separation greater than a few metres, the ground vibrations from pile jacking are indistinguishable from vibrations arising from passing traffic and other construction plant such as generators.

2.3 Sustainability: material and energy use

In urban areas the most commonly-used pile material is concrete, due to the low cost of bored piling and the unsuitability of pile hammers. The recent introduction of high capacity jacking machines has made steel piles a feasible solution for urban areas, and the choice between steel and concrete is once again available.

As raw materials become scarcer, and environmental concerns related to excessive energy use emerge, the choice between steel and concrete is increasingly influenced by environmental factors. In certain regions, these factors are having an increasing effect on the economics of construction through environmental taxes imposed by legislation.

Unlike concrete, steel piles can be easily recycled, although re-use in situ remains an option (Chapman et al. 2001). Embodied energy is a common indicator used to assess the energy use of an object or structure. In the case of foundation piles, this quantity includes the energy used to extract and process the raw materials, then transport and install the foundations. For recycled steel piles the embodied energy is substantially reduced.

Chau et al. (2006) describe a case study comparing the embodied energy of steel and concrete retaining wall systems. For the conditions considered, it was found that the embodied energy of a steel sheet pile wall is halved by the use of recycled steel, and is the optimal solution – from an embodied energy viewpoint – compared to reinforced concrete systems. Other indicators of environmental impact such as the embodied CO₂ emissions provide additional indicators to guide material selection, although standard input parameters and procedures for life cycle analysis assessments are not widely established.

The facility to remove steel piles – unlike bored concrete piles – and release the site for subsequent alternative development is an additional consideration when comparing the long term impact of foundation piles (Dawson 2001).

3 INSTALLATION AND AXIAL CAPACITY

3.1 Pile – CPT analogy for design

As discussed in Section 1.3, the installation method of a pile determines the stress state and level of

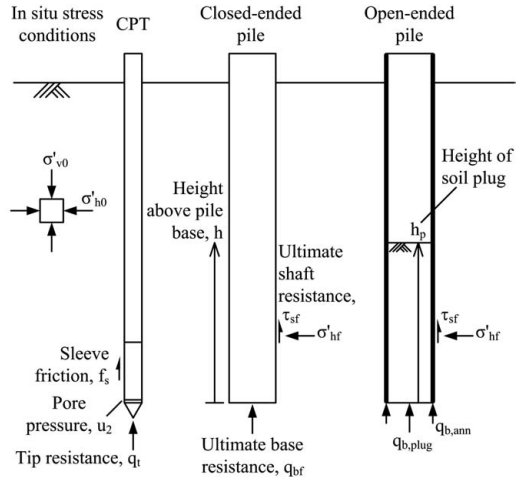


Figure 11. Nomenclature for CPTs and piles.

disturbance of the soil, which in turn has a significant influence on the subsequent strength and stiffness under axial load. This section describes a simple framework for describing the stress changes that take place around a jacked or driven pile during installation. This framework provides a simple basis on which to (i) formulate prediction methods for the strength and stiffness of jacked piles and (ii) understand how the installation process of a jacked pile can be optimised to maximise the axial strength and stiffness (or reduce the required jacking capacity).

Most modern pile design methods directly link CPT parameters to pile capacity, taking advantage of their similar geometry and installation processes (Fig. 11). This analogy is particularly appropriate for jacked piles, which are installed by static force – in the same way as a CPT – in contrast to the dynamic installation of driven piles.

If a jacked pile is considered analogous to a CPT, then the CPT tip resistance, q_t , can be linked to the base resistance during installation, $q_{bf,install}$, and in turn this can be linked to the subsequent static base resistance at failure q_{bf} . The relative size of the pile and the CPT must be accounted for, as discussed in Section 3.3. The CPT sleeve friction, f_s , is analogous to the unit shaft resistance, τ_{sf} , but correlations between these parameters are hampered by the unreliability of sleeve friction measurements, which are often affected by wear and alignment of the sleeve, and by the resolution of subtraction cone devices.

Instead, it is increasingly common to link τ_{sf} to q_t , taking due account of the mechanisms that occur as the soil passes around the base of the advancing pile. Since the soil adjacent to the pile shaft, which governs τ_{sf} , experienced the load q_{bf} (as the pile base passed that horizon) more recently than the in situ stress $\sigma'v_0$, it is

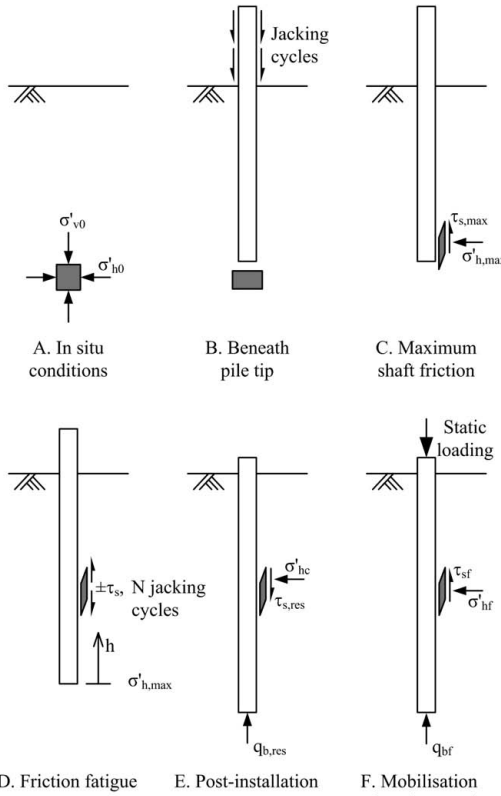


Figure 12. Stages in the loading history of a soil element adjacent to a jacked pile.

more logical to estimate shaft capacity from q_t than from σ'_v0 using a classical earth pressure method.

This approach of breaking down the stress history of a soil element during pile installation is described in detail by Poulos (1988) and White (2005), and is summarised below.

3.2 Soil element 'life cycle' for drained penetration (installation in sand)

The key stages in the stress history of a soil element close to a jacked pile are illustrated in Figure 12. A simple stress path to represent these changes is given in Figure 13. These diagrams represent the case of drained installation – in a sandy soil – so neglect pore pressure effects. Each stage is described in sequence below.

3.3 Base resistance, $q_{bf,install}$, q_{bf}

3.3.1 Mechanisms linking q_p , $q_{bf,install}$, q_{bf}

A soil element that will be in contact with the pile shaft after installation initially lies beneath the pile

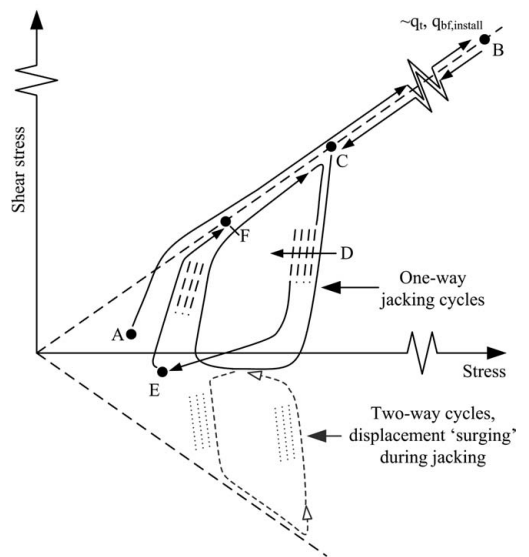


Figure 13. Loading history of a soil element adjacent to a displacement pile.

tip. As the pile or CPT tip approaches, the local stress rises from the in situ value until a stress of $q_{bf,install}$ or q_t acts as the pile or CPT tip reaches that point. The following mechanisms can lead to differences between the profiles of q_t and $q_{bf,install}$ during jacking, and q_{bf} during a subsequent load test:

- During installation, local heterogeneities in ground condition are smoothed out by the large size of a pile compared to a CPT. The zone of deformation around the base of a pile is larger than around a CPT, in proportion to the effective diameter of each. Measurements of q_t are therefore more sensitive to local variations in ground condition.
- The combined effects of the differences in diameter and penetration rate of a pile compared to a CPT may lead to different drainage conditions. The degree of drainage during steady penetration is governed by the dimensionless group vD/c_v , where v = penetration rate, D = diameter and c_v is the relevant coefficient of consolidation. The diameter of a pile is typically an order of magnitude larger than a CPT ($D_{CPT} = 35.7$ mm), whereas the installation rate of jacking machines is comparable to a CPT ($v_{CPT} = 20$ mm/s). Therefore, at sites where the CPT is drained, pile installation may be partially drained, causing excess pore pressure generation and a difference in penetration resistance compared to a CPT.
- During static loading after installation, the plunging, or steady penetration resistance may

not be fully mobilised if q_{bf} is defined by a settlement criterion. However, due to the high base stiffness of jacked piles (described in Section 4), the plunging base capacity is usually mobilised at the conventional settlement criterion of D/10.

3.3.2 Field measurements linking q_c and $q_{bf,install}$

Field measurements at sand and clay sites generally indicate that a unit resistance similar to the CPT tip resistance is mobilised on the base of a closed-ended or plugged pile during jacked installation, such that $\alpha \sim 1$ in Equation 5:

$$q_{bf,install} \approx \alpha q_{t,av} \quad (5)$$

where $q_{t,av}$ is the CPT tip resistance, suitable averaged over a vertical range, to account for the effect of local heterogeneities. At uniform sites a simple arithmetic average of q_t over a vertical range of $+/-1.5D$ is widely used to derive $q_{t,av}$ (Randolph 2003, Jardine et al. 2005 and White & Bolton 2005). However, Xu & Lehane (2005) show that for sites with a strongly layered stratigraphy it is more appropriate to use the 'Dutch Method' (Van Mierlo & Koppejan 1952, Schmertmann 1978). This method gives additional weighting to regions of weaker soil, to which the deformation during penetration will be attracted.

Field tests reported by Dingle et al. (2007) showed that the Dutch method gave a lower bound prediction to $q_{bf,install}$ for a 320 mm diameter closed-ended tubular pile at a highly layered site in Japan. Lehane et al. (2003) report measurements of $q_{bf,install}$ for a 350 mm square precast concrete pile installed through sands and silty clays. It was found that $q_{bf,install}$ was $\sim 80\%$ of the raw q_t profile, but in closer agreement with $q_{t,av}$ found using the Dutch method. Good agreement between $q_{bf,install}$ and q_t has also been reported by Chow (1997) and Lehane (1992) during installation of a 100 mm diameter closed-ended instrumented jacked pile at relatively uniform sites.

A plug usually forms within an open-ended jacked pile after a few diameters of penetration, unless special measures are used, such as vertical cycling ('surging'), water jetting, internal augering or the use of an internal pile shoe. During further jacking the pile remains fully plugged unless a stronger layer is reached, at which point the penetration reverts to a coring manner until sufficient additional plug length is mobilised to balance the increase in base resistance (White et al. 2000, Randolph et al. 1991).

It is difficult to measure the base resistance acting on the enclosed soil plug of an open-ended pile during installation. Lehane & Gavin (2001) present measurements of annular and plug resistance during installation and load testing of a heavily instrumented model jacked pile in sand. During fully plugged

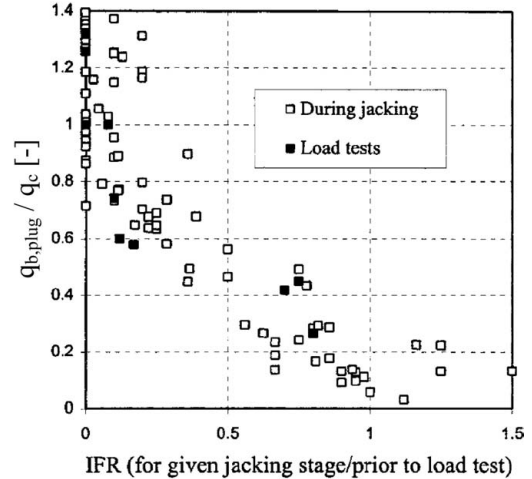


Figure 14. Plug resistance during open-ended pile jacking (Lehane & Gavin 2001).

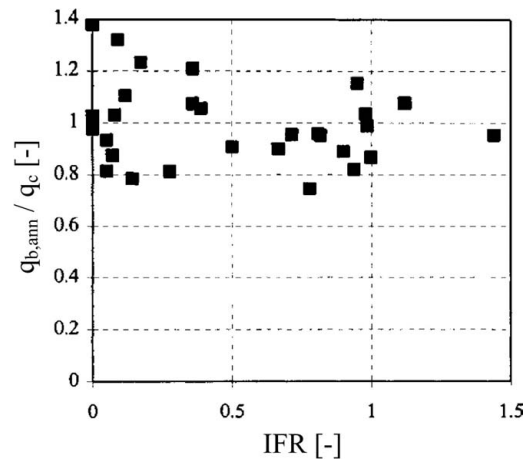


Figure 15. Annular resistance during open-ended pile jacking (Lehane & Gavin 2001).

penetration, $q_{b,plug}/q_c \sim 1$, but reduced values are measured with increasing incremental filling ratio (IFR) (Fig. 14). This observation confirms that when the internal shaft resistance is insufficient to hold the plug in place against the steady penetration resistance, q_t , soil flows into the pile, lengthening the plug. After sufficient lengthening, the increased internal shaft resistance balances the penetration resistance, q_t , and the incremental filling ratio reverts to zero.

Lehane & Gavin's (2001) data of annular resistance, $q_{b,ann}$, confirms that the full local CPT resistance, q_t , is mobilised on the steel area of the pile (Fig. 15). It is usual to assume the same for open-section H-section or sheet piles.

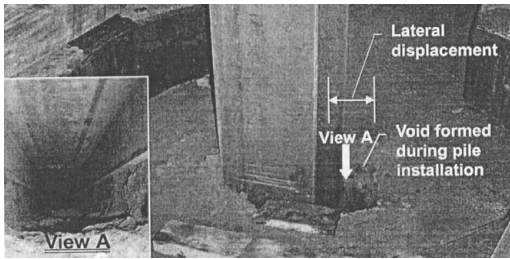


Figure 16. Plugging and buckling of an H-pile (Li et al. 2003).

A back-analysis by White et al. (2000) showed that a vertical arching analysis, following De Nicola & Randolph (1997), can capture the plugging behaviour of a pipe pile during jacking. However, the arching equations are very sensitive to the assumed profile of earth pressure coefficient within the soil plug. For most practical dimensions of tubular pile, a plug will form during jacking, and so the installed pile can be considered as closed-ended under subsequent static loading. This behaviour contrasts with dynamic pile installation methods, during which the inertia of the soil within the pile prevents formation of a plug (Liyanapathirana et al. 2001).

Plugging can also occur during jacking of open-section H-piles. Li et al. (2003) report cases in which jacked H-piles have buckled due to the free-standing length of pile created by downdrag of soil plugs on either side of the H-pile web (Fig. 16). Voids of depth 7–10 m have been reported around H-piles (Li et al. 2003). Sand filling around jacked H-piles is now a standard construction procedure in Hong Kong, to prevent buckling.

3.3.3 Field measurements linking $q_{bf,install}$ and q_{bf}
The jacking load measured during installation is often used to verify the capacity of a jacked pile, based on the assumption that the capacity will not reduce with time after installation. It is well known that the shaft capacity of a displacement pile changes with time after installation due to consolidation and other mechanisms – a process known as ‘set-up’. Set-up of shaft resistance is discussed in Section 3.8.

The base resistance of a pile is less affected by time-dependent processes. Dingle et al. (2007) report the re-mobilisation of $q_{bf,install}$ during static load tests conducted 1–8 hours after installation of a 320 mm diameter closed-ended jacked pile. The base capacity at failure, q_{bf} , was found to be approximately equal to, or greater than – for piles tipped in clay – the base resistance recorded during the final installation stroke. The average ratio of q_{bf} (defined at a settlement of $D/10$) and the load at the end of the final stroke of installation, $q_{bf,fs}$, was 0.99 for the piles tipped in sand (Fig. 17).

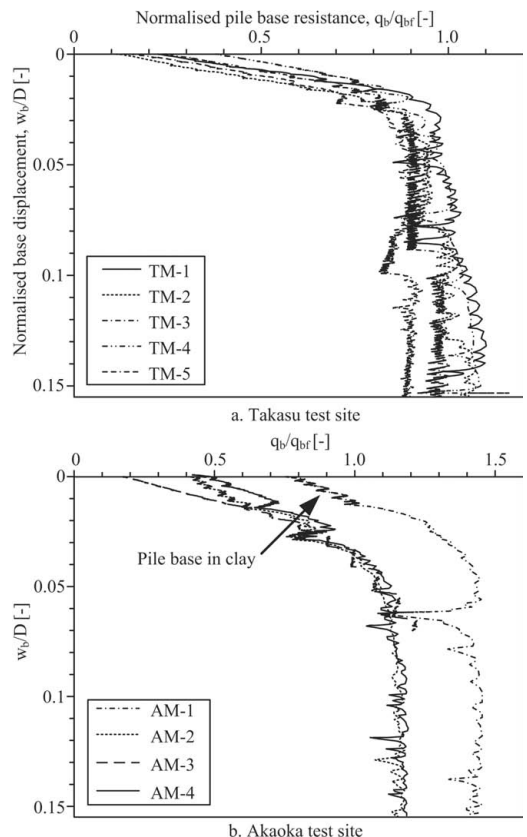


Figure 17. Field measurements comparing load test base response to installation resistance (Dingle et al. 2007).

However, Medzvieckas and Slizyte (2005) report cases in which the base resistance during a load test is lower than during installation – a phenomenon known as relaxation that was also observed by Mitchell & Mander-Jones (2004). This behaviour is not yet fully understood, but could be due to the development of negative pore pressures during shear if the soil is dilatant. This negative pore pressure would create additional effective stress around the pile base during jacking, which would not be present immediately that the jacking force is reapplied, or during a slow maintained load test. Mitchell (2004) describes how relaxation was eliminated at a particular site by cyclic loading of the pile after installation.

Compared to driven piles, jacked piles exhibit a stiffer base response – and a greater base capacity if defined by a settlement criterion – due to the stiffening effect of the final jacking stroke and the resulting residual base load. For closed-ended driven piles in sand, the UWA-05 design method recommends a value of $\alpha = 0.6$ in Equation 5 (Lehane et al. 2005a).

This reduction factor on $q_{t,av}$ is primarily due to partial mobilisation of the full base resistance at D/10 settlement. For closed-ended jacked piles, White & Bolton (2005) and Xu & Lehane (2005) found $\alpha \approx 0.9$ for a database of load tests based on settlement criterion of D/10.

For open-ended driven piles, Lehane et al. (2005a) propose a linear reduction in $q_{bf}/q_{t,av}$ with effective area ratio (defined in Section 3.6) such that $\alpha \rightarrow 0.15$ for a thin-walled pile penetrating in an unplugged manner. Since jacked pile usually plug during installation, these low values of α rarely apply.

3.4 Shaft resistance: general expression

The shaft resistance on a displacement pile is governed by the effective stress friction equation:

$$\tau_{sf} = \sigma'_{hf} \tan \delta \quad (6)$$

where τ_{sf} is the unit shaft resistance, σ'_{hf} is the horizontal effective stress on the pile shaft at failure, and δ is the pile-soil interface friction angle. To exploit the analogy between the CPT and a jacked pile, it is necessary to link σ'_{hf} to the cone tip resistance, q_t . The stress history diagrams shown in Figures 12 and 13 provide this link, and lead to the following general expression for shaft resistance, involving the additional parameters a , b and c :

$$\tau_{sf} = \frac{q_t}{a} A_{r,eff}^b \left[\max\left(\frac{h}{D}, 2\right)^c \right] \tan \delta \quad (7)$$

The mechanisms underlying parameters a , b and c are described in Sections 3.5–3.7.

3.5 Flow around pile tip: 'a' parameter

During installation of a closed-ended jacked pile, as an element of soil flows around the shoulder of the pile the stress level drops from $q_{bf,install}$ (or q_t) to some fraction of this value. This fraction depends on the deformation properties of the soil, and in particular the unloading stiffness. As the soil element comes into contact with the lower part of the pile shaft, an upwards shear stress is mobilised. This maximal value of unit shaft resistance is denoted $\tau_{s,max}$. On the simplified stress path, this stage is marked A – C (Figs. 12, 13) and $\tau_{s,max}$ can be linked to the cone resistance as follows:

$$\tau_{s,max} = \frac{q_t}{a} \tan \delta \quad (8)$$

For the case of a CPT, $\tau_{s,max}$ is similar to the sleeve resistance, f_s , although f_s is actually the average shear

stress over ~ 3 diameters behind the tip of a standard cone. The CPT friction ratio $F_r = f_s/q_t$ is typically 1% in sands, indicating that $a/\tan \delta \sim 100$ for the stress path around a smooth CPT ($\delta \sim 20^\circ$), suggesting an 'a' parameter of ~ 30 . In clays, which have a lower stiffness than sands, so unload less whilst passing around the pile tip, F_r is $\sim 5\%$, which corresponds to a correspondingly lower 'a' parameter. Values of $a = 33$ and 44 for compression and tension loading respectively are recommended in the UWA-05 design method for driven piles in sand (Lehane et al. 2005a). It is assumed that these values also apply for jacked piles. Schneider et al. (2007) discuss in more detail how the 'a' parameter varies with soil type. The difference between compression and tension loading can be attributed to Poisson's strains in the pile and the general unloading of the ground during uplift (de Nicola & Randolph 1993).

3.6 Effective area ratio, A_r ; 'b' parameter

Field-scale open-ended piles rarely plug during driving due to the inertia of the soil column. The pile usually penetrates in an unplugged ('coring') manner instead. In contrast, jacked piles often plug during installation, creating additional soil displacement and horizontal stress acting on the pile shaft. This effect leads to differences in the behaviour of jacked and driven piles.

The degree of plugging during an increment of penetration can be quantified by the effective area ratio, $A_{r,eff}$, which is the ratio of the total volume of material added to the ground (i.e. the gross pile volume minus any soil entering the plug) to the gross pile volume.

$$A_{r,eff} = 1 - IFR \frac{D_i^2}{D^2} \quad (9)$$

$A_{r,eff} = 1$ corresponds to plugged penetration or a closed-ended pile. $A_{r,eff} = 0$ corresponds to a vanishingly thin-walled pile for which there would be negligible soil displacement. The incremental filling ratio (IFR) is the incremental change in plug height (Δh_p) with incremental increase in embedment depth (Δz_{base}), $IFR = \Delta h_p / \Delta z_{base}$.

A multiplicative factor, $A_{r,eff}^b$ is included in Equation 7 to account for the effect of plugging. The difference in shaft resistance on an open-ended pile compared to a closed-ended pile, due to the differing level of soil displacement, is therefore:

$$\frac{\tau_{s,max} [\text{open}]}{\tau_{s,max} [\text{closed}]} = A_{r,eff}^b \quad (10)$$

Cavity expansion analysis provides a theoretical basis for selecting the parameter 'b'. White et al.

(2005) show that a value of $b = 0.3$ is appropriate for sands (drained expansion), whilst a lower value of $b \sim 0.1$ is more appropriate for clays (undrained expansion) (Carter et al. 1980). For a typical thin-walled pipe pile ($D/t = 50$), Equation 10 predicts increases in shaft resistance by factors of 2.1 and 1.3 in sand and clay respectively if plugging occurs. Experimental corroboration of this analysis is provided by Gavin & Lehane (2003), who report a factor ~ 2.5 difference in unit shaft resistance on a model pipe pile when plugged compared to unplugged.

The purpose of these examples is to highlight the possible increase in shaft resistance that can result from permitting a pipe pile to plug during jacked installation. However, site practice is often to prevent plugging by lubricating the inside of the pile or adding a driving shoe, in order reduce the jacking resistance and ease installation. The possible beneficial effect of plugging cannot be utilised in design if plugging is subsequently eliminated by site practices.

3.7 Friction fatigue: ‘c’ parameter

3.7.1 Friction fatigue stress path stage

As a pile is jacked or driven, cycles of loading are applied to the soil adjacent to the pile – as illustrated by stage D on Figures 12 and 13. Jacking involves predominantly one-way cycles of loading, although two-way cycles result if residual base load is trapped after each jacking stroke, leading to the mobilisation of negative shaft resistance. After the final jacking stroke, or hammer blow, some base load may be retained by negative shaft friction on the upper part of the pile, leaving the soil at stress state E. This simple stress path ignores the possible generation of excess pore pressures, but serves to highlight the influence of cycling on σ'_h . Cycles of loading lead to a reduction in normal stress and available shaft resistance – a phenomenon known as friction fatigue. This mechanism has been quantified in laboratory tests, centrifuge models and at field scale.

3.7.2 Laboratory test evidence of friction fatigue

The cyclic loading of each soil element adjacent to the pile shaft is analogous to the response observed in cyclic interface shear box (or ring shear) tests. Cyclic interface shear of sand leads to gradual densification of the shear zone, even if the sample originates in a dense state (DeJong et al. 2003, Porcino et al. 2003 and Ghionna & Mortara 2002). Kelly (2001) describes four tests on sand using the 1 m diameter ring shear apparatus at Sydney University. These results highlight the effect of cycling on interface behaviour (Fig. 18). After initially dilating, each sample continues to shear at constant volume, until 10 displacement-controlled cycles are applied. The number of cycles

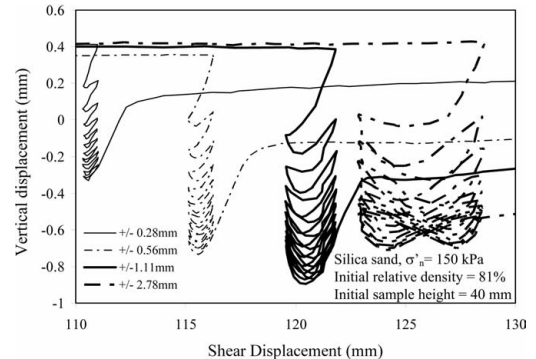


Figure 18. Contraction under cyclic loading in a 1 m diameter interface ring shear test (Kelly 2001).

has a greater influence on the contraction of the interface layer than the net displacement. Also, a higher amplitude of cycling leads to greater contraction.

3.7.3 Centrifuge tests showing friction fatigue

On piles, this behaviour is termed ‘friction fatigue’ and causes the progressive reduction in unit shaft resistance at a given soil horizon as the pile penetrates deeper through further cycles of loading (White & Bolton 2002 and Randolph 2003). Adjacent to the pile, changes in the interface layer thickness, Δt , cause changes in horizontal stress, $\Delta\sigma'_h$. These changes depend on the constraint provided by the far field soil, which can be idealised as an elastic cylindrical cavity (Fig. 19, Equation 11):

$$\Delta\sigma'_h = \frac{4G}{D} \Delta t \quad (11)$$

where G is the operative elastic stiffness of the surrounding soil. Δt is the contraction of the interface layer. Contraction of the interface leads to a reduction in σ'_h , as shown schematically in Figure 19.

Model tests using instrumented piles confirm that friction fatigue is driven by cycles of loading, and that the decay in shaft resistance along a pile shaft is best normalised by the number of cycles experienced by that element, rather than the distance from the pile tip, h . Centrifuge tests involving artificial monotonic pile installation – to the final depth in a single-stroke – show identical values of horizontal stress acting on the pile over the range $1 < h/D < 9$ (Fig. 20). However, the horizontal stress decays when cycles of loading are applied, either during installation, or in a subsequent load test (White & Lehane 2004). Similar data is presented by Schneider & Lehane (2006) and CPT tests using multiple friction sleeves confirm this behaviour (DeJong 2001).

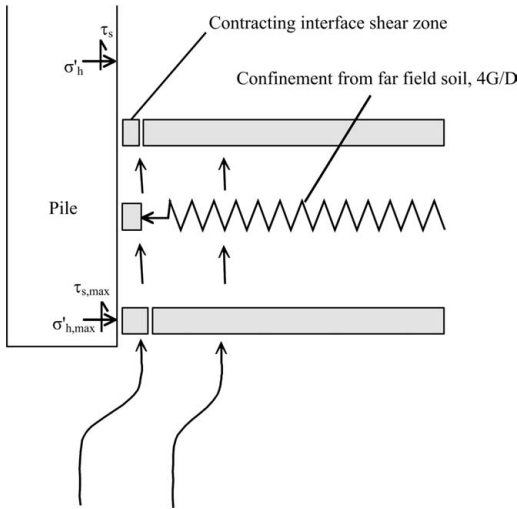


Figure 19. Friction fatigue mechanism (White & Bolton 2004).

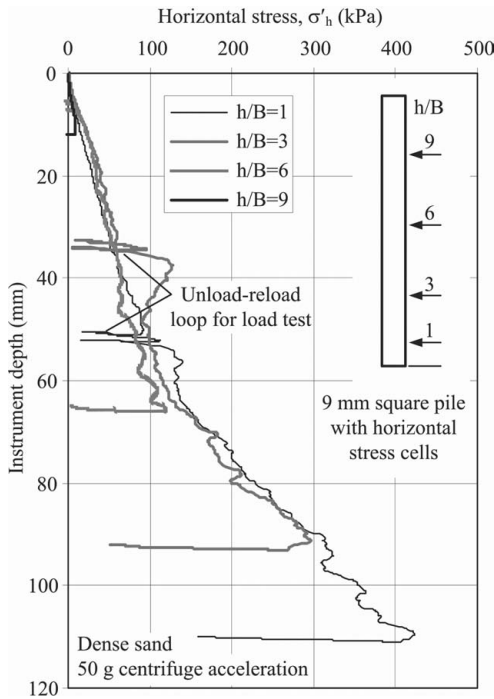
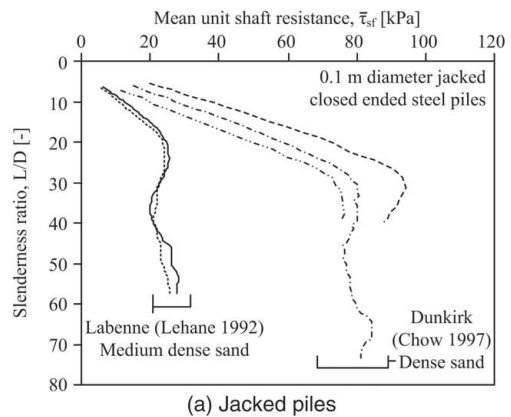


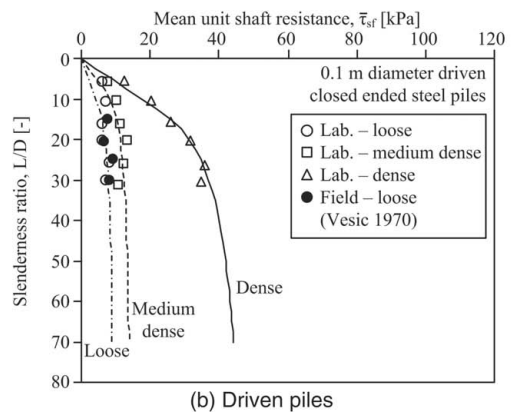
Figure 20. Horizontal stress measurements on a model jacked pile during monotonic installation (White & Lehane 2004).

3.7.4 Field scale tests illustrating friction fatigue

At field scale, the instrumented driven pile tests by Vesic (1970) can be compared with the jacked pile



(a) Jacked piles



(b) Driven piles

Figure 21. Field measurements of mean shaft resistance on jacked and driven piles.

tests reported by Lehane (1992) and Chow (1997) to show the effect of cycles on mean shaft resistance (Fig. 21). These two sets of tests, both on 100 mm diameter closed-ended steel piles, show twice as much shaft resistance for jacked installation compared to dynamic driving.

The instrumented pile tests reported by Dingle et al. (2007) isolated the effect of cycles on mean shaft resistance by installing the same pile at the same site with different numbers of jacking strokes. Figure 22 illustrates the strong influence of installation cycles on mean shaft resistance. The 10 m long piles could be installed with as few as 12 one-way jacking cycles, leading to a mean normalised shaft resistance of $[\tau_{sf}/q]_{av} = 0.006$. However, if installation involved a larger number of cycles, with two-way displacement, the shaft resistance halved.

The mechanism of friction fatigue is well known to operators of pile jacking machines. Large cycles of vertical displacement are commonly used to ease

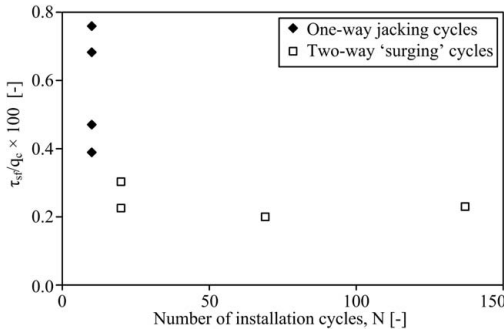


Figure 22. Influence of jacking cycles on shaft resistance (Dingle et al. 2007).

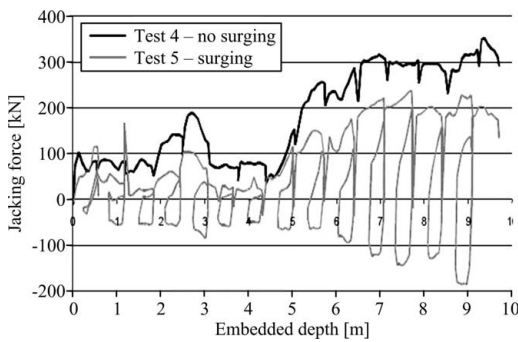


Figure 23. Effect of 'surging' on jacking force at sandy site.

installation – a technique known as 'surging'. Machine operators often aim to reduce the required jacking force in order to counter the tendency for sheet piles to deviate from vertical during hard driving.

Figure 23 shows the effect of 'surging' on the jacking force required to install a sheet pile at a sandy site. In test 4 the pile was installed to a depth of 10 m by one-way jacking strokes of ~700 mm length. In test 5 the pile was cycled by 350 mm after each jacking stroke. These 13 additional displacement cycles reduced the jacking force by 50% at the final embedded depth.

At a different site, with clay layers, the same surging procedure led to a smaller reduction in jacking force of only 10–20 % (Fig. 24). This comparison illustrates that surging is less effective in clay since friction fatigue is reduced. In clay, the pile-soil interface shear zone is thinner than for sand, so can undergo less contraction. In addition, this contraction is hindered by the low permeability which prevents the escape of pore water.

This strong influence of loading cycles on friction fatigue has implications for the design of jacked piles. Compared to driven piles – which are installed by many hundreds of two-way cycles – jacked pile

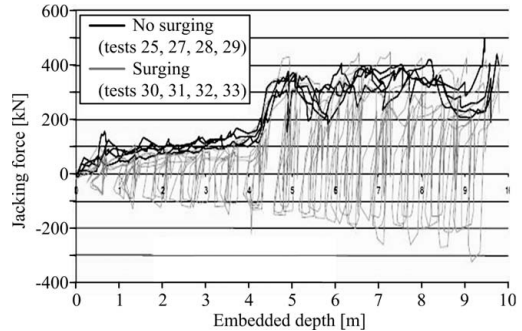


Figure 24. Effect of 'surging' on jacking force at site with clay.

installation involves 10–100 cycles of loading, which is predominantly one-way.

However, although measurements indicate that friction fatigue is caused by cycles of loading, it is not straightforward to include number of cycles – accounting for their amplitude and nature (one-way or two-way) – within a design method. Experimental evidence shows that the rate of friction fatigue depends not only on the number of imposed cycles, but on the mode and amplitude of cycling – which are machine and operator dependent. Two-way cycling leads to a greater degradation than one-way cycling during installation.

These effects are acknowledged in the analysis of in-service cyclic loads – for example during storm loading of offshore piles (Poulos 1988, Jardine 1991). These effects also occur during installation-induced cycles, so affect the resulting shaft capacity and should be acknowledged in design.

3.7.5 Friction fatigue: design approach

A pragmatic approach for design is to follow the format of current CPT-based methods for driven piles. These methods account for friction fatigue through a reduction in unit shaft resistance in proportion to $(h/D)^c$, with a maximum value of h/D being applied very close to the pile tip (typically over the bottom two diameters):

$$\tau_{sf} = \left[\max\left(\frac{h}{D}, 2\right)^c \right] \tau_{s,max} \quad (12)$$

For dynamically-driven piles in sand, a friction fatigue index of $c = -0.5$ is recommended by Lehane et al. (2005a) in the UWA-05 design method, based on a database of > 75 pile load tests. The lower number of cycles imposed during installation of a jacked pile leads to a smaller value of the index c . The horizontal stress measurements shown in Figure 20 imply that $c = 0$ for steady – monotonic – penetration. For piles

installed with a realistic number of jacking strokes, field measurements (in sand) collated by White (2005) and Lehane et al. (2005b) are fitted by values of $-0.2 \geq c \geq -0.4$, reflecting the reduced friction fatigue during installation compared to driven piles.

Soil type also has a strong influence on the rate of friction fatigue and the resulting index c , as discussed in the proceedings of this workshop by Schneider et al. (2007). Clay soils contract less during cycles of interface shear due to the thinner shear zone and the lower permeability. Lehane et al. (2000) report a value of $c \approx -0.2$ for driven piles in clays. Highly compressible soils, such as loose carbonate or micaceous sands are also vulnerable to strong friction fatigue effects, leading to higher values of the parameter ' c '.

In summary, field-scale, centrifuge-scale and element-level tests show that cycles of displacement imposed during pile installation drive friction fatigue, and therefore govern the shaft resistance operative after installation. Pile jacking provides control of this cycling, and allows piles to be installed with a smaller total number of cycles than dynamic driving. Site practices routinely utilise this control to ease installation through 'surging'.

There exists the potential – demonstrated by field data – for jacked piles to offer greater shaft resistance than identical driven piles. However, firm design guidance is not yet established, and careful monitoring of installation would be needed to limit unintended cycles and to check that the final jacking force is in agreement with predictions. As noted previously in relation to plugging, the potential enhancement of shaft resistance that can result from jacked installation cannot be utilised in design unless measures are in place to ensure that the enhancement is not eliminated by site practices that aim to ease installation.

3.8 Effects of time on shaft resistance: 'set-up'

3.8.1 Governing mechanisms

It is well-established that the shaft capacity of displacement piles increases with time (Chow et al. 1998, Axelsson 2000). In clays, this behaviour arises predominantly from the dissipation of positive excess pore pressures that are created by the advancing pile tip. In sands, installation is usually assumed to be drained, but significant set-up is still evident for long periods beyond any plausible dissipation period. Load test data collated by Chow et al. (1998) indicates that shaft capacity typically trebles within 3 years of pile installation. This increase in shaft resistance in the absence of pore pressure dissipation can be attributed to the following mechanisms occurring during the period of set-up:

- (i) *An increase in radial stress, due to creep-induced changes in the hoop and radial stresses*

adjacent to the pile. The stress path during pile installation can be simplified as cylindrical expansion (at the pile tip) then contraction (representing friction fatigue), which leads to lower radial stress than hoop stress close to the pile (Fig. 25). Therefore, any subsequent creep-induced stress equalisation will lead to a reduction in hoop stress and an increase in radial stress and hence available shaft resistance (White et al. 2005). This hypothesised effect will be enhanced if the creep is dilatant, as observed in triaxial tests during creep after a stress path representative of pile installation (Bowman & Soga 2005).

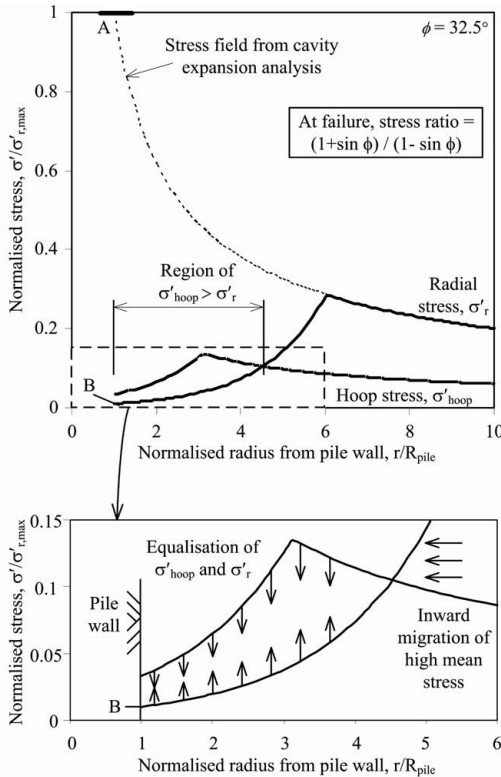
- (ii) *An increase in the stiffness and dilatancy of the soil adjacent to the pile due to creep and aging.* These changes lead to a greater rise in radial stress on loading. Aging of freshly-disturbed sand deposits has been observed to lead to increases in CPT_{qt} (Ng et al. 1998.), and aging of sand leads to a more dilatant response on shearing (Howie et al. 2001)
- (iii) *An increase in pile-soil interface friction angle, due to corrosion of the pile.* This mechanism has been eliminated as a primary cause, since set-up is observed on both corrosive and on-corrosive piles.

These set-up mechanisms apply to both jacked and driven piles. However, according to the hypothesised mechanism shown in Figure 25, the reduced friction fatigue on a jacked pile would lead to a smaller region in which $\sigma_r < \sigma_{hoop}$, and in which creep-induced stress equalisation can drive set-up. The radial profiles of σ_r and σ_{hoop} shown in Figure 25 are calculated based on rigid-plastic cavity expansion theory, with a principal stress ratio of K_p being mobilised at failure. The installation of a pile is simplified as expansion to some maximal value – which would be comparable to q_t – then radial contraction to a value of $(q_c/a)(h/D)^c$, representing soil flow around the pile tip and subsequent friction fatigue (Equation 7). The resulting radial variation in σ_r and σ_{hoop} represents the initial conditions for any subsequent creep-induced equalization of stresses.

This mechanism illustrates how higher friction fatigue creates greater potential for an increase in σ_r due to creep. Conversely, any additional shaft resistance on a jacked pile due to reduced friction fatigue may be partially offset in the long-term by reduced set-up.

3.8.2 Field measurements of jacked-pile set-up

Figure 26 shows collated data of set-up in both sands and clays reported by various authors. These measurements of jacking load and load test capacity are influenced by changes in both base and shaft resistance,



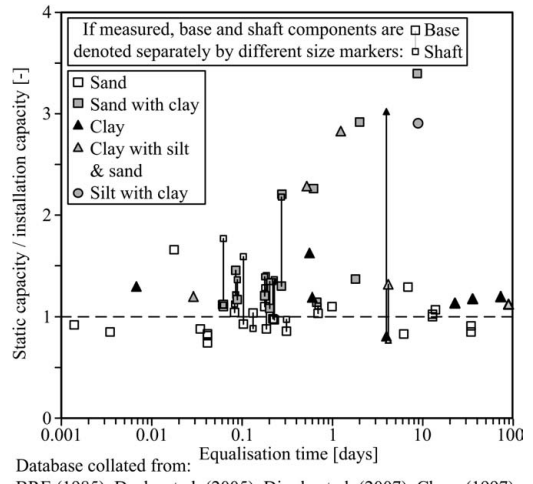
A: Maximum value of radial stress on pile, $\sigma'_{r,\max} \sim q_t$
B: Post-installation radial stress on pile, $\sigma'_{ri} = q_i(h/D)^c/a \sim 0.01\sigma'_{r,\max}$

Figure 25. Hypothesised mechanism for creep-induced set-up based on stress fields from cavity expansion and contraction (after White et al. 2005).

which are separated if known. In contrast, Figure 27, reproduced from Mitchell (2004) shows data of relaxation, collated from a single site.

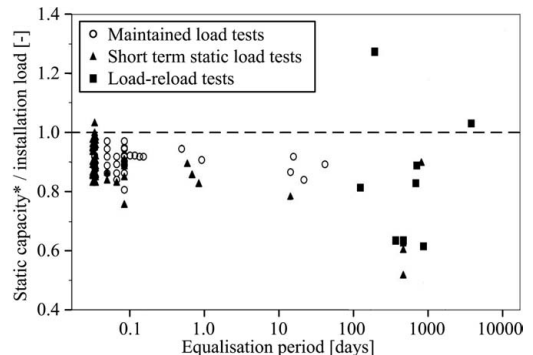
Further evidence of shaft resistance set-up on jacked piles is given by the load test data collated by Zhang et al. (2006). Figure 28 shows collated measurements for ~ 150 jacked piles, including H-piles, square precast concrete piles, and model piles tested in a geotechnical centrifuge. The ratio of load test capacity – usually defined by Davisson's (1972) settlement criterion – to jacking force at the end of installation reveals a scattered trend of increasing set-up with increasing slenderness.

This trend reflects the compensating influences of partial base mobilisation and shaft set-up. The full base resistance may not be re-mobilised at the settlement used to define failure, whereas the shaft resistance encountered during jacking will increase due to set-up prior to the load test. For slender piles (high L/D), the second effect dominates, and the load test



Database collated from:
BRE (1985), Deeks et al. (2005), Dingle et al. (2007), Chow (1997),
Lehane (1992), Medzvieckas & Slizyte (2005), Mitchell & Jones
(2004), Pellew (2002), Powell et al. (2003), Wardle et al. (1992) &
Yetginer (2003)

Figure 26. Set-up of capacity compared to installation resistance.



* evaluated at a normalised load test displacement of $w/D = 0.125$

Figure 27. Effect of time on re-jacking force at a site susceptible to relaxation (Mitchell 2004).

capacity exceeds the installation force; for short piles the converse is true.

3.8.3 Summary of set-up behaviour

The mechanisms governing set-up in sand, and the effect of installation method on set-up, are not yet well understood. Further research is required before the additional capacity that may potentially be available through set-up can be utilised in design.

The use of jacking force measurements to check the installed capacity of jacked piles ignores the beneficial effect of set-up, and so is intrinsically conservative.

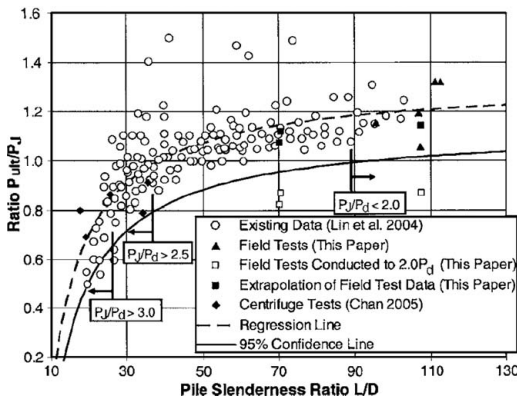


Figure 28. Comparison between set-up, expressed as ratio between load test capacity and jacking force, and pile slenderness (Zhang et al. 2006).

However, ‘set-down’ – or ‘relaxation’ – is occasionally encountered, as shown in Figure 27, and reported by Mitchell (2004). Re-jacking after a pause period provides an indication of any tendency for relaxation.

3.9 Summary of axial capacity

The preceding discussion has highlighted the mechanisms that lead to differences in the axial capacity of jacked and driven piles. The general framework for shaft resistance given by Equations 6 and 7 was adopted by the UWA-05 design method for driven piles in sand, which has been incorporated in the latest revision of American Petroleum Institute (API) design code (API 2006). Table 1 shows the calibrated parameters recommended by UWA-05 and presents tentative modifications for jacked tubular piles, indicating the underlying mechanisms.

For clays, although the same mechanisms apply, the numerical differences will be smaller: friction fatigue is a less significant phenomenon in undrained conditions, and base resistance represents a smaller proportion of capacity in clay, lessening the importance of plugging.

Field measurements indicate that the axial capacity of a jacked pile usually increases with time due to set-up of shaft resistance. However, relaxation has been observed at a small number of sites. Jacking force therefore usually provides a conservative confirmation of the pile capacity. By imposing a short re-jacking stroke after a pause period, relaxation can be identified.

Termination criteria based on jacking force can be used to limit pile length according to the encountered resistance. This approach can lead to shorter piles than if installation is continued to a pre-determined embedment depth based on a conservative design calculation.

Table 1. Comparison of axial capacity parameters for jacked and driven piles in sand

Mechanism	Expression	UWA-05	Jacked pile (tentative)
Base	$q_{bf} = \alpha q_t$ (q_{bf} usually defined at D/10 plugging settlement)	$\alpha = 0.6$ (reducing to 0.15 as $A_{r,eff} \rightarrow 0$ for open-ended)	$\alpha = 0.9$ resistance (assuming during installation)
Maximal shaft resistance	$T_{s,max} = (q_{bf}/a)\tan \delta$	$a = 33$ [comp.] $a = 44$ [tension]	As for UWA-05
Effect of area ratio	$\times A_{r,eff}^b$	$b = 0.3$	As for UWA-05
Friction fatigue	$\times (h/D)^c$	$c = -0.5$	$c = -0.2$ to -0.4

Notes:

Mechanism	Comments (for jacked piles)
Base resistance	Plugging during jacking creates residual base load and a response when reloaded
Maximal shaft resistance	Probably not affected by installation method. Schneider et al. (2007) describe the effect of soil type on the ‘a’ parameter
Effect of Area ratio	Plugging during jacking creates additional lateral soil displacement and a higher $A_{r,eff}$
Friction fatigue	Fewer cycles during jacked installation leads to reduced friction fatigue

4 H-PILE BEHAVIOUR

4.1 H-pile plugging and capacity

Jacked H-piles have been the subject of recent research programmes in Hong Kong reported by Li et al. (2003), Yang et al. (2006) and Zhang et al. (2006). These research programmes were focussed on establishing suitable practices for assuring the performance of H-piles installed into completely decomposed granite (CDG). White et al. (2003) report the use of jacked H-piles to support a 9-storey building in Tokyo.

Yang et al. (2006) and Zhang et al. (2006) report field tests on instrumented H-piles up to 50 m in length, jacked with a force of up to 8 MN through CDG with SPT N-values exceeding 200. Yang et al. (2006) compared driven and jacked piles at the same site, and report higher shaft resistance on the jacked pile, confirming that higher friction fatigue results from increased installation cycles. The test piles were observed to plug during the initial stages of installation, with voids of depth > 4 m reported within the pan of the piles. The degree of plugging during deeper penetration is unknown, and downdrag of a plug close to the pile tip

may not cause observable settlement within the pile pan at the ground surface.

These observations contrast with recent design guidance produced in the UK, based on experience from driven H-piles (Biddle 2005). Design methods for the axial capacity of H-piles are generally based on the limiting values of unit shaft and base resistance developed for tubular piles, but with additional guidance on the appropriate geometry to assume for the failure surfaces.

Biddle (2005) recommend that H-pile shaft resistance is assessed based on the full pile perimeter, assuming that failure occurs at the pile-soil interface. It is stated that ‘plugging is very rare and should not be assumed’, which is inappropriate for jacked piles. As noted earlier for tubular piles, static jacking leads to plugging, whereas the soil inertia prevents plugging during dynamic driving. Additional design considerations for jacked H-piles that result from plugging are:

- (i) Buckling of the free-standing pile length should be prevented by filling the plug void.
- (ii) Predictions (and back-analyses) of axial capacity should consider that base resistance may be mobilised over the gross pile area.
- (iii) In design, the possibility of low shaft resistance on the upper part of the shaft – above any trapped plug, in the filled void – should be considered.

Prediction of H-pile capacity in CDG remains challenging. In situ testing of this material is usually limited to the SPT, since the variable weathering damages CPT devices if hard zones are found. Correlations between SPT N-value and unit shaft resistance show considerable scatter (Fig. 29). In these conditions, the facility to statically test each pile after installation using the jacking machine is highly beneficial. Static load tests involve less uncertainty than the use of a dynamic driving formula, as is current practice in Hong Kong for the termination of driven piles (Yang et al. 2006).

4.2 H-pile walls

A novel technique for enhancing the capacity of H-piles is to install them in a continuous wall, or large ring (Fig. 30). The caisson-type basement foundation used to support the Daido Shinagawa building in Tokyo was constructed from a ring of H-piles installed by the Silent Piler jacking system. Precise control of the jacking machine allowed the separation between adjacent H-piles to be maintained below 5 mm. The completed wall consisted of square box-sections.

The capacity of a completed H-pile wall exceeds the sum of the installation force of each individual pile due to plugging. During installation, the pan of each pile is open (Fig. 31a), whereas during loading the piles form closed box-sections which plug like tubular piles (Fig. 31b). The vertical arching analysis

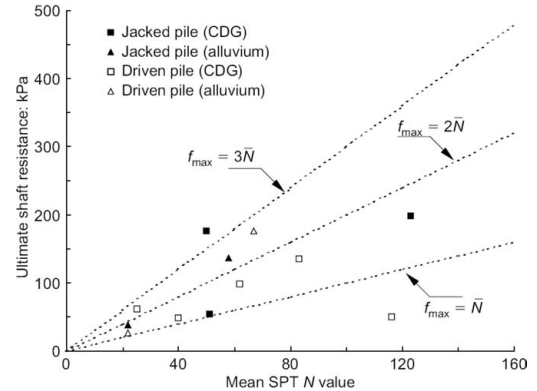
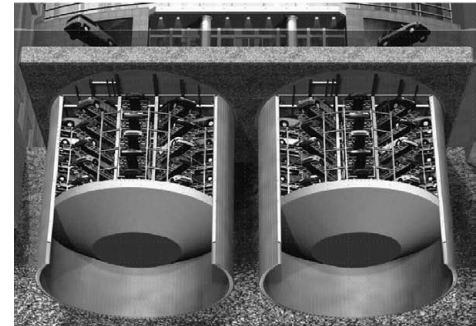


Figure 29. Correlation between H-pile shaft resistance and SPT N-value in Hong Kong alluvium and CDG (Yang et al. 2006).



(a) Continuous H-pile wall



(b) Caisson-type H-pile ring foundation

Figure 30. Foundations from H-pile walls.

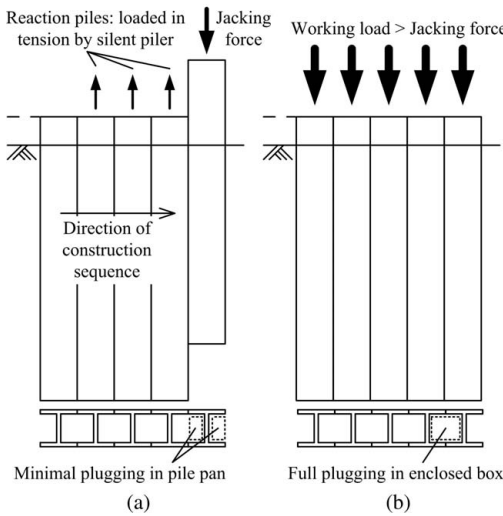


Figure 31. H-pile wall: activation of plugging after installation.

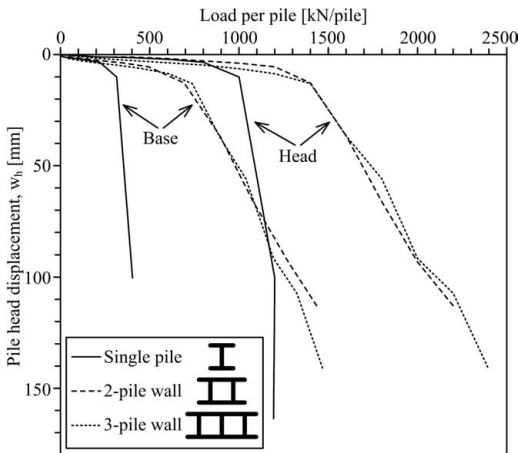


Figure 32. Load tests on H-pile walls (White et al. 2003).

used for tubular pile plugging (Randolph et al. 1991) can be extended to the closed-section boxes formed by an H-pile wall, or the partly-closed pan of individual H-piles (White et al. 2003).

For the Daido Shinagawa building, a set of test piles were installed to assess the axial response of an H-pile wall. An auger was attached to the piler to loosen the soil ahead of the advanced pile, but no spoil was removed. This augering prevented plugging of the test piles during installation. Load tests were conducted on a single pile and on walls of two or three piles (Fig. 32). The stratigraphy consisted of layers of fill, silt and sand and gravel overlying Tokyo mudstone.

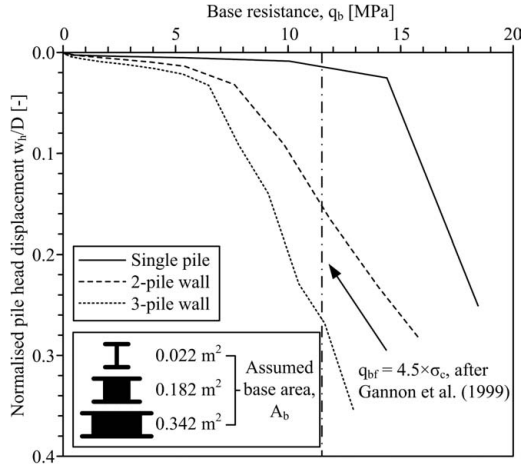


Figure 33. Mobilisation of base resistance on H-pile walls.

The 400 × 400 mm H-piles were embedded by 0.9 m into the Tokyo mudstone, which had an unconfined compressive strength, σ_c , in the range 2.4–2.7 MPa. The piles were instrumented with strain gauges at 6 locations along their length, to allow the load distribution to be deduced. The mean force required to jack the 6 test piles to the final embedded depth of 20 m was 869 kN. The load tests were conducted between 14 and 20 days after installation.

The pile head load-settlement response for each test is shown in Figure 32, with the load expressed per pile. The capacity of the single pile exceeds the installation force, indicating that set-up had occurred during the period between installation and testing. Also, the capacity of each pile within the walls is greater than the single pile. Compared to the single piles, the walls show a 50% higher capacity (per pile) at a failure settlement of $B/10 = 40$ mm.

The strain gauge measurements showed a concentration of shear stress on the lower part of each pile wall, whereas the single pile showed only a gentle increase in shaft resistance close to the pile tip. This concentration of shear stress indicates the mobilisation of high internal shaft friction within the enclosed pile sections, showing that the capacity of the enclosed soil plug is mobilised.

Figure 33 shows the unit base resistance inferred from strain gauges close to the pile base. For the single pile, the force has been normalised by the area of steel, whereas for the walls the plugged cross-sectional area has been used. The convergence of these responses at high loads confirms that the additional capacity of the walls arises from plugging. The mobilised base resistance exceeds $4.5\sigma_c$, which is a typically recommended ultimate bearing capacity for piles in soft rocks (Gannon et al. 1999).

These results confirm that enhanced axial capacity can be activated after the installation of an H-pile wall. However, to mobilise this resistance it is necessary to compress the plug of enclosed soil since the unplugged installation mode does not create beneficial stiffening of the plug. For design, it is necessary to consider the tolerance of the structure to these movements incurred during construction.

5 AXIAL STIFFNESS

5.1 Effect of installation on working behaviour

The final installation stroke of a jacked pile locks in residual base load and pre-loads the surrounding soil, which creates a stiffer base response under working loads. Also, the enhanced shaft resistance resulting from the low number of installation cycles leads to higher stress and therefore stiffness within this region.

5.2 Base response: t-z modelling

Field experiments using jacked piles that have aimed to quantify these effects for use in t-z analyses of axial response are reported by Deeks et al. (2005), Yetginer et al. (2006), Yang et al. (2006) and Dingle et al. (2007). Deeks & White (2007), in the proceedings of this workshop, report centrifuge modelling of the base response.

Parabolic models for the mobilisation of base and shaft resistance closely fit the response of jacked piles (Deeks et al. 2005, Yetginer et al. 2006 and Deeks & White 2007). The field measurements of pile base response reported by Dingle et al. (2007), shown previously in Figure 17, can be recast as secant operative stiffness, normalised by the small strain soil stiffness, G_0 , measured by a seismic CPT (Fig. 34). Good agreement with a parabolic model of the form shown in Equation 13 is evident. The initial operative soil stiffness, $G_{b,\text{init}}$, is back-calculated using the elastic solution for the indentation of a rigid punch into a half space, assuming a Poisson's ratio, ν , of 0.2 (Equation 14). Installation effects are captured by a stiffness multiplier, $\chi_{G_b} = G_{b,\text{init}}/G_0$ which is ~ 1.3 for the load tests reported by Dingle et al. (2007) (Fig. 34).

$$\left(\frac{q_b}{q_{bf}}\right) = -\left(\frac{w}{w_{bf}}\right)^2 + 2\left(\frac{w}{w_{bf}}\right) \quad (13)$$

$$w_{bf} = \frac{\pi(1-\nu)}{4} \frac{q_{bf}}{\chi_{G_b} G_0} D \quad (14)$$

Deeks & White (2007) report centrifuge modelling of jacked piles in sand involving load tests at varying depths, covering different values of CPT rigidity

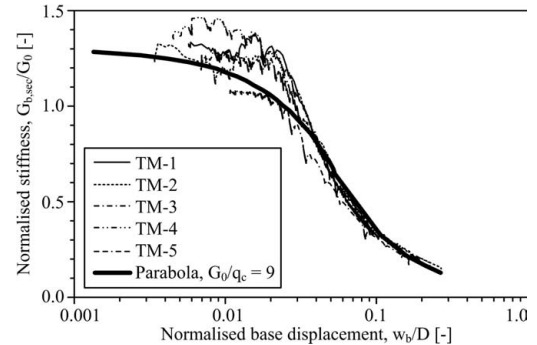
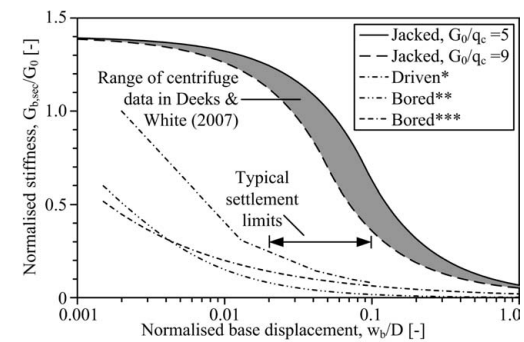


Figure 34. Base response of closed-ended 320 mm diameter jacked piles (Dingle et al. 2007).



*(API 2000), **(Berardi & Bovolenta 2005), ***(Ghionna et al. 1993)

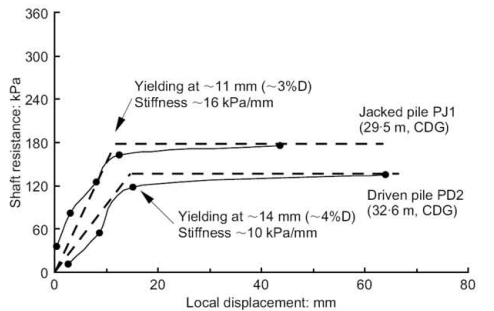
Figure 35. Jacked pile base response compared to guidance for bored and driven piles (Deeks & White 2007).

ratio, G_0/q_d . These tests confirmed that the rigidity of the base response varies with the soil (or CPT) rigidity, and corroborated the high stiffness observed in the field (Fig. 35). The parabolic model given by Equations 13–14 includes the effect of soil rigidity on base response, unlike the models proposed by Ghionna et al. (1993) and Berardi & Bovolenta (2005) – which link $G_{b,\text{sec}}/G_0$ only to w_b/D .

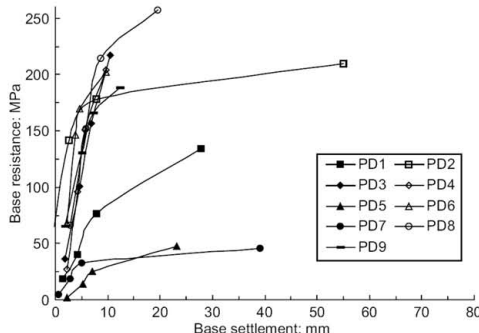
To apply these base response models to open-ended piles it is necessary to account for the small additional settlement that is required to remobilise the plug resistance (Lehane & Randolph 2002).

5.3 Shaft response: t-z modelling

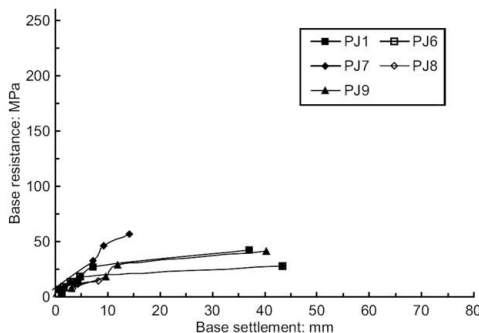
The shaft load-settlement response observed by Dingle et al. (2007) was also parabolic and could be back-analysed using Randolph & Wroth's (1978) analytical solution to link soil stiffness to t-z stiffness. The rigidity of the shaft response was defined as the ratio between the operative soil stiffness at the start of the t-z response, $G_{s,\text{init}}$, and the unit shaft resistance at



(a) Local shaft response of driven and jacked piles in CDG



(b) Base response of driven piles in CDG



(c) Base response of jacked piles in CDG

Figure 36. Shaft and base responses for jacked and driven H-piles (Yang et al. 2006).

failure, τ_{sf} . It was found that $G_{s,init}/\tau_{sf} \approx 30 G_0/q_t$ for two different test sites.

Yang et al. (2006) compared the t-z response of jacked and driven H-piles at the same site in Hong Kong. Load tests identified that jacked piles offer enhanced shaft stiffness, in addition to higher capacity (Fig. 36a). Regarding base resistance, the load test results are less conclusive. The stiffness and strength of 9 driven piles varied over an order of magnitude (Fig. 36b), whereas the jacked piles showed a smaller but more consistent stiffness and capacity (Fig. 36c).

The upper values of base load exceed 200 MPa, which is far higher than the ultimate bearing capacity usually observed in completely decomposed granite (GEO 2006). It is possible that the driving process damaged the strain gauges that were used to infer base load.

5.4 Summary of axial response

Compared to bored and open-ended driven piles, the reported measurements of jacked pile base response are extremely stiff, reflecting the beneficial preloading of the pile base caused by the jacking process. For shaft response, the field evidence is less conclusive, although higher strength and stiffness has been reported. The base response of jacked piles is typically and an order of magnitude stiffer than for bored piles, and a factor ~ 5 stiffer than for driven piles (Deeks et al. 2005, Deeks & White 2007 and Dingle et al. 2007). Further confirmation of these conclusions would allow the enhanced stiffness of jacked piles to be fully utilised in design.

The CPT parameters G_0 and q_t , coupled with a parabolic model, provide a simple method of predicting the base response of a jacked pile. The ratio G_0/q_t typically decreases with relative density, so plunging failure is reached at a higher settlement in denser soils.

6 CONCLUSIONS

6.1 Differences between jacked piles and conventional displacement piles

Pile jacking offers an alternative technique for the installation of displacement piles, instead of dynamic installation using a hammer or vibrator. Pile jacking systems apply static hydraulic load to the pile head, gaining reaction either from deadweight or the negative shaft resistance of previously-installed piles. Compared to driven displacement piles, the installation of a jacked pile involves:

- (i) minimal noise and ground vibration;
- (ii) a reduced number of load cycles;
- (iii) direct measurement of the static resistance.

These differences, coupled with operational aspects of a pile jacking system compared to a conventional rig, have implications both for the construction process and the design process.

6.2 Construction process aspects

Pile jacking machines emit little noise or ground vibrations. Field measurements record disturbance which is comparable to the ambient sources that are generally present in urban areas.

'Self-walking' pile jacking systems – such as the 'Silent Piler' – are limited to installing piles at relatively close spacing, but require minimal temporary works since the machinery is supported by the advancing wall. The jacking capacity of these machines is up to ~ 4 MN, and installation can be eased by jetting, augering, or displacement surging – which increases friction fatigue. The machines typically occupy a working area of < 1 m on either side of the pile wall, so can operate in confined spaces such as adjacent to existing buildings or active roads and railways. The self-walking feature also allows piling on embankment slopes or over water.

Deadweight-based jacking machines – such as the Chinese-manufactured system known as 'G-pile' in Malaysia and Australia – require a strong working platform, and more space and time for mobilisation compared to the lightweight 'self-walking' systems. However, there are no constraints on the layout of a pile group, and the maximum jacking force is ~ 9 MN.

6.3 Design aspects

The axial response of a jacked pile differs from a driven pile due to two principal mechanisms: plugging and friction fatigue. The static jacking process encourages the formation of a plug within tubular piles and also partly-closed sections such as sheet and H-piles.

Plugging leads to additional lateral soil displacement during penetration, creating enhanced horizontal stress on the pile shaft. The low number of cycles during installation leads to reduced friction fatigue compared to dynamically-driven piles. However, the use of displacement surging to ease installation can reduce this effect. The combined influences of plugging and reduced friction fatigue lead to additional strength and stiffness compared to driven or bored piles.

It is logical to link jacked pile capacity to CPT parameters due to the similar installation processes. The general framework for shaft resistance described in this paper allows the differences between jacked and driven piles to be explored. This framework, with parameters calibrated for driven piles in sand, forms the UWA-05 design method. Modified parameters appropriate for jacked piles have been identified and linked to the governing mechanisms.

Under working conditions, the preloading effect created by jacked installation – including compression of any soil plug – leads to enhanced base stiffness. Field measurements and centrifuge tests of jacked piles demonstrate that the base response is typically 10 times stiffer than for a bored pile at typical working settlements. A simple parabolic t-z model linked to CPT parameters captures this behaviour. The initial stiffness of the base response indicates an operative soil stiffness higher than G_0 .

Measurements of jacking force during installation allow the design capacity to be checked. Termination

criteria based on measured jacking force can allow shorter pile lengths to be used where feasible. At most sites, set-up leads to a significant increase in capacity with time, although relaxation has been observed at a limited number of locations.

Novel types of foundation have been proposed, to take advantage of the environmental benefits of jacking, whilst accommodating the limitations of the machines. One example is a caisson of H-piles, in which plugging is activated after installation, leading to high group efficiency.

ACKNOWLEDGEMENTS

Much of the work described in this paper has been supported by Giken Seisakusho Co. Ltd., under a long term research programme at the University of Cambridge, initiated by Mr Akio Kitamura and Professor Malcolm Bolton.

REFERENCES

- API 2000. *RP 2A-WSD Planning, designing and constructing fixed offshore platforms – working stress design, 22nd edition*, Washington DC, USA, American Petroleum Institute.
- Attewell, P. B. & Farmer, I. 1973. Attenuation of ground vibration from pile driving. *Ground Engineering*, 6 (4): 26–29.
- Berardi, R. & Bovolenta, R. 2005. Pile-settlement evaluation using field stiffness non-linearity. *Proceedings of the Institution of Civil Engineers Geotechnical Engineering*, 158 (GE1): 1353–2618.
- Biddle, A. R. 2005. *H-pile design guide*, Ascot, UK, The Steel Construction Institute. SCI publication P335.
- Bowman, E. T. & Soga, K. 2005. Mechanisms of set up of displacement piles in sand: laboratory creep tests. *Canadian Geotechnical Journal*, 42 (5): 1391–1407.
- BRE 1985. *Final report on research on the behaviour of piles as anchorages for buoyant structures*. Department of Energy, UK.
- BS5228 1992. *Noise control on construction and open sites – Part 4: Code of practice for noise and vibration control applicable to piling operations*, London, British Standards Institution.
- Bustamante, M. & Ganeselli, L. 1982. *Pile bearing capacity by means of static penetrometer CPT*. Proceedings 2nd European Symposium on Penetration Testing. Amsterdam: 493–499.
- Carter, J. P., Randolph, M. F. & Wroth, C. P. 1980. Some aspects of the performance of open- and closed-ended piles. *Proceedings, 1st Conference on Numerical Methods in Offshore Piling*. ICE: 165–170.
- Chapman, Y., Marsh, B. & Foster, A. 2001. Foundations for the future. *Proceedings, Institution of Civil Engineers, Civil Engineering*, 144 (1): 36–41.
- Chau, C., Soga, K. & Nicholson, D. 2006. Comparison of embodied energy of four different retaining wall systems. *Proceedings of the International Conference on Re-use of Foundations for Urban Sites*. Watford, UK.

- Chow, F. C. 1997. *Investigations into the behaviour of displacement piles for offshore foundations*. Ph.D., University of London (Imperial College), London, UK.
- Davison, M. T. 1972. High capacity piles. *Proceedings and lecture series in Innovations in Foundation Construction*. ASCE, Illinois section.52.
- Dawson, R. 2001. Foundation piling—steel to replace concrete. *Proceedings, Institution of Civil Engineers, Geotechnical engineering*, 149 (GE4): 205–207.
- De Beer, E. 1988. Different behaviour of bored and driven piles. *Deep Foundations on Bored and Augered Piles I*. Balkema, Rotterdam: 47–82.
- De Nicola, A. & Randolph, M. F. 1993. Tensile and compressive shaft capacity of piles in sand. *ASCE Journal of Geotechnical and Geoenvironmental Engineering*, 119 (12): 1952–1973.
- De Nicola, A. & Randolph, M. F. 1997. The plugging behaviour of driven and jacked piles in sand. *Géotechnique*, 47 (4): 841–856.
- Deeks, A. D., White, D. J. & Bolton, M. D. 2005. A comparison of jacked, driven and bored piles in sand. *Proceedings, XVIIth International Conference on Soil Mechanics & Geotechnical Engineering*. Osaka, Japan. Millpress. 3: 2103–2106.
- DeJong, J. T. 2001. *Investigation of particulate-continuum interface mechanisms and their assessment through a multi-friction sleeve penetrometer attachment*. Georgia Institute of Technology, Atlanta, Georgia, USA.
- DeJong, J. T., Randolph, M. F. & White, D. J. 2003. Interface load transfer degradation during cyclic loading: a microscopic investigation. *Soils and Foundations*, 43 (4): 81–93.
- Dingle, H. R. C., White, D. J., Deeks, A. D. & Nagayama, T. 2007. Field studies of the axial response of closed-ended tubular jacked piles. *Submitted to Géotechnique for publication*.
- Dubbeling, P., Vriend, A. & Nozaki, T. 2006. Press-In piling technology for sustainable construction. *Proceedings Deep Foundations Institute 10th International Conference on Piling and Deep Foundations*. Amsterdam, The Netherlands. DFI: 432–441.
- Eurocode 3 1992. *Eurocode 3. Design of steel structures – Part 5: Piling. BS EN 1993-5:1992 (draft)*, London, British Standards Institution.
- Filip, R. K. 2006. Recent advances in quiet & vibrationless steel pile installation & extraction. *Proceedings Deep Foundations Institute 10th International Conference on Piling and Deep Foundations*. Amsterdam, The Netherlands. DFI: 442–450.
- Gannon, J. A., Masterton, G. G. T., Wallace, W. A. & Muir Wood, D. 1999. *Piled foundations in weak rock*. London, UK, CIRIA. Report 181.
- Gavin, K. & Lehane, B. M. 2003. End bearing of small pipe piles in dense sand. *Proceedings, BGA International conference on foundations*. Dundee, UK. Thomas Telford: 321–330.
- GEO 2006. *Foundation design and construction*. Hong Kong, Geotechnical Engineering Office. GEO publication no. 1/2006.
- Ghionna, V. N., Jamiolkowski, M. & Lancellotta, R. 1993. Base capacity of bored piles in sands from in situ tests. *Deep Foundations on Bored and Auger Piles II*. Balkema: 67–75.
- Ghionna, V. N. & Mortara, G. 2002. An elastoplastic model for sand-structure interface behaviour. *Géotechnique*, 52 (1): 41–50.
- Goncharov, B. V., Karev, V. M. & Troyanovskii, Y. V. 1964. Results of comparative tests of mobile machines for driving piles. *Osnovaniya Fundamenty i Mekhanika Gruntov*, 1 (1): 19–21.
- Head, J. M. & Jardine, F. M. 1992. *Groundborne vibrations arising from piling*. Construction Industry Research and Information Association (CIRIA), UK. Technical note 142.
- Hiller, D. M. & Hope, V. S. 1998. Groundborne vibration generated by mechanized construction activities. *Proceedings, Institution of Civil Engineers, Geotechnical Engineering*, 131: 223–232.
- Howie, J. A., Shozan, T. & Vaid, Y. P. 2001. Effect of ageing on stiffness of loose Fraser River sand. *Proceedings of Advanced Laboratory Stress-Strain Testing of Geomaterials*. Lisse. Balkema. 1: 235–244.
- Jardine, R. J. 1991. Chapter 5: The cyclic behaviour of large piles with special reference to offshore structures. In O'Reilly, M. P. & Brown, S. F. (Eds.) *Cyclic loading of soils*. London, UK: Blackie.
- Jardine, R. J., Chow, F. C., Overy, R. & Standing, J. 2005. *ICP design methods for driven piles in sands and clays*, London: Thomas Telford.
- Kelly, R. 2001. *Development of a large diameter ring shear apparatus and its use for interface testing*. Ph.D., University of Sydney, Sydney, Australia.
- Lehane, B. M., Chow, F. C., McCabe, B. M. & Jardine, R. J. 2000. Relationships between shaft capacity of driven piles and CPT end resistance. *Proceedings, Institution of Civil Engineers, Geotechnical Engineering*, 143: 93–101.
- Lehane, B. M. & Gavin, K. G. 2001. Base resistance of jacked pipe piles in sand. *ASCE Journal of Geotechnical and Geoenvironmental Engineering*, 127 (6): 473–480.
- Lehane, B. M., Pennington, D. & Clark, S. 2003. Jacked end-bearing piles in the soft alluvial sediments of Perth. *Australian Geomechanics*, 38 (3): 123–133.
- Lehane, B. M. & Randolph, M. F. (2002) Evaluation of a minimum base resistance for driven pipe piles in siliceous sand. *ASCE Journal of Geotechnical and Geoenvironmental Engineering*, 128(3):198–205.
- Lehane, B. M., Schneider, J. A. & Xu, X. 2005a. *CPT based design of driven piles in sand for offshore structures*. Perth, Australia, The University of Western Australia. GEO:05345.
- Lehane, B. M., Schneider, J. A. & Xu, X. 2005b. *Evaluation of design methods for displacement piles in sand*. Perth, Australia, The University of Western Australia. GEO:05341.1.
- Li, K. S., Ho, N. C. L., Lee, P. K. K., Tham, L. G. & Lam, J. 2003. Chapter 2: Jacked Piles. In Li, K. S. (Ed.) *Design and construction of driven and jacked piles*. Hong Kong, Centre for Research and Professional Development.
- Liyanapathirana, D. S., Deeks, A. J. & Randolph, M. F. 2001. Numerical modelling of the driving response of thin-walled open-ended piles. *International Journal for Numerical and Analytical Methods on Geomechanics*, 25 (9): 933–953.
- Medzvieckas, J. & Sližyte, D. 2005. Installation of jacked piles in sandy soils. *16th International conference on soil mechanics and geotechnical engineering*. Osaka, Japan. Millpress. 3: 2149–2152.

- Mitchell, P. W. 2004. Jacked piling in a soil subject to relaxation. *Australian Geomechanics*, 39 (4): 25–32.
- Mitchell, P. W. & Manders-Jones, J. 2004. Experiences with Jacked Piles. *Australian Geomechanics*, 39 (4): 11–24.
- Ng, N., Berner, P. & Covil, C. 1998. The ageing effects of sands. *Ground Engineering*, (10): 21.
- Pellew, A. 2002. *Field investigations into pile behaviour in clay*. Ph.D., University of London (Imperial College), London, UK.
- Porcino, D., Fioravante, V., Ghionna, V. N. & Pedroni, S. 2003. Interface behaviour of sands from constant normal stiffness direct shear tests. *ASTM Geotechnical Testing Journal*, 26 (3): 1–13.
- Poulos, H. G. 1988. *Marine geotechnics*, London, UK, Unwin Hyman Ltd.
- Powell, J. J. M., Butcher, A. P. & Pellew, A. 2003. Capacity of driven piles with time – implications for re-use. *Proceedings 13th European Conference on Soil Mechanics and Geotechnical Engineering*. Prague, Czech Republic. 2: 335–340.
- Randolph, M. F. 2003. Science and Empiricism in pile design. *Géotechnique*, 53 (10): 847–875.
- Randolph, M. F. & Wroth, P. 1978. Analysis of deformation of vertically loaded piles. *ASCE Journal of Geotechnical and Geoenvironmental Engineering*, 104 (GT12), 1465–1488.
- Randolph M. F., Leong E. C., & Houlsby G. T. 1991. One-dimensional analysis of soil plugs in pipe piles. *Géotechnique* 41(4): 587–598
- Rockhill, D. J., Bolton, M. D. & White, D. J. 2003. Ground-borne vibrations due to press-in piling operations. *Proceedings, BGA International conference on foundations*: 743–756.
- Sarsby, R. W. 2000. *Environmental geotechnics*, London, UK: Thomas Telford.
- Schmertmann, J. H. 1978. *Guidelines for Cone Penetration Test: Performance and Design*. Washington DC., US Dept. of Transportation, Federal Highway Administration, Offices of Research and Development, Implementation Division. FHWA-TS-78-209 145.
- Schneider, J. A. & Lehane, B. M. 2006. Effects of width for square centrifuge displacement piles in sand. *Proceedings, International Conference on Physical Modelling in Geotechnics*. Hong Kong. Taylor & Francis. 2: 868–873.
- Schneider, J. A., White, D. J. & Kikuchi, Y. 2007. Back analysis of Tokyo port bay bridge pipe pile load tests using piezocene data. *International Workshop on Recent Advances of Deep Foundations (IWDPF07)*. Yokosuka, Japan.
- Selby, A. R. 1997. *Control of vibration and noise during piling*. London, UK, British Steel. Brochure publication.
- Van Mierlo, W. C. & Koppejan, A. W. 1952. Lengte en draagvermogen van heipalen, Bouw.
- Vesic, A. S. 1970. Test on instrumented piles, Ogeechee river site. *ASCE Journal of the Soil Mechanics and Foundations Division*, 96 (2): 561–584.
- Wardle, I. F., Price, G. & Freeman, T. J. 1992. Effect of time and maintained load on the ultimate capacity of piles in stiff clay. *Proceedings, Piling Europe Conference*: 83–90.
- White, D. J. 2005. A general framework for shaft resistance on displacement piles in sand. *Proceedings, International Symposium on Frontiers in Offshore Geotechnics*. Perth: 697–703.
- White, D. J. & Bolton, M. D. 2002. Observing friction fatigue on a jacked pile. *Centrifuge and Constitutive Modelling: Two extremes*: 347–354.
- White, D. J. & Bolton, M. D. 2005. Comparing CPT and pile base resistance in sand. *Proceedings, Institution of Civil Engineers, Geotechnical Engineering*, 158 (GE1): 3–14.
- White, D. J., Finlay, T. C. R., Bolton, M. D. & Bearss, G. 2002. Press-in piling: Ground vibration and noise during pile installation. *International Deep Foundations Congress*. Orlando, USA. ASCE. special publication 116: 363–371.
- White D. J., Bolton M. D. & Wako C. 2003. A novel urban foundation system using pressed-in H-piles. *Proceedings, 13th European Conference on Soil Mechanics & Geotechnical Engineering*. Prague 2:425–432.
- White, D. J., Schneider, J. A. & Lehane, B. M. 2005. The influence of effective area ratio on shaft friction of displacement piles in sand. *International Symposium on Frontiers in Offshore Geotechnics*. Perth, Australia.
- White, D. J., Sidhu, H. K., Finlay, T. C. R., Bolton, M. D. & Nagayama, T. 2000. Press-in piling: The influence of plugging on driveability. *Proceedings, 8th International Conference of the Deep Foundations Institute*. New York: 299–310.
- WorkSafe 2006. *Online article: Successful noise management in construction*. Department of Consumer and Employment Protection, Government of Western Australia. <http://www.safetyline.wa.gov.au/newsite/worksafe/pages/noisgenl0030.html>
- Xu, X. & Lehane, B. M. 2005. Evaluation of end-bearing capacity of closed ended piles in sand from cone penetration data. *International Symposium on Frontiers in Offshore Geotechnics*. Perth: 733–740.
- Yang, J., Tham, L. G., Lee, P. K. K., Chan, S. T. & Yu, F. 2006. Behaviour of jacked and driven piles in sandy soil. *Géotechnique*, 56 (4): 245–259.
- Yetginer, A. G. 2003. *Press-in piling*. M.Eng., Cambridge University, Cambridge.
- Zhang, L. M., Ng, C. W. W., F. C. & H.W., P. 2006. Termination criteria for jacked pile construction and load transfer in weathered soils. *ASCE Journal of Geotechnical and Geoenvironmental Engineering*, 132 (7): 819–829.

Centrifuge modelling of pile foundation

C.F. Leung

Centre for Soft Ground Engineering, Department of Civil Engineering, National University of Singapore

ABSTRACT: Centrifuge modelling has gained wide acceptance as a versatile technique to investigate geotechnical problems. This paper first provides a brief overview on centrifuge model testing of pile foundations conducted in Asia. Details of centrifuge model studies on piles carried out at the National University of Singapore are then presented. Advances in modelling techniques and practical implications of the findings from the studies are also highlighted.

1 INTRODUCTION

Owing to correct simulation of prototype stress levels, significant reduction in soil consolidation duration and repeatability of test results, centrifuge modelling technique has gained wide acceptance as a versatile tool to investigate geotechnical problems. In conjunction with other tools such as numerical modelling and field studies, centrifuge and physical modelling can be a powerful tool in geotechnical design process. Randolph & House (2001) attempted to correlate the different modelling activities in the engineering design process, as illustrated in Figure 1.

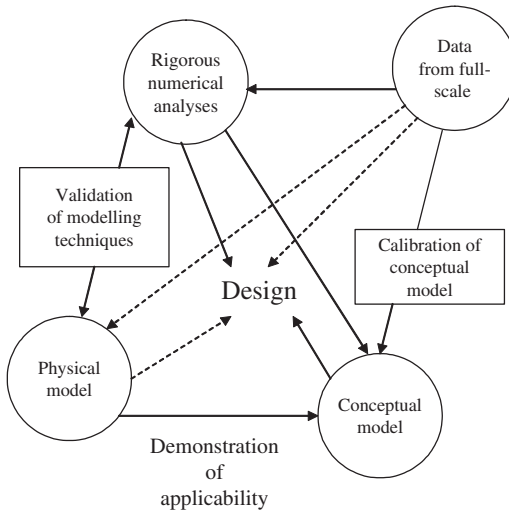


Figure 1. Different modeling activities in engineering design process (after Randolph & House 2001).

Kimura (1998) reported the development of geotechnical centrifuges in Japan and noted rapid increase in the number of new centrifuge facilities in Japan in the 1990s. As of 1998, there were a total of about 40 beam and drum centrifuges in Japan with nominal radius ranging from 0.4 m to 6.5 m and maximum payload ranging from 1 g-t to 500 g-t. Besides Japan, geotechnical centrifuge facilities are also available in many other Asian countries including China, Taiwan, Hong Kong (Shen et al. 1998), Korea (Park et al. 1998), Singapore (Lee et al. 1991) and India. Currently a good number of large geotechnical centrifuge facilities are being built in Korea (Ha et al. 2006, Kim et al. 2006) and China (see for example Ma et al. 2006).

A popular research topic for centrifuge model study is the investigation of pile behaviour. In this review paper, a brief overview on centrifuge model testing of pile foundations in Asia is first presented. This is followed by a detail description on the pile foundation studies performed at the National University of Singapore (NUS) since the early 1990s. Advances in modelling techniques and practical implications of the findings from the centrifuge model studies are also highlighted.

2 CENTRIFUGE MODELLING OF PILES IN ASIA

2.1 Japan

Pile foundations are commonly used to support buildings and other structures worldwide. This is no exception for Japan which also experiences severe earthquakes and typhoons. Thus it is of no surprise that a large number of centrifuge model studies have been carried out in Japan to investigate pile behaviour

under static and dynamic loadings. Researchers from Kyoto University led by M Kimura had published many articles on centrifuge model studies of pile foundations under a variety of configurations and loading situations (see for example Kimura et al. 1998, Kimura & Matsuura 2002).

The advances in pile modelling technique can be demonstrated by a recent interesting centrifuge model study of the Kyoto University group to investigate the performance of caisson foundation reinforced by steel pipe sheet piles (Fig. 2). Various types of connections for the innovative foundation scheme subject to static and dynamic loads were examined. Figure 3 shows the effect of steel pipe sheet pile reinforcement for different types of caisson-pile connections. The effect of reinforcement is defined as the ratio of bearing capacity in a reinforced case over unreinforced

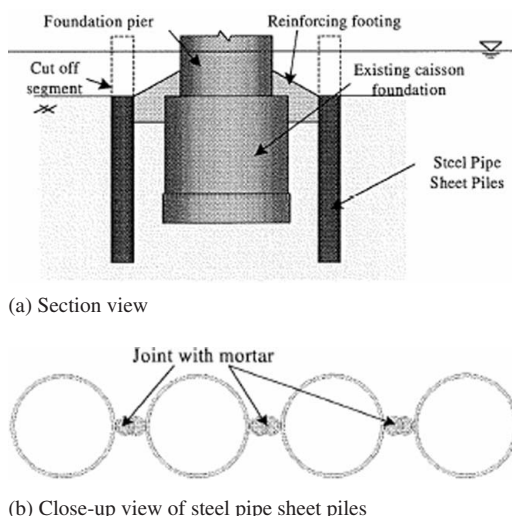


Figure 2. Steel pipe sheet pile reinforcement method (after Isobe & Kimura 2005).

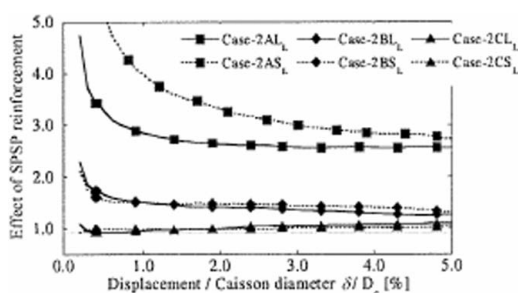


Figure 3. Effect of steel pipe sheet pile reinforcement (after Isobe and Kimura 2005).

case. It is evident that from Figure 3 that the selection of caisson-pile connection is crucial. The study also serves as a good example of research collaboration between research institution and the industry. Detail test results are presented in Isobe & Kimura (2005) and Isobe et al. (2006).

There were also many other useful research studies on pile foundations in Japan. This is particularly so on the investigation of pile performance subject to dynamic and earthquake loads. Examples of such studies included Okawa et al. (2002), Satoh et al. (1998) and Okumura et al. (1994).

2.2 Others

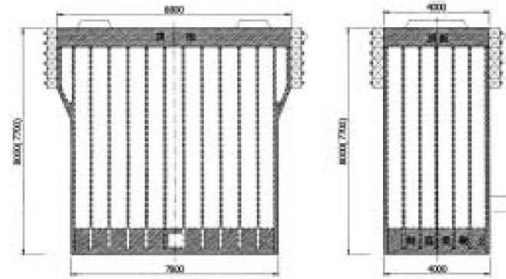
Researchers from China, Hong Kong, Taiwan and Korea had also reported the findings of centrifuge model studies on various pile foundation problems. As an example, during the design stage, Zhang et al. (2006) from the Nanjing Hydraulic Research Institute of China carried out centrifuge model tests to evaluate the suitability of various types of deep foundations to support a heavily loaded bridge, see Figures 4a to 4c. The load-settlement responses of the raft foundation for different types of foundations are shown in Figure 5. As the allowable raft settlement is relatively large, all 3 proposed foundation schemes were found to be acceptable. Further tests were then conducted to evaluate the optimal foundation design for the bridge. The study demonstrated that very useful information can be derived from the investigations of complex geotechnical problems using centrifuge modelling technique.

At the National Central University in Taiwan, Lee et al. (1998) and Lee & Chen (2002) performed a number of centrifuge model studies to investigate pile behaviour under various situations. On the other hand, researchers from Yonsei University (Seo et al. 2006) of Korea reported the findings on the behaviour of pile groups subject to lateral soil movements.

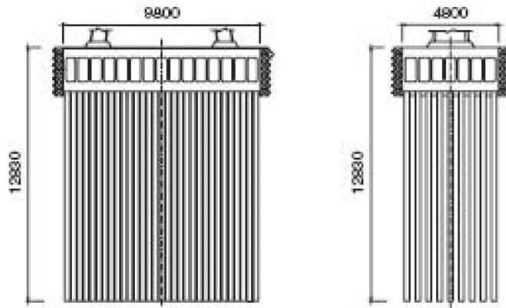
Extensive centrifuge model studies had also been conducted at the Hong Kong University of Science and Technology to investigate foundation problems. A powerful and versatile robot (Ng et al. 2002) called four-axis robot manipulator (Fig. 6) has been developed for centrifuge testing such that the installation, testing and extraction of test objects including model piles and devices can be carried out with relative ease. Su and Li (2006) investigated the pile behaviour under multi-directional earthquake loading. L M Zhang from the same university had also conducted comprehensive centrifuge model studies to investigate pile behaviour. As an example, Zhang & Kong (2006a & b) presented the findings of centrifuge tests on single piles and pile groups subject to torsion in sand. Figure 7 shows typical test results of a single pile subject to torsion and a failure criterion is proposed

to determine the ultimate torsion resistance of a pile in sand.

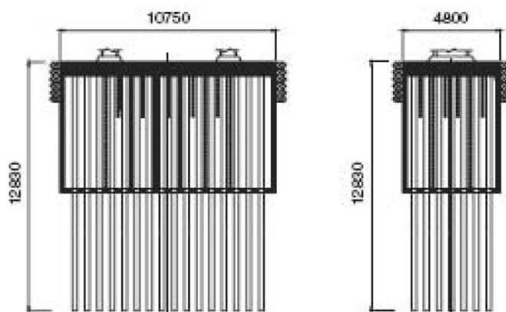
It is indeed pleased to note that a large number of extensive and useful centrifuge model studies on pile foundation have been carried out in many parts of Asia. These studies demonstrate the benefits of centrifuge modelling to investigate pile foundation problems under a wide variety of situations. In the remaining parts of this paper, the studies and findings of centrifuge model studies carried out at NUS will be



(a) Structure of caisson foundation.



(b) Pile-raft foundation.



(c) Steel cofferdam group pile foundation.

Figure 4. Schemes for bridge foundation (after Zhang et al. 2006).

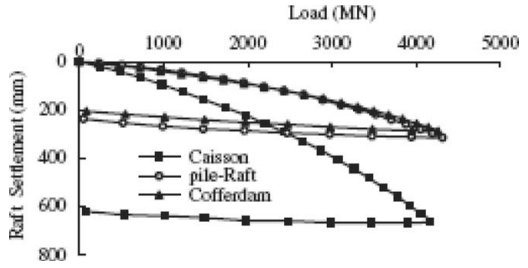
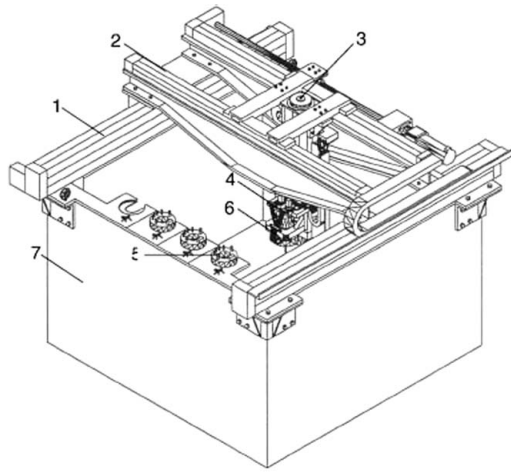


Figure 5. Prototype load-settlement responses of foundation schemes (after Zhang et al. 2006).



- 1. Ball screw on x axis
- 2. Rail on y axis
- 3. Linear driving mechanism in z axis
- 4. Rotary actuator
- 5. Tool adapters stored in the fixture
- 6. Working tool adapter
- 7. Model container

Figure 6. Four-axis robot manipulator (after Ng et al. 2002).

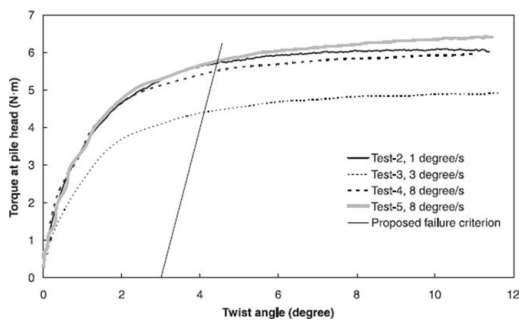


Figure 7. Twist angle versus torque at pile head (after Zhang & Kong 2006a).

presented in detail to further highlight the benefits of centrifuge modelling to investigate the behaviour of piles under axial load, lateral load, and vertical and horizontal soil movements.

3 AXIALLY LOADED PILES

In this section, the results of centrifuge model studies carried out at NUS on different aspects of axially loaded piles are presented. These include the studies on pile creep, lapses during pile installation, comparison of different pile load testing methods, performance of socketed piles, inclined and underreamed piles, piles supporting a large oil tank, and piles subject to negative skin friction. Unless otherwise stated, the centrifuge test results are given in prototype scale hereinafter.

3.1 *Pile creep*

As the design life of structures are typically at least 20 years, pile foundations are often subjected to heavy sustained structural loads. Komornik et al. (1972) reported that piles installed in soft soils and founded in partially cemented sand in Israel continued to settle with time even after most of the loads had been applied. Hannink (1994) also reported that the piles installed in sand supporting buildings ranging from 12 to 41 storeys high in the Netherlands continued to settle up to 30 years after construction. In view of the above, a series of centrifuge model tests has been carried out at NUS to evaluate the variation of pile settlement with time under a constant sustained load in dense sand. Leung et al. (1996) presented details of the test program and results. The tests were conducted at 50 g and a typical test result is shown in Figure 8a, which reveals that the pile continues to settle with time (i.e. pile creep) under a sustained load. A re-plot of the same set of test data on a settlement-log time relationship (Fig. 8b) reveals that the pile settlement increases approximately linearly with logarithmic of time.

The model pile was instrumented with strain gauges to evaluate the load transfer characteristics along the pile. During the tests, the strain gauges mounted close to the pile base and the pressure transducers placed around the pile base area reveal very high pile and soil stresses around the pile base area. To further investigate the pile creep phenomenon, a series of one-dimensional compression tests was performed by placing the same sand of identical relative density in a conventional oedometer cell and subject the sand to similar magnitude of high pressure experienced by the soil in vicinity to the pile base. Microscopic photographs of the sand samples were taken before and after

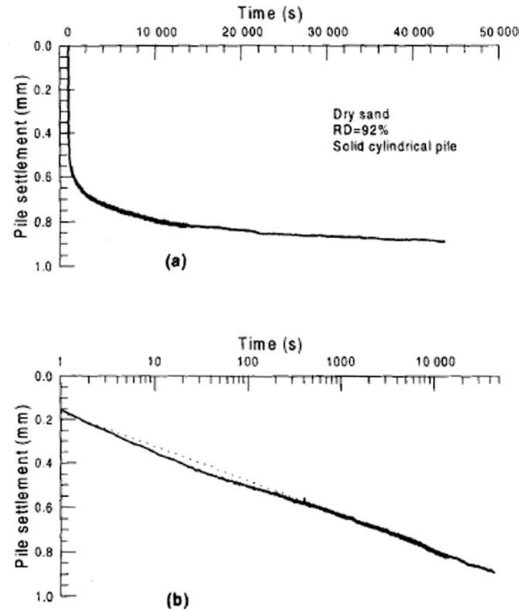


Figure 8. Settlement of pile under sustained load in model scale (after Leung et al. 1996).

the tests. Before sustained loading, the sand particles maintain its original shape and sizes as shown in Figure 9a. Upon sustained loading, the angular protrusions of the sand particles have been chipped off, resulting in a mixture of predominantly more rounded large particles mixed with smaller particles and fines, see Figure 9b. Moreover, microscopic inspection of the particles at an oblique angle reveals the presence of shiny smooth breakage surfaces on the larger rounded particles after sustained loading. Figure 10 shows the grading curves obtained from the sieve analysis on sand samples after two different load durations. Before sustained loading, all the sand particles were retained on the 212 µm sieve. After 290 seconds of sustained loading, about 5% of the particles (by weight) pass through the 212 µm sieve. About 25% of the particles are smaller than 212 µm after 5 days of sustained loading.

Figure 11 shows the variation of creep coefficient with pressure from the results of another 4 one-dimensional compression tests. The sand has been preloaded in 2 tests in which preloading was applied to simulate the initial soil stress levels during pile installation, whilst the reloading pressures represent the stress levels at the pile base under various sustained loads in the centrifuge tests. For sand that has not been subjected to any preloading, Figure 11 reveals that the creep coefficient increases approximately with pressure. On the other hand, preloaded sand behaved

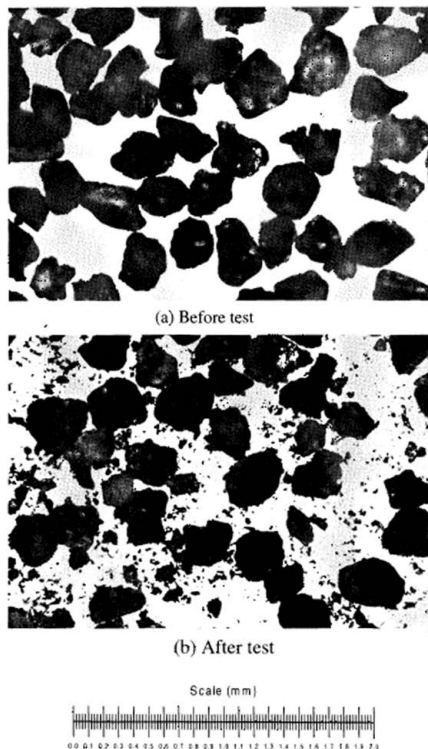


Figure 9. Microscopic pictures of sand particles before and after test (after Leung et al. 1996).

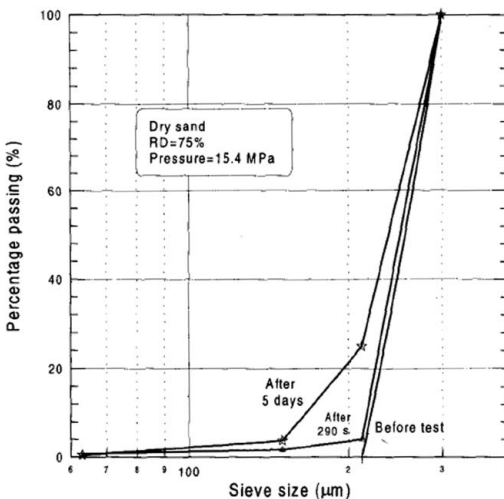


Figure 10. Variation of sand particle size distribution (after Leung et al. 1996).

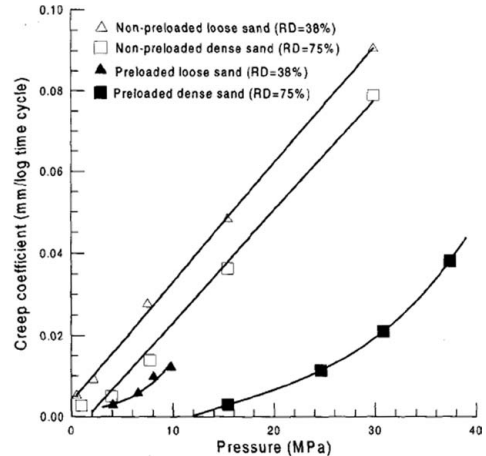


Figure 11. Variation of creep coefficient with pressure for preloaded and non-preloaded load (after Leung et al. 1996).

markedly differently with a trend of creep coefficient following closely with those observed in the centrifuge tests. Thus it can be concluded that the pile creep is due to particle breakage rather than inter-particle slippage. The pile creep is therefore highly dependant on the contact force between particles than the interlocking between particles. Hence pile creep is a combined function of applied load and sand unit weight.

It is evident that the results of centrifuge tests and one-dimensional compression tests essentially show very similar creep settlement-time responses under sustained load. The progressive breakage of sand particles results in a loss of contact between particles, which leads to a gradual decrease in soil resistance and stiffness and an increase in settlement with time. Further test results reveal that pile creep settlement is insignificant if the applied load is less than 50% of ultimate pile bearing capacity. The above findings demonstrate that for pile design in sand, it is prudent to adopt a minimum factor of safety of at least 2 against bearing capacity failure. This is to avoid any excessive long term pile creep settlement under working load as the pile may creep if the stress at the pile base is too high.

3.2 Lapses during pile installation

During pile installation, a pile may experience stoppages during installation due to bad weather, piling machine problems, and incomplete piling before public holiday breaks. In certain situations, the force required to re-install a pile into the soil after installation lapses can be quite different from that without stoppage. Another series of centrifuge model tests has

been conducted at NUS to examine the pile behaviour experiencing stoppages during installation in sand. To simulate an installation lapse, a model instrumented pile was jacked to the desired depth, and then allowed to rest for a desired duration before being jacked deeper into the sand during centrifuge flight. The tests were also conducted at 50 g. The vertical and lateral earth pressures in the soil in the vicinity of the pile were also monitored regularly throughout the tests. Leung et al. (2001a) reported details of the test program and findings.

Figure 12 shows that a pile installed in sand experienced a reduction in penetration resistance between the end of initial installation and the beginning of re-installation. The magnitude of reduction in pile penetration is noticeable even for short lapse duration and increases with the duration of installation lapse. A close-up view of the pile penetration resistance/depth response during the 4th installation lapse is depicted in Figure 13. It is evident that the pile underwent additional penetration when it was reloaded to the previous installation load.

Figure 14 shows the changes in lateral earth pressure at around the one-third, two-third and close to the base of the pile shaft during a typical installation lapse. The miniature pressure transducers are placed fairly close to the pile. The changes in lateral earth pressure are significant and there is a considerable reduction in lateral earth pressure close to the pile base. This observation is consistent with the stress changes in the pile shaft during an installation lapse.

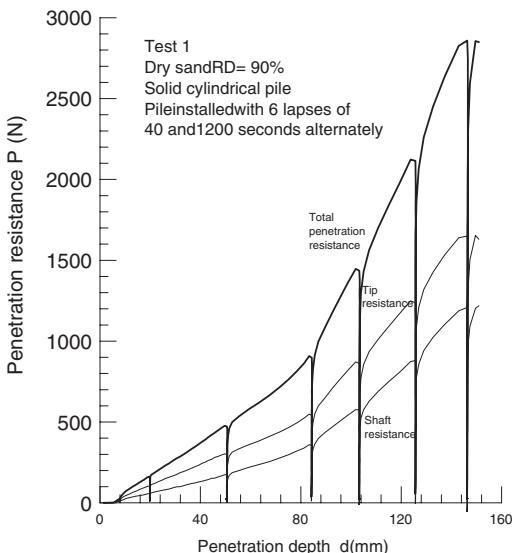


Figure 12. Variation of model penetration resistance with depth (after Leung et al. 2001a).

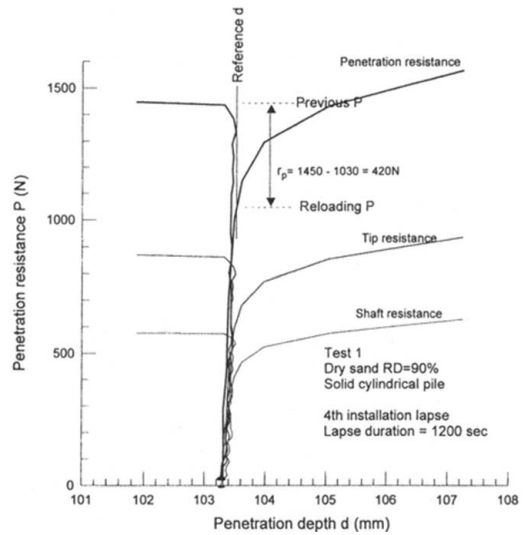


Figure 13. Close-up view of model penetration resistance/depth response (after Leung et al. 2001a).

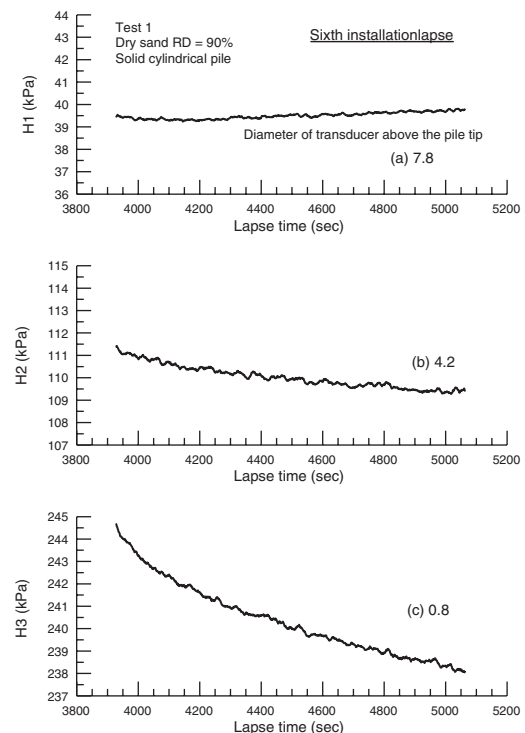


Figure 14. Close-up view of changes in lateral earth pressure (after Leung et al. 2001a).

The strain gauges mounted on the pile shaft reveal that during an installation lapse, there are little changes in the load transfer along the upper pile shaft but considerably more changes in the load transfer along the lower pile shaft. The change in the load transfer is most significant for the strain gauges close to the pile base. The test results illustrate that during a pile installation lapse, there is a progressive stress redistribution in the surrounding soils around the pile, in such a way that it leads to a reduction in pile penetration resistance. Thus it can be deduced that stress reduction in sand around the pile tip and along the lower pile shaft is a cause for the observed reduction in pile penetration resistance during an installation lapse and therefore a possible contributing factor to pile relaxation in the field.

A series of modified one-dimensional compression tests was conducted to examine the stress changes in the sand whereby the sand settlement is restricted. A very stiff triaxial test loading frame was employed as it is crucial that the loading frame itself should have minimal deformation. During tests, the load platen was slowly raised with the sand in contact against a stiff load cell connected to the stiff loading frame. The loading pressure on the sand hence gradually increases and the load platen was stopped immediately at the desired loading pressure. The changes in the load cell readings were monitored frequently until no significant changes in the soil stress were noted.

The changes in the load cell readings with time from the moment the loading platen was stopped are presented as the 'gross response' of the sand in Figure 15. It is evident that the pressure experienced by the sand reduced with increasing time but the rate of reduction in soil pressure decreases rapidly with time. To calibrate the degree of stress relaxation in the loading equipment, the compression test was repeated by replacing the oedometer cell with a rigid box of the same dimension. The pressure change/time response for this test would represent the compression of the loading frame and the response is denoted as the 'equipment response' curve in Figure 15. The 'net specimen response', which is the difference between the gross and equipment responses, is also shown in the figure. The result is very similar to that observed from the centrifuge test as the net response clearly indicates a reduction in pressure experienced by the sand. The rate of soil pressure change gradually reduces with time and becomes insignificant after a period of about 600 sec. The time scale of 600 sec is consistent with that observed in the centrifuge tests. The observation also reinforces the earlier finding that the magnitude of reduction in penetration resistance is noticeable even for short lapse duration, but the rate of reduction in penetration resistance attenuates rapidly with time.

A total of 6 compression tests with different overburden stress levels were carried out and a summary

of the test results is shown in Figure 16. The magnitude of the overburden stress ranges from 60 kPa to 1000 kPa and these stresses are within the same stress range as those measured in the centrifuge tests. For tests with overburden stress levels less than 80 kPa,

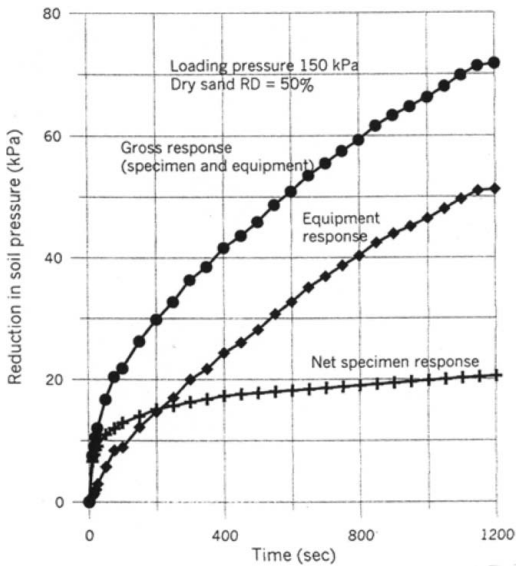


Figure 15. Variation of reduction in soil pressure versus time (after Leung et al. 2001a).

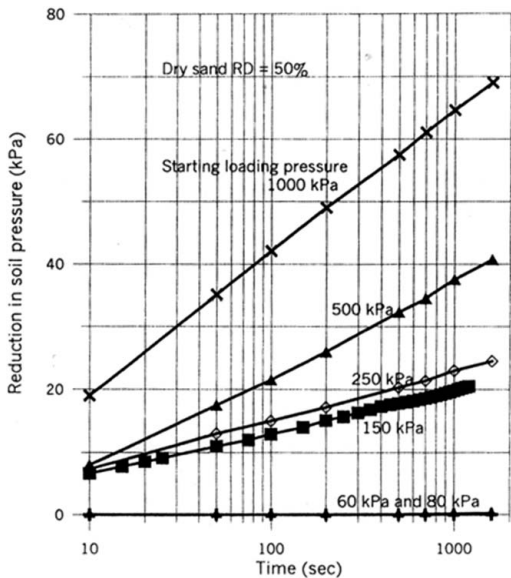


Figure 16. Variation of reduction in soil pressure versus log time (after Leung et al. 2001a).

there is virtually no stress reduction in the sand. This observation is consistent with the measured soil stress changes from the centrifuge tests. For overburden stress in excess of 80 kPa, the results suggest that over the long term, a linear relationship exists between the reduction in soil pressure and logarithm of time. The magnitude of stress reduction for each test can be examined from the gradient of the linear relationship.

Figure 17 illustrates that the magnitude of stress reduction increases with overburden stress. It can thus be concluded that stress reduction would be most critical for the sand located very close to the pile tip area and the magnitude of stress reduction decreases rapidly with distance away from the pile base.

3.3 Comparison of conventional and Osterberg pile load tests

At a piling site, a specified percentage of installed piles will be load tested to verify the pile design. Traditionally static load tests were performed on a test pile such that the pile is loaded at the top resulting in the whole pile shaft experiencing compression. However, providing the relatively huge load reaction system for static load tests in congested areas or in the sea may not be feasible or economical. The Osterberg (1989) load test technique has become popular in recent years. In the test pile, an Osterberg cell is placed at the pile toe or some distance above the pile toe before pile casting or concreting. During a pile load test, the load is applied by pumping fluid into the Osterberg cell. By knowing the equivalent upward and downward forces acting on the pile base and the movement of shaft and pile base, the pile shaft and base resistance and the load-displacement response can be determined. In view of differences in the loading mechanism, the load transfer characteristics along the pile for the 2 pile load test methods can be different. At NUS, a study has been carried out to investigate the above.

In the centrifuge tests, different model piles were used. Figures 17a and b show the details of a

conventionally loaded test pile and an Osterberg cell test pile, respectively. For the conventional test pile, both compression (pile pushed in at the top) and tension (pile pulled out at the top). For the Osterberg cell pile, the model pile body comprises a hollow tube and the internal rod is connected using shear key inside the sliding slot of the hollow tube. During test, the connector is pulled up such that the pile base is lifted, simulating the conduct of Osterberg load test in-flight. All the tests were conducted at 50 g.

The test results are shown in Figure 18. For the pile subjected to compression load at the top, the ultimate shaft resistance is about 1 MN at a pile settlement of 20 mm. For the pile subjected to tension load at the pile top and at the pile base (Osterberg load test), the ultimate shaft resistances are about 0.43 and 0.53 MN, respectively. Thus the compressive shaft friction appears to be considerably larger than the tensile shaft friction. It is noted that the tensile shaft friction of the pile loaded at the pile base is slightly higher than the one loaded at the pile top. This is likely due to the difference in stress level at the loading elevation in the 2 tests.

3.4 Piles socketed in rock

Large diameter cast-in-situ concrete bored piles are often socketed in rock in order to support heavy concentrated structural loads. Though a good number of studies were conducted to evaluate the shaft resistance of rock sockets, relatively few studies have been carried out to examine the failure mechanism of rock below the pile base. A series of centrifuge model tests has been conducted to examine piles socketed in artificial rock made of gypsum cement having the same range of compression and stiffness parameters as the sedimentary rocks in Southeast Asia. The model bored piles were cast using cement mix with an appropriate amount of water at 1 g. The experimental setup and results are described in detail in Leung & Ko (1993). The rock socket shaft friction values obtained from the

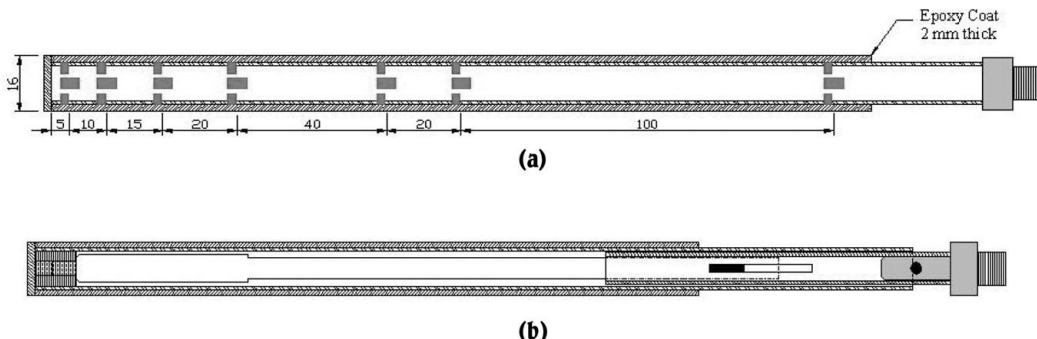


Figure 17. Instrumentation of (a) normal model pile; and (b) Osterberg-cell model pile.

centrifuge tests are found to be comparable with those deduced from existing theories, as illustrated in Figure 19. The results demonstrate the validity of using artificial rock in the model setup.

To investigate the stress bulb below the pile base in detail, the model socketed pile was subject to a huge load such that it settled by over 40% of its pile diameter. After the test, the artificial rock specimen including the model pile was cut open carefully and a failure bulb beneath the pile base was clearly evident,

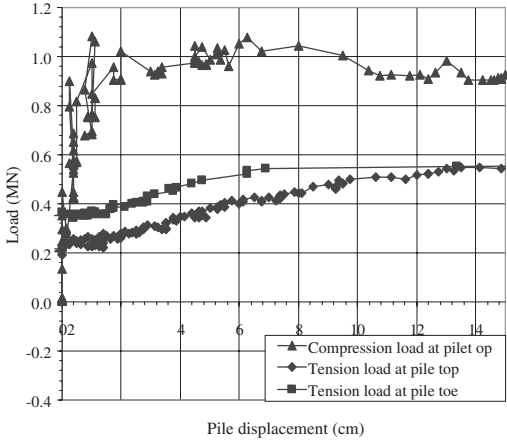


Figure 18. Comparison of shaft resistance of piles in sand.

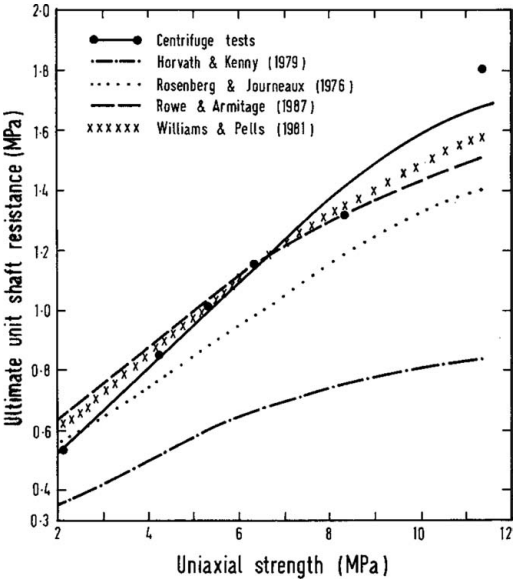


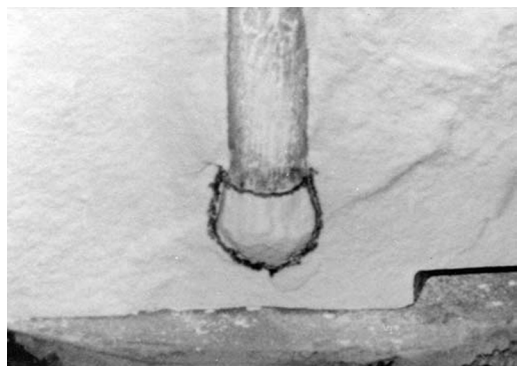
Figure 19. Comparison of test data with existing theories (after Leung & Ko 1993).

as shown in Figure 20. The bulb typically had a height of about 1.35 times the pile diameter and a diameter of 1.25 times the pile diameter at its widest part. There appeared to be no significant differences in the geometry and size of the failure bulbs for pile socketed in rocks of various strengths.

3.5 Pile subject to negative skin friction

The design of piles subject to negative skin friction has always been a concern for geotechnical engineers. Unfortunately codes from different countries often provide widely different recommendations on the above issue. Moreover, the performance of a pile subject to simultaneous downdrag and axial load is not well understood. This issue is important as a pile subject to negative skin friction would simultaneously carry at least the structural dead loads. A centrifuge model study was conducted at NUS to investigate the pile responses due to simultaneous negative skin friction and axial load. The centrifuge model setup is shown in Figure 21. Details of the study are given in Leung et al. (2004).

The results shown in the left hand side of Figure 22 reveals that negative skin friction had developed due to settling of soil under self weight soil consolidation and this negative skin friction remained lock-in even though the self weight soil consolidation has been completed. An axial load was then applied on the pile and the magnitude of negative skin friction gradually reduced and the elevation of the neutral plane (where the shaft friction turns from negative to positive) gradually rose as the applied load increased. Once the applied load reached a certain magnitude, the lock-in negative skin friction has been overcome. This finding re-confirms the conventional wisdom that negative skin friction needs not be considered if there is no further soil settlement under service load provided that the applied load is larger than the lock-in negative skin friction. The applied load was further increased



Failure 20. Failure bulb below pile base (after Leung & Ko 1993).

and the load transfer characteristics along the pile shaft resembled that of a conventional axially loaded pile without negative skin friction. Sand surcharge was again induced into the model container in-flight

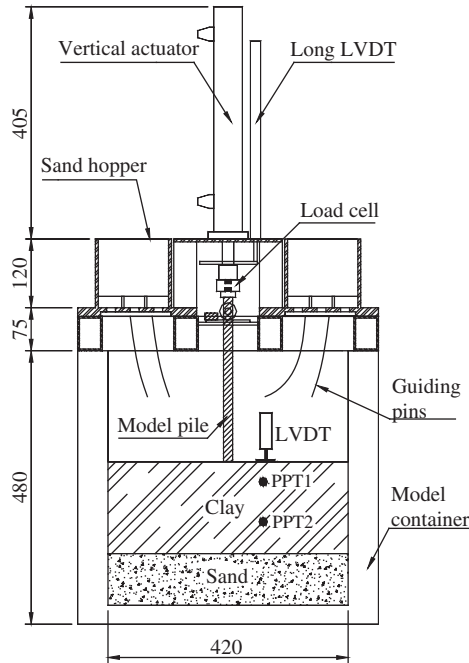


Figure 21. Centrifuge model set-up for negative skin friction study (after Leung et al. 2004).

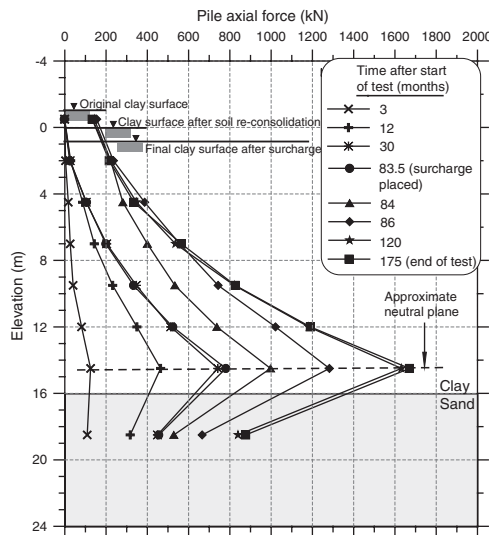


Figure 22. Pile axial force transfer profiles at various times for Test N1 (after Leung et al. 2004).

resulted in further settlement of the in-situ clay. The results shown in the right hand side of Figure 22 reveal that if the soil settles when a pile is in service, negative skin friction would again be induced on the pile.

The effects of pile base condition were examined by comparing the results of test N1 with the pile socketed into a stiff underlying dense sand layer and test N2 with the pile resting on a rigid base. Figure 23 shows that the development of negative skin friction in the upper pile shaft for both tests is similar. For the lower pile shaft, the elevation of the neutral plane for an end-bearing pile (test N2) is at the pile base as compared to around 90% depth of the soft clay layer for test N1.

Figure 24 summarises the test results with various applied load magnitudes on the pile. The results reveal that the magnitude of maximum induced negative skin friction remained fairly constant for the same subsurface soil profile regardless of pile load magnitude. This reveals that the 2 processes of development of negative skin friction along a pile and the load transfer characteristics along the pile shaft under axial load are independent of each other. This observation has important implications in practice as the full magnitude of negative skin friction needs not be considered in the design, as suggested in some design codes. As there will be some load transfer due to the applied load on the pile top, the magnitude of negative skin friction would be reduced.

Preliminary tests were also carried out on pile groups subject to negative skin friction and axial load. Shen et al. (2002) reported that for small size pile groups with the number of piles not more than 5, the

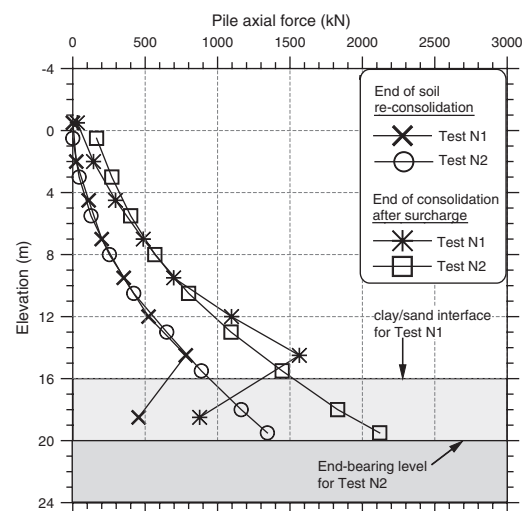


Figure 23. Comparison of pile axial force profiles (after Leung et al. 2004).

group effect appears to be insignificant. Since then, larger pile groups have been carried out and it is established that the group effect becomes significant for larger size pile group. For a 16-pile group, a possible reduction of 30% of negative skin friction per pile is noted. However, the distribution of negative skin friction among the piles is noted to be non-uniform and further interpretations of the test data are currently in progress to examine the distribution of negative skin friction among piles in pile groups of various sizes.

The phenomenon of negative skin friction can be due to different scenarios. The soil settlement adjacent to a pile shaft could be due to self weight consolidation of soft soil, consolidation of clay under new fill such as the case of inner piles underneath a new embankment, or water drawdown below the ground level. Further tests are currently in progress at NUS to investigate the negative skin friction phenomenon under different soil settlement scenarios. The preliminary test results presented by Shen et al. (2006) reveal that the maximum induced negative skin friction appear to be similar for all cases. As such, the design of pile subject to negative skin friction can be unified regardless of the soil settlement scenario.

3.6 Piles supporting oil storage tank

Piles are often installed as the foundation for large oil storage tanks constructed on soft soils. The apportionment of applied loads between the piles and soft

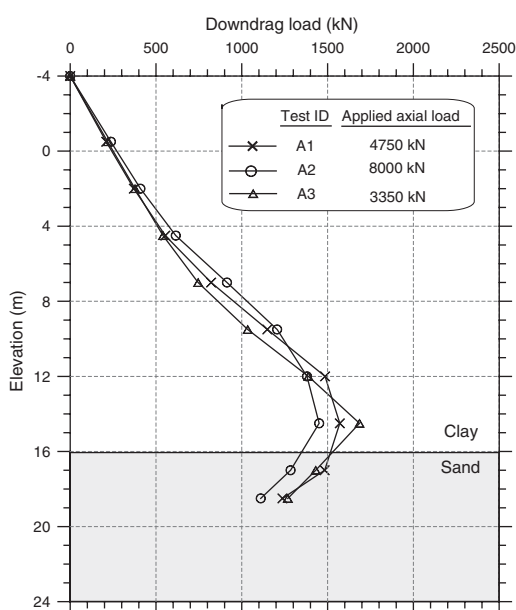


Figure 24. Dragload on piles due to surcharge loading under various applied loads (after Leung et al. 2004).

soils is not well understood. At NUS, a series of centrifuge model tests were conducted to investigate the effects of size of pile cap on the load transfer behaviour of the foundation system. In the tests, the pile size and plan layout were kept constant. Figures 25a and b show the section and plan view of the model setup, respectively. All the tests were conducted at 50 g. The model setup was instrumented such that the load carried by each pile and the settlement at the center and the corner of the tank were obtained. For ease of interpretation of test data, the size of pile cap is expressed as dimensionless pile cap area ratio which is defined as the percentage of pile cap area over the tributary area of one pile. The pile cap area ratio examined in the present study ranges from about 6% to 30%. Details of the study are reported by Lee et al. (2005).

Figure 26 shows the loading pressure-average tank settlement responses from a typical test. Only about 60% of the ultimate tank settlement has occurred at the completion of loading; after which the tank continues to settle with time with the rate of increase in settlement decreases with time. It is noted that about half of the long-term tank settlement has taken place within 1 month upon completion of loading while about 97% of the long-term tank settlement occurs within 9 months after loading. The tank settlement essentially stabilises after 12 months.

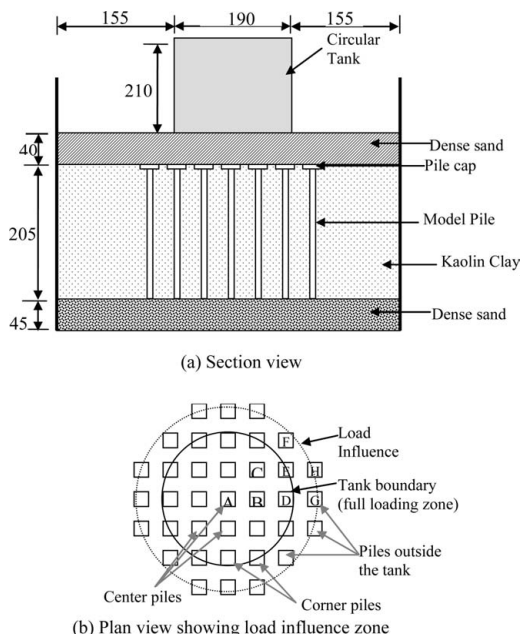


Figure 25. Centrifuge model setup for piles supporting oil tank (after Lee et al. 2005).

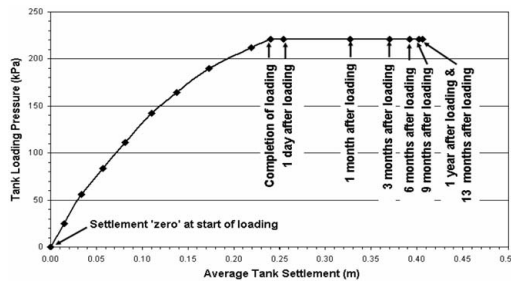


Figure 26. Variation of loading pressure with average tank settlement from a typical test (after Lee et al. 2005).

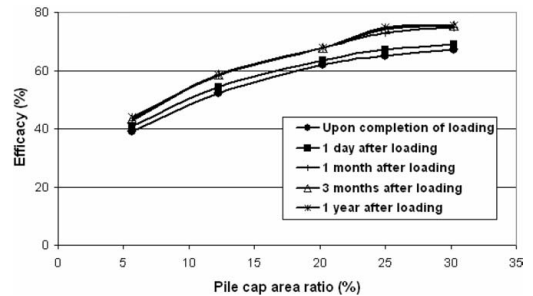


Figure 28. Variation of foundation efficacy with pile cap area ratio (after Lee et al. 2005).

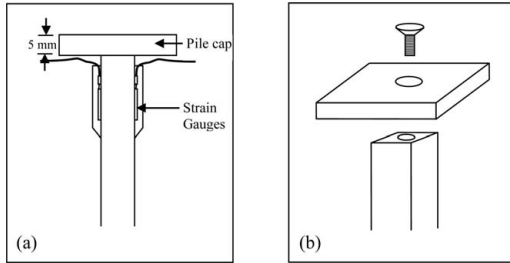


Figure 27. (a) Model instrumented pile; (b) Model pile attached with pile cap.

Figure 27 shows the instrument scheme around the top of selected model piles. Owing to symmetry, only 8 out of a total of 37 piles need to be instrumented to determine the load carried by all the piles. Using the definition proposed by Low et al. (1994), the efficacy of the foundation system is defined as the percentage of total applied loads carried by all the piles. The relationship between the efficacy and pile cap area ratio are shown in Figure 28 which reveals that the efficacy increases with pile cap area ratio. However, it is not beneficial to increase the pile cap area ratio to beyond 25%.

The variation of average tank settlement with pile cap area ratio is shown in Figure 29. It is evident that the tank settlement decreases with increasing pile cap area ratio. An ultimate settlement of 0.84 m was recorded for a pile cap area ratio of 6% as compared to 0.42 m for a pile cap area of 20%. Beyond 20% pile cap area, there are practically little changes in the tank settlement.

3.7 Piles with underream

In certain cases, piles may be subjected to large uplift forces such as those supporting light transmission tower structures. Piles with underream (termed as bell piers in some countries) are employed to resist the large uplift load. Dickin & Leung (1990, 1992) carried out a model study to investigate the performance

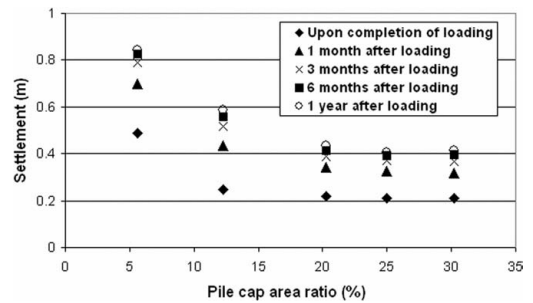


Figure 29. Effect of pile cap area ratio on average tank settlement (after Lee et al. 2005).

of such piles. Centrifuge model tests were conducted to examine the effects of underream diameter (b_b) upon pile shaft diameter (b_s) and the taper angle of the underream (α) on uplift pile capacity, see the inset of Figure 30 for a schematic explanation of the symbols. The test results are expressed in terms of dimensionless breakout factor N_u which is defined as net ultimate uplift resistance (total uplift capacity minus the self weight of pile with underream or anchor) divided by the underream base area and pile embedment depth.

Figure 31 reveals that the influence of α on breakout factor is relatively small for $\alpha < 62^\circ$, beyond which N_u decreases markedly with increase in α . This finding is in broad agreement with Dewaikar (1985) who reported a negligible influence on N_u for α values between 15 and 60° from his finite element analyses.

The uplift failure mechanism of a half-cut underreamed pile was investigated in a transparent model container at 1 g. The model pile or anchor ($\alpha = 0^\circ$) is semi-cylindrical in shape. The failure pattern obtained around an underreamed pile in loose sand, an underreamed pile in dense sand as well as an anchor plate in dense sand subject to uplift are shown in Figures 32a, b and c, respectively. It is evident that underreamed

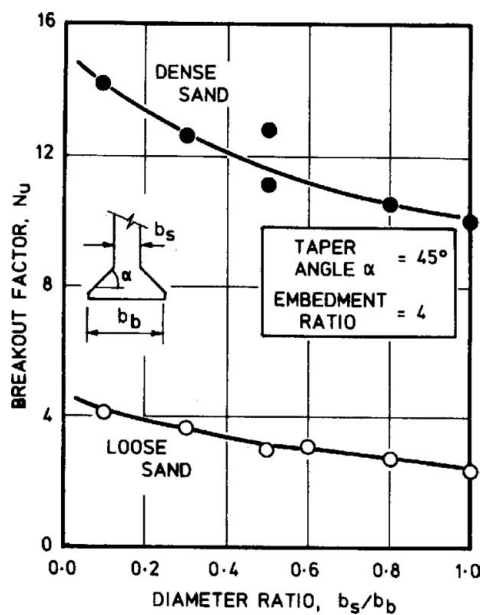


Figure 30. Variation of breakout factor N_u with diameter ratio b_s/b_b (after Dickin and Leung 1992).

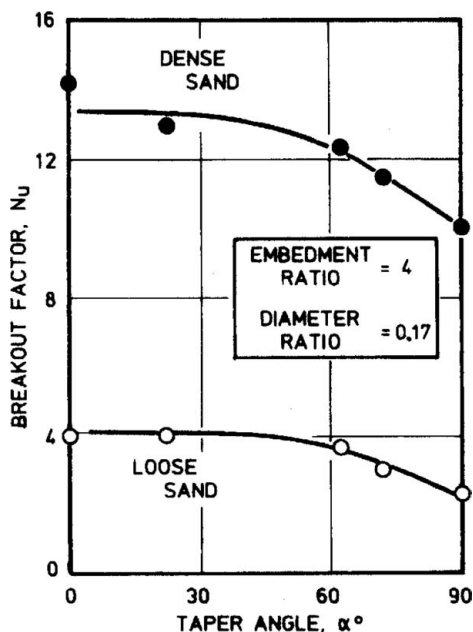


Figure 31. Variation of breakout factor N_u with taper angle α (after Dickin and Leung 1992).

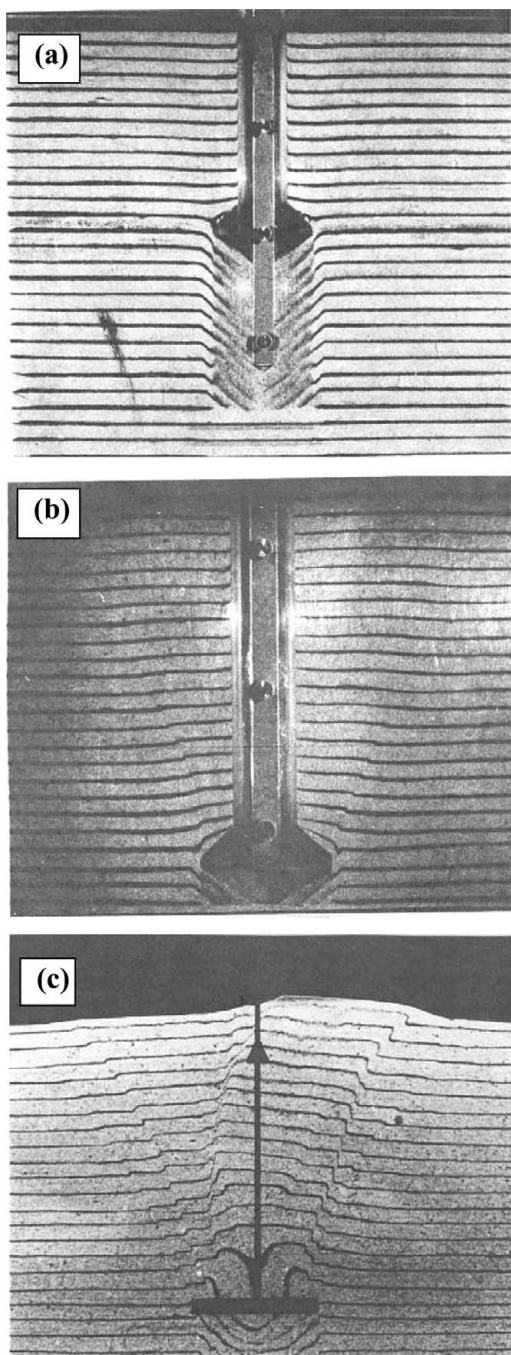


Figure 32. Uplift failure mechanism around (a) underreamed pile in loose sand, (b) underreamed pile in dense sand, (c) an anchor plate in dense sand (after Dickin and Leung 1992).

piles in loose sand had the least distinct failure pattern as compared to that in dense sand illustrating that the uplift resistance in loose sand is much smaller than that in dense sand. The failure pattern for an anchor plate is the most distinct and massive among all the 3 cases indicating an anchor plate offers a much higher uplift resistance as compared to an underreamed pile having the same base diameter. The changes in the failure zones for the 3 cases help to explain the differences in the uplift resistance for various α and b_s/b_b values.

3.8 Inclined piles

Vertical piles installed at a site with nearby deep excavation works may tilt due to excavation-induced soil movement. The performance of inclined piles was investigated using centrifuge modelling technique at NUS. Details of the study are reported in Leung et al. (2001b). Figure 33 shows the centrifuge model setup which comprises 2 actuator systems. The vertical actuator was first activated to jack the instrumented model

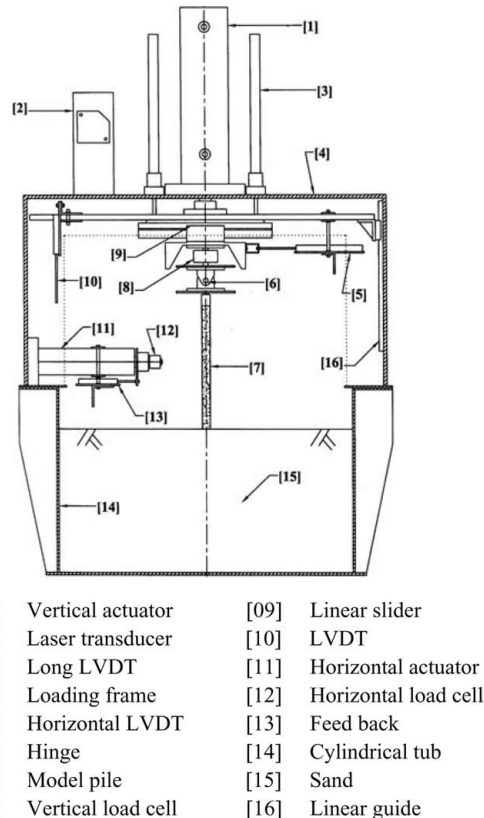


Figure 33. Schematic of model setup for inclined pile study (after Leung et al. 2001b)

pile vertically into the soil. Once the pile reached the desired penetration depth, the horizontal actuator was activated to push the pile laterally to the desired inclination. The vertical actuator was subsequently re-activated to conduct a static vertical load test on the inclined pile.

Figure 34 shows the variation of ultimate pile capacity with pile inclination. The results illustrate that pile capacity is not a concern as it increases with pile inclination except for inclined piles in very dense sand with inclination angle exceeding 12°. This is due to the increase in passive soil resistance beneath the inclined pile shaft. It should be noted that the displacement at

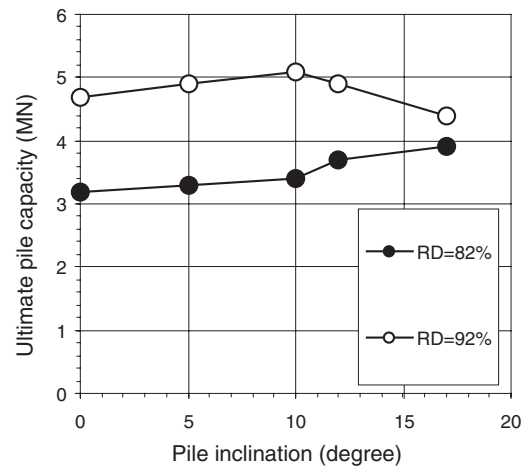


Figure 34. Variation of ultimate pile capacity with pile inclination (after Leung et al. 2001b).

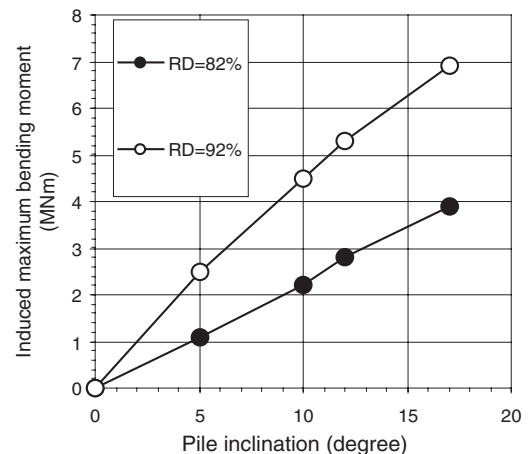


Figure 35. Variation of induced maximum bending moment with pile inclination (after Leung et al. 2001b).

ultimate pile capacity exceeds 200 mm. The variation of maximum bending moment with pile inclination is shown in Figure 35. The induced pile bending moment generally increases approximately linearly with pile inclination. Thus the pile bending moment capacity, rather than bearing capacity, needs to be checked in the design of inclined piles.

4 PILES SUBJECT TO EXCAVATION-INDUCED SOIL MOVEMENT

Deep excavation works would result in lateral soil movement which may have a detrimental effect on the foundation of adjacent buildings. Conventional theories (e.g. Broms 1964a) adopted passive earth pressure as the limiting soil pressure on piles in sand. From the back analyses of centrifuge model test data on piles subject to excavation-induced soil movement, Leung et al. (2000) established that existing theories are capable of predicting the induced pile bending moment and deflection reasonably well at small lateral soil movements. The sand would flow around the piles at large lateral soil movements as in the case near a retaining wall experiencing imminent collapse. As a result, the observed maximum soil pressure on the piles is much lower than that predicted from conventional theories.

Back analysis of centrifuge test data of observed induced pile bending moment in sand using a computer program developed at NUS (Chow and Yong 1996) revealed that a much better agreement between the measured and calculated pile bending moment could be achieved if the limiting soil pressure on the pile is set to be the effective overburden soil pressure. This limiting soil pressure is much lower than the passive earth pressure for a conventional laterally loaded pile proposed by Broms (1964a). Leung et al. (2003) also reported a pile group restrained by a rigid pile cap has a positive effect against soil movement. The back row piles of a pile group could restrain the front row piles from moving forward such that the induced bending moment of the latter is considerably reduced. For larger size pile groups, the inner piles as well as the back row piles are found to experience less induced bending moment due to much smaller soil movements as they are shielded behind the outer piles and the front row piles, respectively.

Centrifuge model tests were also conducted to investigate the behaviour of pile subject to excavation-induced soil movement in clay. The centrifuge model setup for the study is shown in Figure 36. The undrained shear strength profile of the clay at 3 m behind the retaining wall before and after excavation is shown in Figure 37. Detail test setup and results are presented in Ong et al. (2006a) and Leung et al. (2006).

Figures 38a and b show the variations of induced pile head deflection and maximum pile bending moment with log time, respectively. It is noted that the trend of the induced pile responses behind a marginally stable wall (Test 5 shown in Figure 38) and a stable wall (Test 2) is similar. The maximum induced pile bending moment takes place at maximum excavation depth and thereafter the pile bending moment reduces with time. However, the induced pile responses behind the two collapsed walls are markedly different. Figure 38b shows that the maximum induced pile bending moment for the collapsed wall in Test 6 reaches a maximum of 238 kNm at an excavation depth of 1.4 m, and then reduces to 185 kNm at the maximum

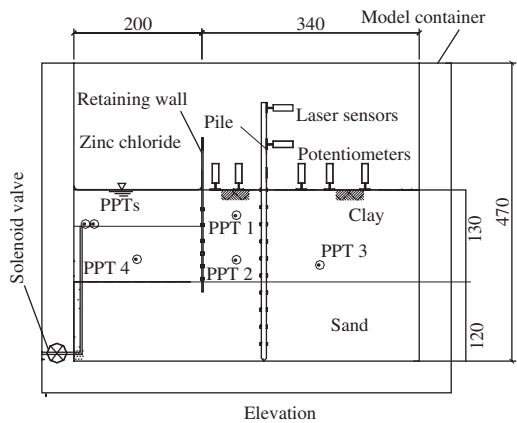


Figure 36. Centrifuge model setup for pile in clay (after Ong et al. 2006a).

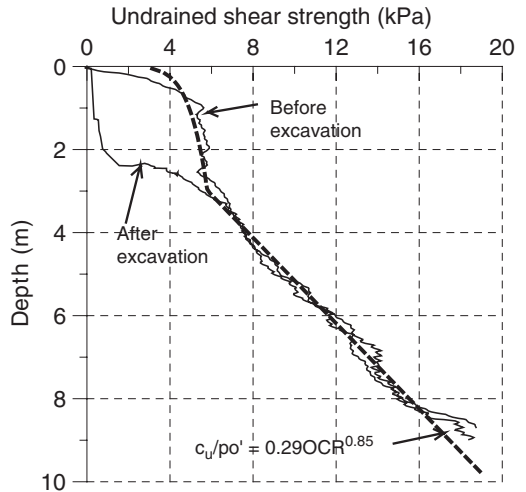


Figure 37. Measured undrained shear strength profiles at 3 m behind retaining wall (after Leung et al. 2006).

excavation depth of 1.8 m. The pile bending moment subsequently reduces further to 80 kNm after a prototype post-excavation period of about 10 months.

On the other hand, the pile head deflection shown in Figure 38a remains unchanged for some time after the wall collapses. With a totally collapsed wall in Test 7, the maximum induced pile bending moment remains fairly constant after reaching its first peak value at an excavation depth of 1.2 m and increases again once the excavation depth exceeds 2 m, as shown in Figure 38b. The pile head deflection over time follows a similar trend as the pile bending moment. Despite a greater excavation depth, the pile head deflection observed in Test 7 is less than that in Test 6 (Fig. 38a). This is attributed to the fact that in Test 7, an underlying dense sand layer restrains the displacement and rotation of the lower pile shaft.

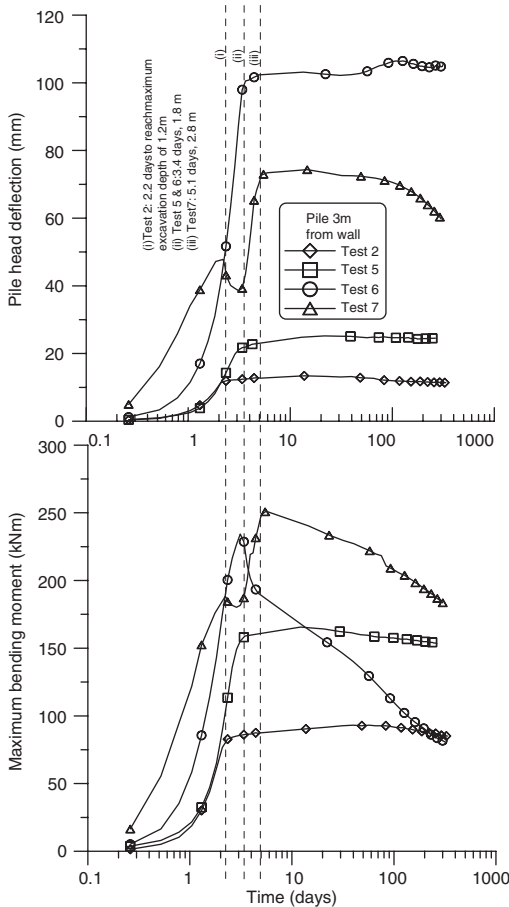


Figure 38. Variations of induced pile head deflection and maximum pile bending moment with time (after Leung et al. 2006).

Back analyses of centrifuge test data reveal that conventional theories also overpredict the induced bending moment on piles in clay, see Figure 39. A ‘flow’ phenomenon is also observed for clay but the development of the phenomenon is quite different from that of sand due to pore pressure dissipation behind the retaining wall and the development of tension cracks observed in clay upon large soil movements, see Figure 40.

Figure 37 reveals that there is stress relief after the excavation of clay in front of the retaining wall resulting in a reduction in undrained shear strength upon excavation. Back analysis of the observed induced pile responses reveal that if the post-excavation undrained soil strength profile is employed, the NUS computer program is capable of predicting the observed induced pile bending moment. However, post-excavation soil

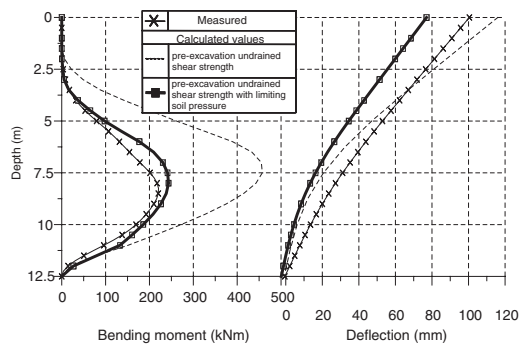


Figure 39. Induced bending moment on piles in clay (after Leung et al. 2006).

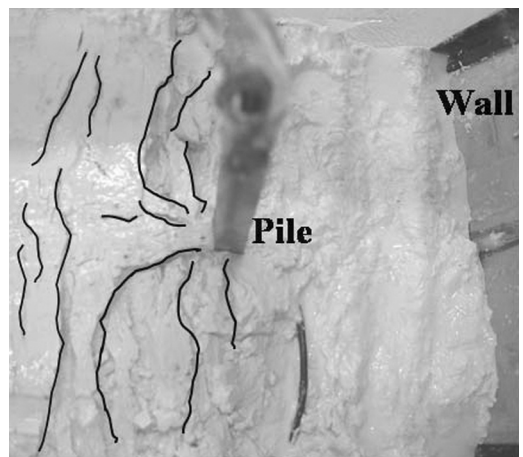


Figure 40. Development of tension cracks observed in clay upon large soil movements (after Leung et al. 2006).

strength profile is not normally available in practice. Further back analysis of the centrifuge test data reveals that if pre-excavation soil strength profile is employed, the limiting soil pressure on the pile would only be about 6 times undrained shear strength c_u . This is considerably smaller than the $9c_u$ value proposed by Broms (1964b).

5 PILES SUBJECT TO LATERAL AND VERTICAL SOIL MOVEMENTS

Figure 41 shows situations in the field where piles may be subjected to simultaneous vertical and lateral soil movements. These cases include piles supporting an embankment, tunnelling with piles nearby and permanent piles supporting an offshore platform with a mobile jack-up rig operating nearby. At NUS, centrifuge model studies were carried out to investigate the problems involving tunnel-pile interaction and jack-up spudcan foundation-pile interaction.

5.1 Tunnel-pile interaction

Figure 42 shows 2 separate scenarios involving ovalisation of tunnel lining and tunnel over-cut. The centrifuge model setup is shown in Figure 43. For the over-cut of tunnel, a technique has been developed to simulate the inward tunnel deformation at the tunnel springline by dissolving the over-cut shaped high density polystyrene foam placed outside a model tunnel lining using

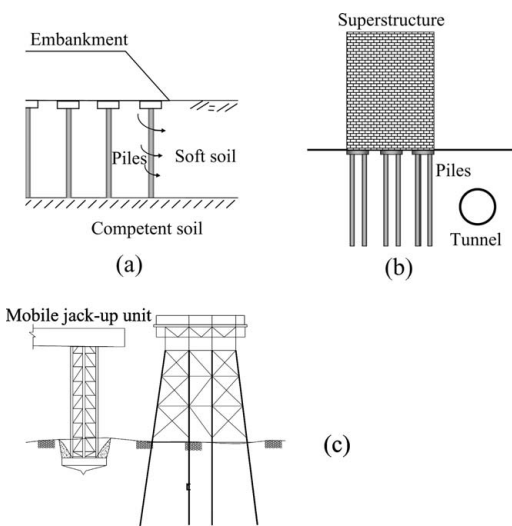


Figure 41. Piles influenced by vertical soil movements: (a) embankment piles; (b) tunnelling; and (c) jack-up spudcan installation (after Leung 2006).

an organic solvent while the centrifuge is in-flight at 100g. Details of the study are given in Ong et al. (2006b).

Particle Image Velocimetry (PIV) technique (White et al. 2003) was employed to evaluate the free field soil movements due to tunnelling. Figure 44 shows the enlarged vector map of the subsurface soil movements at the end of tunnel excavation and after 720 days from a typical test. It is evident that as the soil above the tunnel crown moves vertically downwards, the soil between the tunnel crown and spring elevation gradually moves toward the tunnel due to over excavation. Moreover, at any point within the critical zone, the magnitude of soil settlement above the tunnel is greater than that of horizontal soil movement. As the soil displacements below the tunnel springline are comparatively small in magnitude, these displacements are omitted for the sake of clarity. It is postulated that the soil movement wedge above the tunnel crown serves as an active zone during

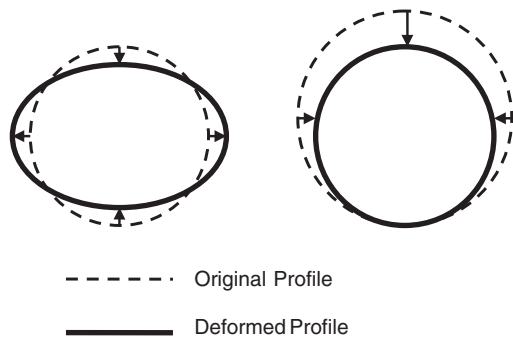


Figure 42. (a) Ovalisation of tunnel lining; and (b) over-cut of tunnel.

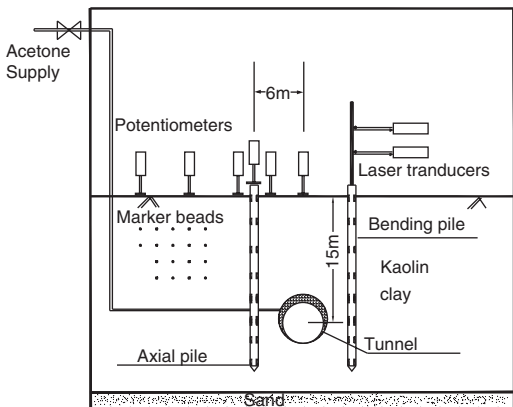


Figure 43. Centrifuge model setup for interaction study between piles and over-cut of tunnel (after Ong et al. 2006b).

tunnelling and the soil wedge falls down to fill the gap upon tunnel excavation. The soil beyond the wedge acts like a passive zone as it helps to support the wedge. As clay is not a rigid body, the soil in the wedge gradually deforms by arching and at the same time overcomes the resistance of the soil in the passive zone, resulting in the observed trough propagation pattern.

The induced axial force profiles for the 2 scenarios of tunnel lining deformation at the completion of tunnel excavation are shown in Figure 45. In both cases, the clearance between the tunnel and the piles is half

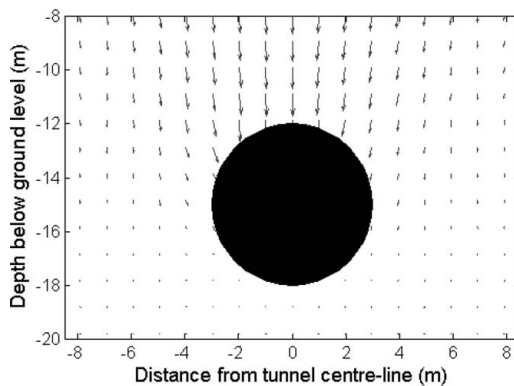


Figure 44. Vectors of soil movements at the end of tunnel excavation (after Ong et al. 2006b).

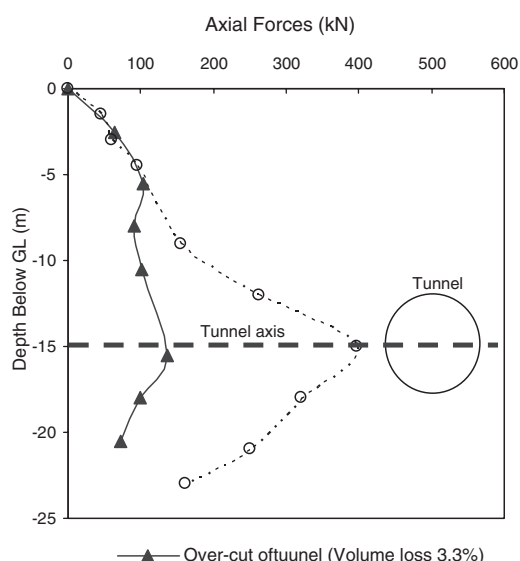


Figure 45. Induced pile axial force profiles at the end of tunnel excavation.

tunnel diameter. It should be noted that the volume loss for the 2 cases is slight different, being 3.3% for the inward tunnel deformation case and 4.2% for the tunnel ovalisation case. Both piles experience negative skin friction due to soil settlement adjacent to the pile shaft and the elevation of the neutral plane is at the tunnel centre-line. This is consistent with the observed free field vertical soil movement shown in Figure 46. The trend of the pile axial force profile for the 2 situations is fairly similar with a larger negative skin friction for the tunnel ovalisation case due to a higher ground loss magnitude.

The induced bending moment profiles of a free head single pile at the completion of excavation for the 2 scenarios of tunnel lining deformation are shown in Figure 46. The pile bends away from the tunnel for the case of tunnel ovalisation while the pile bends toward the tunnel for the tunnel over-cut case. The induced pile bending moment for both cases is noted to increase with depth with a maximum at the tunnel centre-line elevation. The large magnitude of induced pile moment for tunnel ovalisation is mainly due to the large amount of expansion of tunnel lining at the springline; while for inward tunnel deformation, the small void space above the tunnel crown becomes more crucial.

5.2 Spudcan-pile interaction

Mobile jack-up drilling rigs are often employed in seas up to 150 m deep for oil and gas exploration. The foundation supporting the 3 legs of the rig typically

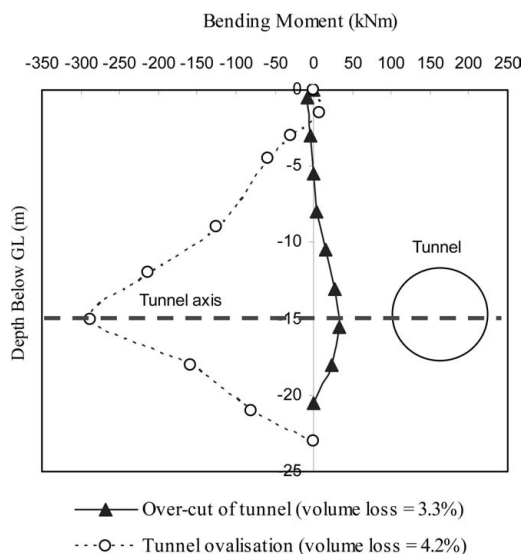


Figure 46. Induced pile bending moment profiles at the end of tunnel excavation.

comprises of 3 spudcans of 10 to 20 m in diameter. The rigs are mobile in nature such that the installation and extraction of the large spudcan foundations may result in vertical and lateral soil movements that could induce excessive bending moment and axial force on the permanent piles supporting the adjacent platform (Fig. 41c).

To date, very few studies have been performed on the issue. Centrifuge model tests had been carried out at NUS to evaluate the bending moment and axial force on a single free head pile due to installation and extraction of a 10-m diameter spudcan in normally consolidated soft clay. The induced pile bending moment profiles at different spudcan penetration depths obtained from a test with a spudcan-pile clearance of half a spudcan diameter are shown in Figure 47. The observed bending moment profiles are very different from those due to excavation and tunnelling induced soil movements. This can be attributed to the difference in the soil movement patterns in the

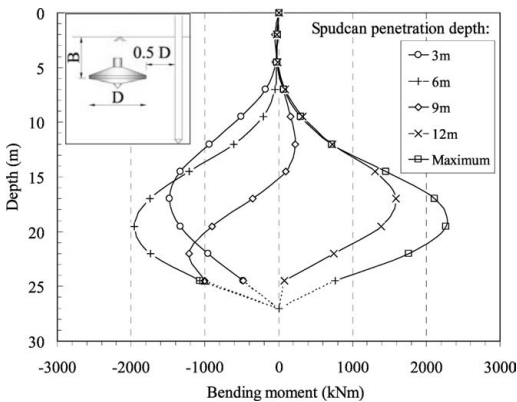


Figure 47. Induced pile bending moment profiles at various spudcan penetration depths.

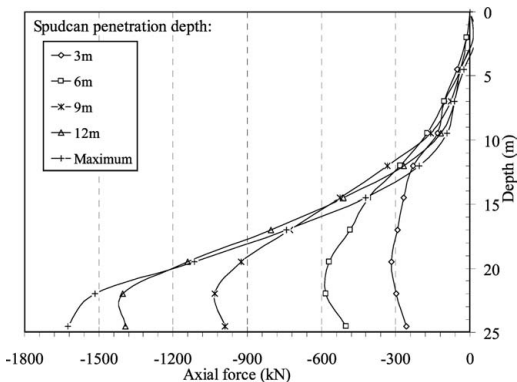


Figure 48. Induced pile axial force profiles at various spudcan penetration depths.

respective case, see detail interpretations presented by Xie et al. (2006).

At shallow spudcan penetration depths, lateral soil movements mainly occur at shallow depths. As the pile head deflection is insignificant at this stage, the soil movements would push the top of the piles to deflect slightly away from the spudcan with the lower pile shaft bending towards the spudcan. As the spudcan penetrates deeper and beyond 9 m depth, the lateral soil movement at mid-depth elevation becomes so great that it pushes the piles away from the spudcan.

Figure 48 shows the induced pile axial force profiles during spudcan penetration. It is noted that the pile is in tension throughout with the magnitude of tension force increases with spudcan penetration depth. The rate of increase in tension force decreases with increasing penetration depth. The observed pile movements confirm that the pile has indeed gradually moving upwards during the spudcan installation process. It should be noted that in this preliminary study, free head piles have been tested while in practice, the pile head condition is fixed.

6 CONCLUSIONS

This paper briefly reviewed the centrifuge model studies on pile foundations conducted in Asia. Details of the centrifuge tests on various pile studies carried out at the National University of Singapore are also presented. This paper demonstrates that if centrifuge modelling is carried out properly with appropriate data interpretations and considerations of scaling laws, it can be a powerful technique to understand pile behaviour under a variety of loadings and situations.

As an example, the studies on excavation-induced soil movement on pile revealed that the limit soil pressures on a pile obtained from conventional theories are on the high side due to 'soil flow around pile' phenomenon at large soil movements. On the other, it is advisable to keep a minimum bearing capacity safety factor of 2 for piles in sand as a pile would creep under sustained load when the stresses around the pile base are very high.

Significant advances in centrifuge modelling of pile have been made by researchers in Asia in the past decade. This trend is set to continue with a good number of new large geotechnical centrifuges in some Asian countries.

ACKNOWLEDGEMENTS

The Author wishes to acknowledge his former and present graduate students Dr N S Yet, Dr Dominic Ong, Mr R F Shen, Mr B K Liao, Mr J K Lim, Mr S Srisakthivel, Mr J Arumongkol, Mr S C Lee,

Mr X Ran, Mr C W Ong for their contributions in the research studies presented in this paper. The efforts of laboratory officers of NUS Centrifuge Laboratory are gratefully appreciated. Last but not least, Mr R F Shen had tirelessly spent time to format this paper.

REFERENCES

- Broms, B.B. 1964a. Lateral resistance of piles in cohesionless soils. *J. Soil Mech. and Found. Div.* 90(3), 123–156.
- Broms, B.B. 1964b. Lateral resistance of piles in cohesive soils. *J. Soil Mech. and Found. Div.* 90(2), 27–63.
- Chow, Y.K. & Yong, K.Y. 1996. Analysis of piles subject to lateral soil movements. *J. of Institution of Engineers Singapore*. 36(2): 43–49.
- Dewaikar, D.W. 1985. Finite element analysis of certain aspects of shallow anchors in a cohesive soil medium. *Proc. 5th Int. Conf. on Num. Mthds. in Geomechanics*, Nagoya. 719–724.
- Dickin, E.A. & Leung, C.F. 1990. Performance of piles with enlarged bases subject to uplift forces. *Can. Geotech. J.* 27: 546–556.
- Dickin, E.A. & Leung, C.F. 1992. The influence of foundation geometry on the uplift behaviour of piles with enlarged bases. *Can. Geotech. J.* 29: 498–505.
- Ha, L.S., Seo, M.W., Jung, W.S., Kim, H.S., Park, D.S., Sobolevsky, A. & Van Laak, P. 2006. Development of a large scale geotechnical centrifuge in KOWACO. *Proc. 6th Int. Conf. Phy. Modelling in Geotech.*, Hong Kong. 1: 135–140.
- Hannink, G. 1994. Settlement of high-rise buildings in Rotterdam. *Proc. 13th Int. Conf. Soil Mech. Fdn. Engr.*, New Delhi. 2:441–444.
- Isobe, K. & Kimura, M. 2005. Mechanical behavior of caisson foundation reinforced by steel pipe sheet piles. *Proc. 15th Int. Conf. Soil Mech. & Geotech. Engr.*, Osaka. 1493–1496.
- Isobe, K., Danno, K., Kimura, M., Zhang, F., Kohno, K., Harata, N., Makino, T. & Kuwajima, T. 2006. Seismic performance of caisson foundation reinforced by steel pipe sheet piles. *Proc. 6th Int. Conf. Phy. Modelling in Geotech.*, Hong Kong. 2: 1001–1006.
- Kim, D.S., Cho, G.C. & Kim, N.R. 2006. Development of KOCED geotechnical centrifuge facility at KAIST. *Proc. 6th Int. Conf. Phy. Modelling in Geotech.*, Hong Kong. 1: 147–150.
- Kimura, T. 1998. Development of geotechnical centrifuges in Japan. *Proc. Centrifuge 98*, Tokyo. 2: 945–954.
- Kimura, M., Adachi, T., Yamanaka, T. & Fukubayashi, Y. 1998. Failure mechanism of axially loaded concrete piles under cyclic lateral loading. *Proc. Centrifuge 98*, Tokyo. 1: 539–544.
- Kimura, M. & Matsuura, Y. 2002. Centrifuge model tests on laterally loaded steel pipe and soil-cement composite pile. *Proc. Phy. Modelling in Geotechnics*, St. John's. 619–624.
- Komornik, A., Wiseman, G. & Zeitlen, J.G. 1972. Building settlement on end-bearing driven piles. *Proc. ASCE Speciality Conf. on Performance of Earth and Earth-supported structures*, Lafayette. 1(2): 1135–1153.
- Lee, C.J., Chen, H.T. & Wang, W.H. 1998. Negative skin friction on a pile due to excessive groundwater withdrawal. *Proc. Centrifuge 98*, Tokyo. 1: 513–518.
- Lee, C.J. & Chen, C.A. 2002. Negative skin friction on grouped piles. *Proc. Phy. Modelling in Geotechnics*, St. John's. 679–684.
- Lee, F.H., Tan, T.S., Leung, C.F., Yong, K.Y., Karunaratne, G.P. & Lee, S.L. 1991. Development of geotechnical centrifuge facility at National University of Singapore, *Proc. Centrifuge 91*, Boulder. 11–17.
- Lee, S.C., Leung, C.F. & Chow, Y.K. 2005. Performance of oil tank foundations. *ASCE Geotechnical Special Publication*. 132: CD volume.
- Leung, C.F. 2006. Performance of piles subject to soil movement. *Proc. 6th Int. Conf. Phy. Modelling in Geotech.*, Hong Kong. 1: 87–98.
- Leung, C.F. & Ko, H.Y. 1993. Centrifuge model study of piles socketed in rock. *Soils and Foundations*. 33(3): 80–91.
- Leung, C.F., Lee, F.H. & Yet, N.S. 1996. The role of particle breakage in pile creep in sand. *Can. Geotech. J.* 33: 888–898.
- Leung, C.F., Chow, Y.K. & Shen, R.F. 2000. Behavior of pile subject to excavation-induced soil movement. *J. Geotech. and Geoenvir. Engr.* 126(11): 947–954.
- Leung, C.F., Lee, F.H. & Yet, N.S. 2001a. Centrifuge model study on pile subject to lapses during installation in sand. *Int. J. of Phy. Modelling in Geotech.* 1(1): 47–57.
- Leung, C.F., Srisakthivel, S. & Chow, Y.K. 2001b. Centrifuge model study of inclined piles. *Proc. 14th Southeast Asian Geotech. Conf.*, Hong Kong, 1: 553–558.
- Leung, C.F., Lim, J.K., Shen, R.F. & Chow, Y.K. 2003. Behavior of pile groups subject to excavation-induced soil movement. *J. Geotech. and Geoenvir. Engr.* 129(1): 58–65.
- Leung, C.F., Liao, B.K., Chow, Y.K., Shen, R.F. & Keg, Y.C. 2004. Behavior of pile subject to negative skin friction and axial load. *Soils and Foundations*. 44(6): 17–26.
- Leung, C.F., Ong, D.E.L. & Chow, Y.K. 2006. Pile behavior due to excavation-induced soil movement in clay. II. collapsed wall. *J. Geotech. and Geoenvir. Engr.* 132(1): 45–53.
- Low, B.K., Tang, S.K. & Choa, V. 1994. Arching in piled foundation. *J. Geotech. and Geoenvir. Engr.* 120(11): 917–938.
- Ma, X.F., He, Z.M., Zhu, H.H. & Lin, N. 2006. Development of a new geotechnical centrifuge at Tongji University in Shanghai. *Proc. 6th Int. Conf. Phy. Modelling in Geotech.*, Hong Kong, 1: 151–156.
- Ng, C.W.W., Van Laak, P.A., Zhang, L.M., Tang, W.H., Zong, G.H., Wang, Z.L., Xy, G.M. & Liu, S.H. 2002. Development of a four-axis robotic manipulator for centrifuge modeling at HKUST. *Proc. Phy. Modelling in Geotechnics*, St. John's. 71–76.
- Okawa, K., Kamei, H., Kimura, M. & Zhang, F. 2002. Dynamic behavior of a group-pile foundation with inclined piles in loose sand. *Proc. Phy. Modelling in Geotechnics*, St. John's. 729–734.
- Okumura, F., Mokutani, S., Okamura, M., Takemura, J., & Kimura, T. 1994. Effects of repeated stress on toe resistance of cast-in-place concrete piles. *Proc. Centrifuge 94*, Singapore. 425–430.

- Ong, D.E.L., Leung, C.F. & Chow, Y.K. 2006a. Pile behavior due to excavation-induced soil movement in clay. I. stable wall. *J. Geotech. and Geoenviron. Engr.* 132(1): 36–44.
- Ong C.W., Leung C.F., Yong, K.Y. & Chow Y.K. 2006b. Pile Responses due to Tunnelling in Clay. *Proc. 6th Int. Conf. Phy. Modelling in Geotech., Hong Kong.* 2: 1177–1182.
- Osterberg, J. 1989. New device for load testing driven piles and drilled shafts separates friction and end bearing. *Proc. Int. Conf. on Piling and Deep Foundations*, London. 421–427.
- Park, J., Park, C., Kim, S., Jeong, H., Kim, Y., Kim, S. & Kim, Y. 1998. Geotechnical centrifuge facility at Daewoo Institute of Construction Technology. *Proc. Centrifuge 98*, Tokyo. 1: 9–12.
- Randolph, M.F. & House, A.R. 2001. The complimentary roles of physical and computational modeling. *Int. J. of Phy. Modelling in Geotech.* 1(1): 1–8.
- Satoh, H., Ohbo, N. & Yoshizako, K. 1998. Dynamic tests on behaviour of pile during lateral ground flow. *Proc. Centrifuge 98*, Tokyo. 1: 325–332.
- Shen, C.K., Li, X.S., Ng, C.W.W. Van Laak, P.A., Kutter, B.L., Cappel, K. & Tauscher, R.C. 1998. Development of a geotechnical centrifuge in Hong Kong. *Proc. Centrifuge 98*, Tokyo. 1: 13–18.
- Shen, R.F., Leung, C.F., Chow, Y.K., Kog, Y.C. & Liao, B.K. 2002. Negative skin friction on piles. *Proc. Physical Modelling in Geotechnics*, St. John's, 673–678.
- Shen R.F., Leung C.F. & Chow Y.K. 2006. Negative skin friction on end-bearing piles. *Proc. 6th Int. Conf. Phy. Modelling in Geotech., Hong Kong.* 2: 875–880.
- Seo, D., Jeong, S. & Kim, Y. 2006. Physical modelling of pile group subjected to lateral soil movements. *Proc. 6th Int. Conf. Phy. Modelling in Geotech.*, Hong Kong. 2: 1043–1048.
- Su, D. & Li, X.S. 2006. Centrifuge modeling of pile foundation under multi-directional earthquake loading. *Proc. 6th Int. Conf. Phy. Modelling in Geotech.*, Hong Kong. 2: 1049–1054.
- White, D.J., Take, W.A. & Bolton, M.D. 2003. Soil deformation measurement using Particle Image Velocimetry (PIV) and photogrammetry. *Geotechnique*. 53(7), 619–637.
- Xie, Y., Leung, C.F. & Chow, Y.K. 2006. Effect of spudcan penetration on adjacent piles. *Proc. 6th Int. Conf. Phy. Modelling in Geotech., Hong Kong.* 1: 701–706.
- Zhang, L.M. & Kong, L.G. 2006a. Centrifuge modeling of torsional responses of piles in sand. *Can. Geotech. J.* 43: 500–515.
- Zhang, L.M. & Kong, L.G. 2006b. Modelling responses of pile groups under torsion. *Proc. 6th Int. Conf. Phy. Modelling in Geotech.*, Hong Kong. 2: 957–962.
- Zhang, W.M., Wang, N.X., Zeng, Y.J. & Li, Y.H. 2006. Application of centrifuge modeling in design of a super bridge foundation. *Proc. 6th Int. Conf. Phy. Modelling in Geotech.*, Hong Kong. 2: 901–906.

Advanced modeling tools for the analysis of axially loaded piles

R. Salgado, M. Prezzi & H. Seo

Purdue University, Indiana, U.S.A.

ABSTRACT: Pile foundations have been used in construction for thousands of years but only in the last few decades has there been significant progress in the technology of pile installation. This progress has not been matched by progress in the analysis and design of these foundation elements. This is in large part due to considerable difficulties in analyzing both pile installation and the response of piles to various types of loadings rigorously. Given these difficulties, the profession has in general used relatively crude design approaches. This is likely to change due to pressures from different directions, particularly the progress in code design (the push towards load and resistance factor design in geotechnical engineering requires a much better grip on all the factors that need to be considered in calculating pile resistances and what the uncertainties in quantities and analyses are, requiring sounder analytical frameworks) and economics (material costs have started to rise, a trend that, if continued, would make it more economically interesting to have optimal designs). In this paper, we will examine the design process for axially-loaded non-displacement piles, focusing on assessing the strength of the underlying analyses. We will show that, for these types of piles, design can be placed on a theoretical basis. We will discuss on-going research on pile analysis that is contributing to the gradual development of the new design methods.

1 INTRODUCTION

While piles have been used literally for millennia, many aspects of piling are not to this day modeled with much rigor. Pile installation, particularly in the case of driven piles, cannot yet be simulated accurately, although it is currently a focus of research. Laterally loaded piles are designed using a semi-empirical technique – the p-y method – which is used almost universally. While more meaningful advances have taken place in axially loaded pile analysis, these advances have not been sufficiently integrated with current knowledge of soil mechanics or tied in a fundamental way with the process by which the tens of pile types in existence are installed in the ground. In this paper, we will examine the analytical basis for calculating the ultimate base and shaft resistances of non-displacement piles subjected to axial loads and the pile head settlement for a given applied load.

The analysis of axially loaded piles appears, on first examination, to be one of the simplest in geomechanics. The total load carried at the pile head, we learn as undergraduate students, is simply the summation of base and shaft resistances:

$$Q = Q_b + Q_s \quad (1)$$

The base and shaft resistances, in turn, are simply the multiplication of shaft and base areas, A_s and A_b , by the respective unit resistances q_b and q_s :

$$Q_b = A_b q_b \quad (2)$$

and

$$Q_s = \sum_{i=1}^n q_{si} A_{si} \quad (3)$$

where i is a soil layer index, and the summation is over the number n of layers crossed by the pile.

The separation of pile resistance in shaft and base resistance is a simplification of the problem, albeit a perfectly acceptable one in most cases. So, up to this point, we would be justified in thinking that this is indeed an easy problem. All we would need to do to proceed is to determine these unit resistances and the problem would be solved. However, the processes used to determine pile unit resistances are far from well developed.

As load on the pile head is gradually increased, the pile settlement increases. This proceeds until a load is reached at which the pile would tend to plunge. This load is known as the plunging or limit load. Given this, a question that arises is how to define the pile base and shaft resistances. Are they the values corresponding to the limit load or those associated with a particular value of pile settlement? There is uncertainty among both practitioners and academics as to how to define pile resistance.

If resistance is used in the classical sense of the word, then it must be associated with an ultimate limit state (ULS), one associated with potentially severe consequences for the supported structure. The plunging of the pile is clearly an ULS but pile settlements

beyond a certain limit would also lead to ULS's. So a resistance defined based on a certain level of settlement is also possible. Since there is some confusion in the literature regarding this, the practice we follow is to use the term limit resistance for the maximum sustainable resistance that can be reached at large strains; i.e., the limit shaft resistance is the maximum shaft resistance and the limit base resistance is the maximum base resistance reached at large pile displacements. When both the limit shaft and limit base resistance are reached, the pile reaches its limit resistance and plunges. Ultimate resistance, on the other hand, is a conventional load associated with an ultimate limit state, but not necessarily a maximum resistance. The most obvious example of an ultimate resistance is the load leading to a pile settlement equal to 10% of the pile diameter, which is favored internationally as an ultimate load criterion. This load has the added advantage that, for the factors of safety typically used in practice, it both separates safe designs from potentially unsafe designs and avoids serviceability limit states.

Now that we have defined precisely what is meant by resistance, we can address its estimation or determination. We will separate soils in sands, clays and transitional soils. In sands, pile resistances can be calculated using drained analysis with soil represented as a frictional material. In clays, pile resistances have typically been estimated using undrained analysis, with the soil modeled as a frictionless, Tresca-like material. Transitional soils, which appear often enough in piling practice, are materials with intermediate behavior, in which partial drainage may be an issue either at the site investigation stage (such as in the interpretation of cone penetration tests) or the pile design stage. Fabric or structure may play a significant role in partially drained soil response. Although extremely interesting and important, we will not discuss transitional soils in this paper.

Piles are typically grouped in two main categories: displacement and non-displacement piles. An ideal non-displacement pile is installed in the soil such that a volume of soil is replaced by the pile (which is in mechanics terms an equal volume of a much stronger, stiffer material, typically concrete) without causing disturbances or changes in the stress or deformation states at any point of the surrounding soil. The classical example of a non-displacement soil is a drilled shaft (bored pile). Drilled shaft installation does cause changes in the surrounding soil; however, these changes are fairly small and very near the pile shaft if installation is done with proper care. Additionally, it is possible to model, even if simply, the effects of the installation on the soil. Displacement piles, in contrast, are piles installed in the ground without any soil removal. This type of pile acquires its space by displacing soil from space it originally occupied, a large-deformation process that is challenging to model.

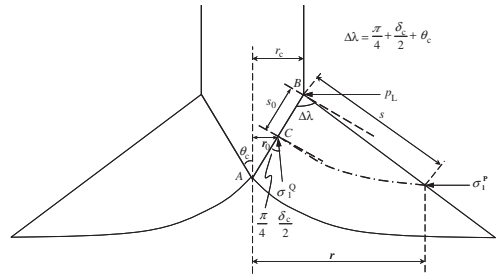


Figure 1. Mechanism of pile base plunge.

2 BASE RESISTANCE

2.1 Sand

2.1.1 Limit base resistance

Ideally, the limit base resistance of piles in sand would be calculated from a large-deformation analysis that would accurately compute the compressive stresses on the pile base as the pile is pushed through the soil. These analyses have become viable but are still challenging, and more so in the case of sands.

Limit base resistance may also be estimated using cavity expansion analysis. The analysis of Salgado and Prezzi (2006) assumes a simplified mechanism to relate the pile base resistance to cylindrical cavity limit pressure. As argued by Salgado et al. (1997), the existence of this relationship is intuitive in that a cylindrical pile, when pushed through the soil, does expand a cylindrical cavity in it, and is backed up by experimental evidence from calibration chamber tests (e.g., Housby and Hitchmann 1988) that show a clear dependence of cone tip resistance q_c , a proxy for pile limit base resistance, on lateral effective stress. Figure 1. shows the mechanism used to calculate limit base resistance, which is obtained by considering the rotation of major principal stresses from the horizontal direction associated with cylindrical cavity expansion to a sub-vertical direction on the cone face. The cylindrical cavity expansion analysis and the stress rotation analysis used to compute q_{BL} are detailed in Salgado and Prezzi (2006) and Salgado and Randolph (2001)¹. An illustration of the values this analysis produces is provided in Figure 2 for two extreme values of the critical-state friction angle.

2.1.2 Ultimate base resistance

Lee and Salgado (1999) performed finite element analyses using ABAQUS to obtain the base resistances of non-displacement piles in sand. They analyzed piles with three different lengths — 5, 10 and 20 m — and a

¹ The program CONPOINT can be used to perform this analysis.

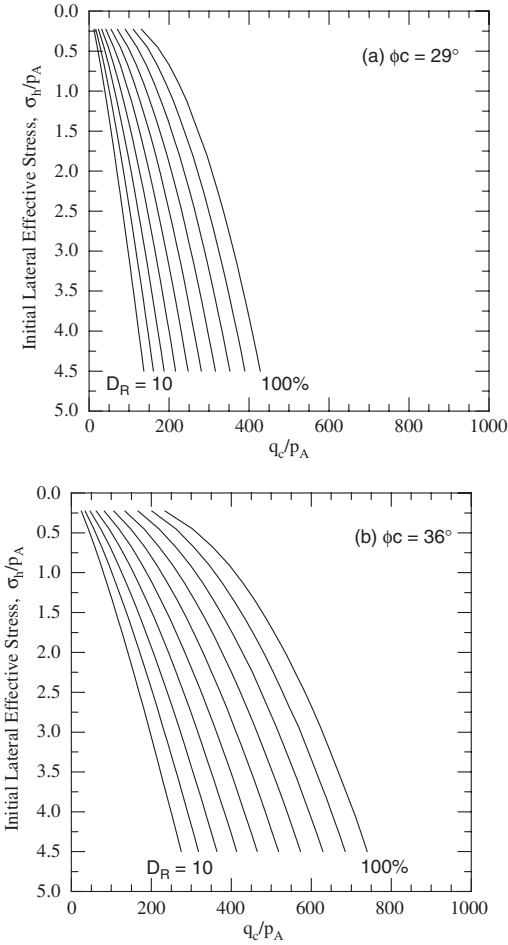


Figure 2. Cone resistance (a proxy for q_{bl}) versus effective lateral stress and relative density for sand with critical-state friction angle equal to 29° and 36° ; p_A = reference stress ($=100 \text{ kPa} = 0.1 \text{ MPa} \approx 1 \text{ tsf}$).

fixed radius of 60 cm, embedded in normally consolidated sand with relative densities of 30, 50, 70 and 90%. Sand parameters were those in Table 1, considered fairly representative of silica sands commonly found in the field. The axisymmetric problem was modeled using eight-noded quadrilateral elements, with interface element of zero thickness at the pile-soil boundary following the Coulomb friction law. The boundaries of the domains were placed far from the pile to minimize boundary effects. The pile was elastic, and the soil, elastic-plastic following a stress-strain model modified after Fahey and Carter (1993) with a nonlinear form of Drucker-Prager criterion to model failure and post-failure response.

Table 1. Basic properties of Ticino Sand (after Ghionna et al. 1994), the sand used in the base resistance analysis of Lee and Salgado (1999).

D_{10} (mm)	D_{50} (mm)	G_s	U	ϕ_c ($^\circ$)	e_{max}	e_{min}	γ_{max} (kN/m ³)	γ_{min} (kN/m ³)
0.36	0.54	2.62	1.5	34.8	0.92	0.57	16.68	13.65

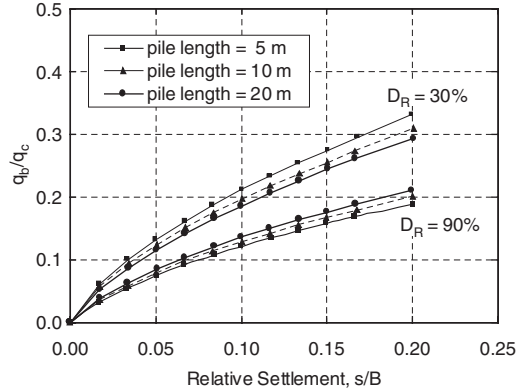


Figure 3. Normalized base load-settlement curves in terms of q_b/q_c and s/B for non-displacement piles.

Unit pile base resistance q_b , normalized with respect to q_c (which is approximately the same as the limit unit base resistance q_{BL}), is shown in Figure 3, as a function of relative settlement s/B (s = pile head settlement, B = pile diameter) for different pile lengths and for the relative densities of 30% and 90%. Cone resistance q_c was estimated using CONPOINT for various values of relative density (D_R) and stress state. The s/B vs. q_b/q_c curves for 90% relative density lie noticeably below those for very loose sand because limit base resistance, which depends mostly on shear strength, increases at a higher rate with increases in relative density than the load associated with a given settlement, which depends on stiffness.

Table 2 shows q_b/q_c for $s/B = 5\%$ and 10% obtained from the analysis. Values of q_b/q_c fall within the 0.07–0.13 range for $s/B = 5\%$ and within the 0.12–0.21 range for $s/B = 10\%$. The values are in general agreement with those observed in the field and laboratory (Table 3).

Figure 4 illustrates the influence of relative density on the normalized base resistance q_b/q_c . The effect is substantial, with q_b/q_c decreasing with increasing relative density. This justifies the presentation of q_b/q_c values for different relative densities in Table 2. The value of q_b/q_c at $s/B = 10\%$ is 0.19–0.21 for $D_R = 30\%$, whereas it is 0.12–0.13 for $D_R = 90\%$. The

Table 2. Values of q_b/q_c for non-displacement piles obtained from FEM analysis.

Pile Length (m)	D_R (%)	q_b/q_c ($s/B = 5\%$)	q_b/q_c ($s/B = 10\%$)
5	30	0.13	0.21
	50	0.1	0.17
	70	0.09	0.14
	90	0.07	0.12
10	30	0.12	0.2
	50	0.1	0.16
	70	0.09	0.14
	90	0.08	0.13
20	30	0.11	0.19
	50	0.1	0.16
	70	0.09	0.15
	90	0.08	0.13

Table 3. Observed and recommended values of q_b/q_c for non-displacement piles.

Author(s)	D_R (%)	q_b/q_c for $s/B = 5\%$	q_b/q_c for $s/B = 10\%$
Franke (1993)	—	—	0.2
Jamiolkowski and Lancellotta (1988)	—	0.2	—
Ghionna et al. (1994)	50	0.09–0.14	0.11–0.19
	90	0.07–0.10	0.10–0.14
Salgado (1995)	—	—	0.15
Mayne and Harris (1993)	—	—	0.26
Teixeira and Albiero (1994)	—	0.18	0.2
Simonini (1996)	—	0.09	0.17

q_b/q_c ratio can be approximated reasonably well by the following equation:

$$\frac{q_{b,10\%}}{q_c} = 0.23 \exp(-0.0066D_R) \quad (4)$$

Eq. (4) indicates that the q_b/q_c ratio decreases with increasing D_R . Alternatively, it expresses the fact that larger settlements are required for soils with higher relative densities to reach a unit base resistance equal to a set percentage of q_c . The results also offer some insight into why most pile design methods that calculate q_b by multiplying q_c by a certain constant (e.g. 0.2 for 10% relative settlement, according to Franke 1989) also place an upper limit (usually in the 4.5–5 MPa range) on possible values of q_b . The results of the present analysis indicate that when piles are embedded in very dense sand layers, a value of q_b , chosen irrespective of relative density (for example, $q_b=0.2q_c$, as proposed by Franke 1989) would yield an excessively large base resistance. Placing a limit on q_b (e.g., 5 MPa) serves a purpose in that case, but if the q_b/q_c values of Table 2

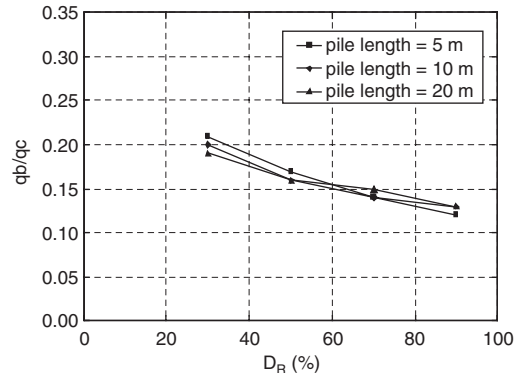


Figure 4. Normalized unit base resistance versus relative density for $s/B = 10\%$.

are used for design, there is no need for setting an upper limit on q_b .

The effect of pile length (i.e. confinement at pile base level) and overconsolidation on q_b/q_c was also studied. The effect of pile length on q_b/q_c was found to be small because q_b and q_c depend on initial confining stress in a similar way. The effect of K_0 on q_b/q_c was found to be inconsequential.

2.2 Clay

2.2.1 Limit base resistance

The ratio of net unit pile base resistance to undrained shear strength in clay has traditionally been taken as 9. This follows from early versions of the bearing capacity equation,

$$q_{bL}^{\text{gross}} = s_{s_u} d_{s_u} N_c s_u + q_0 \quad (5)$$

with shape and depth factors s_{s_u} and d_{s_u} proposed by Skempton (1951) and Meyerhof (1951, 1963); for foundations with $D/B \geq 2.5$, (5) was taken as:

$$q_{bL}^{\text{gross}} = 9s_u + q_0 \quad (6)$$

It is common in pile design in clay to work with net limit unit bearing capacity q_{bL}^{net} . With the assumption that the pile self-weight divided by its cross-sectional area approximately balances q_0 , we arrive at the value of 9 for the ratio q_{bL}^{net}/s_u . Recent research, however, suggests that 9 may be too low. Martin (2001) found a value of approximately 9.3 for this ratio from lower bound analysis. He also determined that this number is essentially the same regardless of the rate of undrained shear strength increase with depth. Salgado et al. (2004) showed, using limit analysis of circular foundations ranging in depth from zero to depths typical of piles, that the unit base

capacity keeps increasing with depth beyond the D/B value of 2.5 used to obtain the earlier estimates of 9 for q_{bL}/s_u . Their lower bound values for unit base resistance in clays is as high as 11 for D/B = 5, with upper bound as high as 13.75 for the same relative depth. It should be noted that the boundary conditions utilized did not account for the constraining effect of shaft resistance on base resistance (by which the soil on the sides of the pile, in order to move up with respect to the pile as the pile is pushed down, must overcome friction with the pile), suggesting the actual values could be higher. On the other hand, limit analysis may not capture well the confined flow mechanism that is operative for deep foundations (which, incidentally, justifies the use of cavity expansion analysis to analyze such problems). A different approach, by Yu et al. (2000), arrives also at higher values for q_{bL}^{net}/s_u (typically in the 10–12 range for realistic conditions). Hu et al. (1999) conducted a large-strain finite element analysis that produced a net limit unit base resistance equal to $12.7s_u$ for a pre-embedded circular foundation with length to diameter ratio of 2 at a displacement of over four pile diameters. This evidence suggests that q_{bL}^{net}/s_u is at least equal to 10 and potentially as high as 12–13.7.

2.2.2 Ultimate base resistance

While in the calculation of collapse loads associated with unrestrained mechanisms the soil stiffness does not matter, in contained plastic flow, the soil stiffness plays an important role. Randolph et al. (2004) argue that, for piles (i.e., for large foundation embedment), a cavity expansion mechanism is in force for the pile base. Even if unrestrained collapse mechanisms can be achieved in clay, the argument can be made that we are not necessarily interested in design in the limit resistance but rather in the value of base load at a specific value of settlement. For 10% relative settlement, Hu and Randolph (2002) obtained q_{bL}^{net}/s_u values ranging from 9.3 to 9.9. In design, their average value of 9.6 could be used.

3 SHAFT RESISTANCE

3.1 Sand

The unit shaft resistance is the product of the normal effective stress on the soil-pile interface ($\sigma'_h = K\sigma'_{v0}$) by an appropriate interface friction coefficient ($\mu = \tan \delta$). Except in the case of floating piles, shaft resistance is fully mobilized along most of the pile length (except very near the base) for a pile subjected to its ultimate load defined according to the 10% relative settlement criterion. It is probably fully mobilized along most of the pile length under service conditions for well designed “end-bearing” piles as well.

Mathematically, the unit limit shaft resistance q_{sL} is written as:

$$q_{sL} = K\sigma'_{v0} \tan \delta \quad (7)$$

where K = coefficient of lateral earth pressure (a function of soil state), δ = interface friction angle, and σ'_{v0} = initial vertical effective stress. We use the notation σ'_{v0} to stress that even if there may be vertical effective stress changes at very close distances from the pile shaft, our reference for calculating σ_h is always the initial vertical effective stress.

Eq. (7) is deceptively simple. Finding appropriate values for K and δ is not trivial, hence the vagueness with which the subject is typically treated in the literature. Values of δ should be expressed in terms of the critical-state friction angle ϕ_c . The argument for using ϕ_c is based on the development of large shear strains near the pile shaft at ultimate load levels. These strains are sufficiently large to cause a certain volume of soil near the pile to reach critical state.² At the ultimate load, critical state will be reached along the pile shaft for both stiff and compressible (slender) piles.

For non-displacement piles, given the high degree of roughness of the concrete placed in-situ, the interlocking of the shaft with the soil is such that shearing will take place within the soil immediately adjacent to the pile. It is therefore appropriate to take $\delta = \phi_c$ for non-displacement piles. This is also illustrated experimentally by the data of Uesugi et al. (1990).

The installation of non-displacement piles preserves to a large extent the pre-existing stress state in the ground. Any limited unloading that may take place is corrected by the placement of the concrete, which has enough fluidity before setting to apply a normal stress on the soil sufficient to reestablish the original lateral stress (in fact, Fleming et al. 1992 argue that the placement of concrete with high fluidity would even lead to an initial K slightly greater than K_0). When the pile is loaded, constant-volume shearing will eventually develop between the pile and the sand. On the way there, the sand, if dilative, will attempt to expand but is constrained from doing so by the presence of the pile shaft; as a result, the normal stress between the pile and sand will increase. The result is that, for loose sands, K is close in value to K_0 , but, for dense sands, K may be significantly greater than K_0 . The literature does not appear to contain any analysis seeking to quantify K as a function of relative density and stress. A relatively simple analysis is possible to illustrate how we currently have the tools to obtain very good relationships for K .

² Geometrically, for a circular pile, this volume would be a hollow cylinder of soil with a thickness of barely a few times the D_{50} of the soil, as we will discuss later.

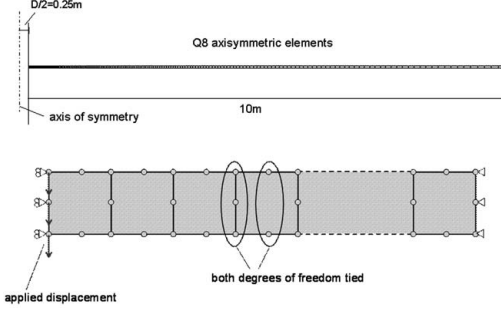


Figure 5. Finite element representation of the application of a displacement to the side of a disc of soil representing a layer of soil around a pile.

A simple finite-element simulation of what happens in the soil as the pile is pushed down and shearing develops along the pile soil interface can be done by considering a disk of soil around the pile (Figure 5), similarly to what was done by Potts and Gens (1984). Where the pile-soil interface would be, a vertical displacement is applied in increments until very large shear strains develop. The soil is modeled using 250 8-noded quadrilateral, axisymmetric elements. Nodes lying in the same vertical are tied together with respect to both vertical and horizontal movement. This means the distortion of the soil disk as the pile is pushed down is captured by vertical shearing of the elements, which cannot rotate nor contract or stretch in the vertical direction. The elements are able to contract or dilate by contracting or stretching in the radial direction. The pile diameter for these analyses was 0.5 m. The sand was modeled using a constitutive model based on work of Papadimitriou and Boukvalas (2002) and Dafalias and Manzari (2004) calibrated with data for Ottawa sand from Salgado et al. (2000) and Carraro et al. (2004). The finite element program SNAC (Abbo and Sloan 2000) was used.

Shear strain is highly localized next to the pile shaft. Considering the dependence of the results on the level of discretization when a strain-softening material is involved, the size (width) of the leftmost element was set to be no less than the shear band thickness that would be observed in reality. Various experimental studies (e.g., Uesugi et al. 1988; Vardoulakis & Sulem 1995, Nemat-Nasser & Okada 2001) on shear strain localization have shown that the shear band thickness is usually in the 5–20 D_{50} range. Most analyses were done for a minimum element size of 10 D_{50} , corresponding to ~4 mm for Ottawa sand, and $K_0 = 0.4$. Sensitivity studies have shown that K/K_0 decreases slightly as the element size drops from 10 to 5 D_{50} and as K_0 increases.

Figure 6 shows the evolution of the shear stress that develops with increasing vertical pile displacement.

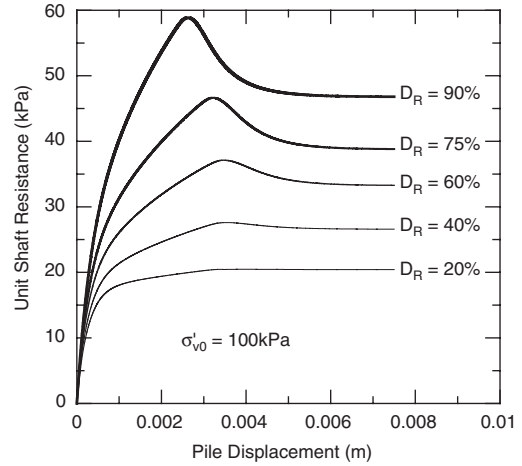


Figure 6. Shear stress versus pile displacement for various D_R values.

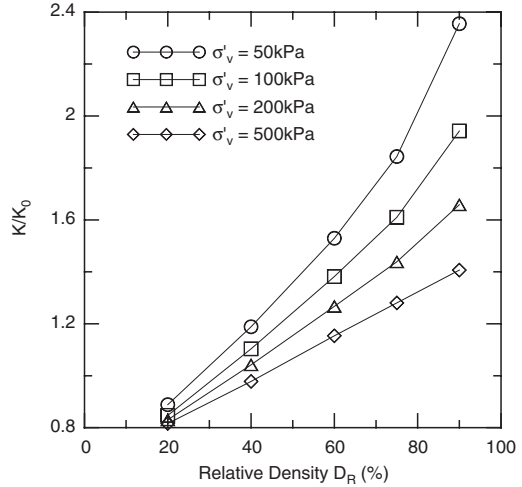


Figure 7. Values of K/K_0 versus D_R for $\sigma'_v = 50$ kPa, 100 kPa, 200 kPa and 500 kPa.

The value of pile movement required for mobilization of q_{SL} is of the order of 4 mm (or about 0.8% of the pile diameter). For loose sand (in the case analyzed here less than about 40% relative density), the final normal stress acting on the pile shaft actually drops due to the contractive nature of the sand. We can obtain K from the ratio of the normal stress at the end of shearing to σ'_v (K is given as a function of D_R in Figure 7). K is less than K_0 for sands looser than about 40% relative density but exceeds K_0 , reaching a value just shy of 2.4 K_0 , for $D_R = 90\%$ and $\sigma'_v = 50$ kPa.

3.2 Clay

Both an effective stress analysis, using Eq. (7), and a total stress analysis can be done of the shaft resistance of a pile in clay. In the more commonly used total stress analysis, q_{sl} is expressed in terms of the undrained shear strength s_u of the soil as:

$$q_{sl} = \alpha s_u \quad (8)$$

There has been little research done on the value of α for drilled shafts. Skempton (1959) argued that α for stiff London clay was lower than 1 due to unloading of the clay at the walls of the shaft and remolding due to drilling operations. He proposed at the time an average $\alpha = 0.45$ for typical sizes of drilled shafts. Reese and O'Neill (1988), based on their own research on drilled shafts installed in stiff clay in Texas, proposed $\alpha = 0.55$. Most publications simply refer to one of these values with little discussion. There is also no clear agreement as to what s_u should be in (8). We will assume s_u in (8) to refer to triaxial-compression, peak undrained shear strength, which may be estimated from the Skempton (1957) correlation:

$$\frac{s_u}{\sigma'_v} = [0.11 + 0.0037(\text{PI})] \text{OCR}^{0.8} \quad (9)$$

We can establish a simple analytical basis for determining α by examining the problem in a conceptual way. The starting point is to recognize that clay is weaker than the relatively rough concrete interface created by drilled shaft installation, and so it is reasonable to assume (as did Fleming et al. 1992) that the shearing takes place within the clay in a direction roughly parallel to the pile shaft, so that interface effects are not a significant factor in determining the value of α . This leaves the process of pile installation as the determining factor for the value of α .

The coefficient α may be expressed quite generally as:

$$\alpha = \frac{s_{u,r}}{s_u} = \frac{\sigma'_{hds} \tan \phi_r}{\sigma'_v [0.11 + 0.0037(\text{PI})] \text{OCR}^{0.8}} \quad (10)$$

where $s_{u,r}$ is the residual shear strength of the clay along the shaft-soil interface that develops upon loading of the pile; ϕ_r is the residual friction angle of the clay (which is operative because the clay particles are aligned with the direction of shearing as a result of auger action during drilling); and σ'_{hds} is the lateral effective stress between the pile shaft and the disturbed soil during axial loading.

It is important to note that ϕ_r decreases with increasing effective normal stress σ' on the plane of shearing (because a larger normal stress forces greater alignment of particles as they are sheared). Figure 8

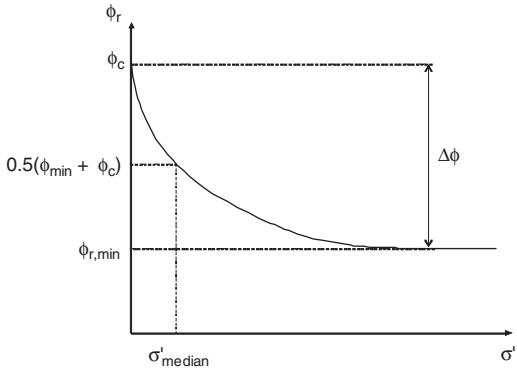


Figure 8. Variation of ϕ_r with normal stress perpendicular to the plane of shearing.

illustrates schematically the decrease in ϕ_r with increasing normal stress on the plane of shearing. At very large stresses, ϕ_r reaches an absolute minimum, denoted by $\phi_{r,min}$. For very small stresses, ϕ_r approaches the critical-state friction angle ϕ_c . The assumption that, at σ' equal to zero, $\phi_r = \phi_c$ is based on the expectation that there would be negligible reorientation of particles in the absence of a normal stress forcing this reorientation to happen.

Following Maksimovic (1989), ϕ_r can be expressed as:

$$\phi_r = \phi_{r,min} + \frac{\phi_c - \phi_{r,min}}{1 + \frac{\sigma'}{\sigma'_{\text{median}}}} \quad (11)$$

where σ' is the normal stress on the plane of shearing, and σ'_{median} is the value of σ' at which the friction angle is exactly equal to the average of the minimum residual friction angle $\phi_{r,min}$ and ϕ_c . From a practical standpoint, for clays containing a large smectite content, such as London clay, ϕ_c might have to be replaced by a lower ϕ value in order for (11) to produce acceptable results. The values from Maksimovic (1989) used in (11) are not necessarily true ϕ_c values. Figure 9, for example, shows data for London clay based on both laboratory and field data. Note that the maximum value of ϕ_{res} at $\sigma' = 0$ extrapolated by Maksimovic (1989) from the data is of the order of 12.5 to 16°, while this clay has ϕ_c in the 20–23° range.

According to Skempton (1985), the residual friction angles of kaolinite, illite and montmorillonite are approximately equal to 15°, 10° and 5°, respectively. Values of the critical-state friction angle for London Clay and kaolinite are given as 23 and 25° by Atkinson (1993). These data are combined with data from Maksimovic (1989) and Kenney (1967), as reported by Maksimovic (1989) in Table 4.

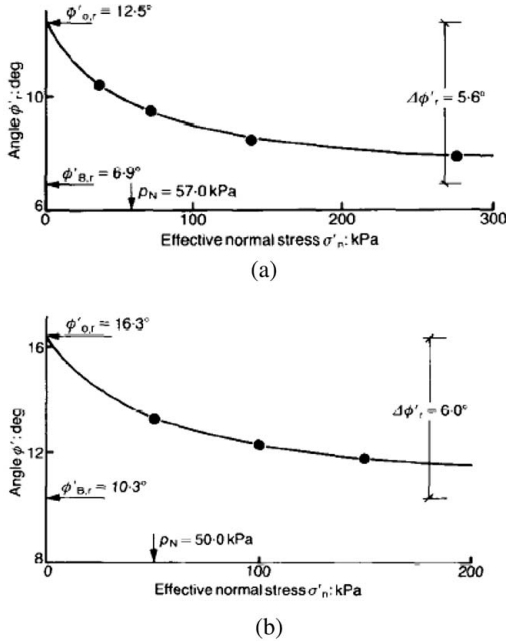


Figure 9. Residual friction angle of London clay versus normal effective stress based on (a) ring shear test data from Bishop (1971) and (b) back-calculation of landslides, after Maksimovic (1989).

We must now tackle the question of how to determine σ'_{hds} . It is difficult to reduce the loading imposed on the soil during excavation and augering to a simple stress path. Naturally, there will be an induced shear stress associated with the excavation and another with the augering. On the way to critical state, we can estimate the pore pressure generated by using the Skempton concept of a pore pressure coefficient or a suitable constitutive model. For simple shear loading, this can be expressed as a ratio a of the pore pressure generated to the applied shear stress τ . If we assume that any changes in volume (under drained conditions) or pore pressure (under undrained conditions) beyond the critical state, towards a residual state, would happen only along the slip surface and would thus be very small, we could neglect additional pore pressure changes to obtain a first-order estimate of σ'_h at the end of installation. The concrete would then be poured, the excess pore pressure dissipated, and σ'_h would (ideally) return to its initial value. Finally, loading of the pile would subject the soil around the pile to a simple shear loading. Having been pre-sheared, its pore pressure generation capability would now be different from that of undisturbed soil (and represented by a pore pressure coefficient a_r). Additionally, the stress path would now be capped by

Table 4. Values of parameters needed to calculate α obtained from Maksimovic (1989), Atkinson (1993) and Skempton (1985).

Clay type	LL (%)	PI (%)	ϕ_c^1 (°)	$\phi_{\text{res,min}}$ (°)	$\Delta\phi$ (°)	σ'_{median} (kPa)
London Clay	75	45	16.3	10	13	50
Kaolinite	65	30	24 ²	13.4 ³	10.6	55

¹Not true ϕ_c but rather extrapolated ϕ_r for zero normal stress (see Figure 9 (b)).

²This compares well with $\phi_c = 25^\circ$ given by Atkinson (1993).

³This compares well with $\phi_r = 15^\circ$ given by Skempton (1985).

the residual strength envelope. The value of σ'_{hds} can now be calculated as:

$$\sigma'_{\text{hds}} = \sigma'_{h0} - 2a_r \tau_r = K_0 \sigma'_v - 2a_r \sigma'_{\text{hds}} \tan \phi_r \quad (12)$$

from which σ'_{hds} can be extracted:

$$\sigma'_{\text{hds}} = \frac{K_0 \sigma'_v}{1 + 2a_r \tan \phi_r} \quad (13)$$

The value of K_0 may be estimated from the often-used Jaky's equation:

$$K_0 = (0.95 - \sin \phi) \text{OCR}^{\sin \phi} \quad (14)$$

We can now calculate α using (14), (13), (11)³ and (10), in succession. The value of a_r can be obtained either by analytical integration of a suitable constitutive model or from simple shear testing. A simple illustration of this analysis can be done here for a stiff clay, for which the stress paths during installation and reloading of the remolded soil would be nearly vertical, such that we may assume for simplicity that $a_r = 0$ and $\sigma'_{\text{hds}} = \sigma'_{h0}$.

The values of α were calculated in this manner for kaolinite for σ'_v ranging from 0 to 500 kPa. Kaolinite was chosen because its fundamental parameters are reasonably well established. Table 4 has values for the parameters required in the calculations. For comparison, we have also included the parameters of London clay; although not done here, calculations of σ for London clay lead to values slightly lower than for kaolinite. As it is customary in practice to plot α versus s_u , we also need to calculate the corresponding value of s_u to develop such plots, which is again done using (9). For anisotropically consolidated clay loaded in simple shear, the value of OCR associated

³Note the iteration between (11) and (13).

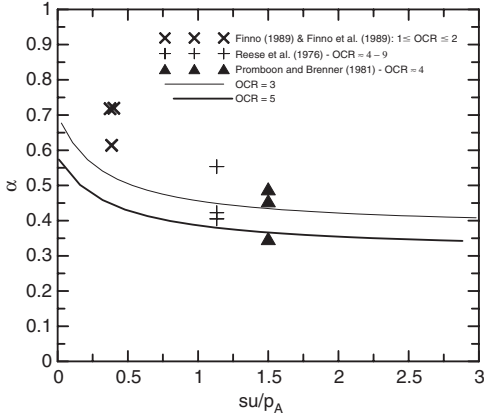


Figure 10. Theoretical values of α and estimated values from field case histories.

with zero a_r is likely to be in the 3–5 range. The corresponding α values are plotted as two lines versus s_u in Figure 10. The value of α will be in this range. We also show in Figure 10 the α values obtained from the relatively few data cases in the literature for which reasonably accurate shaft resistance and s_u values are available and for which OCR can be estimated. The theoretical curves compare well with the data, most of which are for OCR values in the 3–9 range; however, the values associated with low s_u values in the figure are associated with either NC or lightly OC clays, and the theoretical curves are not applicable for those conditions; hence the large difference between the theoretical and field values.

One further consideration regards the clay content or clay fraction CF. Skempton (1985) observed that ϕ_r varies with clay content. For clay content (clay fraction) CF less than approximately 25%, ϕ_r coincides with ϕ_c (note, however, that this is the ϕ_c of the clay-silt-sand soil, not that of the clay); for clay content increasing from 25 to 52%, the residual friction angle drops towards the ϕ_r of the pure clay. For clay content greater than 52%, the residual friction angle remains stable at this minimum value. In order to account for the clay content in the calculation of α , we will assume that the α method will only be used when $CF \geq 25\%$. Based on the numbers provided by Skempton (1985) on the values of CF between which ϕ_r changes from ϕ_c of the soil mix to ϕ_r of the pure clay, we can write the following approximate equation for ϕ_r as a function of CF:

$$\phi_r = \phi_r|_{\text{pure clay}} + \frac{\phi_c|_{\text{pure clay}} - \phi_r|_{\text{pure clay}}}{27\%} [52\% - CF(\%)] \quad (15)$$

Values of α can now be calculated as a function of clay content. The α of soils containing mixtures of

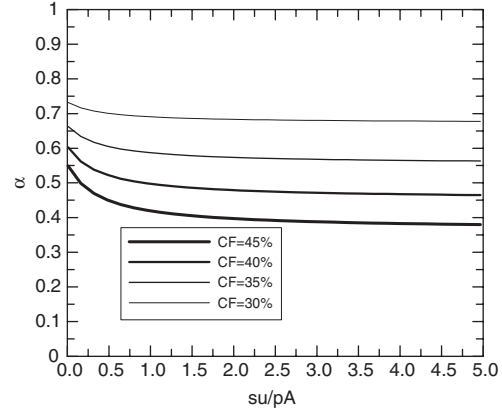


Figure 11. Plots of α versus undrained shear strength s_u for soils with different clay content CF.

sand, silt and clay with more than 25% clay would be expressed as:

$$\alpha = \frac{\sigma'_{\text{uds}} \tan \left\{ \phi_r|_{\text{pure clay}} + \frac{\phi_c|_{\text{mix}} - \phi_r|_{\text{pure clay}}}{27\%} [52\% - CF(\%)] \right\}}{\sigma'_v [0.11 + 0.0037(PI_{\text{mix}})] OCR^{0.8}} \quad (16)$$

Studies on mixtures of clay, sand and silt with high-quality data on the ϕ_c of these soils are few. The presence of sand or non-plastic silt increases ϕ_c by a few degrees. We know that the ϕ_c of most sands, non-plastic silts or mixtures of the two encountered in practice would be in the 30–35° range (e.g., Salgado et al. 2000). The presence of clay reduces ϕ_c from that range to perhaps 28–30°. We will take 28° to be the ϕ_c of a sand-silt-kaolinite mixture with 25% kaolinite, assume it to decrease linearly with clay content as it increases from 25 to 52%, and assume, as before, that $a_r = 0$ for $3 \leq OCR \leq 5$. The PI of the soil drops significantly as CF drops from 52 to 25%. We will assume for simplicity that this drop occurs linearly and that the PI at 25% CF is equal to 10. We can now illustrate the calculation of α for soils with $25 \leq CF \leq 52\%$ using (16). Plots of α versus clay content obtained in this manner are shown in Figure 11, for $OCR = 5$. Note that the plot for $CF = 45\%$ is very close to the corresponding plot of Figure 10. These should be considered preliminary estimates of α , which can be refined with more elaborate determination of all the variables entering the calculations.

4 SETTLEMENT ANALYSIS

While design is often done without explicit settlement checks, analyses that can accurately calculate settlement

for a given load offer an opportunity for more cost-effective design in the future. This section provides an overview of past and current work on this topic.

Poulos and Davis (1968) and Butterfield and Banerjee (1971) obtained analytical solutions for a vertically loaded pile in a homogeneous, single soil layer by integrating Mindlin's point load solution (Mindlin 1936). In reality, however, piles are rarely installed in an ideal, homogeneous, single soil layer. For this reason, analytical solutions for axially loaded piles embedded in a non-homogeneous soil deposit have been sought.

Poulos (1979) presented a series of solutions for the settlement of a pile in a Gibson soil and applied the analysis to a pile in a three-layered soil profile. Lee (1991) proposed solutions for axially loaded piles in finite-layered soil using a discrete layer analysis. In these analyses, only the shear stresses in the equilibrium equation for the soil surrounding the pile were considered (the vertical normal stresses in the soil were neglected).

Randolph and Wroth (1978) using the concept of a "magical radius r_m " (a radius, measured from the pile axis, at which the vertical displacement of soil becomes negligible) proposed an approximate closed-form solution for the settlement of a pile in a Gibson soil (Gibson 1967). Mylonakis (2001) presented solutions accounting for the vertical normal stresses in the equilibrium equation for the soil surrounding the pile. His solutions apply only to an ideal end-bearing pile in a homogeneous elastic soil layer over a rigid base (i.e., settlement at the pile base is taken as zero).

Efforts were made over the last decade to solve the problem of axially loaded piles in multilayered soil with mathematical rigor. Vallabhan and Mustafa (1996) proposed a simple closed-form solution for an axially loaded non-displacement pile installed in a two-layer elastic soil medium based on the principle of minimum total potential energy. Their analyses considered the vertical normal stress and satisfied the radial boundary conditions. Lee and Xiao (1999) expanded the solution of Vallabhan and Mustafa (1996) to multilayered soil and presented semi-analytical solutions. Recently, Seo and Prezzi (2006) provided explicit analytical elastic solutions for a pile in multilayered soil; this analysis is detailed next.

4.1 Mathematical formulation

4.1.1 Problem definition and basic assumptions

We consider a cylindrical pile of length L_p and circular cross section of radius r_p . The pile, which is under an axial load Q_t , is embedded in a total of N horizontal soil layers. The pile itself crosses m layers, while $N - m$ layers exist below the base of the pile. All soil layers extend to infinity in the radial direction, and the bottom (N th) layer extends to infinity downward in

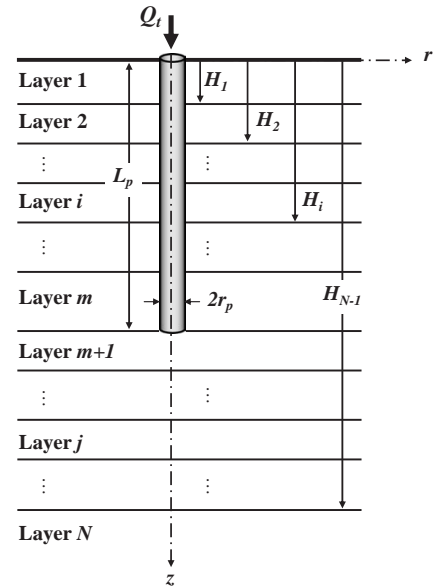


Figure 12. Geometry of the pile-soil system.

the vertical direction. As shown in Figure 12, H_i denotes the depth from the ground surface to the bottom of any layer i , which implies that the thickness of layer i is $H_i - H_{i-1}$ with $H_0 = 0$.

We will refer to the pile cross section at the top of the pile as the pile head and to the pile cross section at the base of the pile as the pile base. Since the problem is axisymmetric, we choose a system of cylindrical coordinates with the origin coinciding with the center of the pile head and the z axis coinciding with the pile axis (z is positive in the downward direction). One of the assumptions in this study is that the pile and the surrounding soil have perfect compatibility of displacements at the pile-soil interface and at the boundaries between soil layers. In other words, it is assumed that there is no slippage or separation between the pile and the surrounding soil and between soil layers. Furthermore, the soil medium within each layer is assumed to be isotropic, homogeneous, and linear elastic. Since radial and tangential strains are very small when compared with the vertical strains, they can be neglected. The vertical displacement at any point in the soil $u_z(r, z)$ is represented as follows:

$$u_z(r, z) = \phi(r)w(z) \quad (17)$$

where $w(z)$ is the vertical displacement of the pile at a depth equal to z , and $\phi(r)$ is the soil displacement dissipation function in the radial direction. The function $\phi(r)$ is a shape function that determines the rate at which the vertical soil displacement decreases in the

radial direction with increasing distance from the pile. Since the vertical displacements within any given cross section of the pile are the same, $\phi(r) = 1$ from $r = 0$ to $r = r_p$. As the vertical soil displacement is zero as r approaches infinity, $\phi(r) = 0$ at $r \rightarrow \infty$.

4.1.2 Governing differential equation

The total potential energy Π of an elastic body is defined as the sum of the internal potential energy (the sum of the strain energy U of the pile and soil) and the external potential energy (equal to minus the work done by the external forces applied to the pile in taking it from the at-rest condition to its configuration under load). The total potential energy of the soil-pile system subjected to an axial force Q_t is given by:

$$\begin{aligned} \Pi = & \frac{1}{2} \int_0^{r_p} E_p A_p \left(\phi \frac{dw}{dz} \right)^2 dz \\ & + \pi \int_0^{r_p} \int_0^{\infty} \left[(\lambda_s + 2G_s) \left(\phi \frac{dw}{dz} \right)^2 + G_s \left(w \frac{d\phi}{dr} \right)^2 \right] r dr dz \quad (18) \\ & + \pi \int_{r_p}^{\infty} \int_0^{\infty} \left[(\lambda_s + 2G_s) \left(\phi \frac{dw}{dz} \right)^2 + G_s \left(w \frac{d\phi}{dr} \right)^2 \right] r dr dz \\ & - Q_t w(0) \end{aligned}$$

where E_p = Young's modulus of the pile; A_p = cross sectional area of the pile; λ_s = Lame's constant of the soil; G_s = shear modulus of the soil.

We can now apply calculus of variations to obtain the equilibrium equations. In order for a stable equilibrium state to be reached, the first variation of the potential energy must be zero ($\delta\Pi = 0$). The governing differential equations for the pile and soil domains follow from imposing this requirement on Eq. (18).

For $0 \leq z \leq L_p$, the following differential equation for the pile displacement in the depth interval associated with any layer i is obtained:

$$-(E_p A_p + 2t_i) \frac{d^2 w_i}{dz^2} + k_i w_i = 0 \quad (19)$$

where,

$$k_i = 2\pi G_{si} \int_{r_p}^{\infty} r \left(\frac{d\phi}{dr} \right)^2 dr \quad (20)$$

$$t_i = \pi(\lambda_{si} + 2G_{si}) \int_{r_p}^{\infty} r \phi^2 dr \quad (21)$$

Since we have m layers in the $0 \leq z \leq L_p$ interval, Eq. (19) is valid for $i = 1 \dots m$. The parameter k_i has units of FL^{-2} (F and L denote force and length, respectively) and represents the shearing resistance of the soil in the vertical direction and hence the change

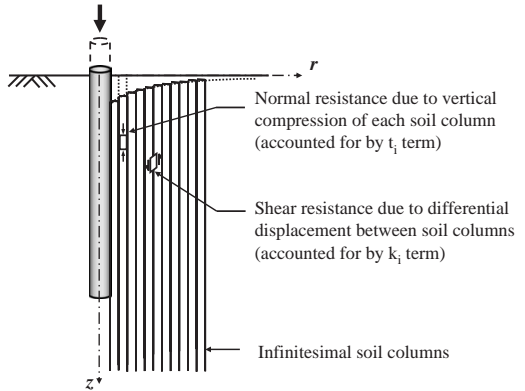


Figure 13. Illustration of two sources of soil resistance.

in shear stress along the radial direction. On the other hand, t_i has units of force and accounts for the soil resistance to vertical compression (Figure 13).

Similarly, we obtain the following differential equation for the soil displacement in layer j beneath the pile ($L_p \leq z \leq \infty$):

$$-\left[\pi r_p^2 (\lambda_{sj} + 2G_{sj}) + 2t_j \right] \frac{d^2 w_j}{dz^2} + k_j w_j = 0 \quad (22)$$

where k_j and t_j are also defined by Eqs. (20) and (21) with j in place of i . Equation (22) is valid for $j = m + 1 \dots N$.

Equations (19) and (22), which were obtained for different domains, can be consolidated into a single governing differential equation. This can be done by noting that $\lambda_{si} + 2G_{si}$ is a function of the Poisson's ratio ν_{si} and the Young's modulus E_{si} of the soil. This leads to:

$$\lambda_{si} + 2G_{si} = \frac{E_{si}(1-\nu_{si})}{(1+\nu_{si})(1-2\nu_{si})} = \bar{E}_{si} \quad (23)$$

where \bar{E}_{si} is the constrained modulus of the soil for a given layer i . Using this notation, we can get the governing differential equation for the pile and soil below it:

$$-(E_i A_i + 2t_i) \frac{d^2 w_i}{dz^2} + k_i w_i = 0 \quad (24)$$

where $E_i = E_p$ and $A_i = A_p$ when $1 \leq i \leq m$; $E_i = \bar{E}_{si}$ and $A_i = \pi r_p^2$ (which coincides with pile cross-sectional area except in the case of a pipe pile) when $m + 1 \leq i \leq N$. This notation for E_i and A_i will be used hereafter unless otherwise stated.

4.1.3 Governing differential equation for the soil surrounding the pile

As done earlier, we obtain the governing differential equation for the soil surrounding the pile by taking the variation of ϕ and then equating these variations to zero:

$$\frac{d^2\phi}{dr^2} + \frac{1}{r} \frac{d\phi}{dr} - \beta^2 \phi = 0 \quad (25)$$

where

$$\beta = \sqrt{\frac{n_s}{m_s}} \quad (26)$$

and m_s and n_s are given by:

$$m_s = \sum_{i=1}^N G_{si} \int_{H_{i-1}}^{H_i} w_i^2 dz \quad (27)$$

$$n_s = \sum_{i=1}^N (\lambda_{si} + 2G_{si}) \int_{H_{i-1}}^{H_i} \left(\frac{dw_i}{dz} \right)^2 dz \quad (28)$$

The parameter m_s has units of FL , and n_s has units of FL^{-1} . Therefore, β has units of L^{-1} , and it determines the rate at which the vertical soil displacement diminishes in the radial direction.

4.2 Solutions of the governing differential equations

4.2.1 Solution for the displacement dissipation function ϕ

Equation (25) is a form of the modified Bessel differential equation, and its general solution is given by:

$$\phi(r) = c_1 I_0(\beta r) + c_2 K_0(\beta r) \quad (29)$$

where $I_0(\cdot)$ is the modified Bessel function of the first kind of zero order and $K_0(\cdot)$ is the modified Bessel function of the second kind of zero order.

As discussed earlier, $\phi(r) = 1$ at $r = r_p$, and $\phi = 0$ at $r \rightarrow \infty$. These boundary conditions lead to:

$$\phi(r) = \frac{K_0(\beta r)}{K_0(\beta r_p)} \quad (30)$$

4.2.2 Solution for the pile displacement function w

The general solution of Eq. (24), which is a second-order linear differential equation, is given by:

$$w_i(z) = B_i e^{\lambda_i z} + C_i e^{-\lambda_i z} \quad (31)$$

where

$$\lambda_i = \sqrt{\frac{k_i}{E_i A_i + 2t_i}} \quad (32)$$

and B_i and C_i are integration constants. We obtain the pile axial strain by differentiating (31) with respect to z . Based on the relationship between the axial strain and force, axial load in the pile at a given cross section is obtained by:

$$Q_i(z) = -a_i B_i e^{\lambda_i z} + a_i C_i e^{-\lambda_i z} \quad (33)$$

where

$$a_i = \lambda_i (E_i A_i + 2t_i) = \sqrt{k_i (E_i A_i + 2t_i)} \quad (34)$$

As we have $2N$ unknown integration constants ($B_1, C_1, B_2, C_2, \dots, B_N, C_N$), we need to identify $2N$ boundary conditions in order to determine their values. First of all, the vertical soil displacement at an infinite depth below the pile base must be zero. Also, the magnitude of the load at the pile head must be equal to the applied external load. Finally, displacement and force should be the same at the interface between any two layers when calculated with the properties of either layer. These give us the $2N$ boundary conditions, and we can determine all the integration constants. These boundary conditions can be expressed as follows:

$$w_N(z)|_{z \rightarrow \infty} = B_N = 0 \quad (35)$$

$$Q_1(z)|_{z=0} = -a_1 B_1 + a_1 C_1 = Q_t \quad (36)$$

$$e^{\lambda_i H_i} B_i + e^{-\lambda_i H_i} C_i - e^{\lambda_{i+1} H_i} B_{i+1} - e^{-\lambda_{i+1} H_i} C_{i+1} = 0 \quad (37)$$

$$-a_i e^{\lambda_i H_i} B_i + a_i e^{-\lambda_i H_i} C_i + a_{i+1} e^{\lambda_{i+1} H_i} B_{i+1} - a_{i+1} e^{-\lambda_{i+1} H_i} C_{i+1} = 0 \quad (38)$$

No matter how many layers we have, Eqs. (35) and (36) always apply and remain unchanged. Please also note that Eqs. (37) and (38) are valid for $1 \leq i \leq N-1$ because we have $N-1$ interfaces between each soil layers. Equations (35) to (38) can be expressed in matrix form as follows:

$$[M][X]=[V] \quad (39)$$

where:

$[M]$ = coefficient matrix consisting of a_i, λ_i, H_i

$[X] = [B_1 \ C_1 \ B_2 \ C_2 \ \dots \ B_{N-1} \ C_{N-1} \ B_N \ C_N]^T$

$[V] = [0 \ Q_t \ 0 \ \dots \ 0 \ 0]^T$

The dimensions of $[M]$, $[X]$, and $[V]$ are $[2N \times 2N]$, $[2N \times 1]$ and $[2N \times 1]$, respectively. If we solve Eq. (39), which can be solved either analytically or numerically, we can determine the integration constants. However, a more efficient way to determine all the integration constants is by finding a recurrence relation based on the boundary conditions. For this purpose, we rewrite Eqs. (31) and (33) in matrix form:

$$\begin{bmatrix} w_i(z) \\ Q_i(z) \end{bmatrix} = \begin{bmatrix} e^{\lambda_i z} & e^{-\lambda_i z} \\ -a_i e^{\lambda_i z} & a_i e^{-\lambda_i z} \end{bmatrix} \begin{bmatrix} B_i \\ C_i \end{bmatrix} \quad (40)$$

From the continuity condition of displacement and force at the interface between layers, we obtain the following:

$$\begin{bmatrix} w_i(H_i) \\ Q_i(H_i) \end{bmatrix} = \begin{bmatrix} w_{i+1}(H_i) \\ Q_{i+1}(H_i) \end{bmatrix} \quad (41)$$

Equations (40) and (41) give us the following recurrence formula for the integration constants:

$$\begin{bmatrix} B_i \\ C_i \end{bmatrix} = \frac{1}{2a_i} \begin{bmatrix} (a_i + a_{i+1})e^{-(\lambda_i H_i - \lambda_{i+1} H_i)} & (a_i - a_{i+1})e^{-(\lambda_i H_i + \lambda_{i+1} H_i)} \\ (a_i - a_{i+1})e^{(\lambda_i H_i + \lambda_{i+1} H_i)} & (a_i + a_{i+1})e^{(\lambda_i H_i - \lambda_{i+1} H_i)} \end{bmatrix} \begin{bmatrix} B_{i+1} \\ C_{i+1} \end{bmatrix} \quad (42)$$

Therefore, if we determine B_N and C_N , we can determine all the B_i and C_i constants in sequence. Using Cramer's rule, B_i and C_i are obtained from:

$$B_i = \frac{|M_{2i-1}|}{|M|} \quad (43)$$

$$C_i = \frac{|M_{2i}|}{|M|} \quad (44)$$

where $|M|$ = determinant of $[M]$; $|M_k|$ = determinant of $[M]$ with the k th column replaced by the vector $[V]$. In order for a given problem to have physical meaning, $|M|$ must not be zero. Therefore, from (35) and (43) we obtain:

$$|M_{2N-1}| = 0 \quad (45)$$

Also, C_N is given by

$$C_N = \frac{|M_{2N}|}{|M|} \quad (46)$$

where the determinant of $|M_{2N}|$ is analytically obtained as:

$$|M_{2N}| = 2^{N-1} Q_t \prod_{i=1}^{N-1} a_i \quad (47)$$

If we substitute Eqs. (43) and (44) into Eq. (42), we get:

$$\begin{bmatrix} |M_{2i-1}| \\ |M_{2i}| \end{bmatrix} = \frac{1}{2a_i} \begin{bmatrix} (a_i + a_{i+1})e^{-(\lambda_i H_i - \lambda_{i+1} H_i)} & (a_i - a_{i+1})e^{-(\lambda_i H_i + \lambda_{i+1} H_i)} \\ (a_i - a_{i+1})e^{(\lambda_i H_i + \lambda_{i+1} H_i)} & (a_i + a_{i+1})e^{(\lambda_i H_i - \lambda_{i+1} H_i)} \end{bmatrix} \begin{bmatrix} |M_{2i+1}| \\ |M_{2i+2}| \end{bmatrix} \quad (48)$$

In order to obtain $|M|$, we will use the boundary condition at the pile head. By substituting $B_1 = |M_1|/|M|$ and $C_1 = |M_2|/|M|$ into Eq. (36), we obtain the following relationship:

$$|M| = \frac{a_1}{Q_t} (|M_2| - |M_1|) \quad (49)$$

Consequently, the numerators in Eqs. (43) and (44) can be recurrently determined from Eq. (48) by using Eqs. (45) and (47) as its ignition terms. The denominators in Eqs. (43) and (44) are obtained from (49). The displacement and force at each layer follow from Eqs. (31) and (33), respectively. Using this procedure, we can obtain explicit analytical solutions for a vertically loaded pile installed in a soil with N layers.

In design, we are interested in estimating the settlement at the pile head when the pile is subjected to the design load. This can be obtained from the solution for the displacement within the first layer:

$$w_t = w_1(0) = B_1 + C_1 = \frac{|M_1|}{|M|} + \frac{|M_2|}{|M|} \quad (50)$$

The explicit analytical solutions presented in this paper offer the advantage that they can be computer-coded easily.

4.3 Solution for a pile embedded in a layered soil resting on a rigid base

Piles are often socketed in a competent layer or rock to obtain a large base capacity. If we know the elastic properties of such a layer, we can use the solution presented in the previous section. We can also obtain analytical solutions for a vertically loaded pile with the base resting on a rigid material that can be used when we do not know the elastic properties of the bearing layer but it is known that it is very stiff. We can do this by restricting the vertical displacement at the base of the pile to zero. The pile-soil system considered here is shown in Figure 14.

In this case, we have zero displacement at the base of the pile instead of at infinity. All other boundary conditions remain the same. Therefore, only Eq. (35) changes to the following:

$$w_N(z) \Big|_{z \rightarrow L_p} = e^{\lambda_N L_p} B_N + e^{-\lambda_N L_p} C_N = 0 \quad (51)$$

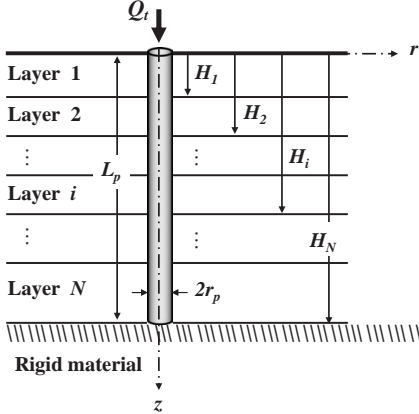


Figure 14. Pile embedded in a multilayered soil with the base resting on a rigid material.

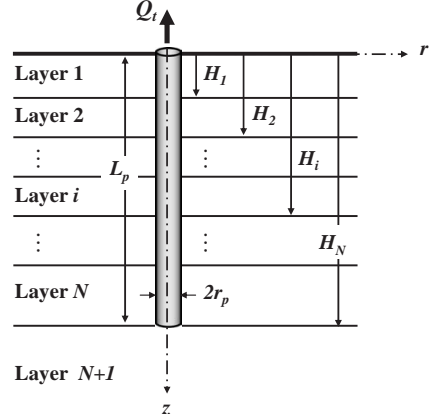


Figure 15. Pile embedded in a multilayered soil under tensile loading.

Now we have a new matrix $[M]$ for the case of an axially loaded pile with the base over a rigid material. As done before, we can calculate $|M_{2N-1}|$ and $|M_{2N}|$:

$$|M_{2N-1}| = -2^{N-1} Q_t e^{-\lambda_N L_p} \prod_{i=1}^{N-1} a_i \quad (52)$$

$$|M_{2N}| = 2^{N-1} Q_t e^{\lambda_N L_p} \prod_{i=1}^{N-1} a_i \quad (53)$$

Using these two ignition terms and (48), we can get explicit analytical solutions for this case.

4.4 Solution for a pile embedded in a layered soil subjected to tensile loading

A limited number of approximate analytical studies are available in the literature on the response of axially loaded piles subjected to tensile loading (Misra et al. 2004, Alawneh 2005). Analytical solutions for an axially loaded pile in a multilayered soil subjected to tensile loading can be easily obtained by changing the pile base boundary condition. The pile-soil system considered here is shown in Figure 15.

In the derivation of the governing differential equations for the pile-soil system within the domain $0 \leq z \leq L_p$, the strain energy from the soil below the pile base is assumed to be negligible (Seo et al. 2006). The governing differential equations remain the same as those derived for the case in which the pile is subjected to a compressive axial load (see equations (19) and (25)).

In the case of tensile loading, the axial load transferred to the base of the pile is zero because the

resistance of the soil below the pile base to tension is negligible, unless we have suction there (in fact, this is obtained as a natural boundary condition following from the minimization of the total potential energy). Instead of Eq. (35), we now have:

$$Q_N(z) \Big|_{z=L_p} = -a_N B_N e^{\lambda_N L_p} + a_N C_N e^{-\lambda_N L_p} = 0 \quad (54)$$

and a new matrix $[M]$. The $|M_{2N-1}|$ and $|M_{2N}|$ matrices are given as follows:

$$|M_{2N-1}| = -2^{N-1} Q_t e^{-\lambda_N L_p} \prod_{i=1}^N a_i \quad (55)$$

$$|M_{2N}| = -2^{N-1} Q_t e^{\lambda_N L_p} \prod_{i=1}^N a_i \quad (56)$$

As done before, using these two ignition terms and (48), we can obtain explicit analytical solutions for this case as well.

4.5 Solution scheme

Since the parameter β appearing in Eq. (30) is not known a priori, an iterative procedure is required to obtain the exact solutions. First, an initial value is assumed for β , and the k_i and t_i values of Eqs. (20) and (21) are calculated. From these values, the pile displacements in each layer are calculated using the appropriate analytical solutions for the problem considered. With the calculated pile displacements in each layer, β is then obtained using Eq. (26) and the resulting value compared with the assumed initial value of β .

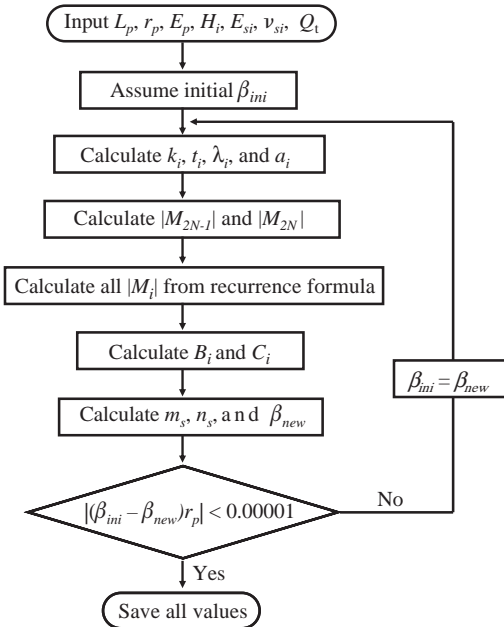


Figure 16. Flowchart for the iterative procedure used to determine the parameter β .

Since β has units of L^{-1} , iterations are repeated until the difference between the values of the dimensionless parameter βr_p obtained from two consecutive iterations falls below the prescribed convergence tolerance. We observed that an exact solution is generally obtained in less than 10 iterations, regardless of the initial value of β assumed. The details of the solution steps are given in the form of a flow chart in Figure 16.

4.6 Case study

We will illustrate how we use these solutions with a case study. Russo (2004) presented a case history on micropiles used for underpinning a historical building in Naples, Italy. The micropiles were installed in a complex soil profile (there are thick layers of man-made materials accumulated over millennia at the site). According to Russo (2004), the installation steps were: (1) drilling of a 200-mm-diameter hole using a continuous flight auger, (2) inserting a steel pipe equipped with injection valves, (3) filling the annular space between the pipe and the soil with grout, (4) grouting the pile shaft through each valve using a double packer, and (5) filling the steel pipe with grout. A micropile (0.2 m in diameter and 19 m in length) was load-tested. Two anchor piles were used to provide reaction to the loading frame, and the compressive load was applied on the test pile with a hydraulic jack.

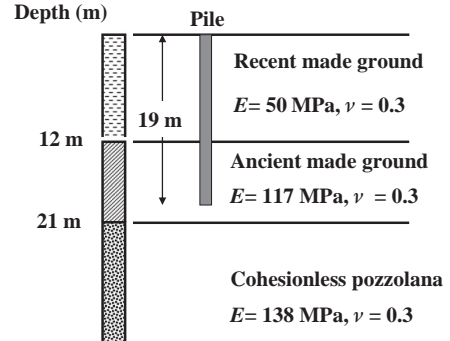


Figure 17. Soil profile and elastic properties of each layer (after Russo 2004).

Table 5. Input values for analysis ($r_p = 0.1 \text{ m}$; $E_p = 27 \text{ GPa}$).

Layer	$H_i \text{ (m)}$	$E_{si} \text{ (MPa)}$	ν_{si}
1	12	50	0.3
2	19	117	0.3
3	21	117	0.3
4	∞	138	0.3

The vertical displacement of the pile head was measured by LVDT's, and the axial strain along the shaft was measured by vibrating-wire strain gages.

Russo (2004) compared the pile load test results with those obtained from finite element analysis. The soil profile and the elastic properties of each soil layer are shown in Figure 17. The Young's moduli of each soil layer were back-calculated from the finite element analysis. The Poisson's ratio was assumed to be 0.3 for all the soil layers. Although Russo (2004) did not provide information on the geometry and properties of the steel pipe left inside the micropile, its outer diameter and inner diameter were assumed to be 33.4 mm and 25.4 mm, respectively. Accordingly, assuming that the Young's moduli of the steel and grout are 200 GPa and 25 GPa, the equivalent Young's modulus of the composite steel-grout cross section is calculated to be approximately 27 GPa.

Table 5 shows the input values used in the analysis. We used four layers with the bottom of the second layer flush with the base of the pile. By following the iterative procedure outlined in Figure 16, we obtained the results summarized in Table 6. All these calculations can be done easily with mathematical software such as MathCAD or MATLAB.

Figure 18 shows measured and calculated load-transfer curves for applied loads equal to 51, 253, and

Table 6. Results of analysis ($Q_t = Q(0) = 542).$

Layer	$w_i(z)$	$Q_i(z)$
1	$-1.239 \times 10^{-5} e^{0.1719z}$ $+3.146 \times 10^{-3} e^{-0.1719z}$	$-2.126 \times 10^3 e^{0.1719z}$ $+5.399 \times 10^5 e^{-0.1719z}$
2	$1.650 \times 10^{-7} e^{0.2399z}$ $+5.327 \times 10^{-3} e^{-0.2399z}$	$4.748 \times 10^1 e^{0.2399z}$ $+1.533 \times 10^6 e^{-0.2399z}$
3	$-2.408 \times 10^{-10} e^{0.4400z}$ $+3.105 \times 10^{-1} e^{-0.4400z}$	$-3.777 \times 10^{-2} e^{0.4400z}$ $+4.871 \times 10^7 e^{-0.4400z}$
4	$2.849 \times 10^{-1} e^{-0.4400z}$	$5.272 \times 10^7 e^{-0.4400z}$

Note: For all layers, $\phi(r) = K_0(0.3344r)/K_0(0.03344)$.

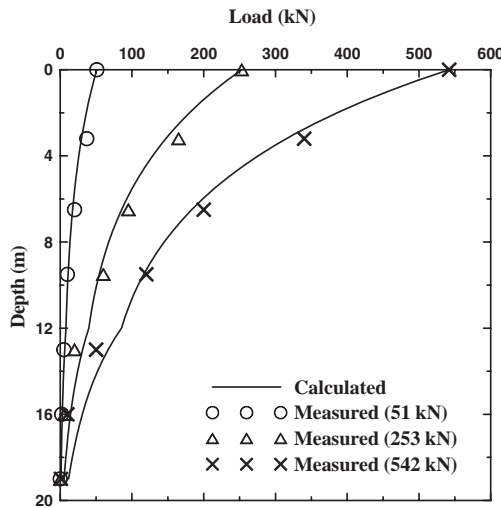


Figure 18. Measured and calculated load-transfer curves for applied loads equal to 51, 253 and 542 kN.

542 kN. Figure 19 shows both the measured load versus settlement curve, and that calculated using the solution presented in this paper. These figures show that there is very good agreement between the calculated and measured values, although the calculated pile head settlement becomes smaller than the measured one for loads greater than about 400 kN.

Figure 20 shows the calculated vertical pile displacement versus depth. The vertical pile displacement decreases exponentially with increasing depth. Figure 21 shows the vertical soil displacement as a function of the radial distance from the pile. Since the present solution satisfies radial boundary conditions, the vertical soil displacement at the level of the pile head becomes negligible at a distance of about 10 m from the pile axis, which corresponds to 50 times the pile diameter.

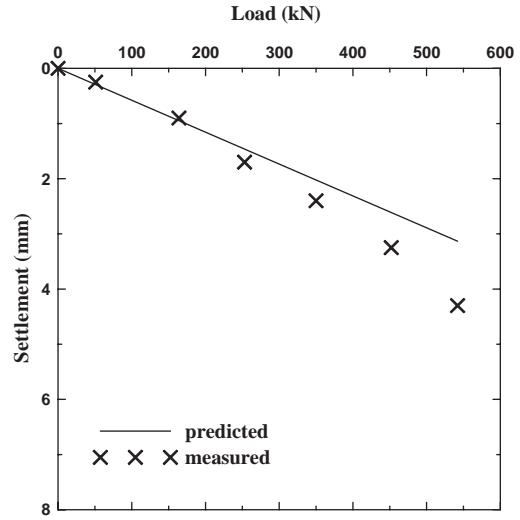


Figure 19. Comparison of the calculated and measured pile head settlement values as a function of the load applied at the head of the pile.

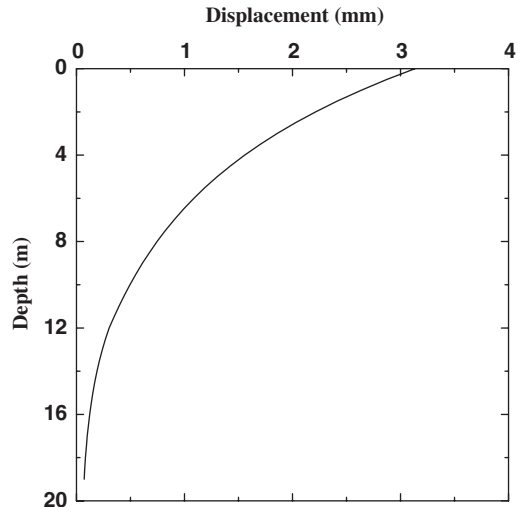


Figure 20. Calculated vertical pile displacement versus depth.

We have reviewed analytical solutions for axially loaded piles under different boundary conditions and its application to a real problem. These solutions were obtained using the same principle with mathematical rigor. These solutions are currently limited to elastic analyses, but research to improve this analysis to account for nonlinearity of the soil behavior is in progress.

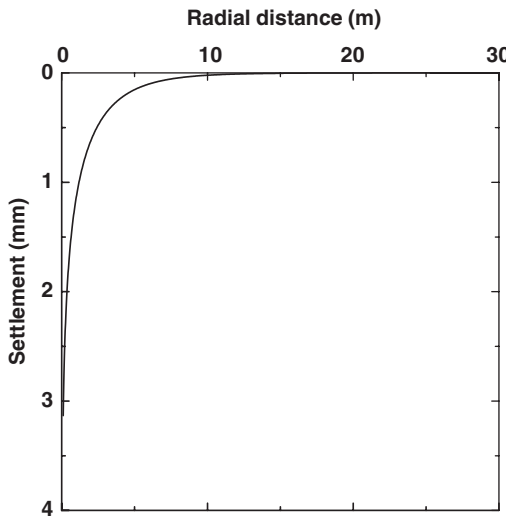


Figure 21. Calculated vertical soil displacement as a function of radial distance from the pile axis at the level of the pile head.

5 CONCLUSIONS

If pile resistance is determined using sound mechanics from a soil model that captures the essence of soil load response without reliance on empiricism or direct correlations, the fundamental basis for rigorous analysis of pile load response is in place. We have shown this to be true for non-displacement piles.

For non-displacement piles installed in sand, the limit base resistance can be calculated with good accuracy using a cavity expansion-based analysis. We have shown using finite element analysis that the ratio of ultimate to limit base resistance is in the 0.13 (for dense sand) to 0.2 (for loose sand) range. The shaft resistance of non-displacement piles in sand is the product of a lateral stress ratio K by the vertical effective stress and the tangent of the critical-state friction angle. We have shown that K lies between just under K_0 for loose sands to about twice K_0 for dense sands.

For non-displacement piles installed in clay, numerical analyses (both finite element and limit analysis) have established accurate bounds on the values of limit unit base resistance. The ratio of net limit unit base resistance to undrained shear strength has been shown convincingly to be in the 10 to 13.5 range. The same ratio for ultimate instead of limit resistance would be less than that; some authors suggest numbers just under 10. The shaft resistance is most frequently calculated using the α method. We have shown that the value of α can be determined analytically if the critical-state and residual friction angles, as well as the relationship between the residual friction angle and

the normal effective stress on the shearing plane, are known. The analysis can also be used to determine α for soils containing clay contents greater than 25%.

In part because of the absence of realistic analysis allowing calculation of settlement given an axial load on the pile, design has relied on calculations of ultimate resistances reduced by factors of safety that would indirectly prevent settlement-based limit states. However, recent work suggests realistic analyses of pile settlement will soon be available, facilitating cost-effective pile design. Explicit analytical solutions for a vertically loaded pile subjected to compressive or tensile loadings and embedded in a multi-layered elastic soil were presented. The solutions satisfy the boundary conditions of the problem. The governing differential equations are derived based on the principle of minimum potential energy and calculus of variations. The integration constants are determined using Cramer's rule and a recurrence formula. The solutions allow calculation of the vertical pile displacement as a function of depth, the load transferred to the pile shaft at any depth, and the vertical soil displacement as a function of the radial direction at any depth if the following is known: radius, length and Young's modulus of the pile, Poisson's ratio and Young's modulus of the soil in each layer, thickness of each soil layer, number of soil layers, and applied load. The use of the analysis was illustrated by obtaining load-transfer and load-settlement curves for a case discussed in the literature for which pile load test results are available.

REFERENCES

- Abbo, A. J. & Sloan, S. W. 2000. SNAC, User manual, Version 2.0. Dept. of Civil, Surveying and Environmental Engrg., University of Newcastle, Callaghan, Australia.
- Alawneh, A. S. 2005. "Modelling load-displacement response of driven piles in cohesionless soils under tensile loading" Computers and Geotechnics, 32(8), 578–586.
- Atkinson, J. 1993. An introduction to the mechanics of soils and foundations through critical state soil mechanics. McGraw Hill publications.
- Bishop, A. W. 1971. Shear strength parameters for undisturbed and remolded soil specimens. Stress-strain behaviour of soils. Roscoe Memorial Symposium: 3–58. Henley: Foulis.
- Butterfield, R. and Banerjee, P. K. 1971. The elastic analysis of compressible piles and pile groups. Geotechnique, 21(1): 43–60.
- Carraro, J. A., Bandini, P. and Salgado, R. 2003. Evaluation of Liquefaction Resistance of Clean and Silty Sands Based on CPT Cone Penetration Resistance. J. of Geotech. and Geoenv. Engineering, ASCE, 129(12): 965–976.
- Dafalias, Y. F. & Manzari, M. T. 2004. Simple Plasticity Sand Model Accounting for Fabric Change Effects. Journal of Engineering Mechanics, ASCE, 130(6): 622–634.
- Finno, R. J. 1989. Surface Conditions and Pile Installation Data. Proc. Pile Prediction Symposium, ASCE, Foundation

- Engineering Congress, Northwestern University, Evanston, IL, R.J. Finno (Ed.): 1–74.
- Finno, R. J., Cosmao, T. and Gitskin, B. 1989. Results of Foundation Engineering Congress Pile Load Tests. Proc. Pile Prediction Symposium, ASCE, Foundation Engineering Congress, Northwestern University, Evanston, IL, R. J. Finno (Ed.): 338–355.
- Franke, E. 1993. Design of Bored Piles, Including Negative Skin Friction and Horizontal Loading. Deep Foundations on Bored and Auger Piles (Van Impe, ed.), Balkema, Rotterdam.
- Gens, A. and Potts, D. M. 1984. Formulation of Quasi-Axisymmetric Boundary Value Problems for Finite Element Analysis. *Engineering Computations*, 1(2), 144–150.
- Ghionna, V. N., Jamiolkowski, M., Pedroni, S. and Salgado, R. 1994. The Tip Displacement of Drilled Shafts in Sands. Proc. of Settlement '94 (Yeung and Félio, eds.), Vol. 2, Geotechnical Engineering Division, ASCE, June: 1039–1057.
- Gibson, R. E. 1967. Some results concerning displacements and stresses in a non-homogeneous elastic half-space. *Geotechnique*, 17(1): 58–67.
- Houlsby, G. T. and Hitchman, R. 1988. Calibration Chamber Tests of a Cone Penetrometer in Sand. *Geotechnique* 38(1), 39–44.
- Hu, Y. and Randolph, M. F. 2002. Bearing Capacity of Caisson Foundations on Normally Consolidated Clay. *Soils and Foundations*, 42(5): 71–77.
- Hu, Y., Randolph, M. F. and Watson, P. G. 1999. Bearing Capacity of Skirted Foundations on Non-Homogeneous Soil. *J. of Geotech. and Geoenv. Engineering*, ASCE, 125(11): 924–935.
- Jamiolkowski, M. and Lancellotta, R. 1988. Relevance of In-situ Test Results for Evaluation of Allowable Base Resistance of Bored Piles in Sands. In: Van Impe(ed), Deep Foundations on Bored and Auger Piles: 107–119. Rotterdam: Balkema.
- Kenney, T. C. 1967. The Influence of Mineralogical Composition on the Residual Strength of Natural Soils. Proc. Oslo Geotech. ConJ on the Shear Strength Prop. of Natural Soils and Rocks, Vol. 1: 124–129.
- Lee, C.Y. 1991. Discrete layer analysis of axially loaded piles and pile groups. *Computers and Geotechnics*, 11(4): 295–313.
- Lee, J. and Salgado, R. 1999. Determination of Pile Base Resistance in Sands. *J. of Geotech. and Geoenv. Engineering*, ASCE, 125(8): 673–683.
- Lee, K-M. and Xiao, Z. R. 1999. A new analytical model for settlement analysis of a single pile in multi-layered soil. *Soils and Foundations*, 39(5): 131–143.
- Maksimovic, M. 1989. On the Residual Shearing Strength of Clays. *Geotechnique*, 39(2): 347–351.
- Martin, C. M. 2001. Vertical Bearing Capacity of Skirted Circular Foundations on Tresca Soil. Proc. 15th Int. Conf. on Soil Mechanics and Geotechnical Engineering, Istanbul, Vol. 1: 743–746.
- Mayne, P. W., and Harris, D. E. 1993. Axial Load-Displacement Behavior of Drilled Shaft Foundation in Piedmont Residuum. Tech. Rep. No. 41-30-2175, Federal Highway Administration, Washington, D.C.
- Meyerhof, G. G. 1951. The Ultimate Bearing Capacity of Foundations. *Geotechnique*, 2(4): 301–332.
- Meyerhof, G. G. 1963. Some Recent Research on the Bearing Capacity of Foundations. *Canadian Geotech. J.*, 1: 16–26.
- Mindlin, R. D. 1936. Force at a point in the interior of a semi-infinite solid. *Physics*, 7: 195–202.
- Misra, A., Chen, C. H., Oberoi, R., and Kleiber, A. 2004. Simplified analysis method for micropile pullout behavior. *J. of Geotech. and Geoenv. Engineering*, ASCE, 130(10): 1024–1033.
- Mylonakis, G. 2001. Winkler modulus for axially loaded piles. *Geotechnique*, 51(5): 455–461.
- Nemat-Nasser, S. & Okada, N. 2001. Radiographic and microscopic observations of shear bands in granular materials. *Geotechnique*, 51(9): 753–765.
- Papadimitriou, A. G. & Bouckovalas, G. D. 2002. Plasticity model for sand under small and large cyclic strains: a multiaxial formulation. *Soil Dynamics and Earthquake Engineering*, 22(3): 191–204.
- Poulos, H. G. 1979. Settlement of single piles in non-homogeneous soil. *Journal of Geotechnical Engineering Division*, 105(5): 627–641.
- Poulos, H. G. and Davis, E. H. 1968. The settlement behavior of single axially loaded incompressible piles and piers. *Geotechnique*, 18(3): 351–371.
- Promboon, S. and Brenner, R.P. 1981. Large Diameter Bored Piles in Bangkok Clay. *Proc. Intern. Conf. Soil Mechs. Found. Engrg.*, Vol. 2: 815–818.
- Randolph, M. F., Jamiolkowski, M. B. and Zdravkovic, L. 2004. Load Carrying Capacity of Foundations. Advances in Geotechnical Engineering – Proc. The Skempton Conference, London, 2004. (Eds.: Jardine, R. J., Potts D. M. & Higgins K. G.). Thomas Telford, London, Vol. 1: 207–240.
- Randolph, M. F., and Wroth, C. P. 1978. Analysis of vertical deformation of vertically loaded piles. *Journal of Geotechnical Engineering Division*, 104(12): 1465–1488.
- Reddy, E. S., Chapman, D. N. and Sastry, V. V. R. N. 2000. Direct Shear Interface Test for Shaft Capacity of Piles in Sand. *Geotechnical Testing Journal*, 23(3): 199–205.
- Reese, L. C. and O'Neill, M.W. 1988. Drilled Shafts: Construction and Design. FHWA Report No. HI-88-042.
- Reese, L. C., Touma, F. J. and O'Neill, M. W. 1976. Behavior of Drilled Piers under Axial Loading. *J. of the Geotech. Engrg. Division*, ASCE, 102(5): 493–510.
- Russo, G. 2004. Full-scale load test on instrumented micropiles. *Proc. of the Institution of Civil Engineers: Geotechnical Engineering*, 157(3): 127–135.
- Salgado, R. 1995. Design of Piles in Sands Based on CPT Results. Proc. 10th Pan-American Conference on Soil Mechanics and Foundation Engineering, Vol. 3: 1261–1274: Guadalajara.
- Salgado, R. and Prezzi, M. 2005. Computation of Cavity Expansion Pressure and Cone Resistance in Sand. *International Journal of Geomechanics*, submitted.
- Salgado, R. and Randolph, M. F. 2001. Analysis of Cavity Expansion in Sand. *International Journal of Geomechanics*, 1(2): 175–192.
- Salgado, R., Bandini, P. and Karim, A. 2000. Shear Strength and Stiffness of Silty Sands. *J. of Geotech. and Geoenv. Engineering*, ASCE, 126(5): 451–462.
- Salgado, R., Mitchell, J. K. and Jamiolkowski, M. 1997. Cavity Expansion and Penetration Resistance in Sand.

- J. of Geotech. and Geoenv. Engineering, ASCE, 123(4): 344–354.
- Salgado, R., Lyamin, A., Sloan, S. and Yu, H.S. 2004. Two- and Three-dimensional Bearing Capacity of Footings in Clay. *Geotechnique* 54(5): 297–306.
- Schmertmann, J.H. 1975. Measurement of In-Situ Shear Strength. Proc. of the ASCE Spec. Conf. on In-Situ Measurements of Soil Properties, Raleigh, Vol.2: 57–138.
- Seo, H., Kim, D., Salgado, R., and Prezzi, M. 2006. Elastic analysis of pile loaded in axial tension in multilayered soil. Internal Geot. Report. No. 2006-01, Purdue University.
- Seo, H. and Prezzi, M. 2006. Analytical solutions for a vertically loaded pile in multilayered soil. *Geomechanics and Geoengineering: An International Journal*, in print.
- Simonini, P. 1996. Analysis of behavior of sand surrounding pile tips. *J. Geotech. Engrg., ASCE*, 122(11): 897–905.
- Skempton, A. W. 1985. Residual Strength of Clays in Landslides, Folded Strata and the Laboratory. *Geotechnique*, 35(1): 3–18.
- Skempton, A.W. 1951. The Bearing Capacity of Clays. Building Research Congress, 1: 180–189.
- Skempton, A.W. 1957. The Planning and Design of New Hong Kong Airport. Proc. ICE, London, 7: 305–307.
- Skempton, A.W. 1959. Cast in Situ Bored Piles in London Clay. *Geotechnique* 9: 153–173.
- Tabucanon, J. T., Airey, D. W. & Poulos, H. G. 1995. Pile Skin Friction in Sands from Constant Normal Stiffness Tests. *Geotechnical Testing Journal*, 18(3): 350–364.
- Teixeira, C. Z., & Albiero, J. H. 1994. A Evolução da Reação de Ponta de Estacas Escavadas Submetidas a Successivas Provas de Carga. Proc., 10th Brazilian Conf. Soil Mech. Found. Engrg., Foz Do Iguacu, Vol. 1: 3–9.
- Uesugi, M., Kishida, H. & Tsubakihira, Y 1988. Behavior of Sand Particles in Sand-Steel Friction. *Soils and Foundations*, 28(1): 107–118.
- Uesugi, M., Kishida, H. & Uchikawa, Y. 1990. Friction between Dry Sand and Concrete under Monotonic and Repeated Loading. *Soils and Foundations*, 30(1): 115–128.
- Vallabhan, C. V. G. & Mustafa, G. 1996. A new model for the analysis of settlement of drilled piers. *International Journal for Numerical and Analytical Methods in Geomechanics*, 20: 143–152.
- Vardoulakis, I. & Sulem, J. 1995. Bifurcation Analysis in Geomechanics: Blackie Academic and Professional.
- Yu, H. S., Herrmann, L. R. & Boulanger, R.W. 2000. Analysis of steady cone penetration in clay. *J. of Geotech. and Geoenv. Engineering, ASCE*, 126(7): 594–605.

CPT-based design of displacement piles in siliceous sands

B.M. Lehane, J.A. Schneider & X. Xu

The University of Western Australia, Perth, Western Australia, Australia

ABSTRACT: This paper provides recommendations for the assessment of the shaft and base capacity of driven and jacked (or ‘pressed-in’) displacement piles in siliceous sand using CPT data. The recommendations related to open and closed-ended driven piles are those proposed by the UWA-05 method and the rationale behind adoption of the selected formulations for this method is provided. The paper also provides guidance on the assessment of the base stiffness of piles in sand.

1 INTRODUCTION

Design correlations linking the capacity of a displacement pile with the Cone Penetration Test (CPT) tip end resistance (q_c) have been in popular use in Europe for over 50 years and are finding increased application worldwide. However, the form of these correlations varies widely, as illustrated by De Cock et al. (2003), primarily because the factors controlling axial pile capacity are influenced by more soil parameters than those affecting CPT q_c . For example, the similarity between the mode of installation of a cone and pile suggests a strong link between the CPT q_c value and the pile end-bearing. However, the relationship

between shaft friction and q_c is less obvious, and even less so, if the displacement pile is open-ended and penetrates the soil in a coring mode.

A database of static load tests in siliceous sands was employed by Schneider et al. (2007) to examine prediction differences between two popular CPT axial pile design methods, LCPC-82 (Bustamante & Gianeselli 1982) and EF-97 (Eslami & Fellenius 1997). Figure 1 plots ratios of calculated to measured capacities (Q_c/Q_m) and illustrates that these methods may, at best, be expected to predict capacity to within a factor of 2. It is also evident that the two methods tend to over-predict the capacity of open ended piles in compression and tension (OEC & OET). Both

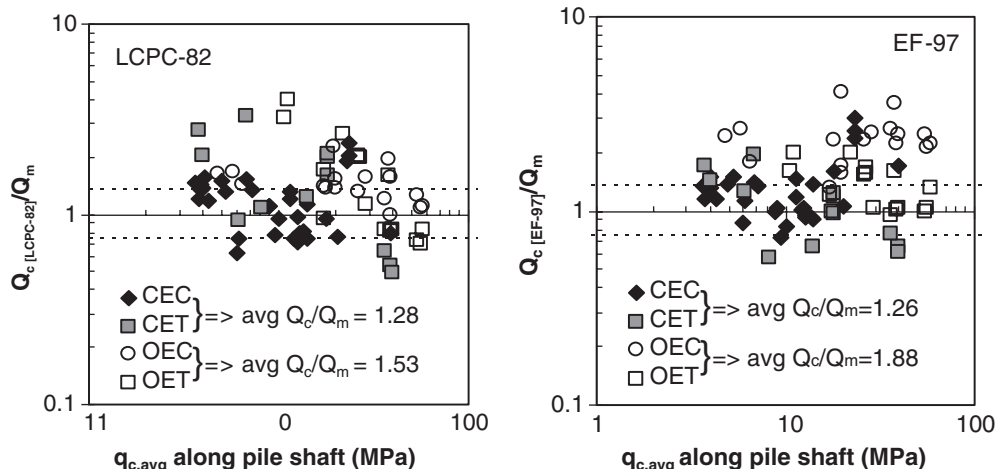


Figure 1. Bias in conventional CPT-based pile design methods, Lehane et al. (2007).

Notation: CEC & CET: Closed ended piles in compression and tension, OEC & OET: Open-ended piles in compression and tension

methods were developed mainly for onshore closed-ended piles and do not make separate recommendations for open ended piles. This shortcoming, in addition to the clear need to improve predictive performance, prompted the development of new CPT-based methods.

Four recently proposed methods were included in the commentary of the 22nd edition of American Petroleum Institute (API) RP2A, Recommended Practice for Fixed Offshore Structures (API 2006). These methods are referred to as *Fugro-05* (Kolk et al. 2005), *ICP-05* (Jardine et al. 2005), *NGI-05* (Clausen et al. 2005) and *UWA-05* (Lehane et al. 2005b). *UWA-05* evolved following a review by the authors of the API RP2A main text method of the 21st edition (API 00) and the three other CPT-based design methods.

Schneider et al. (2007) show that *Fugro-05*, *ICP-05* and *NGI-05* have a broadly similar predictive performance for a newly compiled database of static load tests and are a reasonable improvement on *LCPC-82* and *EF-97*. This similarity is believed to be fortuitous given the significant differences between the formulations adopted for pile end bearing and shaft resistance. While *UWA-05* is shown to predict the capacity of the database piles to an improved level of accuracy (Schneider et al. 2007), this improvement does not provide definitive proof that the method should be used in preference to the any of the other three. It is therefore one aim of this paper to provide the rationale behind the formulations adopted in *UWA-05* and to illustrate that these are a better reflection of the physical mechanisms governing driven pile behaviour in sand. Given the growth and significant promise offered by jacked/pressed-in piles, a second aim of this paper is to provide guidelines for these pile types using the same approach adopted for derivation of the formulations for driven piles.

2 SHAFT FRICTION

Shaft capacity of deep foundations (Q_s) is calculated using the pile geometry and distribution of local shaft friction (τ_f) along the pile shaft, as follows:

$$Q_s = \pi D \int \tau_f dh \quad (1)$$

where D is the pile diameter (πD is the pile perimeter) and h is the height above the pile tip. Assuming a Coulomb failure criterion, local shaft friction is the product of the radial stress at failure (σ'_{rf}) and the interface friction coefficient ($\tan \delta_{cv}$) (Lehane et al. 1993).

$$\tau_f = \sigma'_{rf} \tan \delta_{cv} = \frac{f}{f_c} (\sigma'_{rc} + \Delta \sigma'_{rd}) \tan \delta_{cv} \quad (2)$$

The radial stress at failure is the sum of the radial stress after installation and equalization (σ'_{rc}) and the change in radial stress during pile loading ($\Delta \sigma'_{rd}$). A reduction

in radial stress will occur in tension loading due to a reversal in the loading direction between installation and loading, and also due to a Poisson effect. This difference is simply accounted for in Equation 2 using the f/f_c parameter, which is unity in compression and approximately 0.75 in tension for typical onshore piles.

It is common practice to correlate the average pile shaft friction ($\tau_{f,avg}$) with the average in situ test penetration resistance. For granular soils, Meyerhof (1956) recommended:

$$\frac{\tau_{f,avg}}{p_{ref}} = \frac{N_{avg}}{\alpha_{s,SPT}} \approx \frac{N_{avg}}{50} \quad (3a)$$

$$\tau_{f,avg} = \frac{q_{c,avg}}{\alpha_{s,CPT}} \approx \frac{q_{c,avg}}{200} \quad (3b)$$

where N_{avg} is the average Standard Penetration Test (SPT) N-value, $q_{c,avg}$ is the average CPT cone tip resistance along pile shaft and p_{ref} is a reference stress taken in the above as 100 kPa. When comparing CPT to SPT data, the CPT provides superior vertical stratigraphic profiling as well as measurement repeatability. As a consequence, correlations between $\tau_{f,avg}$ and $q_{c,avg}$ tend to show better reliability than SPT correlations (i.e. Braud & Tucker 1988). However, the reliability of these correlations, as discussed above, is relatively poor, prompting the recent research on factors affecting $\alpha_{s,CPT}$.

The field tests conducted with the Imperial College Model Pile (ICP) is one example of this recent research. Figure 2 shows profiles of average cone tip

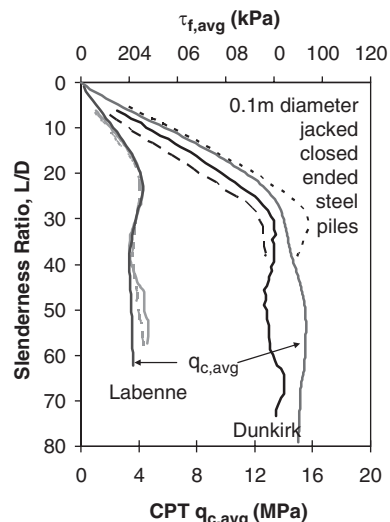


Figure 2. Comparison of average pile shaft friction with average cone tip resistance for Imperial College Model Pile tests in medium dense and dense sands.

resistance and average shaft friction measured during jacking of the ICP at medium dense (Labenne; Lehane et al. 1993) and dense (Dunkirk; Chow 1997) siliceous sand sites. It is evident that:

- $\tau_{f,\text{avg}}$ tends to reach a relatively constant value after 20 to 30 diameters of penetration.
- $\tau_{f,\text{avg}}$ and $q_{c,\text{avg}}$ at Dunkirk are approximately 3 to 4 times higher than at Labenne.
- $\tau_{f,\text{avg}}$ mirrors $q_{c,\text{avg}}$ well at both sites, with $\alpha_{s,\text{CPT}} \sim 170$.

The tendency for the average shaft friction to reach a constant value was discussed by Vesic (1967) based on the results of small diameter driven model piles, and was incorporated into offshore pile design practice using the concept of limiting shaft friction (McClelland et al. 1969). This concept implies that local shaft friction remains constant below a critical depth, which is in marked contrast to observed trend for highest stresses to be recorded closest to pile tip. For example, Figure 3 shows the distribution of local shaft friction recorded during jacked installation of the ICP at the Labenne site. The reduction in local shaft friction with continued pile penetration (or increasing h/D value) is in clear evidence. This phenomenon, which is often referred to as ‘friction fatigue’, is now an accepted characteristic feature of displacement pile design (Randolph 2003) and is one of a number of reasons why $\alpha_{s,\text{CPT}}$ cannot be expected to have a constant value.

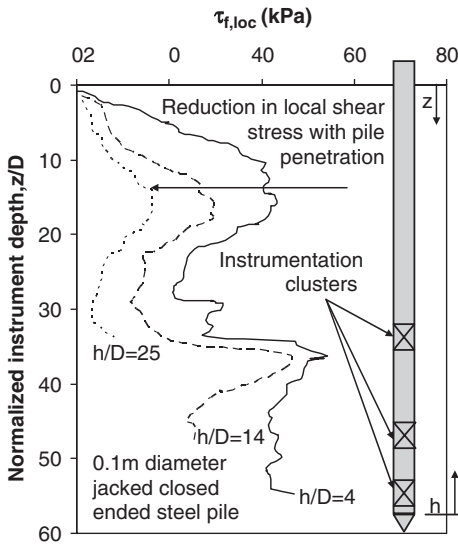


Figure 3. Reduction in local friction with continued pile penetration during pile installation at Labenne (after Lehane et al. 1993).

2.1 Radial stress near the pile tip after installation and equalization

Displacement piles are generally considered to have larger shaft friction values than an equivalent bored pile in siliceous sand due to the increase in radial stress that occurs as the sand is displaced during pile installation. This increase in radial stress may be expected to correlate with the CPT q_c value, which is itself a measure of the lateral stress acting on a pile/penetrometer at $h/D \sim 0$. As insignificant levels of excess pore pressure are typically generated during displacement pile installation (and cone penetration testing) in siliceous sands, the equalized radial stress in the area close to the pile tip may be presumed to be directly proportional to q_c (where a is a constant):

$$\sigma'_{rc} = \frac{q_c}{a} \quad (4)$$

Considering that open-ended pipe piles tend to displace lower relative volumes of soil than closed-ended piles or penetrometers, it is expected that radial stresses developed on the shaft of open ended piles would also be lower. Simply separating piles into ‘open’ or ‘closed’ ended does not adequately capture the potential range of conditions that occur during installation, as open ended piles often exhibit partial plugging during installation. The plugging response is best quantified using the incremental filling ratio (IFR), defined as:

$$\text{IFR} = \frac{\Delta h_{\text{plug}}}{\Delta h_{\text{pile}}} \quad (5)$$

where Δh_{plug} is the incremental change in plug height and Δh_{pile} is the incremental change in pile tip depth. In the absence of detailed IFR data, the plug length ratio (PLR), which is equal to the final plug length divided by the embedded pile length, provides a rough indication of plugging behaviour during installation. The PLR does not correlate well with IFR in layered deposits (Lehane & Gavin 2004).

Figure 4 indicates that PLR tends to increase with diameter for driven piles. There is obviously much scatter in this trend as plugging during installation of driven piles is also strongly influenced by soil layering, plug compression, and plug inertia. Plug inertia leads to significantly different plugging behaviour during installation of jacked and driven piles. While larger diameter driven piles generally penetrate the sand deposit in a fully coring mode, jacked open ended piles tend to plug at an embedment of 5 to 15 diameters (e.g. see Gavin & Lehane 2003a).

Since the increase in radial stress during installation of a displacement pile is controlled by the relative level of soil displaced, it is expected that shaft friction

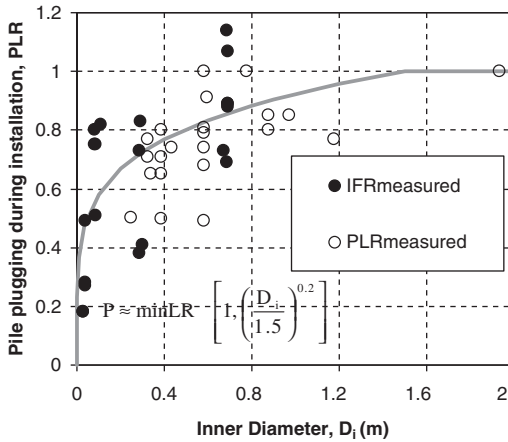


Figure 4. Influence of inner diameter on plugging of driven piles during installation.

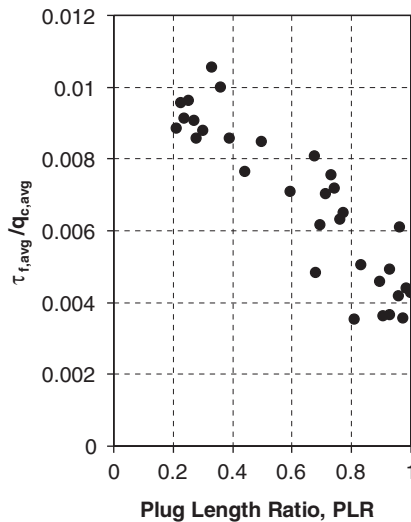


Figure 5. Average normalized ultimate external shear stresses, $\tau_{f,\text{avg}}/q_{c,\text{avg}}$, plotted against corresponding PLR for instrumented double wall piles of Gavin & Lehane (2003b).

reduces as IFR increases. This trend has been observed in calibration chamber tests reported by Gavin & Lehane (2003b), as illustrated in Figure 5, as well as for full scale piles (Paik et al. 2003).

Analytical studies using a cavity expansion analogy (White et al. 2005) showed that the increase in radial stress due to displacement pile installation should be proportional to the relative volume of soil displaced,

which is quantified using the effective area ratio, $A_{rs,\text{eff}}$, i.e.

$$\frac{\sigma_{r,\text{open}}}{\sigma_{r,\text{closed}}} = A_{rs,\text{eff}}^b \quad (6a)$$

where

$$A_{rs,\text{eff}} = 1 - \text{IFR} \times \left(\frac{D_i}{D} \right)^2 \quad (6b)$$

Combining equations (4) and (6a), the following relationship describes the radial effective stress close to the tip of an open or closed ended pile:

$$\sigma'_{rc} = \frac{q_c A_{rs,\text{eff}}^b}{a} \quad (7)$$

Cylindrical cavity expansion theory suggests that the exponent, b , varies from 0.3 to 0.4 for typical sand friction angles.

2.2 Friction fatigue

The reduction in local friction with continued pile penetration i.e. ‘friction fatigue’ has been illustrated in Figure 3. To quantify this effect in design methods for piles in sand, Lehane & Jardine (1994) proposed that σ'_{rc} for jacked piles varies in proportion to $(h/D)^{-0.33}$ (where $h = z_{\text{tip}} - z$, and z_{tip} is the pile tip depth). Friction fatigue in UWA-05 is accounted for by modifying Equation 7 as follows:

$$\sigma'_{rc} = \frac{q_c A_{rs,\text{eff}}^b}{a} \max\left(\frac{h}{D}, v\right)^c \quad (8)$$

where the exponent ‘ c ’ is negative and the constant v prevents the power-law format from reaching excessively high values near the pile tip. The normalisation of the relative height above the pile tip (h) by the pile diameter (D) is presently somewhat arbitrary as no systematic study of the effect of pile diameter on friction fatigue has been performed. The normalisation is adopted by UWA-05 on the basis of the following observations:

- The rate of radial stress and τ_f reduction with h depends largely on the magnitude and type of cycles imposed by the installation method. White & Lehane (2004) show that the rate of decay is stronger for piles experiencing hard driving and much lower for jacked piles, which are typically installed with a relatively low number of (one-way) installation cycles. The absolute value of c for driven piles may therefore be expected to be larger than the value of 0.33 deduced from the ICP tests on jacked piles.

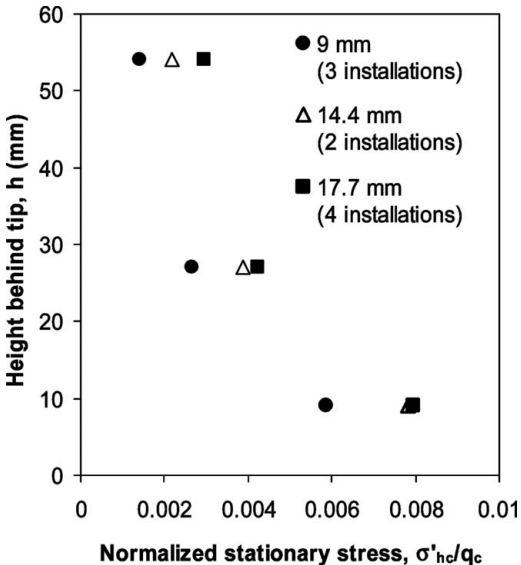


Figure 6. Variation of normalized stationary lateral stress with height above pile tip following monotonic installation (Schneider & Lehane 2006).

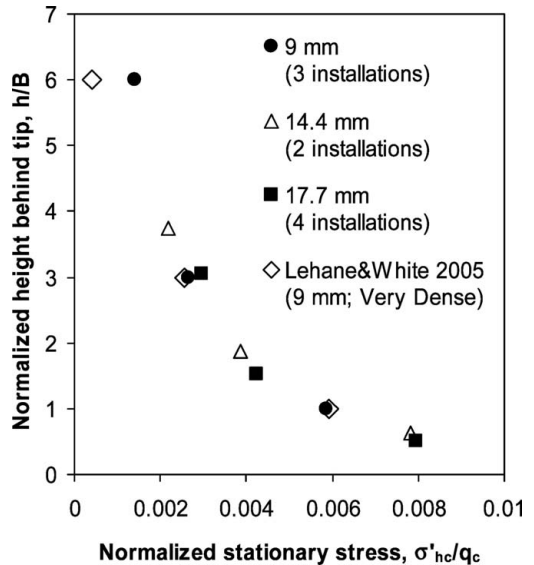


Figure 7. Normalized stationary lateral stress with normalized height above pile tip following monotonic installation (Schneider & Lehane 2006).

- The tendency for hammer selection to be such that the number of hammer blows is broadly proportional to the pile slenderness ratio (L/D), suggests that σ'_{rc} may be tentatively considered a function of h/D .
- White & Lehane (2004) also show that the rate of degradation of σ'_{rc} with h is greater at higher levels of radial stiffness ($4G/D$) and therefore σ'_{rc} at a fixed h value (i.e. after a specific number of installation cycles) reduces with D in a sand having the same operational shear modulus (G).
- Field measurements, such as those described in Lehane et al (2005a), are compatible with the occurrence of a ‘critical depth’ where average shaft friction in uniform soil deposits becomes relatively constant with continued pile penetration beyond a fixed multiple of pile diameters (as defined by Vesic 1967).

A controlled study was performed in the UWA drum centrifuge to evaluate the influence of pile width on the normalized radial stress after monotonic (i.e. one cycle) installation and equalization of jacked piles (Schneider & Lehane 2006). The (square section) piles had side widths (B) of 9 mm, 14.4 mm and 17.7 mm were instrumented with lateral stress cells at various heights above the pile tip. Figure 6 illustrates that, at an equivalent height behind the pile tip (h), wider piles tend to have higher stationary horizontal stress (σ'_{hc}) normalized by q_c . However, as shown on Figure 7, a unique variation of σ'_{hc}/q_c with h/B is observed - supporting the format of Equation 8.

2.3 Interface friction angle

Friction coefficients ($\mu = \tan\delta$) increase with the roughness of construction materials (i.e., Potyondy 1961). Uesugi & Kishida (1986a, 1986b) performed shear tests between sands and steel interfaces, and observed that the coefficient of friction correlates strongly with the average roughness (R_a) normalized to the median particle size (D_{50}); this ratio is referred to as the normalized roughness (R_n). These trends have been verified by additional studies into interface shear behaviour (i.e., Jardine et al. 1993, Tabucanon 1997, Dietz 2000, Frost et al. 2002).

Measurements obtained in laboratory interface shear testing are summarized in Figure 8. These indicate:

- Above a critical normalized roughness (typically between 0.05 and 0.3), shear failure occurs within the soil itself and δ is independent of the properties of the interface.
- As for soil-soil shearing, peak interface friction angles are generated and these depend on soil density and stress level. After continued shearing, interface friction angles reduce to a constant volume/critical state values (δ_{cv}) that are independent of stress level and density.
- At a relatively constant average roughness, such as 10 μm for lightly rusted steel piles, the interface friction angle tends to reduce with increasing median particle size. Increasing particle size is analogous to decreasing normalized roughness.

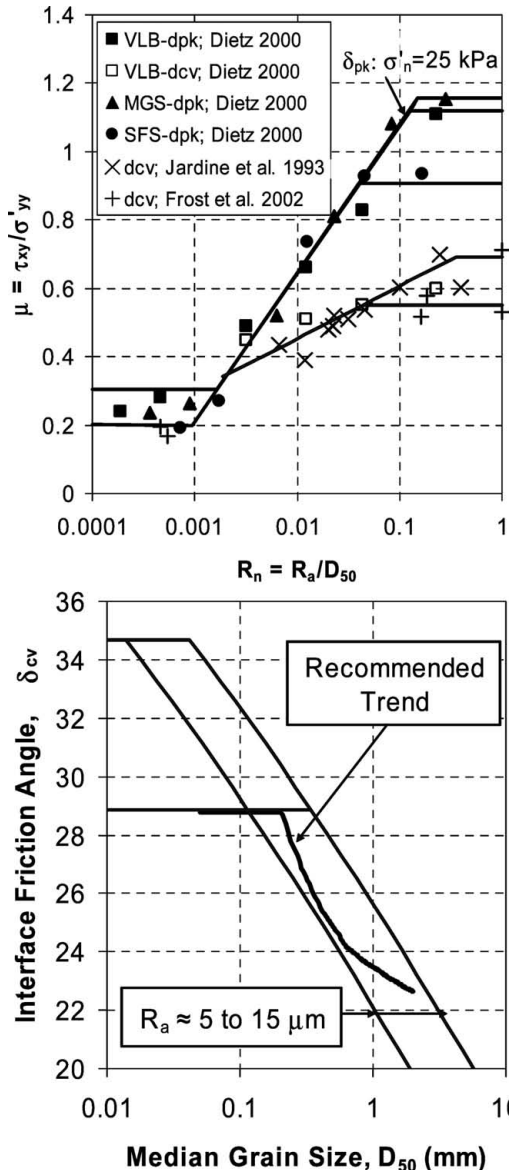


Figure 8. Influence of median grain size (D_{50}) and normalized roughness (R_n) on interface friction angle (δ_{cv}).

Lehane et al. (1993) and Chow (1997) have shown that δ_f varies in proportion to $\tan\delta_{cv}$. Figure 8 shows that δ_{cv} value, which should be measured routinely, increases as the normalised roughness, $R_n = R_a/d_{50}$, increases.

2.4 Changes in radial stress during loading

Changes in radial stress during loading of a pile can arise due to a Poisson effect as well and due to dilation

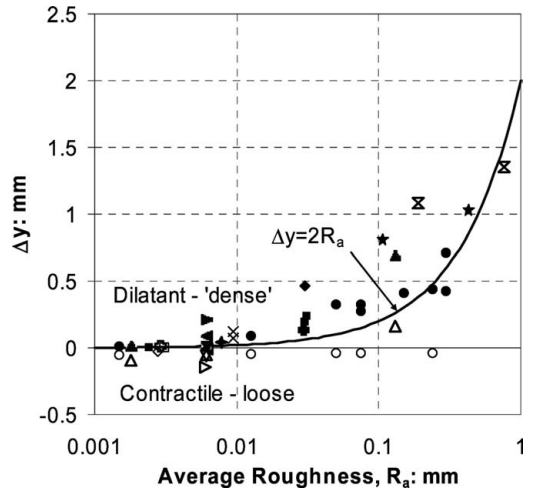


Figure 9. Relationship between average interface roughness and the normal sand displacement after dilation has ceased.

of the soil at the interface during shear. The magnitude of the changes in radial stress may be estimated using the cavity expansion analogy as:

$$\Delta\sigma'_{rd} = 4G \frac{\Delta y}{D} \quad (9)$$

where Δy is the dilation (= radial displacement) of the sand at the pile interface and G is the operational shear modulus of the sand surrounding the pile shaft, which reduces as $\Delta y/D$ increases.

Some insights into the likely value of Δy may be obtained from interface shear tests. Figure 8 indicates that the difference between the peak and constant volume friction angle increases with normalized roughness. This implies that the maximum dilation angle (ψ_{pk}) and the maximum Δy value are also a function of R_n . Figure 9 compares these maximum Δy values against the average roughness (R_a), while Figure 10 presents the same data but with both these parameters normalised by D_{50} . A summary of the properties of the sands used in both figures is presented in Table 1.

The reduced scatter in Figure 10, compared to Figure 9, indicates that Δy may be expressed as a function of soil density, D_{50} , and interface roughness for dense sand at the same stress level. Additionally, as expected, laboratory data also show that Δy reduces with an increase in normal stress.

These data demonstrate that the existing simple relationships currently employed for evaluating Δy in ICP-05 and UWA-05 are over-simplistic and require improvement. Fortunately, observed values of $\Delta\sigma'_{rd}$ tend to be relatively small for most field scale piles (but are very significant for laboratory model piles;

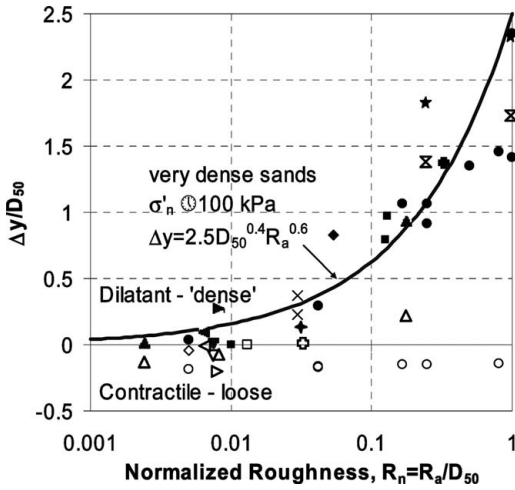


Figure 10. Influence of normalized roughness on normalized displacement after dilation has ceased.

Table 1. Laboratory reference sands used in Figure 9.

Sand	Symbol		D ₅₀ (mm)	Reference
	Loose	Very Dense		
Labenne	NA	×	0.32	Jardine et al. 1993
Sydney	○	●	0.30	Tabucanon 1997
Dunkirk	NA	+	0.25	Chow et al. 1998
Ticino	◇	◆	0.56	
Toyoura	□	■	0.24	Fioravante et al. 1999
FF	⊕	⊗	0.09	
MGS	NA	★	0.44	
VLB	NA	☒	0.78	Dietz 2000
Ottawa	△	▲	0.74	
Q Rok	▷	▶	0.75	
Legendre	▽	▼	0.82	Westgate 2005
Glass	◀	◀	0.95	

see Lehane et al. 2005c), and therefore the accuracies of the Δy and equivalent G values selected for input to Equation 9 are not usually significant. It would appear, based on arguments put forward in Lehane et al. (2005c), that both ICP-05 and UWA-05 over-predict the value of G and under-predict Δy , resulting in a reasonable estimate for $\Delta\sigma'_{rd}$.

2.5 UWA-05 design equations for shaft friction

The UWA-05 design equations for shaft capacity of driven piles arose from the foregoing considerations and are expressed as follows:

$$Q_s = \pi D \int \tau_f dh \quad (10a)$$

$$\tau_f = \sigma'_{rf} \tan \delta_{cv} = \frac{f}{f_c} (\sigma'_{rc} + \Delta\sigma'_{rd}) \tan \delta_{cv} \quad (10b)$$

$$\sigma'_{rc} = \frac{q_c A_{rs,eff}}{33}^{0.3} \max\left(\frac{h}{D}, 2\right)^{-0.5} \quad (10c)$$

$$A_{rs,eff} = 1 - IFR\left(\frac{D_i^2}{D^2}\right) \quad (10d)$$

$$IFR_{mean} \approx \min\left[1, \left(\frac{D_i}{1.5}\right)^{0.2}\right] \text{ with } D_i \text{ in metres} \quad (10e)$$

$$\Delta\sigma'_{rd} = 4G_0 \cdot \Delta y / D \quad (10f)$$

where:

$$\delta_{cv} = \text{constant volume interface friction angle}$$

$$\sigma'_{rf} = \text{radial effective stress at failure}$$

$$\sigma'_{rc} = \text{radial effective stress after installation and equalization}$$

$$\Delta\sigma'_{rd} = \text{change in radial stress due to loading stress path (dilation)}$$

$$f/f_c = 1 \text{ for compression and } 0.75 \text{ for tension}$$

Despite reliance on compensating errors, $\Delta\sigma'_{rd}$ is currently assessed using G_0 and $\Delta y \approx 2R_a$ (Jardine et al. 2005).

$$G_0/q_c = 185 \cdot q_{cIN}^{-0.7}$$

$$q_{cIN} = (q_c/p_{ref})/(\sigma'_{v0}/p_{ref})^{0.5}$$

$$p_{ref} = \text{a reference stress equal to } 100 \text{ kPa}$$

$$\sigma'_{v0} = \text{in situ vertical effective stress}$$

$$\Delta y = \text{interface dilation (assumed as } 0.02 \text{ mm for steel piles)}$$

2.6 Increases in shaft capacity with time

The increase in the shaft capacity with time of displacement piles in sand is now well established, although no design method specifically caters for time effects in its formulations. This is primarily because of the lack of data arising from the fact that static load tests are generally performed only once, and usually within about one to three months of installation. The database of pile load tests with adjacent CPT profiles discussed by Schneider et al. (2007) primarily contains first time load tests performed within 90 days of installation.

Increases in pile capacity with time are usually attributed to gains in shaft capacity i.e. existing base capacity data do not exhibit an ageing effect. Figure 11 provides an indication of the observed increases with time and combines the tension test data set discussed by Chow et al. (1998) with O-Cell retests presented in Bullock et al. (2005) and the first time tests

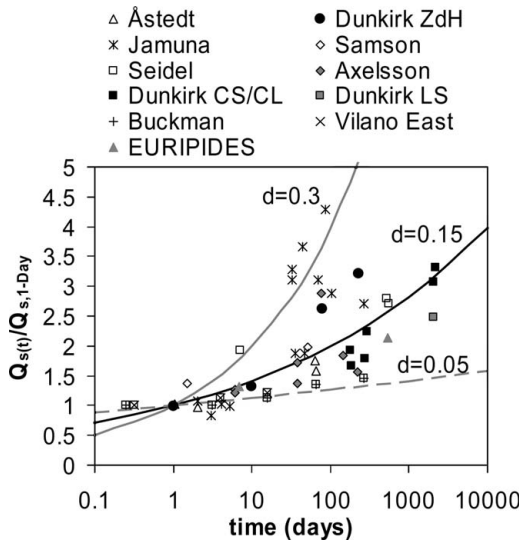


Figure 11. Database of tension pile load tests with time.

discussed by Jardine et al. (2006). The trend lines shown on the figure are of the following form:

$$\frac{Q_{s(t)}}{Q_{s,\text{ref}}} = \left(\frac{t}{t_{\text{ref}}} \right)^d \quad (11)$$

where t_{ref} is a reference time, $Q_{s,\text{ref}}$ is the shaft capacity at that reference time and d is an empirical parameter which varies from 0.05 to 0.3. Evidently, shaft capacity can increase by a factor of between two to three over a period of 3 years.

Increases in any of the parameters in equation (2) result in increases in pile shaft friction. These increases are currently understood to be due to:

- Increases in σ'_{rc} due to equalization of hoop and radial stress (Åstedt et al. 1992, Jardine et al. 2006)
- Increases in σ'_{rc} due to equalization of free field radial stress with that adjacent to pile (White & Bolton 2004, White et al. 2005)
- Increases in σ'_{rc} due to constrained dilatant creep (Bowman & Soga 2005)
- Increase in $\Delta\sigma'_{rd}$ due to an increase in Δy (Chow et al. 1998)
- Increase in $\Delta\sigma'_{rd}$ due to increase in G (Chow et al. 1998, Axelsson 2002)
- Increase in δ as the sand's dilation angle increases (Bullock et al. 2005)
- Increases in D , δ_f , and Δy from sand 'welding' to steel piles (Bea et al. 1999)

Further research, which should include the acquisition of additional measurements of τ_f and σ' distributions over time, are necessary before time

effects can be reliably incorporated in axial pile design methods.

3 END BEARING

Factors that were considered in the development of the UWA-05 proposals for base capacity evaluation of closed and open-ended piles are listed in the following. These proposals are based on the analyses reported by Xu & Lehane (2005) and Xu et al. (2005). The base capacity is defined as the pile end bearing resistance at a pile base displacement of 10% of the pile diameter, $q_{b0.1}$.

3.1 End bearing capacity of closed-ended piles

The strong direct relationship between the end bearing resistance of a closed ended driven pile and the cone tip resistance, q_c , has been recognised for many years and arises because of the similarity between their modes of penetration. Prior to assessing pile end bearing resistance $q_{b0.1}$, the CPT q_c value needs to appropriately averaged to account for differences in diameter between a pile and penetrometer ($D_{CPT} = 36$ mm). Xu & Lehane (2005) present a discussion of q_c averaging techniques, which is summarized here. The following three q_c averaging techniques were examined:

- simple arithmetic average over a zone extending from 1.5D above to 1.5D below the pile tip (e.g. simplified LCPC approach, Bustamante & Ganeselli 1982).
- the geometric mean of q_c measured over a given zone in the pile tip vicinity, as recommended by Eslami & Fellenius (1997), i.e. 4D below to 8D above when a pile is installed through a loose layer into a dense layer, but from 4D below to 2D above when a pile is installed through a dense layer into a loose layer.
- the 'Dutch' q_c averaging technique (van Mierlo & Koppejan 1952, Schmertmann 1978) commonly employed in North American and European practice, where q_c values are averaged over an influence zone extending 8D above, and between 0.7D and 4D below the pile toe following a 'minimum path rule'. This method is less straightforward than the other two and is illustrated in Figure 13.

The q_c profiles for all case histories in the UWA database were digitised and a computer code was written to examine the implications of these q_c averaging methods. The averaged q_c values ($q_{c,\text{avg}}$) are plotted against the cone resistance at pile tip level, $q_{c,\text{tip}}$ for each method on Figure 12 for both closed and open-ended piles. It was found that:

- (i) As shown in Figure 12a, arithmetic averaged q_c values over $\pm 1.5D$ are very close to the cone

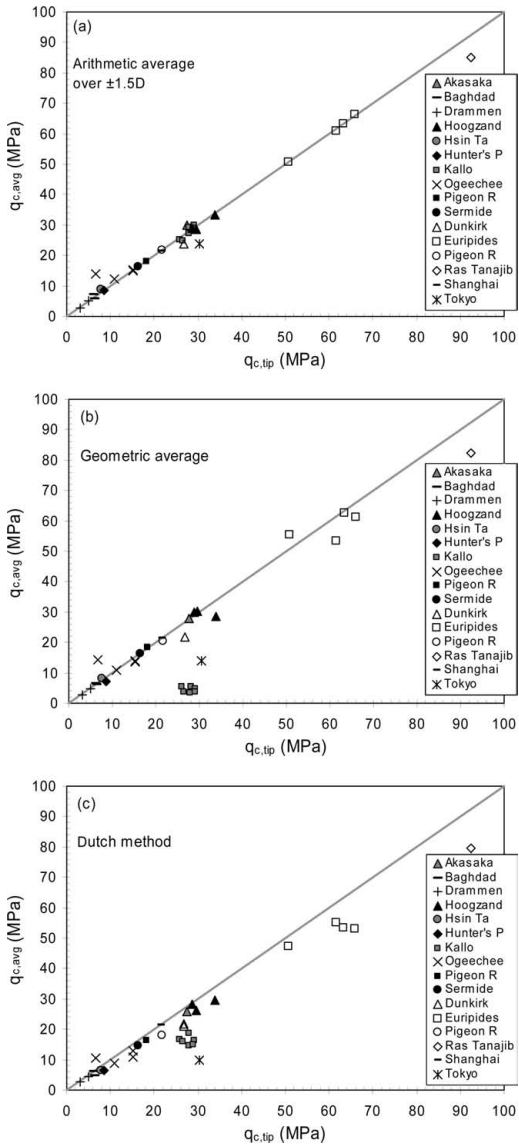


Figure 12. Comparisons of $q_{c,\text{avg}}$ with $q_{c,\text{tip}}$: (a) arithmetic average, (b) geometric mean, and (c) Dutch method.

resistances at the pile tip $q_{c,\text{tip}}$, with averaged ratios of $q_{c,\text{avg}}/q_{c,\text{tip}}$ equal to 1.03. It is obvious that this method does not reflect the strongly layered stratigraphies at sites such as Kallo and Tokyo Bay; such layering is likely to be significant for piles, which have a much larger diameter than a cone penetrometer.

(ii) In contrast, as seen on Figure 12b and Figure 12c, the use of the geometric mean and the 'Dutch'

approaches lead to $q_{c,\text{avg}}/q_{c,\text{tip}}$ ratios significantly different to unity at 'non-homogeneous' sites, with $q_{c,\text{avg}}/q_{c,\text{tip}}$ being as low as 0.2 at the Kallo site when the geometric average is employed. In the relatively homogeneous deposits (i.e. excluding the Kallo and Tokyo Bay sites), the average ratio of $q_{c,\text{avg}}/q_{c,\text{tip}}$ is 1.0 and 0.9 for the geometric mean and Dutch approaches respectively.

A case history reported by Lehane et al. (2003) provides an opportunity to investigate the suitability of averaging techniques as it includes the base resistance measured during continuous jacked installation of a 350mm square concrete pile. On inspection of the comparisons on Figure 14, it appears that, of the three averaging techniques considered, $q_{c,\text{avg}}$ derived using the 'Dutch' method provides a better match to the general shape and magnitude of the pile end bearing profile. This match with 'steady state resistance' suggests that the static pile end bearing, $q_{b0,1}$, is more uniquely related to the Dutch value of $q_{c,\text{avg}}$.

Numerical studies complimented by centrifuge investigations, reported in Xu & Lehane (2007), indicate that the end bearing of a pile founded in a dense layer is potentially reduced if a loose layer is present within a distance of up to 12 pile diameters of the tip, but that end bearing in a loose sand layer is un-affected by the presence of a dense layer if the dense layer is more than 2 pile diameters away. The reduction in pile end bearing in a given dense sand layer depends both on the relative depth of pile tip with respect to the loose layer and on the ratio of the 'steady state' q_c values in the respective layers. An example of a numerical prediction of the variation of end bearing with embedment depth is illustrated in Figure 15, where it is compared with the empirical averaging techniques. It is evident that the 'Dutch' method provides the closest match to the prediction. Based on (i) this observation, (ii) the similarity between the centrifuge end bearing data and the numerical predictions and (iii) comparisons such as shown on Figure 14, the Dutch averaging technique is adopted for calculation of end bearing by UWA-05.

Recent research into the end bearing of closed ended piles suggests:

1. The values of $q_{b0,1}$ for driven piles are typically less than $q_{c,\text{avg}}$ because the displacement of 0.1D is insufficient to mobilise the ultimate value (i.e. $q_{c,\text{avg}}$). The UWA base capacity database of measured $q_{b0,1}$ values normalised by the Dutch $q_{c,\text{avg}}$ values are presented on Figure 16. It is evident that, apart from the Ogeechee River and Baghdad sites, $q_{b0,1}/q_{c,\text{avg}}$ for all test piles is relatively constant at ≈ 0.6 and is independent of pile diameter.
2. Since jacked piles usually have higher locked-in base stresses and base stiffness, $q_{b0,1}$ for these piles tends to be a higher ratio of $q_{c,\text{avg}}$. The authors compiled a database of field and centrifuge load tests on

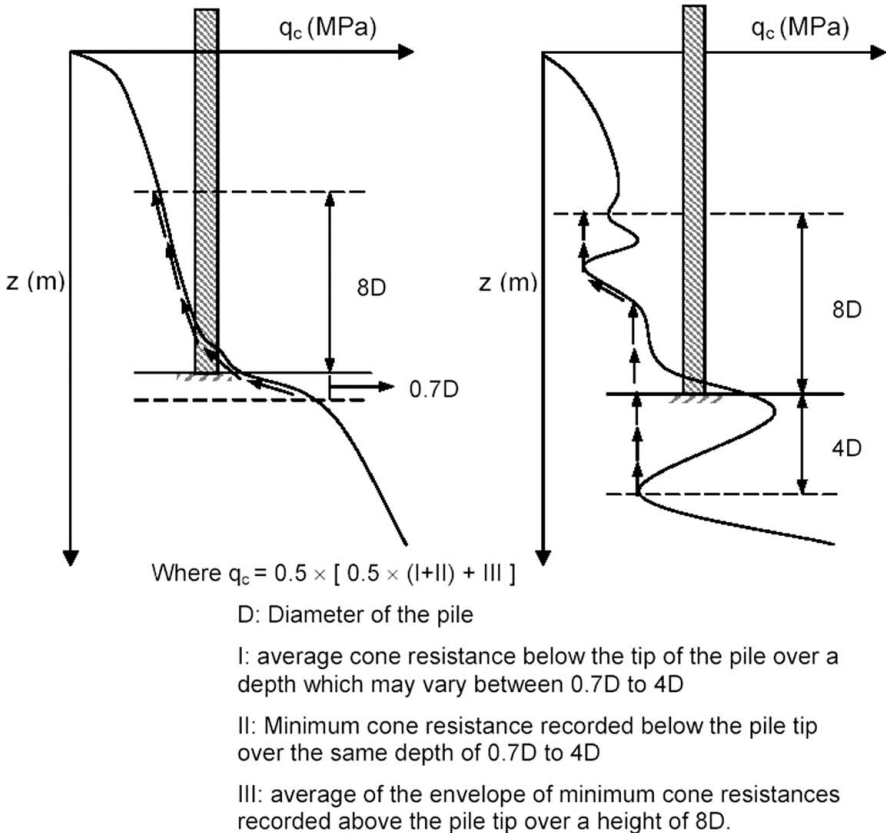


Figure 13. Calculation of the average cone tip resistance in Dutch method (van Mierlo & Koppejan 1952, Schmertmann 1978).

jacked piles. The centrifuge tests, which are reported in Xu (2007), were conducted using model piles of different diameters ($D = 6\text{ mm}, 9.5\text{ mm} \& 16\text{ mm}$) at various stress levels (σ'_{v0} from 65 kPa to 190 kPa) and samples of various relative densities (D_r from 0.36 to 0.93). Figure 17 presents a summary of the centrifuge and field ratios of $q_{b0.1}/q_{c,\text{avg}}$ ratios. The mean $q_{b0.1}/q_{c,\text{avg}}$ ratio is seen to be about 0.9 (i.e. about 50% higher than the value of 0.6 for driven closed-ended piles), and there is no systematic variation of this ratio with $q_{c,\text{avg}}$, D & D_r .

3. The findings of Randolph (2003), White & Bolton (2005), and others, are consistent with the UWA-05 proposal to adopt a constant ratio of $q_{b0.1}/q_{c,\text{avg}}$ for both driven and jacked closed-ended piles.

On the basis of the foregoing, the UWA-05 method proposes the following equations for closed-ended displacement piles:

$$Q_b = q_{b0.1} \frac{\pi}{4} D^2 \quad (12a)$$

$$q_{b0.1}/q_{c,\text{avg}} = 0.6 \text{ for driven piles} \quad (12b)$$

$$q_{b0.1}/q_{c,\text{avg}} = 0.9 \text{ for jacked piles} \quad (12c)$$

3.2 End bearing capacity of open-ended piles

The end bearing formulation adopted by UWA-05 for open ended piles was based predominantly on the following observations:

1. Salgado et al. (2002), Lehane & Gavin (2001, 2004), and others, have shown that a relatively consistent relationship between $q_{b0.1}$ for a pipe pile and the CPT q_c value becomes apparent when the effects of sand displacement close to the tip during pile driving are accounted for. This installation effect is best described by the incremental filling ratio (IFR) measured over the final stages of installation- and is referred to here as the final filling ratio (FFR). As the FFR approaches zero, $q_{b0.1}$

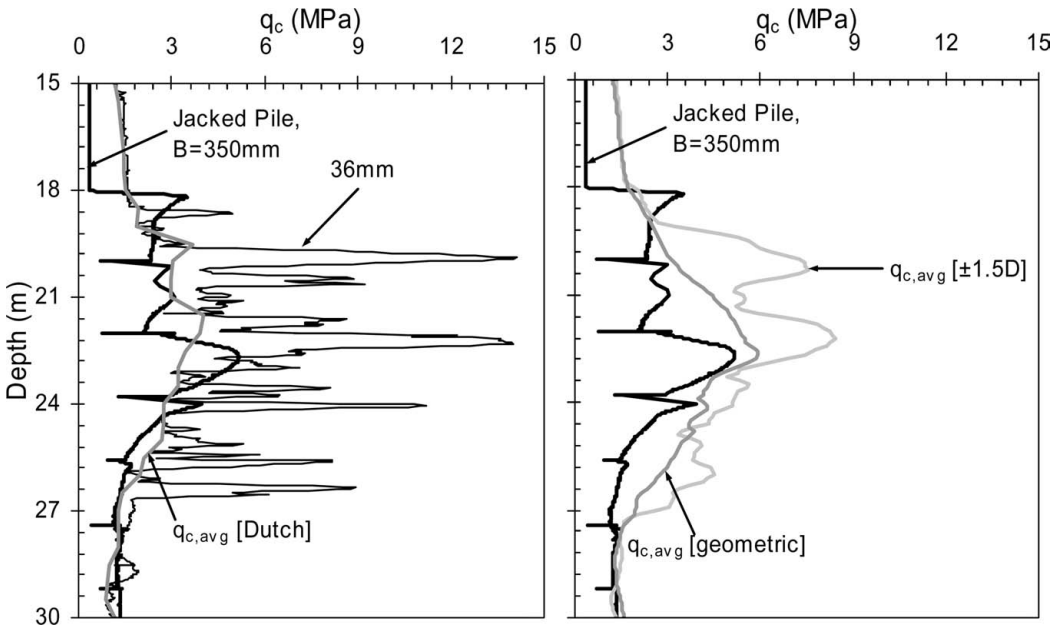


Figure 14. Measured and predicted q_c profiles at Perth, Australia site (Xu & Lehane 2005).

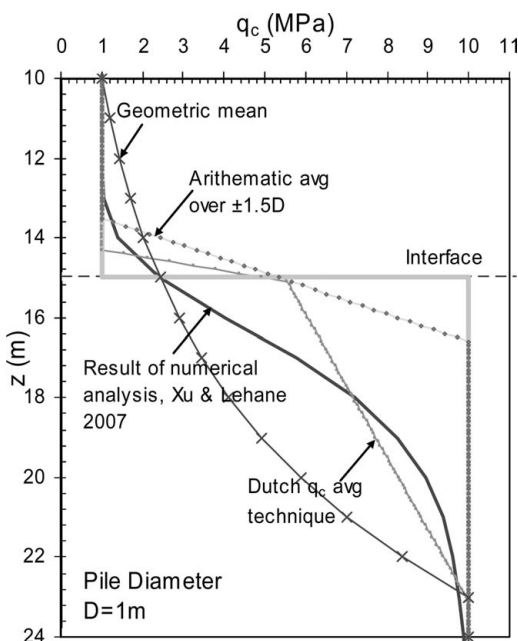


Figure 15. Comparison of q_c averaging techniques in an idealized two-layered soil profile with a 1 m diameter closed-ended pile.

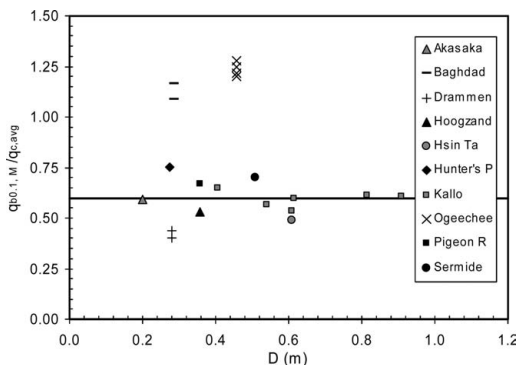


Figure 16. Measured $q_{b0,1}$ normalised by Dutch $q_{c,avg}$ for closed-ended piles, (Xu & Lehane 2005).

- approaches that of a closed-ended pile with the same outer diameter. Examples of measured IFR profiles for eight pile tests in the UWA database are shown in Figure 18.
2. The displacement induced in the sand in the vicinity of the base is most conveniently expressed in the terms of the effective area ratio $A_{rb,eff}$, defined in Equation 13d. This ratio ($A_{rb,eff}$) depends on the pile's D/t (outer diameter to wall thickness) ratio

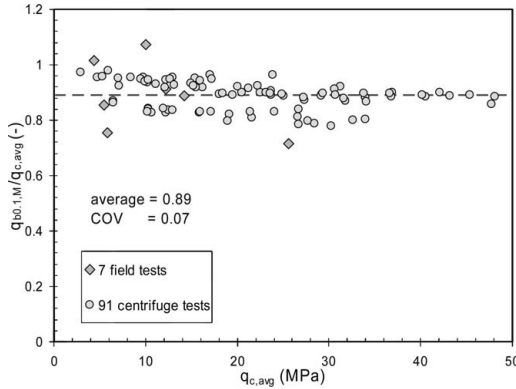


Figure 17. Ratios of $q_{b0.1,M}/q_{c,avg}$ for closed-ended jacked piles based on field and centrifuge tests, (Xu 2007).

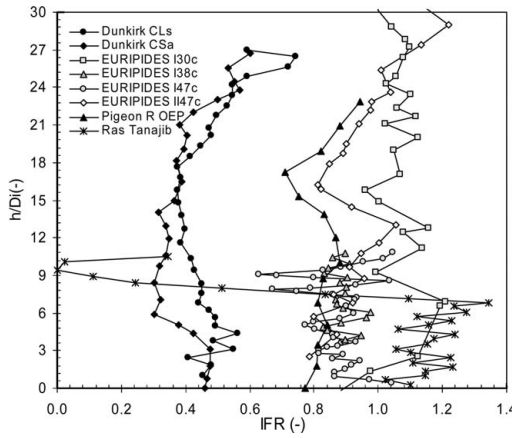


Figure 18. Examples of IFR measurements during pile driving (Xu et al. 2005).

- and the FFR value, and varies from unity for a pile installed in a fully plugged mode to about 0.08 for a pile installed in a coring mode with D/t of 50.
3. Despite the fact that most full scale driven pipe piles exhibit a low level of partial plugging during installation (i.e. coring predominates), Lehane & Randolph (2002), and others, have shown that, if the length of the soil plug is greater than 5 internal pile diameters ($5D_i$), the plug will not fail under static loading, regardless of the pile diameter.
 4. The controlling influence of the level of soil displacement on end bearing means that replacing a soil plug with concrete will not influence its end bearing; this has been proven by Beringen et al. (1979), and others.

5. Experimental data and numerical analyses indicate that the resistance that can develop on the tip annulus at a base movement of 0.1D varies between about 0.6 and 1.0 times the CPT q_c value (e.g. Bruno 1999, Salgado et al. 2002, Lehane & Gavin 2001, Paik et al. 2003, Jardine et al. 2005).
6. Lehane & Randolph (2002) suggest that the base resistance provided by the soil plug for a fully coring pile (with $FFR = 1$) is approximately equivalent to that of a bored pile.
7. Recommended values of $q_{b0.1}/q_{c,avg}$ for bored piles range from 0.15 to 0.23 (Ghionna et al. 1993). These ratios are not dependent on the pile diameter.
8. The value of $q_{c,avg}$ should be evaluated in the same way as that employed for closed-ended piles, but using an effective diameter (D^*) related to the effective area ratio, A_{rb}^* i.e. $D^* = D \times (A_{rb})^{0.5}$. Case histories described by Xu et al. (2007) involving large diameter open-ended piles in strongly layered profiles support this recommendation.
9. There are relatively few documented case histories that report the incremental or final filling ratios. In the absence of FFR measurements, a rough estimate of the likely FFR may be obtained using Equation 13e (see also Figure 4).
10. Very few publications provide guidance on the end bearing developed by open-ended jacked piles. The data reported by Gavin & Lehane (2005) and White et al. (2000) indicate that fully plugged open-ended jacked piles behave like closed-ended jacked piles (with $q_{b0.1}/q_{c,avg}$ ratios of around unity), and that no significant difference exists between the end bearing characteristics of jacked and driven piles that partially plug during installation.

The UWA-05 proposal for end bearing of pipe piles is provided in Equation 13. This proposal is developed in Xu et al. (2005, 2007) and shown to compare favourably with the existing database of base capacity measurements for open-ended driven piles (e.g. see Figure 19). Further verification (and possible refinement) of the formulae is required for open-ended jacked piles.

$$Q_b = q_{b0.1} \frac{\pi}{4} D^2 \quad (13a)$$

$$q_{b0.1}/q_{c,avg} = 0.15 + 0.45A_{rb,eff} \quad \text{for driven piles} \quad (13b)$$

$$q_{b0.1}/q_{c,avg} = 0.15 + 0.75A_{rb,eff} \quad \text{for jacked piles} \quad (13c)$$

$$A_{rb,eff} = 1 - FFR \left(\frac{D_i^2}{D^2} \right) \quad (13d)$$

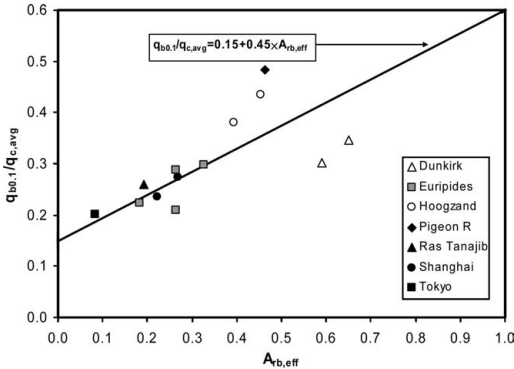


Figure 19. Ratio of $q_{b0,1}/q_{c,avg}$ versus effective area ratio $A_{rb,eff}$ for open-ended driven piles.

$$FFR \approx \min \left[1, \left(\frac{D_i}{1.5} \right)^{0.2} \right] \quad \text{with } D_i \text{ in metres} \quad (13e)$$

3.3 Base stiffness of displacement piles

3.3.1 Base stiffness of jacked closed-ended piles
 Xu (2007) back-analysed data from a testing series comprising 91 static load tests on jacked centrifuge model closed-ended piles in uniform and layered sand samples. The base stress (q_b)-base displacement (w_b) response observed in these tests was approximately linear up to a normalised base displacement (w_b/D) of at least 0.5%. Residual loads for all cases were less than 20% of the capacity at $w/D = 0.1$.

Figure 20 presents the equivalent shear moduli (G_{IN}) representative of this initial portion of the q_b - w/D relationship. It is seen that the G_{IN}/q_c^1 values follow the average trendline proposed by Rix & Stokoe (1992) for the very small strain in-situ stiffness (G_0) of freshly deposited sand. However, values of G_{IN} appear to be higher than G_0 in relatively dense sand (i.e. $q_{c1N} > 250$ in Figure 20). Nevertheless, the similarity between G_{IN} and G_0 may arise because of the high degree of over-consolidation induced in the sand below the pile base by the final jacking stroke prior to the static load test. As soil/sand is not linear elastic up to $w_b/D \sim 0.5\%$, it would appear that the initial linearity over such a large strain range arises because any decrease in shear stiffness with strain

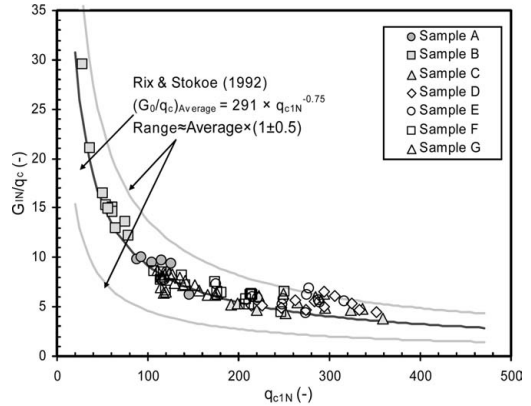


Figure 20. Initial shear stiffness ratios for jacked centrifuge piles (Xu 2007).

from the very small strain value (at $w_b/D \sim 0.01\%$) is compensated for by the increase in stress level.

It may be inferred from Figure 20 that the base stiffness of jacked piles at working levels of displacement can be approximated by employing the in-situ G_0 value as the operational shear stiffness (which is now measured routinely).

The measured variation of the equivalent elastic shear stiffness of the soil (G) at the pile base with w/D and with the resistance ratio (q_b/q_c) is summarised in Figure 21 for all the centrifuge static load tests; these tests are categorized in terms of their G_{IN}/q_c values. (Note that G_{IN}/q_c reduces with an increase in the relative density). The degree of stiffness reduction with the displacement/strain level (i.e. w/D) depends on the G_{IN}/q_c ratio, while the relationship between G/G_{IN} and q_b/q_c is relatively unique and independent of G_{IN}/q_c . Stiffness decay curves and hence the full pile base load-settlement response may therefore be derived from a measurement of G_0 ($\sim G_{IN}$) and q_c . In fact, as shown in Figure 21a, the relatively unique relationship between G/G_{IN} and q_b/q_c can be reproduced using an equation with a modified hyperbolic form. This relationship is likely to only be applicable to jacked piles (with relatively low residual stresses) because of the influence of the installation method.

3.3.2 Base stiffness of open-ended piles

Gavin & Lehane (2007) examined the effect of soil displacement (as measured by the filling ratio) on the base stress (q_b)-normalised base displacement (w_b/D) response of jacked and driven piles in sand. Typical data recorded are plotted on Figure 22, which shows how the equivalent base modulus varies not only with the base displacement (w_b/D), but also with the final

¹ It is noteworthy that these “ q_c ” values were taken as the model pile base resistance mobilised during the jacking stage preceding the static load test. For tests in non-homogeneous profiles, these q_c values are affected by the presence of weaker/stronger layers and should be considered as the corrected steady state pile end bearing value.

filling ratio (FFR) for open-ended piles. They also show how the stiffness of a bored pile (which essentially has a FFR of unity) in the same soil conditions is lower than all other pile types at a given w_b/D value i.e. base stiffness falls systematically with FFR.

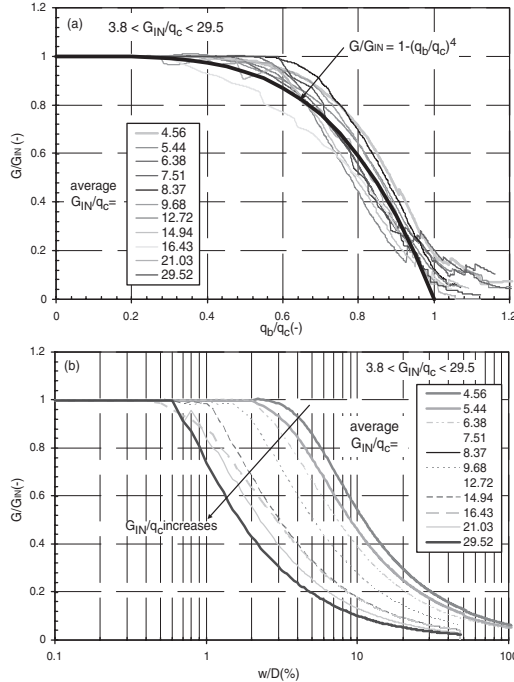


Figure 21. Categorized stiffness reduction curves based on similar ratios of G_{IN}/q_c for jacked piles (Xu 2007).

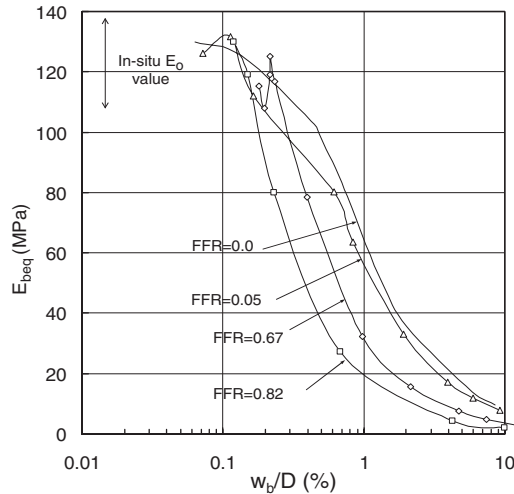


Figure 22. Base stiffness dependence on soil displacement during pile installation (Gavin & Lehane 2007).

Their data review indicated that virtually no pile base movement occurs during static loading of closed or open-ended piles until the residual base stress generated during pile installation is exceeded. Once the residual pressure is exceeded, a stiff, linear base load-displacement response is exhibited, during which the operational stiffness is approximately equivalent to the small strain in-situ elastic stiffness (E_0 or G_0) measured prior to pile installation. This is the same result deduced independently by Xu (2007). The onset of significant stiffness degradation occurs at a normalised base displacement level which is controlled, for a displacement pile, by the level of pre-stress imparted during installation (which depends on the filling ratio for a pipe pile) and, for a bored pile, by the sand's over-consolidation ratio. At this stage, the base load-displacement response of the model pile may be approximated as a parabola up to a displacement of 10% of the pile diameter.

Equation (13) under-estimates the base resistance of displacement piles for $w_b/D > 0.1$ and a database study compiled by Gavin & Lehane (2005) indicated that the base stress mobilised at displacements of up to one diameter (referred to here as q_{bulk}) may be estimated as:

$$q_{bulk} = q_c \text{ for closed-ended driven piles} \quad (14a)$$

$$q_{bulk} = (q_{plug} \times A_{plug}) + (q_{ann} \times A_{ann}) \text{ where} \quad (14b)$$

$$q_{ann} = q_c \quad (14c)$$

$$q_{plug} = (0.8 - 0.7 \text{ FFR})q_c \text{ with } \text{FFR} \leq 1 \quad (14d)$$

where A_{ann} is the annular area and q_{ann} is the unit base resistance at the base of the annulus. Equation (14) may then be used to assess the degree of pre-stressing induced by installation. Gavin & Lehane (2007) propose that the initial linear portion of the base stress-displacement relationship can be described by:

$$q_b = [k(w_b/D)] + q_{bres} \quad (15a)$$

$$\text{where } k = (4/\pi) E_0 / (1 - v^2) \quad \text{for } w_b/D < w_{by}/D \quad (15b)$$

$$\text{and } w_{by}/D = (\pi/4) q_{bulk} (1 - v^2) / E_0 \leq 1.5 \% \quad (15c)$$

When w_b/D exceeds w_{by}/D and is less than 10%, the base stress, q_b , is expressed as:

$$q_b = [k(w_{by}/D)^{1-n} (w_b/D)^n] + q_{bres} \quad (15d)$$

with $w_{by}/D \geq 0.003$

The value n in Equation 15d is determined by equating its prediction for $q_{b0.1}$ (i.e. q_b at $w_b/D = 0.1$) with that predicted using the appropriate $q_{b0.1}$ formulation for the particular pile type. As Equation 15c cannot be applied when w_{by}/D is zero, based on the stiffness values indicated by static load tests on the bored piles, Gavin & Lehane (2007) suggest a lower bound w_{by}/D value of 0.3% for virgin loading. They also show that the n values backcalculated for the laboratory and field tests reduce as w_{by}/D increases from a value of about 0.33 for a bored pile with no pre-loading to about 0.1 for a closed-ended driven pile.

4 COMPARISON OF DRIVEN AND JACKED PILES

The low noise and vibration levels associated with jacked or ‘pressed-in’ piles have led to their increasing popularity in recent years. Factors causing differences in the axial capacity of jacked and driven piles in sand include:

- Driven piles have a larger number of installation cycles which may lead to higher levels of friction fatigue.
- Closed ended jacked piles have a greater base stiffness than comparable driven piles and a higher $q_{b0.1}/q_{c,avg}$ ratio (compare equations 12b and 12c)
- Open ended jacked piles tend to plug to a greater degree than open ended driven piles, influencing both installation resistance and static capacity.

The *UWA-05* method (originally formulated for driven piles) has been extended to account for these differences. Table 2 summarizes parameters used in the assessment of the database of driven (Schneider et al. 2007) and jacked (Xu 2007) piles. The a and b parameters for both pile types are assumed to be the same but the ‘ c ’ exponent is modified for jacked piles to a value that leads to a less severe reduction in local friction and is the same value deduced by Lehane & Jardine (1994) for jacked piles in the medium dense sand at Labenne. In addition, the proposed $q_{b0.1}/q_{c,avg}$ ratio leads to a higher base capacity for jacked piles.

Table 2. *UWA-05* parameters for piles in siliceous sands.

Instal- lation	a				
	Comp.	Tens.	b	c	$q_{b0.1}/q_{c,avg}$
Driven	33	44	0.3	-0.50	$0.15 + 0.45A_{rb,eff}$
Jacked	33	44	0.3 ^a	-0.33	$0.15 + 0.75A_{rb,eff}$

^a parameter currently not calibrated for open ended jacked piles

Figures 23 and 24 use the UWA database of static load tests to investigate predictive performance using the parameters in Table 2 and the potential bias of *UWA-05* predictions with sand relative density (which varies with normalized cone tip resistance, q_{c1N}) and pile slenderness ratio (L/D). Only data on closed ended jacked piles are available and the same database subsets used in Figure 1 are examined. It is evident that, despite the shortage of data for jacked piles, the predictive performance for both driven and jacked piles is reasonable, given the range of sites, soil conditions, pile geometries and pile types. Statistical analyses summarised in Schneider et al. (2007) and Xu et al. (2007) provide clear evidence that *UWA-05* performs better than other existing design methods for the available database of static load test.

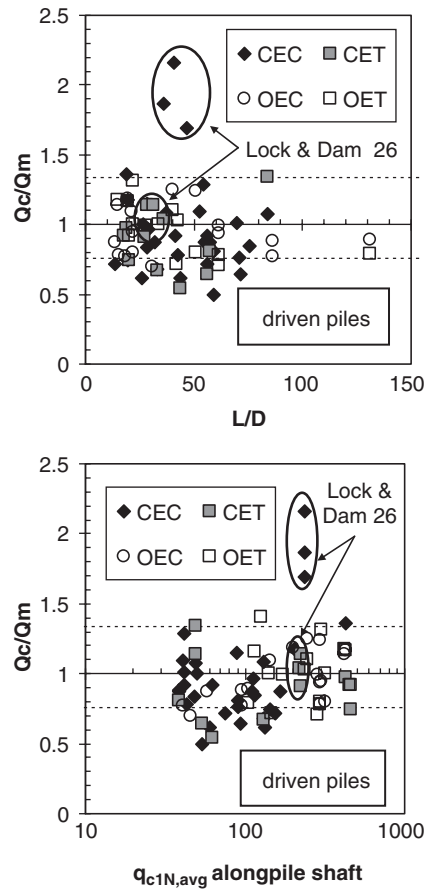


Figure 23. Ratios of capacities calculated using *UWA-05* to measured capacities for database of driven piles with adjacent CPT profiles.

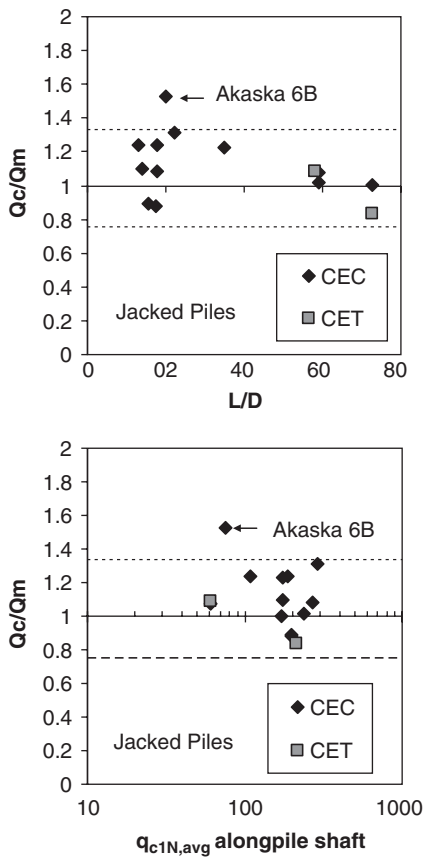


Figure 24. Ratios of capacities calculated using UWA-05 (with parameters in Table 2) to measured capacities for database of closed-ended jacked piles with adjacent CPT profiles.

5 EXTRAPOLATION TO LARGE DIAMETER PILES

For full scale offshore driven piles, as IFR = 1 and the dilation term ($\Delta\sigma'_{rd}$) can be ignored, the UWA-05 formulations simplify to:

$$Q_{comp} = Q_b + Q_s = q_{b0.1} \frac{\pi}{4} D^2 + \pi D \int \tau_f dz \quad (16a)$$

$$Q_{tens} = 0.75 \cdot \pi D \int \tau_f dz \quad (16b)$$

$$q_{b0.1} = q_{c,avg} \times (0.15 + 0.45 A_r) \quad (16c)$$

$$\tau_f = \frac{q_c A_r^{0.3}}{33} \left[\max \left(\frac{h}{D}, 2 \right) \right]^{-0.5} \tan \delta_{cv} \quad (16d)$$

$$A_r = 1 - \left(\frac{D_i^2}{D^2} \right) \quad (16e)$$

Although the predictive performance of UWA-05 for the database piles is adequate, achieving a satisfactory prediction for large offshore piles is less certain given that most database piles have a diameter lower than that commonly employed offshore. Lehane et al. (2005a) examined the implications of the offshore form of UWA-05 (i.e. equation 16) and assessed its performance against existing API recommendations and ICP-05 (the best performing of the three other CPT based methods included in API (2006)). This examination indicated that Equation (16) provides a more conservative extrapolation than ICP-05 for shaft capacity from the existing database to typical offshore piles used in practice. Equation (16) also predicts higher base capacities than ICP-05 because of its assumption that a pile plug with a length greater than 5 diameters will not fail under static loading. As a consequence UWA-05 and ICP-05 predict similar axial capacities for offshore piles in compression. It follows that ICP-05 is potentially un-conservative for short term tension capacity (which is critical for the new generation of moored offshore structures).

It is also noteworthy that Equation (16) tends to provide lower capacities than API-00 in loose sands, but higher capacities for dense sands in compression. API-00 and UWA-05 predictions for tension capacity in dense sands are broadly similar for pile lengths in excess of 25 m. However, the UWA-05 method, unlike API-00, does not show any prediction bias with L, D, L/D and D_r.

6 CONCLUSIONS

This paper has provided the background and basis for the formulations proposed in the CPT-based displacement pile design method, referred to as UWA-05. It is shown how this method incorporates a variety of recent research findings in a way that enables most of the significant factors that affect the capacity of displacement piles in sand to be incorporated in relatively simple design formulations. These formulations allow assessment of the shaft and base capacity of jacked and driven, open and closed-ended displacement piles in siliceous sand. A simple means of estimating the base stiffness of displacement piles is also provided.

ACKNOWLEDGEMENTS

The second and third authors would like to acknowledge the financial assistance provided by the International Postgraduate Scholarship scheme at the

University of Western Australia and by the Australian Research Council.

REFERENCES

- API 2000. Recommended Practice for Planning, Designing, and Constructing Fixed Offshore Platforms – Working Stress Design, API RP2A. 21st Edition, American Petroleum Institute, Washington, D.C.
- API 2006. Recommended Practice for Planning, Designing, and Constructing Fixed Offshore Platforms – Working Stress Design, API RP2A. 22nd Edition, American Petroleum Institute, Washington, D.C.
- Axelsson, G. 2002. Conceptual model of pile set-up for driven piles in non-cohesive soil. Deep Foundations 2002, Geotechnical Special Publication No. 116, Reston, VA, 64–79.
- Bea, R.G., Jin, Z., Valle, C., and Ramos, R. 1999. Evaluation of reliability of platform pile foundations. *J. Geotech. Geoenviron. Eng.*, ASCE, 125(8), 696–704.
- Beringen, F. L., Windle, D., and Van Hooydonk, W. R. 1979. Results of loading tests on driven piles in sand. In Proceedings of the Conference on Recent Development in the Design and Construction of Piles, ICE, London. 21–22 March 1979, 213–225.
- Bowman, E.T., and Soga, K. 2005. Mechanisms of setup of displacement piles in sand: laboratory creep tests. *Canadian Geotech. J.*, 42(5), 1391–1407.
- Briaud, J. L., and Tucker, L. M. 1988. Measured and predicted axial response of 98 piles. *Journal of Geotechnical Engineering*, 114(9): 984–1001.
- Bruno, D. 1999. Dynamic and static load testing of driven piles in sand. PhD Thesis, University of Western Australia.
- Bustamante, M., and Gianesselli, L. 1982. Pile bearing capacity prediction by means of static penetrometer CPT. Proc., 2nd European Symp. on Penetration Test., Amsterdam, 493–500.
- Bullock, P.J., Schmertmann, J.H., McVay, M.C., and Townsend, F.C. (2005). Side shear setup II: Results from Florida test piles. *J. Geotech. Geoenviron. Eng.*, ASCE, 131(3) 301–310.
- Chow, F.C. 1997. Investigations into the behaviour of displacement piles for offshore foundations. PhD Thesis, Univ. of London (Imperial College).
- Chow, F.C., Jardine, R.J., Brucy, F., and Nauroy, J.F. 1998. Effects of time on capacity of pipe piles in dense marine sand. *J. Geotech. & Geoenv. Engrg.* ASCE, 124(3), 254–264.
- Clausen, C.J.F., Aas, P.M., and Karlsrud, K. 2005. Bearing capacity of driven piles in sand, the NGI approach. Proc., Int. Symp. Frontiers Offshore Geomech. ISFOG, Perth, 677–681.
- De Cock, F., Legrand, C., and Huybrechts, N. 2003. Overview of design methods of axially loaded piles in Europe - Report of ERTC3-Piles, ISSMGE Subcommittee. Proc., 8th European Conf. on Soil Mech. and Geotech. Eng., Prague, 663–715.
- Dietz, M.S. 2000. Developing an holistic understanding of interface friction using sand within the direct shear apparatus. *PhD Thesis*, University of Bristol, 282.
- Eslami, A., and Fellenius, B. 1997. Pile capacity by direct CPT and CPTu methods applied to 102 case histories. *Canadian Geotech. J.*, 34, 886–904.
- Fioravante, V., Ghionna, V.N., Pedroni, S., and Porcino, D. 1999. A constant normal stiffness direct shear box for soil-solid interface tests. *Rivista Italiana di Geotecnica*, 33(3), 7–22.
- Frost, J.D., DeJong, J.T., and Recalde, M. 2002. Shear failure behavior of granular-continuum interfaces. *Engineering Fracture Mechanics*, 69, 2029–2048.
- Gavin, K., and Lehane, B. 2003a. End bearing of small pipe piles in dense sand. In BGA International Conference on Foundations, Innovations, Observations, Design and Practice, Dundee, United Kingdom, pp. 321–330.
- Gavin, K., and Lehane, B. M. 2003b. The shaft capacity of pipe piles in sand, *Canadian Geotech. J.*, 40(1), 36–45.
- Gavin, K., and Lehane, B. M. 2005. Estimating the end bearing resistance of pipe piles in sand using the final filling ratio. Proc., Int. Symp. Frontiers Offshore Geomech. ISFOG, Perth, 717–723.
- Gavin, K., and Lehane, B. M. 2007b. The base stiffness of piles in sand, submitted to *Canadian Geotech. J.*, 40(1).
- Ghionna, V.N., Jamiołkowski, M., Lancellotta, R. and Pedroni, S. 1993. Base capacity of bored piles in sands from in situ tests. In Deep Foundation on Bored and Auger Piles, ed. V. Impe, Balkema, Rotterdam: 67–75.
- Jardine, R.J., Lehane, B.M., and Everton, S.J. 1993. Friction coefficients for piles in sands and silts. Proc. Int. Conf. on Offshore Site Investigation and Foundation Behaviour, SUT, London, 661–677.
- Jardine, R.J., Chow, F.C., Overy, R.F., and Standing, J. R. 2005. ICP design methods for driven piles in sands and clays. Thomas Telford, London, 97.
- Jardine, R.J., Standing, J.R., and Chow, F.C. 2006. Some observations of the effects of time on the capacity of driven piles in sand. *Géotechnique*, 56(4), 227–244.
- Kolk, H.J., Baaijens, A.E., and Senders, M. 2005. Design criteria for pipe piles in siliceous sands. Proc., Int. Symp. Frontiers Offshore Geomech. ISFOG, Perth, 711–716.
- Lehane, B.M., Jardine, R.J., Bond, A.J., and Frank, R. 1993. Mechanisms of shaft friction in sand from instrumented pile tests. *J. Geotech. Eng.*, 119 (1), 19–35.
- Lehane, B.M., and Jardine, R.J. 1994. Shaft capacity of driven piles in sand: a new design approach. Proc., 7th Int. Conf. on Behaviour of Offshore Struct., MIT, Cambridge, MA, 23–36.
- Lehane, B.M. and Gavin, K.G. 2001. Base resistance of jacked pipe piles in sand. *J. of Geotech. and Geoenv. Engrg.* ASCE 127(6), 473–480.
- Lehane B.M. and Gavin K. 2004. Discussion to: Determination of bearing capacity of open-ended piles in sand. *J. Geotech. & Geoenv. Engrg.* ASCE 130 (6), 656–658.
- Lehane, B.M. and Randolph, M.F. 2002. Evaluation of a minimum base resistance for driven pipe piles in siliceous sand. *J. of Geotech. and Geoenv. Engrg.*, ASCE 128(3): 198–205.
- Lehane, B.M., Pennington, D., and Clark, S. 2003. Jacked end-bearing piles in the soft alluvial sediments of Perth. *Australian Geomechanics*, 38(3): 123–133.
- Lehane, B.M., Schneider, J.A., and Xu, X. 2005a. A review of design methods for offshore driven piles in siliceous sand. UWA Report GEO 05358, The University of Western Australia, 105.
- Lehane, B. M., Schneider, J. A., and Xu, X. 2005b. The UWA-05 method for prediction of axial capacity of driven piles in sand. In International Symposium on Frontiers in Offshore Geotechnics, Perth. pp. 683–689.

- Lehane, B.M., Gaudin, C., and Schneider, J.A. 2005c. Scale effects on tension capacity for rough piles buried in dense sand, *Géotechnique*, 55(10), 709–719.
- Lehane, B.M., and White, D.J. 2005. Lateral stress changes and shaft friction for model displacement piles in sand, *Canadian Geotech. J.*, 42(4): 1039–1052.
- Lehane, B.M., Schneider, J.A., and Xu, X. 2007. Development of the UWA-05 design method for open and closed ended driven piles in siliceous sand, *Proc. GeoDevner 2007*, ASCE.
- McClelland, B., Focht, J.A., & Emrich, W.J. 1969. Problems in design and installation of offshore piles. *J. Soil Mech. Found. Div.*, ASCE, 95(SM6), 1491–1514.
- Meyerhof, G.G. 1956. Penetration tests and bearing capacity of cohesionless soils. *J. Soil Mech. and Foundation Div.*, ASCE, 82(SM1), Paper 886, 19.
- Paik, K., Salgado, R., Lee, J., and Kim, B. 2003. Behavior of open- and closed-ended piles driven into sands. *J. Geotech. Geoenviron. Eng.*, 129(4), 296–306.
- Potyondy, J.G. 1961. Skin friction between various soils and construction materials, *Geotechnique*, 11(4), 339–353.
- Randolph, M. F. 2003. Science and empiricism in pile foundation design. *Géotechnique*, 53(10), 847–875.
- Rix, G. J., and Stokoe, K. H. 1992. Correlation of initial tangent modulus and cone resistance. In *Proceedings of the International Symposium on Calibration Chamber Testing*, Potsdam, New York, pp. 651–362.
- Salgado, R., Lee, J. And Kim, K. 2002. Load tests on pipe piles for development of CPT-based design method. Final report, FHWA/IN/JTRP-2002/4.
- Schneider, J.A., and Lehane, B.M. 2006. Effect of width for square centrifuge displacement piles in sand, *Proc. Int. Conf. on Physical Modeling in Geotechnics*, Hong Kong, Taylor & Francis: 867–873.
- Schneider, J.A., Xu, X., and Lehane, B.M. 2007. Database assessment of CPT based axial pile design methods in siliceous sands: Part I – overview of methods, database and predictive performance. *J. Geotech. Geoenviron. Eng.*, submitted.
- Schmertmann, J.H. 1978. Guidelines for cone test, performance, and design. U.S. Federal Highway Administration, FHWATS-78209.
- Tabucannon, J.T. 1997. Shaft resistance on piles in sand, *PhD Thesis*, University of Sydney.
- Uesugi, M., and Kishida, H. 1986a. Influential factors of friction between steel and dry sands, *Soils and Foundations*, 26(2), 33–46.
- Uesugi, M., and Kishida, H. 1986b. Frictional resistance at yield between dry sand and mild steel, *Soils and Foundations*, 26(4), 139–149.
- Van Mierlo, W.C. and Koppejan, A.W. 1952. Lengte en draagvermogen van heipalen bouw. January.
- Vesic, A.S. 1967. A study of bearing capacity of deep foundations, *Final Report Project B-189*, Georgia Institute of Technology, Atlanta, GA, USA, March, 241 pp.
- Westgate, Z.J. 2006. Analysis of granular soil-structure interface evolution using particle image velocimetry, *MS Thesis*, University of Massachusetts-Amherst, 248.
- White, D.J., Sidhu, H.K., Finlay, T.C., Bolton, M.D., and Nagayama, T. 2000. Press-in piling: the influence of plugging on driveability. In *Proceedings of the 8th International Conference of the Deep Foundations Institute*, New York, pp. 299–310.
- White, D.J. and Bolton, M.D. 2004. Displacement and strain paths during plane-strain model pile installation in sand. *Géotechnique*, 54(6), 375–397.
- White, D.J., and Lehane, B.M. 2004. Friction fatigue on displacement piles in sand. *Géotechnique*, 54(10), 645–658.
- White, D.J. and Bolton, M. D. 2005. Comparing CPT and pile base resistance in sand. *ICE, Geotechnical Engineering* 158, 3–14.
- White, D.J., Schneider, J.A., and Lehane, B. M. 2005. The influence of effective area ratio on shaft friction of displacement piles in sand. *Proc., Int. Symp. Frontiers Offshore Geomech. ISFOG*, Perth, 741–747.
- Xu, X., and Lehane, B.M. 2005. Evaluation of end-bearing capacity of closed-ended pile in sand from CPT data. *Proc., Int. Symp. Frontiers Offshore Geomech. ISFOG*, Perth, 733–739.
- Xu, X., Schneider J. A. and Lehane B.M. 2005. Evaluation of end-bearing capacity of open-ended piles driven in sand from CPT data. *Proc., Int. Symp. Frontiers Offshore Geomech. ISFOG*, Perth, 725–731.
- Xu, X., Schneider, J.A., and Lehane, B.M. 2007. CPT-based design methods for end bearing of driven piles in siliceous sand. *Canadian Geotech. J.*, submitted.
- Xu, X., and Lehane, B.M. 2007. Numerical and experimental study of end bearing resistance in layered soil, *Géotechnique*, submitted.
- Xu, X., 2007. Investigation of the end bearing performance of displacement piles in sand, PhD thesis, the University of Western Australia.
- Åstedt, B., Weiner, L., and Holm, G. 1992. Increase in bearing capacity with time for friction piles in silt and sand. *Proc. Nordic Geotech. Meeting*, 411–416.

Recent advances in designing, monitoring, modeling and testing deep foundations in North America

C. Vipulanandan

Department of Civil and Environmental Engineering, University of Houston, Texas, U.S.A.

ABSTRACT: Based on the challenges in supporting structures on difficult ground conditions and advancement in various technologies, deep foundation engineering has seen rapid advances in designing, monitoring, modeling and testing in recent years. Full-scale tests coupled with innovative monitoring and numerical modeling has helped to better understand the behavior of deep foundations in difficult soils and rocks. Static and dynamic loading systems have been used to load relatively larger diameter single and group pile foundations and monitor the performances in various ground conditions. Construction and monitoring techniques have been improved to ensure the quality of augered cast-in-place piles. Osterberg load cell with better instrumentation have been used to understand the behavior of rock socketed drilled shafts in soft rocks. Tools are being developed to better characterize condition in the borehole of a drilled shaft using downhole penetrometer and laser based roughness profiler. Numerical methods are being used to model the behavior of single and group piles. There is increased interest in understanding the lateral behavior of piles under dynamic loading conditions. Nondestructive test methods are being used to investigate the integrity and bearing capacity of the piles. Load and Resistance Factor Design concept is used more and more in designing deep foundations.

1 INTRODUCTION

In recent years, studies have focused on understanding the behavior of driven piles, drilled shafts, augered cast-in-place (ACIP) piles and micropiles designed to carry much higher vertical and lateral static and dynamic loads with limited deflection in various geological conditions. Noteworthy improvement in recent times in north America include better understanding of the soil-pile interaction under static and dynamic conditions, development of computer codes to deal with complex loading and geological conditions, design methods and innovative instrumentation and monitoring systems used during construction and service conditions. Plastic composites and self consolidating concrete have been used in the construction of driven piles and drilled shafts respectively. With the complexity of the problems encountered in the field, it is critical that numerical methods must be used and this is particularly true when nonlinear soil models are used. More attention is paid to better quantify the load-settlement behavior of piles in addition to the bearing capacity.

Non-displacement augered cast-in-place (ACIP) piles are being increasingly used for supporting buildings, bridges, sound barrier walls and many other structures around the world because they can be installed

relatively rapidly with minimum environmental impact and have the flexibility to quickly adjust pile length for varying soil conditions as compared to the other deep foundation systems. Due to lack of understanding of ACIP pile behavior, in many instances, the design capacity of the ACIP pile must be verified by performing one or more full-scale load test on site before installing the production ACIP piles. Hence there is a need to better quantify the performance of ACIP piles in various soil conditions.

Compared to the drilled shafts and driven piles of equivalent size, augered cast-in-place (ACIP) piles can be installed more rapidly with relatively less disturbance to the surroundings in favorable geological conditions. Hence the installation procedure and the quality of the material used in the construction have significant effects on the behavior of the ACIP piles. Construction quality can be monitored using the automated monitoring system where the volume of grout pumped and the pressures are monitored with depth. Also the maximum and minimum pressure required to advance the auger was monitored with time. All these data can be used to control the quality of the pile installation. The grout used in the construction of ACIP piles is rich in cement and it is critical to monitor the curing of the pile with time in order to determine the development of residual strains in the pile

and to determine the appropriate time for load testing the pile.

A fair number of theoretical and empirical methods for analyzing load-displacement behavior have been proposed for the various types of deep foundations. These methods, however, seem not to be widely used in engineering practice mainly because the input data required is difficult to determine from the results of common site investigations. Since number of design procedures limit the deflection in deep foundation supporting load bearing structures, it is essential to predict the load-displacement behavior of piles based on the simple relationship of in-situ soil properties and dimensions of the pile.

Drilled shafts are used increasingly as foundations to support bridges and other transportation structures in many geographical areas in the U.S., where rock lies near the ground surface. Drilled shafts are constructed by excavating into the rock, forming a cylindrical socket, and constructing the socket with reinforced concrete. In general, clay shale rocks can be cemented, uncemented and/or with seams of bentonite or calcareous materials. Designing of the drilled shafts socketed in uncemented clay shale and weakly cemented sandstone is a challenge partly because only limited information is available in the literature on the ultimate unit side resistance and ultimate unit end bearing in soft rocks.

Recent advances in deep foundation engineering in North America are as follows:

- Full-scale testing, instrumentation (including Osterberg cell) and long-term monitoring of large diameter piles and pile groups (Rollins et al. 2004, Moon 2004, Paikowsky et al. 2005, Vipulanandan et al. 2005c, Fellenius, B.H. 2006, Vipulanandan et al. 2007a)
- Modeling the load-displacement behavior of piles (Kulhawy & Chen 2005, Vipulanandan et al. 2005a)
- Lateral behavior of piles and pile groups under static and seismic loading conditions (Rollins, 2003, Anderson et al. 2003, Ashour & Norris 2003, Ashour et al. 2004, Rollins et al. 2004)
- Behavior of rock socketed drilled shafts and augered cast-in-place piles (Kulhawy et al. 2005, Vipulanandan et al. 2005b, Vipulanandan et al. 2007b)
- Correlation between piles parameters and in-situ test methods (Samtani & Liu 2005, Vipulanandan & Kaulgud 2005a)
- Construction monitoring and pile materials (Vipulanandan et al. 2000, Iskander et al. 2001, Brown 2005; Brettmann & NeSmith 2005, Vipulanandan et al. 2007a)
- Nondestructive evaluation of piles (Hussain & Liking 2005)

- Reliability based design for piles (Kulhawy & Phoon 2002)
- Numerical modeling of pile and pile group behavior (Duncan et al. 2005, Sellountou et al. 2005, Tand & Vipulanandan 2005)

The overall objective of this paper was to highlight some of the advances in deep foundations in North America in recent years.

2 ACIP PILES

ACIP piles are becoming popular in both private and public sectors due to their rapid construction and environmentally friendly installation. Due to lack of design methods it was important to load test selected number of piles to verify the designed capacity and deflection in the pile. In recent years over 50 load tests have been performed on ACIP piles, as documented in the literature, with diameters in the range of 300 to 760 mm.

2.1 *Pile instrumentation*

In a recent study in central Texas, two 760 mm diameter ACIP piles, one socketed into very dense sand and the socketed into very hard clay, were instrumented to investigate the curing process and load distribution in the pile during the static load tests (Vipulanandan et al. 2007a). The monitoring of the grout curing process was important determine the earliest time for the static load test the ACIP piles. The vibrating wire strain gages were attached to the steel reinforcing cage and lowered into the grout filled bore hole to measure the temperature and strains at various locations in the pile. Total of 10 gages were installed axially at four different levels along the pile. Besides this, 2 strain gages were installed horizontally at two different locations. Because the strain gages had their sensors at the center of the vibrating wire strain gages, readings taken from these gages were from the center of the pile cross section. Instrumentation used in this pile can be seen in Figure 1 (Vipulanandan et al. 2007a).

2.2 *Construction monitoring*

One of the key concerns when using ACIP (also known as Continuous Flight Auger — CFA) piles is that the soil surrounding the pile not be decompressed during drilling. If the velocity of penetration is less than the critical velocity, decompression can occur.

In fact, decompression can occur even if the above condition is satisfied, if the soil being excavated is water-bearing sand with sufficient ground-water head to force the cuttings up the auger. A contractor must provide a drilling rig with sufficient torque and crowd to obtain the required velocity of penetration. This

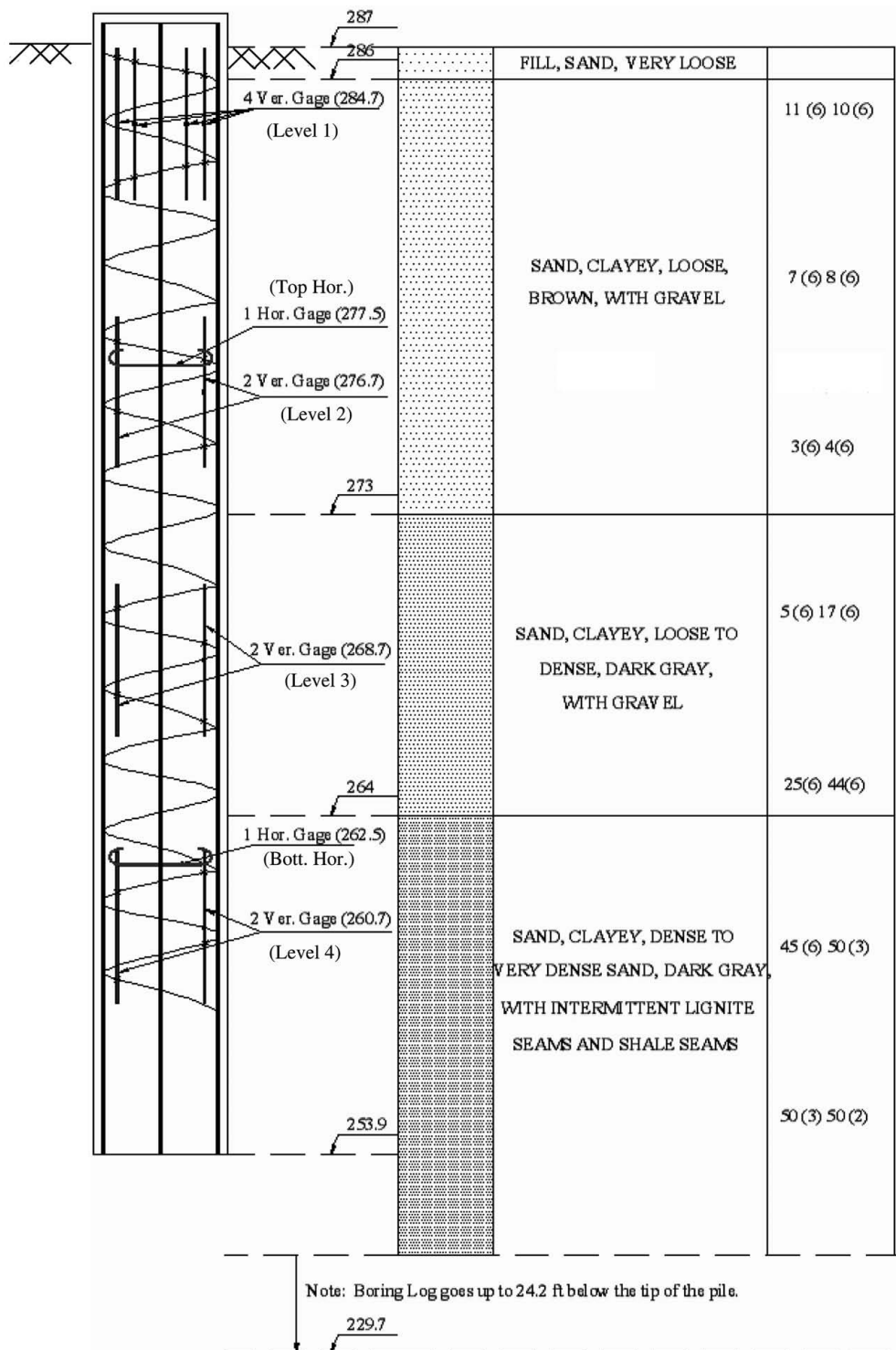


Figure 1. Instrumentation used in an ACIP pile and the geotechnical profile.

critical rate of penetration of the auger used was found to be 30 mm/sec with an auger revolution of 5 rpm which was held nearly constant during the drilling and the critical velocity is shown in Figure 2, and this condition was satisfied (Vipulanandan et al. 2007a). The drill rig used was capable to drill loose to very dense sand layers (Manufacturer's specification). Drill rig gearbox had a maximum torque of 50 kN.m (36,000 ft-lb.) and 4.45 kN (5000 lb.) total crowd. It can be observed (Figure 3) that the required torque for deepest layer augured was more than twice the top layer. It can be concluded that the TCP test data (TxDOT Geotechnical Manual, 2000) are in good agreement with the required torque values in terms of penetration resistance of the soil layers. Required torque to drill the soil increased significantly at approximately 4.6 m (15 ft) depth which was also the

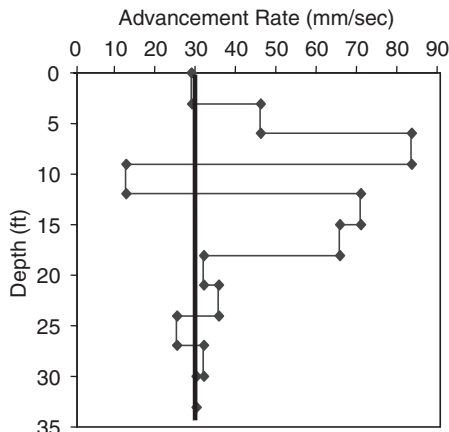


Figure 2. Advancement rate during drilling (1 m = 3.3 ft.).

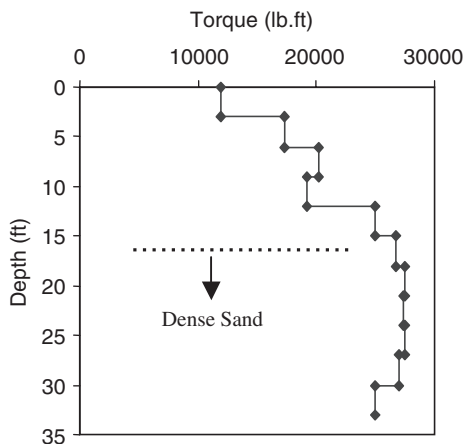


Figure 3. Applied torque to drill the bore hole (1 kip.ft = .135 kN.m).

starting depth for the dense sand according to the TCP test.

Pile integrity may be the most important aspect of the quality control item in an ACIP pile installation. It can directly affect the structural capacity of the pile or the soil resistance around the pile. The ratio of the actual volume of grout pumped to the theoretical volume of the pile is defined as the grout ratio. Minimum ratio suggested by the Deep foundation Institute is 1.15 (DFI 1994) which means 15% extra volume is required in addition to the nominal volume of the borehole. Pumped grout volume was measured for every 1 m (3 ft) withdrawal which was considered accurate enough to assure pile integrity. Figure 4 shows that the 1.15 grout ratio condition was satisfied at every depth except between 1–2 m (3–6 ft.) Grout ratio was 0.94 at this interval and not considered a problem since about 2.5 m (8 ft.) of grout head was used in the bore hole. The successfully performed pile load test after 7 days also proved that this was not a problem. Figure 5 shows the minimum and maximum grouting pressure measured during the grouting phase. The grout pressure level is important to prevent any soil collapse during the withdrawal of the auger. Maximum grout pressure was held almost constant and was around 1380 kN/m² (200 psi). Minimum grout pressure was fluctuating along the depth. The average minimum pressure was higher at deeper levels due to the higher soil confinement.

2.3 Curing

The Temperature readings with time are used to evaluate the strength gain of the grout. This technique is called the maturity method assumes that the strength is dependent both on temperature and time. In this

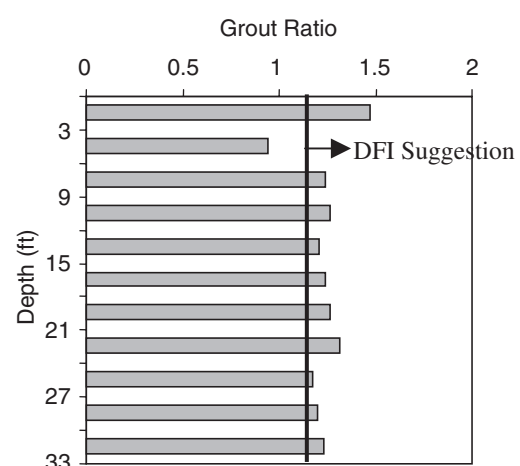


Figure 4. Pumped grout ratio by depth.

study the temperature was measured four times over a period of 7 days. Hence a nonlinear relationship was used to best approximate the temperature-time relationship (Eqn. 1). Integration the temperature-time relationship will give the maturity. A typical integrated curve for a vibrating strain gage is given in Figure 6.

$$T = \left[\frac{\frac{t}{t_p}}{q + (1 - p - q) \frac{t}{t_p} + p \left(\frac{t}{t_p} \right)^{\frac{(p+q)}{p}}} \right] T_p \quad (1)$$

where p, q are material parameters, T_p and t_p represent the peak temperature and the corresponding time respectively. Parameter "q" is defined as the ratio of

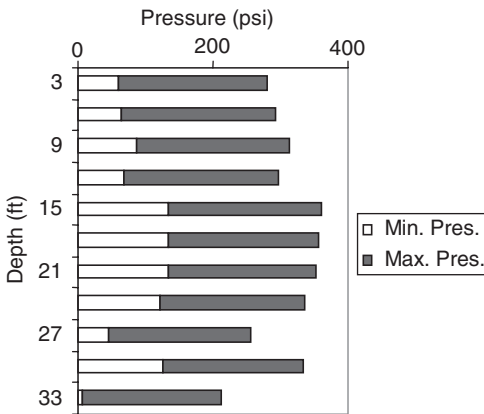


Figure 5. Applied grout pressures ($1 \text{ kPa} = 7 \text{ psi}$).

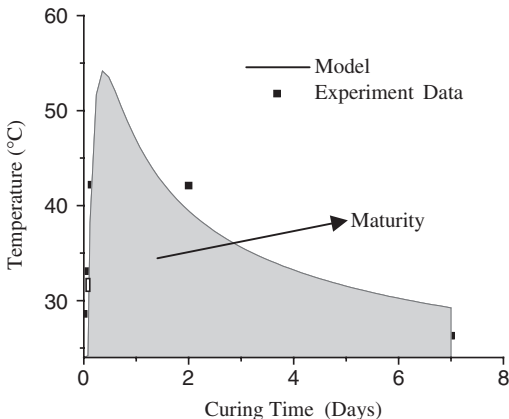


Figure 6. Typical time-temperature relationship and model prediction (Top Strain Gage Level).

secant slope at peak temperature to initial tangent slope ($0 < q < 1$ and $(p + q)/q > 0$).

Maximum and average temperatures measured in the pile were 63.15°C and 54.63°C respectively. Average time to reach the maximum temperature was 8.4 hours which was very similar for the entire pile. The maximum temperature measured was over 40°C higher than the surrounding ground temperature. Maximum and average maturities were $2667^\circ\text{C}\text{-hrs}$ and $2251^\circ\text{C}\text{-hrs}$ respectively. Similar to CB site, for both temperature and maturity, maximum values were obtained from the horizontal strain gages. A typical to an integrated curve for one strain gage is given in Figure 6 (Vipulanandan et al. 2007a).

Grout samples were collected from the site and tested under compression seven days after the installation of the pile. The $2'' \times 2''$ cube samples yielded an average strength of 4250 psi compressive strength and the average maturity was $2251^\circ\text{C}\text{-hrs}$. which agreed with the design chart published in the literature.

2.4 Residual strain

Average strain was computed at each level (Figure 1) by simply averaging the readings from the gages at each level and plotted with time in Figures 7 and 8 for vertical and horizontal gages respectively. Maximum residual strain was read at level 4 and it was about 90 microstrain in compression. Compression strains increased with time and were higher at deeper levels two days after casting. The tensile strains at the center of the pile may be due to temperature expansion at the center. General trend is almost same at the three bottom

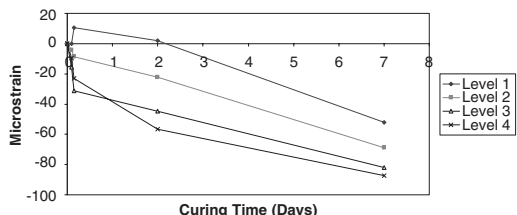


Figure 7. Variation of vertical strain at different levels with time.

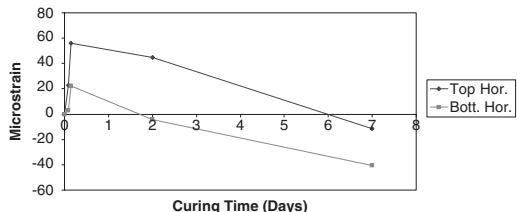


Figure 8. Variation of horizontal strain at different levels with time.



Figure 9. Load test on 760 mm diameter ACIP pile using a single beam with 8 reaction piles for a designed capacity of over 5 MN.

levels, but top level strain gages gave tension strain with an average 10 microstrain during the setting of the pile. Tension strains were more significant in the horizontal strain gages at the center. Top horizontal strain gage gave a maximum 60 microstrain tension deformation which had a decreasing trend with time. After 6 days it showed lower compression strains. Bottom horizontal strain gage behavior was more like top level vertical strain gages which were tension strain in the first two days then compression with a maximum value of 40 microstrain at the end of the seven days. The residual vertical strain in the pile after 7 days of curing was compressive and increased with depth from 40 to 80 microstrains.

2.5 Grout tests

Quality of the grout was evaluated in the field using the flow cone method and flow cylinder method. Some grout mixes had problem with the flow cone method since the opening was limited to 19 mm. Cube and cylindrical samples were collected to measure the strength at specified time periods (Vipulanandan et al. 2007a).

2.6 Load test

Since expected pile capacity was high, eight reaction piles were used for the full-scale load test (Figure 9). Figure 10 shows the entire measured load displacement behaviors including the unloading phases at both the test sites. The pile head load at a displacement of 9 mm (0.36 in) was 320 tons in East Cohino Bayou (ECB) (very dense sand) and 380 tons for the hard clay site. The pile at the Cochino Bayou (CB) site which was seated on hard clay soil showed a stiffer behavior compared to the pile seated on very dense sand. The end bearing at CB was 82 tons (about 25.6% of the total load) and at ECB, it was 40.5 tons which was about 13% of the total load. Pile base

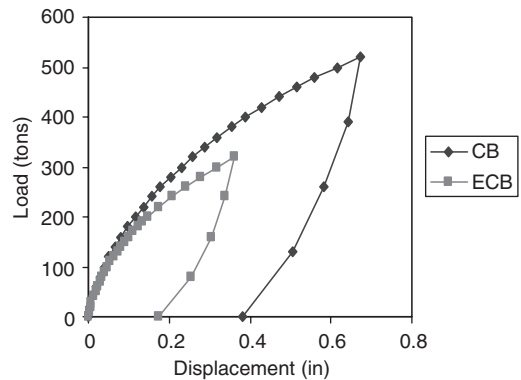


Figure 10. Load-displacement relationships for ACIP piles.

seated on hard clay gave a stiffer end bearing response compared to the pile seated on very dense sand. The pile in hard clay was loaded to 520 ton at a displacement of 16 mm (0.66 inches). Based on the test results, two highway bridges were built using 760 mm diameter ACIP piles. These two bridges are the second and third highway bridges totally support on ACIP piles in Texas and in the U.S.

2.7 Modeling load-displacement relationships

Based on the inspection of the load (Q)-displacement (ρ) relationships for the ACIP piles, hyperbolic equation has been proposed which can be represented as follows:

$$Q = \frac{\rho}{A + B\rho} \quad (2)$$

The hyperbolic relationship is preferred over exponential equations and bi-linear relationships due to the simplicity in using the equation and correlating of the two parameters to geotechnical properties at the pile location. This does not agree with the observation of Kulhawy (2004), where the initial portion of the load-displacement relationship was assumed to be linear. The entire system of pile material, soil and soil-pile interaction are nonlinear and hence initial load-displacement relationship will be nonlinear as observed in number of studies (Vipulanandan & Kaulgud 2005).

The parameter A is the reciprocal of the initial tangent (Equation (1)) but the initial tangent is not very easy to determine since it is very sensitive to the construction method. Hence an alternative parameter must be defined and Equation (2) can be further modified by rearranging the terms and obtaining a relationship with non-dimensional terms as follows:

$$\frac{Q}{Q_{ult}} = \frac{\rho/d}{C + \rho/d} \quad (3)$$

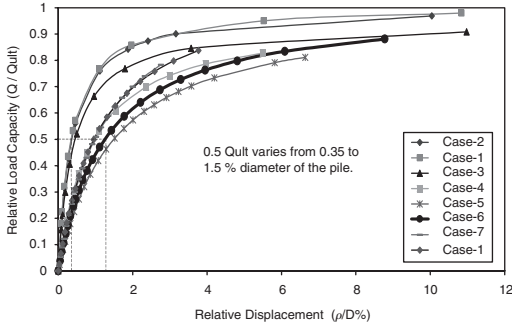


Figure 11. Relative load capacity versus relative displacement.

When $Q = 0.5Q_{\text{ult}}$ the displacement $\rho = \rho_{50}$, then it can be shown that $C = \rho_{50}/d$. Hence Equation (3) can be written as follows:

$$\frac{Q}{Q_{\text{ult}}} = \frac{\rho/d}{\rho_{50}/d + \rho/d} \quad (4)$$

Figure 11 shows the typical plot of Q/Q_{ult} versus ρ_{50}/d for several ACIP piles and the ρ_{50}/d varied from 0.35 to 1.5%. If the Q_{ult} and ρ_{50}/d can be estimated correctly for the site from geotechnical data then $Q-\rho$ relationship for the ACIP pile can be obtained using Eqn. (4).

2.8 Estimation of Q_{ult}

The variation of Q_{ult} with CPT- q_c is shown in Fig.8. Based on limited data, the relationship can be represented as a linear relationship as follows:

$$Q_{\text{ult}} / LD = 0.019q_c + 0.2 \quad (5)$$

or as hyperbolic variation and can be represented as follows:

$$\frac{Q_{\text{ult}}}{LD} = \frac{q_c}{7.8 + 1.9q_c} \quad (6)$$

The predictions of Q_{ult} using the above two relationships are compared in Vipulanandan and Kul (2005). The ratio of pile capacity at 5% deflection (using hyperbolic relationship) to ultimate capacity varied from 0.79 to 0.97 with mean of 0.89. The ratio of pile capacity at 10% deflection (using the hyperbolic relationship (Equation (4))) to the ultimate capacity varied from 0.88 to 1.03 with mean of 0.96.

2.9 Estimation of ρ_{50}/d

It should be noted that the value of ρ_{50}/d will depend on many factors including interface conditions,

stress-strain behavior of the surrounding soils, soil characteristics, in-situ stresses in the ground, construction methods and loading procedures. For the ACIP piles investigated in this study, ρ_{50}/d varied from 0.35% to 1.5%. The variation of ρ_{50}/d with CPT- q_c and friction ratio was investigated. Of the two CPT parameters investigated, better correlation was observed with friction ratio and the relationship is as follows:

$$\rho_{50}/d \% = \frac{0.015}{f_s/q_c} \quad (7)$$

Hence using the CPT test results both parameters for the non-dimensional hyperbolic model (Eqn. (4)) can be estimated and hence the load-displacement relationship can be predicted.

2.10 Rock socket

ACIP piles are being socketed in limestone in Florida and clay shale in Texas. In Texas, the Texas Cone Penetrometer (TCP) is used to characterize the site. The TCP test that is performed by driving a 3.0-inch diameter, 60-degree solid steel cone into rock at the bottom of a standard borehole. The cone is affixed to the bottom of a string of steel rods and driven by a 170-pound hammer dropped 24 inches onto a flat steel plate at the head of the steel rod successively for 100 blows. The driving energy per blow is similar to a standard penetrometer test (SPT), and the TxDOT cone is used in preference to the split spoon because of its robustness. The cone penetration resistance is the distance that the tip of the cone advances in 100 blows. The test procedure is available in Tex Method 132-E (TxDOT 2000). A correlation between unconfined compressive strength (q_u) and TCP was developed using 218 data for uncemented clay-shale in Dallas, Texas (Nam 2004). The variation of unconfined compressive strength with TCP is shown in Figure 12. The strength varied from 100 to 3000 kPa, the relationship can be represented as follows:

$$q_u (\text{kPa}) = 7500[\text{TCP}(mm)]^{-0.4} \quad (8)$$

Most of the load tests were performed to a displacement of less than 5% of diameter and hence a model should be used to best estimate the ultimate capacity of the piles at appropriate deflection. A preliminary review of the load-displacement relationship from load test data may be represented by hyperbolic relationship and will be verified in this study (Vipulanandan & Kaulgud 2005b).

The ratio ρ_{50}/d for all eight ACIP piles socketed in clay-shale varied from 0.5% to 1.2% as shown in Figure 13, the variation of ρ_{50}/d is relatively small considering the geological diversity of the cases studied

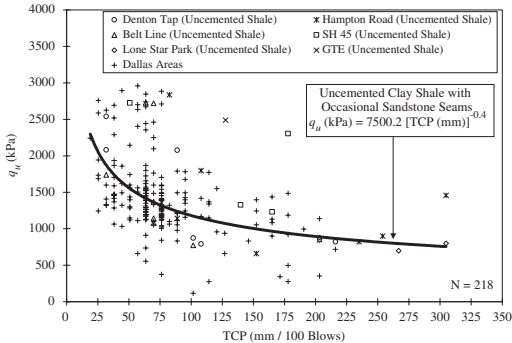


Figure 12. Correlation between TCP (Texas Cone Pentrometer) and q_u (Modified after Nam 2004).

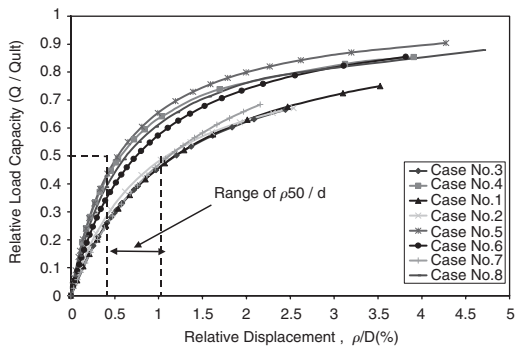


Figure 13. Variation of relative displacement and relative load capacity.

and load capacities achieved by the various piles. Theoretically, Q will reach to ultimate value when displacement is at infinity (Eqn.4).

With the limited load test data on ACIP piles socketed in clay-shale the variation of normalized ‘rough estimate of peripheral friction factor’ ($Q_{ult}/q_u * \Pi^* D^* L$) with L/D ratio of the rock socket can be expressed as follows,

$$\frac{Q_{ult}}{q_u \Pi^* D^* L} = -0.11(L/D) + 0.96 \quad (9)$$

The term ‘ $q_u * \Pi^* D^* L$ ’ represents the maximum side friction that can be generated in the rock socket when $\alpha = 1$, ($f_s = \alpha q_u$). Further more to mobilize the ultimate skin friction (f_s) in the case of the bored piles it requires displacement of 0.5–2% of pile diameter.

The variation of Q_{ult} with TCP can be represented as follows,

$$\frac{Q_{ult}}{LD} = \frac{99216}{TCP} \quad (10)$$

By knowing in-situ TCP penetration resistance (per 100 blows) and assuming the length and diameter of pile, Eqn. 10 can be used to determine the Q_{ult} .

The variation of ρ_50/d with q_u can be expressed as follows,

$$\rho_{50}/d = \frac{15.8}{q_u/P_{1,Atm}} \quad (11)$$

Hence both parameters for the non-dimensional hyperbolic model can be estimated from the rock strength, TCP and pile dimensions.

3 DRILLED SHAFTS

3.1 Rock socket

In order to understand the load transfer within the rock socket, studies are being performed using Osterberg Load cell and other instruments. During a load test, the strain distribution along the socket was measured using the sister bars. The Osterberg Cell was used to measure the load. Forty-eight (48) days after constructing the test sockets, axial load was applied to the rock socketed drilled shaft in 100 kN (11.2-ton) increments every five minutes until the plunging failure was observed. It was clear that both the test and reaction sockets reached plunging failure at a load of 2.7 MN. The maximum load for the test socket was determined to be about 2.5 MN at the upward movement of 10 mm (0.4 inches) and downward movement of 60 mm inches by taking double tangent lines. Based on the test data, load transfer distributions were obtained along the shaft and socket.

From this information the distribution of maximum side resistance and base resistance were determined using the measured qualities. The corresponding side and base deflections were measured at the top plate and bottom plate of the Osterberg Cell. Also, the unit side load transfer curves, the so-called “ $f-w$ ” curves, were developed according to the O’Neill and Reese method (1999). The locations for developing the $f-w$ curves were at the middle of the test and reaction shafts. The local displacement w at the middle of the shafts was determined by subtracting the elastic shaft shortening from the measured displacement at the Osterberg Cell (Moon 2004).

3.2 Bearing capacity in soft rock

Drilled shafts are frequently used as foundations to support bridges and other transportation structures in many geographical areas around the world, where rock lies near the ground surface. Drilled shafts are constructed by excavating into the very soft rock, forming

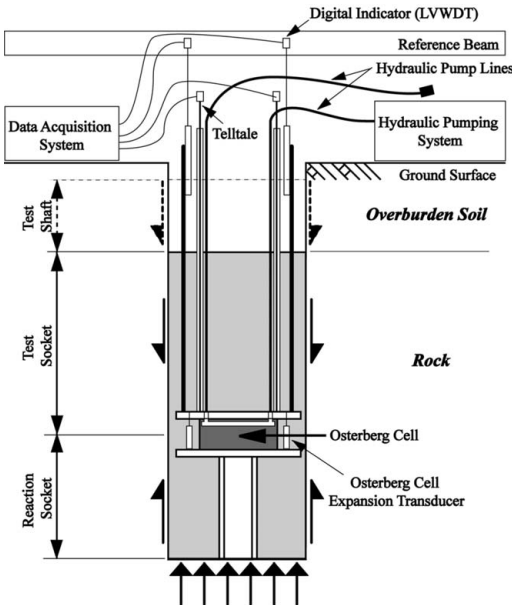


Figure 14. Osterberg cell used in rock socket test.

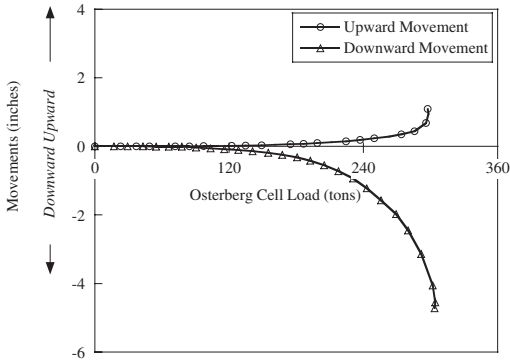


Figure 15. Upward and downward movements versus load (Osterberg cell) at the test site (1 ton = 10 MN; 1 inch = 25 mm).

a cylindrical socket, and constructing the socket with reinforced concrete. Designing of drilled shafts socketed in soft rock (compressive strength less than 2.5 MPa) is a challenge partly because only limited information is available in the literature on the ultimate unit end bearing in soft rocks.

A total of 21 documented cases were used to develop the relationship between the ultimate unit end bearing (q_{ult}) and the unconfined compressive strength of soft rock (q_u), unconfined compressive strength less than 2.5 MPa. The CASES are summarized in Vipulanandan et al. (2007a), with information on

test location, type of rock, date of test, shaft geometry, rock strength and ultimate unit end bearing capacity.

(i) Ultimate Unit End Resistance (q_{ult})

The unconfined compressive strength of soft rocks in which the load tests were performed varied from 1.44 tsf (0.14 MPa) to 26 tsf (2.5 MPa) the ultimate unit end bearing varied from 10 tsf (0.96 MPa) to 96 tsf (9.2 MPa). The ratio of q_{ult} -to- q_u varied from 2.39 to 19.82 with an average of 5.71.

Past studies have investigated the relationship between q_{ult} and unconfined compressive strength (q_u) of soft rocks. The relationship generally used is as follows:

$$q_{ult} = \alpha_q (q_u)^m \quad (12)$$

Where, magnitudes of parameters m and α_q depend on the rock type, unconfined compressive strength and defects in the rock. Based on the least square fit of the 21 data points the nonlinear relationship shown in Fig. 1 is as follows:

$$q_{ult} = 13.1 \cdot (q_u)^{0.56} \quad (13)$$

Where q_{ult} and q_u are in tsf (1 tsf = 98.9 kPa).

Limited studies have suggested using Eqn. (3) with $m = 1$ for relating the ultimate unit end resistance to the unconfined compression strength (Rowe and Armitage 1987). Based on the linear least square fit of the data (Fig. 1) for the soft rocks in this study, the relationship was as follows:

$$q_{ult} = 3.80 q_u = N_c C \quad (R = 0.57 \text{ and } N = 21, N_c = 2\alpha_q) \quad (14)$$

where q_{ult} = ultimate unit base resistance in tsf and N_c is the end bearing capacity factor. It must be noted that Rowe & Armitage (1987) suggested a linear relationship with the parameter α_q equal to 2.5 (or N_c equal to 5). Vipulanandan & Moon (2005) suggested a linear relationship (based on 4 data) for uncemented clay shale in the Dallas, Texas area with the parameter α_q equal to 4.04 (or N_c equal to 8.08).

3.3 Core hole effect

Due to uncertainty in characterizing the soft rock below the bottom of the bore hole a number of states including Alabama, Colorado, Connecticut, Florida, Georgia, Hawaii Kansas and Texas require a core-hole length of 1.7 m (5 ft) beyond the bottom of the shaft. It is of interest to note that a few SDOTs such as Arizona and New York don't have any recommendation regarding core-holes. Also no diameter for the core holes are specified, but in practice diameter of 50 mm (2 inch) or higher are used. A commercially

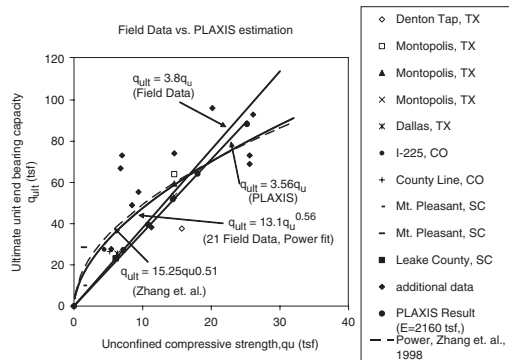


Figure 16. Experimental and numerical analyses relationships between q_{ult} and q_u for soft rocks.

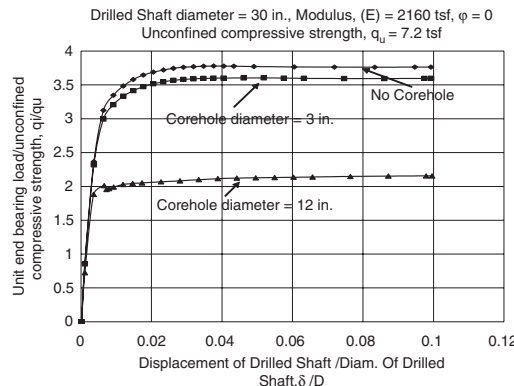


Figure 17. Effect of core-hole diameter on the normalized unit end bearing displacement relationship (1tsf = 0.096 MPa).

available geotechnical finite element program (PLAXIS) was used to develop the FEM models (Vipulanandan et al. 2007b).

(i) No Core-hole

The effects of rock cohesion and friction angle on α_q ($N_c/2$) were investigated. A typical response (unit end bearing versus displacement) for a rock with cohesion of 3.6 tsf (0.34 MPa) is shown in Figure 4. By varying the cohesion, the different ultimate unit end bearing capacities were determined. The relationship between q_{ult} and undrained shear strength of rock was approximated with a linear relationship. The α_q factor for the soft rock with zero friction ($\phi = 0$) and zero dilatancy ($\psi = 0$) was 3.56 (Figure 17). The α_q (from FEM) was 6.3% lower than the value obtained from the field tests. When the friction angle was increased to 20° , the relationship between q_{ult} and undrained shear strength of rock was linear and the N_c factor

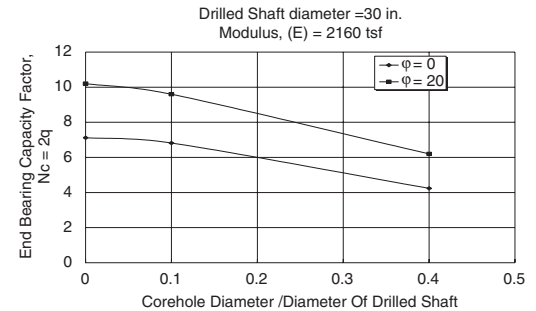


Figure 18. Effect of open core-hole diameter on the N_c factor (1tsf = 0.096 MPa).

increased to 10.2, an increase of 43% over the no friction case.

(ii) With Core-hole

The effects of rock cohesion, friction angle and core-hole diameter on the N_c factor were investigated. The relationship between q_{ult} and undrained shear strength was linear. The core-hole length was 5 ft (1.6 m). The N_c factor for the soft rock with zero ($\phi = 0$) and 20° friction reduced with core-hole diameter (Figure 18).

When the open core-hole diameter was 0.1D, the N_c factor was reduced by 4% and 6% for friction angles of zero and 20° respectively. When the core-hole diameter was 0.4D the N_c factor was reduced by about 40% in both cases. It must be noted that the trends observed in this study are very much related to constitutive relationship used for the rock behavior.

3.4 Downhole penetrometer

During construction of deep foundation in soft rock layers under hard soils, it is essential to locate the rock stratum, especially when drilling with slurry. When slurry is used for drilling, the bottom of the borehole cannot be seen; thereafter soil cuttings cannot be differentiated from soft rock. A new static penetrometer, known as a Downhole Penetrometer, is a simple mechanical device that is attached to the bottom of the Kelly bar to identify rock stratum. The downhole penetrometer is now being field calibrated to be used to identify the soil or rock strata in the boreholes.

3.5 Laser borehole roughness profiler (lbrp)

One of the factors known to affect the side resistance in a rock socket is the roughness of the borehole wall. Roughness was profiled using a laser borehole roughness profiler (LBRP). However, the laser borehole roughness profiler (LBRP) needed to be adapted to operate off the Kelly bar of a drill rig, and a laser-based

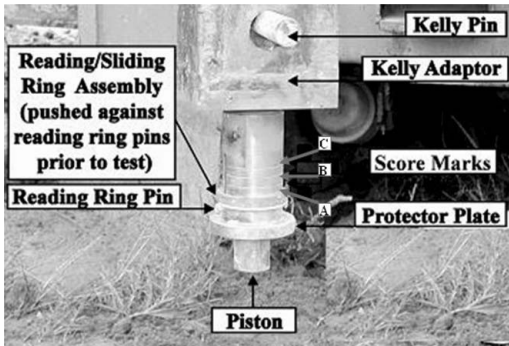


Figure 19. Downhole penetrometer attached to the Kelly bar.

technique for accurately recording the depth had to be developed (Moon 2004). The laser borehole roughness profiler (LBRP) was based on the laser triangulation principle. The hardware included a laser generator, a position sensitive device (PSD) as laser detector, signal processing circuits, laser control circuits, data acquisition, and digital control units. The distance measuring device was attached to the Kelly bar to record the vertical distance. The laser borehole roughness profiler (LBRP) measured the roughness at a speed of 100-kilo samples per second while the Kelly bar moved up from the bottom of the borehole.

The system was calibrated in the laboratory and found to have an accuracy of approximately 0.01 inches on both vertical distance and interface roughness (radial distance). It was then tested under field conditions and found to provide reasonable roughness profiles of a borehole.

4 DRIVEN PILES

4.1 Lateral load test on pile groups

To improve the understanding of lateral resistance of pile group, a series of lateral load tests were performed on a full-scale pile group using static and dynamic loads. In the cyclic static pile group test, 9 steel pipe piles (610 mm diameter) spaced 3.0 pile diameters on centers, were placed in clay. The load was applied using two 1.3 MN hydraulic jacks. During the static test, load was cycled fifteen times to evaluate the drop in capacity under repeated loading and the formation of gap. The peak load typically reduced by 15% from the initial cycle to the final cycle. There was significant drop in resistance in the trailing row compared to the leading row. The dynamic load was applied using the Statnamic system which produced a lateral force up to 3.5 MN (345 tons) in about 15 seconds. Several combinations of static and dynamic loading conditions were investigated. When the dynamic loading followed

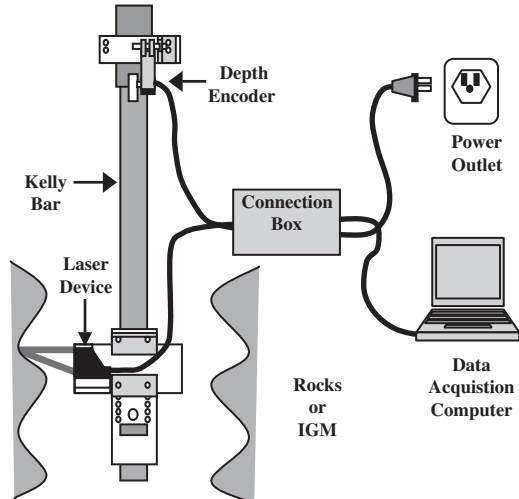


Figure 20. Schematic of Laser Borehole Roughness Profiling System hardware.

the static loading, the dynamic lateral resistance was the same as the static resistance. In the cases when dynamic loading was applied before the static loading, the dynamic resistance was 30 to 60% higher than the static resistance. The group loading reduction effects were not significant during the dynamic loading as they were for the static loading (Rollins et al. 2004).

4.2 Fiber-reinforce (FRP) piles

The durability of concrete and corrosion of steel are serious hindrance in constructing in aggressive soil and waterfront environments. Composite piles are being used for waterfront barriers and bearing piles for light structures. Most composite piles are made of high density polyethylene with glass or steel reinforcement. Fiber-reinforced polymer (FRP) composite represents an alternative material without many of the durability disadvantages of traditional materials. But the driving of the piles can become a challenge because of the mechanical properties of the pile (Iskander et al. 2001). The recycled FRP piles can be a solution to the sustainable engineering concept that is becoming a popular approach.

5 NONDESTRUCTIVE TESTS

The quality of the deep foundations must be evaluated through various stages of construction and also monitored during its service life. Standardized nondestructive methods are being used more widely in evaluating the structural integrity and load capacity of

ACIP piles, concrete piles, concrete filled steel pipe piles, steel piles and timber piles. The ASTM standards that are of relevance are as follows: ASTM D-5882 – Low-strain integrity testing; ASTM D-6760 – Cross-hole sonic logging; and ASTM D-4945 – Dynamic load testing. Extension of the basic methods is being investigated with improved instrumentation and time-dependent computational tools (Hussein & Likins 2005). Also wireless methods are being used for collecting and transmitting data.

6 RELIABILITY DESIGN

Load and Resistance Factor Design (LRFD) is being considered as an alternative design for the working or allowable stress design (WSD/ASD). The LRFD requires that all limit states to be checked using specific multiplier-factor format involving load and resistance factors. The LRFD is similar to the “Limit State Design” in Canada and the partial factor approach used in Europe, although a different multiple-factor format involving factored soil parameters is used. All these approaches primarily redistribute the original global factor of safety into separate load and resistance factors (or soil parameter partial factor). There is increasing interest in introducing more reliability based factors for loads, soil parameters, calculation models and factors of safety (Kulhawy & Phoon 2002).

7 NUMERICAL MODELING

7.1 Construction and performance

Construction processes are being modeled to better understand the changes in the ground stress conditions and its effect on the ultimate bearing capacity of ACIP piles (Sellountou et al. 2005). Load-displacement behavior of drilled shafts in slickenside clays were investigated using the finite element method. In this modeling, suction effect, slickenside clay behavior, soil strength, permeability and in-situ stress conditions were investigated (Tand & Vipulanandan, 2005).

7.2 Laterally loaded group piles

Although p-y method, elastic continuum and finite element analysis are used for analysis of laterally loaded pile behavior new models are being developed to handle more complex ground conditions such as layered soils. The current version of Strain Wedge Method (SWM) programs allow consideration of the behavior of piles and shafts and the pile or shaft cap in layered soil taking into account the nonlinear material behavior of the pile as well as the soil and the development of the associated p-y curves including

partial or full liquefaction in sand layers. AASHTO now recognizes SWM as an alternative to traditional p-y curve solutions (Ashour et al. 2004, Ashour & Norris 2003). Effect of pile head fixity on the behavior of laterally loaded piles has been investigated (Duncan et al. 2005).

8 CONCLUSIONS

Due to increasing demand for deep foundations to support larger and larger loads in unfavorable ground conditions there has been notable amount of growth in many areas has resulted in growth in many areas. Based on the information collected on the recent development in deep foundations in North America, following conclusions can be advanced:

- (1) Full-scale load tests are not only used to verify the load-displacement relationships for various types of piles but also help understand the load transfer mechanisms based on the type of construction. Osterberg Load cells are increasingly used for load tests.
- (2) Monitoring the important parameters (torque, rate of advance, grout pressure and volume and curing temperature) during the installation of the ACIP pile is critical to ensure quality. Flow cylinder and flow cone are being used to quantify the flow properties of the grout. Cubic and cylindrical specimens are used to determine the compressive strength of grout used in ACIP piles.
- (3) Hyperbolic relationship can be used to represent the load-displacement behavior of ACIP piles in soils and in the rock socket. Model parameters have been related to the in-situ test parameters.
- (4) Nondestructive tests methods are being increasingly used in determining the integrity and capacity of the piles.
- (5) Numerical methods coupled with different concepts are being used model the behavior of piles and pile groups in complex ground conditions. Strain wedge models the behavior of laterally loaded piles in layered soils.
- (6) Load and Resistance Factor Design (LRFD) are being used in designing deep foundations.
- (7) Downhole penetrometer and laser borehole roughness device can become very helpful tools to better quantify the condition in the bore-hole base and side wall before concreting.

ACKNOWLEDGEMENT

The study was supported by the Center for Innovative Grouting Materials and Technology (CIGMAT) at the University of Houston, Houston Texas. The sponsor is not responsible for any of the findings in this study.

REFERENCES

- Abu-Hejleh, N. & Attwooll, W. J. 2005. Colorado's Axial Load Tests on Drilled Shafts Socketed in Weak Rocks: Synthesis and Future Needs, *Report # CDOT-DTD-R-2005-4*, Colorado Department of Transportation Research Branch, July, Denver, CO.
- Anderson, J.B., Townsend, F. C., & Grajales, B. 2003. Case Histories Evaluation of Laterally Loaded Piles. *Journal of Geotechnical & Geoenvironmental Engineering*, ASCE, 129(3): 187–196.
- Ashour, M., Pilling, P. & Norris, G. 2004. Lateral Behavior of Pile Groups in Layered Soils. *Journal of Geotechnical & Geoenvironmental Engineering*, ASCE, 130(6): 580–592.
- Ashour, M. & Norris, G. 2004. Lateral Behavior of Pile Groups in Layered Soils. *Journal of Geotechnical & Geoenvironmental Engineering*, ASCE, 129(6): 404–414.
- Brown, D. A. 2005. Practical Considerations in the Selection and Use of Continuous Flight Auger and Drilled displacement Piles. C. Vipulanandan & F. Townsend (eds), *GSP 132, Advances In Deep Foundations*, ASCE. (CD-ROM).
- Brettmann, T. & NeSmith, W. 2005. Advances in Auger Pressure Grouted Piles: Design, Construction and Testing. C. Vipulanandan & F. Townsend (eds), *GSP 129, Advances In Deep Foundations: Construction, Design, And Testing-In Memory of Michael W. O'Neill*, ASCE: 290–307.
- DFI 1994. Augered Cast-in-Place Manual, Deep Foundation Institute, Sparata, NJ, 29 pp.
- Duncan, M., Robinette, M. & Mokwa R. L. 2005. Advances in Auger Pressure Grouted Piles: Design, Construction and Testing. C. Vipulanandan & F. Townsend (eds), *GSP 129, Advances In Deep Foundations: Construction, Design, And Testing-In Memory of Michael W. O'Neill*, ASCE: 235–250.
- Fellenius, B. H. 2006. Results from Long-term Measurement in Piles of Drag Load and Downdrag. *Canadian Geotechnical Journal*, 43(4): 409–430.
- Frizzi, R.P. & Meyer, M.E. 2000. "Augercast Piles – South Florida Experience", New Technological and Design Developments in Deep Foundations, *Proceedings of sessions of Geo-Denver 2000 held in Denver, Colorado, August 5–8, 2000*, edited by Norman Dennis, Jr., Ray Castelli and Michael W. O'Neill: 382–395.
- Hussein, M. H. & Liking, G. 2005. Deep Foundations Quality Control and Quality Assurance Testing Methods. *Journal of Florida Engineering Society*: 12–16.
- Iskander, M., Hanna, S. & Stachla, A. 2001. Drivability of FRP Composite Piling. *Journal of Geotechnical and Geoenvironmental Engineering*. 127(2): 169–176.
- Kulhawy, F. H. & Phoon, K. K. 2002. Observations on Geotechnical Reliability-Based Design Development in North America. *Fndn. Design Codes & Soil Investigation in View of Intl. Harmonization & Performance Based Design*, Ed. Y Honjo, O Kusakabe, K Matsui, M Kouda & G Pokharel, Balkema, Lisse-Netherlands: 31–48.
- Kulhawy, F.H. 2004. On the Axial Behavior of Drilled Foundations", *GeoSupport 2004: Drilled Shafts, Micropiling, Deep Mixing, Remedial Methods, & Specialty Foundation Systems (GSP 124)*, Ed. JP Turner & PW Mayne, ASCE, Reston: 34–51.
- Kulhawy, F. H., Prakoso, W. A. & Akbas, S.O. 2005. "Evaluation of Capacity of Rock Foundation Sockets", *Alaska Rocks 2005 (Proc., 40th US Symp. Rock Mech.)*, Ed. G Chen, S Huang, W Zhou & J Tinucci, Anchorage, Alaska, Paper 05–767, 8 p. (CD-ROM).
- Moon, N. S., O'Neill, M. W. & Vipulanandan, C. 2004. Correlation between Texas Cone Penetrometer (TCP) Values and the Compressive Strength of Clay Shale in Texas. Proceeding. *CIGMAT 2004 Conference and Exhibition*, Houston, Texas (<http://www2.egr.uh.edu/civeb1/CIGMAT/04-poster/12.pdf>).
- Moon, N. S. 2004. Improved Design for Drilled Shafts in Rocks. *Ph.D. Dissertation*, Department of Civil and Environmental Engineering, University of Houston, Houston, Texas.
- O'Neill, M. W., & Reese, L. C. 1999. Drilled Shafts: Construction Procedures and Design Methods. *FHWA Publication No. FHWA-IF-99-025*. Department of Transportation, Federal Highway Administration, Office of Implementation, McLean, VA.
- O'Neill, M. W., Vipulanandan, C., Ata, A. & Tan, F. 1999. *Axial Performance of Continuous Flight Auger Piles for Bearing, Project Report No. 7-3940-2*, Texas Department of Transportation, Austin, Texas, 253 pp.
- O'Neill, M. W., Ata, A., Vipulanandan, C. & Yin, S. 2002. Axial Performance of ACIP Piles in Texas Coastal Soils. *Deep Foundation Congress 2002, GSP 116*, ASCE: 1290–1304.
- Paikowsky, S.G, Hajduk, E. L. & Hart, L. J. 2005. Comparison Between Model and Full Scale Pile Capacity Gain in Boston Area. C. Vipulanandan & F. Townsend (eds), *GSP 132, Advances In Deep Foundations*, ASCE. (CD-ROM).
- Rollins, K. M., Olsen, R. J., Garrett, B. H. & Broderick, R. D. 2004. Dynamic Lateral Load Behavior of a Full-Scale Pile Group. SDEE/ICEGE.
- Rollins, K. M. 2003. Response, Analysis and Design of Pile Groups Subjected to Static and Dynamic Lateral Loads, *Final Project Report*, Utah Department of Transportation 350 p.
- Rowe, R.K. & Armitage, H.H. 1987. A Design Method For Drilled Piers in Soft Rock. *Canadian Geotechnical Journal*, 24: 126–142.
- Sellountou, E. A., O'Neill, M. W. & Vipulanandan, C. 2005. Construction effects on ACIP Pile Behavior in Texas Coastal Soils. C. Vipulanandan & F. Townsend (eds), *GSP 132, Advances In Deep Foundations*, ASCE. (CD-ROM).
- Tand, K. & Vipulanandan, C. 2005. Modeling the Load-Displacement Behavior of Underreamed Footings in Jointed Clays Using FEM. C. Vipulanandan & F. Townsend (eds) *GSP 129, Advances In Deep Foundations: Construction, Design, And Testing-In Memory of Michael W. O'Neill*, pp. 290–307.
- TXDOT 2000. *Geotechnical manual (online version)*, Texas Dept. of Transportation, Bridge Division, Austin, Texas.
- Vipulanandan, C., O'Neill, M. W., & Weng, Y. 2000. Mechanical Properties and Chemical Resistance of Auger Grout, *Geotechnical Special Publication, No. 100*, ASCE: 433–446.
- Vipulanandan, C., Kim, M. G., & O'Neill, M. W. 2004. *Axial Performance of Continuous Flight Auger Piles for Bearing, Project Report No. 7-3940-2*, Texas Department of Transportation, Austin, Texas, 253 pp.

- Vipulanandan, C., Kim, M. G., & O'Neill, M. W. 2004 Axial Performance of Continuous Flight Auger Piles for Bearing, Project Report, *CIGMAT 2004-6*, 253 pp. <http://cigmat.cive.uh.edu>.
- Vipulanandan, C., Tand, K. & Kaulgud, S. 2005a. Axial Load-Displacement Relationship and CPT Correlation for ACIP Piles In Texas Gulf Coast Soils. C. Vipulanandan & F. Townsend (eds), *GSP 132, Advances In Deep Foundations: Construction, Design, And Testing*, ASCE. (CD-ROM).
- Vipulanandan, C. & Kaulgud, S. 2005b. Behavior of ACIP Piles Socketed in Clay Shale. C. Vipulanandan & F. Townsend (eds), *GSP 129, Advances In Deep Foundations: Construction, Design, And Testing-In Memory of Michael W. O'Neill*, (CD-ROM).
- Vipulanandan, C. & Moon, N. 2005c. Case Studies on Testing Drilled Shafts Socketed In Uncemented Clay Shales in Texas, *Proceedings, Geo³*, ADSC, Dallas, Texas: 259–270.
- Vipulanandan, C. Liu, R. & Moon, N. S. 2005c. Improved Design for Drilled Shafts in Rocks, *Final Report 0-4372*, Texas Department of Transportation, Austin, Texas (under review).
- Vipulanandan, C., Guvene, O. & McClelland, M. 2007a. Monitoring the Installation and Curing of a Large Diameter ACIP Pile in Very Dense Sand. *Proceedings GeoDenver 2007*, ASCE. (CD-ROM).
- Vipulanandan, C., Hussain A. & Usluogulari, O. 2007b. Parametric Study of Open Core-hole on the Behavior of Drilled of Shafts Socketed in Soft Rock. *Proceedings GeoDenver 2007*, ASCE. (CD-ROM).
- Zhang, L. and Einstein, H. H. 1998. End Bearing Capacity of Drilled Shafts in Rock. *Journal of Geotechnical and Geoenvironmental Engineering*, 124(7): 574–584.

Current design practice for axially loaded piles and piled rafts in Germany

C. Vrettos

Technical University of Kaiserslautern, Kaiserslautern, Germany

ABSTRACT: The new generation of German DIN standards for geotechnical works adopted the philosophy of the Eurocode EC7 introducing the limit state design approach. A summary of the relevant national standards for pile design and construction is given. The design rules and the respective code provisions are presented in detail, both for ultimate and serviceability limit states. Two illustrative pile design examples are described. The second part of the paper provides an overview of the guideline contents for the design and construction of piled raft foundations.

1 INTRODUCTION

Traditional pile design in Germany was based on the global safety factor approach that uses a lumped factor applied notionally to either the ultimate strength or the applied load. This is deemed to account for all the uncertainties inherent in the design. This was the philosophy of the German DIN standards until recently. The general code for geotechnical design referring to the permissible loading of foundation soils was the DIN 1054:1976-11 issued in 1976. The standards for piles were the DIN 4014:1990-03 for bored piles, DIN 4026:1975-08 for driven piles and DIN 4128:1983-04 for grouted piles.

In the frame of harmonisation of industrial standards within the European Union the member states agreed to adjust their national codes to the Eurocodes within a specified period of time. The introduction of the Structural Eurocodes established the limit state design (LSD) approach. A limit state is usually defined as any limiting condition beyond which the structure ceases to fulfil its intended function. Limit state design considers the performance of a structure, or structural elements, at each limit state. Typical limit states are strength, serviceability, stability, fatigue. Different factors are applied to loads and material strengths to account for their different uncertainty. The new DIN standards generation adopted that principle assuring compatibility with the Eurocodes.

The ultimate limit states are verified by applying partial factors to the main variables of the calculation model, and by verifying that the fundamental inequality $E_d \leq R_d$ is fulfilled, where E_d denotes the design value of the action effects and R_d denotes the design value of the resistance.

A review with focus on practical aspects and design methods is given by Kempfert et al. (2003). The Working Group 2.1 on Piles of the German Geotechnical Society (DGGT) is presently preparing a detailed report with recommendations covering all major aspects of piling technology, design methods, and quality control.

In the following, the basic design principles of the Eurocode and the relevant DIN standards as applied to axially loaded pile foundations are presented and two illustrative examples are given to demonstrate the application of the new DIN standards. Furthermore, the design principles for piled raft foundations that constitute a novel foundation system for settlement-sensitive high-rise building are given.

2 CODES AND DESIGN FUNDAMENTALS

2.1 Eurocodes and DIN standards

While Eurocodes (EC) 2, 3, 4, 5, 6, and 9 refer to a given construction material (reinforced concrete, steel, etc.), EN 1990 (Basis of design), Eurocode 1 (Actions), Eurocode 7 (Geotechnical design) and Eurocode 8 (Earthquake resistance) are relevant to all types of construction, irrespective of the material used. Eurocode 7 (EC7) consists of two parts: EN 1997-1 Geotechnical design – Part 1: General rules, and EN 1997-2 Geotechnical design – Part 2: Ground investigation and testing. Part 1 describes in a general form the principles for geotechnical design in the frame of the LSD concept as applied to the calculation of the geotechnical actions on the structural elements in contact with the ground (footings, piles,

basement walls, etc.), as well as to the deformations and resistances of the ground submitted to the actions from the structures. Pile foundations are treated there in Section 7. Some detailed design rules or calculation models, i.e. formulae or diagrams, are given only in Annexes that are informative except Annex A that is mandatory in the normative sense. Annex A defines the partial factors for ultimate limit state in persistent and transient design situations (“fundamental combinations”), as well as correlation factors for the characteristic values of pile bearing capacity. The numerical values for the partial or correlation factors are merely recommended values. These values can be changed in the National Annex to EN 1990-1, which is published by each country.

Part 2 of EC 7 makes the link between the design requirements of Part 1, in particular Section 3 “Geotechnical data”, and the results of a number of laboratory and field tests. The standardisation of the tests themselves is published by the TC 341 of CEN. All field and laboratory tests common in geotechnical practice are treated. A number of informative Annexes with examples of correlations and derivations of values of geotechnical parameters from field test results are included.

In Germany pile design is presently specified in the DIN 1054:2005-01, issued in the year 2005 that replaced the old DIN 1054:1976-11. In addition, pile design is regulated by the DIN EN 1997-1:2005-10 that is the German version EC7-1. For steel piles the DIN EN 1993-5 (EC3-5) also applies.

The following standards that establish the general principles for the construction of the various pile systems are issued as German versions of European codes (EN):

- DIN EN 1536:1999 Execution of special geotechnical works – Bored piles
- DIN EN 12794:2005 Precast concrete products – Foundation piles. It covers both single length and segmental piles for which the larger transverse dimension is not more than 1.5 times the smaller transverse dimension.
- DIN EN 12699:2001 Execution of special geotechnical works – Displacement piles. This document covers piles driven using impact, vibration, pressing, screwing or a combination of these methods.
- DIN EN 14199:2005 Execution of special geotechnical works – Micropiles. This covers piles with outside diameter smaller than 300 mm for bored piles and smaller than 150 mm for displacement piles.

Since diaphragm wall elements are often used in the sense of pile foundations the following construction standards are also relevant:

- DIN EN 1538:2000 Execution of special geotechnical works – Diaphragm walls. This document

includes cast in situ concrete diaphragm walls, precast concrete diaphragm walls, and reinforced slurry walls.

- DIN 4126: Stability analysis of diaphragm walls.

Some additional ISO-standards that are developed specifically for piles are not expected to be introduced officially by the building control authority in Germany.

Standards that concern the public safety need in Germany approval by the building control authority. In this spirit and in order to enable the introduction of European standards that are often less binding in content than the German ones, special technical reports (DIN-Fachberichte) are prepared as application documents containing the necessary additional provisions that render the European standard more precise. Presently, only the “DIN – Fachbericht 129:2005-02 Application document to DIN EN 1536:1999-06, Execution of special geotechnical works – Bored piles” is published, the other reports being in preparation.

At the end of 2004 a two year period started during which the National Annex (NA) to EC7-1 had to be prepared. This Annex will contain the values of the design parameters required by EC7-1. At the same time a five-year period started at the end of which the EC7-1 in combination with the NA EC7-1 will be introduced nationwide removing all inconsistencies of national codes with respect to EC7-1.

For the transition period a number of national standards have been prepared that are concurrently valid with the new ones. In that sense the old standard for geotechnical design DIN 1054:1976-11 that is based on the global safety factor approach will be withdrawn at the end of 2007 being replaced by the DIN 1054:2005-01 that is based on the partial safety factor concept. A supplement standard DIN 1054:~2007 to be issued in 2007 will contain solely specifications compatible to EC7-1. The DIN 1054 will be redrawn at the earliest in 2009.

2.2 Limit states

Two limit states are considered when undertaking a limit state design for foundations: ultimate (ULS) and serviceability limit states (SLS).

The ultimate limit state governs the safety of a structure against collapse or excessive deformation of a foundation leading to the collapse of the structure it supports. It should have a very low probability of occurrence. In DIN 1054:2005 it is referred to as GZ 1 and is further divided into three cases depending on the failure mechanism involved:

- GZ 1A: Loss of equilibrium of structure or ground without failure of the ground (uplift, buoyancy, hydraulic heave, internal erosion, piping)

- GZ 1B: Failure of structure/structural element or failure of the ground supporting the structure (sliding, bearing resistance failure of foundations, failure of piles, retaining walls, anchors etc.)
- GZ 1C: Loss of global stability induced by failure of the ground and/or supporting elements such as anchors or nails

The serviceability limit state, denoted by GZ 2 in DIN 1054:2005, governs situations beyond which specified functions of a structure or structural elements can no longer be satisfied, e.g. deformation, settlement or vibration exceeding specific values under normal working conditions. The analysis usually involves the estimation of deformation.

Eurocode EC7 defines the following limit states in place of the states GZ1A, GZ1B, and GZ1C of the DIN 1054:2005: EQU, STR, GEO, UPL, HYD denoting “equilibrium”, “internal failure of structure”, “geotechnical failure”, “uplift”, and “hydraulic failure”, respectively. This implies that for compatibility the state GEO has to be split into two sub-cases GEO-1 and GEO-2.

2.3 Actions and resistances

DIN 1054:2005 considers design situations for specific combinations of combinations of actions EK 1 to EK 3 and safety classes of resistances SK 1 to SK 3 yielding load cases 1 to 3 (LF 1 to LF 3). More specifically it distinguishes between:

Combinations of actions (EK):

- Regular combination of actions (EK 1): Permanent and variable actions which occur regularly during the lifetime of the structure;
- Rare combination of actions (EK 2): Actions of EK1 plus rare or onetime actions;
- Exceptional combination of actions (EK 3): Actions of EK1 plus exceptional actions occurring at the same time, e. g. accidents, earthquakes or other catastrophic events.

Conditions of safety classes of resistances (SK):

- SK 1: Conditions valid for the lifetime of the structure;
- SK 2: Conditions valid during repair or construction of the structure or of nearby structures;
- SK 3: Conditions which may most likely occur only once or never during the life time of the structure.

Load cases:

- Load case 1 (LF 1): Permanent or temporary design situations during the lifetime of the structure;
- Load case 2 (LF 2): Temporary design situations during construction or repair;
- Load case 3 (LF 3): Accidental design situations.

The relevant combinations are defined in DIN 1054:2005. For example, LF 1 is obtained by combining EK 1 and SK 1, LF 2 by combining either EK 2 and SK 1 or EK 1 and SK 2. Partial safety factors are defined for the particular load cases. LF 3 when resulting as combination of EK 3 and SK 3 may require unit valued partial safety factors for actions and resistances. Numerical values for the partial safety factors for pile foundations are given in the following sections of the paper.

Basic for the design are the characteristic values for actions and resistances denoted by the index “k”. They are obtained from experiments, measurements, calculations or experience by considering the type of structure and design method, the quality and size of sample, and the sensitivity of the particular parameter. The characteristic values of actions are multiplied while these of the resistances are divided by appropriate partial safety factors. The resulting values are the so-called design values denoted by the index “d”.

2.4 Partial safety factors

Due to the novelty of limit state design in most of the European countries and the wide variety of soil conditions, soil testing and design methods, EC 7 allows for three different so-called Design Approaches (DA 1, DA 2 and DA 3) when assessing R_d and E_d for persistent and transient situations. The selection of the design approach and of the values of the partial factors is left to national determination. Discussion and comparisons of results using the 3 DAs may be found in Frank et al. (2004). The basic principle for the selection of design approach in Germany was to maintain the safety level of the former global safety factor approach.

3 PILE DESIGN ACCORDING TO DIN 1054:2005

3.1 General

In pile design it is distinguished between internal and external bearing capacity. The former refers to check against failure of the pile material (concrete, steel etc) itself while the latter refers to bearing capacity check of the ground supporting the pile. According to DIN 1054:2005 this corresponds for piles to the ultimate limit state GZ 1B (in EC7-1: STR for the internal, GEO-2 for the external bearing capacity). For tension piles the Limit state GZ 1A of DIN 1054:2005 (UPL in EC7-1) has to be checked in addition.

3.2 Actions

For piles it is distinguished between:

- Foundation loads, e.g. from the superstructure building;

- Soil-specific loads (e.g. from downdrag, bending due to settlement, lateral earth pressure);
- Dynamic and cyclic loads.

From these characteristic actions one obtains the characteristic loads E_k on the piles:

$F_{G,k}$ and $F_{Q,k}$, and, $H_{G,k}$ and $H_{Q,k}$, from permanent (index “G”) and variable loads (index “Q”) on the pile head in axial and transverse horizontal direction, respectively, as well as bending moments $M_{G,k}$ and $M_{Q,k}$, due to various permanent and variable actions.

All these loads have to be transferred to the ground fulfilling the internal and external capacity check.

3.3 Characteristic resistances

It is customary in Germany to determine the axial pile resistances not via calculation methods but on the basis of

- Static load tests
- Dynamic load tests
- Empirical correlations

3.4 Pile resistance from static load tests

Following the DIN 1054:2005, when piles are designed from static load tests the measured resistance values $R_{1m,j}$ are obtained from the in-situ experimental resistance vs. settlement/heave curves (RSC/RHC). From these data one then determines the characteristic RSC/RHC curves that are the basis for the design and the capacity check.

3.4.1 Characteristic resistance for ULS

Characteristic values of resistance for the limit state GZ 1 are obtained from the measured ones $R_{1m,j}$ by dividing them with a correlation factor ξ . This corresponds to the recommendation given in EC7-1. The characteristic value $R_{1,k}$ is obtained as the minimum of the pile load test results according to equation (1):

$$R_{1,k} = \min \{R_{1m,\min} / \xi; \bar{R}_{1m} / \xi\} \quad (1)$$

where $R_{1m,\min}$ and \bar{R}_{1m} are the minimum and average values of measured resistance, respectively, ξ is the correlation factor as given in Table 1, and

$$s_N = \sqrt{\sum_{i=1}^N (\bar{R}_{1m} - R_{1m,i})^2 / (N-1)} \quad (2)$$

If more than one pile contributes to the load transfer to the ground, e.g. when using a rigid pile cap, and if the dispersion coefficient $S_N/\bar{R}_{1m} \leq 0.25$, it is allowed to use from Table 1 the average value \bar{R}_{1m} of the pile load test results. For intermediate values a linear interpolation is applied.

Table 1. Correlation factor ξ in dependence on the number of pile load tests N and the dispersion of the measured values according to DIN 1054:2005.

Number of tests N	Correlation factor		
	Average value \bar{R}_{1m}		Minimum value $R_{1m,\min}$
	$S_N/\bar{R}_{1m} = 0$	$S_N/\bar{R}_{1m} = 0.25$	
1	–	–	1.15
2	1.05	1.10	1.05
>2	1.00	1.05	1.00

The use of the correlation factor was not customary in Germany and is a compromise with respect to the future introduction of the Eurocode. The values of the correlation factor in the DIN 1054:2005 are different from those given in the EC7-1 in combination with the National Annex, cf. Frank (2006). The procedure defined in the DIN basically corresponds to the experience in Germany with the global safety factor concept.

In the event where the limiting resistance is not explicitly identified from the measured resistance vs. settlement curve it is assumed that it occurs at a settlement of

$$s_1 = 0.10 \cdot D_b \quad (3)$$

where D_b is the diameter of the pile base.

3.4.2 Characteristic resistance for SLS

The transfer of the rules defined in Table 1 to the derivation of characteristic resistance vs. settlement curves (RSC) for the serviceability limit state could produce undesirable jumps in the characteristic RSC. DIN 1054:2005 recommends a qualified weighting of the results of pile tests at the SLS enabling the derivation of a characteristic RSC that should be continuous.

A practicable solution is the following: If the measured RSC show relatively uniform dispersion with values smaller than $S_N/\bar{R}_{1m} = 0.25$ or $S_N/\bar{R}_{1m} = 0.25$ a single correlation factor ξ is determined using the average value $\bar{R}_{m,\min}$, whereas for values larger than 0.25 the correlation factor is determined using $\bar{R}_{m,\min}$. Only for non-uniform dispersion with values lying below and above the limiting value 0.25 would jumps in the curve be produced. A meaningful correction is then applied to the experimental curve that has to be verified by a geotechnical expert.

3.4.3 Static axial load tests

The performance of pile tests of static or dynamic nature is standardised in Germany in the Recommendations for Static and Dynamic Pile Tests

of the German Geotechnical Society, Working Group 2.1, DGGT (1998).

One pile test should be carried out for each uniform subsoil condition, whereas for foundations with more than hundred piles two pile tests are recommended. For sensitive buildings and buildings of geotechnical category GK 3 (for the definition of GK see below) the number of pile tests is defined in cooperation with the geotechnical expert. For micropiles DIN 1054:2005 requires at least 2 piles to be tested, at minimum at 3% of all piles.

The testing load shall be large enough in order to reach the limit state GZ1 fulfilling one of the following criteria:

a) Limiting settlement:

$$R_{g1} = R(S_g)$$

with $s_g = 0.1 \cdot D$ whereby D is the pile diameter for uniform cylindrical piles, the diameter of the pile base for piles with widened base, and the equivalent pile diameter (same area) for piles with rectangular cross section.

b) Creeping behaviour:

$$R_{g1} = R(k_s)$$

where k_s is an individually specified amount of creep.

With respect to the necessary instrumentation separate monitoring of shaft and base resistance is required when soil is strongly nonhomogeneous, shaft resistance after reaching peak value drops to a much lower residual value, and when strict criteria are imposed on limiting displacement values. In standard cases recording of pile head settlement is considered sufficient.

3.5 Pile resistance from dynamic load tests

Under certain circumstances DIN 1054:2005 allows the determination of pile resistances from dynamic load tests. Correlation factors ξ have also to be considered as given in Table 1. The required number of dynamic tests as well as the increase in the value of the ξ factors is summarized in Table 2 in dependence on the available data from comparable static tests and the testing procedure used.

With respect to the data reduction procedure it is distinguished between direct and extended methods. The former are based on one-dimensional wave propagation theory and allow the direct on-site estimation of the bearing capacity reached, while the latter incorporate the complete model of the pile embedded in the soil. Typical examples are the CASE and TNO formulae and the CAPWAP – TNOWave, respectively. In the Rapid Load Test the direct method is performed by means of the Unloading Point Method.

Table 2. Increase of correlation factor ξ according to Table 1 when evaluating dynamic pile load tests.

(1) Calibration on static pile load tests		
Location of pile test	Analysis procedure	Increase
Same site	Extended method (e.g. CAPWAP)	None
	Direct Method (e.g. CASE-formula)	$\Delta\xi = 0.10$
Different project	Extended method	$\Delta\xi = 0.05$
	Direct method	$\Delta\xi = 0.15$
(2) Deduction from general empirical values (only extended method permitted)		$\Delta\xi = 0.15$

Note: When applying the correlation factors ξ from Table 1 to dynamic load tests, the double number of tests must be available in the first column in Table 1 (e.g. static $N = 1$, dynamic $N = 2$).

This procedure is however not allowed by the DIN 1054:2005.

3.6 Pile resistance from empirical correlations

This applies mainly to bored piles and corresponds to the traditional practice followed in Germany. Characteristic values for base resistance $q_{b,k}$ and shaft friction at each layer $q_{s,k,i}$ are directly determined from values of soil parameters using appropriate charts and tables. The variation of pile resistances with settlement s underlying the design procedure is depicted in Figure 1, with $R_k(s)$, $R_{b,k}(s)$, and $R_{s,k}(s)$ denoting the characteristic values of total, base, and shaft resistance of the pile, respectively. The characteristic axial pile resistance is

$$R_k(s) = R_{b,k}(s) + R_{s,k}(s) = q_{b,k} \cdot A_b + \sum_i q_{s,k,i} \cdot A_{s,i} \quad (4)$$

where A_b and $A_{s,i}$ are the pile base area and shaft surface in layer i .

In Figure 1 s_g denotes the limiting settlement with

$$s_g = 0.10 \cdot D_b$$

that is set equal to the settlement at the ultimate limit state GZ 1.

For the pile settlement at the SLS the relevant parameter is the pile shaft diameter D_s .

The limiting settlement for the mobilisation of shaft resistance is defined by the following equation with settlements given in [cm] and resistance in [MN]:

$$s_{sg} = 0.50 \cdot R_{s,k}(s_{sg}) + 0.50 \leq 3.00 \quad (5)$$

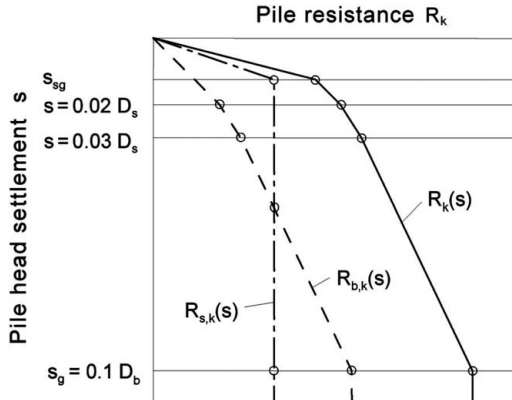


Figure 1. Elements of characteristic resistance vs. settlement curves for bored piles according to DIN 1054:2005.

Table 3. Pile base resistance for bored piles in cohesionless soils according to DIN 1054:2005.

Relative pile head settlement s/D_s and s/D_b	Pile base resistance $q_{b,k}$ in [MPa]			
	10	15	20	25
0.02	0.70	1.05	1.40	1.75
0.03	0.90	1.35	1.80	2.25
0.10 ($=s_g$)	2.00	3.00	3.50	4.00

Intermediate values are obtained by linear interpolation. For bored piles with widened base values shall be reduced to 75%.

When determining the characteristic axial pile resistance vs. heave curve for bored piles it is set

$$s_{sg,tension} = 1.30 \cdot s_{sg} \quad (6)$$

The informative Annex B to DIN 1054:2005 summarizes empirical correlations as determined from a large number of static pile load tests both for pile shaft and pile base resistance. They are valid for bored piles with diameter D_b or D_s from 0.30 to 3.00 m that are embedded at least over 2.50 m in bearing layer. These empirical values are given in dependence on the CPT tip cone resistance q_c for cohesionless and on the characteristic value of undrained shear strength for cohesive soils $c_{u,k}$, respectively, cf. Tables 3 to 6. When applied for estimating the pile base resistance the tip cone resistance of the CPT is usually determined as an average value over a depth from $1 \cdot D$ above to $4 \cdot D$ below the pile base for pile diameters

Table 4. Pile base resistance for bored piles in cohesive soils according to DIN 1054:2005.

Relative pile head settlement s/D_s and s/D_b	Pile base resistance $q_{b,k}$	
	At an average shear strength $c_{u,k}$ of the undrained soil in [MPa]	0.10 0.20
0.02	0.35	0.90
0.03	0.45	1.10
0.10 ($=s_g$)	0.80	1.50

Intermediate values are obtained by linear interpolation. For bored piles with widened base values shall be reduced to 75%.

Table 5. Pile shaft resistance for bored piles in cohesionless soils according to DIN 1054:2005.

Average tip resistance of CPT in [MPa]	Ultimate value $q_{s,k}$ of pile shaft friction in [MPa]
0	0
5	0.040
10	0.060
≥ 15	0.120

Intermediate values are obtained by linear interpolation.

Table 6. Pile shaft resistance for bored piles in cohesive soils according to DIN 1054:2005.

Shear strength $c_{u,k}$ of undrained soil in [MPa]	Ultimate value $q_{s,k}$ of pile shaft friction in [MPa]
0.025	0
0.10	0.040
≥ 0.20	0.060

Intermediate values are obtained by linear interpolation.

$D \leq 0.6$ m, and $1 \cdot D$ above to $3 \cdot D$ below the pile base for $D > 0.6$ m. For pile shaft friction the average over a layer with small scatter in the data is taken. Values for rocks are reproduced in Table 7.

For displacement piles and micropiles equation (4) is valid accordingly, however only for the limit state GZ 1.

$$R_{1,k}(s) = R_{b1,k}(s) + R_{s1,k}(s) = q_{b1,k} \cdot A_b + \sum_i q_{s1,k,i} \cdot A_{s,i} \quad (7)$$

Table 7. Pile base and pile shaft resistance for bored piles in rock according to DIN 1054:2005.

Uniaxial compression strength $q_{b,k}$ in [MPa]	Pile base resistance $q_{b,k}$ in [MPa]	Pile shaft friction $q_{s,k}$ in [MPa]
0.50	1.50	0.08
5.00	5.00	0.50
20.00	10.00	0.50

Intermediate values are obtained by linear interpolation.

Table 8. Partial safety factors for actions for the ultimate limit state GZ1B according to DIN 1054:2005.

Action	Factor	LF1	LF2	LF3
Permanent	γ_G	1.35	1.20	1.00
Unfavorable variable	γ_Q	1.50	1.30	1.00

Table 9. Partial safety factors for pile resistances for the ultimate limit state GZ 1B according to DIN 1054:2005.

Pile resistance	Factor	LF1-LF3
Resistance in compression from pile load test	γ_{Pc}	1.20
Resistance in tension from pile load test	γ_{Pt}	1.30
Resistance in compression and tension from empirical correlations	γ_P	1.40

Some recommended empirical values are summarized in Annex C and D of DIN 1054:2005.

3.7 Bearing capacity check for axial loading

In limit state GZ 1 the characteristic values of the loads imposed by the superstructure on the piles F_k are multiplied by the partial factors on actions to obtain the design values:

$$F_{1,d} = F_{k,G} \cdot \gamma_G + F_{k,Q} \cdot \gamma_Q \quad (8)$$

where γ_G and γ_Q are the partial safety factors for unfavourable permanent and variable actions, respectively. The partial factors depend on the load case (LF 1 to LF 3) considered as given in Table 8.

The design value of the pile resistance is determined from equation (9) using the partial safety factor for pile resistance γ_R as given in Table 9:

$$R_{1,d} = R_{1,k} / \gamma_R \quad (9)$$

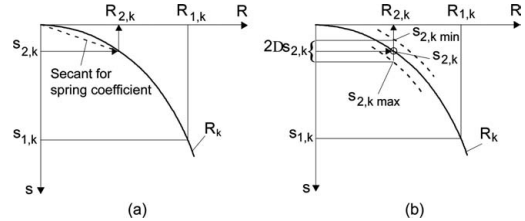


Figure 2. Resistance of single pile $R_{2,k}$ at SLS from a characteristic resistance vs. settlement curve according to DIN 1054:2005 for small (a) and considerable (b) expected differential settlements between piles.

Finally, the bearing capacity for the ultimate limit state is checked requiring

$$F_{1,d} \leq R_{1,d} \quad (10)$$

Note that for load case LF 1, that describes persistent situations, the average partial factor for actions $\gamma_{G,Q} \approx 1.4$, and the partial factor for resistance $\gamma_R \approx 1.4$ when pile resistance is determined from empirical correlations. This yields $1.4 \cdot 1.4 \approx 2.0$, that corresponds to the value of the traditional global safety factor.

3.8 Serviceability check for axial loading

The serviceability check for limit state GZ 2 requires

$$F_{2,d} \leq R_{2,d} = R_{2,k} \quad (11)$$

Crucial to the serviceability is the estimation of the differential settlements between the individual piles within a pile group or between supports consisting of single piles or pile groups. They may result in an ultimate limit state for the superstructure. The amount of differential settlement Δs depends mainly on the pile type and the absolute settlement s_2 . Typical values for $\Delta s/s_2$ range from 1/3 for bored piles to 1/4 for displacement pile foundations.

The method suggested by the DIN 1054:2005 is schematically shown in Figure 2 with $s_{2,k}$ denoting the allowable settlement, as defined e.g. from the structural analysis of the superstructure. The restraint inducing differential settlement is estimated as

$$\Delta s_{2,k} = \kappa \cdot s_{2,k} \quad (12)$$

whereby the factor κ depends on the pile installation method, the soil stratigraphy, and the position of the piles within the foundation system and shall be determined in agreement with a geotechnical expert. In absence of specific investigations a first estimate $\kappa = 0.15$ is often used in practice.

3.9 Pile groups

Due to the interaction of piles in a pile group the resistance vs. settlement curves of the individual piles are different than those of the single isolated pile strongly depending also on the position within the group. It may also happen that for large settlements the resistance of the piles in a group is larger than that of the isolated single pile. At working loads conditions, however, a group pile will settle more than the single one. Although the application of computational method for the assessment of resistance vs. settlement curve is not allowed by the DIN 1054:2005 the prediction of group behaviour is feasible only by means of an appropriate mechanical model. This in turn is difficult to be defined due to the influence of the installation method, and of the prevailing soil conditions. A practicable solution consists in using the resistance curve for a single pile and applying a theoretical model that describes as close as possible the group effects. In this sense, a distinction between bored and displacement piles is necessary. While the installation for displacement piles makes the reliable prediction of group effects almost impossible due to the induced soil displacement, the careful installation of bored piles affects the ground to a much lesser extent. In general, due to the pre-stressing of the soil between the piles and the influence of the induced driving energy the expected settlement of displacement piles will be smaller than that of bored piles. The distance, beyond which the interaction two neighboring piles becomes negligible is often set equal to 6 to 8 pile diameters.

DIN 1054:2005 does not require for pile groups the verification of bearing capacity. An alternative approach is based on the suggestions of EC7 and examines two failure mechanisms: (i) compressive and pull-out resistance of the piles individually, and (ii) compressive or pull-out failure of the piles and the soil contained between them acting as a block. For the prediction of settlements and the verification of serviceability a number of computational methods are available in the literature that should be used with engineering judgement because of the difficulty in assessing the effects of pile ground geometry, soil properties, and pile cap stiffness. For pile foundations consisting of end-bearing piles the total settlement may be calculated by adding the parts due to the settlement of an equivalent deep sited raft foundation at the level of the pile base, and the settlement of the individual piles. The calculation of differential settlements, that are crucial to potential distortion of the superstructure, requires, however, more elaborate methods.

3.10 Special pile types

Shaft-grouted bored piles are often used to enhance shaft resistance in soils of low relative density or soft

consistency and also as remedial measure when the vicinity of the pile is disturbed due to the pile construction. Often, base-grouting is also performed for increasing load carrying capacity. Grouting is carried out using tube-a-manchette in stages after casting the bored piles. Site-specific instrumented trial piles are usually carried out to confirm the design parameters and verify the construction method. For preliminary design one may use the empirical relations for shaft resistance of grouted micropiles (Annex D of DIN 1054:2005) or increase by 50% the shaft resistance values of conventional bored piles given in the tables above.

Resistance of tension piles shall be determined solely by static load tests, except for the case that a certified geotechnical expert allows it.

4 GROUND INVESTIGATION FOR PILES

The results of the ground investigation shall be sufficient to provide information for the proper installation of piles according to the respective DIN EN construction standards. The extent of these investigations depend according to DIN 4020:2003-9 "Geotechnical investigations for civil engineering purposes" on the geotechnical category of the project and are set-up in detail by a geotechnical expert.

According to DIN 1054:2005 foundations are classified into the geotechnical categories (GK) whereby the lowest category GK1 is not applicable to piles.

GK 2 is relevant e.g. when pile settlement is important for the structural system, pile resistance is determined from empirical correlations and simple soil conditions, or negative friction is expected. The highest category GK 3 includes among other situations with highly loaded piles at low values of permissible settlements and/or shaft and base grouting, estimation of resistance from empirical correlations at difficult soil conditions, piled-raft foundations, and cyclically loaded piles when sufficient experience is not available for the particular type of pile. The depth of investigation is defined by the DIN 4020:2003.

Bearing capacity of cohesionless soils should be determined on the basis of the tip resistance of the CPT. Correlations between q_c and the blow count numbers N of SPT or Dynamic Probing Heavy (DPH), e.g.

$$q_c (\text{CPT}) \approx N_{10} (\text{DPH})$$

or other correlations based on the relative density have been proven in practice.

The undrained shear strength of cohesive soils is usually determined from undrained triaxial tests and verified by empirical relations based on soil consistency or CPT results. For soft soils the field vane tests is also used.

5 DESIGN EXAMPLES FOR PILES

5.1 Pile design from empirical correlations

The example is taken from the DIN 4014:1990-03. We consider an axially loaded bored pile to be designed from the empirical correlations given in the Annex B of DIN 1054:2005. Pile geometry, soil stratigraphy, and soil properties are given in Figure 3. The clay layer is characterized by the undrained shear strength $c_{u,k}$ while for the sandy layer the profile of the CPT tip cone resistance is given. First, the depth profile of the CPT is divided into sublayers of constant cautious estimates of the average values.

From Tables 5 and 6 one obtains the ultimate values of pile shaft friction for sand and clay, and with the mantle area the pile shaft resistance values $R_{s,k,i}$ as listed in Table 10.

From the ultimate value of pile shaft friction $R_{s,k}$ we obtain using equation (5) the settlement for the

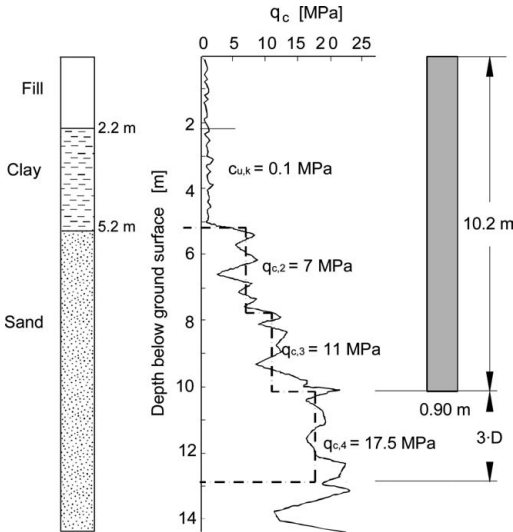


Figure 3. Design situation for example of pile design from empirical correlations: soil profile, CPT tip resistance, and pile geometry.

Table 10. Ultimate values for pile shaft friction for design example.

Layer i [m]	$A_{s,i}$ [m^2]	$c_{u,k,i}$ [MPa]	$q_{c,i}$ [MPa]	$q_{s,k,i}$ [MPa]	$R_{s,k,i}$ [MN]
2.20–5.20	8.48	0.10		0.040	0.339
5.20–7.70	7.07		7.00	0.056	0.396
7.70–10.20	7.07		11.00	0.088	0.622
				$R_{s,k} =$	1.357

mobilisation of shaft friction s_{sg} in [cm] with $R_{s,k}$ in [MN]

$$S_{sg} = 0.50 \cdot R_{s,k} + 0.50 = 1.20 \text{ cm.}$$

In order to determine the pile base resistance $R_{b,k}$ an average value of the soil strength is derived over a depth of $3 \cdot D$ (here $3 \cdot D = 2.70 \text{ m}$) below the pile base level. From the CPT-profile an average value of $q_{c,m} = 17.5 \text{ MPa}$ is obtained.

By applying the numerical values given in Table 3 for $q_{c,m}$ we get the settlement-dependent values of the pile base resistance as summarized in Table 11.

Since the values for pile resistances given in the Annex B of DIN 1054:2005 are already characteristic ones, the correlation factor ξ does not need be considered.

The characteristic resistance vs. settlement curve is finally determined by the addition of the two resistance components, as depicted in Figure 4 with the numerical values given in Table 12.

5.2 Pile design from static pile load test results

The pile foundation as depicted in Figure 5 with a pile diameter $D = 0.90 \text{ m}$, permanent load $F_{G,k} = 1.20 \text{ MN}$

Table 11. Pile base resistance for design example.

Relative settlement s/D	$q_{b,k}$ [MPa]	$R_{b,k}(s)$ [MN]
0.02	1.225	0.784
0.03	1.575	1.008
0.10	3.250	2.080

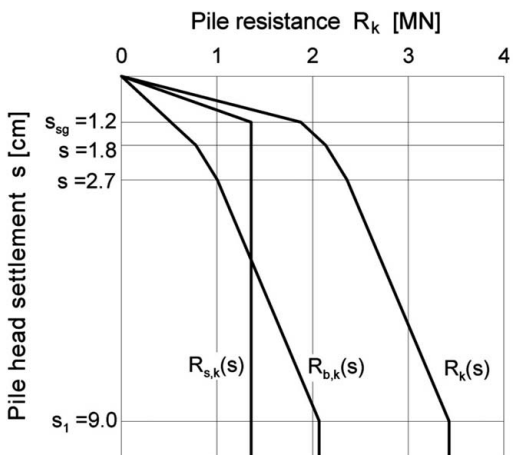


Figure 4. Resistance vs. settlement curve from empirical correlations for the design example.

Table 12. Pile resistance in dependence on pile head settlement for design example.

Relative settlement s/D	Pile head settlement [cm]	$R_{s,k}$ (s) [MN]	$R_{b,k}$ (s) [MN]	R_k (s) [MN]
s_{sg}	1.2	1.357	0.509	1.866
0.02	1.8	1.357	0.784	2.141
0.03	2.7	1.357	1.008	2.365
0.10	9.0	1.357	2.080	3.437

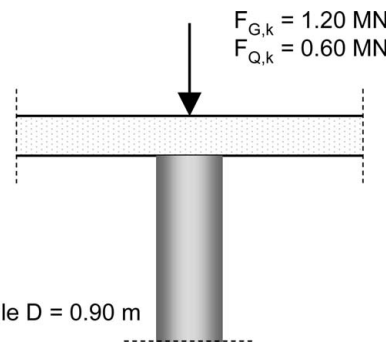


Figure 5. Design situation for example of pile design from static load tests.

Table 13. Results of two pile load tests together with the derived numerical values of the characteristic resistance vs. settlement curves for a flexible and a rigid structural system.

s	[cm]	0	1	2	4	6	9
$R_{m,min}$	[MN]	0	1.60	2.20	3.15	3.60	3.95
$R_{m,max}$	[MN]	0	1.80	2.65	3.50	4.00	4.40
R_m	[MN]	0	1.70	2.43	3.33	3.80	4.18
ξ_{flex}	[–]		1.05	1.05	1.05	1.05	1.05
$R_{k,flex}$	[MN]	0	1.52	2.10	3.00	3.43	3.76
$S_N R_m$	[MN]	0	0.08	0.13	0.07	0.07	0.08
ξ_{rigid}	[–]		1.07	1.08	1.07	1.07	1.07
$R_{k,rigid}$	[MN]	0	1.59	2.25	3.12	3.57	3.92

and variable load $F_{Q,k} = 0.60 \text{ MN}$ is considered. The results of the two pile load tests carried out are given as values $R_{m,min}$ and $R_{m,max}$ in Table 13. The settlement giving the limit load is defined according to equation (3) as $s_1 = 0.1 \cdot 90 \text{ cm} = 9 \text{ cm}$. The prescribed allowable pile settlement is $s_2 = 2.0 \text{ cm}$.

5.2.1 Characteristic pile resistance

The characteristic pile resistance vs. settlement curve is determined according to DIN 1054:2005 as follows. If it is assumed that the load from the superstructure is not distributed to more than one pile (i.e. load

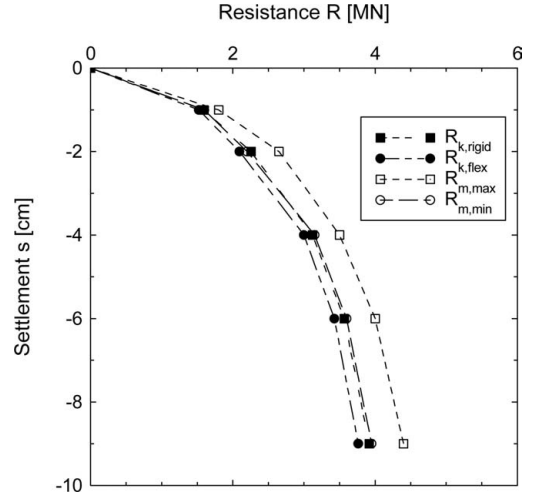


Figure 6. Derivation of characteristic resistance vs. settlement curves from the pile load tests.

transfer from “weak” to “strong” piles), the design departs from a flexible pile cap, and the characteristic values of the resistance vs. settlement curve is determined from the minimum values of the test results $R_{m,min}$. The correlation factor is $\xi = 1.05$, cf. Table 1. The resulting pile resistance is given in Table 13 and Figure 6.

If on the other hand the pile cap is rigid enabling the redistribution of pile loads, the characteristic pile resistance is allowed to be determined from the average value from all pile tests conducted. For relative values of the data dispersion $S_N / R_m \leq 0.25$ the correlation factor ξ is obtained by linear interpolation and is applied to the entire resistance vs. settlement curve thus avoiding discontinuities in the curve. The resulting resistance vs. settlement curve is depicted in Figure 6 with the numerical values summarized in Table 13.

5.2.2 Bearing capacity check

At the ultimate limit state GZ 1B the condition

$$E_{1,d} \leq R_{1,d}$$

has to be verified. For load case LF 1 we have:

(a) Independently acting piles (flexible system):

$$\begin{aligned} E_{1,d} &= G_{G,k} \cdot \gamma_G + F_{Q,k} \cdot \gamma_Q = \\ &= 1.2 \cdot 1.35 + 0.6 \cdot 1.50 = 2.52 \text{ MN} \end{aligned}$$

$$R_{1,d} = R_{1,k} / \gamma_{P_c} = 3.76 / 1.20 = 3.14 \text{ MN} > 2.52 \text{ MN}$$

(b) Load distribution by rigid cap (rigid system):

$$E_{1,d} = 2.52 \text{ MN}$$

$$R_{1,d} = R_{1,k} / \gamma_{Pc} = 3.92 / 1.20 = 3.27 > 2.52 \text{ MN}$$

5.2.3 Serviceability check

From the characteristic loads $F_{2,k}$ resulting from the structural analysis we have

$$E_{2,d} = E_{2,k} = F_{G,k} + F_{Q,k} = 1.20 + 0.60 = 1.80 \text{ MN}$$

The allowable characteristic pile resistance in the serviceability limit state is obtained from Figure 6:

$$R_{2,d} = R_{2,k} = 2.10 \text{ MN} > 1.80 \text{ MN} \text{ (flexible system)}$$

$$R_{2,d} = R_{2,k} = 2.25 \text{ MN} > 1.80 \text{ MN} \text{ (rigid system)}$$

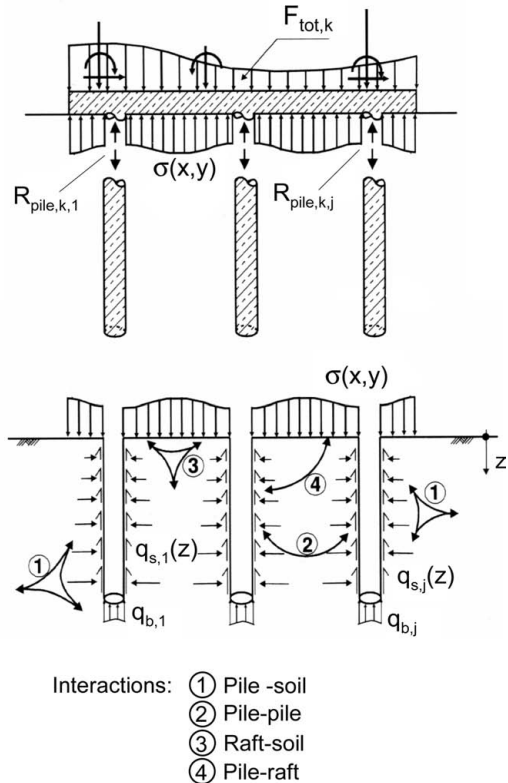
Hence, for both cases the SLS check is fulfilled.

The serviceability limit check can be also performed via the pile settlement: From Figure 6 we obtain for the characteristic pile load $F_{2,k} = 1.80 \text{ MN}$ the settlement for a flexible system $s_2 = 1.50 \text{ cm}$, while for a rigid system $s_2 = 1.30$. Both values are smaller than the allowable settlement of 2.00 cm.

6 PILLED RAFT FOUNDATIONS

6.1 General and design methods

Piled rafts are a new foundation concept for important high-rise buildings and have been successfully used in Germany since the beginning of the 90's, Katzenbach et al. (2000). This foundation type is a viable alternative to conventional pile or raft foundations in competent ground. The combined foundation is able to support the applied axial loading with an appropriate factor of safety at a tolerable level of settlement under working loads. The implementation of this foundation type led to an abolition of complicated settlement-correction techniques. During the last years the computational methods available in combination with measurements on real projects allowed the realistic modelling of the complicated bearing behaviour of that composite foundation system. The bearing behaviour is described by means of the pile raft coefficient α_{pr} that defines what amount of the total force $F_{tot,k}$ is carried by the piles. Hence, α_{pr} ranges from 0 for a raft to 1 for a pile foundation. Due to the strong nonlinearity of the pile bearing behaviour the pile raft coefficient depends on the stress level and accordingly also on the amount of settlement of the piled raft foundation. The piles can be loaded up to their ultimate bearing capacity, and are spaced strategically to achieve a more uniform settlement thus reducing sectional forces in the raft and leading to a more economical solution.



- Interactions:
- ① Pile -soil
 - ② Pile-pile
 - ③ Raft-soil
 - ④ Pile-raft

Figure 7. Interactions in a piled raft foundation (Hanisch et al., 2001).

This new foundation concept has been introduced very recently in the DIN 1054:2005 in Section 8.5.5. For the design reference is made to the corresponding guideline (Hanisch et al., 2001) and to the fact that a project specific approval by the building control authority is required.

The guideline requires the computational model applied to be able to simulate: (i) the bearing behaviour of a single pile taking into account the shearing along the pile shaft and the compression at the pile base, and (ii) the interaction effects between individual piles and between pile and raft as schematically shown in Figure 7. Back analysis of a static pile test is commonly used to verify the assumptions of the model and the values of the parameters.

The design work consists in estimating the deformation behaviour of the composite system and the distribution of the load into its two components, pile group and raft. The available methods may be divided into (i) approximate analytical, (ii) approximate numerical, and (iii) refined numerical, the choice being dictated by the importance of the project. An overview is given by Poulos (2001).

The aim of the design process is to optimize the position and the geometry of the piles. The solution of the soil-structure interaction problem is obtained by means of a pseudo-coupled procedure that is based on an interaction between the designers of the superstructure and the foundation system, resp. The interface in this design procedure is defined in terms of the modulus of subgrade reaction for the raft and the spring coefficients for the individual piles.

For the preliminary design, where different foundation alternatives are compared, a flexible simplified method is required to assess the influence of the pile group configuration and of the soil parameters. An approximate method that is an extension of the method outlined by Randolph (1994) has been presented by the author (Vrettos, 2006). The method allows the accommodation of the variable pile distance and length as well as the different stiffness of central, peripheral, and corner piles.

For the final design a nonlinear finite element analysis with an appropriate soil model is usually carried out for important projects. In the past, the majority of these calculations used an elastoplastic Drucker/Prager – cap model mainly due to the fact that this formulation is already implemented in numerical codes.

6.2 Ultimate limit state

The guideline for piled rafts adopted the limit state design philosophy and distinguishes for limit state GZ 1 between external and internal bearing capacity. The methodology defined by the EC7-1 for piles can not be directly applied to piled rafts.

6.2.1 External bearing capacity

The calculation of the resistance vs. settlement curves for the overall foundation system is carried out using a computational model accounting for the interaction effects and applying a global safety factor η to the characteristic values of actions.

$$\eta \cdot \sum_{i=1}^n F_{k,i} \leq R_{l,tot,k} \quad (13)$$

with η equal to 2.0, 1.75, and 1.50 for load case LF 1, LF 2, and LF 3, respectively.

Assessment of the characteristic value of the total resistance $R_{l,tot,k}$ is made on the basis of the induced total settlement, i.e. the point at which the settlement starts to increase at a higher rate.

If the check is not performed by an adequate realistic computational model it is allowed in simple cases to calculate the total resistance $R_{l,tot,k}$ by means of the characteristic value of the base resistance of the foundation raft, i.e. ignoring the vertical bearing capacity of the piles. Dowel resistance of the piles

along the failure surface may be considered in the analysis.

Simple cases are defined as follows:

- Geometrically uniform piled raft, i.e. identical pile length and diameter, constant pile spacing, rectangular or circular raft, overhang of less than three pile diameters at the edges of the raft;
- Homogeneous soil conditions with no abrupt changes in soil stiffness;
- Foundation loaded at its center of gravity with no dynamic effects.

It should be noticed that the check of the external bearing capacity of the individual piles is not required.

6.2.2 Internal bearing capacity

All foundation elements shall be checked against material failure for all relevant combinations of actions. In particular, piles shall be designed for compression combined with bending and shear, tension during construction stages, and downdrag. The raft shall be checked for bending, shear, and punching shear at the slab-column and slab-pile connections.

The partial resistances of raft and piles depend on the stress level induced by the actions. Therefore it is required that the pile raft coefficient α_{pr} be calculated both for the ultimate and the serviceability limit state. The sectional forces of the raft and of the piles are computed for the load distribution on piles and raft corresponding to the pile raft coefficient. The more unfavourable results are then used for the structural design.

6.3 Serviceability limit state

Checking is carried out for limit state GZ 2 in analogy to the bearing capacity check by setting for the partial safety factor a value equal to 1.

6.3.1 External serviceability

The requirements of serviceability of the system are fulfilled when

$$E \left(\sum_{i=1}^n F_{k,i} \right) \leq C \quad (14)$$

The effects E dependent on the actions $F_{k,i}$ are computed by an adequate model based on characteristic values of the material properties.

The resistance parameter C is in most cases the tolerable settlement of the piled raft foundation. It is defined e.g. from the requirements referring to connections of service pipes in the building, the settlement of adjacent buildings, or the bending and tilting of the superstructure itself. In practice, for the serviceability of elevators but also for optical reasons tilting shall be limited to 1:1000. It should also be noted

that according to observations – even for homogeneous soil conditions, symmetrical building and loading – differential settlements may reach values in the order of 30% to 50% of the total settlement.

DIN 1054:2005 specifies for the serviceability check a value of the safety factor for the actions equal to 1.0 both for permanent and variable loads. However, relevant for serviceability are the settlement-inducing loads. It is therefore recommended here – when consolidation effects are of minor importance – to reduce the permanent load of the superstructure by the own-weight of the foundation slab and to add – in absence of detailed information – 30% of the variable load.

6.3.2 Internal serviceability

Piles have to be checked for the allowable crack width. The raft has to be checked in addition for the amount of differential settlements that may lead to structural distortion of the superstructure.

6.4 Checking of design and supervision of construction

Design and construction shall be approved by a geotechnical expert particularly qualified for this job. The following works have to be done:

- Examination of the ground investigations and laboratory testing program and the interpretation of the results
- Plausibility check of the characteristic values of soil parameters used in the computational model
- Examination of the computational model adopted for the design and of the numerical results using an independent calculation method
- Set-up and supervision of the monitoring program, and verification of design assumptions against field observations.

The construction of the piled raft foundation shall be supervised by a geotechnical expert assigned by the client and approved by the building control authority.

It should be noted that for quality control purposes the DIN requires that designs be subjected to review by “checking engineers” who need a special official registration. However, responsibility for the design remains with the design engineer.

6.5 Monitoring

The bearing behavior and the load transfer have to be monitored under the supervision of a qualified geotechnical expert. Monitoring may comprise the excavation, the foundation and the adjacent buildings. The monitoring program is an indispensable component of the safety concept and serves the following needs:

- Verification of the computational model and the assumptions made regarding soil parameters;

- Timely detection of critical situations;
- Observation of the evolution of settlements during the construction.

The program includes measurement of:

- Load-settlement behaviour of the foundation by geodetic methods;
- Load share between raft and piles by recording soil-raft contact pressure and pile loads;
- The bearing behaviour of typical piles (central, edge, corner) comprising the pile head and pile base force as well as the distribution of skin friction along the pile shaft;
- The variation of soil deformation with depth.

In simple cases measuring only the load-settlement behaviour will be sufficient.

7 CONCLUSIONS

The adoption of the Eurocodes by the national DIN standards resulted in important changes in the design philosophy with a unified set of principles for all geotechnical design. It motivates a systematic thought about uncertainty in soil parameters and makes clear distinction between ultimate and serviceability limit states. In German standards the basic principle for selecting numerical values for the partial safety factors is maintaining the safety level of the former global safety concept. The methodology for piles outlined in the DIN 1054:2005 standard follows past experience and provides guidance by specifying pile resistances for a variety of pile types and soil conditions.

The design methodology for piled rafts is embedded in the limit state design philosophy. Design work requires the close cooperation between the structural and the geotechnical engineer in order to optimize the foundation with respect to the settlements and construction costs.

REFERENCES

- DGKT – German Geotechnical Society. 1998. Recommendations of the Working Group 2.1 on Static and Dynamic Pile Testing (in German).
- Frank, R. 2006. Design of pile foundations following Eurocode 7, *Proc. XIII Danube-European Conference*, Ljubljana.
- Frank, R., Bauduin, C., Driscoll, R., Kavvadas, M., Krebs Ovesen, N., Orr, T. and Schuppener, B. 2004. *Designers' Guide to EN 1997: Geotechnical design-General rules*. London: Thomas Telford.
- Hanisch, J., Katzenbach, R. and König, G. 2001. *Kombinierte Pfahl-Plattengründungen*. Berlin: Ernst & Sohn.

- Katzenbach, R., Arslan, U., and Mooramann, C. 2000. Piled raft foundation projects in Germany. In J.A. Hemsley (ed.), *Design Applications of Raft Foundations*: 323–391. London: Thomas Telford.
- Kempfert, H.G., Eigenbrod, K.D. and Smoltczyk U. 2003. Pile Foundations. In U. Smoltczyk (ed.), *Geotechnical Engineering Handbook*, 3: 83:227: Berlin: Ernst & Sohn/Wiley.
- Poulos, H.G. 2001. Piled raft foundations – Design and applications, *Geotechnique* 50(2): 95–113.
- Randolph, M.F. 1994. Design methods for pile groups and piled rafts. *Proc. 13th Int. Conf. Soil Mech. Found. Engng.*, New Delhi, 5: 61–82.
- Vrettos, C. 2006. Ein Näherungsverfahren zur Berechnung von Pfahl-Plattengründungen mit unregelmäßiger Geometrie. In F. Rackwitz (ed.), *Entwicklungen in der Bodenmechanik, Bodendynamik und Geotechnik*: 303–312. Berlin: Springer.

Recent advances in the analysis of pile foundation in China

M. Huang, F. Liang & Z. Li

Department of Geotechnical Engineering, Tongji University, Shanghai, China

ABSTRACT: The purpose of this paper is to give a brief review of recent advances in the analysis of pile foundation practiced in China. Emphasis is given to the analysis methods for composite piled raft with cushion and pile responses due to tunneling. In particular, an integral equation approach is discussed first to analyze the problems of composite piled raft with cushion, followed by an introduction of a simple analytical two-stage method for evaluating the pile responses due to tunneling. Numerical examples have demonstrated the performance of the proposed analytical methods. Such analytical approaches are quite efficient for the engineering computation, and provide a useful tool for engineers due to its simplicity.

1 INTRODUCTION

Since the reform and open policy was carried out in the late 1970s, China has been in strong economic growth continuously. Especially, in the 21st century, based on the rapid economic growth for the past twenty years, Beijing will host the next Olympic Games in 2008 and Shanghai will host the World Expo in 2010. Recently, rapid construction in China has provided great opportunities for geotechnical engineers to use their knowledge and talents to solve many challenging problems involving foundations, ground improvement, excavations, and tunnels with innovative technologies.

As the buildings become more and more high, consequently, load transmitted to the foundation also become heavier. The design of foundation becomes more complex and important. To bear the heavy load or control the settlement of foundation, it is customary to consider first the use of shallow foundation such as a strip foundation or a raft foundation, which was possibly combined with ground improvements. If it is not adequate, deep foundation such as a fully piled foundation is used instead. Universal practices promote the design level and construction technology of pile foundations. Some innovative types of pile are adopted in practice and new analysis methods are proposed.

The type of piles is often chosen dependent of the type of subsoil. Most type of piles, such as cast-in-place concrete piles, precast concrete square or pipe pile, H-type steel pipe piles, mini-piles and others, are already used in China. Table 1 gives the maximum scale of the main type of piles applied in China (Shi & Hong 2005). Since the rapid development of pile engineering, some new problems, such as the design

method of the new types of piles and the testing method for the bearing capacity of super-length piles, are faced in China.

Another important problem involving the analysis of pile foundations is pile response due to deep excavation or tunneling. With the development of underground construction due to lack of available space in Shanghai, the influence of tunneling or deep excavation on adjacent building becomes an important problem. Various analysis methods of pile responses caused by tunneling or deep excavation have also

Table 1. Maximum scale of piles practiced in China.

Type of pile	Max. length of piles /m	Width (diameter) of piles /m	Applied instance
Bored cast-in-place concrete piles	104	4.0	Bridge
Manual excavated pile	53	4.0	Building
Precast concrete square pile	75	0.6	Building
Steel pipe pile	83	1.2	Building
Precast prestressed concrete pipe piles ($d \geq 1.0\text{ m}$)	65	0.8	Building
Precast prestressed concrete pipe piles ($d > 1.0\text{ m}$)	40	1.2	Bridge
Driven cast-in-place concrete piles	35	0.7	Building
Deep soil-cement mixing columns	30	0.7	Oil tank

been developed, over recent years in particular, but there is currently almost no simple analytical method available for a preliminary routine design in the engineering.

This paper will present a brief review of some recent advances in the analysis of pile foundations in China. Emphasis has been placed on the analysis methods for composite piled raft with cushion and pile responses due to tunnelling.

2 RECENT ADVANCES IN THE ANALYSIS FOR PILE FOUNDATIONS PRACTICED IN CHINA

2.1 *Piled raft foundation*

In a traditional design of piled foundations, it is customary to assume that all design loads are carried by the piles beneath the raft, even though competent soil strata may exist immediately beneath the raft. This conservative approach appears to be due to a limited understanding of the raft-piles-soil interaction in such a complex three-dimensional problem. In the past few years, there has been an increasing recognition that the raft or pile cap has significant contribution to the performance of piled foundation. In situations where a shallow foundation alone does not satisfy the design requirements, it may be possible to enhance performance of the raft by the addition of piles. The use of a limited number of piles, strategically located, may improve the ultimate load capacity and reduce the settlement of the raft foundations. It is called piled raft foundation or settlement reducing piled foundation (Poulos 2001). The conception of designing foundation based on the principle of controlling settlement was proposed by Burland et al. in 1977, who stated that fewer piles can be used to reduce the settlement of foundation when the bearing capacity is sufficient and the deformation is intolerable. Significant developments in this area have been made by a number of researchers in the last three decades. It has been recognized that the piled raft foundation can be regarded as an alternative intermediate between shallow and deep foundations (Cooke 1986, Horikoshi & Randolph 1996; et al.). The concept of piled raft foundation has been used extensively in Europe and Asia, and has been proven to be an economical way to improve the serviceability of foundation performance by reducing settlements to an acceptable level.

Due to the economical benefit, more attention has been paid to the piled raft foundation in China. Back to 1979, Tong (1979) discussed the possibility of applying the conception of settlement-reducing piles in Shanghai. Later, Huang et al. (1991) proposed a simple method for the design of settlement-reducing pile foundation, which was based on an analytical

method derived from the Geddes's stress solution (Geddes 1966). In order to promote the application of settlement-reducing pile foundation, a seminar on the design philosophy based on controlling deformation was held at Tongji University in 1996 (Hou & Yang 1996). After the seminar, such a settlement-reducing pile foundation has been widely applied in Shanghai and other coastal cities in China such as Shanghai, Ningbo, Wenzhou, Tianjing, Shenzhen, and the others. The Construction Committee of Shanghai Municipal Government demanded that all piled raft foundation of high-rise buildings in Shanghai should be designed with the settlement-controlling principle. Furthermore, the guide for the design of settlement-reducing pile foundation has been complied not only in the local code such as Design code of foundation in Shanghai but also in the National code for design of foundation in China. Yang (2000) gave a comprehensive review concerning the research and engineering practices of piled raft foundation in China.

As well known, such a complex problem can be analyzed only by a few numerical methods due to the three dimensional nature of piled raft foundations. All the methods require the discretization of raft and piles along pile shaft in the analysis, which will affect their efficiency when performing analysis of large pile groups commonly used in practice.

In an attempt to overcome some of the limitations of the existing methods, a variational approach was developed by Shen et al. (2000) to investigate the behaviour of piled rigid raft foundations, while an extension of the variational solutions for the analysis of piled flexible foundation was reported by Chow et al. (2001). In their researches, the free-body for analysis was usually whole piled raft or pile group-soil system isolated from piled raft foundation, the pile group-soil interaction was calculated by Mindlin's solution or other complex methods, and the flexural behaviour of the raft is described by Poisson-Kirchhoff thin plate theory.

Further development of the variational method was made by Liang & Chen (2004). The proposed approach was similar to that of Chow et al. (2001), while some important modifications were made to improve it. First, the free-body for the analysis is a flexible raft isolated from piled raft foundation instead of pile group-soil system or whole piled raft system, and then only the deflections of raft and the contact stress at the raft-pile and raft-soil interfaces are required to be solved. It will simplify the solution procedures. Secondly, pile group-soil interaction is calculated with a simplified model, in which the discretization of piles along pile shaft is not needed either. Compared to other rigorous approaches, the proposed method is computationally efficient and inexpensive. Hence, it is feasible to perform the analysis of large piled raft foundations.

2.2 Composite piled raft with cushion

The design concept of piled raft foundation has been proved to be an economical way to improve the performance of foundation by reducing settlements to acceptable levels. However, the piled raft foundation might not be applied in some circumstances. Poulos (2001) outlined the unfavourable situations that involve the presence of soft clay layer or loose sand layer near the surface, soft compressible layers at relatively shallow depths and some others. In the former cases, the raft might not be able to provide significant loading capacity and stiffness, while in the latter case, long-term settlement of the compressible underlying layers might reduce the contribution of raft to the long-term stiffness of foundation.

However, in the coastal regions of China, building construction often meets with deep soft soil deposit soft and hence the piled raft foundation is unfavourable. In order to use the piled raft foundations in such unfavourable cases, engineers have developed various practical methods in China. However, most of the engineering practices applied the equal length of piles in the piled raft foundation. The stiffness profile of piles does not match with the distribution of contact pressure beneath foundation. From an economical point of view, the parameters of piles should be chosen according to the soil properties and contact pressure of foundation, and etc. For this purpose, a new type of piled raft foundations was developed in the engineering practices. Liang et al. (2003) proposed a type of foundation as is shown schematically in Figure 1. It is named as "composite piled raft with cushion" (for short as "CPRC"). For this new type of foundation, short piles composed of relatively flexible materials such as mixed soil-cement or sand-gravel columns were applied to improve the bearing capacity of shallow natural subsoil. Long and rigid piles were embedded in deep stiff clay or other supporting stratum to reduce the settlement, while the gravel cushion placed on top of the piles plays an

important role in mobilizing the bearing capacity of subsoil and modifying the stresses transferred to piles.

CPRC is an innovative concept for the use of piles with non-uniform properties below a raft foundation in order to improve its performance. More and more buildings with such a new composite foundation were practiced in the coastal cities of China. Due to its complicated constitution, it is rather difficult to perform an accurate analysis with existing analysis methods. The development in theory drops behind practices evidently. Liang et al. (2005a) summarized the origins, developments and practices of the new composite foundation.

Numerous investigations have shown that the behaviour of group piles is not identical to that of a single pile under the average load of the piles in the group. Using different length or diameter of piles could be a beneficent decision for high-rise buildings, since both the bearing capacity of the slab and that of the piles will be fully mobilized. Ahner & Sukhov (1996) reported several projects with the non-uniform piles in Germany. Most of them locate in Frankfurt Main, where the top soil layer consists of settlement-active clay. Lee et al. (2002) presented a 2500 ton oil storage tanks supported by 137 piles with varying length. The lengths and arrangements of piles have significant effect on the stresses and deflections distributed over the raft, and a rational design of piles may greatly improve the performance of piled raft foundations.

However, the application of non-uniform piles has been restricted in China in view of the safety of foundation. In the Technical Code for Building Pile Foundation of China, it specifies that the non-uniform piles should not be used in one unit of the same building. Despite of the restriction of the Technical Code, raft foundation with non-uniform piles has been practiced in China. Gong (2002) presented a simple analytical method and case histories for the non-uniform piles. Liang et al. (2003) developed a finite element model for the CPRC foundation.

CPRC acts as a composite structure consisting of raft, cushion and non-uniform piles. In the new type of foundation, the cushion made of gravels on top of the piles plays an important role. Firstly, gravel cushion between the raft and piles can adjust the load-sharing ratios of piles and subsoil, and enhance the strength of subsoil among piles. Particularly, it could avoid the separation between raft and subsoil effectively, which occurred occasionally in the practices of coastal cities in China such as Shanghai (Zhao 1989). Secondly, the setting of gravel cushion makes the assumption of analysis more close to the real boundary conditions of piled raft foundation. In the analysis of piled raft foundation, the interface between raft and soil is commonly assumed to be smooth and continuous, and the connection between the raft and the pile

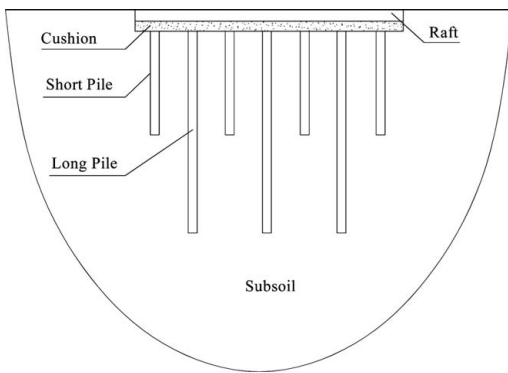


Figure 1. Sketch of composite piled raft foundation.

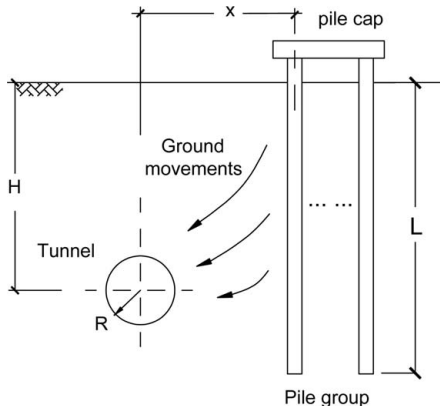


Figure 2. Pile group adjacent to tunnel.

is assumed to be a sliding ball joint for only the vertical forces transmitted from the raft to the head of piles (Hain & Lee 1978). The two assumptions imply that only the vertical component of the contact stress is presented. The presence of gravel cushion makes only the vertical forces be transmitted.

2.3 Pile responses due to tunneling

Unavoidable ground movements due to tunneling will impose additional axial and lateral internal forces on pile which may lead to structural distress or failure of the piled foundation as shown in Figure 2. Morton & King (1979) and Loganathan & Poulos (2002) carried out the static ‘1 g’ laboratory testing and centrifuge model testing respectively to investigate the effects of tunneling on the bearing capacity and pile deformation. They found that the influence of tunneling on adjacent piled foundation in weak soil may be a great concern to geotechnical engineers. Bezuijen & Schrier (1994) found that the pile settlement can be significant, if the volume loss caused by tunnelling is 1% or more and the distance between the pile and the tunnel is less than 1 tunnel diameter.

3 ANALYSIS METHOD FOR CPRC AND PILE RESPONSES DUE TO TUNNELING

3.1 Analysis method for CPRC

CPRC is rather complex and no design method be followed so far, several investigations for the design of CPRC have been reported (Ma et al. 2001, Liu et al. 2003, Song et al. 2003, Liang et al. 2003, Liang et al. 2005b).

Ma et al. (2001) discussed the basic conception of CPRC and proposed an extended composite modulus

method to calculate the bearing capacity and deformation of CPRC. Composite modulus method is a simplified method for the design of composite ground recommended by the China Technical Standard for Foundation Treatment. Piles are considered as equivalent subsoil according to the compress modulus ratio of piles to subsoil. It is only suitable for piles made of low strength materials. Long piles in CPRC are made of rigid materials, and hence the method based on composite modulus is not appropriate for CPRC.

To study the variation of the pile-soil stress ratio and the failure mode for this new type of composite foundation, Liu et al. (2003) conducted a field plate load test for CPRC. Reactions on the top of piles and subsoil were measured in the test. By comparing with the in-situ test data, the paper analyzed the reduction coefficient and the influence factor for the bearing capacity of each type of pile and the subsoil.

Song et al. (2003) proposed a analysis method for the settlement and internal force of rigid pile composite raft foundation. In this method, the raft is modelled with Mindlin plate element, and the soil-pile-cushion system is modelled through a semi-analytical solution. Besides an algorithm is proposed to consider the rigidity of the super-structure, the choices of its parameters are discussed in details. Numerical examples are presented to compare the calculated results with field measurements and with those obtained by truly three-dimensional finite element method calculations.

Analytical approach is usually not suitable for dealing with the problem of CPRC. Most of the studies carried out so far do not incorporate the effect of cushion in the analysis and all the piles have the equal length. In order to clarify behaviours of this new type of foundation, especially the influences of cushion, Liang et al. (2003) performed three-dimensional finite element analyses of CPRC. It is well known that the finite element method is versatile for studying complex boundary-value problems. The paper presented the factors affecting the behaviour of the CPRC foundation, which include the ratio of length to diameter and elastic moduli of piles, thickness and elastic modulus of cushion, etc. Load-sharing ratios of piles and subsoil as well as settlement of foundation were also investigated. Since most foundation is in elastic state under common working load conditions, the raft, cushion, piles and subsoil were all assumed to be weightless linearly elastic media. Compared with the foundation without cushion, the maximum axial stress shifts lower from the head of piles to a certain depth. The bearing capacities of shallow subsoil can be properly mobilized through an appropriately applied cushion technique, especially for ground containing hard crust in shallow layers. There exists an optimum thickness of cushion to make best use of the capacities of short pile and subsoil as well as to alleviate the stress concentration of long piles effectively. The thickness

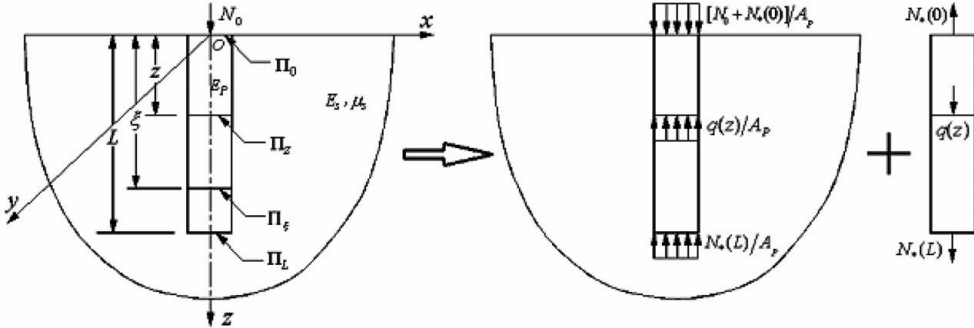


Figure 3. Scheme of imaginary piles model.

of cushion has considerable effects on adjusting the load-sharing ratio of piles to subsoil.

Finite element method is often limited in the size of problem that can be addressed due to three-dimensional nature of pile groups, especially for large pile groups. For the purpose of practical application, Liang et al. (2005b) developed an approximate approach for the analysis of CPRC. Based on an imaginary piles model shown in Figure 3 (Muki & Sternberg 1970), an integral equation approach was applied to analyze CPRC. As shown in Figure 3, let $\{0, x, y, z\}$ be a rectangular Cartesian coordinate frame spanning the homogeneous semi-infinite elastic soil medium. The embedded piles in the group are assumed to have the length of L , diameter of d , and circular cross-sectional regions of Π_z ($0 < z < L$). Following the approach proposed by Muki & Sternberg (1970), the embedding soil medium is extended throughout the half space and fictitious piles. The Young's modulus E_p^* of fictitious pile is equal to the difference of that between the real pile and the extended soil, i.e.

$$E_p^* = E_p - E_s \quad (1)$$

where E_p is the Young's modulus of real piles, and E_s is the Young's modulus of soil. The extended soil was treated as a three-dimensional elastic continuum which is represented by the material constants E_s and μ_s (the Possion ratio of soil). $q(z)$ is the "bond force" per unit pile-length exerted by the extended soil on the fictitious pile at depth z . A is the cross-sectional area of the pile. The fictitious pile is also subjected to the external axial forces $N^*(0)$ and $N^*(L)$, concentrated within the terminal cross-sections Π_0 and Π_L , respectively.

Here $N^*(0)$ is the portion of applied force $N(0)$ transmitted to the fictitious pile, and $N^*(L)$ is the bond-force exerted by extended soil on the fictitious pile. The axial strain ϵ_z^* in the fictitious pile is assumed

to be equal to that of the centre point in the cross-section in the extended soil. The Fredholm integral equations of the second kind were set up to solve the question of the interaction between piles and soil. Details of this approach can refer to the paper written by Muki & Sternberg (1970).

By simulating the cushion with the Winkler spring, the effect of cushion was taken into consideration, and then the second kind Fedholm's equations were deduced to solve the problems as shown in Fig. 4 (Liang et al. 2006).

In Figure 4, n and n' are the total number of piles and soil elements respectively ($i = 1, 2, \dots, n$; $k = n + 1, n + 2, \dots, n' + n$). p_s is the pressure acting on the spring between the raft and subsoil, N_{oi} is the resultant load acting on the spring between raft and the head of pile i , L_i is the length of pile i , d_i is the diameter of pile i , S_{ji} is the distance between the center of pile j and that of pile i , and S_{mk} is the distance between the center of soil element m and that of soil element k .

In order to verify the accuracy of the present approach, Liang et al. (2005) compared the calculated results, including compression of cushion, loads shared by piles and subsoil, load transfer characters and stress distribution of subsoil, with those from the finite element analysis (Liang et al. 2003). The analyzed model is shown in Figure 5. In the analysis, it is assumed that the long piles are made of concrete, while the short piles and cushion are made of sand-gravel. The raft is made of concrete and assumed rigid. The geometric sizes are listed as follows (Fig. 5). $d_1 = d_2 = d = 0.45$ m, $s = d$, $B = 2.7$ m, $\delta = 0.3$ m, $L_1 = 50d = 22.5$ m, $L_2 = 25d = 11.25$ m. Material properties are given as the elastic modulus of subsoil $E_s = 5$ MPa, the Poisson's ratio of subsoil $\mu_s = 0.35$, the elastic modulus ratio of long piles to subsoil $k_1 = 5100$, the elastic modulus ratio of short piles to subsoil $k_2 = 100$, the elastic modulus of cushion $E_m = 50$ MPa, and the Poisson's ratio of cushion

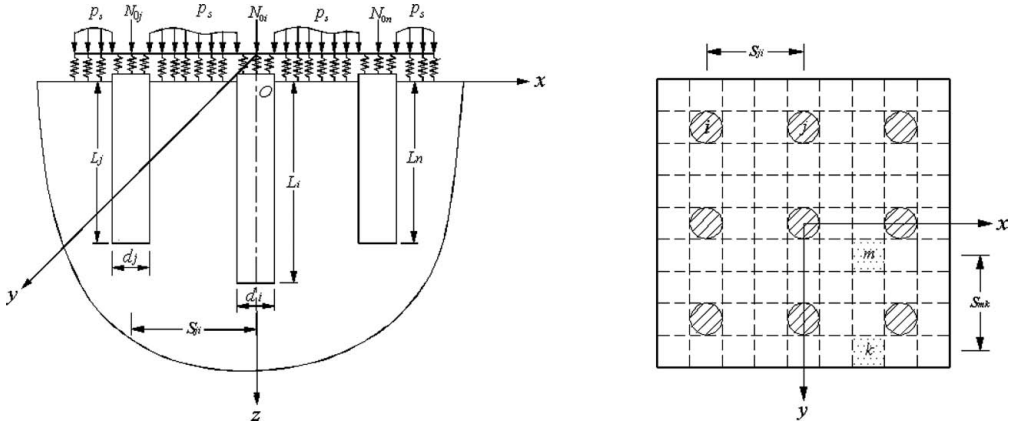


Figure 4. Scheme of CPRC.

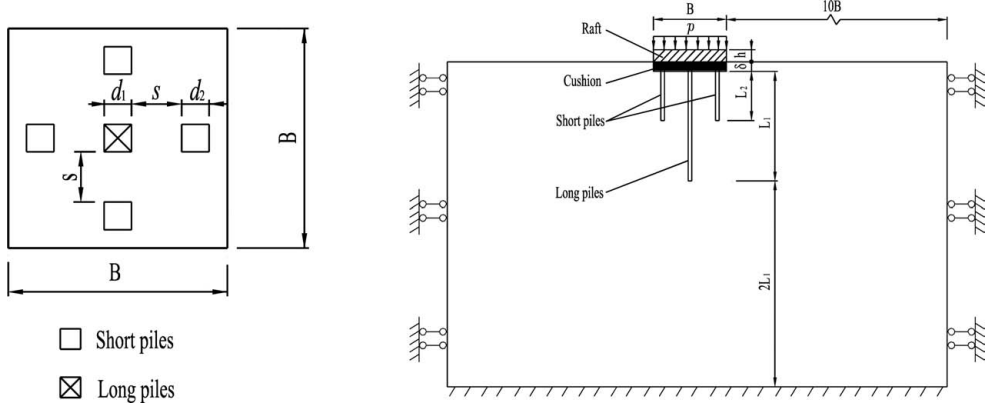


Figure 5. Schematic diagram of calculating model to be analyzed.

$\mu_m = 0.3$. The force uniformly acted on the raft is $p = 100 \text{ kPa}$.

Results of the present method were compared with those of the finite element method. Figure 6 showed the comparison of axial stress and the settlement of piles. The influences of pile length on the working behaviour of the foundation were also studied by Liang et al. (2005b). The space does not permit here the details of comparisons.

3.2 Analytical method for pile responses due to tunneling

Analysis methods to analyze pile responses due to tunneling may be classified broadly into two categories so far. The first of them is a complete three-dimensional analysis method which treats the piles and their surrounding soil as a whole during tunnel

excavation, and usually the finite element method (FEM) was used (Mroue & Shahrouz 2002, Gordon & Ng 2005, Lee & Jacobsz 2006). FEM can consider the interaction between pile and its surrounding soil, pile-to-pile interaction (PPI), the nonhomogeneous of soil and complicated boundary conditions. However, it requires substantial computational effort and professional software. It is only suitable for obtaining some detail in final design of foundation rather than a preliminary routine design tool (Kitiyodom et al. 2005). The second class is so-called two-stage approach. First, free-field soil movements induced by tunnelling (vertical and lateral) are estimated by a simple, analytical method, and, second, these estimated soil movements are imposed on the pile in the analyses by using the finite element method, boundary element method or finite-difference method, etc. to compute the pile responses (Chen 1999, Loganathan et al. 2001,

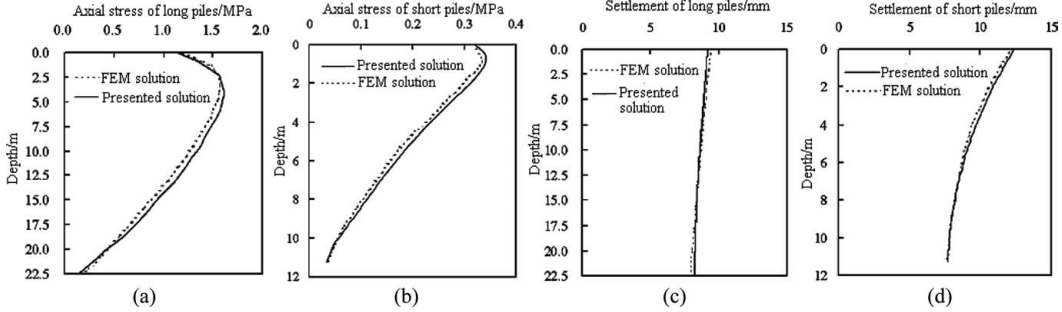


Figure 6. Comparison of the present method with FEM.

Kitiyodom et al. 2005, Xu & Poulos 2001). Obviously, two-stage method is acceptable easily by engineering designer. However, there is currently almost no simple analytical method available to evaluate pile responses due to tunneling especially considering the pile-to-pile interaction in pile groups.

Li & Huang (2007) presented a simplified analytical two-stage method to determine the deformation and internal force (both vertical and lateral) of piles due to tunnelling base on the Winkler model. The free-field soil movement due to tunnelling is calculated by the closed-form solution proposed by Loganathan & Poulos (1998) as given in equations (2) and (3)

$$U_z = \varepsilon_0 R^2 \left(-\frac{z-h}{x^2 + (z-h)^2} + \frac{(3-4v_s)(z+h)}{x^2 + (z+h)^2} - \frac{2z[x^2 - (z+h)^2]}{[x^2 + (z+h)^2]^2} \cdot e^{-[\pi(38x^2/(h+R)^2] + [0.69z^2/h^2]}) \right) \quad (2)$$

$$U_x = -\varepsilon_0 R^2 x \left(\frac{1}{x^2 + (z-h)^2} + \frac{3-4v_s}{x^2 + (z+h)^2} - \frac{4z(z+h)}{[x^2 + (z+h)^2]^2} \right) \cdot e^{-[\pi(38x^2/(h+R)^2] + [0.69z^2/h^2]}) \quad (3)$$

where U_z and U_x are the subsurface settlement and lateral movement of the soils due to tunnelling; R is the tunnel radius; z is the depth below ground surface; h is the depth of tunnel horizontal axis level; v_s is the Poisson's ratio; x is the lateral distance from tunnel centerline; ε_0 is equivalent ground loss ratio which is defined as

$$\varepsilon_0 = \frac{\pi \left(R + \frac{g}{2} \right)^2 - \pi R^2}{\pi R^2} \times 100\% = \frac{4gR + g^2}{4R^2} \times 100\% \quad (4)$$

where g is gap parameter (Lee and Row, 1992).

By imposing displacement compatibility between the pile and its surrounding soil, the vertical and

lateral governing equilibrium equation of a single pile is given by

$$\frac{d^2 W_i(z)}{dz^2} - \delta^2 [W_i(z) - U_z(z)] = 0 \quad (5)$$

$$\frac{d^4 U_i(z)}{dz^4} + 4\lambda^4 [U_i(z) - U_x(z)] = 0 \quad (6)$$

where $W_i(z)$ and $U_i(z)$ are the pile settlement and the lateral deflection due to tunnelling respectively. $U_z(z)$ and $U_x(z)$ are the vertical and lateral free-field soil movement at pile location respectively. δ and λ are the dimensionless Winkler parameters. By solving the equation (5) and (6), the single pile responses due to tunnelling can be obtained.

Mrouech & Shahrou (2002) found that the presence of the pile reduces the soil lateral deformation especially in the pile section located at the level of the tunnelling axis. This phenomenon is often regarded as shielding effects, i.e. the real displacement of the pile is equal to the free-field soil movement plus the shielding movement, in which the shielding movement is opposite to the free-field soil movement.

For the case of a piled group with n identical piles, the total displacement response of a single pile in the group both in vertical and lateral directions can be estimated from the sum of the following two components:

- (1) Displacement of the pile due to the free-field soil movement caused by tunnelling;
- (2) Shielding displacement induced by the pile-to-pile interaction (shielding effect) which decreases the displacement response of single pile due to tunnelling.

Considering an arbitrary pile i of the group, the total displacement (both in vertical and lateral directions) could be obtained by superimposition

$$W_n(z) = \sum_{j=1}^n W_{nj}(z) \quad (7)$$

$$U_{ii}(z) = \sum_{j=1}^n U_{ij}(z) \quad (8)$$

Loganathan & Poulos (2001) analyzed the elastic response of a 2×2 pile group to the soil movement induced by tunneling with ground loss ratio 1% in the problem as shown in Figure 7. The depth of tunnel centerline from the ground surface is 20 m and the tunnel diameter is 6 m. Piles in the group are spaced at 2.4 m with 0.8 m diameter and 25 m length. The horizontal distance between the “front” row pile and the tunnel centerline is 4.5 m.

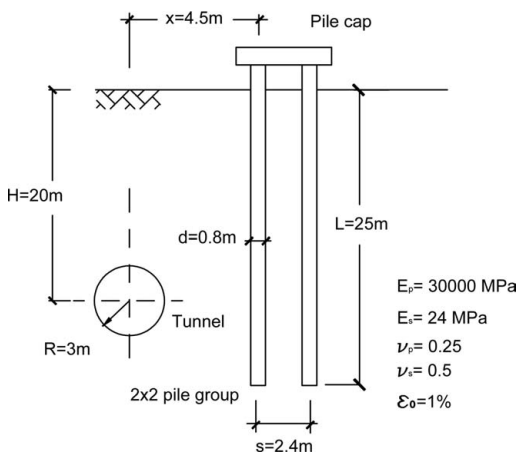


Figure 7. 2×2 pile group with cap adjacent to tunnel (Loganathan et al., 2001).

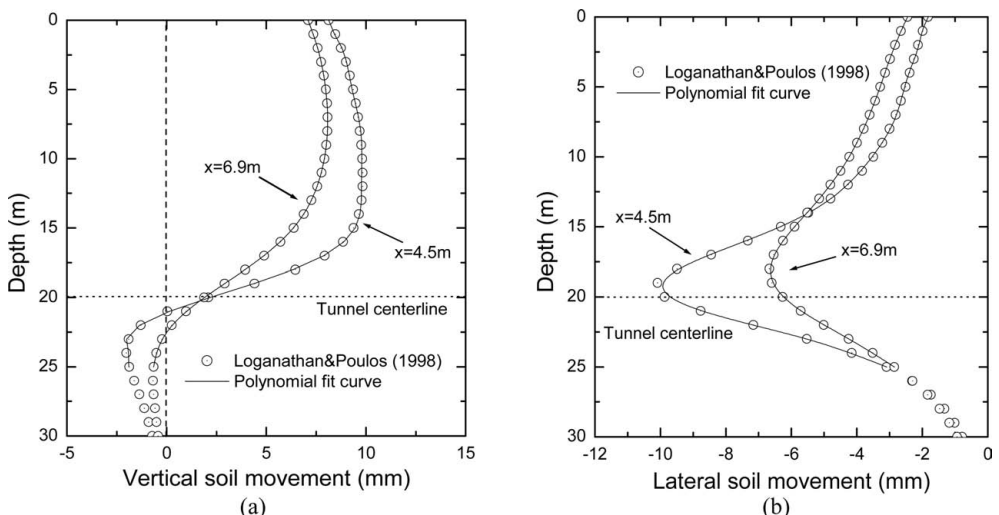


Figure 8. Free-field ground movements: (a) vertical ground movement; (b) lateral ground movement.

Figure 8 shows the free-field soil movement induced by tunnelling and its polynomial fit curve along the whole pile length at the “front” and “rear” pile. It can be found that both vertical and lateral free-field ground movement decrease with distance from tunnel centreline.

Figure 9 and Figure 10 shows the comparisons of the responses of front pile and rear pile in the piled group calculated using the proposed method with those computed by GEPAN in Loganathan & Poulos (2001) respectively. The responses of a single pile at an identical horizontal distance were also presented to illustrate the shielding effect of the pile group. It can be seen that the response profiles obtained from the proposed method match with the result calculated by GEPAN both in front pile and rear pile. The lateral deflection and bending moment profiles of pile with depth for both a single pile and a pile in piled group are almost identical, while the settlement and axial force profiles show divergence. The maximum axial force estimated for a single pile is about 20% higher than that for a front pile in piled group and about 50% for a rear pile. The settlement of a single isolated pile is slightly higher than that of a front and rear pile within piled group. It means the shielding effect of pile group subjected to soil movement induced by tunnelling in vertical direction is remarkable compared with that in lateral direction. Although the shape of profiles is identical, the maximum axial force and bending moment were underestimated compared with that calculated by GEPAN, especially for front pile.

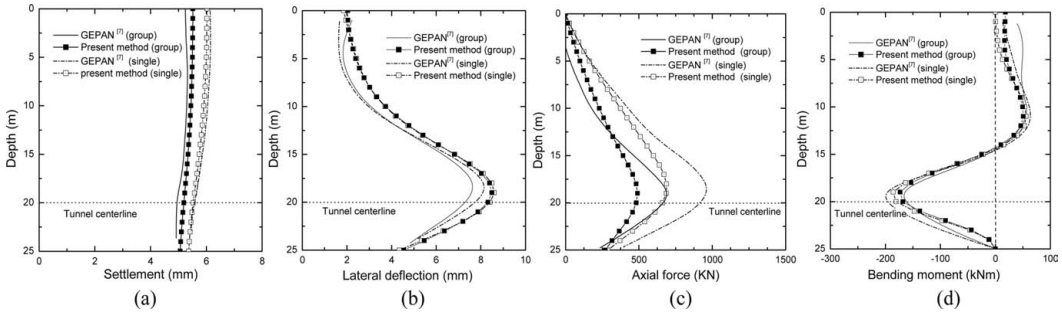


Figure 9. Computed response of front pile in 2×2 pile group: (a) settlement; (b) lateral deflection; (c) axial force; (d) bending moment.

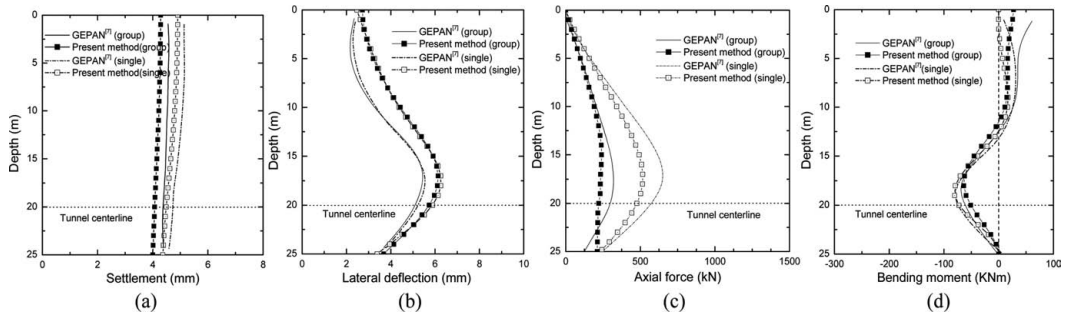


Figure 10. Computed response of rear pile in 2×2 pile group: (a) settlement; (b) lateral deflection; (c) axial force; (d) bending moment.

4 CONCLUSIONS

This paper has reviewed recent advances of the analysis of pile foundation in China. Two typical problems involving a new type of piled raft foundation – composite piled raft with cushion and the effects of tunneling on existing piles and pile groups are of particular interest in this paper. For the analysis of composite piled raft with cushion subjected to vertical load, an integral equation approach has been introduced based on an imaginary model. The effect of cushion was taken into consideration by simulating it with the Winkler spring. The accuracy of the present method was verified by the comparison with the finite element method. For the analysis of piles and pile groups subjected to ground movements induced by tunneling, a simple analytical two-stage method has been introduced. The analytical solution proposed by Loganathan & Poulos (1998) was used to estimate the free-field ground movement induced by tunneling. The free-field displacements estimated were then imposed on single piles and pile groups in simple analytical analyses to compute pile and pile group response. The proposed method was verified through the comparison with published solutions by the

boundary element program GEPAN in Loganathan & Poulos (2001). Based on this review, it has been suggested that such analytical approaches are quite efficient for the engineering computation, and provide a useful tool for engineers due to its simplicity.

REFERENCES

- Ahner, C. & Sukhov D. 1996. Combined piled-raft foundation (CBRF)—safety concept. *Leipzig annual civil engineering report—LACER* No.1. Leipzig: University of Leipzig, 333–345.
- Bezuijen, A. Schrier, J.V.D. 1994. The influence of a bored tunnel on pile foundations. *Centrifuge 94*, Leung, Lee & Tan (eds), 681–686.
- Burland, J.B. & Broms, B.B., et al. 1977. Behavior of foundations and structures. In: *Proceeding 9th International Conference on Soil Mechanics and Foundation Engineering*, Tokyo, 2: 495–546.
- Chow, Y.K. & Yong, K.Y. et al. 2001. Analysis of Piled Raft Foundations Using a Variational Approach. *International Journal of Geomechanics*, 1(2): 129–147.
- Chen, L.T. & Poulos, H.G. 1999. Pile responses caused by tunneling. *J. Geotech. Geoenviron. Eng.*, ASCE, 125(3): 207–215.

- Chen, L.Z., Liang, F.Y. et al. 2004. Field studies on behavior of composite piled raft foundation for high-rise buildings. *Chinese Journal of Geotechnical Engineering*, 26(2): 167–171 (In Chinese).
- Cooke, R.W. 1986. Piled raft foundation on stiff clays—a contribution to design philosophy. *Geotechnique*, 36(2): 169–203.
- Gordon, T.K. & Ng, C.W.W. 2005. Effects of advancing open face tunneling on an existing loaded pile. *J. Geotech. Geoenvir. Eng., ASCE*, 131(2):193–201.
- Gong, X.N. 2002. Theory and applications of composite foundation . Beijing: Press of building industry of China (In Chinese).
- Hain, S.J. & Lee, I.K. 1978. The analysis of flexible raft-pile systems. *Geotechnique*, 28(1): 65–83.
- Hou, X.Y. & Yang, M. 1996. The design theory and engineering of foundations in soft soil based on controlling settlement principle. Shanghai: Press of Tong university (In Chinese).
- Horikoshi, K. & Randolph, M.F. 1996. Centrifuge modeling of piled raft foundation on clay. *Geotechnique*, 46(4), 741–752.
- Huang, S.M. & Wang, D.M., et al. 1991. The design and preliminary practice of reducing settlement pile foundation. In: *the 6th symposium on soil mechanics and foundation engineering*, Shanghai: 405–414(In Chinese).
- Jee, C.J. & Jacobsz, S.W. 2006. The influence of tunneling on adjacent piled foundation. *Tunnelling and Underground Space Technology* 21(3–4): 430.
- Kitiyodom, P. & Matsumoto, T. & Kawaguchi, K. 2005. A simplified analysis method for piled raft foundations subjected to ground movements induced by tunneling. *Int. J. Numer. Anal. Meth. Geomech.* 29:1485–1507.
- Jee, C.J. & Jacobsz, S.W. 2006. The influence of tunneling on adjacent piled foundation. *Tunnelling and Underground Space Technology* 21(3–4): 430.
- Lee, K.M., Rowe, R.K. & Lo, K.Y. 1992. Subsidence owing to tunneling I: estimating the gap parameter. *Canadian Geotechnical Journal* 29:929–940.
- Lee, K.M. & Rowe, R.K. 1990. Finite element modeling of the three-dimensional ground deformations due to tunneling in soft cohesive soils: Part I-method of analysis; Part II-result. *Computers and Geotechnics* 10: 87–138.
- Li, Z. & Huang, M. 2007. Analysis of settlement and internal forces of grouped pile due to tunneling. *Chinese Journal of Geotechnical Engineering* , 29(3) (In Chinese).
- Liang, F.Y. & Chen, L.Z. 2004. A modified variational approach for analysis of piled raft foundation. *Mechanics research communications*, 31(5): 593–604.
- Liang, F.Y., Chen, L.Z. & Shi, X.G. 2003. Numerical analysis of composite piled raft with cushion subjected to vertical load. *Computers and Geotechnics*, 30(6): 443–453.
- Liang, F.Y., Li, J.P. & Chen L.Z. 2005a. Recent progress of composite piled raft with cushion practiced in china. In: *Proceedings of the Second China-Japan Geotechnical Symposium*, Shanghai: 609–613.
- Liang, F.Y., Chen L.Z. & Li, J.P. 2005b. An approximate approach for the analysis of composite foundation with hybrid piles. *Chinese Journal of Geotechnical Engineering*, 27(4): 459–463 (In Chinese).
- Liang, F.Y., Li, J.P. & Chen, L.Z. 2006. Optimization of composite piled raft foundation with varied rigidity of cushion. In: *GeoShanghai International Conference 2006*, ASCE, GSP153: 29–34.
- Liew, S.S. & Gue, S.S. & Tan, Y.C. 2002. Design and instrumentation results of a reinforcement concrete piled raft supporting 2500-ton oil storage tank on very soft alluvium deposits. *The 9th International Conference on Piling and Deep Foundations*, Nice, 263–269.
- Liu, F.Y., Yang X.B. & Liu, X. 2003. Field test of a composite foundation including mixed pile. *Chinese Journal of Geotechnical Engineering*, 25(1): 71–75 (In Chinese).
- Loganathan, N. & Poulos, H.G. & Stewart, D.P. 2000. Centrifuge model testing of tunneling-induced ground and pile deformations. *Geotechnique* 50(3): 283–294.
- Loganathan, N. & Poulos, H.G. & Xu, K.J. 2001. Ground and pile-group response due to tunneling. *Soil and foundations* 41(1): 57–67.
- Loganathan, N. & Poulos, H.G. 1998. Analytical prediction for Tunneling-induced ground movement in clays. *J. Geotech. Geoenvir. Eng., ASCE* 124(9): 846–856.
- Ma, J. & Zhang, D.G. & Zhang, Z. 2001. Design of the composite foundation with long short pile. *Geotechnical Engineering Technique* 15(2): 86–91(In Chinese).
- Mroueh, H. & Shahroor, I. 2002. Three-dimensional finite element analysis of the interaction between tunneling and pile foundations. *Int. J. Numer. Anal. Meth. Geomech.* 26: 217–230.
- Morton, J.D. & King, K.H. 1979. Effect of tunneling on the bearing capacity and settlement of piled foundation. *Proc. Tunneling 79, IMM, London* 57–68.
- Muki, R. & Sternberg, E. 1970. Elastostatic load-transfer to a half-space from a partially embedded axially loaded rod. *International Journal of Solids and Structures*, 6(7): 69–90.
- Peck, R.B. 1969. Deep excavations and tunneling in soft ground. *7th Int. Conf. on Soil Mech. and Found. Engng.* 225–290.
- Poulos, H.G. 2001. Pile raft foundations: design and applications. *Geotechnique*, 51(2), 95–113.
- Xu, K.J. & Poulos, H.G. 2001. 3-D elastic analysis of vertical piles subjected to “passive” loadings. *Computer and Geotechnics* 28: (349–375).
- Yang, M. 2000. Study on reducing-settlement pile foundation based on controlling settlement principle. *Chinese Journal of Geotechnical Engineering* 22(4): 482–486.
- Shi, P.D. & Hong, Y.X. 2005. The origin, practices and development of piles in China. In: *the 7th Chinese National Conference on Pile Engineering*, Ningbo, 38–47(In Chinese).
- Shen, W.Y. & Chow, Y.K. et al. 2000. A variational approach for the analysis of pile group-pile cap interaction. *Geotechnique*, 50(4): 349–357.
- Song, E.X. & Shen, W. & Jin, H. 2003. A practical method for the analysis of rigid pile composite foundation raft system . *Chinese Journal of Geotechnical Engineering*, 25(3): 268–272 (In Chinese).
- Tong, Y.X. 1979. The practiced experiences and design method of piles foundation in Shanghai. Shanghai: Electric designing institute of East China (In Chinese).
- Zhao, X.H., Li, B. & Yang, G.X., et al. 2005. Practice and theory for specially big and deep excavation engineering. Beijing: China Communications Press.
- Zhao, X.H. 1989. Design theory of piled raft and piled box foundation for the practices of high buildings in Shanghai. Shanghai: Press of Tongji university (In Chinese).

Current status of deep and pile foundations in Korea

S. Jeong

School of Civil & Environmental Eng., Yonsei Univ., Seoul, Korea

C. Cho

Samsung Corporation, Kyonggido, Korea

D. Seo, J. Lee, H. Seol, Y. Kim & J. Lee

School of Civil & Environmental Eng., Yonsei Univ., Seoul, Korea

ABSTRACT: In Korea, deep foundations such as large-diameter drilled shafts and large-section caissons are commonly used to support high-rise buildings and heavy weight structures. These piles and caissons are usually embedded in weathered- and soft-rocks of granite-gneiss with typically end-bearing type piles. This paper presents the brief summary of current status of deep foundations such as the techniques of design and analysis of pile systems, construction techniques, and quality control techniques available for last decade in Korea. In addition, new techniques such as time effect of driven pile, rock-socketed drilled shafts, single shaft-single column drilled shafts, and raft foundations are investigated and reported.

1 INTRODUCTION

In Korea, a number of huge construction projects such as land reclamation projects for many harbor terminals, offshore grand bridges, and lifeline systems are in progress in urban and costal areas. In these areas, deep foundation such as pile foundations and caissons are frequently used to support high-rise buildings and heavy weight structures for ensuring structural safety rather than serviceability limit capacity. They are: driven piles, bored piles, cast-in-place piles and open and pneumatic caissons.

With the geological characteristics and the rapid progress of economy, Korea experienced shortage of good quality land for the construction of industrial plants and hence many reclamation projects along the shorelines of western and southern coasts have been performed. Pusan clays are widely deposited varying from 20 m to 70 m thick in Nakdong River plain. The coastal area between the island Gadukdo and Noksan is reclaimed for construction of New Pusan Port in which many bridge constructions are in progress.

Recently, advanced pile techniques are being developed in Korea. The time effect of driven piles was applied in the design and practice of pile foundations. In addition, much work has been performed for the optimal design of rock-socketed drilled shaft, single column drilled shaft, soil nailed drilled shaft, piled raft foundation, and piled foundation subjected to lateral soil movements, etc.

To provide better understanding on the present status of deep and pile foundations, the authors gather the general information through comprehensive literature review, which covers over 20 publications reported in Korea. This paper describes the state-of-the-art and -practice of the deep foundations in Korea.

2 TYPES OF PILES AND THEIR STRUCTURAL CHARACTERISTICS

In Korea, different types of piles are used in construction work, depending on the type of load to carry, the subsoil conditions, and the water table. Piles can generally be divided into two categories: steel piles and PHC (Pretensioned spun High strength Concrete) piles. Table 1 shows a record of the amount of piles used in European countries in 1994 (Van Impe 1996). At the same period, there was a record in using about 5000 MN of steel piles (corresponding to 3500 km in lengths of diameter 508 mm pile) and 40,000 MN of PHC piles (14,600 km in lengths of diameter 500 mm pile) in Korea. Based on this, it was found that our products are comparable to European country and a little less than that of Japan.

Steel piles generally used are pipe piles (SPS400, SPS490) without filling with concrete after driving or preboring. When necessary, steel piles are spliced by welding and can be fitted with driving points or shoes with hard driving conditions. On the other hand,

Table 1. Record of the amount of piles used in European countries in 1994.

Data on different type of piles in the indicated countries															
		Italy		Germany		The Netherlands		U.K.		France		Belgium		Austria	
		A	B	A	B	A	B	A	B	A	B	A	B	A	B
in (%) in (km)															
15,000 km															
Cast In Place		12	1800	15	2250	8	960	7	700	27	1650	32	320	6	120
Driven	Prefabricated	Steel	1	150	5	750	—	4	400	1	60	2	20	3	60
	Concrete	5	750	10	1500	44	5280	11	1100	0.2	12	10	100	5	100
<i>With soil displacement</i>	Timber	0	—	0	—	15	1800	0	—	0	—	0	—	1	20
	Lost auger head + cast in situ or prefabricated	—	—	9	1350	8	960	6	600	6	240	30	300	2	40
Large dia (>0.65 m) bentonite															
Large dia. with lost steel casing		41	6150	28	4200	0.1	10	30	3000	40	2400	2	20	53	1060
<i>With soil excavation</i>	Auger + Bored Piles	15	2250	15	2250	23	2760	40	4000	20	1200	15	150	10	200
	Continuous flight auger Jet grouted columns and related techniques	10	1500	12	1800	2	220	—	—	2	120	7	120	10	200
Root piles and grouted micro pile		16	2400	6	900	2	200	4	240	2	20	10	200		

concrete piles are precast piles, especially PHC pile with compressive strength of about 80,000 kN/m².

3 DESIGN AND ANALYSIS OF PILE FOUNDATION

3.1 Rock-socketed drilled shafts

As discussed, in Korea, a number of huge construction projects such as land reclamation projects for an international airport, high-speed railways and many harbor constructions are in progress in urban and coastal areas. Since 1990, drilled shafts are frequently used in those areas as a viable replacement for driven piles for two applications: Deepwater offshore foundations, and foundations in urban areas where the noise and vibration are associated with pile driving. Over 90% of the drilled shafts constructed in Korea are embedded in weathered rocks. The weathered rocks, which occupy two-thirds of the total land area of the Korean peninsula, are generally the results of the physical weathering of granite-gneiss of varying thicknesses ranging up to 40 m.

Many specifications such as FHWA, AASHTO and ADSC have been reported as a design guideline of drilled shafts, however, the current design methods for rock-socketed drilled shafts are mainly based on the knowledge derived from observation of the load tests or the empirical methods related to the unconfined compressive strength (UCS) of intact rocks. However, it is known that such a design of piles is generally overconservative by as much as an order of magnitude (Osterberg, 1998). In Korea, many cases of using drilled shafts have been reported on the field of on- and off-shore piles and high-rise buildings (Seol & Jeong 2006).

According to the studies by Reese & O'Neill (1988) and Ghionna et al. (1994), the bearing capacity of rock-socketed drilled shafts should be determined by far more serviceability limit capacity within the limit of allowable settlements of superstructures than ultimate bearing capacity. In addition, because the ultimate shaft resistance is generally mobilized at smaller displacements of interface between the shaft and surrounding rock than ultimate toe resistance, piles typically carry most of their working load in shaft resistance. Therefore, for optimum designs of rock-socketed drilled shafts, predicting the shear load transfer pile into surrounding soil or rock is as important as, or possibly more critical than, doing the ultimate bearing capacity.

The capacity and shear load-movement performance of rock-socketed drilled shafts are critically dependent upon construction details and geometry conditions. A comprehensive study of these details has been reported by Horvath et al. (1983), O'Neill et al. (1995), and Seidel et al. (2001). They report that the

shear behavior of rock-socketed drilled shafts is highly influenced by the following parameters: (i) rock strength (drained intact and residual strength parameters are generally used), (ii) borehole roughness, (iii) rock mass modulus and Poisson's ratio, (vi) structure of discontinuity and surface condition of rock mass, (v) pile diameter, (vi) initial normal stress between concrete and rock prior to loading, and (vii) construction practices. However, it is difficult to implement, based on empirical methods, interaction between those factors in determining the performance of socketed pile reliably due to complexity of the interaction. A conservative approach to design is therefore rather pursued.

In Korea, some work on shaft resistance in rock sockets has been done in one of the following three ways: (1) through shearing of the bond between the concrete and the rock that develops when cement paste penetrates into the pores of the rock (bond); (2) sliding friction between the concrete shaft and the rock when the cement paste does not penetrate into the pores of the rock and when the socket is smooth (friction); and (3) dilation of an unbonded rock-concrete interface, with an inevitable increases in the normal stress $\Delta\sigma_n$ in the rock asperities around the interface until those asperities shear off, one by one (dilation). In consequence of an increase in stress normal to the interface produced by constant normal stiffness (CNS) boundary condition, the frictional resistance between pile and rock increases. As a result, the shear behavior of rock-socketed drilled shafts can be modeled better under CNS condition rather than the constant normal load (CNL) condition. Therefore, many research based on CNS direct shear tests has been progressed to analyze characteristics of shear load transfer for rock-socketed drilled shafts in Korea since 1990's. These phenomena are illustrated schematically in Figure 1.

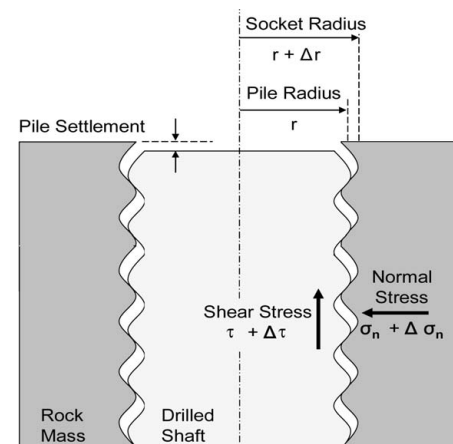


Figure 1. Behavior of pile socketed in rock.



Figure 2. Incheon 2nd bridge.

3.1.1 Axial load design concept

The geotechnical design of drilled shafts requires the consideration of both the serviceability and strength limits.

The serviceability limit ensures that the function of the structure under normal service conditions performs satisfactorily. This limit requires the determination of the top load-settlement curve in order to ensure that the settlement (wall) developed under the design allowable load (Q_{all}) is less than the tolerable settlement.

The strength limit ensures that the design provides adequate margin of safety against geotechnical failure. This limit requires determination of the ultimate unit base resistance (q_{max}) of the rock layer beneath the shaft, ultimate unit side resistance of the rock around the shaft (f_{max}), the average load factor and resistance factor (f) in the load and resistance factor design (LRFD) method, and the factor of safety (FS) in the allowable stress design (ASD) method.

In Korea, firstly, LRFD method has applied to design the Incheon 2nd bridge. Here, the LRFD approach applies separate factors (load factor and resistance factor) to account for uncertainty in load and resistance. This will provide a more reliable approach for the design of highway structures and achieves a more consistent level of safety in both structure and sub-structure design.

3.1.2 Field case study

Since 1990's, active development of the coastal areas has brought increased pressure to build coastal bridges such as the Seohae, the Youngjong and Kwangan grand bridges. Interestingly among them, the Incheon 2nd bridge project is now being performed for connecting between the Incheon international airport and new Songdo city in Korea. The total length of incheon 2nd bridge is 11.6 km including 1.5 km cable stayed bridge, which were socketed to rocks. If the Incheon 2nd bridge is completed, it will be the 5th longest cable stayed bridge in the world. Pile foundations of Inchoen

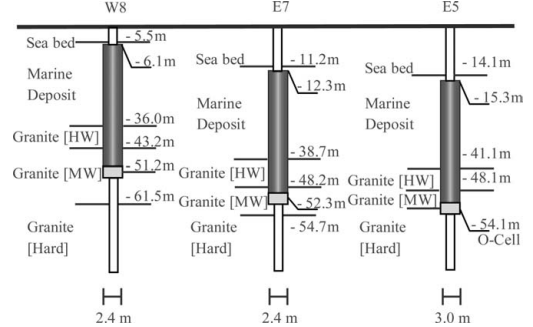


Figure 3. Subsurface profile and shaft embedments for test piles.

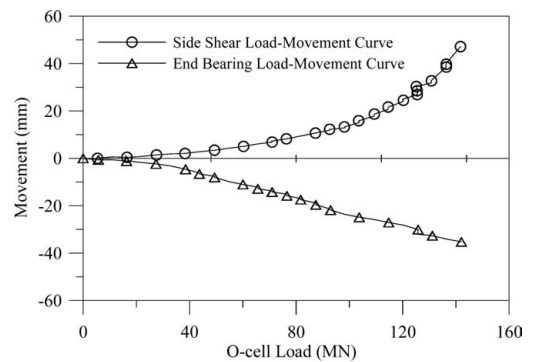


Figure 4. Load-deformation curve of test shaft, E5.

2nd bridge consist of large diameter drilled shafts, up to 3 m in diameter and 55 m in embedded length.

Figure 3 shows the subsurface profile and shaft embedment of test piles constructed for loading test. Both of test piles W8 and E7 are 2400 mm in diameter and 45.1 and 40.0 m in length, respectively. Test pile E5 is 3000 mm in diameter and 40.1 m in length. All test piles were performed using bi-directional loading test (Osterberg cell test) suited for the high bearing capacity of large-diameter pile. They were loaded enough to quantify ultimate shaft resistance (f_{max}). Applied loads of test piles W8, E7, and E5 were 240 MN, 170 MN, and 284 MN, respectively. Especially 284 MN of test pile E5 corresponds to a new world record of loading using the Osterberg cell test. Figure 4 shows Load-deformation curve of test shaft E5.

Prior to starting the load testing program, borings were approximately carried out as deep as 70 m to; identify the subsurface materials, differentiate the in-situ characteristics of the soil and rock layers, and obtain samples for testing. In addition, pressuremeter test (PMT), elastic-wave tomography, borehole shear test (BST), borehole image processing system (BIPS),

Table 2. Summary of site investigation.

	Fill	Deposit	Residual	HWR	MWR	Soft Rock	Hard Rock
γ_t (kN/m ³)	18.1	18	(18.5)	20	21	25	26
N value [TCR]	1~ 20	2~20	30~ 50/1	~50/1	~50/1	[100]	[100]
U_s (MPa)	–	–	–	(10)	(20)	37	65~95
D (MPa)	–	–	–	140~ 1250	300~ 3100	5200	10700
E_{mass} (MPa)	–	–	–	650~ 2500	5700	10400	–
v (0)	(0.32)	(0.4)	(0.32)	0.3	0.28	0.25	0.22
C (MPa)	0	0.08	0	0.10	0.10	0.15	–
Φ (Deg)	(27)	0	(30)	32	33	(35)	(38)
R.M.R	–	–	–	–	–	20~60	–
R.Q.D	–	–	–	0~5	0~10	0~68	0~100

Note : () means general reference value presumed without performing field tests.

and many other tests were additionally performed to investigate for rock layers in detail. Results based on site investigations are summarized in Table 2.

3.2 Piled raft foundation

In Korea, to date, conventionally capacity based design has been performed for the pile foundation. This means that the total structural load is transferred by piles, considering the factor of safety against a bearing capacity failure. Moreover, the contribution of the raft for the transmission of the load directly to the supporting soils is usually neglected.

However, piled raft foundation concept differs from conventional foundation design. It is a composite construction consisting of the three bearing elements piles, raft and subsoil. In this concept the piles are usually not required to ensure the overall stability of the foundation but to act as settlement reducers. A major design question is how to design the pile elements optimally to minimize the settlements of the piled raft foundation. So piled raft foundations is considered an economical foundation type compared to conventional foundation. But no standards or design regulations are available for the reliable design and analysis of piled raft foundations in almost countries in the world.

In Korea, a south-west coastal area has been developed since the 1990's. In this area, a soft clay layer, about 20~30m thick, has been deposited over the bearing layer. So foundation designs based on piled raft foundation concept are adopted for preventing an excessive amount of pile used and an increasing number of structures are founded on piled raft.

In the past decade, various researches have been developed with field measurements, model tests and numerical analyses. In Korea, various numerical

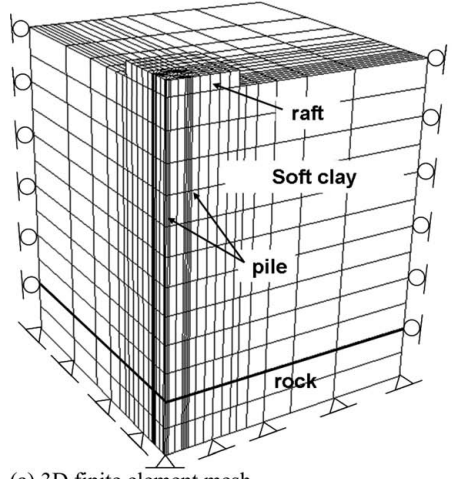


Figure 5. Test shafts on the offshore area.

analyses and model tests to analyze the behavior of piled raft have been developed. Among these methods, field measurement has been considered as the most appropriate method for investigating the real behavior of a piled raft but they needs lots of costs and time. Although numerical methods were an approximate methods and they must be additionally verified, but there are less costly and simply than model and field testing so numerical methods have been developed in the last two decades.

Numerical methods of the piled raft have been summarized by Poulos (2001). There were three broad classes of methods of analysis: simplified calculation methods; approximate computer-based methods; and more rigorous computer-based methods. In most numerical analyses, the piled raft was modeled by a thin plate on springs where interactions of pile-raft-ground were simplified using interaction factors obtained from parametric study. This modeling had the priority in the calculation time, but did not consider a complex soil-structure interaction in the analysis. Recently, because of the development of computer technology as well as computational methods, 3D finite element problems can be analyzed on personal computers. In addition, there are several finite element programs available for the analysis. Thus, the authors believe that the modeling of the raft, piles, and supporting soil as a soil structure interaction using 3D nonlinear finite element method is a feasible method for the analysis of this complex foundation.

There is an example of 3D finite element analysis of “floating” piled raft on soft clay (Fig. 6). In general, the piled raft has proved to be an economical foundation type, compared to the conventional pile foundations. However, there is a reluctance to consider the use of piled raft on soft clay, because of an excessive settlement and insufficient bearing capacity. Despite these reasons, the settlement of the piled



(a) 3D finite element mesh

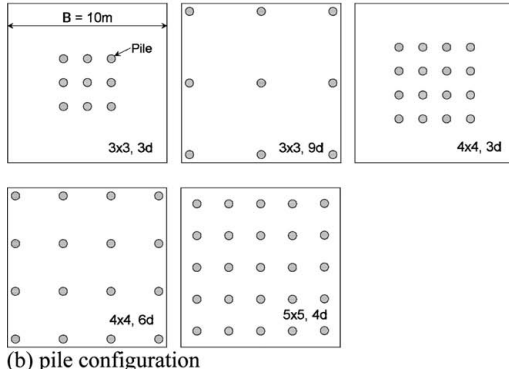


Figure 6. 3D finite element mesh and pile configuration used in the analysis.

raft may be effectively reduced by using an optimal arrangement of piles in a group.

Figure 6 shows the 3 Dimensional behavior of piled raft on soft clay based on a numerical study using 3D finite element method considered in this study. In soft clay condition, the soil-structure interaction is so complex that simplified methods cannot model problem correctly because of large settlement and nonlinear load-settlement behavior. Thus, the modeling of the raft, piles, and supporting soil as a soil-structure interaction problem using 3D FEM is a suitable method. A series of numerical analysis was performed for a various pile lengths and pile configurations on the raft subjected to vertical loading.

Based on the results of the parametric study, comparisons were made among unpiled raft, freestanding pile group (FPG) and piled raft (Fig. 7).

The influence of the pile lengths and configurations were important to reduce the average settlement

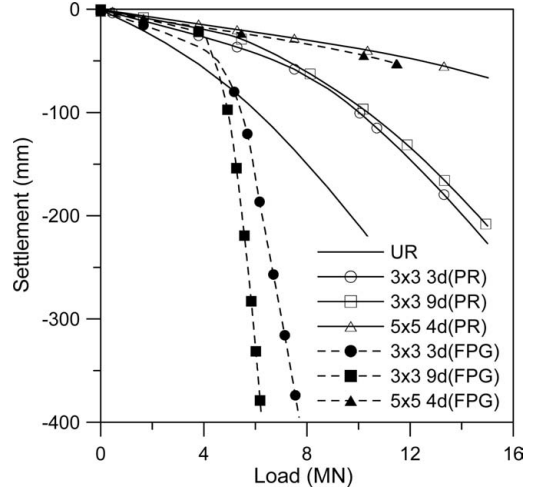


Figure 7. Unpiled raft (UR), Freestanding pile group (FPG) an piled raft (PR):load-settlement curves.

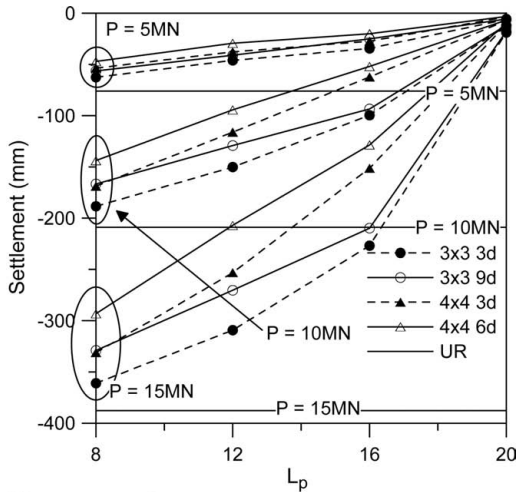
(differential settlement) of the raft. For all cases, it is shown that the average settlement generally decreases with an increase in pile length and spacing. The differential settlements are much more sensitive to the pile length and configuration than the average settlement (Fig. 8). Importantly, the floating piled raft on soft clay effectively reduces the settlement, compared to the piled raft supported by end bearing piles.

3.3 Design of single column bents

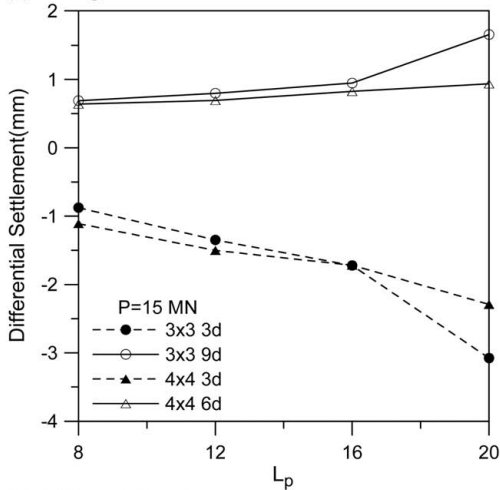
3.3.1 Introduction

Single column bent is a drilled shaft that is continuous with the column. Single column bents have been broadly increased to use for the support of highway and railway structures in Korea and elsewhere due to their cost-effective and spacing-saving features. These structural elements typically consist of a continuous shafts/column with either a constants cross section, or a reduced cross section, above grade. This type of foundation has the advantage of avoiding problems associated with the column-pile caps-piles and the fact that the excavation can be readily inspected and the competency of the bearing material can be verified. Because of this interest, single column bents were constructed for a few civil engineering projects (Inchon 2nd Bridge, Geoga grand Bridge).

Two kinds of single column bents are widely encountered in bridge construction in Korea. The pile shaft is either Cast-In-Drilled Hole (CIDH) pile shafts, or Cast-In-Steel-Shell (CISS) pile shaft. The maximum moment in single column bent occurs at a depth of one to two pile diameters below grade, and thus



(a) average settlement



(b) differential settlement

Figure 8. Average settlement and differential settlement with pile length (L_p) and configurations.

inelastic flexural deformations are expected below ground line (Fig. 9). The resulting plastic hinge may be relatively long compared with commonly used relations to estimate plastic hinge length as a consequence of the gradual variation in moment.

Typical design guidelines of single column bent allow variable ductility levels depending on the bridge importance and the redundancy of the structural system (Caltrans 1999). However, while these design procedures often address strength and capacity of such structures to prevent collapse, they remain poorly calibrated for large diameter shafts.

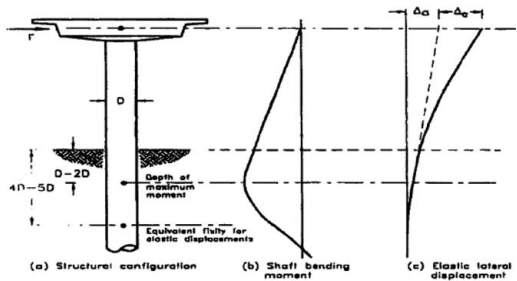


Figure 9. Response of single column bent to lateral loading (Priestly et al., 1996).

3.3.2 Design for axial load

Single column bents were originally designed resist load only in end bearing. Thus, the design involved the use of the equation of bearing capacity. Numerous loading tests conducted on instrumented drilled shafts showed that single column bents can often produce a substantial amount of resistance in side shear. Concurrently, design method has been developed to predict the skin friction resistance. This concept of axial load for design is widely accepted by the engineering profession for the computation of the ultimate resistance of single column bents. To aid in the design, variable load tests performed to assess single column bents performance and soil response. Results of a number of loading test under compressive loads reflect the design in construction projects of Korea. Field testing should be more considered to be a part of the design with site conditions.

3.3.3 Design for lateral load

Single column bent is employed most frequently either to support heavy loads, to minimize settlement, to support uplift loads, or to support lateral loads. The performance of single column bent under lateral loading is important consideration in design. Single column bent subjected to lateral loads should be designed so that they satisfy three conditions: (1) Single column bent should be able to carry the imposed load with an adequate margin of safety against failure in bending; (2) the deflection of the foundation under load should not be larger than the tolerable deflection for the structure it supports; and (3) the soil around the pile or shaft should not be loaded so heavily that it reaches its ultimate load-carrying capacity.

Such large displacements are required to mobilize the ultimate capacity of the soil that soil failure does not control the design in most cases. Principal interest usually are the lateral deflection of single column bent and the maximum bending moment in most heavily loaded single column bent. Specifically, observation of single column bent during past earthquakes has shown that the integrated shaft/column bridge bents

tend to develop large deflections when subjected to earthquake loads.

Two relatively simple methods that can be used to analyze laterally loaded single column bent approximately are the Equivalent Cantilever Method (Davisson 1970), and Broms' Method (Broms 1965). The Equivalent Cantilever Method is well-suited for estimating the buckling load for freestanding single column bent. Broms' Method can be used to estimate ultimate strength-state resistance. Another method, so called the p-y method (McClelland & Focht 1958), which can deal better with the nonlinear aspects of the problems. The p-y method is an extension of the subgrade reaction approach as soil is represented by a series of nonlinear springs. The reaction of the soil against the shaft is related to the deflection of the shaft by means of nonlinear p-y curves.

Analytical methods can be employed to compute the deflection and rotation of the shaft at grade and the bending moment and shearing force within the shaft as a function of depth. Such information is necessary so as to assess deformation in the superstructure and to design the single column bents. Allowable lateral displacement based on Specification for highway bridges (Korea Road Association reformed in 2005) is not over 50 mm. In order to evaluate the effect of the soil-shaft interaction and to gain better understanding of p-y behavior for single column bents that are commonly used in Korea, a full-scale, reinforced concrete shaft was recently constructed and tested in the field under static and cyclic lateral loading (Inchon 2nd Bridge project).

3.3.4 Behavior prediction of single column bent

Several theoretical and numerical approaches have been developed and implemented to consider slightly different assumptions for design and analysis of single column bent. Load transfer curve methods, based on the assignment of a set of p-y, t-z and q-z curves, provide approximate, yet accurate soil-single column bent interaction analysis. To carry out structural analysis, beam-column method, one of the most practical approaches, is used for numerical modeling of the shaft-soil system. Finite difference techniques are used to solve the non-linearity differential equations governing compatibility between the shaft displacement and the load transfer along the shaft.

The behavior of single column bent subjected to axial loads was evaluated by load transfer curve method. The axial behavior of soil-shaft interaction is modeled by beam-columns, with discrete nonlinear soil spring in form t-z curves for side friction, and q-z curves for end bearing. The soil is represented by a set of nonlinear load-transfer curves representing the soil resistance as a function of shaft displacements at several discrete points along the shaft. The load distribution and deformation of shafts to axial load are estimated by the analytical method.

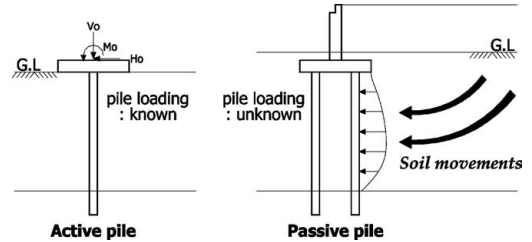


Figure 10. Active piles and passive piles.

Analysis for single column bent commonly involves the use of a beam on the nonlinear Winkler foundation analysis in which the soil reaction (p) is related to shaft lateral deflection (y). The lateral analysis of the system based on the beam-column model and nonlinearity in p-y curves was developed to consider material non-linearity and $p\Delta$ effect.

To investigate the accuracy, efficiency, and applicability of the analytical method, its results are compared with the results obtained from field case studies and commercial codes. For the comparison study, the prediction by present study simulates well the general results on axial and lateral loads. It is found that the maximum bending moment is located within a depth approximately 1.5D (D: shaft diameter) below ground surface when material non-linearity and $p\Delta$ effects are considered.

3.4 Piles subjected to lateral soil movements

Pile problems subjected to lateral soil movements and lateral pressures are one of the hot topics encountered in soft clay in Korea for last decade. A distinction can be made between the two following groups (Fig. 10) of these problems:

1. piles which are expected to transmit lateral loads to the soil;
2. piles which are subjected to lateral loading along their shafts by horizontal movements of the surrounding soil.

In the first group the horizontal load on the piles is the cause and the horizontal soil movements are the consequence; we can call these piles "active piles". In the second group the horizontal soil movements are the cause and the horizontal loads along the pile shaft are the consequence. We can call these piles "passive piles". Examples of passive piles include piles adjacent to tunneling and excavation, piles adjacent to pile driving, piles for stabilizing a slope, and pile-supported bridge abutments adjacent to approach embankments (Jeong, 1998).

Two problems were mainly occurred for the passive piles: (1) structural distress or breakage due to

significant lateral loads and (2) lateral pile displacement exceeding serviceability criteria. In Korea, problems related to this phenomenon were publicly reported since the 1980s. In recent years, field cases related to the occurrence and measurements on reclamation areas were reported because of the big projects for new land development (New Incheon Port, Pyeongtaek-Dangjin Port, Gwangyang Port, New Busan Port, New Ulsan Port, and so on). Since early 1980s, theoretical and experimental studies in Korea have been carried out on the passive piles (Hong 1984, 1999, KHC 1996, Jeong et al. 2002). In this study, various researches conducted in Korea were briefly reviewed according to three categories: field study, centrifuge study, and numerical study. Also, the design guidelines used in Korea were discussed.

3.4.1 Field study

In Korea's field studies, special attention has been given to the bridge abutment movements (Hong et al. 2001, Jeong et al. 2002, Lee et al. 2003). Korea Highway Corporation (1996) reported on 140 cases of bridge abutment movement on highway construction sites in Korea and suggested the design guideline (Modified I index, M_{IL}) for the lateral movement of bridge abutments as follows.

$$M_{IL} = \alpha \cdot \frac{\gamma \cdot H}{c} \quad (1)$$

where, c is average value of undrained shear strength in soft clay layer, $\alpha (= (b \times D)/(B \times A))$ is the area ratio of piled bridge abutment to soft clay layer subjected to lateral soil movements, γH is surcharge load, b is sum of pile width normal to the longitudinal axis of embankment, D is soft clay layer depth, and BA is piled bridge abutment area. According to this method, the lateral movement of piled bridge abutments was occurred by unsymmetrical surcharge loads if the value of M_{IL} index is less than 1.5. Based on the limit of 15 mm, the lateral movement was occurred at the 38% of measured bridge abutments.

Chung-Ang University research team (12 cases in Hong et al. (1994); 30 cases in Hong et al. (2001)) was reported various field data and suggested that the lateral movement of bridge abutments may occur when the safety factor of slope is less than either 1.5 in case without the pile effect or 1.8 in case with the pile effect.

3.4.2 Centrifuge study

Based on the field studies, it is difficult to examine the mechanism of piles or piled bridge abutments subjected to lateral soil movements due to the site-specific characteristics in field data. While centrifuge modeling, because of its ability to produce the same stress level in a small-scale model as those in an equivalent

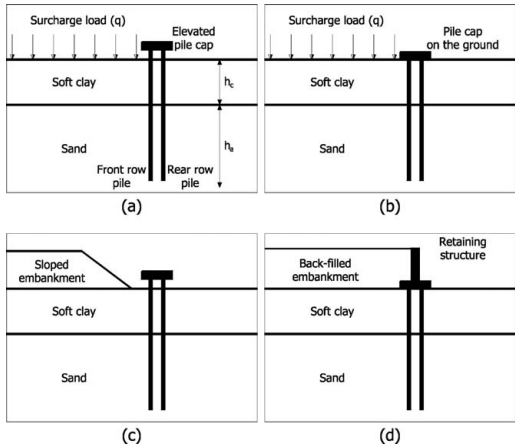


Figure 11. Centrifuge model test configuration.

full-scale prototype, is a powerful tool in studying soil-structure interaction problems.

The schematic centrifuge model test configurations of pile groups on soft clay subjected lateral soil movements are illustrated in Figure 11. Based on the previous studies in foreign and domestic research field, in this study, elevated pile cap (Fig. 11a) was used in Springman's (1989) and Jeong's (2004) tests, Bransby (1993) carried out four tests with the pile cap contact with the soil surface (Fig. 11b), Stewart's (1992) tests are applicable to a sloped embankment (Fig. 11c), and Kimura et al.'s (1994) and Ellis's (1997) tests corresponded to a back-filled embankment using an abutment wall (Fig. 11d).

Table 3 describes detailed information on centrifuge model tests carried out until now (Jeong et al., 2004). Here all data were converted to equivalent full-scale values. The soft clay layer is identified by the depth (h_c), initial undrained shear strength at mid-depth (c_u), and stress condition. Surcharge loading category was divided into pressure systems (which do not model shear loading along the clay layer surface) and inflight simulation of a sand embankment. The pile group is characterized by the pile diameter (d_p), total length (L), length of embedment in a stiff substratum (h_a), pile flexural rigidity ($(EI)_p$), pile arrangement (s_1, s_2), and pile tip fixities.

Three geotechnical centrifuges are already operating at National University of Chungbuk, National University of Kangwon, and Daewoo Institute of Construction Technology in Korea. The centrifuge (600 g-ton) at Korea Water Resources Corporation (KOWACO) was installed at September 2006 and is operating now. This facility is designed to have 8 m arm radius to the platform and the large scale earthquake hydraulic shaker. Also, the other centrifuge facility (240 g > ton) is now being constructed at Korea

Table 3. Representative studies of centrifuge model tests.

Researcher	Springman(89)	Stewart (92)	Kimura et al. (94)	Bransby (95)	Ellis (97)	Jeong et al. (04)
No. of tests	8	7	8	4	4	5
Acceleration level (g)	100	110	100	100	100	40
Clay layer properties						
h_c (m)	6.0, 8.0	8.0, 18.0	10.0	6.0	6.0, 10.0	5.3, 11.2
c_u (kPa)	15	15	15	40	25	15
Surcharge loading system						
q (kPa)	200–250	100	160	210–220	140	110
Fill or pressure	Pressure	Fill	Fill	Pressure	Fill	Pressure
Construction period (days)	100–500	1000	Not available	14, 30	21, 158, 210	75, 150
Pile group properties						
Pile-head	Free/fixed	Fixed	Fixed	Fixed	Fixed	Fixed
Pile-tip	Free	Free	Free/fixed	Free	Free	Fixed
h_a (m)	10, 8	14, 4	3, 0	10, 13	9, 13	2, 8.2
L (m)	20	24	13	19	19	16
d_p (m)	1.27	0.43	1.00	1.27	1.27	0.8
$(EI)_p$ (MN/m ²)	5131	85.6	1180	5131	5131	1069.6
S_1/d_p	3.15, 5.25	–, 4.9	3.5, 7.5	5.25	5.25	3.3
S_2/d_p	–, 3.94	–, 6.5	3.0	3.94	3.94	3.3
Structure						
Retaining wall	No	No, yes	No, yes	No	Yes	No

Advanced Institute of Science and Technology (KAIST). This centrifuge facility will include an inflight biaxial shaking table, 4 degree-of-freedom inflight robot and general modelling equipments. In Korea, Jeong et al. (2000) were conducted centrifuge model tests on stabilizing piles in weathered slopes. Also, a series of centrifuge model tests of pile groups subjected to lateral soil movements were performed by Jeong et al. (2004). Due to state-of-the-art facilities, the centrifuge studies will be actively conducted on the static and dynamic behavior of pile foundations.

3.4.3 Numerical study

In Korea, 2D or 3D numerical studies have been carried out at design stage in order to check the lateral movement of piled bridge abutments. Simultaneously, slope stability checks were conducted to examine the general stability of piled bridge abutments. The FE codes such as ABAQUS (Jeong & Kim 2000, Seo et al. 2001), PLAXIS (Jeong et al. 2000), AFFIMAX, FLAC, PENTAGON and the slope stability programs such as GEO-SLOPE, TALREN97, SLOPILE (Hong 1999) were widely used in Korea.

4 CONSTRUCTION OF PILE FOUNDATION

Driven piles are traditionally used in Korea. Especially, long driven piles have been often installed on the

onshore or offshore. For example, steel piles, up to 1852 mm in diameter and 88 m in embedded length, were installed on the Pusan new port and the Namhang bridge of south coast in Korea.

Since some problems in environment are caused in the use of driven piles, the demands of low-noise and low-vibration pile methods such as bored piles and drilled shafts are increasing as a substitute. In addition, the usage of PHC piles is gradually increased because of improved capabilities. For instance, PHC piles, having of 600 mm in diameter and 60 m in length, were founded on the Jinhe, which is located on south coast in Korea.

General low-noise and low-vibration pile methods are summarized in Table 4. In Korea, SIP (Soil-cement Injected Pile) method, in which ready-made pile is inserted into borehole after excavating, and PRD (Percussion Rotary Drilled) method, in which auger with ready-made pile excavates soil and then installs that pile simultaneously, are mainly used. On the other hand, small-diameter (≤ 600 mm) drilled shafts method have been used in Europe and North America. Small-diameter drilled shafts method have some difference according to regions. Displaced piles are mainly used in Europe, whereas non-displaced piles by using ACIP (Augered Cast-in-Place) method are done in North America. In Korea, non-displaced small-diameter drilled shafts by using Omega method were introduced from Europe, but not applied due to

Table 4. Low-noise and low-vibration pile methods.

Pile type	Construction method
Bored Precast Pile	SIP, SDA(DRA), PRD
Small-dia. drilled shafts	ACIP, Atlas, Fundex, Omega
Large-dia. drilled shafts	RCD, All casing
Micro Pile	Micro Pile

difficulty in quality control and difference in construct condition.

Recently, large-diameter drilled shafts are used as a viable replacement for driven piles since structures become more larger and heavier. This tendency more grows because a cost of steel rises and low-pollution advantage of drilled shafts are raised.

Large-diameter drilled shafts in Korea are mostly founded on rock using reverse circulation drilling (RCD) method, all casing method, or combination of those methods. Stability of the excavated soil wall is maintained either by the use of temporary casings and water or bentonite. For circular piles, the latter is less common. Casings are installed using hydraulic oscillators, pneumatic swingheads or vibratory hammers. The water level within the casing is normally maintained above ground water level and dry excavated piles are rare. In stiff ground and in rock, the bottom section of the bore may be completed with no casing. To minimize the difficulty in withdrawing the temporary casing during concreting, daily twisting, lifting and pushing down the casing by an oscillator is a common practice. Inevitably, the capacity of side shear resistance of piles will be affected by this kind of operation. After excavation, concreting is normally accomplished by gravitational tremie pipe under water/bentonite. Piles of diameter up to 3.0 m are common and depths may extend to over 80 m. Heavy self-guiding rope-operated and hydraulic rectangular grabs, clamshell mechanical grabs and hydrofraise reverse circulation trench excavating machines (i.e., hydromills) are commonly used for the excavation of drilled shafts. With the aid of chisels, rock mills or hard rock cutter tools, excavations are possible through any type of hard soil or rock in order to reach the bearing layer to establish the end-bearing point. During the mixing of the fresh bentonite prior to concreting, the quality and properties of the bentonite slurry are monitored and closely controlled to meet the specifications. After excavation and before cleaning the spoil at the base of the trench with a grab, scraping of the filter cake from the vertical sides of the trench with a modified clamshell mechanical grab with a wire brush is sometimes practiced during the trench excavation. Base cleaning, reinforcement cage lowering and concreting are commonly consecutively executed to form the shafts.

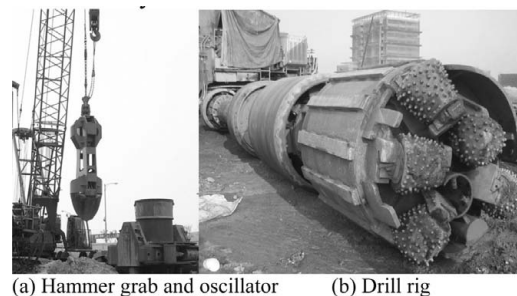


Figure 12. Drilling equipment.

5 LOAD TEST AND QUALITY CONTROL OF PILE FOUNDATION

5.1 Axial load test

In Korea, load tests used are classified into static load test, statnamic loading test, pile driving analyzer (PDA), osterberg cell test, and pseudo static loading test. Since 1994, the most general load test is performed using the PDA, which has been used as an effective tool for the construction control of pile foundation, measured force and particle velocity in pile due to driving, and calculated several control parameters based on the 1-D wave propagation theory. The SPT involves stress wave propagation in a slender rod due to hammer impact, like pile driving, and thus, the principle of wave mechanics is applicable to this dynamic penetration test.

PDA acquires the time histories of force and particle velocity due to driving of sampler, and also calculates the transferred energy through both square force and force-velocity integration method. The force and velocity measurements during SPT are similar to the routine measurements performed during dynamic testing of piles. Rod energy ratio(ER_r) is defined as the ratio of the calculated energy to theoretical energy, and is in turn expressed by multiplication of velocity energy ratio(ER_v) and dynamic efficiency(η). Selecting the measuring location below anvil removes the inconvenience to consider velocity energy ratio and dynamic efficiency separately.

However, the PDA is an indirect method, restricted to driven pile. Set-up (freeze) and relaxation are typical accuracy problems from the PDA (Fig. 13). As a number of huge constructions are being in progress in urban and coastal areas, large diameter drilled shafts are frequently used as a viable replacement for the driven piles.

Generally the high capacity of large diameter drilled shaft, in combination with the high cost of top load systems providing over 10MN reaction, make conventional load testing too costly or otherwise impractical

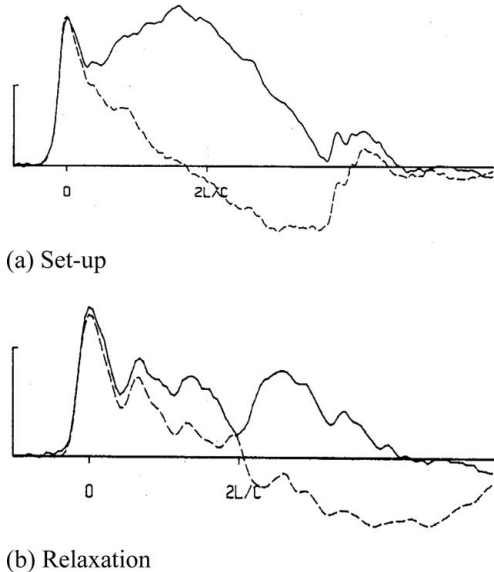


Figure 13. Time effect (PDA).

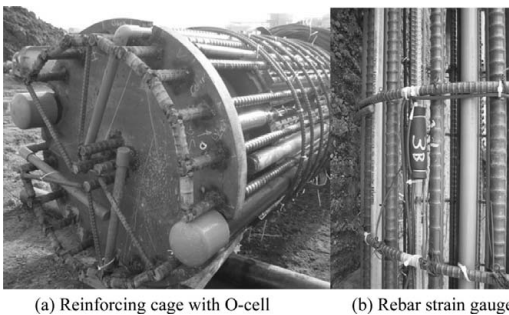


Figure 14. Instrumentations of test shaft.

for routine testing. Bi-directional loading test (osterberg cell test), providing high capacities at affordable cost, has therefore become an attractive alternative method for testing drilled shafts in Korea.

The bi-directional loading test provides the opportunity not only to confirm the design assumptions used to calculate the capacity of the shaft, but to determine the distribution of shaft resistance dissipation over the length of the shaft and to isolate the end-bearing capacity.

Figure 14 shows a reinforcing cage with osterberg load cell (O-cell) used in field load tests. The O-cell, a static-loading test device for drilled shafts, is a hydraulic jack used to induce an upward and downward

vertical load at the bottom of the shaft. The O-cell is pressurized using a compressed air driven pump with diluted automotive antifreeze as the hydraulic fluid. The soil and/or rock surrounding the shaft or pile provide the reaction for the load test. As the cell is pressurized, the bottom of the cell moves downward, causing end bearing forces, while the top of the cell moves upward, causing shaft resistance.

In this study, all drilled test shafts were instrumented with rod extensometers (Fig. 14a) and strain gages (Fig. 14b) installed in groups of four separate gauges along the length of the shafts to obtain information on the shaft resistance distribution as well as O-cell. The strain-gauge readings at the start of the test were taken to be zero. Therefore, strain recorded during the test corresponds to the increase of load (for each gauge level) and reflects the load generated by the O-cells after the transfer of self-weight is completed.

The testing procedure followed ASTM 1143-81 quick load test method, applying small, approximately equal increments of load at equal short time intervals. The load increments were applied by increasing the pressure in the O-cells in steps. The increments were applied approximately every 15min until the observations showed excessive displacement of either the shaft (upward) or the base (downward), or until the maximum capacity of the particular O-cell combination had been reached. Readings of all gauges were taken into each load increment. A graph of total cell separation versus applied hydraulic pressure is plotted as the test progressed, and the loading is terminated when distinct steepness of the load-displacement curve took place, characteristic of imminent failure. The load test is generally performed to load the drilled shafts up to three times the anticipated working capacities of the test shafts.

5.2 Axial test results

The O-cell loads drilled test shafts in compression similar to a conventional top load test and thus the data from an O-cell test could be analyzed in much the same way as data from a conventional top load test. The only significant difference is that the O-cell provides two load-deformation curves, one for shaft resistance and one for end bearing.

In this study, the three assumptions made to reconstruct the equivalent top load-settlement curve at the pile top from an O-cell load test results are as follows: First, the shaft resistance-deformation curve for upward movement of the pile is the same as the downward movement of a conventional head-down static pile load test. Second, the end bearing load-deformation curve obtained from an O-cell test is the same as the end bearing-load deformation component curve of a conventional head-down test. Finally, the pile is

assumed to be rigid so that the top and bottom have the same deformation, but sustaining different loads.

By adding the shaft resistance to the mobilized end bearing at the same deformation, a single point on the equivalent top load curve can be obtained. The equivalent head-down load-settlement curve can then be determined by repeating this step to all data. Points beyond the maximum displacement of the component that does not reach an ultimate could be obtained by conservatively assuming that at greater displacements it remains constant at the maximum applied load. There is another method that, but less conservatively, extrapolate the non-ultimate component by using hyperbolic curve fitting, and then use this extrapolated curve in the calculations to produce the equivalent top load-deformation curve.

5.3 Lateral load test

Large diameter drilled shaft have been widely used for the support of long span bridges in Korea and elsewhere due to their cost-effective and multipurpose features. The behavior of the drilled shaft foundations under lateral loading is an important consideration in non-linear analysis ($p-y$ curve) for design.

In this study, describes a series of lateral load tests were performed on offshore large diameter drilled shafts in marine clay with static and cyclic loading types. Four case were considered: Case 1 and Case 2 were performed on small-scale piles ($D = 1.016\text{ m}$, $L = 26\text{ m}$) by static loading; Case 3 were performed on small-scale piles ($D = 1.016\text{ m}$, $L = 26\text{ m}$) by cyclic loading; Case 4 was performed on a full-scale pile ($D = 2.4\text{ m}$, $L = 45\text{ m}$) by static loading. The test pile and procedure are designed according to ASTM D-3966. Lateral loads were connected through a load cell and reaction piles. A schematic illustration of the loading system is shown in Figure 15.

Testing of the shaft/column was displacement controlled. Cyclic lateral loading was applied across an amplitude range of 50 mm to 2.75 m. Two loading cycles were performed at most displacement levels; however, 12 loading cycles were performed at two displacement amplitudes (152 and 457 mm) to investigate the effects of cyclic degradation. Cycles at displacement amplitudes $>152\text{ mm}$ included 16 stops to enable measurements of the shape of hysteretic response curves.

5.4 Lateral test results

In order to develop $p-y$ curve, first of all, bending moment and lateral displacement were obtained from lateral load test. In this study, the $p-y$ curves were evaluated from experimental data in Korea. Two types of measurements are used for these analyses: slope (s

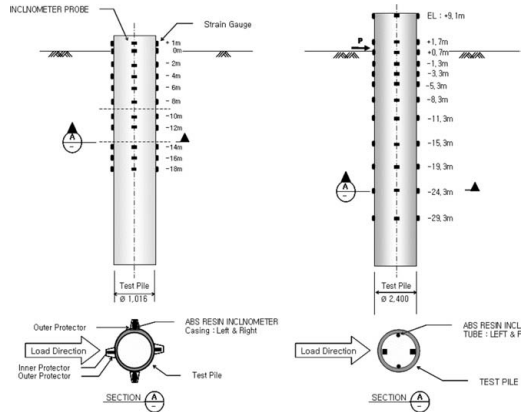


Figure 15. A schematic illustration of the loading system.

TEST PILE along the shaft (measured from inclinometers) and curvature (ϕ) (measured from extensometer pairs on opposite ends of the shaft section, or inferred based on differentiation of slope with depth). Bending moment is proportional to curvature (ϕ), with the constant of proportionality being the nonlinear stiffness of the concrete section (EI),

$$EI\phi(z) = M(z) \quad (2)$$

where, z denotes depth. The lateral soil reaction on the shaft, p , is calculated by double differentiating the shaft bending moment distribution (Hetenyi, 1946),

$$p(z) = \frac{d^2}{dz^2} M(z) \quad (3)$$

The shaft deflected shape, y , is obtained by a single integration of the slope, or a double integration of the curvature. Expressed in terms of differentials,

$$\phi(z) = \frac{d^2 z}{dz^2} y(z) \quad (4)$$

$$s(z) = \frac{d}{dz} M(z) \quad (5)$$

A complete solution of the differential equations yields a set of profiles such as shown in Figure 16. Several features of the profiles in Figure 16 are noteworthy. First, the y and p profiles crossover zero at identical depths. Second, boundary conditions used to develop the solution typically include y , s , M , and V at depth zero, and y at the shaft toe (typically assumed to be zero).

In this study, the bending moment data from the lateral load test were used to derive $p-y$ curves for the pile in a manner similar to that used on physical

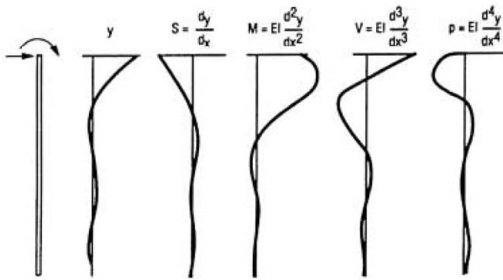


Figure 16. Form of results obtained from a complete solution of a laterally loaded shaft.

experiments. The values of bending moment along with the known moment of zero at the top of the pile were fitted with fifth degree polynomial using the least squares technique. The polynomial curve representing the bending moment data was twice differentiated to obtain soil resistance values (p) and deflection (y) was obtained directly from inclinometer.

Plotted on Figure 17 are developed p - y curves at various depths which were derived from the lateral load test results. As is evident from these plots, there exist increasing due to soil resistance in the changing depth which can be mobilized.

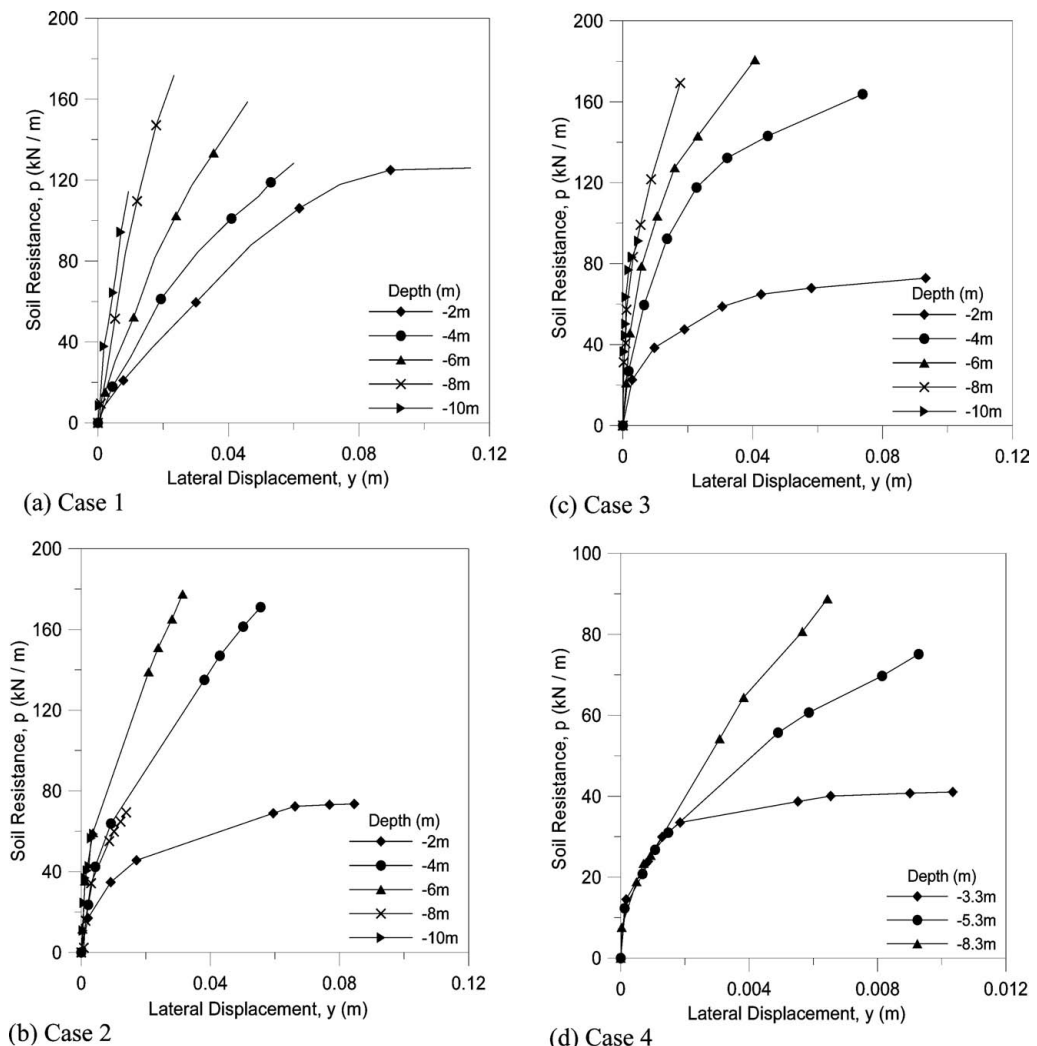


Figure 17. P - y curves in marine clay.

5.5 Defects in drilled shafts

Quality assurance of pile is important not only bearing capacity by pile load test but also integrity test in pile. Specially, integrity test is the most important quality assurance factor in case of drilled shaft pile in Korea. Drilled shafts can have defects because of complicated construction process that makes difficult to control the quality control. There are three principal defects that can occur at the base of a drilled shaft.

- Weak soil or rock at the base because the drilling was not carried to the appropriate depth or because the founding stratum was not present at the particular location.
- Loose sand or other sediment at the base because the excavation was not cleaned properly or because sediment was deposited from slurry.
- Weak concrete at the base because the concrete was allowed to fall through water or drilling slurry. In the supposedly dry construction method, excessive water could have collected before the concrete was placed.

5.6 Detection of defects

Typically quality assurance for drilled shafts classified into direct examination techniques and indirect examination techniques. Direct examination techniques include visual examination during and after

installation, load testing, and drilling or boring alongside the shaft or into the shaft. Indirect examination techniques include internal tests utilizing drill holes or pre-performed ducts within the shaft for example sonic logging or nuclear techniques, external tests from top or side of exposed shaft for example sonic echo tests or resistivity techniques, and finally remote tests conducted alongside shaft for example parallel seismic techniques. Integrity tests mean in a broad sense the indirect examination techniques which are nondestructive tests (NDT).

It has reviewed the use of following four methods that are commonly in use in Korea for drilled shaft inspection, with a view to defining the limits of the tests so they may be utilized in a rational fashion.

1. Cross hole sonic logging (CSL)
2. Nuclear density testing through the use of gamma-gamma testing (gamma)
3. Sonic echo testing (sonic)
4. Impulse response method

In this report, the brief descriptions about the four methods as well as the limitations were shown in Table 5.

The Korea Highway Corporation (2001) recommended cross hole sonic logging in integrity test of drilled shafts. Also, it is regulated that the test pile number should be approximately 30% of total installed piles.

Table 5. Summary of integrity method for Drilled Shafts (G-I of ASCE, 2000).

Method	Description	Advantages	Disadvantages	Comments
Sonic Echo	Instrumented or noninstrumented hammer strikes pile top adjacent to an accelerometer (receiver) Generate low Strain wave Reflected wave analyze Analysis done in time domain	Faster, cheaper test No preparation required Can verify "good" shaft No need to preselect prior to installation of shaft	Interpretation of results necessary to deal with such issues as external damping Long slender shafts damp reflected wave (L/D limited to 30/1) Accurate depth to defect difficult \pm 5–20% May identify shape changes(bulges, casing steps) as defects Rapid load transfer may be interpreted as a defect Few technicians available	Should never be sole bases for rejection of shaft
Impulse response	Similar to sonic echo Instrumented hammer and receiver Reflected wave is analyzed not only in velocity domain but also frequency	Same as sonic echo Can derive comparative information on dynamic stiffness of shaft head	Same as sonic echo Hard to detect toe defects Better at differentiating necking from bulges	Should never be sole bases for rejection of shaft

(Continued)

Table 5. (Continued)

Method	Description	Advantages	Disadvantages	Comments
CSL	Water-filled steel tubes place in drilled shafts at regular intervals Sonic pulse generator lowered in one tube Receiver lowered in another tube Analysis of velocity of wave transmission	Noninvasive Reasonably economic Can spot multiple defected No depth limitation No soil stiffness effect Easy interpretation Accurate depth to defect determination	Hard to check concrete quality outside reinforcing Difficult to place tubes within tolerances Must preselect shafts to be inspected Cannot find fine cracks Slow test speed Debonding/coupler problems interfere with readings Few technicians available	Test results should be reviewed in conjunction with results of visual inspection
Gamma-gamma	Dry plastic or steel tubes placed in drilled shafts at regular intervals Gamma radiation source and receiver probe lowered into tubes Density plot of concrete surrounding tubes Range of examination 2 in. to 10 in.	Noninvasive Reasonably economic Can locate defects Can spot multiple defects No soil stiffness effect Accurate depth to defect determination Better quantification of concrete density No depth limitation	Slow test speed Difficult to transport equipment due to nuclear precautions Must preselect shafts to tested Difficult to place tubes within tolerances Test limited to a few inches around tube Coupler problems interfere with readings Cannot determine extent of defect	Test results should be reviewed in conjunction with results of visual inspection

6 CONCLUDING REMARKS

The main objective of this study was to gather the general information on the current status of design and construction techniques available for deep foundations in Korea.

Since 1990's, much work has been done in many fields in Korea: the techniques of design and analysis of pile systems, construction and quality control techniques. Lately there have also been advanced research focusing on the new techniques such as time effect of driven pile, rock-socketed drilled shafts, single shaft-single column drilled shafts, and raft foundations and research concerning with environmental matters.

ACKNOWLEDGEMENTS

The authors would like to acknowledge the contribution of Dr. Lee(Piletec Co.), Dr. Kim(Incheon 2nd bridge project of Samsung Eng & Con), Daewoo Institute of Construction Technology and Korea Highway Co.

REFERENCES

- AASHTO. 2004. *AASHOTO LRFD Bridge (II) Design Specification*, ISBN No. 1-56051-251-2, American Association of State Highway and Transportation Officials, Washington, D.C.
- Ashour, M., Norris, G. and Shamsabadi, A. 2001, Effect of the non-linear behavior of pile material on the response of laterally loaded piles, *Forth international conference on Recent Advances in Geotechnical Earthquake Engineering and soil Dynamics*, San Diego, California, March 26–30:6–10.
- Baker, C. N., Jr., Parikh, G., Briaud, J-L, Drumright, E. E., and Mensah, F. 1993. *Drilled Shafts for Bridge Foundations*, Report No. FHWA-RD-92-004. Federal Highway Administration, McLean, VA, August.
- Broms, B. 1964, Lateral Resistance of Piles in Cohesive Soils, *J. Soil Mechanics and Foundation Div.*, ASCE, 90(4):27–63.
- Broms, B. B. 1965. Design of Laterally Loaded Piles. *Journal of the Soil Mechanics and Foundation Division*. ASCE, 90(3):79–99.
- California Department of Transportation Division of Engineering Services. 1999. *CALTRANS SEISMIC DESIGN CRITERIA*
- Davission, M. T. 1970. *Lateral Load Capacity of Piles*. Highway research Record No.333, Highway Research Board, Washington, D. C.:104–112.

- Evans, L. T. and Duncan, J. M. 1982, *Simplified Analysis of Laterally Loaded Piles*, Report No. UCB/GT/82-04, Geotech Engineering, Department of Civil Engineering, California Univ., Berkeley.
- Georgiadis, M. Development of P-Y Curves for Layered Soils, *Proceedings of Geotechnical Practice in Offshore Engineering*, American Society of Civil Engineers:536–545.
- Ghionna, V. N., Jamiolkowski, M., Pedroni, S. & Salgado, R. 1994. The tip displacement of drilled shafts in sands. *Vertical and horizontal deformations of foundations and embankments*, Geotech, Spec Publ. 40(2):1039–1057.
- G-I Deep Foundations Committee. 2000. Nondestructive Evaluation of Drilled Shafts, Report of a Task Force Sponsored by the G-I Deep Foundations Committee, *Journal of Geotechnical and Geoenvironmental Engineering*, 126(1):92–95.
- Hetenyi, M. 1946. *Beams on Elastic Foundation*, The University of Michigan Press, Ann Arbor.
- Hong, W. P. 1984. Earth pressures acting on a row of piles due to lateral soil movements., *J. of the Korean Soc. of Civil Eng.*, 4(1):59–68.
- Hong, W. P., Kwon, O. H., Han, J. G., and Cho, S. H. 1994. A study on lateral movement of bridge abutment on soft ground, *J. of the Korean Geotech. Soc.*, 10(4):53–65.
- Hong, W. P. 1999. Computer programs to analyze stability of slopes containing piles, *Proc. of the 1999 Slope Stability Conf.*, Korean Geotech. Soc., 7(4):75–87.
- Hong, W. P., Song, Y. S., Shin, D. S., and Son, K. M. 2001. Stability of bridge abutments on soft ground undergoing lateral flow, *J. of the Korean Geotech. Soc.*, 17(4):199–208.
- Horvath, R. G., Kenny, T. C. & Kozicki, p. 1983. Method of improving the performance of drilled piers in weak rock, *Canadian Geotechnical Journal* 20:758–772.
- Jeong, S. S. 1998. Analysis of passive piles, *Proc. of the KGS Fall '98 National Conf.*:86-89.
- Jeong, S. S., Won, J. O., and Kim, B. C. 2000. Analysis method of passive piles considering group effect, *Proc. of the KGS Spring 2000 National Conf.*:151–158.
- Jeong, S. S., Kim, B. C. 2000. Interaction factors of one-row pile groups subjected to lateral soil movements, *J. of the Korean Geotech. Soc.*, 16(3):157–162.
- Jeong, S. S., Suh, J. J., and Jang, B. S. 2000. Behavior of piled abutment adjacent to surcharge loads, *Proc. of the KGS Fall 2000 National Conf.*:25–32.
- Jeong, S. S., Lee, J. H., Seo, D. H., Kim, Y. S., and Jang, B. S. 2002. Design guidelines of piled bridge abutment subjected to lateral soil movements, *Proc. of the KGS Spring 2002 National Conf.*:381–388.
- Jeong, S., Seo, D., Lee, J. & Park, J. 2004. Time-dependent behavior of pile groups by staged construction of an adjacent embankment on soft clay, *Canadian Geotechnical Journal*, 41:644–656.
- Kim, S.I., Jeong, S.S., Cho, S.H., and Park, I.J. 1999. Shear Load Transfer Characteristics of Drilled Shafts in Weathered Rocks, *Journal of Geotechnical and Geoenvironmental Engineering*, ASCE:999–1010.
- Korea Highway Corporation: Highway & Transportation Technology Institute 1996. *A study on protection method for lateral movement of abutment (II)*, Korea Highway Corporation, Seoul.
- Korea Highway Corporation. 2001. Design standard of single drilled shaft.
- Korea Road Association. 2005. Specifications for highway bridges (in Korean).
- Lee, J. H., Suh, J. J., Jeong, S. S., and Jang, B. S. 2003. The behavior of piled bridge abutments subjected to lateral soil movements – Design guidelines, *J. of the Korean Geotech. Soc.*, 19(1):21–29.
- McClelland, B., and Focht, J. A. Jr. 1958. Soil Modulus for Lateral Loaded Piles. *Transactions*. ASCE, 123: 1049–1086.
- O'Neill, M. W., Townsend, F. C., Hanssan, K. M., Buller, A. and Chan, P. S. 1995. *Load transfer for drilled shafts in intermediate geomaterials*, FHWA-RD-95-XXX Draft report: U.S. Department of Transportation.
- Osterberg, J. O. 1998. The Osterberg Load Test Method for Bored Driven Piles. The First Ten Years, *Proc., 7th Int. Conf. and Exhibition on Piling and Deep Foundations*, Foundation Institute, Vienna, Austria:1.28.1–1.28.11.
- Poulos, H.G. 2001. Piled raft foundations : design and applications. *Geotechnique* 51(2):95–113.
- Priestly, M., Seible, F., and Calvi, G. 1996. *Sesismic Design and Retrofit of Bridges*. John Wiley & Sons, New York.
- Reese, L. C. and O'Neill, M. W. 1988. *Drilled shafts: Construction procedures and design methods*, Publ. No. FHWA-HI-88-042, Federal Highway Administration, Washington, D.C.
- Seidel, J. P. and Collingwood, B. 2001. A new socket roughness factor for prediction of rock socket shaft resistance, *Canadian Geotechnical Journal*, 38(1):138–153.
- Seol, H. I., Jeong, S. S., Kim, Y. K., Kim, Z. C. 2006. Load-settlement characteristics of offshore drilled shafts using the static bi-directional loading tests. *International Offshore and Polar Engineering Conference*. San Francisco:508–514.
- Turner, M. J. 1997. *Integrity Testing in piling practice*, CIRIA, London.
- Van Impe, W.F. 1996. Deep Foundations on Screw Piles. *Proceeding of International Conference on Pile Foundation*, Korean Geotechnical Society, Seoul, Korea.

Trend of research and practice of pile foundations in Japan

T. Matsumoto, P. Kitayodom & T. Shintani

Graduate School of Natural Science and Technology, Kanazawa University, Kanazawa, Japan

ABSTRACT: This paper first reviews the trend of research and practice of pile foundations in Japan, which were presented in the annual meetings of Japanese Geotechnical Society (JGS) in the last 5 years from 2002 to 2006. Of course, various researches have been carried out for pile foundations. Among them, developments of new pile load test methods and their applications, researches on piled raft foundations, and researches on bearing mechanisms of open-ended pipe piles are highlighted in this paper.

1 INTRODUCTION

There are more than hundred pile makers or pile construction companies at present in Japan. Four big companies are members of Japan Association for Steel Pipe Piles (JASPP), 55 companies are members of Concrete Pile Installation Association (COPITA), 44 companies are members of Nihon Kiso Kyoukai (Japanese Foundation Association), 3 companies construct timber piles, and several companies construct small-diameter pipe piles for foundations of houses.

Product of steel pipe piles in 2005 was about 0.55 million tons (sales proceeds of about 50 million US\$). Product of prefabricated concrete piles was about 3.7 million tons in 2005.

Various new pile construction methods have been developed in the last decade. However, methods to confirm the performance of the constructed piles, design methods of pile foundation structures and corresponding design codes or specifications do not seem to have developed sufficiently.

This paper first reviews the trend of research and practice of pile foundations in Japan, which were presented in the annual meetings of Japanese Geotechnical Society (JGS) in the last 5 years from 2002 to 2006.

Thereafter, among various researches on pile foundations, developments of new pile load test methods and their applications, researches on piled raft foundations, and researches on bearing mechanisms of open-ended pipe piles are highlighted. Finally, discussions are made on technical circumstances that seem to be needed to enhance the use of the new developments and technologies in practice.

2 TREND OF RESEARCH IN THE LAST 5 YEARS IN JAPAN

Pile engineers in Japan are divided into civil engineering field (mainly bridge foundations) and architectural field (mainly building foundations). There are three annual meetings of Japan Society of Civil Engineers (JSCE), Architectural Institute of Japan (AIJ) and Japanese Geotechnical Society (JGS). Pile engineers from both fields gather in the annual meeting of JGS.

Table 1 is the breakdown of the papers relating pile foundations presented in the annual meetings of JGS from 2002 (37th) to 2006 (41st). The number of papers relating pile foundations is increasing year by year. In the last 5 years, 40% of the papers are related

Table 1. Breakdown of papers relating pile foundations presented in the JGS annual meeting from 2002 to 2006.

Year	Total number	Horizontal loading	Liquefaction	Seismic loading	Piled raft	Load test	Suction foundation	Screw pile	Open-ended pipe pile
2002	92	16	17	19	12	4	3	0	0
2003	113	14	12	10	10	10	3	0	3
2004	117	11	22	12	11	8	3	9	2
2005	131	10	19	16	28	19	3	11	15
2006	137	19	17	16	16	20	0	8	5

to horizontal loading or piles in liquefied ground or piles subjected to seismic loading.

The number of papers relating pile load test and piled raft tend to increase. The papers relating screw piles that are new types of steel pipe pile are found from 2004.

In 2005, many papers were presented for open-ended steel pipe piles. These papers are related to vertical bearing capacity and horizontal resistance of large diameter steel pipe piles that will be used for foundations of bridges in Tokyo port seaside road project under planning. Estimation of the end-bearing capacity of large diameter pipe pile due to plugging was one of important design issues. Static, dynamic and rapid pile load tests were carried out for this project.

Various approaches are used in the researches; are theory, numerical analysis, laboratory test, field test. However, as for design of pile foundations, bearing capacity based design seems to be still predominant in Japan.

In the below, among the various researches on pile foundations, developments of pile load test methods, researches on piled rafts and bearing mechanisms of open-ended pipe piles in Japan are introduced briefly.

3 DEVELOPMENTS OF PILE LOAD TEST METHODS IN JAPAN

Various pile load methods such as the conventional static load test method, the Osterberg cell method, the dynamic load test method and the rapid load test method, are available now in Japan.

Most pile load tests are carried out to obtain assessment or approval of a newly developed pile construction method from the authorised institutes such as the Building Center of Japan and so on. Bearing capacity of the newly developed pile is estimated from an empirical equation using the SPT N -values. Once the new pile construction method is approved, pile load test for constructed piles in practice is exempted. This system does not seem to be rational, because only one or two borehole investigations are conducted in a pile construction site, which is not enough to grasp the ground conditions of the whole construction area. Another reason for the current authorisation system may be attributed to the fact that the conventional static load test is rather time and cost consuming.

3.1 Influence of reaction piles on test pile in static load test

The conventional static load test has been believed to be the most reliable test method to obtain the load-settlement relation of a single pile. However, centrifuge modelling of a static load test with use of reaction piles by Latotzke et al. (1997) showed that the true load-settlement relation is not obtained from

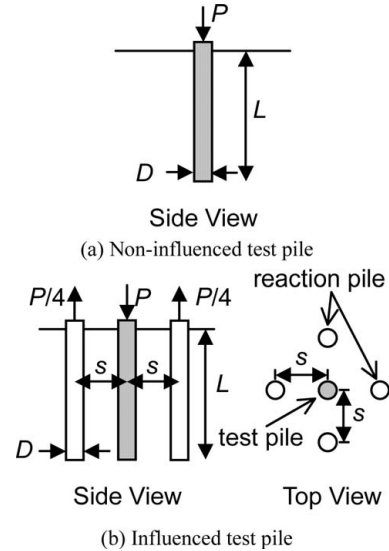


Figure 1. Analytical conditions of vertical load test.

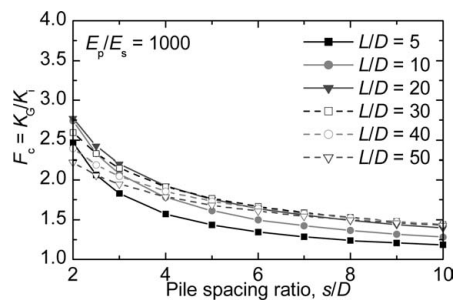


Figure 2. Correction factor, F_c , for piles embedded in semi-infinite homogeneous ground (after Kitiyodom et al. 2004a).

the static load test due to the interaction between the test pile and the reaction piles. Kitayodom et al. (2004a) carried out a parametric study to investigate the influence of the reaction piles on the load-settlement curve of a test pile. In the parametric study, a computer program PRAB for simplified three-dimensional deformation analysis of a piled raft which is described in detail in Section 4. In the parametric study of vertical load test, a true single pile (non-influenced test pile) and a test pile with reaction piles (influenced test pile) were analysed for various pile diameter, D , pile length, L , and pile spacing, s , and pile-soil stiffness ratio, E_p/E_s , as shown in Figure 1.

Figure 2 shows an example of the results of the parametric study. Here, the correction factor, F_c , is defined as the ratio of the pile head stiffness of the

influenced test pile, K_G , to that of the non-influenced test pile, K_I . The value of K_G is larger than K_I due to the interaction between the test pile and the reaction piles, which means that the pile head settlement of the influenced test pile become smaller than that of the non-influenced test pile.

It can be seen from Figure 2 that F_c is about 2 even when pile spacing ratio $s/D = 3$ that is usually employed in static load tests in Japan. An important conclusion from the parametric study is that analysis of the test pile with reaction piles is needed to obtain a true load-settlement curve of the test pile from the load-settlement measured in the static load test.

3.2 Use of dynamic load test

Use of dynamic load test in Japan is predominant in driven steel piles, because most piles constructed in urban areas are bored, auger and cast-in-place concrete piles, or steel piles constructed by push-in or screwed-in construction methods.

Dynamic load tests have been mainly used for steel pipe piles for foundations of bridges, for examples, the access bridge of Kansai International Airport (Matsumoto & Takei 1991), Tokyo Trans-Bay highway (Momiya et al. 1992), a highway bridge constructed in a soft rock (Matsumoto et al. 1995, Matsumoto et al. 1997, Hayashi et al. 2000), the access bridge of new Kita-Kyushu Airport (Ochiai et al. 1997).

It is important to allow for the influence of the soil inside a pipe pile (internal soil) as well as the external soil resistance when analysing pile driving and response subjected to static load of the pipe pile. Commercial programs, CAPWAP (Rausche et al. 1972) and TNOWAV (TNO 1977) are used in Japan for analysing pile driving. However, these programs do not explicitly take into account of the existence of the internal soil.

A computer program Kwave was developed by Matsumoto and Takei (1991), in which the influence of the internal soil is explicitly considered. The pile/soil system shown in Figure 3 is employed in Kwave. In this pile/soil system, the internal soil is modelled by series of masses and springs according to Heerema & de Jong (1980).

The characteristic solutions of the wave equation are used to calculate wave propagation in the pile, whereas the Smith method is used to calculate dynamic behaviour of the internal soil.

Rational soil resistance models have been implemented in Kwave. Figure 4 shows the shaft resistance model proposed by Randolph & Simons (1986). The values of the shaft spring, k_s , and the radiation damping, c_r , per unit area are approximately obtained from the work of Novak et al. (1978) as follows:

$$k_s = \frac{2.75G}{2\pi r_0} \quad (1)$$

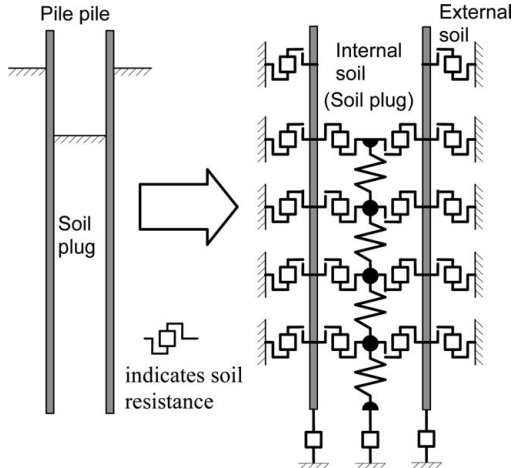


Figure 3. Pile/soil system used in Kwave.

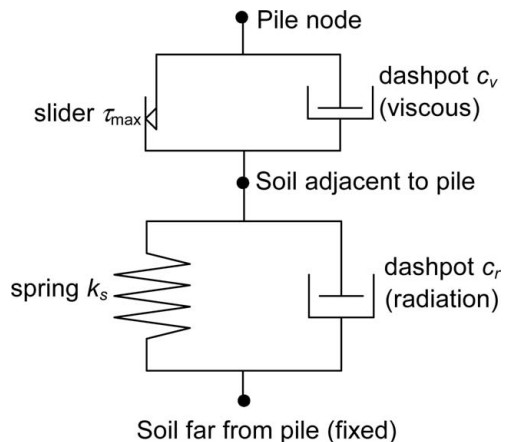


Figure 4. Shaft resistance model (after Randolph & Simons 1986).

$$c_r = G/V_s \quad (2)$$

where G and V_s are the shear modulus and the shear wave velocity of the surrounding soil respectively, and r_o is the outer radius of the pile.

The dynamic friction, τ_d , is generally taken as a non-linear function of velocity, according to

$$\tau_d = \tau_{\max} \left\{ 1 + \alpha \left(\frac{\Delta v}{v_0} \right)^\beta \right\} \quad (3)$$

where τ_{\max} is the static maximum shaft friction, v_0 is a reference velocity (taken for convenience as 1 m/s),

and Δv is the relative velocity between the pile and the adjacent soil. Non-linear viscous laws similar to Eq. (2) have been proposed by Gibson & Coyle (1968), Heerema (1979) and Litkouhi & Poskitt (1980), all of whom suggest a value of β close to 0.2, with the parameter α varying from about 0.1 for sand, to unity for clay soils. The relation of Eq. (2) was introduced into the viscous damping in Figure 4.

The shaft spring under static loading, $k_{s(\text{static})}$ is estimated according to the following equations (Randolph 1991):

$$k_{s(\text{static})} = (2\pi/2.75\zeta) \cdot k_s \quad (4)$$

$$\zeta = \ln[5.0(1-\nu)l_d/d_o] \quad (5)$$

where l_d is the embedded pile length, d_o is the outer pile diameter and ν is the Poisson's ratio of the soil.

Figure 5 shows the pile base resistance model. The value of the soil spring, k_b , the damping, c_b ($c_{b1} = c_{b2}$), and the lumped soil mass, m_b , per unit base area can be estimated as follows (Randolph & Deeks 1992): for soil plug base:

$$k_b = \frac{4G}{\pi(1-\nu)r_i} \quad (6)$$

$$c_b = \frac{3.2\rho V_s}{\pi(1-\nu)} = \frac{3.2G}{\pi(1-\nu)V_s} \quad (7)$$

$$m_b = 16r_i \frac{0.1-\nu^4}{\pi(1-\nu)} \rho \quad (8)$$

for annular pile base:

$$k_b = \frac{4G}{\pi(1-\nu)(r_o + r_i)} \quad (9)$$

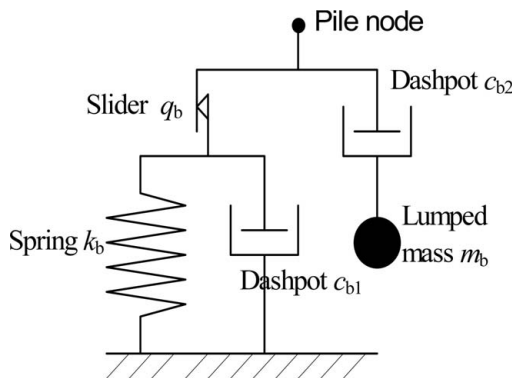


Figure 5. Base resistance model (after Randolph & Deeks 1992).

$$c_b = \frac{3.2\rho V_s}{\pi(1-\nu)} = \frac{3.2G}{\pi(1-\nu)V_s} \quad (10)$$

$$m_b = 16 \frac{r_0^2 + r_0 r_i + r_i^2}{r_o + r_i} \frac{0.1 - \nu^4}{1 - \nu} \rho \quad (11)$$

where r_i is the inner radius of the pipe pile.

One of advantages of the use of the rational soil resistance models is that the parameter except for the maximum static shaft resistance, τ_{\max} , and the maximum static base resistance, q_b , can be estimated from the soil properties, G , ν , ρ , V_s and the pile radii, r_o and r_i . The rational soil resistance models have been implemented also in KWAVE-FD in which finite difference scheme is employed to calculate wave propagation in the soil and in the soil plug (Wakisaka et al. 2004).

Although reliability of the dynamic load test has been demonstrated through comparisons of the results of static load tests and dynamic load tests, the dynamic load test is not so popular in Japan. The first author has heard the following opinions for the dynamic load testing from piling engineers in Japan:

- i) It is difficult to understand the wave propagation phenomena in a pile.
- ii) Dynamic load test is not reliable.
- iii) When dynamic load test is conducted on bored or auger or cast-in-place concrete piles, it is difficult to determine configurations and mechanical properties of the test pile.
- iv) Time for dynamic load test is very short, but it takes several days to get the results of the wave matching analysis and the corresponding static load-settlement curve from the testing company.
- v) Dynamic load test is difficult because of the problems of vibration and noise especially in urban areas.
- vi) In cases of bored, auger and cast-in-place concrete piles, extra cost is needed to prepare pile driving device.
- vii) In case of cast-in-place concrete pile, it is rather difficult to measure dynamic signals.
- viii) Even if dynamic load test is carried out during initial pile driving, it is difficult to estimate bearing capacity of the pile after 'set-up' phenomena. Re-striking test is needed for such case.
- ix) Reliability of dynamic load test would be lower than that of the static load test. But, it is possible to carry out dynamic load test on a large number of piles in a site with the cost for a conventional static load test. Therefore, dynamic load test is useful to confirm performance of many constructed piles in the site and to assess the safety of the constructed foundation.

Although the authors do no agree with i) and ii), they cannot help but agree with iii) to viii). Opinion ix) is a big advantage of the dynamic load testing.

3.3 Developments of rapid pile load test methods

Piling engineers had been seeking for a new pile load test method that is reliable, time and cost effective, prompt for output of the test results, and does not require reaction system. One of such test methods, Statnamic, was developed of the Joint of Birmingham Hammer Corporation, Canada, and TNO, the Netherlands (Birmingham et al. 1989). Loading mechanism of the Statnamic load test method is launching a mass on the top of a pile by gas explosion force that pushes the test pile into the ground at the same time. Loading duration of the Statnamic test is typically 80 to 120 ms that is about 20 times that of the dynamic load test. The Statnamic load test method is one of rapid pile load test methods.

The first Statnamic test in Japan was performed in 1991 by Takenaka Corporation against a cast-in-place concrete pile. In 1992, a research group of rapid pile load test methods was established led by Prof. Osamu Kusakabe, Tokyo Institute of Technology. Behaviours of pile and surrounding soil during the Statnamic loading were investigated, and number of comparative tests of static load test and Statnamic test were carried out in the activity of the research group. The achievements of the research group were presented in the *Proceedings of the 1st and the 2nd International Statnamic Seminars* in 1995 and 1998.

Rapid pile load test method was implemented in *Standards for Vertical Load Tests of Piles* (Japanese Geotechnical Society 2002), and the research group served their purpose in 2002.

Poulos (1998) pointed out advantages of the Statnamic test over other test types as follows:

- i) the test is quick and easily mobilised
- ii) high loading capacity if available
- iii) the loading is accurately centred and can be applied to both single piles and pile groups
- iv) the test does not require any pre-installation of the loading equipment
- v) it can be adapted to apply lateral loading
- vi) the test is quasi-static, and does not involve the development of potentially damaging compressive and tensile stresses in the test pile
- vii) the test can be carried out on both uninstrumented and instrumented piles
- viii) the load is measured via a calibrated load cell and does not rely on pile material and cross-section properties.

Poulos (1998) pointed out also some potential shortcomings, including:

- i) certain assumptions need to be made in the interpretation of the test
- ii) the Statnamic can only be used for cyclic or repetitive loading in conjunction with a newer generation of catching system

- iii) it cannot provide information on time-dependent settlements or movements. While this may not be of great importance for single piles, it can be a major limitation when testing pile groups, especially if compressive layers underlie the pile tips.

Other rapid pile load test methods have been developed, e.g. Dynatest by Gonin & Leonard (1984) and Pseudo-static pile load tester by Schellingerhout & Revoort (1996). These rapid pile load test methods utilise a falling mass and coil springs on the pile top to prolong loading duration. The falling mass type rapid load test methods offer advantages over the Statnamic, including:

- i) time for preparation of test equipment for a pile is very short, less than 10 min in usual
- ii) it is very easy to conduct cyclic or repetitive loading for a pile
- iii) loading duration is easily adjusted by changing combination of mass of the hammer and stiffness of the spring
- iv) maximum load is easily controlled by changing the falling height of the hammer mass
- v) cost of the test may be cheaper than that of the Statnamic.

Falling mass type rapid load test methods have been developed also in Japan: Soft Cushion Method by System Keisoku Corporation, Spring Hammer test method by the joint of Kanazawa University and Marubeni Material Lease Corporation (Matsumoto et al. 2004b) and Hybridamic Load Test Method by JibanShikenjo Corporation. Loading principle of these test methods is basically identical to that of Dynatest and Pseudo static test methods, although some devial are made for spring or cushion on the pile top.

Figure 6 shows the Soft Cushion Test device having a loading capacity to measure a static capacity of about 16 MN.



Figure 6. Soft cushion rapid load test method by System Keisoku Corporation.

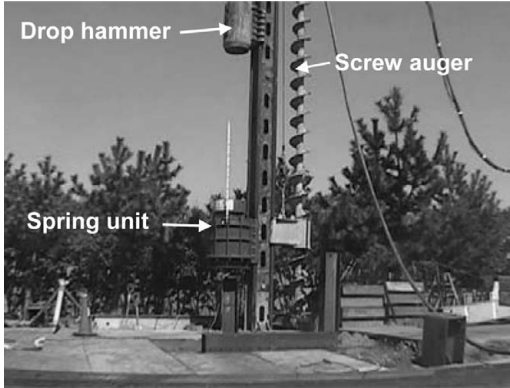


Figure 7. The Spring Hammer test device mounted on a pile construction machine.

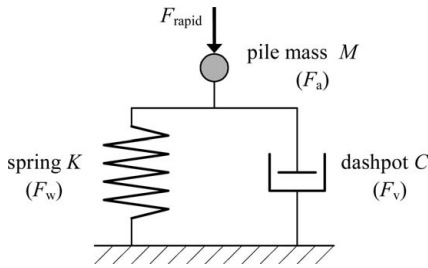


Figure 8. Modelling of pile and soil during rapid loading.

Figure 7 shows the Spring Hammer loading device having a loading capacity of 2 MN. The hammer and the spring unit are mounted on a leader of a pile construction machine together with a screw auger. An advantage of this test device is that rapid pile load tests can be done promptly after the completion of an auger pile. Of course, the Spring Hammer device can be used for rapid load test on any constructed pile.

One of advantages of the rapid load test is that simplified interpretation methods, in which the pile is treated as a rigid mass neglecting wave propagation phenomena in the pile, could be used to derive a static load-settlement relation from the measured dynamic signals.

Figure 8 shows the modelling of pile and soil during rapid pile load testing. The pile is assumed as a rigid mass having mass of M , and the soil is modelled by a spring and a dashpot. This modelling is advocated by Middendorp et al. (1992) and Kusakabe & Matsumoto (1995). The Unloading Point Method (Kusakabe & Matsumoto 1995) is widely used in the interpretation of rapid load test signals in Japan, in which the damping value, C , is assumed to be linear while soil spring is treated as non-linear. Within the

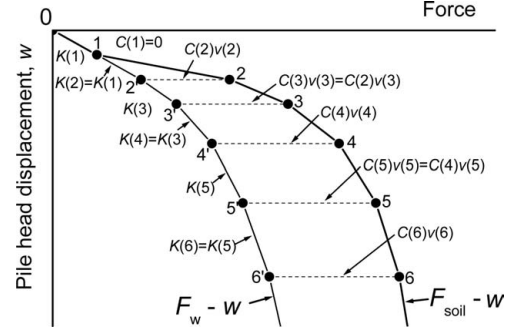


Figure 9. Notations used in non-linear damping interpretation method.

first author's experiences, the Unloading Point method tends to overestimate the pile head stiffness of the test pile in many cases.

Matsumoto et al. (1994) have proposed a simplified interpretation method of rapid load test signals, in which both of the soil spring, K , and the damping value, C , are assumed to be non-linear. This method is called 'non-linear damping method' (note that the method was called 'modified initial stiffness method' in the original paper).

The non-linear damping method to obtain the 'static' load-settlement relation' of a test pile is as follows:

Figure 9 shows the notations used in the non-linear damping method. The applied load, F_{rapid} , is equal to the sum of the soil resistance, F_{soil} , and the inertia of the pile:

$$F_{\text{soil}}(i) = F_{\text{rapid}}(i) - M \cdot \alpha(i) \quad (12)$$

where M is the mass of the pile and $\alpha(i)$ is the measured pile acceleration at time step i .

The soil resistance, F_{soil} , is the sum of the spring resistance (static resistance), F_w , and the dashpot resistance, F_v .

$$F_{\text{soil}}(i) = F_w(i) + F_v(i) = F_w(i) + C(i) \cdot v(i) \quad (13)$$

where $C(i)$ is the damping coefficient and $v(i)$ is the pile velocity at time step i .

At the first step ($i = 1$), the initial stiffness, $K(1)$, is calculated by the initial static load, $F_w(1)$, divided by the initial displacement, $w(1)$.

$$K(1) = F_w(1)/w(1) = F_{\text{static}}/w_{\text{static}} \quad (14)$$

At the next step (at step $i + 1$), the soil spring, $K(i+1)$ is assumed to be equal to $K(i)$ as indicated by Eq. (15). Hence, the static resistance, $F_w(i+1)$, at

step $i + 1$ is calculated by Eq. (16). The value of $C(i + 1)$ can be determined by means of Eq. (17).

$$K(i+1) = K(i) \quad (15)$$

$$F_w(i+1) = F_w(i) + K(i+1) \cdot \{w(i+1) - w(i)\} \quad (16)$$

$$C(i+1) = \{F_{\text{soil}}(i+1) - F_w(i+1)\} / v(i+1) \quad (17)$$

At the following step $i + 2$, $C(i + 2)$ is assumed to be equal to $C(i + 1)$ as indicated by Eq. (18). Therefore, the values of $F_w(i + 2)$ and $K(i + 2)$ can be determined by means of Eqs. (19) and (20), respectively.

$$C(i+2) = C(i+1) \quad (18)$$

$$F_w(i+2) = F_{\text{soil}}(i+2) - C(i+2) \cdot v(i+2) \quad (19)$$

$$K(i+2) = \frac{F_w(i+2) - F_w(i+1)}{v(i+2) - w(i+1)} \quad (20)$$

By repeating the procedure from Eq. (15) to Eq. (20), the values of K and C for following steps are alternately updated consecutively. Finally, whole static load-displacement relation, F_w vs w , is constructed as shown in Figure 9.

3.4 Comparisons of results of static load tests and rapid load tests using Spring Hammer device

Comparisons of static load tests and rapid load tests were carried out to validate the rapid load testing using the Spring Hammer device (Nakashima et al. 2006, Matsuzawa et al. 2006a). The results of these comparative tests are briefly introduced.

Figure 10 shows the profiles of the soil layers and SPT N -values at the test site. The ground at the test site blow a depth of 2 m consists of alternating layers of silt and sand. The SPT N -values are less than 7 to a depth of 7 m, and about 15 from 8 m to 11 m in depth. A total of 7 test piles were constructed.

Each test pile was steel H-shaped pile with an end circular plate so as to increase the end-bearing capacity, as shown in Figure 11.

Construction procedure of the test pile is as follows:

- i) borehole is made by a screw auger
- ii) fresh cement mortar is poured in the borehole
- iii) pile is inserted into the borehole
- iv) the inserted pile is driven by a drop hammer. During this stage, rapid pile load test is carried out using the Spring Hammer device
- v) when the required end-bearing capacity is obtained, driving and testing are terminated.

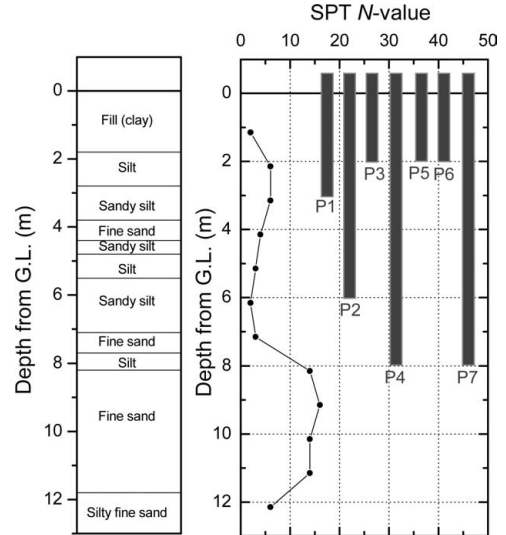


Figure 10. Profiles of soil layers and SPT N -values, together with seating of the test piles.

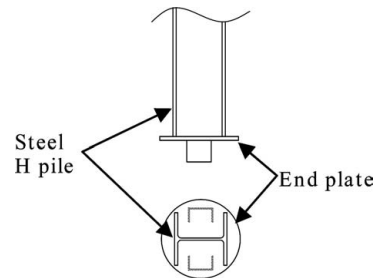


Figure 11. Steel H pile with end-plate.

Table 2. Specifications of piles 1, 3 and 7.

	Pile 1	Pile 3	Pile 7
Length (m)	4.0	3.0	9.0
Embedment length (m)	3.0	2.0	8.0
Diameter of borehole (m)	0.45	0.45	0.55
Diameter of end plate (m)	0.45	0.45	0.47
Load test type at construction	Rapid	Rapid	Rapid
Load test type 7 days after the end of construction	Static and Rapid	Static and Rapid	none

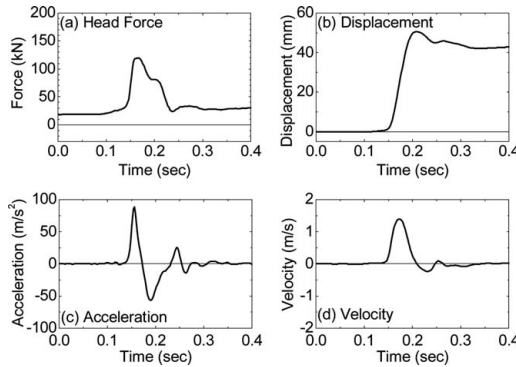


Figure 12. Examples of measured dynamic signals (construction stage of pile No. 3).

One of advantages of this pile and construction procedure is that performance of all the constructed piles can be obtained promptly at the site. The pile is called MSSP (Marubeni Super Safety Pile).

Figure 12 shows the measured dynamic signals during rapid load test of pile No. 3 during construction. The force on the pile top is measured by a load cell, the displacement and accelerations at the pile head are measured by an optical displacement transducer and accelerometers. In this test, load duration is 0.14 s (140 ms) that can be regarded as rapid loading according to the *Standards of JGS for Vertical Load Tests of Piles*.

Static load tests of piles No. 1 and No. 3 were carried out 7 days after the end of construction. Note that bearing capacity of the test piles increased during this rest period, because the fresh cement mortar hardened during this period. Rapid load tests were carried out soon after the end of static load tests. The non-linear damping method was used to derive static load-settlement curve of the test pile for each blow.

Figure 13 shows the comparison of load-settlement curves from the static load test and the rapid load tests on pile No. 1. Three rapid load tests were carried out after the static load test by falling the hammer mass of 2 tons from heights, h , of 0.1, 1.0 and 1.5 m. It can be seen from Figure 13 that the envelop curve of the curves from the static and rapid load tests is consistent.

Figure 14 shows the comparison of load-settlement curves from the static load test and the rapid load tests on pile No. 3. A consistent envelop curve of the curves from the static and rapid load tests can be seen again.

The results of Figures 13 and 14 encourage the use of the rapid pile load test with the non-linear damping interpretation method as an alternative to the static load test.

Figure 15 shows the results of the rapid load tests on pile No. 7 during construction stage. A total of 10

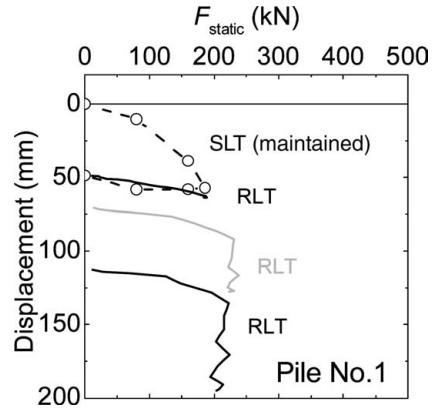


Figure 13. Comparison of results of static and rapid load tests on pile No. 1 conducted at 7 days after the end of pile construction.

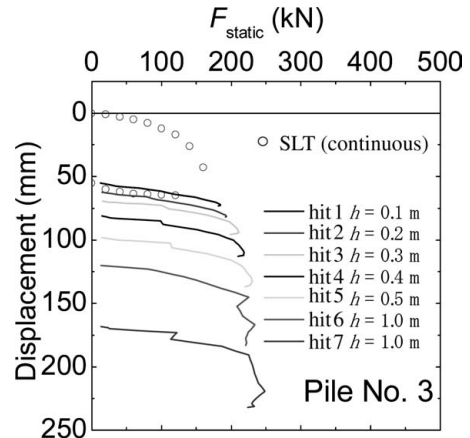


Figure 14. Comparison of results of static and rapid load tests on pile No. 3 conducted at 7 days after the end of pile construction.

blows were applied to the pile. The pile tip penetrated in a silt layer until the 5th blow, while the pile tip penetrated into a sand layer from the 6th blow. It is interesting to note that increase in end bearing capacity of the pile was not clearly seen when the pile tip was in the silt layer, whereas end bearing capacity of the pile was rapidly improved by consecutive blows when the pile tip penetrated in the sand layer. This result encourages the use of rapid load test to improve the performance of a pile as well as to confirm the improved performance of the pile.

The Spring Hammer test method has been used to investigate variation of load-settlement relations of

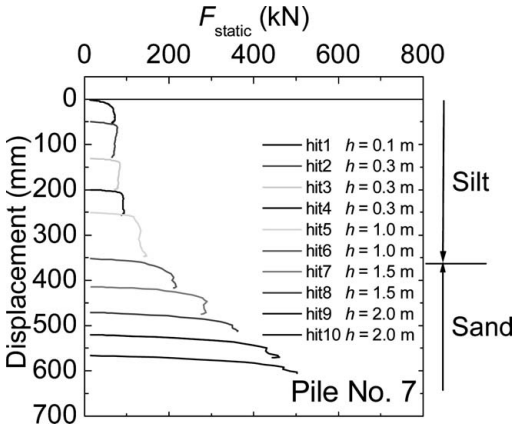


Figure 15. Increase in end bearing capacity of pile No. 7 during construction stage due to consecutive blows.

25 small-diameter steel pipe piles constructed in a site (Matsumoto et al. 2006a), and also applied to plate load tests to investigate effects of sizes of circular plates on the bearing capacity of a ground (Matsuzawa et al. 2006b).

3.5 Dynamic horizontal load test method

Assessment of behaviour of a single pile subjected to static or dynamic horizontal loading is one of seismic design issues of a pile foundation in Japan.

A dynamic horizontal load test method has been developed by the joint of Civil Engineering Research Institute for Cold Region, Japan Pile Corporation and Kanazawa University (Matsumoto et al. 2005b, Kojima et al. 2006).

Figure 16 shows the dynamic horizontal load test method. The pile is hit horizontally by a hammer. Horizontal force, accelerations and displacement are measured via a load cell, accelerometers and displacement transducers. Bending strains of the pile are measured optionally.

Advantages of the dynamic horizontal load test method are:

- reaction piles are not needed
- impact can be applied by human power
- cyclic or repetitive loading is easily performed.

Figure 17 shows the horizontal load and the horizontal displacement near the pile head measured in a dynamic horizontal load test on the steel pipe pile with specifications listed in Table 3. The dynamic signals are similar to those measured in vertical rapid load tests. However, simplified interpretation methods cannot be applied to the dynamic horizontal load test, because wave propagation in the pile and inertial

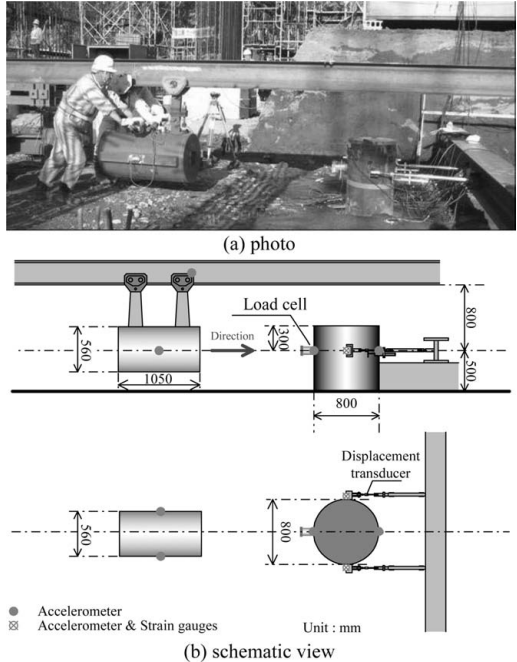


Figure 16. Dynamic horizontal load test method.

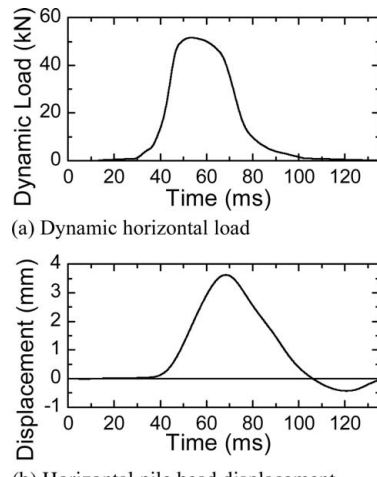


Figure 17. Measured dynamic signals.

effects of the surrounding soils are not appropriately corrected by using simplified interpretation methods where the pile is treated as a single mass. Hence, wave matching analysis of the dynamic horizontal load test is needed to estimate a 'static' horizontal load-displacement relation.

Table 3. Specifications of steel pipe pile.

Property	Value
Length (m)	30.0
Embedment length (m)	29.2
Outer diameter (mm)	800
Inner diameter (mm)	*770, **782
Cross-sectional area (cm^2)	*369.2, **223.7
Young's modulus (kN/m^2)	2.06×10^8
Bending rigidity (cm^2)	* 5.87×10^5 , ** 3.60×10^5
Shear wave velocity (m/s)	3187
Density (ton/ m^3)	7.8
Mass (ton)	5.9

* Upper part ($z < 6 \text{ m}$), ** Lower part ($z > 6 \text{ m}$)

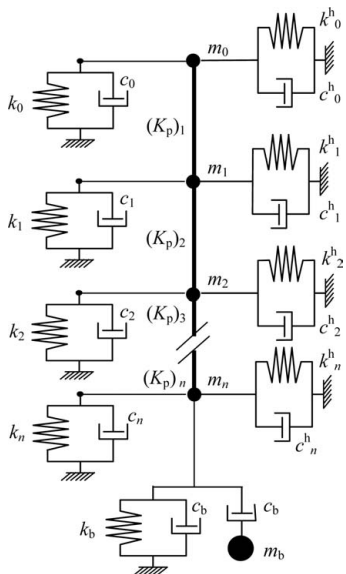


Figure 18. Hybrid modelling of the pile and the soil.

Figure 18 shows a hybrid modelling of the pile and the soil used for wave matching analysis of dynamic horizontal load test. For details of the analysis method, refer to Matsumoto et al. (2005a) and Kitayodom et al. (2006). Comparative tests of static and dynamic horizontal load tests have been carried out in two sites of bridges foundations (Kojima et al. 2006, Kitayodom et al. 2007).

4 PILED RAFTS

Piled raft foundations have been used since 1980s in Japan by Takenaka Corporation (Kakurai 1987,

Kakurai 2003, Kakurai et al. 1987, Tanaka et al. 1987; Yamashita and Kakurai 1991; Yamashita et al. 1994; Yamashita et al. 1998; Yamada et al. 2001). In most these applications of piled raft foundations, piles were bell bottomed type and were designed as primarily end-bearing piles. Two cases of piled rafts using reverse (top-down) construction method were included in the above cases. Detail field observations including settlements and load transfer to piles were carried in these cases (Kakurai 2003).

Several general contractors started to use piled rafts from the end of 1990s (for example, Majima & Nagao 2000), and the number of applications of piled rafts is increasing.

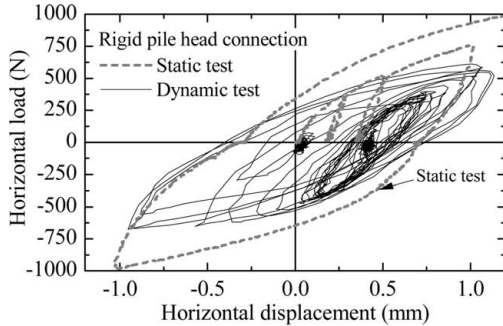
One of issues in design of a piled raft in Japan is estimation of behaviour of the piled raft subjected to horizontal external force and/or an earthquake. However, most seismic designs of piled rafts were substantially treated as rafts alone by ignoring the existence of the piles due to the detailed behaviour of the piled raft foundations subjected to horizontal loads still has not been well clarified.

With an aim to clarify this behaviour, Horikoshi et al. (2003a, 2003b) conducted a series of static and dynamic centrifuge model tests for piled raft foundation models on dry sand in a centrifugal field of 50 g. An influence of the rigidity of the pile head connection on the horizontal behaviour of the foundation was investigated by designing two model piled rafts with two different pile head connections, i.e., rigidly fixed and hinged pile head connections. It was found that comparable behaviours of the piled rafts were obtained in the static and dynamic centrifuge model tests.

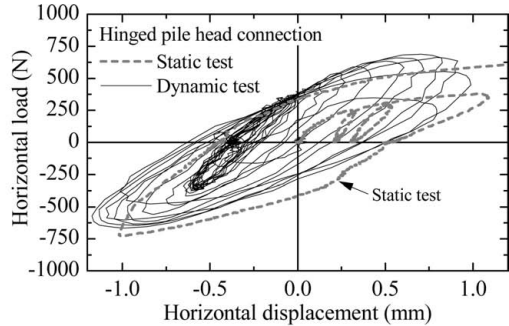
The horizontal load-displacement behaviour of model piled rafts subjected to dynamic loading is compared with that observed in the static test in Figure 19. The horizontal load in the dynamic test was calculated as the product of the raft mass and the acceleration measured on the raft. The figure shows that the overall load displacement behaviour was consistent between the static and the dynamic tests, although the loading-unloading hysteresis curves shifted gradually in the dynamic tests due to the occurrence of the residual displacements.

The proportion of the load carried by the piles in model piled rafts subjected to dynamic loading is compared with those obtained from the static loading tests in Figure 20. The results from the dynamic tests and the static loading tests were consistent in both piled rafts.

Figure 21 compares the bending moment distributions along the pile shaft. The applied horizontal load of 600 N (26% of the raft weight) was chosen for both models. In the shaking table tests, unlike the static loading where only the upper structure is loaded, the ground itself has a dynamic response which can influence the structural responses. However, in their test

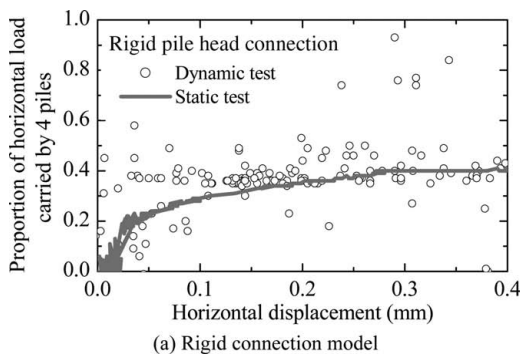


(a) Rigid connection model

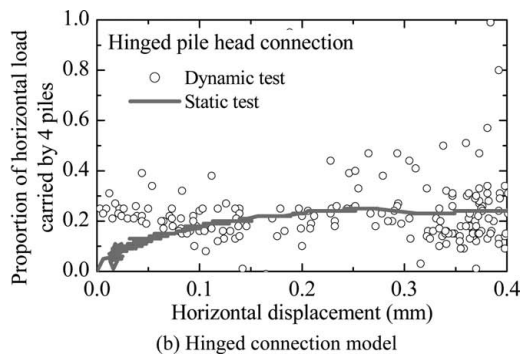


(b) Hinged connection model

Figure 19. Horizontal load-displacement relationship of piled raft compared with static test result.

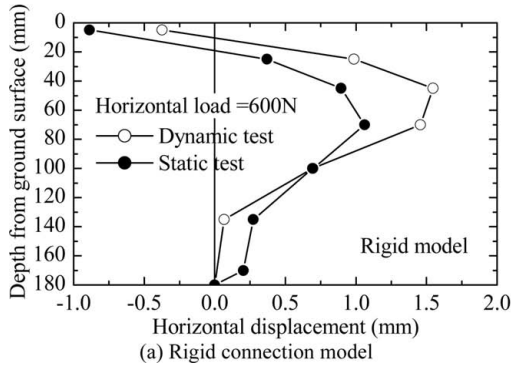


(a) Rigid connection model

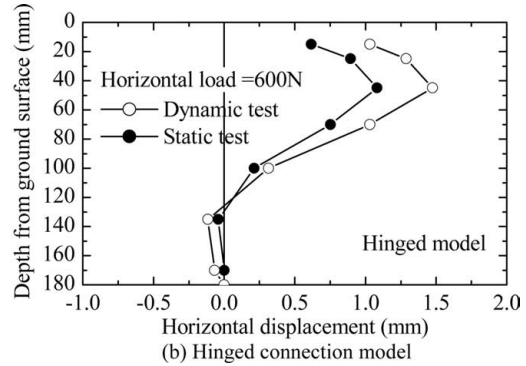


(b) Hinged connection model

Figure 20. Proportion of horizontal load carried by 4 piles during shaking period in comparison with static test result.



(a) Rigid connection model



(b) Hinged connection model

Figure 21. Distributions of bending moments along pile shaft.

since the mass of the raft model was relatively large, inertia effects seemed to be much dominant compared with the kinematic effects, thus the dynamic responses were similar to the static responses.

These results support the idea of a traditional seismic design method of a foundation in which dynamic

loads acting on the foundation are modelled by an equivalent static horizontal load.

Considering current trends toward the limit state design or performance based design in the area of foundation engineering, precise estimation of deformation of a pile foundation and of stresses of their

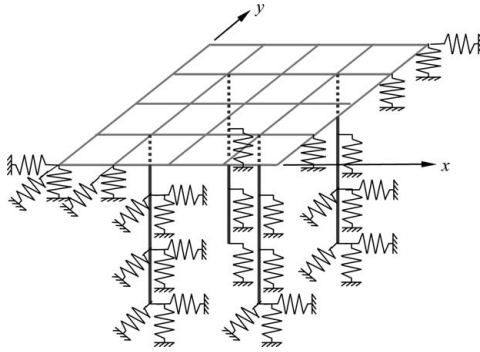


Figure 22. Plate-beam-spring modelling of a piled raft.

structural members is a vital issue in the frame-work of these new design criteria. In the preliminary design stage, a number of alternative calculations are required, varying the number of piles, the pile length, the pile spacing, the locations of the piles, and so on. Hence, a feasible but reliable deformation analysis method of piled raft foundations would be useful. As a preliminary routine design tool of piled raft foundations subjected to vertical, horizontal and moment loads, a computer program PRAB (Piled Raft Analysis with Batter piles) has been developed by Kitayodom & Matsumoto (2002, 2003).

In this program, a hybrid model is employed in which the flexible raft is modelled as thin plates, the piles as elastic beams, and the soil is treated as springs (Figure 22). Both the vertical and horizontal resistances of the piles as well as the raft base are incorporated into the model. The interactions between structural members, pile-soil-pile, pile-soil-raft and raft-soil-raft interactions are taken into account based on Mindlin's solutions for both vertical and horizontal forces. The considered soil profile may be homogeneous semi-infinite, arbitrarily layered and/or underlain by a rigid base stratum. The estimation of non-linear deformation of the foundations is calculated by employing the bilinear (elastic-perfectly plastic) response of soil springs.

The validity of PRAB was verified through comparisons with several published solutions and three-dimensional finite element analysis. These comparisons suggest that PRAB is capable of predicting reasonably well the deformation and the load distribution of single piles, pile groups and piled rafts. In addition, in order to examine the applicability of the computer program PRAB, analyses of the static centrifuge model test were carried out by Kitayodom et al. (2005b).

Analyses of the centrifuge tests were carried out using the geometrical and mechanical properties given in Table 4. The soil was treated as finite homogeneous layer in the analysis. The Young's modulus of the soil

Table 4. Analysis conditions.

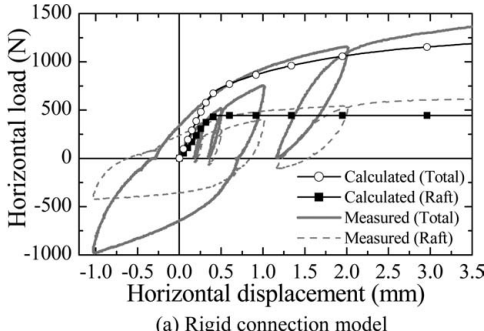
Pile	Pile length = 180 mm Outer diameter = 10 mm, Inner diameter = 8 mm Young's modulus = 70.6 GN/m ² Poisson ratio = 0.16
Raft	Mass = 4.69 kg Width = 80 mm, Breadth = 80 mm Thickness = 25 mm (substantially rigid) Young's modulus = 70.6 GN/m ² Poisson ratio = 0.16
Soil	Layer depth = 460 mm Density = 1.52 t/m ³ , Internal friction angle = 35° Void ratio = 0.76, Poisson ratio = 0.3 Finite homogeneous layer

was obtained by fitting the measured load-displacement curves at the initial loading stage. And it was found that the value of the Young's modulus was 17.4 GN/m². Although cyclic horizontal loads were applied to the model piled raft in the centrifuge tests, the horizontal load was applied in one direction in the analysis. The analysis was conducted for only horizontal loading stage. The vertical load carried by the raft base just before the horizontal load was taken into account as the initial condition. The friction coefficient at the raft base of 0.42 was obtained from the horizontal load test of the raft alone. The limit yield pressure of the piles was assumed to increase linearly with depth and was a product of the Rankine passive pressure coefficient and the effective overburden pressure.

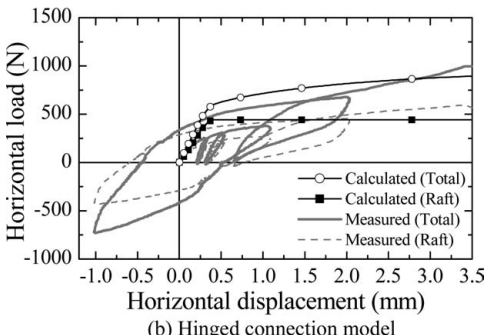
Figure 23 shows the comparisons between the load-displacement behaviour of horizontally loaded model piled raft calculated using PRAB and those obtained from the centrifuge test. It can be seen from both the calculated results and the centrifuge results that the piles in the piled raft with the hinged pile head connection carry smaller amount of the horizontal load than those in the piled raft with the rigid pile head connection, while the amount of the horizontal load carried by the raft is almost the same.

Figure 24 shows the comparisons between the proportions of the horizontal load carried by four piles calculated using PRAB and those obtained from the centrifuge tests. The higher proportion of the horizontal load carried by the piles is shown in the case of the piled raft with the rigid pile head connection. The bending moment profiles at a horizontal displacement of 0.25 mm calculated using PRAB are compared with the centrifuge results in Figure 25. As a whole, the analysis results match well with the measured values obtained from the centrifuge tests.

Moreover, in Nemoto et al. (2006), Mikami et al. (2006) and Yaegashi et al. (2006), a series of experimental and analytical study on the behaviour of model piled rafts in dry sand subjected to static vertical load



(a) Rigid connection model



(b) Hinged connection model

Figure 23. Horizontal load-displacement relationships.

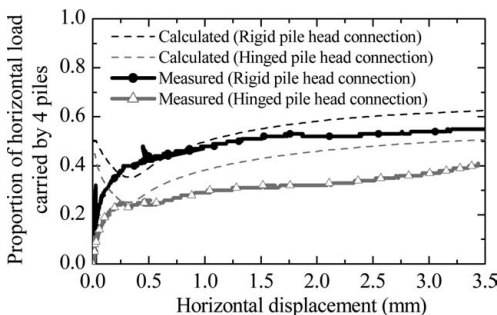


Figure 24. Proportion of horizontal load carried by piles.

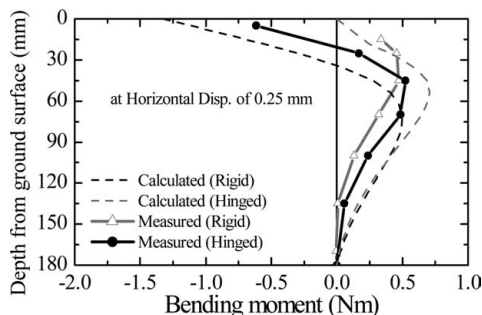


Figure 25. Distributions of bending moment.

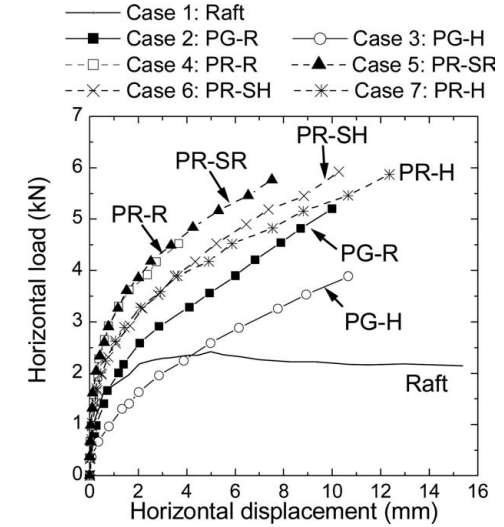


Figure 26. Horizontal load vs horizontal displacement.

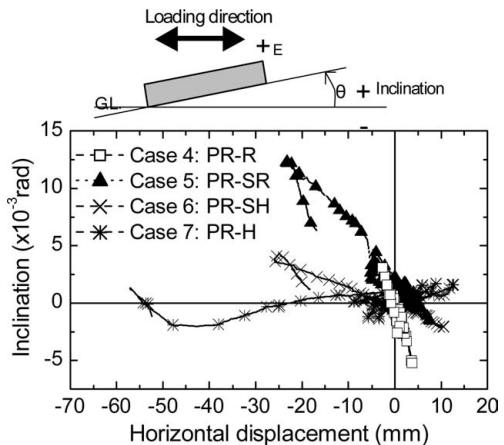


Figure 27. Inclination of raft vs horizontal displacement.

and static horizontal load were carried out, in order to investigate the influence of various pile head connection conditions on the behaviours of model pile groups and model piled rafts. Four different pile head connection conditions were modelled and denoted as ‘rigid’, ‘semi-rigid’, ‘semi-hinged’ and ‘hinged’.

Figure 26 shows the influence of the pile head connection condition on the horizontal load versus the horizontal displacement. Horizontal stiffness of the piled raft is larger than that of the pile group and becomes lower as the pile head connection rigidity becomes lower.

Figure 27 shows the relationships between the inclination of the raft and the horizontal displacement. It

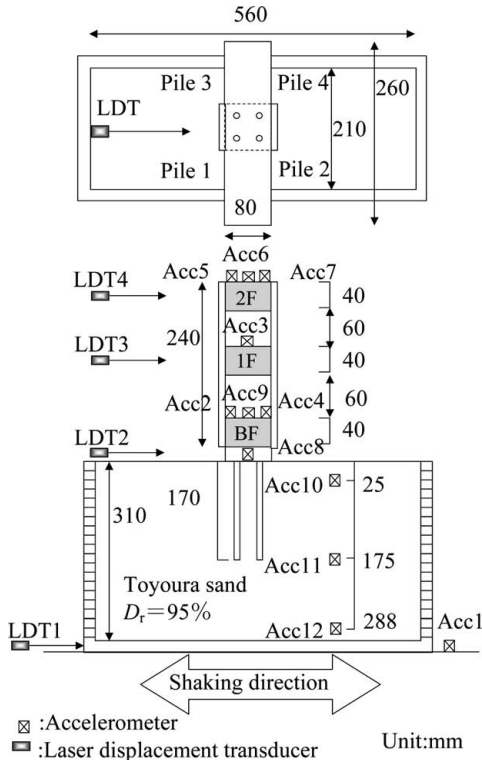


Figure 28. Test set-up.

can be seen that the inclination of the raft increases as the pile head connection rigidity becomes higher. It can be said that lower pile head connection rigidity suppresses the rotation of the foundation compared with higher pile head connection rigidity for a given horizontal displacement, although lower pile head connection rigidity results in larger horizontal displacement for a given horizontal load.

Analyses of the horizontal load test results of model foundations with different pile head connection conditions were carried out using PRAB. Reasonable agreements between the calculated results and the measured values were obtained.

In the above-mentioned experimental works, moment load associated with the horizontal load was not explicitly taken into account. In actual structures such as bridges, the height of centre of gravity is generally higher than the foundation breadth. In such cases, moment loads can have a significant influence on the behaviour under static and seismic loading. Matsumoto et al. (2004ab, 2005c) carried out static horizontal load tests and shaking tests of model piled raft in dry sand, in which rigid superstructures having the same mass but different heights of gravity centre were placed on the model raft. The results of their

experiments showed that the height of gravity centre of the superstructure affects greatly the behaviour of the whole structure consisted of the superstructure and the piled raft during shaking.

When applying the piled raft to foundation of a building, the flexibility of superstructure (building) may be rather flexible, compared with bridge piers for example. In Matsumoto et al. (2006b), a series of shaking tests of model piled rafts with flexible superstructures on them were carried out. Figure 28 shows an illustration of the final stage of the test set-up just before starting shaking. It was found that responses of the superstructure such as horizontal accelerations and rocking motions become largest when input acceleration frequency conforms the primary resonant frequency of the superstructure. Total horizontal load acting on the superstructure becomes small, even though relatively large horizontal accelerations are generated on each floor, due to secondary vibration mode of the superstructure.

In practice, pile foundations may be subjected to soil movements induced by nearby excavation operations, settling embankments, pile driving operations, tunnelling operations, moving slopes, or landslides. In Kitayodom et al. (2005a), the computer program PRAB was extended to accommodate the three-dimensional simplified analysis of piled raft foundations subjected to soil movements.

5 OPEN-ENDED PIPE PILES

Open-ended steel pipe piles are widely used for foundations both on land and offshore. During driving process of these piles into the soil, a soil column known as the soil plug is formed inside the pile. As penetration continues, the frictional resistance between the inner pile shaft and the soil plug may develop, and may prevent further soil intrusion. Depending on the relative movement between the pile and the soil plug, the pile is considered to be perfectly plugged, imperfectly plugged or unplugged. The question then arises how is the effects of the soil plug on the pile performance during pile driving and during static loading in compression.

Bearing capacity of open-ended pipe piles would be still one of unsolved problems in foundation engineering.

5.1 Bearing mechanism of open-ended pipe pile

It is widely accepted that the bearing capacity of an open-ended pipe pile in static compressive loading is the sum of the outer shaft capacity, Q_{out} , the toe capacity, Q_{toe} of the annular pile base, and the soil plug capacity, Q_{plug} , assuming that each component is independent (Figure 29). From the force equilibrium,

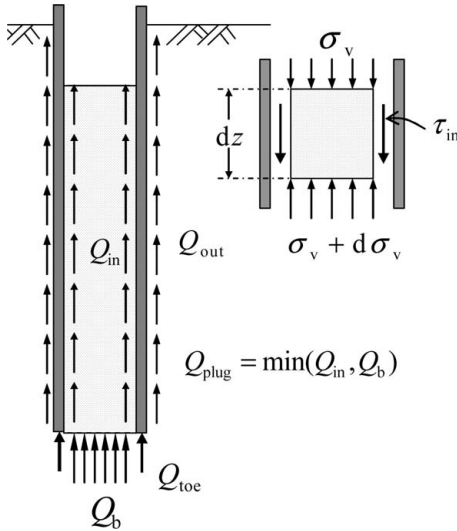


Figure 29. Components of bearing capacity of open-ended pile, and force equilibrium of forces in soil plug element.

the soil plug capacity, Q_{plug} , is the smaller value of the potential inner shaft capacity, Q_{in} , or the bearing capacity of the soil beneath the plug base, Q_b . Thus, if Q_{in} is greater than Q_b , the pile will fail in plugged mode. In pile driving, the inner shaft resistance, R_{in} , can exceed the end-bearing resistance of the soil beneath the plug, R_b , because the inertia force of the soil plug is mobilised. The inertia of the soil plug encourages slip relative to the pile, preventing plugging of the pipe pile as pointed out by Smith, To & Wilson (1986). Most open-ended piles will be filled up with soil during driving, but fail in plugged mode as close-ended piles during static loading (Paikowsky, Whitman & Baligh 1989). However, open-ended piles having larger diameters will fail in imperfect plugged mode even during static loading.

The soil plug has been modelled as a thin disk element by many researchers (*e.g.* Yamahara 1964a) as shown in Figure 29, since the increment of radial strain of the soil plug can be neglected due to high rigidity of the pile compared to that of the soil plug.

5.2 Design practice of open-ended pipe pile in Japan

Most pile foundations for highway bridges are designed based on the *Specifications for highway bridges* by the Japan Road Association (2002) (called JRA specifications hereafter).

According to the JRA specifications, the bearing capacity of an open-ended steel pipe pile is estimated as the sum of the outer shaft capacity, Q_{out} , and the

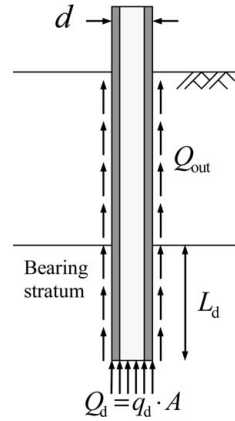


Figure 30. Notations and components of bearing capacity of pile defined in the JRA specifications.

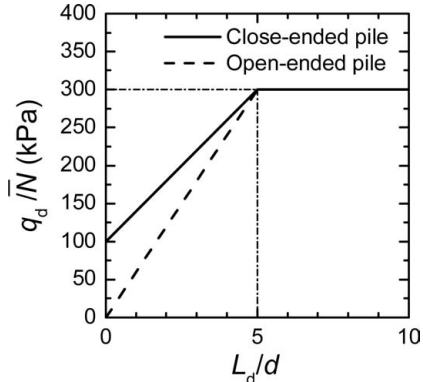


Figure 31. q_d/\bar{N} versus L_d/d proposed in the JRA specifications.

end-bearing capacity, Q_d . The value of Q_d is calculated as the product of the net cross-sectional area of the pile (*i.e.* cross-sectional area of close-ended pile), A , and the ultimate bearing capacity per unit area, q_d . The value of q_d is calculated from the blow count from the Standard Penetration Test (SPT N -value) and the ratio of the embedment length into the bearing stratum, L_d (see Figure 30), to the outer diameter of the pile, d , using the empirical relations shown in Figure 31. Two empirical relations are proposed for close-ended pile and open-ended pile, respectively. For open-ended piles, q_d/\bar{N} is linearly proportional to L_d/d and reaches the limit value of 300 kPa at $L_d/d = 5$. The limit value of 300 kPa is the same for both close-ended pile and open-ended pile, *i.e.* an open-ended pile is regarded as plugged if L_d/d

Table 5. Empirical relations to estimate maximum outer shaft friction (in kPa).

Soil type	Construction method		
	Driven	In-situ	Inner augered
Sandy	$2N$ (limit = 100)	$5N$ (limit = 200)	N (limit = 50)
Clayey	$10c_u$ or $10N$ (limit = 150)	$10c_u$ or $10N$ (limit = 150)	$5c_u$ or $5N$ (limit = 100)

exceeds 5. Here, \bar{N} is the average of SPT N -values along the embedment length, L_d .

The maximum outer shaft friction, $\tau_{\text{out(max)}}$, is estimated from the empirical relations listed in Table 5.

5.3 Researches of open-ended pipe pile in Japan

The pioneering research work on plugging mechanism of open-ended piles is the theoretical approach of Yamahara (1964a, b). After that, a number of experimental, numerical and theoretical researches and field tests have been done in Japan. These research works have been summarised and reviewed by Matsumoto et al. (2004). Some of these researches are picked up again in this paper, and a new challenging research on plugging is introduced.

5.3.1 Theoretical research by Yamahara (1964a, 1964b)

Yamahara (1964a) derived equations for estimating the vertical pressure, p , of the uniform soil plug and the inner shaft capacity, Q_{in} , for sand and clay, based on the force equilibrium of a thin soil plug element (Figure 32) as follows:

For sand (fully drained condition):

$$p(x) = \frac{\gamma' A}{\mu \nu U} \left(e^{\frac{\mu \nu U}{A} x} - 1 \right) = \frac{\gamma' d}{4 \mu \nu} \left(e^{\frac{4 \mu \nu}{d} x} - 1 \right) \quad (21)$$

In Eq. (21), γ' is the effective unit weight of the soil, μ the coefficient of friction between the pile and the soil, ν the coefficient of the lateral pressure ($\nu = q/p$), d the inner diameter of the pile, A the sectional area of the soil plug ($A = \pi d^2/4$), U the inner perimeter of the pile ($U = \pi d$), and x is the distance from the top of the soil plug (see Fig. 32).

The total inner shaft capacity, Q_{in} , is obtained from multiplying A to Eq. (21) in which x is replaced by the total length of the soil plug, l .

$$Q_{\text{in}} = \frac{\gamma' A^2}{\mu \nu U} \left(e^{\frac{\mu \nu U}{A} l} - 1 \right) = \frac{\pi \gamma' d^3}{16 \mu \nu} \left(e^{\frac{4 \mu \nu}{d} l} - 1 \right) \quad (22)$$

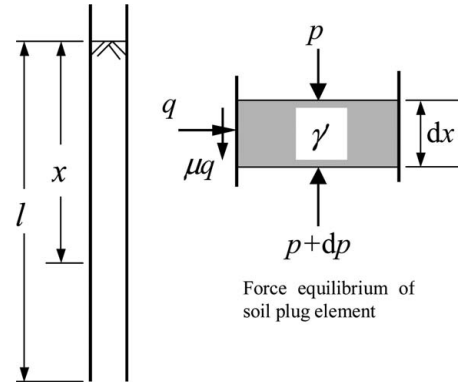


Figure 32. Notations and force equilibrium of soil plug element used in Yamahara (1964a).

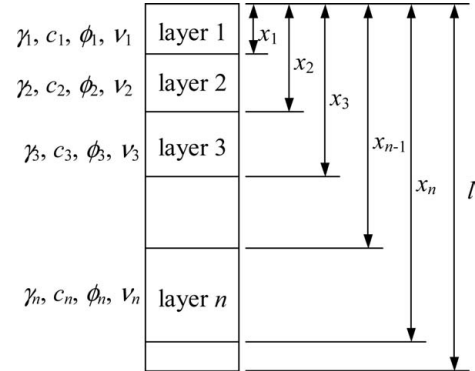


Figure 33. Notations used for multi-layered ground in Yamahara (1964a).

For clay (fully undrained condition):

Fully undrained condition is assumed for clays and it is also assumed that the inner shaft resistance is limited to the undrained shear strength, c . Thus,

$$p(x) = \frac{cU + \gamma' A}{A} x = \left(\frac{4c}{d} + \gamma' \right) x \quad (23)$$

$$Q_{\text{in}} = (cU + \gamma' A)l = \frac{\pi d^2}{4} \left(\frac{4c}{d} + \gamma' \right) l \quad (24)$$

Yamahara (1964a) extended the above solutions to treat a multi-layered ground (Fig. 33) as below.

For the n th soil layer where the soil is sand:

$$p_n(x) = \frac{1}{UV_n \tan \phi_n} \times \\ \left\{ (c_n U + \gamma'_n A + UV_n \tan \phi_n p_{n-1}(x)) e^{\frac{UV_n \tan \phi_n}{A} (x - x_{n-1})} - (c_n U + \gamma'_n A) \right\} \quad (25)$$

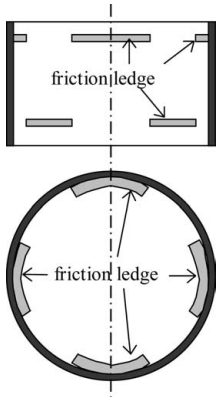


Figure 34. Use of friction ledges to increase the friction coefficient at the inner shaft interface (Yamahara, 1964b).

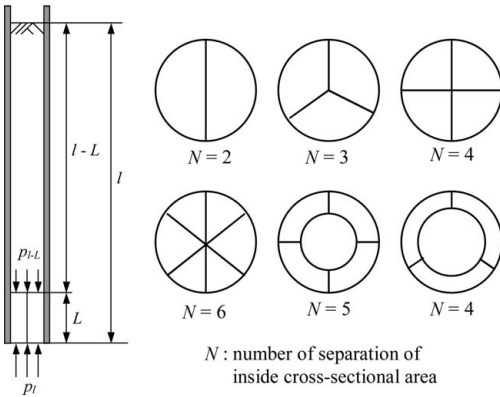


Figure 35. Use of separation walls and/or smaller pipe pile to increase the inner shaft capacity (Yamahara, 1964b).

In Equation (25), $p_{n-1}(x)$ can be estimated successively from the boundary condition (stress condition) at the top of the soil plug.

Methods for increasing the inner shaft capacity were proposed also in Yamahara (1964b), as shown in Figures 34 and 35. Friction ledges are welded on the inner shaft of an open-ended steel pile to increase the coefficient of friction between the inner shaft and the soil inside the pile (Figure 34).

Another method is division of the inside of a pipe pile along a length of L from the pile tip by using separation walls and/or an additional pipe pile with smaller diameter (Fig. 35). The idea of this method is increasing the interface area between the devised pile section and the inner soil to increase the vertical pressure, p_i , of the inner soil in each separated pile inside area, based on Eq. (21).

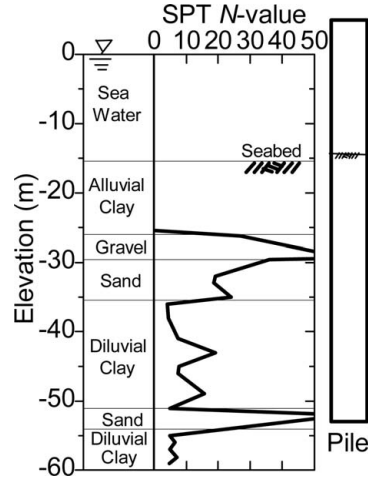


Figure 36. Test pile at final seating, together with ground condition.

5.3.2 Access bridge for kansai international airport

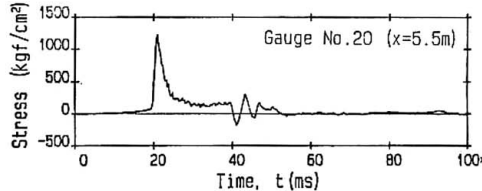
An offshore pile testing was carried out in 1986 in association with the design of foundation piles for the access bridge that spans the Kansai International Airport in Osaka Bay, 5 km offshore, and the mainland (Shibata et al. 1989). A test steel pipe pile having a length of 58 m, an outer diameter of 1500 mm and a wall thickness of 22 mm was driven by a diesel hammer to a depth of 37.1 m below the seabed (Fig. 36). The level of the top surface of the soil inside the pile rose up 1.1 m above the original surface of the seabed. The re-driving test and the static load test were performed 35 days after the final driving.

Matsumoto & Takei (1991) analysed the final pile driving and the static load test by using KWAVE program. The results of the final matching analysis are shown in Figure 37. The wave propagation analysis showed that the permanent settlement per blow was 4 mm, whereas the top of the soil plug did not have permanent settlement. The calculated results conformed well to the measured pile and soil plug behaviours during driving.

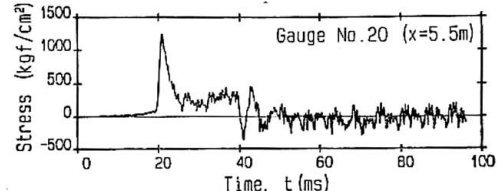
Static load-settlement curves of the pile were calculated using the soil parameters identified from the wave matching analysis, and are compared with the measured values in Figure 38. The calculated (predicted) load-settlement curves for the pile head and the pile base are in good agreements with the measured ones.

The analyses of the pile driving and the static load test indicated the following influence of the soil plug on the pile behaviour:

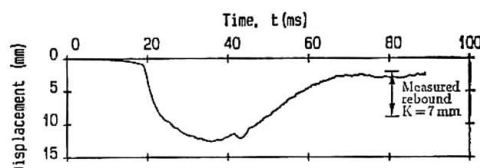
- i) The inner shaft resistance is effectively mobilised during driving due to the inertia of the soil plug



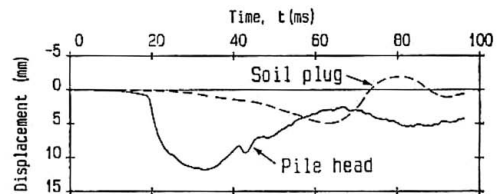
(a) Measured stress-wave of the pile



(b) Calculated stress-wave of the pile



(c) Measured pile head displacement



(d) Calculated displacements of the pile head and the top of the soil plug

Figure 37. Results of wave matching analysis of the re-driving test.

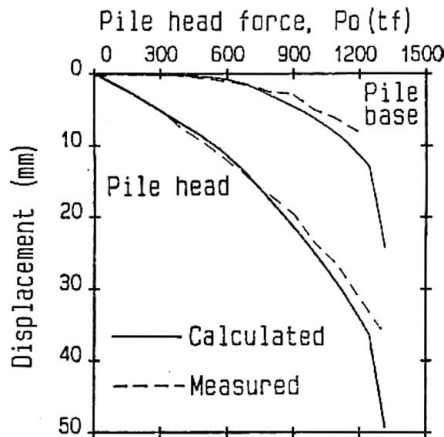


Figure 38. Comparison of measured load-settlement curves and those derived from the wave matching analysis.

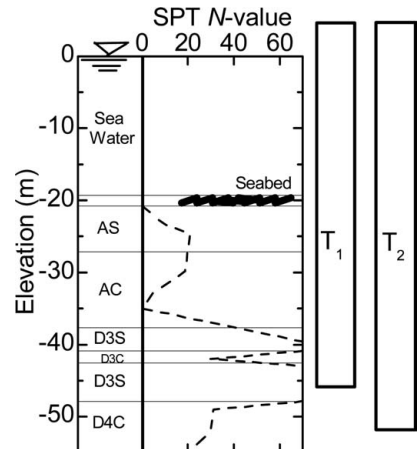


Figure 39. Final seating of the test piles, together with the soil profile and SPT N-values.

- ii) Only imperfect plugging of the pipe pile occurs during driving
- iii) In the static load test, the outer shaft resistance is predominantly mobilised at initial loading stage until it reaches the ultimate state. After the outer shaft resistance is fully mobilised, the inner shaft resistance starts to mobilise
- iv) Hence, wave matching analysis with consideration of wave propagation in the soil plug and the inner shaft resistance is important to derive the behaviour of the pile under static loading from the dynamic load test results.

5.3.3 Tokyo trans bay highway bridge

Trans-Tokyo Bay Highway (TTBH) connects Kawasaki City and Kisarazu City over the Tokyo Bay. TTBH consists of the tunnel section (9.4 km) and the bridge section (4.7 km). The bridge piers are supported by driven open-ended steel pipe piles. The test piling was performed in 1989 through 1990 at a point of the bridge route about 3 km offshore from Kisarazu City (Momiyama et al. 1992). Two test piles, designated as T_1 and T_2 , were driven by a steam hammer.

Figure 39 shows the final seating of the test piles, together with the soil profile and SPT N -values. The

soil that intruded into the pile T_2 was excavated during interruption of pile driving so that pile T_2 had no soil inside it (had no internal shaft resistance).

The compression load tests of pile T_1 and pile T_2 were performed after 2 months from the end of pile driving. The tension load test was conducted on pile T_1 after 1 year from the end of the compression load test. The load-displacement relations of piles T_1 and T_2 are compared in Figure 40. It is seen from Figure 40 that the load-displacement curves of piles T_1 and T_2 were almost identical until the pile load of 12 MN was reached, indicating that the mobilisation of the internal shaft resistance was negligible in pile T_1 .

The distributions of axial forces along the piles at the ultimate state are compared in Figure 41. It is seen from

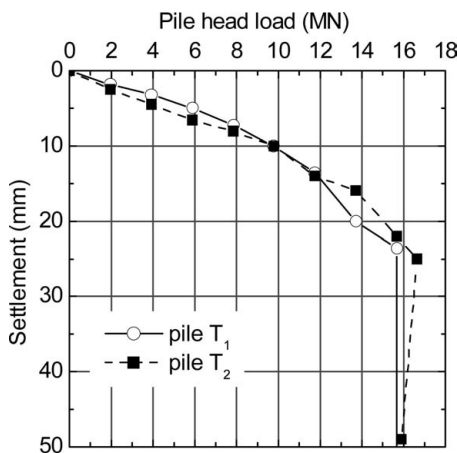


Figure 40. Load-displacement relations of pile T_1 and pile T_2 .

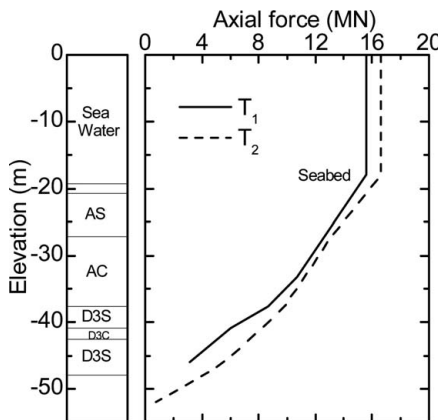


Figure 41. Measured distributions of the axial forces of the piles at the ultimate state.

Figure 41 that the rate of decrease in the axial force down the pile shaft is similar for piles T_1 and T_2 , which means that the mobilisation of the shaft resistance including the internal and external shaft resistances was almost identical in piles T_1 and T_2 . This result indicated again that the internal shaft resistance of pile T_1 was negligible, if we remind that pile T_2 had no soil plug.

The results of the test piling showed that the internal shaft resistance is smaller than the external shaft resistance, even if the set-up phenomena would have occurred in the soil inside the pile.

Detailed analyses of the pile load tests have been carried out by Matsumoto & Kitayodom (2005e).

5.3.4 Highway bridge in a soft rock, Noto Peninsula

A new highway was constructed in Noto Peninsula, Japan, in 1994 and 1995 with the start of operation in 1997. A diatomaceous mudstone that is a kind of hard clay widely distributes in Noto Peninsula. A series of pile load tests were performed in 1991 in association with the design of foundation piles (open-ended steel pipe piles) for the new highway bridges (Matsumoto et al. 1995). Three test piles designated as T_1 , T_2 and T_3 were driven into a relatively uniform diatomaceous mudstone ground. All the test piles had the same geometrical properties; length of 11.0 m, an outer diameter of 400 mm and a wall thickness of 12.1 mm. Compression load tests were performed on piles T_1 and T_2 , while the tension test was performed on pile T_3 . The soil plug inside pile T_2 was excavated prior to the static load test so that pile T_2 had the outer shaft resistance alone.

For pile T_1 , generation of pore water pressures around and inside the pile were measured during driving and the static load test by means of pore water pressure transducers which had been instrumented in the ground prior to the pile driving process (Fig. 42).

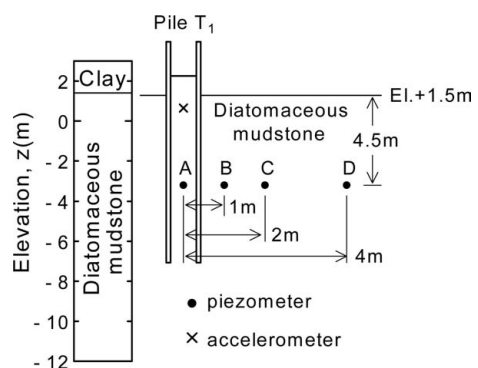


Figure 42. Instrumentation of pore water pressure transducers around pile T_1 .

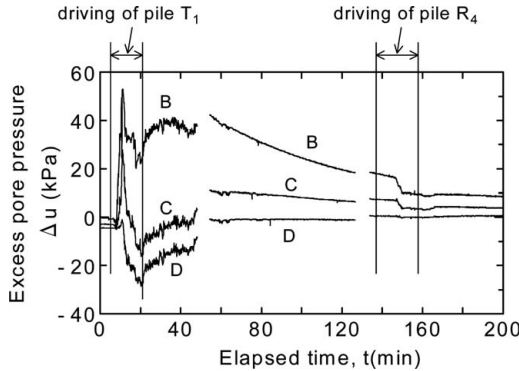


Figure 43. Pore pressure phenomena around pile T_1 during and after pile driving process.

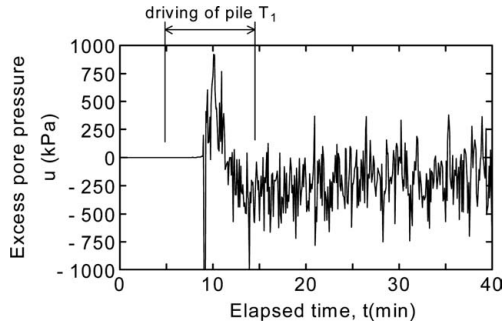


Figure 44. Pore pressure phenomena inside pile T_1 during and after pile driving process.

Figure 43 shows the measured pore pressures during and after pile driving process.

It is seen from Figure 43 that positive (compression) pore pressure was generated first at positions B, C and D, followed by the decrease in pore pressure.

Matsumoto et al (1995) discussed that the positive and negative pore pressures can be generated according to the position of the pile tip relative to position of the ground during pile driving. The dissipation of the pore pressures after the end of pile driving indicated that the increase in bearing capacity of the pile was significantly controlled by the effective stresses of the ground around the pile.

The pore pressure measured inside the pile (at position A) is shown in Figure 44. Very large pore pressure of 880 kPa was generated in the soil plug during driving. This indicates that the soil plug deformed in fully undrained condition during driving.

The comparison of load-displacement curves obtained from the static load tests on pile T_1 and pile T_2 is shown in Figure 45. The ultimate capacity of

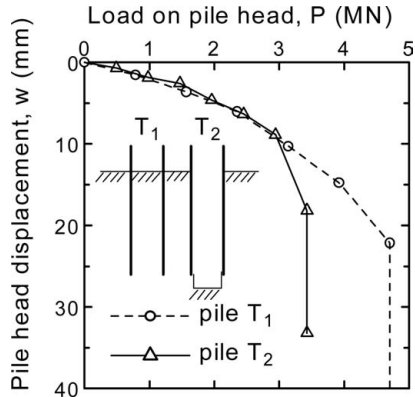


Figure 45. Comparison of load-displacement curves from static load tests on pile T_1 and Pile T_2 .

pile T_1 was 4.7 MN, while that of pile T_2 was 3.7 MN. An axial force of 0.4 MN was transmitted to the pile tip when pile T_1 reached the ultimate state. Note that pile T_2 had the outer shaft resistance alone. Hence the inner shaft capacity of pile T_1 was estimated as 0.6 MN.

It is seen from Figure 45 that the load-displacement curves of pile T_1 and pile T_2 are identical until the pile head load reaches 2.9 MN. This result indicates that the outer shaft resistance was predominantly mobilised in pile T_1 . A safety factor of 3 is commonly adopted in pile design in Japan. Therefore, precise estimation of the outer shaft resistance is important to estimate the load-displacement curve for the working load.

5.3.5 Wharf structures in Nagoya Bay

Steel pipe piles were employed for the wharf structures in Nagoya Bay (Kikuchi et al, 2000). Series of Statnamic and dynamic load tests were carried out to estimate the bearing capacity of the piles in order to establish a site-specific driving formula used for driving control of production piles at the site. Three test piles designated as V1, V2 and V3 were driven into relatively uniform alluvial clay. The pile toes were seated in a thin dense gravel sand stratum. All the test piles had a length of 50 m and a diameter of 1.5 m. The wall thickness of the pile was 17 mm at the pile head and 15 mm at the pile toe. Two test piles, V1 and V3, were simple open-ended piles while the cross-rib plates were installed at the pile toe of test pile V2 as shown in Figure 46.

Dynamic load tests were performed at the end of driving and re-driving after 23, 25 and 28 days on the test piles V1, V2 and V3 respectively. Statnamic tests were carried out by a 30 MN loading capacity device

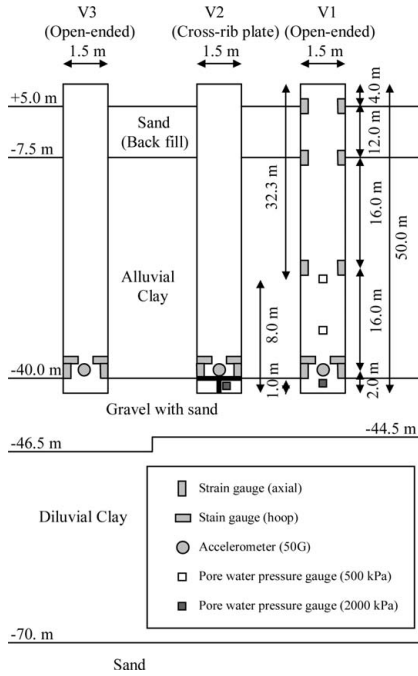


Figure 46. Schematic diagram of test condition.

at 42, 49 and 51 days after the end of driving on the test piles V1, V2 and V3, respectively.

Kikuchi et al. (2000) suggested that

- The pile shaft resistance in the alluvial clayey stratum shows large recovery behaviour (set-up) after pile driving
- The pore water pressure around the pile in the alluvial clayed stratum increased at the time of dynamic and Statnamic tests and settled down to natural pressure within 46 days
- The pile with the cross-rib plates at the pile toe indicated large stiffness than that of without the cross-rib plates in the load-displacement curves.

5.3.6 Application of DEM to research of piles

Dynamic load tests, static compression load tests and static tension tests of open-ended model pipe piles in a model ground of dry sand were carried out by the joint of JASPP and Kanazawa University (Kitiyodom et al. 2004b).

Dry silica sand was used for the model ground throughout this study. The physical properties of the sand are summarized in Table 6. The sand was prepared in a rigid cylindrical chamber having dimensions of 1.2 m in diameter and 1.8 m in depth (as shown in Figure 47). The sand was poured into the chamber and compacted to nearly its maximum relative density. Weights were placed on the model

Table 6. Physical properties of silica sand.

Property	Value	
Relative density at test	D_r	>90%
Peak friction angle	ϕ'	45 deg.
Residual friction angle	ϕ'_r	41 deg.
Density of soil particle	ρ_s	2.676 t/m ³
Maximum density	ρ_{dmax}	1.692 t/m ³
Minimum density	ρ_{dmin}	1.383 t/m ³
Mean grain size	D_{50}	0.25 mm
Coefficient of uniformity	U_c	2.268

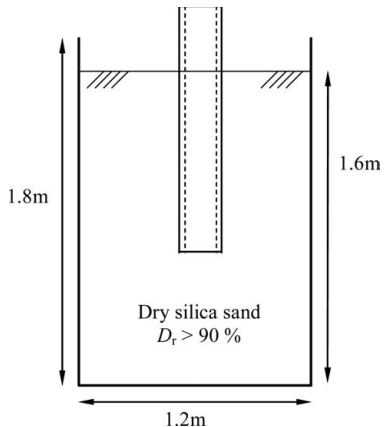


Figure 47. Model ground.

ground surface prior to driving process of the pile, resulting in an additional vertical surcharge pressure of 1.67 kPa.

The uniformity of the soil strength of the model ground was examined through the tests by using a miniature cone penetrometer with a diameter of 16.2 mm and an apex angle of 60 degrees. The cone penetration tests (CPT) were conducted twice near the centre point of the model ground. The penetration rate was set at 2 mm/s. The measured strengths are shown in Figure 48. The figure shows that the strength increases with depth.

One of model piles which is named P1H had a length of 1500 mm, an outer diameter of 101.6 mm, and an inner diameter of 97.26 mm and a wall thickness of 2.17 mm. This model pile was driven into the model ground by means of a falling hammer until the pile toe reached the prescribed depth. Then the static axial compressive pile load test was carried out. Thereafter the static axial tensile pile load test was conducted.

During the pile driving process, the pile embedment length, L_d , and the height of soil plug, H_{sp} , were measured. The model pile P1H was driven until the

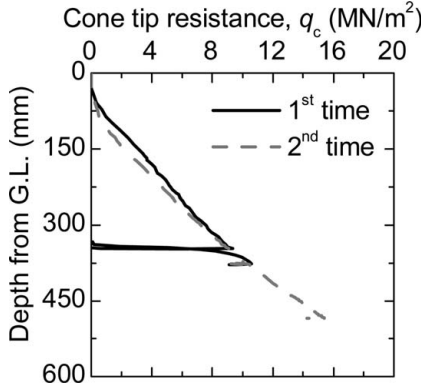


Figure 48. Distributions of cone tip resistance.

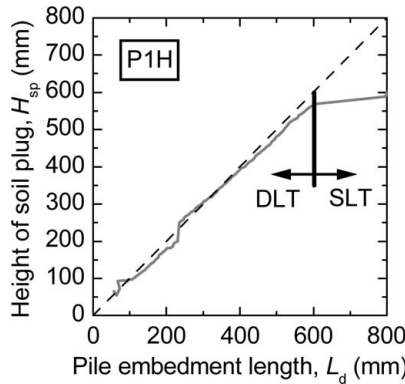


Figure 49. Pile embedment length vs soil plug height.

pile toe reached a depth of 603 mm. The height of soil plug, H_{sp} , attained to 568 mm at the end of pile driving as shown in Figure 50, indicating that only imperfect plugging of pipe pile occurred during driving. This was caused by the inertia of the soil plug inside the pile, which encouraged the slippage between the soil plug and the pile and prevented perfect plugging of the pile.

Figure 50 shows the relationship between the pile head load, P , and the pile head displacement, w . In Figure 50, the outer shaft resistance, Q_{out} , vs w which was measured in the tension test is also shown.

The end resistance of the annual pile toe, Q_{toe} , was estimated as follows. The ratio of the end-bearing pressure to the cone tip resistance, q_b/q_c , at any normalized pile base displacement, w_b/D may be expressed as Eq. (26) following de Nicola & Randolph (1997):

$$\frac{q_b}{q_c} = \left(\frac{\lambda m (w_b/D)}{(w_b/D) + c} \right) \quad (26)$$

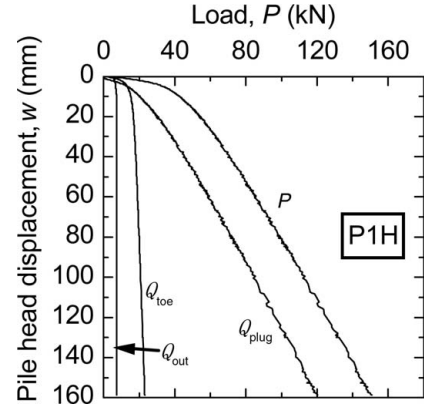


Figure 50. Results of the static axial compressive pile load test and static axial tensile pile load test.

where $m = 0.7$, $c = 0.015$, D is the pile diameter, and λ is related to the effective stress by

$$\lambda = \begin{cases} 1.75 - \left(\frac{\sigma'_v}{2p_a} \right) & \text{for } \sigma'_v < 200 \text{ kPa} \\ 0.75 & \text{for } \sigma'_v \leq 200 \text{ kPa} \end{cases} \quad (27)$$

where $p_a = 100$ kPa.

In this study, the length of the model pile was not so long, so the pile base displacement, w_b , was assumed to be the same as the pile head displacement, w . The effective stress of the soil at the pile base, σ'_v , including the vertical surcharge pressure of 1.67 kN/m² due to weights placed on the ground surface was 11.53 kPa, and the cone tip resistance, q_c , was 21344 kPa.

The pile base resistance, Q_{toe} , is then calculated from the product of the end bearing pressure, q_b , and the cross sectional area of the pile, A_p .

$$Q_{toe} = q_b A_p \quad (28)$$

The soil plug resistance, Q_{plug} , may now be calculated by

$$Q_{plug} = P - Q_{out} - Q_{toe} \quad (29)$$

In Figure 50, Q_{toe} and Q_{plug} thus obtained are also shown. It is seen that most of the total load, P , was the soil plug resistance, Q_{plug} , that was equal to the end bearing resistance of the ground beneath the bottom of the soil plug.

It is seen from Figure 50 that the soil plug height increased only 30 mm during the static load test, although the pile displacement of 160 mm was given to the pile. Hence, the pile was considered to be perfectly plugged during the static load test.

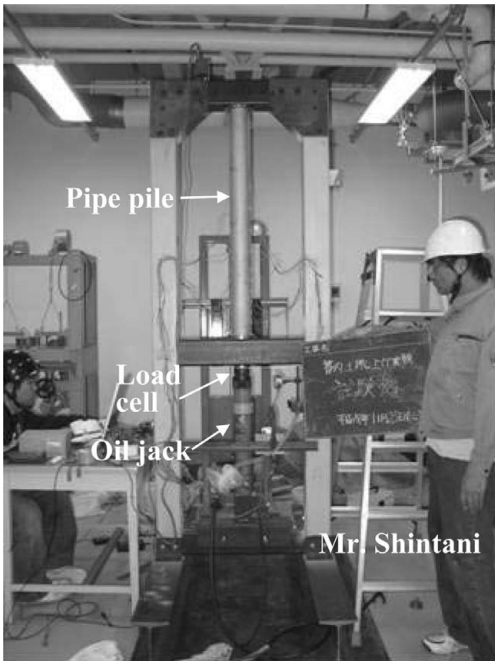


Figure 51. Push-up load test apparatus.

In order to investigate the soil plug behaviour in more detail, push-up load tests of soil plug and their analyses using Discrete Element Method (DEM) were carried out (Shintani 2007).

Figure 51 shows the push-up load test apparatus. The silica sand was poured in the pipe pile so that the sand plug had a relative density of about 90%. The bottom of the sand plug was pushed-up by an oil jack quasi-statically. Push-up force and displacements of the top and bottom of the sand plug were measured. Strain gauges were mounted down the outer shaft of the pipe pile to measure the axial forces of the pile, from which distributions of inner shaft resistance were obtained.

Push-up load tests were carried out for sand plugs having the aspect ratio, H/D , ranging from 3 to 6, where H is the height of soil plug and D is the inner diameter of the pipe pile of 97 mm.

Figure 52 shows the relationships between the push-up force and the push-up displacement at the bottom of sand plug for $H/D = 3$ to 6. In cases of $H/D = 3$ and 4, the peak push-up force was obtained. In cases of $H/D = 5$ and 6, loading was terminated before the peak push-up force was obtained because of the capacity of the loading device. But, it may be inferred that the soil plug resistance (push-up force) increases exponentially with increasing H/D .

In the static compression load test of pile P1H, H/D was 5.8. The soil plug resistance attained to

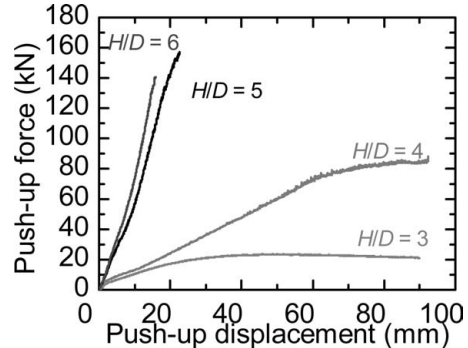


Figure 52. Push-up displacement vs push-up force.

120 kN when the pile displacement attained to 160 mm (see Fig. 50).

In the push-up test of the sand plug of $H/D = 6$, push-up force of 120 kN was mobilised by a push-up displacement of 12 mm that is much smaller than the pile head displacement in the static compression load test. This difference is reasonable, because a large displacement of the bottom of the soil plug is required to mobilise the end bearing resistance of the ground beneath the bottom of the soil plug in the static compression load test.

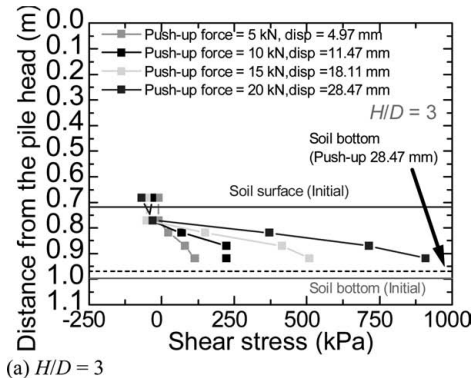
Figure 53 shows the distributions of shear stress (inner shaft resistance) measured in push-up load tests in cases of $H/D = 3$ and 6. The inner shaft resistance increases exponentially with distance from the top of the soil plug as expected from the theory by Yamahara (1964a).

Analysis of penetration of the pipe pile into the ground from the ground surface will be useful to investigate the mechanisms of formation of the soil plug and its capacity. The soils surrounding and inside the pipe pile undergo very large deformations and failures during pile installation process. Discrete Element Method (DEM) is one of useful numerical methods to analyse such behaviour of the soils.

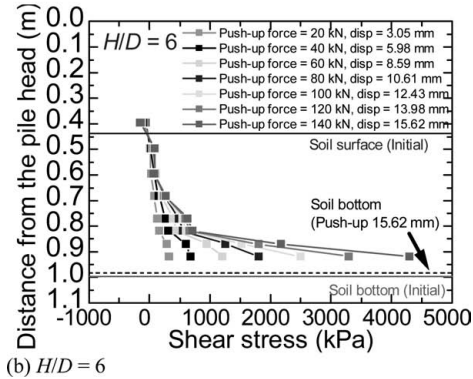
DEM analyses of the push-up load tests were attempted by the authors (Shintani et al. 2006, Shintani 2007) as the first step to investigate the bearing mechanism of open-ended pipe piles.

The DEM code used in this study was PFC3D (Itasca 2003). ‘Clump’ that is shown in Figure 1 was employed in the DEM analyses. A clump is composed of spheres that are overlapping partly to form a non-spherical particle. In this parametric study, the sand was modelled by peanut-shaped clumps composing of two spheres as shown in Figure 54, following Katzenbach & Schmitt (2004).

It is desirable to use the same particle size as the real sand in DEM simulation. However, such modelling is



(a) $H/D = 3$



(b) $H/D = 6$

Figure 53. Distributions of shear stresses down the internal pile surface.

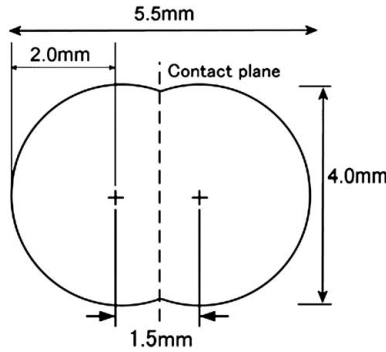


Figure 54. Peanut-shaped clump used in the DEM analyses.

practically impossible, in view of capacity and time of calculation. In centrifuge tests, no scale effect was observed for model footings that had ratios of footing diameter to soil particle size ranging from 30 to 180 (Ovesen 1979).

Diameter of the soil plug in parametric calculation in this paper is about 100 mm. According to the above

Table 7. Analysis parameters of clump.

Property	Value
Particle size (Long axis)	5.5 mm
(Short axis)	4.0 mm
Density of soil particles, ρ_s	2.73 ton/m ³
Friction angle between clumps, ϕ_μ	35 degrees
Normal and tangential spring stiffness between clumps	5×10^5 N/m
Normal and tangential spring stiffness between clump and wall	5×10^5 N/m

observation in centrifuge tests, the particle size used in DEM should be less than 3 mm. However, the use of clumps consisting of 2 spheres having a diameter of 3 mm took a very long calculation time. Hence, the authors decided to use peanut-shaped clumps having a diameter of 4 mm as shown in Figure 54.

The values of normal spring, tangential spring and the friction coefficient between the clumps were determined through matching analyses of the element tests (results are shown later). The identified analysis parameters are summarised in Table 7. Note that local damping value (Itasca 2003) of 0.7 was employed and any other damping was not used through the analyses. Calculation timestep used was $5 \mu\text{s}$ for all the DEM analyses except for the analysis of direct shear test where timestep of $2 \mu\text{s}$ was used.

Maximum density and minimum density tests were carried out. The minimum density test followed the standard method by Japanese Geotechnical Society (1992). On the other hand, non-standard method was used in the maximum density test. In the standard method, the sand is poured into the mould (40 mm high) with a collar (20 mm high) in 10 layers, and 100 impacts are applied to the mould after pouring each soil layer. In non-standard method used in this research, the sand was poured into the mould with the collar at once, and 1000 impacts were applied to the mould, as shown in Figure 55. Figure 55 shows the analytical models for the minimum and maximum density tests. The hopper, mould and collar were modelled by 'wall elements'. A total of five DEM analyses of minimum and maximum density tests were carried out.

Clumps were created every time randomly inside the hopper (Fig. 55(a)). Afterwards, the hopper was pulled-up at a speed of 5 mm/s. After the clumps had dropped into the mould with collar (Fig. 55(b)), the clumps in the collar were deleted (Fig. 55(c)) to obtain the maximum void ratio, e_{\max} .

DEM analysis of the maximum density test was started from the state of Figure 55(b). In order to model the impact on the mould, sinusoidal horizontal displacement having a frequency of 5 Hz and an amplitude of 5 mm was applied to the mould. The

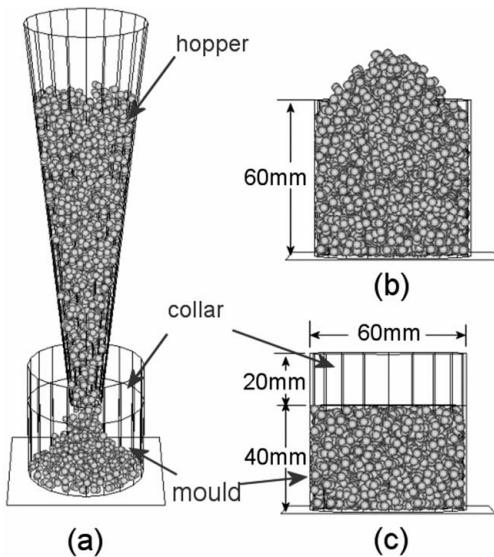


Figure 55. Analysis models used for minimum density test and maximum density test.

Table 8. The calculated results of minimum density tests.

Analysis	Maximum void ratio	Minimum dry density
1st	0.976	1.384 ton/m ³
2nd	0.946	1.405 ton/m ³
3rd	0.944	1.406 ton/m ³
4th	0.962	1.394 ton/m ³
5th	0.960	1.395 ton/m ³
Mean	0.958	1.397 ton/m ³

shaking direction was changed by 36 degrees every 10 cycles of shaking, to simulate the test procedure.

The results of DEM analyses of the minimum density tests are summarised in Table 8. The mean values of maximum void ratio and minimum dry density are 0.958 and 1.397 ton/m³, respectively. These values may be comparable with those obtained from the minimum density test (see Table 6).

The results of DEM analyses of the maximum density tests are compared with the test results in Figure 57. Changes in void ratio are plotted against the number of shaking cycles in Figure 57 until the shaking cycle of 200, although 1000 shaking cycles were analysed. The void ratio rapidly decreased with increasing shaking cycle to about 100 cycles and then almost levelled off for further shaking cycles in the non-standard maximum density tests. The results of DEM analyses simulate this measured behaviour well. The minimum void ratio and the corresponding maximum dry density obtained from the DEM analyses are summarised in Table 9.

Table 9. The calculated results of maximum density tests.

Analysis	Minimum void ratio	Maximum dry density
1st	0.678	1.629 ton/m ³
2nd	0.672	1.635 ton/m ³
3rd	0.682	1.625 ton/m ³
4th	0.671	1.636 ton/m ³
5th	0.676	1.631 ton/m ³
Mean	0.676	1.631 ton/m ³

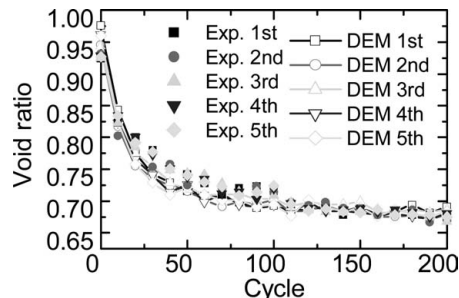


Figure 56. The calculated and experimental results of maximum density tests until 200 shaking cycles.

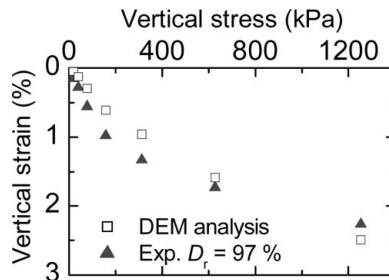


Figure 57. The calculated and experimental results of one-dimensional compression test.

The one-dimensional compression tests and the direct shear tests of the sand were carried out using the consolidation ring and the shear ring having an inner diameter of 60 mm and a height of 20 mm. However, in the DEM analyses, the height of the soil specimen was set at 40 mm in the DEM analyses, because the size of clump (Fig. 54) seemed to be large compared to the actual ring height of 20 mm.

The friction between the clumps and the walls was neglected. The initial void ratio prior to compression was set at 0.693 in the DEM analysis. In the process of DEM analysis of the one-dimensional compression test, a total of 8 loading steps, 9.8 to 1254.4 kPa, were applied to the top loading plate.

Figure 57 shows the comparison between the one-dimensional test results and the DEM analysis results.

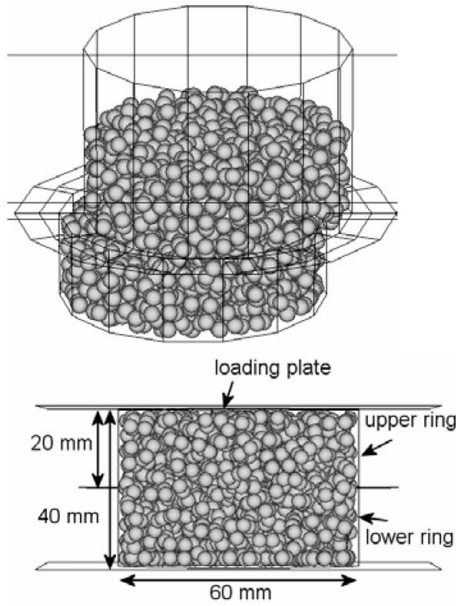


Figure 58. DEM modelling of direct shear test.

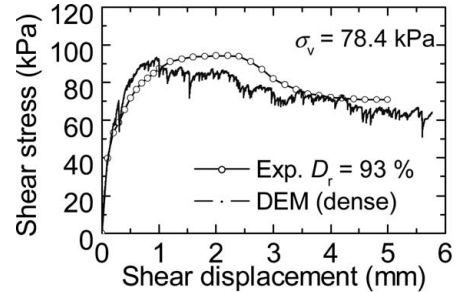
It can be seen from the figure that the test results are well simulated by the DEM analysis.

Direct shear test was carried out with a vertical stress of 78.4 kPa for the dense sand having $D_r = 93\%$ ($e = 0.608$). In the DEM analysis, the initial void ratio prior to compression was set at 0.693 and vertical stress of 78.4 kPa was applied to the specimen through the top loading plate. After completion of the analysis of the vertical loading, horizontal displacement was applied to the upper ring at a displacement rate of 0.4 mm/min (Fig. 58).

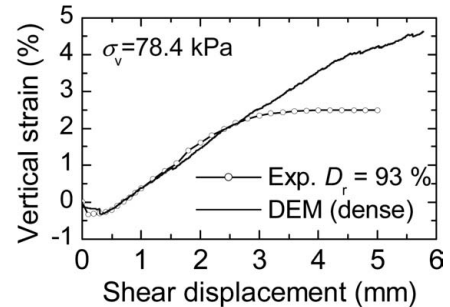
Figure 59 shows the comparison between the results of the direct shear test and the DEM analysis. Figure 59(a) shows the relationships between the shear displacement and the shear stress. Figure 59(b) shows the relationships between the shear displacement and the vertical strain. It can be seen from Figure 59(a) that the experimental result was simulated well by the DEM analysis and that ϕ_{peak} value is estimated as 49 degrees that is larger than the grain-to-grain friction angle, ϕ_μ of 35 degrees. The dilatancy behaviour observed in the experiment was also simulated well by the DEM analysis (Fig. 59(b)).

As the element tests of the sand were well simulated by DEM as mentioned in the above, DEM analyses of the push-up load tests were attempted using the analytical parameters identified through DEM analyses of the element tests.

Figure 60 shows the analysis model of push-up loading of soil plug. Considering axi-symmetrical



(a) Shear displacement vs shear stress



(b) Shear displacement vs vertical strain

Figure 59. The calculated and experimental results of direct shear test.

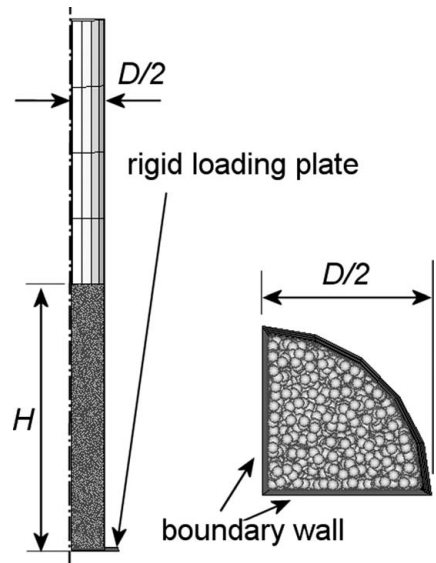


Figure 60. Analysis model of push-up load test of soil plug.

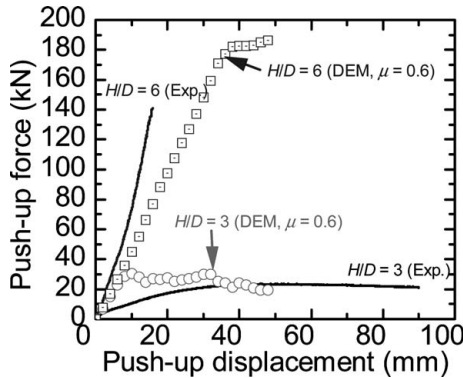


Figure 61. Results of DEM simulations of push-up load tests of soil plug.

condition of the problem, only one-fourth of the pile and the soil plug were modelled. The pile was modelled by rigid walls. Hence the deformation of the pile body was not taken into account in the analysis. The soil particles (clumps or spheres) were generated inside the model pile in order to create the soil plug. Then, self-weight analysis was conducted without friction between the soil and the inner pile shaft. Finally, the analysis of push-up loading was carried out by applying an upward velocity of 5 mm/s to the rigid loading plate, taking into account the friction between the soil and the inner pile shaft.

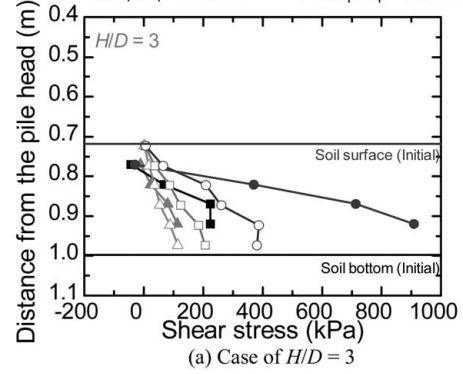
Figure 61 shows the comparisons of the results of the push-up load tests and the DEM analyses. In the DEM analyses, coefficient of friction between the pile and the soil particle, μ , was set to be 0.6.

Figure 62 shows the distributions of inner shaft resistance calculated from the DEM analyses, compared with the experimental results.

The results of Figures 61 and 62 may encourage the use of DEM to investigate behaviours of the pile and the ground which accompany large deformation and failure of the ground.

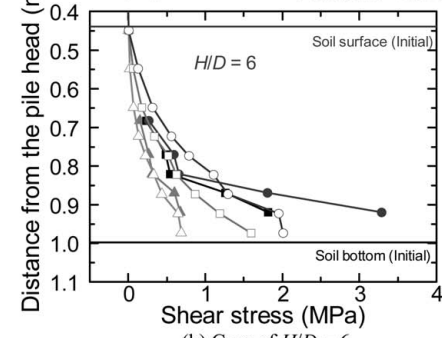
Figure 63 shows the distributions of mobilised coefficient of friction between the soil and the inner pile shaft calculated from the DEM analyses. Here, the mobilised coefficient of friction is defined as the ratio of shear stress (inner shaft resistance) to the radial stress acting on the inner pile shaft. The coefficient of friction between the soil particle and the pile was set to be 0.6. However, the mobilised coefficient of friction ranges from 0.4 to 0.55 which are less than the coefficient of friction between the soil particle and the pile. It may be inferred from this result that rotation of the soil particles adjacent to the pile shaft, rather than slippage between the soil particles and the pile shaft, controls the inner shaft resistance.

Legend for Figure 62(a):
 —▲— Exp. Push-up force = 5 kN, —△— DEM Push-up force = 5 kN, Push-up disp = 4.97 mm
 —■— Exp. Push-up force = 10 kN, —□— DEM Push-up force = 10 kN, Push-up disp = 11.47 mm
 —●— Exp. Push-up force = 20 kN, —○— DEM Push-up force = 20 kN, Push-up disp = 28.47 mm



(a) Case of $H/D = 3$

Legend for Figure 62(b):
 —▲— Exp. Push-up force = 40 kN, —△— DEM Push-up force = 40 kN, Push-up disp = 5.98 mm
 —■— Exp. Push-up force = 80 kN, —□— DEM Push-up force = 80 kN, Push-up disp = 10.61 mm
 —●— Exp. Push-up force = 120 kN, —○— DEM Push-up force = 120 kN, Push-up disp = 13.98 mm



(b) Case of $H/D = 6$

Figure 62. Distributions of inner shaft resistance calculated from the DEM analyses.

The authors are attempting DEM analyses of the penetration of an open-ended pipe pile into the ground from its surface, using analytical models as shown in Figure 64, where the pile is modelled by the rigid walls or particles to allow for the deformation of the pile.

6 BARRIERS IN APPLICATIONS OF NEW TECHNOLOGIES TO PRACTICES

A number of new technologies and new design methods have been developed in Japan, as have been mentioned so far. However, it seems that there are difficulties or barriers in applying the new developments

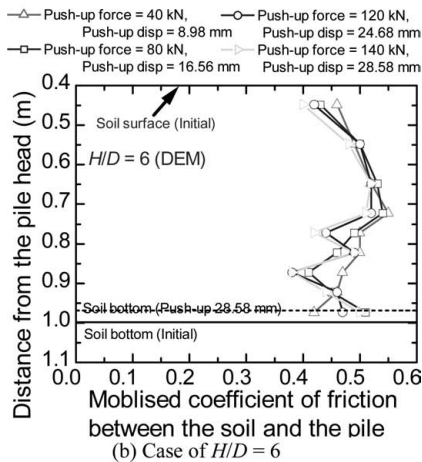
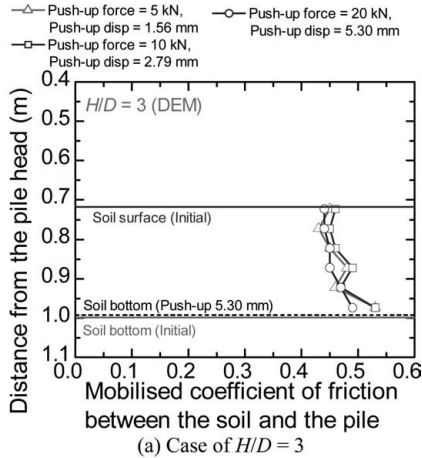


Figure 63. Mobilised coefficient of friction along the inner pile shaft.

to practices, because of a number of reasons, including:

- too many codes or specifications
- codes or specifications are not flexible to accommodate new developments
- excessive persistence of governmental officers and foundation designers on codes or specifications
- current system of approval or authorisation of bearing capacity of new pile type
- foundation and superstructure are designed separately
- lack of education of foundation engineering to students.

There are four main pile design codes in Japan: Japan Road Association code for bridge foundations, Architectural Institute code for building foundations,

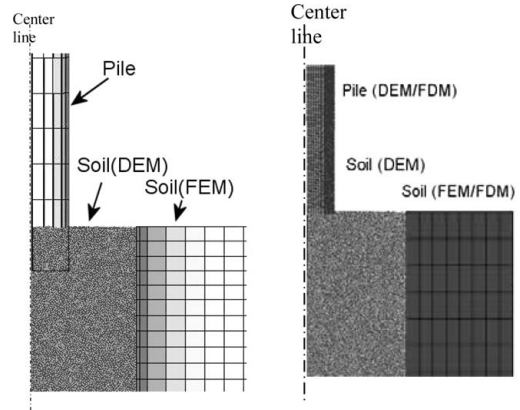


Figure 64. Ongoing analysis of penetration of an open-ended pipe pile into the ground surface.

Japan Railway code and code for Port and Harbour facilities. In addition, there are several local pile design codes. Even if a pile is constructed in a site, bearing capacity of the pile estimated using the above codes are different. This situation often confuses pile designers and pile engineers. In the authors' opinion, the safety factor could be varied according to type of superstructure, but the design codes to estimate the bearing capacity should be unified.

The current pile design codes sometimes refuse the use of new developments in practice. For example, in the Japan Road Association code, it is specified that all external loads on the foundation must be supported by piles alone. Therefore, use of piled rafts for foundations of bridges is not possible at present, although most actual bridge abutments are piled rafts from a view point of their bearing mechanisms.

Safety factor used for piles is typically three in the design codes. If a load test is performed in a construction site, safety factor of 2.7 can be applied to the piles in the site. However, number of load tests is not considered to reduce the value of safety factor more rationally. If the number of load tests in a site is taken into account in pile design properly, rapid pile load testing will play an important role in pile design and guarantee the safety of the constructed foundation.

In the first author's experience, government officers and pile designers tend to persistent excessively to the design codes, even if a load test is carried out. If the bearing capacity of the pile is less than the value from the design codes, most government officers and pile designers have no idea to respond it. Sometimes they doubt of the reliability of the test or tend to neglect the test results. Allowance of the number of load tests in the design may improve such situation. And, education of new design concepts to government officers and pile designers would be needed.

As mentioned earlier, if new pile construction method is approved or authorised, pile load test is not needed for the constructed piles. This system should be improved, because it is widely recognised that bearing capacity of piles in a site is variable largely. Pile load tests on a few piles may be useful to confirm the performance of the constructed piles, even if they have been authorised.

Foundation and superstructure are designed separately in usual. Designer for superstructure designs the superstructure assuming that no settlement of foundation occurs. Much more communication between structural designer and geotechnical designer is of a benefit for rational design. And a design tool for design of whole structure including superstructure and foundation structure will be useful.

In most text books of soil mechanics used in universities in Japan, description and discussion about pile foundation seems to be insufficient. Methods to estimated deformation of pile foundations and pile dynamics are scarcely mentioned. Education of deformation analysis of pile foundations to students would be desired to accommodate new design frameworks where estimation of deformation of the foundation structure is one of important design issues.

7 CONCLUDING REMARKS

Trend of research and practice of pile foundations and new developments of pile technologies in Japan were reviewed. And, discussion was made to utilise new technologies in practice more effectively.

The authors would like to express their appreciation to JASPP, COPITA, Civil Engineering Research Institute for Cold Region, Japan Pile Corporation, System Keisoku Corporation, Marubeni Construction Material Lease Corporation, JibanShikenjo Corporation for their supports in summarising this paper.

REFERENCES

- Bermingham, P. & Janes, M. 1989. An innovative approach to load testing of high capacity piles. *Proc. of the Int. Conf. on Piling and Deep Foundations*, London: 409–413.
- de Nicola, A. & Randolph, M. F. 1997. The plugging behaviour of driven and jacked piles in sand. *Géotechnique*, 47(4): 841–856.
- Gibson, G. & Coyle, H.M. 1968. Soil damping constant related to common soil properties in sands and clays. *Report No. 125-1*, Texas Transport Institute, Texas A & M University.
- Gonin, H.G.C. & Leonard, M.S.M. 1984. Theory and performance of a new dynamic method of pile testing. *Proc. of 2nd Int. Conf. of Application of Stress-Wave Theory to Piles*, Stockholm: 403–410.
- Hayashi, M., Matsumoto, T. & Suzuki, M. 2000. Dynamic load testing on 102 steel pipe piles for bridge foundations on mudstone. *Proc. 6th Int. Conf. on the Application of Stress-Wave Theory to Piles*, São Paulo, Brazil: 697–705.
- Heerema, E.P. 1979. Relationships between wall friction, displacement, velocity and horizontal stress in clay and in sand for pile driveability analysis. *Ground Engineering*, 12(1).
- Heerema, E.P. & de Jong, A. 1980. An advanced wave equation computer program which simulates dynamic pile plugging through a coupled mass-spring system. *Proc. Int. Conf. on Numerical Methods in Offshore Piling*, London, ICE: 37–42.
- Horikoshi, K., Matsumoto, T., Hashizume, Y., Watanabe, T. & Fukuyama, H. 2003a. Performance of piled raft foundations subjected to static vertical loading and horizontal loading. *Int. Journal of Physical Modelling in Geotechnics*, 3(2): 37–50.
- Horikoshi, K., Matsumoto, T., Hashizume, Y. & Watanabe, T. 2003b. Performance of piled raft foundations subjected to dynamic loading. *Int. Journal of Physical Modelling in Geotechnics*, 3(2): 51–62.
- Itasca. 2003. PFC3D Manual, Itasca Corporation.
- Japanese Geotechnical Society. 2002. Standards of Japanese Geotechnical Society for Vertical Load Tests of Piles. Japanese Geotechnical Society, Tokyo.
- Kakurai, M. 1987. Field measurements of load transfer in piled raft foundation. *Proc. of the 8th ARCSMFE*, Kyoto, 1: 327–329.
- Kakurai, M. 2003. Study on vertical load transfer of piles. *Dr. Thesis of Tokyo Institute of Technology*: 304. (in Japanese).
- Kakurai, M., Yamashita, K. & Tomono, M. 1987. Settlement behavior of piled raft foundations on soft ground. *Proc. of the 8th ARCSMFE*, Kyoto, 1: 373–376.
- Katzenbach, R. & Schmitt, A. 2004. Micromechanical modelling of granular materials under triaxial and oedometric loading. *Proc. 2nd Int. PFC Symp. on Numerical Modeling in Micromechanics via Particle Methods*: 313–322.
- Kikuchi, Y., Nishimura, S. & Tatsuta, M. 2000. Statnamic and dynamic load tests for large diameter steel pipe piles supported by thin a bearing layer at Nagoya port in Japan. *Proc. 6th Int. Conf. on the Application of Stress-Wave Theory to Piles*, São Paulo, Brazil: 599–607.
- Kitiyodom, P. & Matsumoto, T. 2002. A simplified analysis method for piled raft and pile group foundations with batter piles. *Int. Journal for Numer. and Anal. Methods in Geomech.*, 26: 1349–1369.
- Kitiyodom, P. & Matsumoto, T. 2003. A simplified analysis method for piled raft foundations in non-homogeneous soils. *Int. Journal for Numer. and Anal. Methods in Geomech.*, 27: 85–109.
- Kitiyodom, P., Matsumoto, T. & Kanefusa, N. 2004a. Influence of reaction piles on the behaviour of test pile in static load testing. *Canadian Geotechnical Jour.*, 41(3): 408–420.
- Kitiyodom, P., Matsumoto, T., Hayashi, M., Kawabata, N., Hashimoto, O., Ohtsuki, M. & Noji, M. 2004b. Experiment on soil plugging of driven open-ended steel pipe piles in sand and its analysis, *Proc. 7th Int. Conf. on the Appl. of Stress-Wave Theory to Piles*, Selangor, Malaysia: 447–458.

- Kitiyodom, P., Matsumoto, T. & Kawaguchi, K. 2005a. A simplified analysis method for piled raft foundations subjected to ground movements induced by tunnelling. *Int. Journal for Numer. and Anal. Methods in Geomech.*, 29: 1485–1507.
- Kitiyodom, P., Matsumoto, T., Horikoshi, K. & Watanabe, T. 2005b. Analyses of vertical and horizontal load tests on piled raft models in dry sand, *Proc. 16th ICSMFE*, Osaka: 2005–2008.
- Kitiyodom, P., Matsumoto, T., Kojima, E., Kumagai, H. & Tomisawa, K. 2006. Analysis of static and dynamic horizontal load tests on steel pipe piles, *Proc. 10th International Conference on Piling and Deep Foundations*, Amsterdam, The Netherlands: 690–699.
- Kitiyodom, P., Matsumoto, T., Tomisawa, K., Kojima, E. & Kumagai, H. 2007. Dynamic and static horizontal load tests on steel pipe piles and their analyses. *Proc. of Int. Workshop on Recent Advance of Deep Foundations (IWDPF 07)*, Yokosuka, Japan (submitted).
- Kojima, E., Tomisawa, K., Matsumoto, T., Kitiyodom, P. & Kumagai, H. 2006. Dynamic horizontal load tests on steel pipe piles having different sizes in the same construction site and their analyses, *Proc. 10th International Conference on Piling and Deep Foundations*, Amsterdam, The Netherlands: 700–708.
- Kusakabe, O. & Matsumoto, T. 1995. Statnamic tests of Shonan test program with review of signal interpretation, *Proc. 1st Int. Statnamic Seminar*, Vancouver, Canada: 13–122.
- Latotzke, J., König, D. & Jessberger, H.L. 1997. Effects of reaction piles in axial pile tests. *Proc. of the 14th Int. Conf. on Soil Mech. and Foundation Eng.*, Hamburg, Germany, 2: 1097–1101.
- Litkouhi, S. & Poskitt, T.J. 1980. Damping constant for pile drivability calculations. *Geotechnique*, 30(1), 77–86.
- Majima, M. & Nagao, T. 2000. Behaviour of piled raft foundation for tall building in Japan. *Design applications of raft foundations* (Hemsley, J.A., Ed.), Thomas Telford: 393–410.
- Matsumoto, T. & Takei, M. 1991. Effects of soil plug on behaviour of driven pipe piles, *Soils and Foundations*, JSSMFE, 31(2): 14–34.
- Matsumoto, T., Tsuzuki, M. & Michi, Y. 1994. Comparative study of static loading test and Statnamic on a steel pipe pile driven in a soft rock. *Proc. 5th Int. conf. and Exhibition on Piling and Deep Foundations*, Bruges, Belgium: 5.3.1–5.3.7.
- Matsumoto, T., Michi, Y. & Hirano, T. 1995. Performance of axially loaded steel pipe piles driven in soft rock, *Jour. of Geotech. Eng.*, ASCE, 121(4): 305–315.
- Matsumoto, T., Michi, Y. & Hayashi, M. 1997. Reliability of dynamic load testing on steel pipe piles in soft rock, *Proc. 14th ICSMFE*, Hamburg, Germany, 2: 1185–1188.
- Matsumoto, T., Kitiyodom, P., Wakisaka, T. & Nishimura, S. 2004a. Research on plugging of open-ended steel pipe piles and practice in Japan, *Proc. 7th Int. Conf. on the Appl. of Stress-Wave Theory to Piles*, Selangor, Malaysia: 133–152.
- Matsumoto, T., Wakisaka, T., Wang, F.W., Takeda, K. & Yabuuchi, N. 2004b. Development of a rapid pile load test method using a falling mass attached with spring and damper, *Proc. 7th Int. Conf. on the Appl. of Stress-Wave Theory to Piles*, Selangor, Malaysia: 351–358.
- Matsumoto, T., Fukumura, K., Kitiyodom, P., Oki, A. & Horikoshi, K. 2004c. Experimental and analytical study on behaviour of model piled rafts in sand subjected to horizontal and moment loading. *Int. Journal of Physical Modelling in Geotechnics*, 4(3):1–19.
- Matsumoto, T., Fukumura, K., Oki, A. & Horikoshi, K. 2004d. Shaking table tests on model piled rafts in sand considering influence of superstructures. *Int. Journal of Physical Modelling in Geotechnics*, 4(3): 20–37.
- Matsumoto, T., Kitiyodom, P., Kojima, E., Kumagai, H., Nishimoto, S. & Tomisawa, K. 2005a. Analysis of pile driving in vertical and horizontal directions using a hybrid model, *Proc. the 2nd Sino-Japan Symposium on Geotechnical Engineering*, Shanghai, China: 503–510.
- Matsumoto, T., Fukumura, K. & Oki, A. 2005d. Influence of superstructure on behaviour of model piled rafts in sand under Seismic Loading, *Proc. 16th ICSMFE*, Osaka: 2017–2021.
- Matsumoto, T. & Kitiyodom, P. 2005e: Case study on soil plugging of open-ended steel pipe piles in Tokyo Bay, *Proc. Int. Symp. on Frontiers in Offshore Geotech.*, Perth, Australia: 791–797.
- Matsumoto, T., Tamura, M., Matsuzawa, K. & Kubo, Y. 2006a. Variation of load settlement relations of 25 steel pipe piles constructed in a site from rapid pile load testing. *Proc. 10th International Conference on Piling and Deep Foundations*, Amsterdam, The Netherlands: 727–736.
- Matsumoto, T., Oki, A., Kitiyodom, P. & Tachibana, T. 2006b. Influence of flexibility of superstructure on the behaviour of piled rafts on dry sand during shaking table test, *Proc. the 2nd Int. Conf. on Physical Modelling in Geotechnics*, Hong Kong: 1021–1027.
- Matsuzawa, K., Shimizu, S., Nakashima, Y., Isobe, Y. & Matsumoto, T. 2006a. Load tests on end bearing steel H piles (Part 1: Test outline). *Proc. of the Annual Meeting of Architectural Institute of Japan 2006*, Yokohama: CD-ROM (in Japanese).
- Matsuzawa, K., Sakihama, H., Nemoto, H. & Matsumoto, T. 2006b. Size and loading rate effects observed in plate load tests on a loam ground. *Proc. 10th Int. Conf. on Piling and Deep Foundations*, Amsterdam, Netherlands: 737–746.
- Middendorp, P., Bermingham, P. & Kuiper, B., 1992. Statnamic loading testing of foundation piles, *Proc. of 3rd Int. Conf. of Application of Stress-Wave Theory to Piles*, The Hague, Netherlands: 581–588.
- Mikami, H., Sakihama, H., Horii, H., Arai, T., Matsumoto, T. & Kitiyodom, P. 2006. Horizontal load tests of model piled rafts with different pile head connection conditions, *Proc. the 2nd Int. Conf. on Physical Modelling in Geotechnics*, Hong Kong: 937–943.
- Momiyama, Y., Honma, M., Katayama, T. & Maruyama, T. 1992. Vertical loading test on large-diameter steel-pipe piles for Trans-Tokyo Bay Highway, *TSUCHI-TO-KISO JSSMFE* 40(2): 47–52 (in Japanese).
- Nakashima, Y., Shimizu, S., Isobe, Y., Matsuzawa, K. & Matsumoto, T. 2006. Load tests on end bearing steel H piles (Part 1: Test outline). *Proc. of the Annual Meeting of Architectural Institute of Japan 2006*, Yokohama: CD-ROM (in Japanese).
- Nemoto, H., Yaegashi, K., Takeuchi, Y., Nishimura, N., Matsumoto, T. & Kitiyodom, P. 2006. Vertical load tests

- of model piled rafts with different pile head connection conditions, *Proc. the 2nd Int. Conf. on Physical Modelling in Geotechnics*, Hong Kong: 853–859.
- Novak, M., Nogami, T. & Aboul-Ella, F. 1978. Dynamic soil reactions for plane strain case. *Jour. of Mechanical Eng. Div.*, ASCE, 104(EM4): 953–959.
- Ochiai, H., Kusakabe, O., Sumi, K., Matsumoto, T. & Nishimura, S. 1997. Dynamic and Statnamic load tests on offshore steel pipe piles with regard to failure mechanisms of pile-soil interfaces at external and internal shafts. *Proc. of Int. Conf. on Foundation Failures*, Singapore: 327–338.
- Ovesen, N.K. 1979. Discussion 9.3 on ‘The use of physical models in design,’ *Proc. 7th European Conf. on SMFE*, Brighton, 4: 319–323.
- Paikowsky, S.G., Whitman, V.R. & Baligh, M.M. 1989. A new look at the phenomenon of offshore pile plugging. *Marine Technology* 8: 213–230.
- Poulos, H.G. 1998. Pile testing -From the designer’s viewpoint. *Proc. of 2nd Int. Statnamic Seminar*, Tokyo: 3–21.
- Randolph, M.F. & Deeks, A.J. 1992. Dynamic and static soil models for axial pile response. *Proc. of 4th Int. Conf. on Application of Stress-Wave Theory to Piles*, The Hague: 3–14.
- Rausche, F., Moses, F. & Goble, G.G. 1972. Soil resistance predictions from pile dynamics. *Jour. of the Soil Mech. and Found. Div.*, ASCE, 98(SM9).
- Schellingerhout, A.J.G. & Revoort, E. 1996. Pseudo static pile load tester. *Proc. of 5th Int. Conf. on Application of Stress-Wave Theeory to Piles*, Orlando: 1031–1037.
- Shibata, T., Sekiguchi, H., Matsumoto, T., Kita, K. & Motoyama, S. 1989. Pile drivability assessment by waveform analysis, *Proc. 12th ICSMFE*, Rio de Janeiro, 3: 1105–1108.
- Shintani, T., Matsumoto, T., Kitiyodom, P., Kawano, H. & Haneda, K. 2006. Parametric study on push-up loading of sand plug in open-ended pipe pile using DEM, *Proc. International Symposium on Geomechanics and Geotechnics of Particulate Media (IS Yamaguchi 06)*: 253–259.
- Shintani, T. 2007. Push-up load tests of sand plug and their DEM analyses. Master Thesis of Kanazawa University.
- Smith, I.M., To, P. & Willson, S.M. 1986. Plugging of pipe piles. *Proc. 3rd Int. Conf. Numerical Methods in Offshore Piling*, Nantes: 53–73.
- Tanaka, T., Segawa, T., Katoh, Y., Kakurai, M. & Tomono, M. 1987. A design of foundation and the behaviour of a tall building at Kobe Port Island. *Proc. of the Int. Symp. on Geotechnical Engineering of Soft Soils*: 389–396.
- The Japan Road Association. 2002. *Specifications for highway bridges, Part IV: Substructures*. The Japan Road Association, Tokyo (in Japanese).
- TNO. 1977. *Dynamic pile testing*. Report No. BI-77-13.
- Wakisaka, T., Matsumoto, T., Kojima, E. & Kuwayama, S. 2004. Development of a new computer program for dynamic and static pile load tests, *Proc. 7th Int. Conf. on the Appl. of Stress-Wave Theory to Piles*, Selangor, Malaysia: 341–350.
- Yamahara, H. 1964a. Plugging effects and bearing mechanism of steel pipe piles. *Trans. of the Architectural Inst. of Japan*, 96: 28–35.
- Yamahara, H. 1964b. Plugging effects and bearing mechanism of steel pipe piles (Part 2). *Trans. of the Architectural Inst. of Japan*, 97: 34–41.
- Yaegashi, K., Kitiyodom, P., Fujita, M., Arai, T., Hasei, H. & Matsumoto, T. 2006. Analyses of vertical and horizontal load tests of model piled rafts in sand using a hybrid model, *Proc. the 2nd Int. Conf. on Physical Modelling in Geotechnics*, Hong Kong: 1579–1585.
- Yamada, T., Yamashita, K., Kakurai, M. & Tsukatani, H. 2001. Long-term behaviour of tall building on raft foundation constructed by top-down method. *Proc. of the 5th Int. Conf. on Deep Foundation Practice*, Singapore: 411–417.
- Yamashita, K. & Kakurai, M. 1991. Settlement behavior of raft foundation with friction piles. *Proc. of the 8th Int. Deep Foundation Institute Conference*, Stresa: 461–466.
- Yamashita, K., Kakurai, M. & Yamada, T. 1994. Investigation of a piled raft foundation on stiff clay. *Proc. of ICSMFE*, New Delhi, 3: 543–546.
- Yamashita, K., Yamada, T. & Kakurai, M. 1998. Simplified method for analyzing piled raft foundations. *Proc. of Deep Foundations on Bored and Auger Piles*, Ghent: 457–464.

Technical papers

Axial and lateral bearing capacity of piles

Vertical bearing capacity of large diameter steel pipe piles

Y. Kikuchi

Foundations Division, Port & Airport Research Institute, Yokosuka, Japan

M. Mizutani

Tokyo Port Office, Ministry of Land, Infrastructure and transport, Tokyo, Japan

H. Yamashita

Japanese Association for Steel Pipe Piles, Tokyo, Japan

ABSTRACT: The Tokyo Port Seaside Road has been designed so that the Tokyo Coastal Highway Bridge will cross over Channel No. 3 of the port. At the site, various load tests, including static axial compressive load tests, were carried out using large diameter steel pipe piles. The results show that the toe resistance could be divided into the inner friction and the resistance of a pile body. It is also shown that the maximum resistance of a pile body can be reached with a relatively small settlement, whereas a large settlement is required for exhibiting the inner resistance. However, as there were some uncertain factors when applying this idea to the actual design, the apparent plugging ratio should be taken into account when considering the end bearing capacity of a pile. In this case, the apparent plugging ratio was larger than the value obtained in an existing test results. The frictional resistance can be estimated from an SPT-N value, as indicated in the Specifications for Highway Bridges.

1 INTRODUCTION

The Tokyo Port Seaside Road has been designed so that the Tokyo Coastal Highway Bridge will cross over Channel No. 3 of the port. The subject of this study is a steel-pipe-sheet pile foundation that features large-diameter steel pipe piles serving as the pier foundation between the principal meridians of the Tokyo Coastal Highway Bridge. As its bearing capacity has not been fully proved, load tests (including a static axial compressive load test, a rapid load test, and a dynamic load test) were conducted to obtain information about the bearing mechanism of the foundation piles at the site where bridge construction has been planned, and the test results were used for designing the bridge. This report discusses the characteristics of vertical bearing capacity obtained from in-situ tests on actual size large diameter open-ended steel pipe piles which were constructed in the same way as in the actual construction.

2 OVERVIEW OF THE STATIC AXIAL COMPRESSIVE LOAD TEST

Figure 1 shows the conditions of the ground where the tests were conducted, and the embedded depth of test piles. It is found from the figure that the water

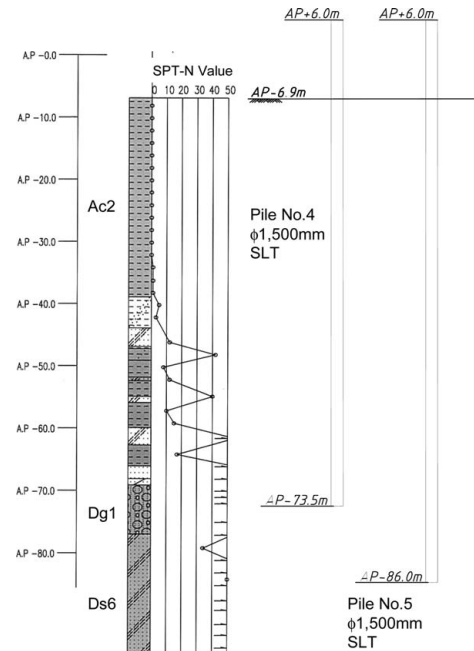


Figure 1. Overview of the soil boring log and the embedment of the test piles.



Photo 1. View of the static axial compressive load test.

depth at this site is about AP-7 m. A soft, cohesive alluvium layer continues down to AP-40 m, followed by a laminated ground (alternating sandy and cohesive layers) down to AP-65 m, and then a dilluvial sandy gravel layer (the Tokyo gravel layer) appears around AP-69 m. Following a few weak layers in the sandy gravel layer around AP-80 m, a solid sandy layer appears around AP-82 m.

The results of static axial compressive load tests are presented here. In the tests, steel pipe piles of 1,500 mm in diameter were hammer-driven into a sandy gravel layer and a sandy layer, in order to obtain the characteristics of bearing capacity of these piles under two conditions (i.e. inserted to sandy gravel layer and sandy layer). Photo 1 shows a view of the static axial compressive load test.

In these load tests, the axial force that acted on a pile was measured by attaching strain gauges to the pile; at the same time, the settlement of the pile (both at the pile toe and the pile head) was measured using settlement gauges. Multi-stage repeated loading was conducted in accordance with the static axial compressive load test method proposed by the Japanese Geotechnical Society (2002). Particular care was taken when a virgin load was applied; that is, the load was maintained for 30 minutes or longer to wait for the settlement of the pile, before moving to the next loading stage.

3 VERTICAL BEARING CAPACITY

3.1 Results of load tests

Figure 2 shows the axial force distribution when a virgin load was applied to Pile No. 4. What should be noted here is the axial force distribution around the lower end of the test pile. As the lower end was being embedded into the sandy gravel layer, the subgrade resistance increased, with a large change in the axial force in the depth direction. At the point where the pile head load exceeded 22,000 kN, the axial force

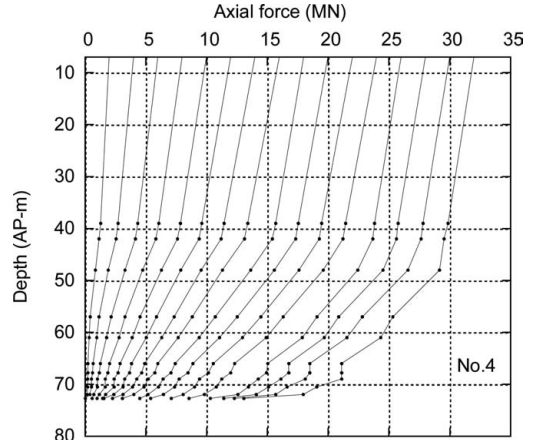


Figure 2. Axial force distribution in the load test on Pile No.4.

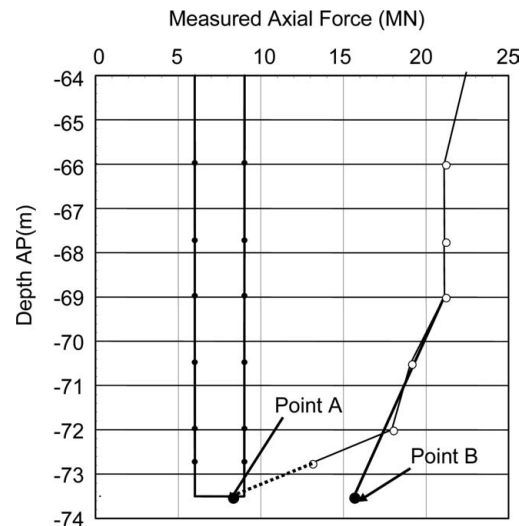


Figure 3. Axial force distribution at the pile base (Pile No. 4).

distribution showed a large bent around the pile toe. This suggests that transferred axial pile force was rapidly decreased toward the pile toe.

Figure 3 shows an enlarged view of the situation around the pile toe. Here, assuming the load at Point B in Figure 3 to be the toe resistance, load settlement curves for both the head and lower end of the pile can be obtained as shown in Figure 4.

The loading test results of Pile No.5 are shown in from Figure 5 to Figure 7. Although embedded length was different from Pile No.4, the pile was inserted to stiff sandy layer. The feature of the axial force distribution was similar to the results of the load test on Pile No.4; such that transferred axial pile force was rapidly

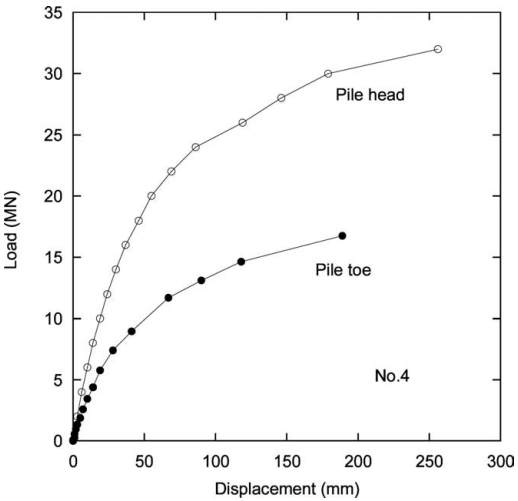


Figure 4. The relation between load and displacement (Pile No.4).

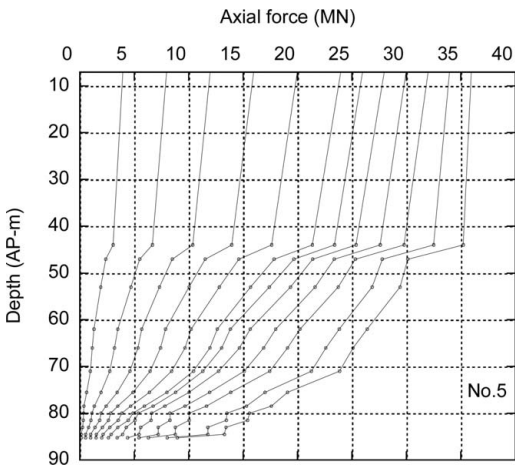


Figure 5. Axial force distribution in the load test on Pile No.5.

decreased toward the pile toe when the applied load to the pile head is close to the bearing capacity.

3.2 Critical resistance

Based on the relation between the vertical axial compressive load and the displacement of a pile shown in Figure 4 and Figure 7, the primary critical resistance and the secondary critical resistance (when the displacement of the toe is 10% of pile diameter) were obtained as shown in Table 1.

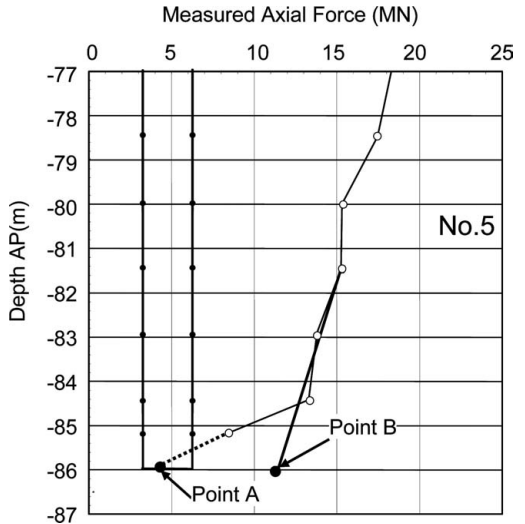


Figure 6. Axial force distribution at the pile base (Pile No.5).

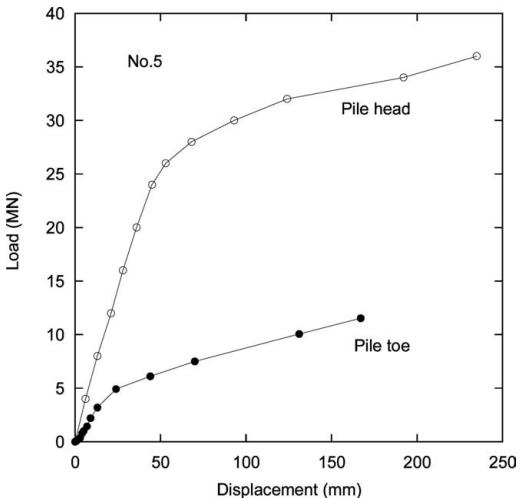


Figure 7. The relation between load and displacement (Pile No.5).

3.3 End bearing capacity of a pile

The axial forces distribution around a pile end under the secondary critical resistance are shown in Figure 4 and Figure 5.

Axial force suddenly became smaller than at the upper part at the point where a strain gauge was set near the lower pile end. The point showing a sharp change in the axial force was 1D (D: pile diameter) above the lower pile end. Around the lower pile end, the solidity of

Table 1. Critical resistance (MN).

	Pile No.4	Pile No.5
Primary critical resistance	20	26
Secondary critical resistance	32	36

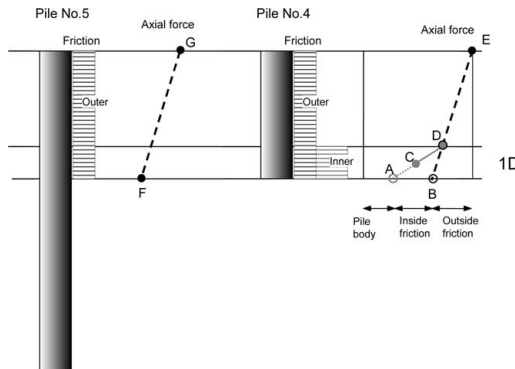


Figure 8. Relation between axial force distribution and friction.

ground did not change. Judging from the test results from Pile No. 5 which was more deeply embedded, it was unlikely that the peripheral friction became large only at this point (see Figure 5). Moreover, the results of a cone penetration test (CPT) showed that the penetration resistance of the inner soil of a pile base clearly became larger than the outer ground after the loading test (Nishimura et al. 2005). Thus, it can be concluded that a sharp change in the axial force might have been caused by skin friction of the inner side of a pile. As shown in Figure 8, the total bearing capacity at the pile toe could be obtained by extrapolating the measured values of axial force within the assumed bearing layer to the level of the lower pile end (Point B).

Assuming that the load at Point A obtained by extrapolating the measured value that curved at the pile end should be the resistance of the pile body, the difference between the load at Point B and the load at Point A could be regarded as the plug resistance due to inner friction. Figure 9 and Figure 10 show the relation between the total base resistance, the resistance of inner friction, and the resistance of a pile body. In both figures, at the secondary critical resistance, the total base resistance shows an increase. The resistance of a pile body reached nearly the maximum level when the settlement of a pile end was about 50 mm, about 3% of settlement, while the resistance of inner friction was still increasing.

Yamagata and Nagai (1973), Nicola, and Randolph (1997) proposed an equation to obtain the ultimate resistance of a unit sectional area, based on their assumption that the base resistance of the open-ended

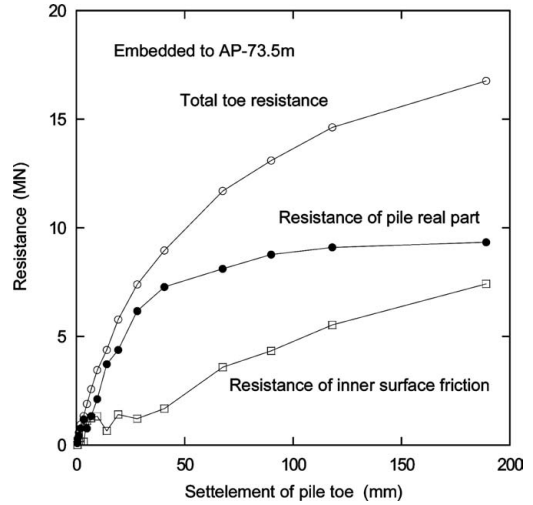


Figure 9. Resistance of a pile base (Pile No. 4).

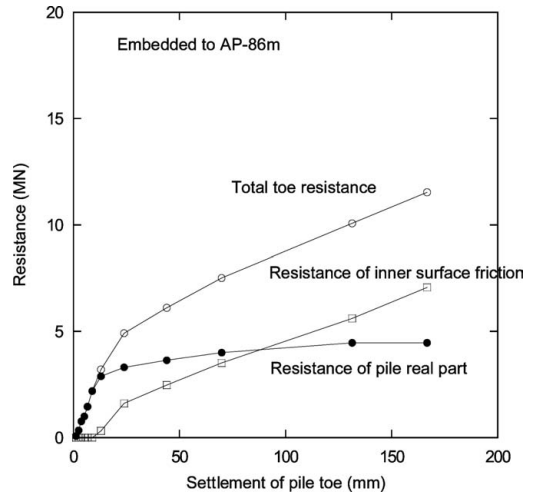


Figure 10. Resistance of a pile base (Pile No. 5).

pile can be expressed as the sum of resistance at the sectional area of the lower end of a pile A_t , and inner friction. Yamagata and Nagai (1973) proposed the following equation to estimate this resistance from an SPT-N value: $q_t = 0.4 N A_t (\text{MN/m}^2)$.

From the loading test results of a full-scale open ended pile, Nicola and Randolph (1997) proposed a correlation between the resistance of the real portion of a pile of an open ended pile q_t and CPT resistance q_c :

$$q_t = \left(\frac{\lambda m(w_t/D)}{(w_t/D) + c} \right) q_c A_t$$

where, $m = 0.7$, $c = 0.015$, w_t/D : normalized settlement of the pile toe

$$\begin{aligned}\lambda &= 1.75 - (\sigma'_v/200) \quad (\sigma'_v \leq 200 \text{ kPa}) \\ &= 0.75 \quad (\sigma'_v \geq 200 \text{ kPa})\end{aligned}$$

When converting the equation proposed by Nicola and Randolph under the test pile embedment condition and the secondary critical load condition, the resistance of a unit sectional area q_b can be obtained from the cone penetration resistance q_c as follows: $q_b = 0.46 q_c (\text{kN/m}^2)$. Thus, the ultimate resistance R_t of the sectional area of a pile can be obtained using the proposed equations, based on the SPT-N value measured at a pile base and the CPT results, as shown in Table 2.

The loads at Point A on Pile No. 4 and No.5 in Figure 3 and Figure 6 under the secondary critical load condition were 8.2 MN and 4.6 MN respectively as shown in Figures 9 and 10. Both loads were close to R_t values shown in Table 2.

It might appear to be somewhat less accurate to assume that the end bearing capacity of a pile at Point C is the sum of the resistance of the sectional area of a pile end and the inner friction, and that the load at Point B is the resistance of the sectional area of a pile end, as shown in Figure 8. However, the results coincide relatively well with the existing proposals, so the above assumption can be considered to be fairly correct. Table 3 shows the results obtained from load tests. The resistance of inner friction was estimated to be 7.5 MN on Pile No. 4 (accounting for 48% of the end bearing capacity of the pile), 6.7 MN on Pile No. 5 to be (accounting for 59% of its bearing capacity). The resistance of inner friction showed similar values whether the bearing layer was the sandy gravel layer or the sandy layer. Thus, it can be said that the difference in the pile base resistance under the secondary critical load in a sandy gravel layer and a sandy layer largely depends on the difference in the pile body resistance.

As shown in Table 2, the pile body resistance depends on the penetration resistance (a CPT q_c value or a converted SPT-N value) of a relatively limited area around a pile base. However, the inner friction in a sandy gravel layer and a sand layer can apparently be determined independently regardless of the penetration resistance.

3.4 Apparent plugging ratio

The bearing mechanism of an open-ended pile is considered to be as mentioned in the above section 3.3. Here, the results of load tests are compared with those obtained from the conventional method used in design. Table 3 shows the apparent plugging ratios obtained from the bearing capacity at a pile toe (the value

Table 2. Resistance of the sectional area of a pile end R_t (MN).

Proposed by	Yamagata and Nagai(1973)		Nicola and Randolph (1997)	
	R_t proposed equation	$0.4NA_t$	$0.46q_cA_t$	
Pile No.	4	5	4	5
Strength of the ground measured at a pile toe	Converted SPT-N Value (125)	Converted SPT-N Value (68)	CPT: q_c Value (97 MPa)	CPT: q_c Value (50 MPa)
Resistance R_t	(8.6)	4.7	7.7	4.0
Load at Point B	8.2	4.6	8.2	4.6

Table 3. Bearing capacity at a pile toe (based on the results of a static axial compression load test).

	Pile No.4	Pile No.5
Pile Diameter (mm)	$\varphi 1,500$	$\varphi 1,500$
Type of Bearing Layer	Gravel	Sand
Embedded depth into a bearing Layer	$3D(4.5 \text{ m})$	$3D(4.5 \text{ m})$
Axial force at the position of a gauge at the lower end of a pile (MN)	13.0	9.0
Bearing capacity at a pile base (MN)	15.7	11.3
Apparent plugging ratio (%)*	74	53

*Apparent plugging ratio $\alpha = \text{Bearing capacity at a pile base}/(0.3NA_p)$, where $N = 40$ and A_p = Sectional area of a pile

obtained by dividing the bearing capacity at a pile base by $0.3NA_p[N: \text{SPT}-N(\leq 40)]$, where $N = 40$ and A_p = the sectional area of a pile]. The value of apparent plugging ratio of Pile No. 5 is larger than the one obtained from the existing load tests (Momiyama et al. 1992) using a sand layer as a bearing layer (27% [pile diameter: 1,600 mm], 40% [pile diameter: 2,000 mm]).

3.5 Frictional resistance

In order to obtain the frictional resistance of each layer, the ground was divided into a sandy layer, a clayey layer, and a sandy gravel layer. Each value was linked with SPT-N values, and averaged by Piles No. 4 and No. 5, as shown in Table 4. The frictional resistance of the clayey and sandy layers were relatively close to the value indicated in the Specifications for Highway Bridges (JRA 2002). Therefore, for the sandy gravel layer, it was proposed to make the value larger than the one in the Highway Bridge Specifications (JRA 2002),

Table 4. Frictional resistance (obtained from the static axial compressive load test) (kN/m^2).

Type of layer	Value obtained from the test	Equation in the highway bridge specifications	Proposed value
Sandy	$3.1N$	$2N$	$2N$
Clayey	$9.2N$	$10N$	$10N$
Sandy gravelly	$4.0N$	$2N$	$3N$

taking into account of the frictional resistance obtained from the static load test.

3.6 Estimation of the ultimate resistance

It was proved that the mechanism of end bearing capacity of a pile can be explained by the sum of the inner frictional resistance and the resistance of the pile body. However, there are some uncertain factors when estimating the inner resistance. Therefore, in the design, the pile toe resistance should be evaluated as the comprehensive resistance including the apparent plugging ratio as shown in Eq. (1). In other words, the ultimate resistance of a pile (the secondary critical resistance) is assumed to be the combination of the end bearing capacity (see Table 3) and the proposed frictional resistance value (see Table 4), as shown in Eq. (1).

$$R_u = \alpha \cdot 300NA_p + U\Sigma L_i f_i \quad (1)$$

where, R_u : Ultimate bearing capacity of a pile (kN), α : Apparent plugging ratio, N: Design N value of the ground at a pile base (≤ 40), A_p : Projected sectional area of a pile end (m^2), U : Peripheral length of the pile (m), L_i : Thickness of the layer exhibiting frictional resistance (m), f_i : Proposed value of frictional resistance (kN/m^2).

Figure 11 compares the axial force distribution obtained from Eq. (1) with the measured axial force distribution. It is clear from the figure that the calculated values do not exceed the measured values, thereby indicating that the design axial force at the pile head is the safer side.

4 CONCLUSIONS

At the site where the construction of the Tokyo Port Seaside Road has been planned, various load tests, including static axial compressive load tests, were carried out using large diameter steel pipe piles. As a result, valuable data on vertical bearing capacity were obtained. The results show that the toe resistance could be divided into the inner friction and the resistance of a

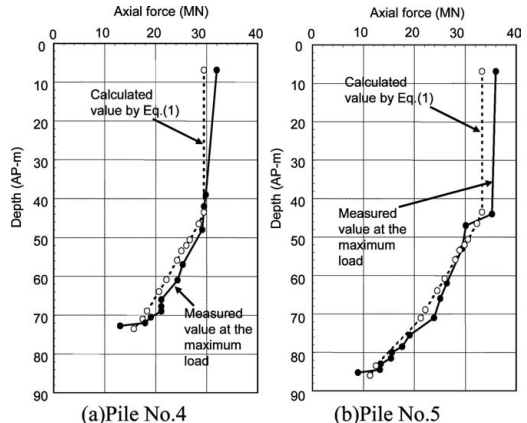


Figure 11. Comparison of axial force distribution.

pile body. It is also shown that the maximum resistance of a pile body can be reached with a relatively small settlement, whereas a large settlement is required for exhibiting the inner resistance. However, as there were some uncertain factors when applying this idea to the actual design, the apparent plugging ratio should be taken into account when considering the end bearing capacity of a pile. In this case, the apparent plugging ratio was larger than the value obtained in an existing test results (Momiyama et al. 1992). The frictional resistance can be estimated from an SPT-N value, as indicated in the Specifications for Highway Bridges (JRA 2002). The bearing capacity of large diameter steel pipe piles has not yet been sufficiently studied, so it should be further studied.

REFERENCES

- Japan Road Association. 2002. *Specifications and Comments for Highway Bridges Vol. IV Substructures*. (in Japanese)
- Japanese Geotechnical Society. 2002. Standard for Method for Static Axial Compressive Load Test of Single Piles. JGS1811-2002.
- Momiyama, Y., Honma, M., Katayama, T., and Maruyama, T. 1992. Vertical loading tests on large-diameter steel-pipe piles for the Trans-Tokyo Bay Highway. *Tsuchi-to-Kiso* 40(2): 47 to 52. (in Japanese).
- Nicola, A. and Randolph, M.F. 1997. Plugging behaviour of driven and jacked piles in sand. *Geotechnique* 47(4): 84–856.
- Nishimura, N., Kusakabe, O., Kikuchi, Y., Fukui, J., Sasaki, H., Geshi, H. 2005. Cone penetration tests for inside soil of driven open-ended steel pipe piles in Tokyo port seaside road project, *Proc. of 40th JNCGE*. (in Japanese).
- Yamagata, K. and Nagai, K. 1973. Consideration of an open ended steel pipe pile (No.2). *Journal of Architecture and building engineering*. No.213. (in Japanese).

Back analysis of Tokyo port bay bridge pipe pile load tests using piezocone data

J.A. Schneider & D.J. White

The University of Western Australia, Perth, Australia

Y. Kikuchi

Foundations Division, Port & Airport Research Institute, Yokosuka, Japan

ABSTRACT: This paper reports and back-analyses the results of two static load tests on 1.5 m diameter instrumented pipe piles, conducted to aid the design of the Tokyo port bay bridge. The site investigation included high quality piezocone testing (CPTU), which is used to back-analyze the pile response in light of recently-developed design methods for axial pile capacity. Local shaft friction (τ_f) in sands, silts, and lightly overconsolidated clays, as well as unit base resistance (q_b) of pipe piles in Tokyo gravel and Edogawa sand are evaluated using CPT q_t . A simple expression for shaft resistance, which is an extension of the UWA approach for piles in sand, is shown to provide good predictions for the shaft resistance through the mixed sand, silt and clay layers at this site. The base resistance at a tip settlement of $D/10$ is a combination of resistance on the pile annulus and the enclosed soil plug. The unit annulus resistance is fully mobilized and comparable to CPT q_t at the pile tip. The plug resistance is only $\sim 0.2q_{t,\text{avg}}$ at the end of the load test, but steadily increasing, which highlights the conservatism in limiting pipe pile base capacity by a settlement criterion if the structure can tolerate additional movement.

1 INTRODUCTION

The complex deformation processes during the installation and loading of a driven pile, prevent accurate theoretical modeling of axial pile capacity. Instead, design methods must be calibrated using databases of load tests. Offshore and nearshore driven piles are typically 0.76 m to >2 m in diameter, whilst databases of load tests used for design method calibration typically have a mean diameter less than 0.5 m. A recently-compiled database of 77 pile load tests with adjacent CPT profiles at sandy sites contained only four load tests on piles with a diameter greater than 1 m (Schneider et al. 2007a). Since the application of a calibrated design method to a nearshore or offshore pile involves significant extrapolation from existing databases, it is essential that the equations in the design method correctly capture the mechanisms that influence pile capacity; in particular the effects of pile diameter and end-condition.

Cone penetration tests (CPTs) are routinely undertaken during an offshore site investigation and are increasingly common for nearshore and onshore surveys. Various CPT-based design methods for axial capacity have been developed and the 2006 revision of

the American Petroleum Institute (API) recommended practice for fixed offshore structures (RP 2A) will include four alternative methods for assessing the axial capacity of piles in siliceous sand (API 2006).

The piezocone penetration test (CPTU) provides three measurements of soil behaviour which are nearly continuous with depth: (i) cone tip resistance, q_c , (ii) sleeve friction, f_s , and (iii) penetration-induced pore pressure measured behind the cone tip, u_2 . These measurements are controlled by aspects of soil strength, stiffness, and the coefficient of consolidation of the soil deposit. Not only is the CPTU useful for detailed profiling in soft soils, but newer technologies allow near continuous penetration in very dense sands and gravels with tip resistance in excess of 100 MPa. Testing in hard soils often requires alternating drilling with wireline cone penetration testing (Fugro 2001), but these techniques are relatively routine in practice, particularly for offshore and nearshore site investigations.

In addition to profiling of soil type and engineering parameters, a CPT can be considered as a model pile, so the CPT parameters provide a sound basis for predicting axial capacity. The static axial bearing capacity, Q_t , of a deep foundation is given as the sum of the shaft capacity, Q_s , and the base capacity, Q_b .

Pile weight is subtracted for piles in compression and Q_b is taken as zero in tension.

$$Q_t = Q_s + Q_b = P \int_{h=0}^{h=L_{emb}} \tau_f dh + q_b A_b \quad (1)$$

where:

- P = pile perimeter, πD ,
- A_b = gross pile base area
- L_{emb} = total embedded length of pile
- z_{tip} = tip depth of the pile
- h = height above the pile tip

Since the unit shaft and base resistance, τ_f and q_b , are influenced by soil strength and compressibility, pile geometry, installation method, direction of loading, and time between installation and load testing, many correlations have evolved relating these parameters to CPT tip resistance, q_c . The predictive performance of recent CPT-based design methods indicates that simple equations based on penetrometer parameters can better capture the variation of τ_f and q_b with soil conditions and pile geometry than traditional earth pressure methods (based on the in situ stress multiplied by an earth pressure coefficient for shaft resistance or a bearing capacity factor for base resistance).

This paper describes the back-analysis of two recent load tests on 1.5 m diameter pipe piles conducted in Tokyo Bay (Kikuchi et al. 2005) using adjacent CPTU data. As there is a dearth of static load test data on large

diameter piles, these case histories offer valuable evidence of the behaviour of pipe piles. A discussion of the site characterization using the CPTU results is presented, followed by back-analysis of static load tests.

2 SITE CHARACTERISATION BY CPTU

The geotechnical investigation undertaken during the design of the new Tokyo port bay bridge aimed to assess the available axial pile capacity, and provide information to allow back-analysis of the subsequent load tests (Kikuchi et al. 2005). The investigation consisted of standard penetration tests (SPT), piezo-cone penetration tests (CPTU), as well as sampling and laboratory triaxial testing.

Historically, it has been observed that an acceptable design assumption for the unit base capacity (q_b in MPa) for pipe piles in Tokyo Bay is approximately 10% of the SPT N-value. However, pile performance at neighbouring sites has implied that lower bearing capacities can be encountered for piles founded in the Tokyo Gravel layer. As CPT q_c has been shown to correlate well with pile base resistance (e.g. Delft 1936, White & Bolton 2005, Xu. et al. 2005), and the CPT is analogous to a model pile, it is anticipated that q_c provides a more reliable indicator of base resistance than SPT N-value.

The measured profiles of each CPTU parameter are shown in Figure 1, as well as the hydrostatic water

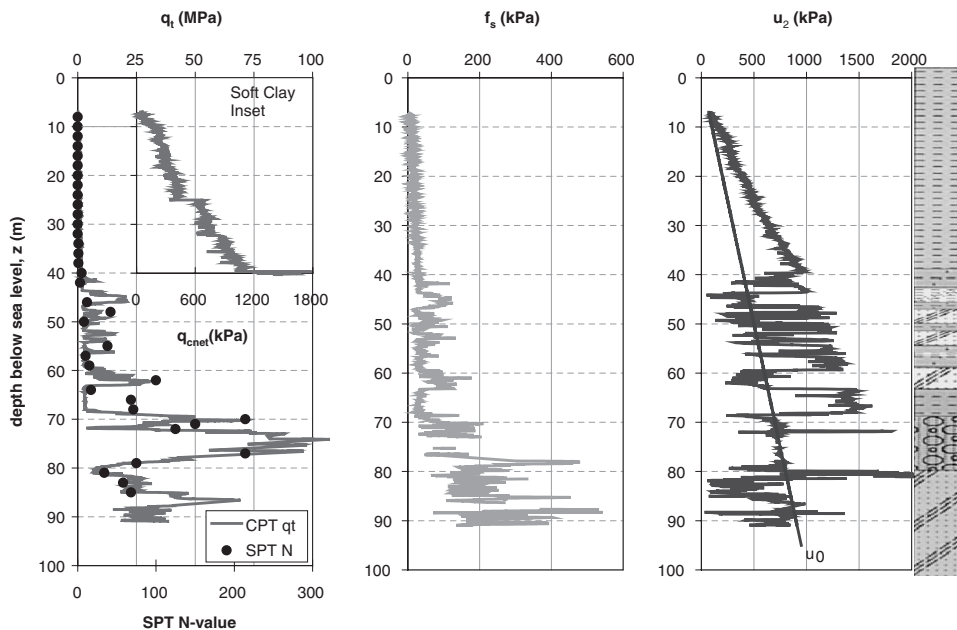


Figure 1. In situ test data at Tokyo Bay load test site.

pressure, u_0 , starting from sealevel, $z = 0$ (to match the zeroing of the CPTU pore pressure device). In this figure, the cone penetration tip resistance, q_c , has been corrected for pore pressure effects to total cone tip resistance, q_t , following the standard procedure given by Lunne et al. (1997). The SPT-N values are equivalent values defined as $50 \times (30/s_{N50})$, where s_{N50} is settlement measured at SPT-N value is 50. The ratio of q_t/p_{ref} (where p_{ref} is a reference stress of 0.1 MPa) to SPT N-value is approximately 2 to 4, but the main distinction between the two in situ test parameters is the more detailed profile of vertical variability revealed by the cone penetration test. The local variation in q_t is of paramount importance when calculating the axial capacity of piles.

When evaluating soil layering and soil behaviour type from in situ test data, it is rational to use normalized (dimensionless) parameters (Wroth 1984). Four common normalized CPT parameters are:

$$Q = \frac{q_t - \sigma'_{v0}}{\sigma'_{v0}} = \frac{q_{cnet}}{\sigma'_{v0}} \quad (2)$$

$$F_r = \frac{f_s}{q_t - \sigma'_{v0}} = \frac{f_s}{q_{cnet}} \quad (3)$$

$$B_q = \frac{u_2 - u_0}{q_t - \sigma'_{v0}} = \frac{\Delta u_2}{q_{cnet}} \quad (4a)$$

$$\frac{\Delta u_2}{\sigma'_{v0}} = \frac{u_2 - u_0}{\sigma'_{v0}} \quad (4b)$$

The parameters in these expressions are named as follows: q_{cnet} is the net tip resistance, Δu_2 is the excess penetration pore pressure, Q is the normalized cone tip resistance (and is equivalent to the bearing capacity factor, N_q in drained conditions), F_r is the friction ratio, and B_q is the pore pressure parameter. When evaluating soil behaviour type (SBT) in layered deposits using the piezocone, it is often clearer to use recent correlations based on the normalized excess pore pressure, $\Delta u_2/\sigma'_{v0}$ (Schneider et al. 2007b) instead of the traditional correlations based on B_q (e.g. Robertson 1990). Profiles of the normalized piezocone parameters are shown in Figure 2. The soil layer boundaries become more distinct when the normalized parameters are used compared to the measured parameters (Figure 1). The properties of the individual layers are given in Table 1.

The CPTU data for the soil layers shown in Table 1 are plotted on a $Q-\Delta u_2/\sigma'_{v0}$ SBT chart in Figure 3. Piezocone SBT charts are useful for evaluating differences in soil behaviour for each 'layer', particularly for assessing whether cone penetration is drained or undrained. Penetration in clays is usually undrained, while penetration in sands is usually drained. In silty soils, penetration often occurs under conditions of partial consolidation, which complicates interpretation.

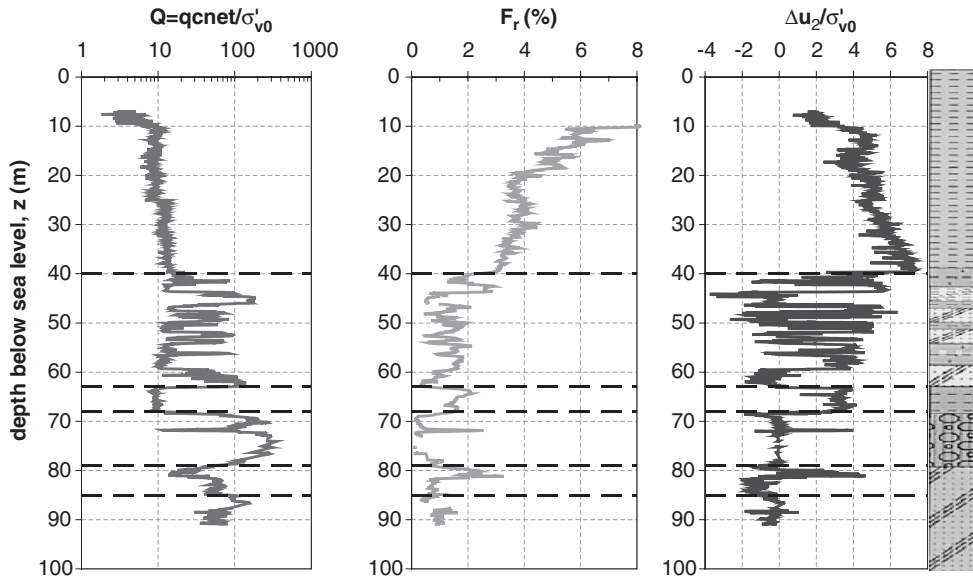


Figure 2. Profiles of normalized piezocone parameters at Tokyo Bay load test site.

Table 1. Soil layers evaluated from Figure 2 supplemented with soil properties based on lab testing of the sands and silts.

Layer	Depth (m)	ρ_d (g/cm ³)	d_{50} (mm)	ϕ'	Q_{avg}^1 [stdev]
Yurakucho CLAY	7–40	—	—	—	10.5 [2.7]
Interlayered SAND and CLAY	40–63	—	—	—	54.5 [47.5]
Yurakucho CLAY	63–68	—	—	—	9.3 [0.46]
Tokyo GRAVEL	68–79	2.01	2.94	41 (CD)	192.5 [77.5]
Edogawa SILT	79–85	1.28	0.075	38 (CU)	46.3 [16.0]
Edogawa SAND	85–90	1.55	0.168	34 (CU)	83.1 [31.3]

¹ $s_u/\sigma'_{v0} = Q/N_{kt}$; N_{kt} typically 12 to 15 in lightly OC clays

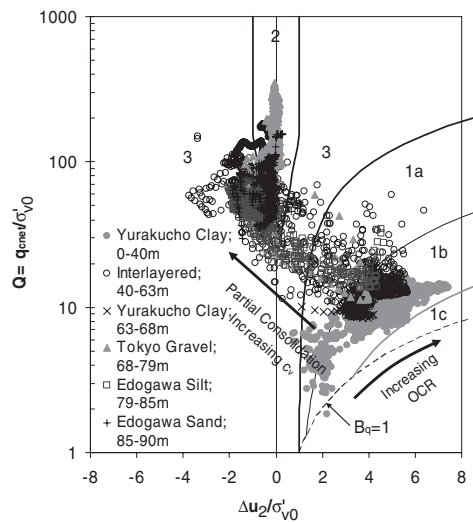


Figure 3. Soil behaviour type from CPTU using generalized charts of Schneider et al. (2007b).

The Yurakucho clay exists as two layers, which both predominantly plot in Zone 1b of this SBT chart. High penetration pore pressure and low cone tip resistance characterize these clayey soils. Tokyo gravel and Edogawa sand have relatively high Q values, and near hydrostatic penetration pore pressures. These soils predominantly plot in Zone 2 of this SBT chart,

indicating essentially drained penetration. The inter-layered sands, silts, and clays, between 40 and 63 m, as well as the Edogawa silt, tend to plot between Zone 1b and to the left of Zone 2, or in Zone 3: ‘Transitional soils.’ Soils within this area of this SBT chart are often partially drained during cone penetration tests (Schneider et al 2007b). Both Q and $\Delta u_2/\sigma'_{v0}$ are necessary for the assessment of SBT and are useful when predicting pile behaviour.

3 LOAD TEST SETUP AND RESULTS

Two piles were statically load tested to aid the design of foundations for the new Tokyo port bay bridge. In addition, statnamic load tests and dynamic load tests were performed, which are outside the scope of this paper but are discussed by Kikuchi et al (2005). A summary of the test pile dimensions and load conditions is presented in Table 2, and a photograph of the static load test setup is shown in Figure 4. The parameters in Table 2 are pile diameter, D , wall thickness, t , tip depth below sea level, z_{tip} , embedded length, L_{emb} , time period between installation and load testing, plug length ratio (PLR) at end of driving, associated effective area ratio ($A_{r,eff}$), compressive load at a tip displacement of 0.1D, $Q_{t,0.1D}$, and pile head displacement, w_{head} , at the end of the load test.

The effective area ratio, $A_{r,eff}$, during an increment of penetration of an open-ended pile is the ratio of the added volume (i.e. the gross pile volume minus any soil entering the plug) to the gross pile volume.

$$A_{r,eff} = 1 - IFR \frac{D_i^2}{D^2} \quad (5)$$

$A_{r,eff} = 1$ corresponds to plugged penetration or a closed-ended pile. $A_{r,eff} = 0$ corresponds to a vanishingly thin-walled pile for which there would be negligible radial movement. The incremental filling ratio (IFR) is the incremental change in plug height (Δh_p) with incremental increase in driving depth (Δz_{tip}), $IFR = \Delta h_p / \Delta z_{tip}$. In the absence of measurements of IFR, the plug length ratio (PLR = plug length / embedded pile length) provides an indication of the mean IFR during installation. An equivalent pile diameter (D_{eq}) can be calculated based on pile geometry and plugging during installation, $D_{eq} = (D^2 - IFR \cdot D_i^2)^{0.5} = D \cdot (A_{r,eff})^{0.5}$.

The piles were installed using an IHC S280 hydraulic hammer, with a maximum rated energy of 280 kN-m at a stroke of 2.1 m. Measurement of the plug length within the pipe pile at the end of driving showed a soil level above the seabed, indicating that installation occurred primarily in a coring (unplugged) manner. Plug heights greater than the penetration depth are typically due to dilation of the soil plug in

Table 2. Pile load test parameters.

Pile ID	D (m) [t (mm)]	Z_{tip} [L_{emb}] (m)	Time (days)	PLR [$A_{r,eff}$]	$Q_{t,0.1D}$ (MN)	Final w_{head} (mm)
TP-1	1.5 [28]	73.5 [66.5]	35	>1.0 [0.073]	32.0	255
TP-2	1.5 [28]	86.0 [79.0]	60	>1.0 [0.073]	36.0	240



Figure 4. Static load test setup.

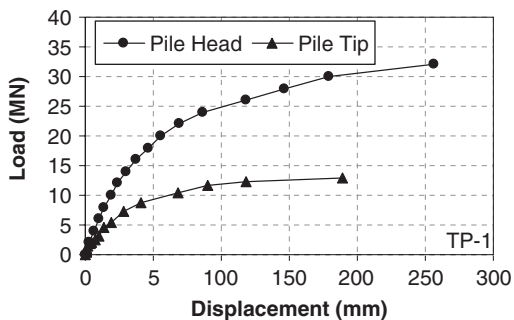


Figure 5. Load settlement behaviour of TP-1 tipped in gravel.

dense soils (Foray et al. 1998) and a maximum IFR of unity is used in analyses.

During load tests, the head load was measured as the jacking force, and the axial load distribution was monitored using 12 to 14 levels of strain gauging. The first two levels of strain gauges corresponded to the seabed and the bottom of the thick Yurakucho clay layer at 40 m depth. Internal channels were used to protect the strain gauges during installation.

The piles were loaded in 4 MN increments until a load of 24 MN was reached, and then loaded in 2 MN increments until a pile tip displacement of approximately 0.1D. Each load step was maintained for at least 30 minutes, resulting in the duration for each

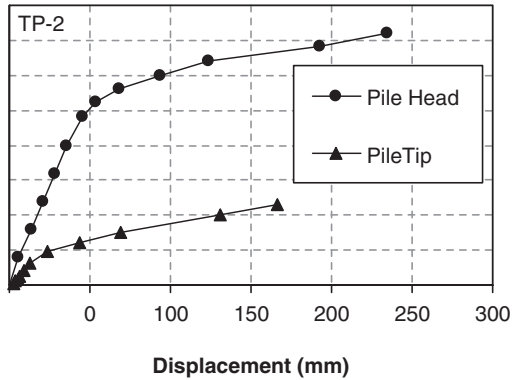


Figure 6. Load settlement behaviour of TP-2 tipped in sand.

load test of approximately 12 hours. Pile head and base load-displacement curves are presented for TP-1 and TP-2 in Figure 5 and 6, respectively.

Load tests were performed 35 to 60 days after installation (Table 2). Assuming a coefficient of consolidation for the clay layers of approximately $10 \text{ m}^2/\text{yr}$, normalized time factors ($T_{eq} = c_h \cdot \text{time}/D_{eq}^2$) of 5 to 10 are calculated. T_{eq} factors between 5 and 10 relate to 80 to 90 percent consolidation of the clay layers at the time of load testing (Randolph 2003).

4 BACK-ANALYSIS METHODOLOGY

4.1 Shaft resistance in sand

Piezocene data, combined with an extension of the UWA method for predicting axial pile capacity in siliceous sands (UWA-05; Lehane et al. 2005, 2007), has been used to evaluate the shaft friction and base resistance of the test piles. The general expression for unit shaft resistance, τ_f , is based on a Coulomb failure criterion (Lehane et al. 1993).

$$\tau_f = (\sigma'_{rc} + \Delta\sigma'_{rd}) \tan \delta_f = \sigma'_{rf} \tan \delta_f \quad (6)$$

where σ'_{rc} is the radial stress after installation and equalization, $\Delta\sigma'_{rd}$ is the change in radial stress during pile load, δ_f is the soil-pile interface friction angle, and σ'_{rf} is the radial stress at failure. For large diameter piles, the influence of $\Delta\sigma'_{rd}$ becomes small (e.g. Lehane et al. 2005, 2007), and τ_f can be estimated directly from CPT tip resistance, q_t , using modification factors a , b and c , in Equation 7.

$$\tau_f = \frac{q_t}{a} A_{r,eff}^b \left[\max\left(\frac{h}{D}, 2\right)^c \right] \tan \delta \quad (7)$$

Table 3. UWA-05 method parameters in siliceous sand.

Loading	a	b	c	$\tan \delta$
Compression	33	0.3	-0.5	Measured or $f(d_{50})$
Tension	44			

White (2005) suggested the general form of Equation 7, linking the parameters a, b and c to the main mechanisms governing shaft resistance as follows:

- a: relates to the drop in stress from q_t to a maximum value of normal stress on the pile wall after the pile tip has passed a soil horizon.
- b: relates to the partial displacement of soil around the tip of an open-ended pile, which leads to a lower radial stress and unit shaft resistance at the pile shoulder compared to a closed-ended pile (or CPT). Cavity expansion analysis provides a theoretical basis for this parameter in clays (Carter et al 1980) and in sands (White et al 2005).
- c: relates to the local degradation of horizontal stress due to friction fatigue as the pile tip penetrates deeper (Heerema 1980, Lehane 1992, White & Lehane 2004).

Based on the methodology outlined in Lehane et al. (2005, 2007), the calibration of UWA-05 using a database of load tests with adjacent CPT profiles resulted in the parameters summarized in Table 3. At present, UWA-05 is the only CPT-based pile design method within API (2006) which specifically caters for all the mechanisms mentioned above that influence pile capacity in sands.

The UWA method was originally developed for piles embedded in sand. These Tokyo Bay test piles pass through layers of clay, silt and sand, and so the UWA method cannot be directly applied to estimate shaft resistance without further calibration. The framework given by Equation 7 and the subsequent bullet points are equally applicable to clay. However, account should be made of the effects of drainage and consolidation which lead to additional differences between pile and CPT behaviour and differences in the a, b and c parameters given above.

4.2 Modified $q_t - \tau_f$ correlations for this site

For the purposes of back-analysing the Tokyo Bay piles, which pass through clays and silts before being tipped in sand or gravel, it is necessary to reconsider the parameters given in Table 3, which were calibrated only for sands. The task is to assess how the parameters a, b and c may differ in other soils.

In materials finer than sand, cone tip resistance may be undrained, or partially consolidated, while axial pile

capacity during static load testing is essentially drained. To illustrate this behaviour, it is helpful to reduce Equation 7 to a single parameter, $k_1 = q_{t,\text{avg}}/\tau_{f,\text{avg}}$, which has been used previously to compare average CPT tip resistance and pile shaft capacity (e.g. Almeida et al. 1996, Eslami & Fellenius 1997):

$$\frac{1}{k_1} = \frac{A_{r,\text{eff}}^b \tan \delta_f}{a} \left[\frac{1}{L_{\text{emb}}} \int_{h=0}^{L_{\text{emb}}} q_t(h) \cdot \max\left(\frac{h}{D}, 2\right)^c dh \right] \quad (8)$$

Equation 8 shows that k_1 tends to increase with pile slenderness as friction fatigue has a more significant influence on mean unit shaft resistance: increased slenderness (i.e. higher L_{emb}/D) leads to a reduction in the bracketed term of Equation 8. Also, partial consolidation or undrained behaviour during cone penetration leads to higher values of k_1 in sands compared to silts, which are in turn higher than those in clays (Lehane 1992, Eslami & Fellenius 1997). Since the cone parameter Q also increases with coefficient of consolidation (or soil type) for a constant overconsolidation ratio (OCR) (Figure 3), k_1 can be estimated as a function of Q. The purpose of such a link is to allow shaft resistance in all types of soil to be estimated from q_t .

Typical values of k_1 have previously been proposed for particular soil types and for typical ranges of in situ state (i.e., Q). These values of k_1 range from 15 to 40 in clays and 100 to 250 in silts and sands, respectively (e.g. Almeida et al. 1996, Eslami & Fellenius 1997). For this Tokyo site, Q is typically in the range of 5 to 15 in the clay layers, 50 in the silts, and 100 to 200 in the sands and gravels. The following equation links these measurements with previous suggested values of k_1 :

$$k_1 \approx \min\left(\frac{4}{3}Q + 10, 250\right) \quad (9)$$

The resulting values of k_1 range from 17–30 in the clay layers, increasing to 75 in the silts, and up to 250 in the Tokyo gravel. It should be noted that Equation 9 has been calibrated for ranges of Q at this site, and may be *unconservative* in softer NC clays or loose sands and *overly conservative* in heavily overconsolidated clays.

Lehane et al (2000) note that k_1 is influenced by factors other than simply soil type. In clays, k_1 is affected by s_u/σ'_{v0} (or OCR), sensitivity (S_s), plasticity index (I_p), and relative voids index (I_{rv}), in addition to friction fatigue, end condition and interface friction angle, as mentioned previously for sands. Equations 7 and 8 separately account for the influence of end condition and friction fatigue on the k_1 parameter via the $A_{r,\text{eff}}^b$ and $(h/D)^c$ terms.

It is more rigorous to separate out these mechanisms rather than use a single correlation to capture the effect of soil type – indicated by the parameter Q – on all mechanisms affecting shaft resistance. Equation 10 links Q to the ‘ a ’ parameter (in Equation 7) and interface friction angle for this site.

$$\frac{a}{\tan \delta_f} \approx \min \left(\frac{2}{3} Q + 5, 78 \right) \quad (10)$$

Values of $a/\tan \delta_f$ are approximately half to one third of k_1 due to the influence of friction fatigue, as expressed in Equation 8. For Q values greater than 117, Equation 10 is limited by $a/\tan \delta_f$ equal to 78. This value ties in with the UWA-05 method for piles in compression using values of $a = 33$ and $\delta_f = 23$ degrees. Lower interface friction angles are associated with coarser grained sands and gravel (e.g. Lehane et al. 2005). Slightly lower values of $a/\tan \delta_f$ equal to 60 apply in the Edogawa sand layer, with Q_{avg} of 83. These values tie in with the UWA-05 method for δ_f between 28 and 29 degrees, which is typical for fine sands.

Equation 10 therefore allows an improved back-analysis of the load test shaft resistance to be made, using the full expression for shaft resistance (Equation 7). By changing the ‘ a ’ parameter into a function of Q , the effect of soil type is modeled.

There is less information available on the influence of soil type on the ‘ b ’ and ‘ c ’ parameters for Equation 7, but it is desirable to account for these differences. A binary distinction between ‘drained’ and ‘undrained’ CPTU penetration resistance is tentatively made at $\Delta u_2/\sigma'_{v0} = 1$ for simplicity. ‘Drained’ parameters were taken based on the UWA-05 method for sands. For ‘undrained’ CPTUs, the area ratio parameter, ‘ b ’, was taken as 0.1 based on Carter et al’s (1980) study into the difference between open and closed-ended piles (for $A_{ref,eff} > 0.05$), while ‘ c ’ was taken as −0.2 (Lehane et al 2000).

In summary, a back-analysis of the measured distribution of shaft resistance through the mixed soils of Tokyo Bay has been achieved by extending existing empirical relationships for pile capacity in sand by evaluating the mechanisms influencing CPT q_t and pile τ_f in other soils. The revised parameters used in Equation 7 are given in Table 4. The purpose of this modification is to allow the effect of soil type to be incorporated into a simplified correlation between τ_f and q_t , using only normalised CPT parameters as inputs. This back-analysis is compared to the measured data in section 5, after discussion of factors influencing calculation of base resistance.

4.3 Base resistance in sand

To estimate the base resistance of large diameter piles from in situ test data requires consideration

Table 4. Parameters used in Equation 7 for back analysis of compression load tests at the Tokyo Bay site.

CPT Penetration	$\Delta u_2/\sigma'_{v0}$	$a/\tan \delta_f$	b	c
‘Drained’	<1	$\min(2/3Q+5, 78)$	0.3	−0.5
‘Undrained’	>1		0.1	−0.2

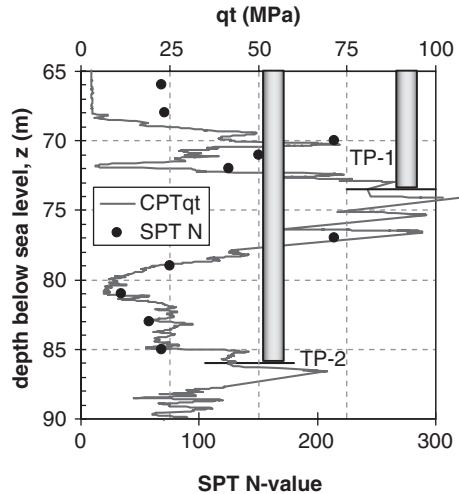


Figure 7. Cone tip resistance and SPT data in founding strata.

of: (i) averaging of the in situ parameters to account for the differing zones of influence of the in situ test and the pile; (ii) plugging: piles plug statically in uniform deposits if the plug length is at least 5D in that layer (e.g. Randolph et al 1991; Lehane & Randolph 2002), but the static plugging behavior may differ in layered deposits; (iii) the stiffness of the soil below the pile will influence the fraction of the ultimate (plunging) capacity that can be mobilized at acceptable levels of settlement (typically 0.1D).

SPT N-values are usually measured at a vertical separation of 1.5 m to 2 m. There are usually insufficient N-values in the zone influenced by the pile tip to conduct meaningful averaging or to detect thin strata. This is a serious limitation in heavily layered deposits, such as Tokyo Bay, since vertical as well as horizontal variability may significantly influence the available pile base resistance.

As shown in Figure 1 and expanded for Figure 7, CPTs provide a much more detailed vertical profile of soil strength. Due to differences in the diameter of a CPT and a pile, q_t must be appropriately averaged. A discussion of different averaging techniques is presented by Xu & Lehane (2005) and Lehane et al. (2007).

Figure 7 highlights the variation in q_t close to the tips of the test piles. Table 3 summarizes the average cone tip resistance for the two test piles using three common methods:

- (i) the arithmetic mean over a vertical range of $\pm 1.5D$ (i.e., Bustamante & GIANESELLI 1982);
- (ii) the effective geometric average using pile outer diameter over up to $+4D$ to $-8D$ (Eslami & Fellenius 1997);
- (iii) the minimum path Dutch averaging technique over up to $+4D$ to $-8D$ (Van Mierlo & Koppejan 1952, Schmertmann 1978).

For open-ended pipe piles, it is necessary to choose an appropriate effective diameter when applying these methods. The total base resistance is the sum of the annular resistance on the steel of the pile, Q_{ann} , plus any plug resistance, Q_{plug} , mobilized on the soil within the pile (Lehane & Gavin 2001, Paik et al. 2003). As loading begins, the annular resistance is mobilized first, whilst the soil below the plug undergoes compression. If these mechanisms are considered separately, the zone of the influence of the annulus is much smaller than the plug, and correspondingly more sensitive to local layering.

Annular resistance is often linked directly to local cone tip resistance without additional averaging, since the pile wall thickness is comparable to the CPT diameter ($q_{\text{ann}} = \alpha q_t$, $\alpha = 0.6$ to 1.0 ; DNV 1992). When calculating installation resistance for a coring or partially plugged open-ended pile, the effective diameter, D_{eff} , calculated by considering the effective area ratio is most logical. However, under static loading, failure occurs in a plugged manner, so an area ratio of unity is appropriate, implying that the full diameter of the pile should be used for averaging q_t . Table 5 shows the averaged values of q_t found using the methods described above.

The following observations arise from Table 5:

- (i) Averaged q_t over $\pm 1.5D$ leads to slightly higher values than q_t at the pile tip;
- (ii) The Dutch method, when applied using D_{eq} , leads to values of $q_{t,\text{avg}}$ that are 70 to 85% of q_t ;
- (iii) The Dutch method, when applied using the inner pile diameter (which is more logically applicable

Table 5. Average cone tip resistance for evaluation of pile end bearing.

Tip depth (m)	q_t (MPa)	$\pm 1.5D$ (MPa)	effective geometric average (MPa)	Dutch $D_i =$ (MPa)	Dutch $D_{\text{eq}} =$ (MPa)
73.5	80.7	84.4	50	23.8	57.2
86	42.1	47.9	35.4	19.6	36.0

for static load testing), leads to values of $q_{t,\text{avg}}$ in the range 30–50% of q_t .

These contrasting values of $q_{t,\text{avg}}$ highlight the need for additional research into q_t averaging for the assessment of pile base resistance for large diameter pipe piles in layered deposits.

5 BACK-ANALYSIS RESULTS

5.1 Summary of back-analysis approach

The back analysis of the piles is addressed in two stages:

1. Assess appropriate $q_b/q_{c,\text{avg}}$ for the annulus and plug based on strain gauging near the pile tip;
2. Apply modified $\tau_f - q_c$ correlations developed for the range of Q in sands, silts, and clays at this site, as discussed in Section 4.2.

The shaft resistance is added to the base resistance to develop back-analysed axial load transfer curves for test piles TP-1 and TP-2, which are compared to measured strain gauge data.

5.2 Measured vs. back-analysed base resistance

Annulus and plug resistance were separated by studying the strain gauge responses close to the pile tip. A sharp increase in the apparent local shaft resistance was observed 1.5D above the pile base on both test piles. This deviation was attributed to the onset of load transfer via internal shaft resistance, and was used to evaluate the resulting plug resistance, as described by Kikuchi et al (2005).

Table 6 summarizes the components of base capacity at a pile tip displacement (w_{tip}) of 0.1D. It can be seen that despite the plug having an area more than ten times greater than the annulus, the resistance on the annulus provides the majority of the base capacity at w_{tip} of 0.1D for TP-1 and approximately 40% of the base resistance for TP-2. These surprising results arise because:

- (i) for this layered site the average cone tip resistance applicable to the annulus is up to 4 times

Table 6. Measured base resistance at $w_{\text{tip}} = 0.1D$ on the pile annulus and the soil plug.

Pile	Tip depth (m)	Annular resistance ¹ (MN)	Plug resistance ² (MN)
TP-1	73.5	8.2	7.5
TP-2	86	4.6	6.7

¹Area of pile annulus 0.13 m^2

²Area of pile plug 1.64 m^2

- greater than that applicable to the plug due to the different zones of influence (Table 5);
- (ii) base resistance on the annulus is mobilized at smaller displacements than on the plug due to compression of the soil near the tip of the pile, and the relative dimensions of the plug compared to the pile wall.

Figures 8 and 9 summarize the mobilization of pile base resistance normalized to cone tip resistance values for TP-1 and TP-2, respectively. Annular resistance is normalized using a non averaged CPT q_t . Plug resistance is normalized using the Dutch method averaged with the internal pile diameter, D_i . Despite higher average q_t values, a much higher proportion of $q_{t,avg}$ is mobilized along the annulus as compared to that on the plug. These observations are in agreement with Lehane & Gavin (2001) and Paik et al. (2003) who separated the components of plug and annular resistance using strain gauged double walled piles. Annular resistance on TP-1 plateaus at approximately $0.8q_t$, while TP-2 shows much higher resistance at $1.5q_t$. The higher resistance on TP-2 is attributed to potentially higher q_t values at the pile location as compared to those measured by the CPT. This natural variability near the tip of TP-2 is indicated in Figure 7,

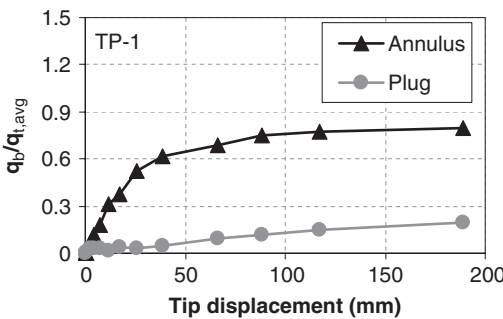


Figure 8. Mobilization of base resistance for TP-1.

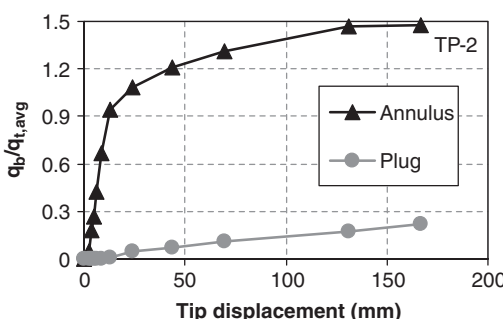


Figure 9. Mobilization of base resistance for TP-2.

which shows q_t increases from 40 MPa to 70 MPa within 1 m of the base of TP-2.

The plug resistance for both piles is approximately 0.15 to 0.2 $q_{t,Dutch}$ averaged over the pile inner diameter, in agreement with observations of Xu et al. (2005), among others. For these low displacement piles, base stiffness is similar to that of a bored pile (Lehane & Randolph 2002) and would require significant displacement to mobilize $q_{t,avg}$ despite the pile failing in a plugged manner.

The following equation was used for end bearing in the back analysis.

$$Q_{b0.1} = 1.0q_t A_{ann} + 0.15q_{t,avg,plug} A_{plug} \quad (11)$$

The average cone tip resistance on the soil plug was calculated using the Dutch averaging technique over the internal pile diameter. The cone tip resistance was not averaged for calculating annular resistance.

Neither test reached a steady value of plug resistance. Reviews of closed-ended pile capacity indicate that an ultimate (plunging) capacity of $q_b/q_{t,avg}$ in the range 0.6–1.0 is achieved after sufficient settlement, often no more than 0.1D (White & Bolton 2005). Since open-ended piles fail in a plugged manner, a similar plunging capacity should be achieved after compression of the soil beneath the pile and within the soil plug. However, these load tests, and all other published load tests on open-ended piles of diameter >1.5 m, were halted prior to the full mobilization of plunging capacity.

At the end of these load tests, the unit plug resistance was continuing to increase approximately linearly at a rate of $>1.0q_b/q_{t,avg}$ per diameter. For applications in which significant settlement can be tolerated this observation suggests that there may be significant reserves of base capacity that are not exploited if capacity is defined by a settlement criterion. In the case of these test piles in Tokyo Bay, the tangent base stiffness at the end of each load test was ~ 1 MN per 10 mm of settlement.

5.3 Axial load transfer curves

The back-analysed axial load transfer curves for test piles TP-1 and TP-2 are shown in Figures 10 and 11 respectively. These profiles correspond to a tip displacement of $D/10$. As discussed in section 4, the shaft resistance profile has been calculated using an extension of the UWA-05 method based on Equations 7 and 10, and the parameters given in Table 4. The base resistance has been calculated using Equation 11 after assessment of strain gauge response near the pile tip. Comparisons of the calculated and measured capacity are given in Table 7.

The calculated base resistance matches the measurements well when using the full value of q_t on the

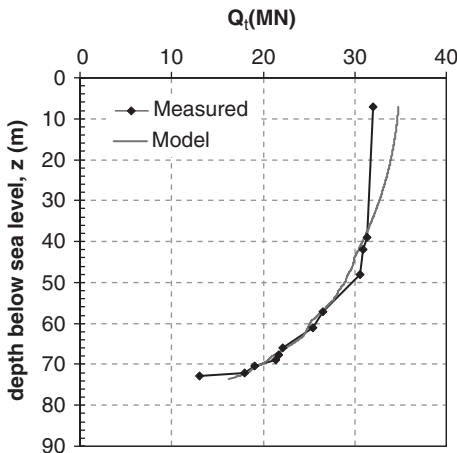


Figure 10. Comparison of predicted to measured axial load transfer along TP-1 for tip displacement of 0.1D.

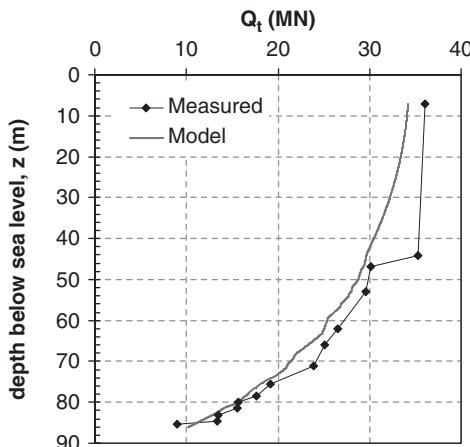


Figure 11. Comparison of predicted to measured axial load transfer along TP-2 for tip displacement of 0.1D.

Table 7. Comparison of back-analysed capacity at $w_{tip} = 0.1D$.

	TP-1 (MN)			TP-2 (MN)		
	Q_s	Q_b	Q_t	Q_s	Q_b	Q_t
Calculated, Q_c	18.5	16.3	34.8	24.0	10.2	34.2
Measured, Q_m	16.3	15.7	32.0	24.7	11.3	36.0
Ratio, Q_c/Q_m	1.13	1.04	1.09	0.97	0.90	0.95

annulus and 15% of the Dutch averaged (using the inner pile diameter) q_t value on the pile plug. Variability in cone resistance near the pile tip may have resulted in higher apparent proportions of q_t on

the annulus. The magnitude and distribution of shaft friction is predicted reasonably well over the length of the pile, particularly considering the simple expression used for the sand, silt and clay layers. This expression relies only on CPT parameters without supplementary laboratory data, although, supplemental laboratory data would help refine input parameters and increase the level of knowledge related to mechanisms influencing pile capacity.

In places along the profile, the predicted and measured shaft friction distribution tends to be vertically offset, which can be attributed to natural soil variability. Matching of trends in driving resistance with trends in the CPTU profile could be used to update a model after pile installation. Additionally, shaft friction in the Yurakucho clay above 40 m tends to be overpredicted. This may have resulted from strain softening due to pile compression or partial consolidation of the clay following pile driving.

Whilst this back-analysis has been conducted after the event, the resulting approach has a robust basis since it captures the governing mechanisms influencing shaft resistance, including:

- the influence of end condition on the increase in radial stress due to pile installation;
- the effect of drainage and partial consolidation during cone penetration testing on the relationship between CPT q_t and radial stress at the pile wall after installation and consolidation; and
- the reduction in local shaft resistance with continued pile penetration (friction fatigue) and strain softening of soft clay layers near pile head.

6 CONCLUSIONS

This paper describes the back-analysis of two static load tests on large-diameter pipe piles in Tokyo Bay, and discussed factors influencing cone penetration tip resistance and the relationship between CPTU parameters and pile capacity. It is concluded that:

- Piezocone testing provides superior profiling of soil type and strength in a cost effective manner compared to SPTs complemented by sampling and laboratory testing. This comparison highlights the value of CPTU tests in order to aid the design of long piles in layered soil deposits, such as those for the Tokyo port bay bridge.
- Combined drilling and wireline CPTU tests provides near continuous profiles of soil strength in very dense sands and gravels. This information is of significant value when evaluating the influence of soil layering in the vicinity of a pile tip.
- Degree of consolidation during cone penetration testing and pile installation effects the correlation between CPTU and pile (i.e., q_b and τ_f) parameters.

- A correlation between $a/\tan\delta$ and Q has been developed to assess τ_f for typical CPTU parameters in sands, silts, and clays at this site. Results agree well with existing empirical correlations as well as site specific data, and further exploration of this approach appears promising.
- The base resistance of open-ended piles is influenced by resistance on the annulus as well as resistance on the soil plug. Prior to full mobilization of the soil plug, it is necessary to assess annular resistance as a direct fraction of CPT q_t without local averaging, due to the small zone of influence. However, local variability will therefore significantly influence q_t , and thus estimates of annular resistance, as observed for this site.
 - The correlation between CPT q_t and base resistance on the pile plug needs to account for the larger diameter of piles. The 'Dutch' averaging technique using the inner pile diameter appears to be appropriate for the layered soil profiles at this site.
 - Open-ended piles require greater displacement to mobilize base capacity as compared to a closed-ended pile of the same diameter. At the end of these load tests, the plug resistance remained only partially mobilized and the tangent base stiffness was significant. If structures can tolerate larger settlements, addition base capacity may be available for design, but load tests to higher displacement are necessary to prove this hypothesis.
- ## ACKNOWLEDGEMENTS
- The first and second authors acknowledge the generosity of PARI in providing the data from the Tokyo port bay bridge project. Additionally, the first author thanks the Australian Research Council (ARC) as well as support through an International Postgraduate Research Scholarship (IPRS), a University Postgraduate Award (UPA), and a Convocation travel scholarship to Cambridge University.
- ## REFERENCES
- Almeida, M., Danziger, F., and Lunne, T. 1996. The use of the piezocone test to predict the axial capacity of driven and jacked piles. *Canadian Geotech. J.*, 33: 23–41.
- American Petroleum Institute (API) 2006. *Recommended Practice for Planning, Designing, and Constructing Fixed Offshore Platforms – Working Stress Design*, API RP2A, 22nd Edition, American Petroleum Institute, Washington, D.C.
- Bustamante, M., and Gianeselli, L. 1982. Pile bearing capacity prediction by means of static penetrometer CPT. *Proc., 2nd Europ. Symp. on Penetration Test.*, Amsterdam: 493–500.
- Carter, J.P., Randolph, M.F., & Wroth, C.P. 1980. Some aspects of the performance of open- and closed-ended piles. *Num. Methods in Offshore Piling, ICE*:165–170.
- Delft Laboratory of Soil Mechanics (Delft) 1936. The pre-determination of the required length and the prediction of the toe resistance of piles. *Proc. 1st Int. Conf. on Soil Mech. and Foundation Eng.*, Cambridge: 181–184.
- Det Norske Veritas (DNV). 1992. *Classification Notes No. 30.4, Foundations*, February: 54.
- Eslami, A., and Fellenius, B. 1997. Pile capacity by direct CPT and CPTU methods applied to 102 case histories. *Canadian Geotech. J.*, 34: 886–904.
- Foray, P., Balachowski, L., and Colliat, J.-L. 1998. Bearing capacity of model piles driven into dense overconsolidated sands, *Canadian Geotech. J.*, 35: 274–385.
- Fugro. 2001. *Geophysical and Geotechnical Techniques for the Investigation of Near-Seabed Soils and Rocks*, Fugro NV, Leidschendam, NL: 51.
- Heerema, E.P. 1980. Predicting pile drivability: Heather as an illustration of the friction fatigue theory, *Ground Eng.*, 13: 15–37.
- Kikuchi et al. 2005. Vertical bearing capacity of large diameter steel pipe piles for Tokyo port seaside road, *Journal of Structural Engineering*, 1571–1578.
- Lehane, B.M. 1992. Experimental investigations of pile behaviour using instrumented field piles, *PhD Thesis*, Imperial College, University of London: 615.
- Lehane, B.M., Jardine, R.J., Bond, A.J., and Frank, R. 1993. Mechanisms of shaft friction in sand from instrumented pile tests. *ASCE J. Geotech. Eng.*, 119 (1): 19–35.
- Lehane, B. M., Chow, F. C., McCabe, B. A., and Jardine, R. J. 2000. Relationships between shaft capacity of driven piles and CPT end resistance. *Proc. of the Institution of Civil Eng., Geotech. Eng.*, 143(2): 93–101.
- Lehane, B.M., and Gavin, K. 2001. Base resistance of jacked pipe piles in sand, *ASCE J. Geotech. & Geoenv. Eng.*, 127(6): 473–480.
- Lehane, B. M., & Randolph, M. F. 2002. Evaluation of a minimum base resistance for driven pipe piles in siliceous sand. *ASCE J. of Geotech. and Geoenv. Eng.*, 128(3): 198–205.
- Lehane, B.M., Schneider, J.A., and Xu, X. 2005. The UWA-05 method for prediction of axial capacity of driven piles in sand. *Proc., Int. Symp. Frontiers Offshore Geomech. ISFOG*, Perth: 683–689.
- Lehane, B.M., Schneider, J.A., and Xu, X. 2007. CPT based design of displacement piles in siliceous sands. *Proc., Int. Workshop on Recent Advances of Deep Foundations*, Yokosuka, Japan.
- Lunne, T., Robertson, P.K., and Powell, J.J.M. 1997. *Cone Penetration Testing in Geotechnical Practice*, Blakie Academic and Professional, Melbourne: 312.
- Paik, K., Salgado, R., Lee, J., and Kim, B. 2003. Behavior of open- and closed-ended piles driven into sands. *ASCE J. Geotech. Geoenvir. Eng.*, 129(4): 296–306.
- Randolph, M.F., Leong, E.C., and Housby, G.T. 1991. One-dimensional analysis of soil plugs in pipe piles, *Géotechnique*, 41(4): 587–598.
- Robertson, P.K. 1990. Soil classification using the cone penetration test, *Canadian Geotech. J.*, 27(1): 151–158.
- Schmertmann, J. H. 1978. *Guidelines for cone test, performance, and design*: U.S. Federal Highway Administration, FHWA-T-78209.

- Schneider, J.A., Xu, X., and Lehane, B.M. 2007a. Database assessment of CPT based axial pile design methods in siliceous sands: Part I – overview of methods, database and predictive performance, *ASCE J. Geotech. Geoenviron. Eng.*, in review.
- Schneider, J.A., Randolph, M.F., Mayne, P.W., and Ramsey, N.J. 2007b. Soil behaviour type evaluated using normalized piezocone parameters, *ASCE J. Geotech. Geoenviron. Eng.*, submitted.
- Van Mierlo, W.C., and Koppejan, A.W. 1952. Lengte en draagvermogen van heipalen bouw.
- White D.J. 2005. A general framework for shaft resistance on displacement piles in sand. *Proc., Int. Symp. Frontiers Offshore Geomech. ISFOG*, Perth: 697–703.
- White, D.J., and Lehane, B.M. 2004. Friction fatigue on displacement piles in sand. *Géotechnique*, 54(10): 645–658.
- White, D.J. and Bolton, M.D. 2005. Comparing CPT and pile base resistance in sand, *Proc. of the Institution of Civil Eng., Geotech. Eng.*, 158: 3–14.
- White, D. J., Schneider, J. A., and Lehane, B. M. 2005. The influence of effective area ratio on shaft friction of displacement piles in sand. *Proc., Int. Symp. Frontiers Offshore Geomech. ISFOG*, Perth: 741–747.
- Wroth, C.P. 1984. The interpretation of in situ soil tests, *Géotechnique*, 34 (4): 449–489.
- Xu, X., and Lehane, B.M. 2005. Evaluation of end-bearing capacity of closed-ended pile in sand from cone penetration data, *Proc. of the Int. Symp. on Frontiers in Offshore Geotechnics*, Perth, Australia, Taylor & Francis Publishers, pp. 733–739.
- Xu, X., Lehane, B.M., and Schneider, J.A. 2005. Evaluation of end-bearing capacity of open-ended driven piles in sand from CPT data, *Proc. of the Int. Symp. on Frontiers in Offshore Geotechnics*, Perth, Australia, Taylor & Francis Publishers, pp. 725–731.

Pile foundation design of the connecting bridge for New-Kitakyushu airport

H. Ochiai & N. Yasufuku

Kyushu University, Department of Civil Engineering, Fukuoka, Japan

Y. Maeda

Kyushu-Kyoritsu University, Department of Civil Engineering, Fukuoka, Japan

S. Yasuda

Tokyo-Denki University, Department of Civil and Environmental Engineering, Tokyo, Japan

ABSTRACT: In this paper, an importance of integrating the geotechnical investigations with pile foundation design was clarified through a case study in terms of investigation, design and construction of the connecting bridge for New-Kitakyushu airport. The basic policy and concepts for geotechnical investigations and pile foundation design of the connecting bridge for New-Kitakyushu airport are introduced. The changes of geotechnical engineering profile are briefly mentioned based on the density of in-situ investigations and laboratory tests. A method used for evaluating the vertical bearing capacity of driven piles in the actual design is explained based on the geotechnical considerations. The applicability is also verified by comparing the predicted results with the results from the full-scale pile load tests, whose results derived the reduction of the safety factor for design. Finally, the significance of geotechnical investigations including in-situ and laboratory tests and full scale pile load tests were discussed in terms of the cost performance of the construction of pile foundations for supporting the connecting bridge of New-Kitakyushu airport.

1 INTRODUCTION

A connecting bridge was constructed on the sea as an access road for New Kitakyushu airport, which was opened in 2006. The length of the bridge is about 2 km and 24 piers are mounted for supporting the bridge. The location of New-Kitakyushu airport at Kyushu area in Japan and an overview of the connecting bridge under construction are shown in Figures 1

and 2. In order to clarify the geological and mechanical characteristics of the ground for supporting the bridge and the manmade airport island, a large number of in-situ and laboratory tests had been performed for five years from 1991 to 1995.

In this paper, the basic policy and concepts for geotechnical investigations and design of this project are introduced. The changes of geotechnical engineering profile are briefly mentioned based on the density

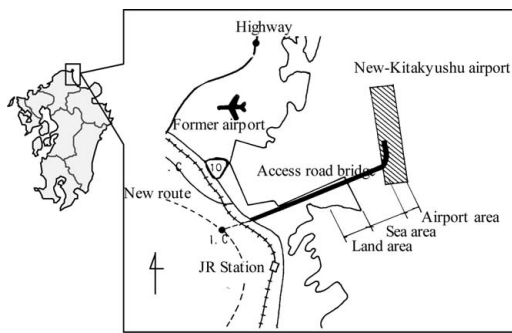


Figure 1. Location of New-Kitakyushu airport and the connecting bridge.

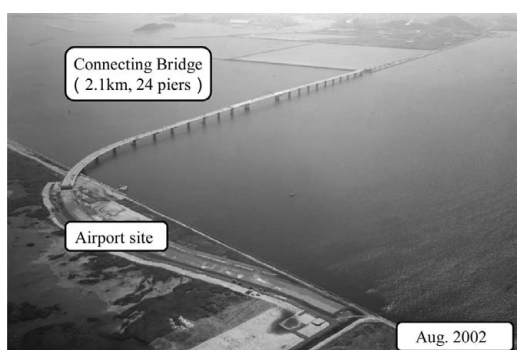


Figure 2. Overview of connecting bridge under construction.

of in-situ investigations and laboratory tests. The process of producing a model ground for design is also made clear, which is used for estimating the bearing capacity of driven piles. Further the method used for predicting the vertical bearing capacity of driven piles is discussed based on the geotechnical considerations. The applicability is also verified by comparing the predicted results with the results from the full-scale pile load tests, whose results are linked with the reduction of the safety factor for design. Finally, the significance of in-situ investigations and full scale pile load tests are indicated related to the cost performance of the construction of pile foundations for supporting the connecting bridge.

2 GEOTECHNICAL INVESTIGATION AND DESIGN

Figure 3 shows the policy and concept of geotechnical investigation and design for constructing the connecting bridge for New-Kitakyushu airport. As shown in this figure, the field and laboratory investigations, and the engineering design are conducted based on the clear policy, which includes that:

- 1) The actual collaboration between geotechnical investigators and designers is effective for a rational design and construction in this project,

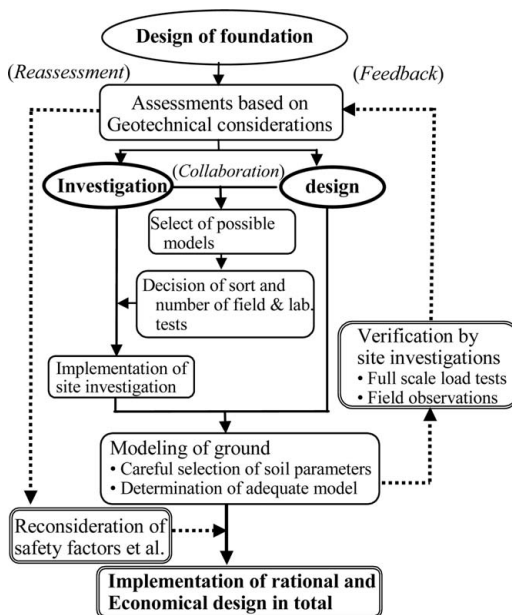


Figure 3. Collaboration of geotechnical investigations with design.

- 2) The design parameters are determined based on the geotechnical considerations, which reflect the results obtained from the geotechnical investigations and laboratory soil tests. The model for estimating the bearing capacity of piles in design is presented based on the geotechnical considerations.
- 3) A rational bearing stratum should be carefully selected based on the geological and geotechnical point of view.
- 4) The predicted performance in design was checked by a full-scale model tests. The results were reflected to the reduction of factor of safety for design as mentioned below.

Such treatment seems to be important to linked with the performance based design, which may become the mainstream in foundation design near future.

3 GEOTECHNICAL ENGINEERING MAP FOR DESIGN

Figure 4 shows the history of the geotechnical engineering profile mainly by the field investigations from 1991 to 1995, which covers the land, sea and airport areas. Figure 4 was drawn by adding the boring data in each pier of the access road, where the total number of borings became more than 65 with 3500 m in total length, and the geological investigations on the diatom earth and also volcanic ash deposit with the results of the seismic exploration. The boring

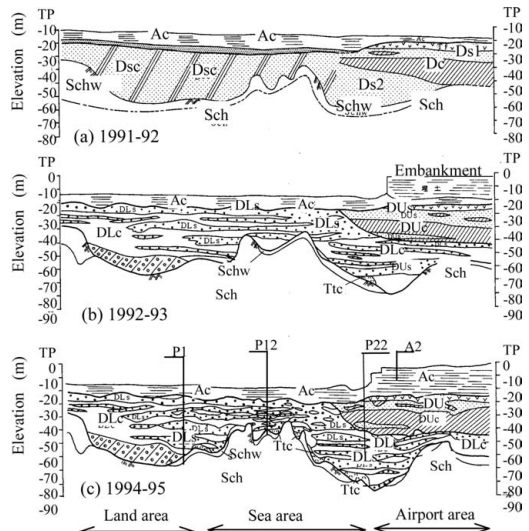


Figure 4. History of geotechnical engineering profile.

densities of each area in 1992, 1993 and 1995 are roughly 350 m, 180 m and 70 m respectively.

It is judged that the geotechnical engineering profile becomes more precise with the increasing boring density and quality of in-situ investigations. The accuracy of geotechnical investigations is believed to lead to the economical and rational design and construction, even if the percentage of investigation cost to the total one might be somewhat increased (see Table 2). Figure 4 clarified that 1) the investigated ground consists of alluvial clayey layers with 7–9 m thickness and Pleistocene layers laminated by sandy and clayey soils with 20–60 m thickness below the alluvial layers and also weathered crystalline schist as the base layer. The corresponding ground is therefore roughly divided into 3 layers. 2) The undulation of base layer is extremely high in which the difference becomes more than 45 m. 3) The structure of Pleistocene layers is complicated and the continuities in horizontal direction are not so clear, and so the lens shape layers are found here and there. 4) The surface of unconformity in Pleistocene layers is clearly found from sea area to airport area of which inclination is about 15 degrees in the longitudinal direction.

3.1 Geological profile with increases of site investigation

When determining a good bearing stratum for pile foundation, Japanese design code by Japan Road Association recommends that the N-values of sandy or sand-gravel layers are greater than 30 blow counts, and also N-values of clayey layers are more than 20. Figure 5 shows the characteristics of N-values in Pleistocene sandy and clayey layers obtained from the SPT. The N-values of both layers tend to become more than 30 in average when the depth is roughly deeper than 30 m T.P. level. Based on the results, the

following guideline for pile foundation design was determined such that:

1. The layer at 30 m T.P level was judged as an effective bearing stratum for driving the pile foundation. A steel pipe sheet-pile foundation was selected as a type of pile foundation in this project, where, all of pile tips are set up in Pleistocene laminated ground at around 30 m T.P. levels. 2) As shown in Figures 4 and 5, the scatters of N-values seems not to be small and also it is not easier to distinguish from the sandy and clayey layers from N-values obtained because the site consists of a complicated laminated sandy and clayey layers. In this circumstances, the uniform and empirical method based on the N-values is not rational and precise to evaluate the pile bearing capacity. Thus, a method for evaluating the pile vertical bearing capacity should be introduced together with a proper geotechnical engineering map for foundation design, which is derived by geotechnical considerations based on the results of the large numbers of in-situ and laboratory tests. The resultant geotechnical engineering map and the soil constants of each layers as characteristic values are summarized in Figure 6 and Table 1, in which the soil constants are mainly obtained by the standard consolidation and triaxial undrained and drained compression tests. The detail derived process and explanation have already been reported by Ochiai and Yasufuku(2003). 3) Full-scale pile load tests are conducted to confirm the validity of the predicting method used for foundation design. The possibility of reducing the safety factor for design to 2.5 from 3.0 is considered through the geotechnical point of view based on the field investigations, laboratory test results and the accuracy of the predicting method with full scale pile load tests.

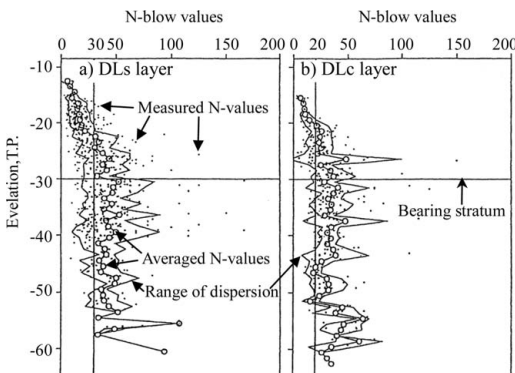


Figure 5. Distribution of N-values in DL layer against depth.

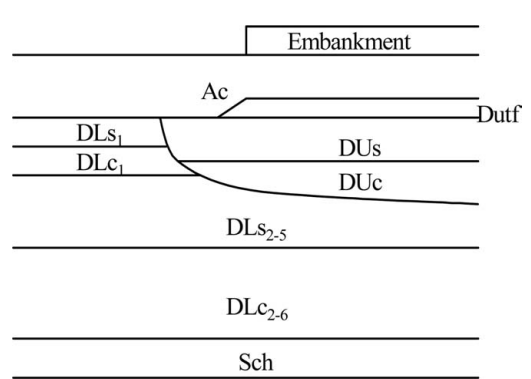


Figure 6. Model geotechnical engineering map for design.

Table 1. Soil constants of each layer.

		Strength parameters					
		N-value	γ' (tf/cm ³)	c' (tf/m ²)	ϕ' (degs.)	ϕ'_{cv} (degs.)	OCR*
Alluvial clay	AC	0.0	0.53	0.292	0.0	33.0	1
Pleistocene (Upper)	Volcanic	Dutf	11.0	0.66	0.6	30.0	33.7
	Sandy	DUs	30.4	0.90	0.0	37.0	34.6
	Clayey	DUc	0.0	0.53	8.1	24.0	36.9
Pleistocene (Lower)	Sandy	DLS ₁	17.0	0.90	2.6	35.4	35.7
		DLS ₂₋₅	40.0	0.53	5.5	32.6	35.7
	Clayey	DLC ₁	27.0	0.94	2.6	34.8	35.5
		DLC ₂₋₆	32.4	0.97	4.4	29.6	36.4
	Gravel	DLg	47.5	0.99	0.0	36.0	1
Metamorphic rocks		Sch-w	29.7	0.90	5.7	22.7	—
		Sch	98.3	0.90	5.7	22.7	1

* OCR is strongly dependent on the depth.

4 EVALUATION OF VERTICAL BEARING CAPACITY OF DRIVEN PILES

4.1 Basic idea

Specification for Highway Bridge gives a following equation as an estimating method of the ultimate pile bearing capacity based on the results of the field and laboratory investigations (JRA, 1996):

$$R_u = U \sum L_i f_i + q_d A \quad (1)$$

Where R_u : ultimate bearing capacity of pile, A : pile tip area, q_d : pile end bearing capacity, U : pile circumference, L_i : thickness in each layer, f_i : maximum skin friction of pile. The first and second terms are related to the skin friction of pile and pile-tip bearing capacity, respectively. However, the main part of the vertical bearing capacity of a pile is often mobilized from the skin friction in practical designs within the limits of allowable displacement, because relatively large displacements are needed to mobilize the end bearing capacity. In addition, as a normal open-end pile is used as a type of pile foundation, the end bearing capacity strongly depends on the degree of the blockade effect and thus the precise prediction of the end bearing capacity was considered to be quite difficult. Then, as shown in Figure 7, the skin friction mobilized through the internal face of the pile under the bearing stratum was assumed as the equivalent end bearing capacity in the design. Therefore, the second term $q_d A$ is expressed as $U \Delta L f_i$.

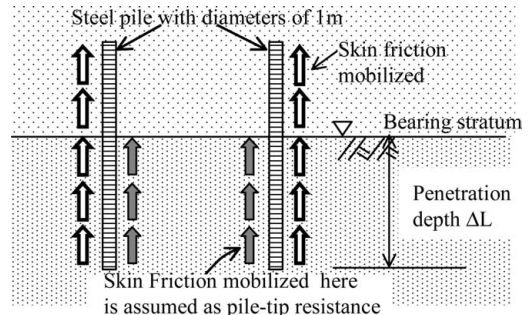


Figure 7. Basic idea of pile bearing capacity.

4.2 Evaluation of skin friction

4.2.1 Basic equation

The following basic equation is therefore used for calculating the skin friction of piles which is determined as the sum of pile to soil adhesion and friction components:

$$f = c'_s + \sigma'_h \tan \phi'_s \quad (2)$$

where, c'_s and ϕ'_s are the adhesion and friction parameters between pile and soil, and σ'_h is the effective lateral stress acting on the pile.

4.2.2 Soil constants as characteristic values

An idea that the adhesion between pile and soils is roughly equal to the apparent cohesion of soils c' is

widely used for a practical design. It is mentioned that the applicability of this idea is effective, irrespective of type of soils such as clay and sand (e.g. Tomlinson, 1980). Therefore, c'_δ in eq. (2) was assumed to be equal to the apparent cohesion of soils surrounding the pile such that:

$$c'_\delta = c' \quad (3)$$

In practical design, the axial pile capacity is estimated for the settlements of approximately 10% of the pile diameter. The 10% settlements usually exceed those for mobilizing the maximum skin friction of pile. Further, when considering that the mobilized mechanism of skin friction between pile and soils surrounding the pile, it is reasonable to use the friction angles at the critical state corresponding to sufficiently large displacement ϕ'_{cv} as ϕ'_δ (Yasufuku et al., 1997). Here ϕ'_δ is assumed to be conservatively two-third of $\phi' \cdot \phi'_\delta$ is thus given by

$$\phi'_\delta = \frac{2}{3} \phi' \quad (4)$$

where, ϕ' : effective friction angle at peak strength state.

4.2.3 Coefficient of lateral effective stress

The mobilization of the skin friction is dependent on the lateral effective stress σ'_h and thus in turn is dependent on the overburden pressure σ'_v . When considering σ'_h is given by $K\sigma'_v$, Eq.(2) is rewritten by

$$f = c'_\delta + K\sigma'_v \tan \phi'_\delta \quad (5)$$

K is a coefficient of lateral effective stress and σ'_v is vertical effective stress. The coefficient of lateral effective stress K was estimated from the previous research findings related to the K_0 -value. K -values in Pleistocene clayey layers were determined by the following equation (Mayne and Kulhawy, 1982).

$$K = (1 - \sin \phi') \text{OCR}^{\sin \phi'} \quad (6)$$

where, OCR is over-consolidation ratio defined as the ratio of the consolidation yield stress p_c to the overburden pressure σ'_v . Figure 8 shows the measured values of OCR, ϕ' in average and the calculated K -values in Eq.(6) against elevation. It is clear that applying this equation into the Pleistocene clayey layers, most of K -values became more than 1.0. Based on the experimental evidence, K -value for design was decided as 1.0, irrespective of type of Pleistocene layers. Thus, the presented model for evaluating the vertical bearing capacity is expressed as

$$R_u = U \sum L_i f_i + U \Delta L f_i \quad (7)$$

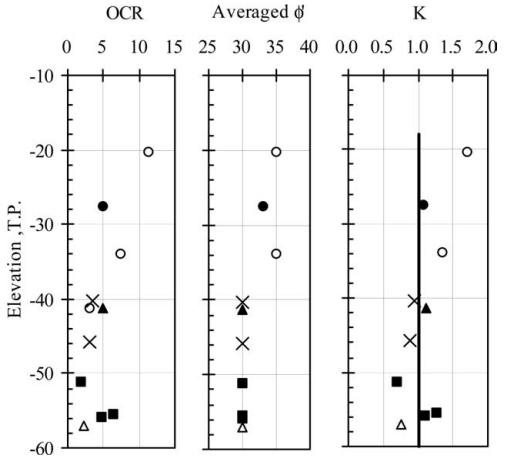


Figure 8. Measured values of OCR, ϕ' and calculated K -values against elevation from T.P. level.

$$f_i = c' + 1.0 \gamma' z \tan \left(\frac{2}{3} \phi' \right) \quad (8)$$

where, z is an arbitrary depth from the surface and ΔL is a penetration depth from the bearing stratum (see Fig. 7).

5 VERIFICATION OF VERTICAL BEARING CAPACITY OF DRIVEN PILES

In order to verify the applicability of the presented model and to confirm the characteristics of the pile bearing capacity of each layer, full scale pile load tests were conducted at two representative sites, which locate at 12P and 22P sites shown in Figure 4. As an important engineering judgment in this project, the reduction of the factor of safety from 3.0 to 2.5 for pile foundation design was discussed through comparing the predicted results with the results of full scale pile load tests.

Figure 9 shows the soil profiles and N values with depth for 12P site. N-values can be seen to widely change with depth from nearly zero to more than 20 and also N-values at pile tips are roughly 30. The steel piles with a diameter of 1.0 m were carefully driven using vibration and hydraulic hummers. The effective length of each pile was about 30 m. Tests were conducted based on the multi-cycles method, which is recommended by the JGS (1993). Four strain gauges were located at each of the cross sections as shown by the dots in Figure 9.

Figure 10 shows the comparison of the estimating total vertical bearing capacities with those of full-scale pile load tests at 12P and 22P sites, in which

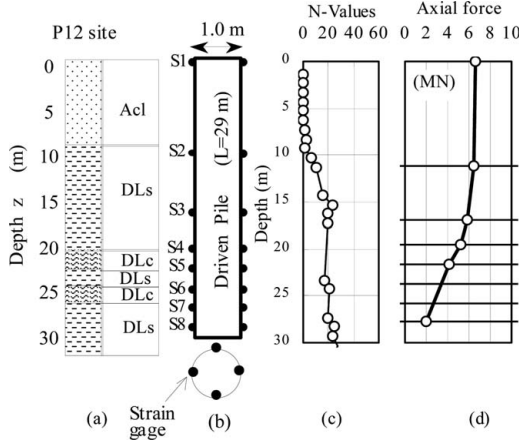


Figure 9. Soil profile, N-values and measured axial force in pile load test at P12 site.

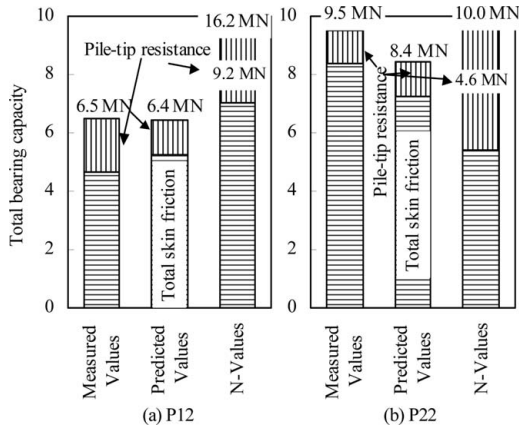


Figure 10. Comparison of predicted total bearing capacities with those of pile load tests.

Eqs (7) and (8) was used to calculate the predicted values. The bearing capacity calculated by the empirical model based on the measured N-values recommended by JRA is also depicted in this figure. The model used here can reasonably estimate both total skin friction and pile tip resistance at both sites, comparing with those from JRA recommendation. As shown in Table 1 and Figure 4, we have a clear grasp of the soil characteristics values for each layer and a practically efficient geotechnical profile. Therefore, the model can apply very well to evaluate the pile bearing capacity according to the ground profile at each site, with the consequence that the accuracy of the prediction clearly increased and these facts became an important evidence to reduce the factor of safety for pile foundation design from 3.0 to 2.5.

Table 2. Total cost benefit.

	Method by N-values	Method proposed here
Cost for geotechnical investigations*	1	2.11
Construction cost of piles	1	0.82
Total cost	1	0.84

The cost includes full scale load tests.

6 EFFECT OF A REDUCTION IN TOTAL COSTS

The comparison of the cost performance in terms of the construction of pile foundations driven in P1 to P24 sites is summarized in Table 2, which is a result of trial calculation. Note that the cost is normalized by the cost obtained by the standard manner for evaluating the pile bearing capacity using N-values (JRA, 1993) without any full scale pile load tests. For comparison, the layer of the bearing stratum for each case was assumed to be same, however, the penetration depth ΔL was considered to depend on the calculation manner. Total cost are divided by 2 parts, in which one is the part for the cost related to the geotechnical investigations which include in-situ and laboratory soil tests, and full scale pile load tests, and the other is related to the normalized total pile construction cost in terms of P1 to P24 piers. The presented manner used here is expected to cut the cost more than 15% comparing with the total cost by the standard approach using N-values. Thus even if the cost of the geotechnical investigations became roughly two times higher comparing with the general manner, the appropriate in-situ and laboratory investigation with a reasonable considerations can reduce the total cost in the project, because they produced the highly accurate ground profile and the proper evaluation method of pile bearing capacity and also the full scale pile load tests gave the decreasing factor of safety from 3.0 to 2.5. It is believed that the geotechnical considerations and manner treated here can give an important information for the geotechnical investigators, structural designers and construction engineers.

7 CONCLUSIONS

An importance of integrating the geotechnical investigations with pile foundation design was clarified through a case study in terms of investigation, design and construction of the connecting bridge for New-Kitakyushu airport. The following major conclusions were drawn:

- 1) A rational method for evaluating the pile bearing capacity was presented which reflected the soil

- characteristic values and geological environmental history. In addition, the applicability of the presented method was confirmed through full-scale pile load tests, with the consequence that the safety factors for pile foundation design were reduced from 3.0 to 2.5.
- 2) In-situ and laboratory investigation with reasonable geotechnical considerations can reduce the total cost of the construction of the bridge for New-Kitakyushu airport.

REFERENCES

- JSSMFE. 1993. *Standards for Vertical Load Tests of Piles*: 113–121.
- Japan Road Association. 1996. *Specifications for Highway Bridge Part IV*: 330–337(in Japanese).
- Mayne, P.W. & Kulhawy, F.H. 1982. K_0 -OCR relationships in soils. *J. Geotech. Eng. Div. ASCE*. 108(GT6): 851–872.
- Ochiai, H. & Yasufuku, N. 2003. Investigation, design and construction of the connecting bridge for New-Kitakyushu airport. *9th Annual Meeting of Chinese Soil Mechanics and Geotechnical Engineering*. Vol.1: 214–22

Numerical prediction for long-term displacements of pile foundation

K. Danno & K. Isobe

Department of Urban Management, Kyoto University, Kyoto, Japan

M. Kimura

International Innovation Center, Kyoto University, Kyoto, Japan

ABSTRACT: Recent introduction of performance-based design into infrastructure, including pile foundation, is on process. For performance-based design, it is necessary to develop the practical prediction method for long-term displacements of pile foundation. In this paper, the applicability of soil-water coupling FEM with the pile model which can express pile volume is validated in comparison with actual load test. And the prediction of long-term displacements of actual pile foundation with soil-water coupling analysis is conducted.

1 GENERAL INSTRUCTIONS

1.1 Research background

Recently, an introduction of performance-based design into infrastructure is on process. It means that, in pile foundation, we have to examine not only bearing capacity, but also displacements occurring in usual time and in emergency time. For performance-based design of pile foundation, it is necessary to develop practical prediction method for long-term displacements of pile foundation.

Many prediction methods have been proposed, however, they still need to be developed, because of the difficulty in considering the interaction of pile-soil-pile system and complicated ground condition. At present, it is seemed that FEM is the most powerful method to predict the long-term displacements of pile foundation, which can solve above problems.

1.2 The applicability of FEM

In the analysis using FEM, it is rather easy to consider the complicated ground condition, if appropriate constitutive model is chosen. But it is still a problem how to express the pile volume.

Generally, there are two ways in pile modeling method using FEM. One is method with solid element, and the other is with beam element.

In solid element method, pile volume is expressed by solid element. But usually, the solid element is modeled as linear elastic model and it is hard to consider non-linear behavior of pile, such as bending.

In beam element method, it is pretty easy to calculate the non-linear behavior of pile. But it is difficult to express pile volume. In this method, the rigidity of pile is concentrated into beam element, and the stress transmitted through pile is concentrated at the node shared by soil element and beam element. This stress-concentration leads to over-deformation.

In this paper, the pile model which is able to express pile volume in FEM is adopted. The model is composed as combination of beam elements, like framed structure. The behavior of actual pile is considered by the beam element at the heart of pile body. The node positioned at heart of pile is jointed with other nodes composing pile body by rigid beam elements. The displacements of the nodes composing pile body follow the displacements of the node at heart of pile, and the Navier hypothesis is satisfied. The elements composing pile body are assumed to be elastic body, whose rigidity is assumed to be 1/10 times smaller than the beam element at the heart of pile, according to the concept of hybrid element (Zhang et al, 2000). Through this modeling, the pile volume is fully considered (shown in Figure 1).

The applicability of FEM with the adopted pile model is validated through comparison of numerical prediction by FEM and actual load tests. Further more, the numerical prediction of long-term displacements of actual pile foundation with soil-water coupling FEM is conducted. The pile foundation is actual pile foundation of load viaduct, now under design for the expansion of Nihonkai Tohoku Highway in Murakami-shi, Niigata Prefecture, Japan. As a result, the long-term behavior of pile foundation, the mechanism of uneven

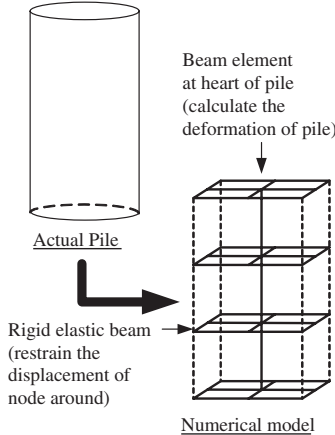


Figure 1. The concept of adopted pile model.

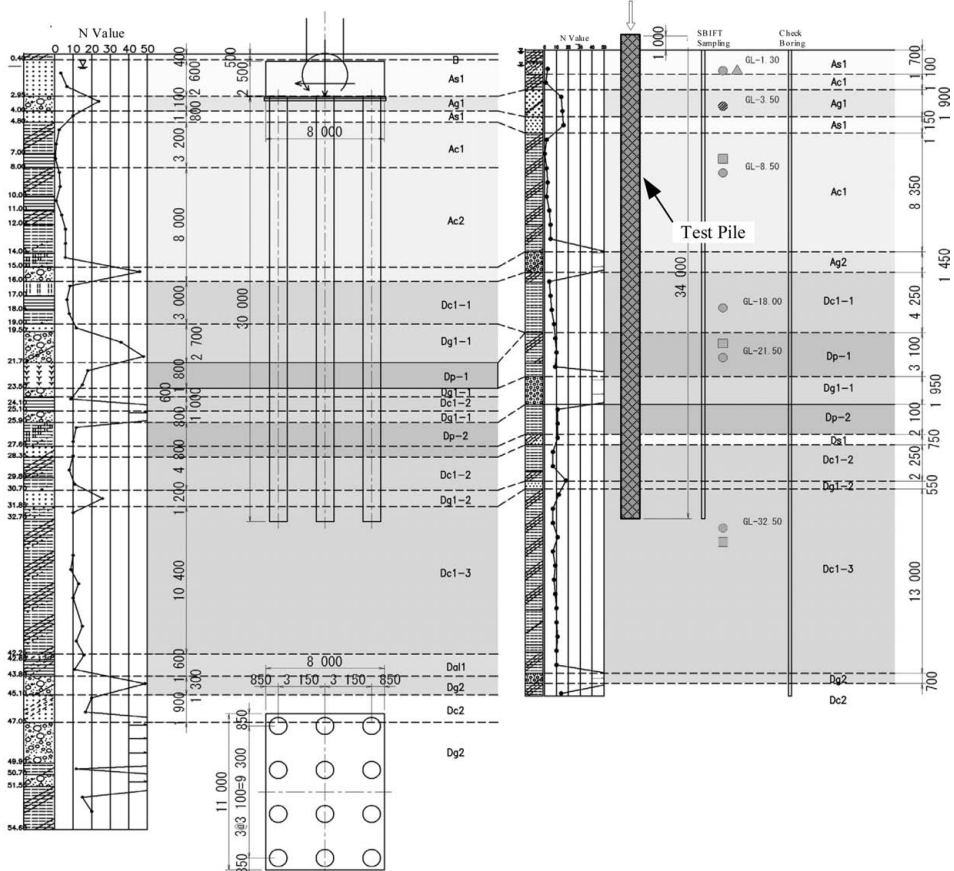
settlement, the load sharing system in pile foundation is clarified.

2 VALIDATION OF NUMERICAL MODEL

2.1 Actual load tests for single pile

The actual load tests were conducted to examine the long-term stability of designed pile foundation in advance. The designed pile foundation above mentioned (named P28 viaduct foundation) is close to rail way structure, however, the load test was conducted at the P29 ground, which is nearby P28 ground. The geotechnical condition of the grounds is shown in Figure 2.

The pile is designed as steel tube pipe pile with soil cement, which is injected into inner space of pile and also outer space (the thickness is 100 mm).



(a) P28 ground and designed pile foundation

(b) P29 ground

Figure 2. Geotechnical condition.

The load tests were planned to be conducted as; (1) long-term load test (examination of long-term stability), (2) short-term load test (examination of bearing capacity), (3) horizontal load test (examination of horizontal resistance of the ground).

2.2 Numerical prediction of the load tests

The prediction with soil-water coupling FEM is conducted by using ‘DGPILE-3D’, numerical analysis code developed by Kimura & Zhang (2000). The applicability of DGPILE-3D for static and dynamic problem has been validated through many practical numerical analyses.

The constitutive model for soils is *subloading* t_{ij} model (Nakai & Hinokio, 2004), which is able to express the behavior of normally and over-consolidated soils. The soil parameters are determined by tri-axial compression test under constant minor principal stress and consolidation test. The soil parameters are shown in Table 1.

The pile is modeled by the modeling method above mentioned (see Figure 1). The parameters are determined by the property of the material used for pile (shown in Table 2). The pile body is assumed to be non-permeable element.

The boundary condition is assumed as following; the ground surface is drained while the bottom and the side of the ground are non-drained. The boundary condition of displacement is assumed to be; fixed at

the bottom, free at the ground surface and roller at the side boundaries.

2.3 Result of validation

The loading condition and the displacements of pile in all load tests are shown in Figure 3 to Figure 5. All results in Figure 5 to Figure 7 are shown as comparison between computed results and observed results.

Figure 3 (a) and (b) shows the loading condition and the displacement at pile head in long-term load test. The calculated displacement over-estimates observed displacement a little, but the calculation express the behavior of actual pile appropriately.

Table 2. Parameters of pile model.

(a) Parameters of beam element

EA [kN]	EI [kN-m]	M _y [kN-m]	Poisson's ratio
1.31 × 10 ⁷	1.35 × 10 ⁶	3996	0.20

(b) Parameters of solid element

E [kN/m ²]	I [m ⁴]	γ [kg/m ²]	Poisson's ratio
8.71 × 10 ⁵	0.173	8.08	0.20

Table. 1. Parameters of soils.

N	Value	Thickness m	Density g/cm ³	E ₀ kN/m ²	I _p	ϕ	λ	κ	K ₀	ν	k m/sec	e ₀	OCR
As1-1	3	1.70	1.83	2.11e4	—	33.1	3.80e-3	2.80e-3	0.50	0.30	1.00e-06	1.00	10.0
Ac1	1	1.10	1.84	—	45.5	25.1	3.04e-1	4.14e-2	0.63	0.30	1.20e-09	1.68	4.31
Ag1	14	1.90	1.94	4.89e4	—	23.4	1.50e-3	1.20e-3	0.50	0.30	1.00e-04	0.65	20.0
As1-2	16	1.15	1.73	6.35e4	—	36.0	1.40e-3	1.00e-3	0.50	0.30	1.00e-06	0.85	20.0
Ac1	2	8.35	1.63	—	40.7	25.8	1.65e-1	1.73e-2	0.57	0.30	8.23e-10	1.10	4.00
Ag2	60	1.45	1.94	1.40e5	—	39.8	1.60e-3	1.20e-3	0.50	0.30	1.00e-04	0.65	20.0
Dc1-1	6	4.25	1.73	—	34.8	26.8	2.13e-1	4.07e-2	0.59	0.30	2.95e-10	1.24	2.45
Dp-1	9	3.10	1.58	—	65.9	38.2	6.90e-1	7.20e-3	0.38	0.30	1.02e-09	2.69	1.80
Dg1-1	108	1.95	2.04	1.40e4	—	39.8	2.00e-3	1.70e-3	0.50	0.30	1.00e-04	0.65	20.0
Dp-2	11	2.10	1.73	—	45.8	25.0	1.56e-1	7.90e-3	0.63	0.30	3.69e-10	0.92	2.82
Ds1	11	0.75	1.94	1.90e4	—	30.2	1.60e-2	1.20e-2	0.50	0.30	1.00e-06	0.85	20.0
Dc1-2	7	2.25	1.73	—	45.8	25.0	1.56e-1	7.90e-3	0.63	0.30	2.48e-10	0.92	2.63
Dg1-2	18	0.55	2.04	2.88e4	—	32.2	1.20e-2	8.00e-3	0.50	0.30	1.00e-04	0.65	20.0
Dc1-3	9	13.00	1.83	—	33.4	27.2	2.00e-1	3.17e-2	0.54	0.30	4.87e-10	1.08	1.82
Dg2	49	0.70	2.04	5.68e5	—	35.5	1.00e-2	6.00e-3	0.50	0.30	1.00e-04	0.65	20.0
Dc2	14	0.70	1.84	—	32.0	27.3	2.39e-1	2.76e-2	0.57	0.30	7.32e-11	1.21	1.16

(Above parameters are written by averaged value in each soil layer).

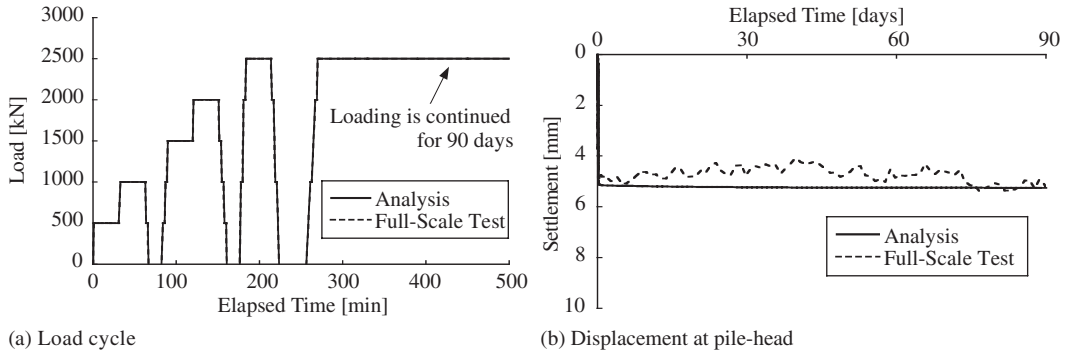


Figure 3. Long-term load test.

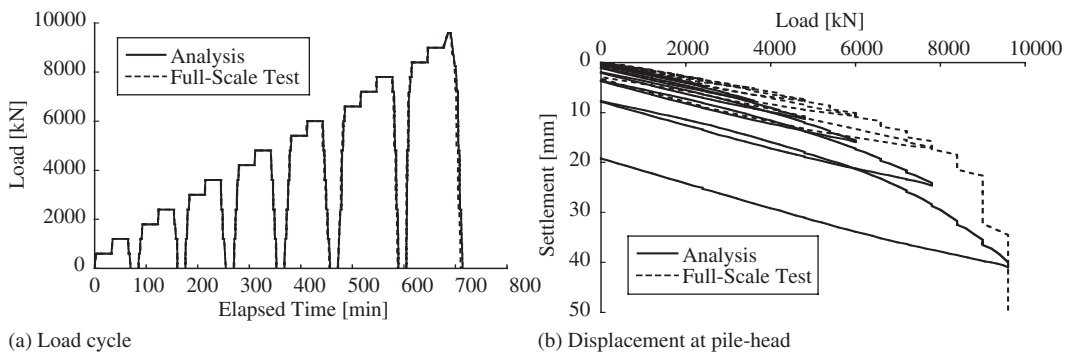


Figure 4. Short-term load test.

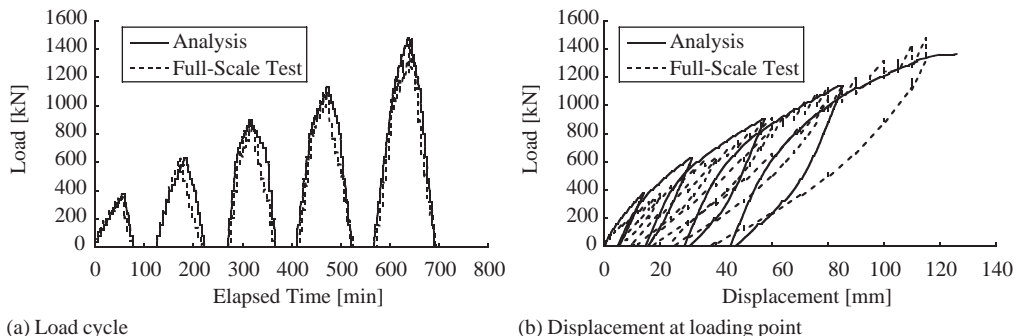


Figure 5. Horizontal load test.

Figure 4 (a) and (b) shows the loading condition and the displacement at pile head in short-term load test. The calculated displacement over-estimates the observed displacement a little, as same as in long-term load test. The rebound of displacement is rather under-estimated in computation. It is considered that, the boundary condition of pile body in the calculation,

which is assumed to be non-drained, is different from the actual condition. Actually, the permeability around pile is likely to increase due to the sliding of the pile. In the calculation, which is under completely non-drained condition around pile body, the deformation of soil around pile body is restrained because of the continuity of water.

Figure 5 (a) and (b) shows the loading condition and displacement at loading point. In the area of the displacement under 30 mm, the computed result overestimated the observed result a little. In the area of displacement of 30 mm to 80 mm, the difference between both results becomes small, and in the area of displacement over 80 mm, the computed result underestimated the observed result. This is caused by the characteristic of the constitutive model for soils.

Subloading t_{ij} model is able to consider the shear force dependency to stress, and the rigidity is underestimated under low stress like in the soil layer nearby ground surface.

2.4 Conclusions

The validation of FEM with adopted pile model is conducted through comparison of actual load tests and numerical prediction. Using appropriate constitutive model for soils, soil parameter, pile model and pile parameter, the behavior of actual pile is expressed not only qualitatively but also quantitatively.

3 NUMERICAL PREDICTION OF LONG-TERM DISPLACEMENTS OF PILE FOUNDATION

3.1 Design of pile foundation

The pile foundation targeted in numerical prediction is planned to be constructed for load viaduct of Nihonkai Tohoku Highway at Murakami-shi, Niigata Prefecture, Japan. The ground is very soft clayed ground, because it was originally seashore-lake, and land reclamation was done 200 years ago. Considering the ground condition, the pile foundation is designed as frictional pile. But complete obeying the design standard leads to increase in construction expense, because in the design of frictional pile, the end-bearing capacity is not

expected and there is need to adopt a high safety rate for bearing capacity and number of pile or pile length increases in order to satisfy designing allowable bearing capacity.

But if the displacement occurring in the future is predicted appropriately in advance, and some displacement is allowed to occur within the range where harmful displacements for super-structure does not occur, it is possible to expect end-bearing capacity and adopt low safety rate using in the design of end-bearing pile. This leads to decrease the number of pile or the length of pile, and the rationalization in construction expense or in structuring becomes possible (The pile foundation designed under this concept is called ‘Rationalized Pile’).

To design rationalized pile foundation, there is need to predict long-term displacements occurring in the future in advance. In this chapter, the result of numerical prediction is reported. The long-term stability and the appropriateness of rationalized pile foundation are estimated.

3.2 Numerical condition of the analysis

Numerical conditions, including numerical code, constitutive model and soil parameters, pile model and pile parameters are the same as previous chapter. The boundary condition is also the same as previous chapter. The loading condition is assumed to obey actual construction process.

3.3 Result of numerical prediction

Figure 6 shows the settlement curve at pile-head up to 700 days and 50 years. The displacements are same at all point because of the rigidity of footing. The amount of settlement is 22 mm just at completion of construction (251 days), and 45 mm at 50 years. Under completely non-drained condition at side boundaries, the consolidation settlement has at most 50% finished just

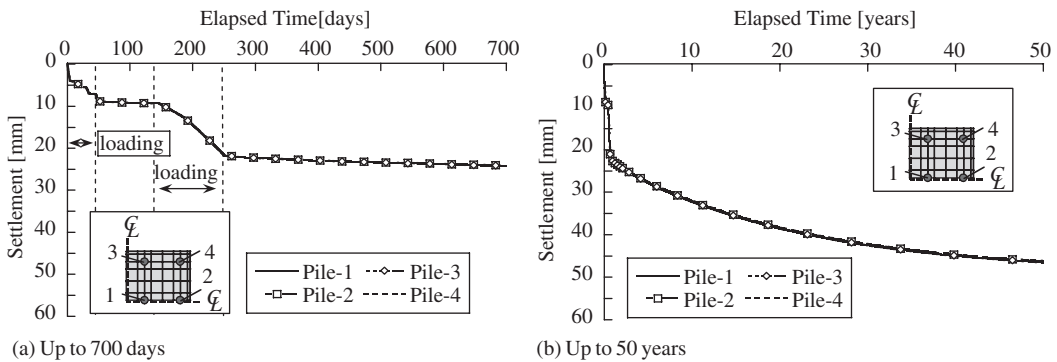


Figure 6. Settlement curve at pile-heads.

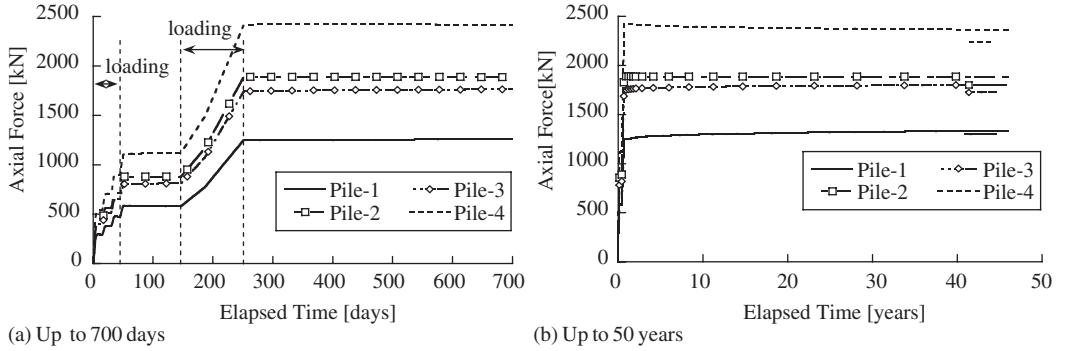


Figure 7. Changing of shared load by piles.

at completion of construction. If there is some problem with permeability of ground, there is need to pay attention for the progress of settlement. In this case, however, the settlement is at most 45 mm, and that is possible to respond by simple maintaining method. It is said that the design with rationalized pile is appropriate in this case.

Figure 7 shows the changing of shared load by piles (=axial force occurring at pile just under footing). According to loading, the shared load by Pile-4 (outer pile) increases, and the shared load is the largest among piles. The shared loads are Pile-4 > Pile-2 > Pile-3 > Pile-1, and the shared load by pile increases when distance from the center of pile increases. Usually, piles are designed assuming that each pile share the same load. It is necessary to consider this mechanical behavior of load sharing by piles when designing pile foundation.

Figure 8 shows the distribution of excess pore water pressure (=EPWP) at completion of construction. It is shown that big EPWP remains around the end of inner pile. This is caused by the emphasis of stress transmitted by pile-end. In this analysis, uneven settlement is not observed because the rigidity of footing is assumed to be enough high. But in actual foundation, where the footing is rather soft, there is a possibility of uneven settlement occurring. Considering this mechanism of EPWP occurring, the completion of consolidation settlement near the center of pile foundation delays from around. There is a possibility of the settlement of inner pile-head becoming larger than outer pile due to the emphasis of stress transmitted from pile-end and delayed dissipation of EPWP. This is important notice to manage settlement of pile foundation.

3.4 Conclusions

In this pile foundation, the settlement predicted likely to occur in the future is within allowable range, and the concept of rationalized pile is confirmed to be

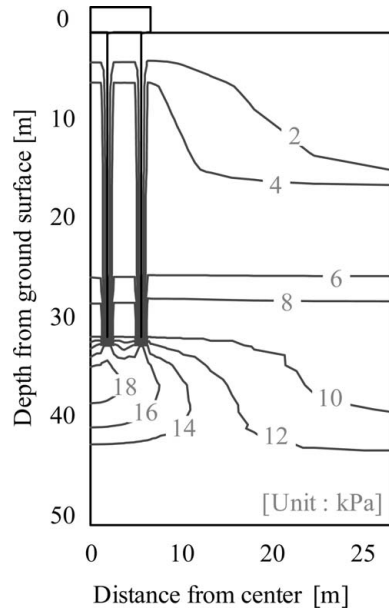


Figure 8. Distribution of Excess Pore Water Pressure.

efficient in this case. Further more, the load sharing system (outer pile shares larger load than inner pile) and mechanical behavior of uneven settlement (larger settlement is likely to occur in inner pile than in outer pile) are clarified.

4 SUMMARY

In this paper, the applicability of soil-water coupling FEM with the pile model which can express pile volume appropriately is validated through comparison of actual

load tests and numerical prediction. Further more, the long-term stability of pile foundation is examined by numerical analysis with soil-water coupling FEM, using the same numerical model.

The finding obtained from the validation is as follows.

(1) FEM with the adopted pile model is able to express the behavior of actual single pile.

The findings obtained from the numerical prediction of long-term displacements of pile foundation are as follows.

(2) Under completely non-drained condition at side boundaries, the consolidation settlement has at most 50% finished just at completion of construction. If there is some problem with permeability of ground, there is need to pay attention to the progress of settlement.

(3) The settlement predicted by calculation is within the range of allowable displacements. The concept of rationalized pile is efficient in this case.

(4) In pile foundation, outer pile share larger load than inner pile.

(5) Large EPWP occurs around pile-end of inner pile and the completion of consolidation settlement of soils around inner pile-end delay from soils around outer pile-end, because of the emphasis of pile-end stress and delay of dissipation of EPWP. This phenomenon can possibly lead to the occurrence of

uneven settlement, and the settlement at inner pile-head will be bigger than outer pile.

ACKNOWLEDGEMENT

In conducting numerical simulation, a lot of helpful advice about FEM analysis is given by Professor Feng Zhang (Nagoya Institute of Technology, JAPAN).

The actual load tests for single pile have been conducted by East Nippon Expressway Company Limited (JAPAN) and Expressway Technology Center Foundation (JAPAN).

We are very thankful to the parties concerned to this study on this occasion.

REFERENCES

- Zhang, F., Kimura, M., Nakai, T. & Hoshikawa, T. 2000. Mechanical Behavior of Pile Foundations Subjected to Cyclic Lateral Loading Up to the Ultimate State. *Soils and Foundations* 40(5): 1–17.
- Kimura, M. & Zhang, F. 2000. Seismic Evaluations of Pile Foundations with Three Different Methods based on Three-Dimensional Elasto-Plastic Finite Element Analysis. *Soils and Foundations* 40(5): 113–132.
- Nakai, T. & Hinokio, M. 2004. A Simple Elastoplastic Model for Normally and Over Consolidated Soils with Unified Material Parameters. *Soils and Foundations* 44(2): 53–70.

Side resistance of piles considering strain levels

M. Suzuki

Shimizu Corporation, Tokyo, Japan

M. Shirato, S. Nakatani & K. Matsui

Public Works Research Institute, Tsukuba, Japan

ABSTRACT: This paper describes how to draft a formula for estimating the side resistance of a pile by reviewing a great number of in situ pile loading tests conducted in the past. This will improve the formula used in the current Specifications, which is considered to be an overestimation. Furthermore, the magnitude of safety margin excluding the safety factor of the current Specifications is also unclear. The reliabilities of two SPT-N values normalized unit side resistances in each layer are examined: f_y/N at the yield point of a P_o-S_o curve and f_p/N at the peak side resistance, by using the reliability index, β . The results show that f_y/N has higher reliability than f_p/N ; this finding should be useful when revising the Specifications in the near future.

1 INTRODUCTION

“Specifications for Highway Bridges, Part IV: Substructures” is the Japanese mandatory code for designing bridge foundations, and provides various formulae for estimating the pile resistance. Recently, these have been proposed by empirical formulae based on the results of a large number of in situ pile loading tests. This is mainly because geotechnical theories cannot accurately estimate the actual bearing resistance of piles derived from in situ tests due to the complexity of ground conditions in Japan and so on. When drafting a new empirical formula for the Specifications, we need to use reliability theory since the magnitude of the maximum loads in the tests are all different and/or most test piles have uncertainty in estimating their resistance behavior.

When considering the effectiveness of an in situ pile loading test, we need to consider information on the magnitude of the maximum load and with or without measurement devices such as strain-meters for the division of side and base resistances. Recent research has shown that the ultimate bearing resistances of piles are mobilized at the displacement of more than 10% of the pile diameter at the pile top in in situ loading tests. The magnitude of the maximum load, which causes displacement of more than 10% of the pile diameter, should be ideal in the tests, accordingly. Furthermore, test piles often have measurement devices for the division of resistances. On the other hand, most loading tests in the past were performed to confirm the design resistance (= allowable resistance \times safety factor),

and so their magnitude of the maximum loads were relatively small (in general, displacement of up to 2 to 5% of pile diameter). However, we need to adopt the data of even these tests in order to increase the number of tests for analyzing the pile resistance provided that information on the division of resistances is available.

The mechanism of resistance of the mobilized ultimate resistance of a pile is complex. We know that the resistance of a pile can reach its ultimate value with the displacement of 10% of the pile diameter, and that the side and base resistances do not increase in proportion to the load at the pile top up to the ultimate value. Side resistance reaches its ultimate value at a displacement of just under 5% of the pile diameter whereas the base resistance continues to increase at more than 10%. Taking account of this behavior, there may be a relationship between the peak of the side resistance and yield point of a load P_o -displacement S_o curve at the pile top. The relationship has not been well understood because there have been few in situ loading tests with fully mobilized side resistance and indefinite yield point of the curve, so we tried to quantify the relationship by using reliability theory.

In this paper, we describe how to draft a formula for estimating the side resistance of a pile by reviewing a great number of in situ pile loading tests conducted in the past. This will improve the formula given in the current Specifications, which is considered to be an overestimation due to the fact that design values of the unit side resistance normalized by the average SPT-N value in each layer (f_d/N) were determined by respective peak values from the relation of unit side

resistance, f , to displacement, S , in each layer. Furthermore, the magnitude of the safety margin excluding the safety factor in the current Specifications is unclear.

We examine the reliability of two SPT- N value normalized unit side resistances in each layer: f_y/N at the yield point of a P_o-S_o curve and f_p/N at the peak side resistance at pile tops based on the in situ pile test results, by using the reliability index, β .

2 RESULTS OF PILE LOADING TEST

Design values of the unit side resistance by an average SPT- N value (f_d/N) provided as estimation formulae in the Specifications were determined by selecting respective peak values of unit side resistances in each layer from the relation of the unit side resistance, f , and displacement, S , during a test. Consequently, it has been pointed out that estimated side resistances using f_d/N tend to overestimate the resistances observed in the tests. To determine the yield point of the P_o-S_o curve, a Weibull curve as well as conventional methods such as the $\log P_o-\log S_o$ rule, were used here. It was found in advance of this analysis that yield points estimated by both methods were almost the same.

The resistances observed in the test piles based on past tests have been collected for the purpose above, in which SPP means driven steel piles and CCP means cast-in-place bored piles. These tests all had measurement devices for dividing the resistance into the side and base, although their magnitude of the maximum loads were different. In these tests, there are few test results with displacement of more than 10% of the pile diameter at pile tops, and there are not many results with displacement of more than the yield point of the P_o-S_o curve.

Figure 1 shows side views, including the axial forces in each section of the pile, A-4, with displacements of more than 10% of the pile diameter, and Figure 2 shows the relations of total resistance, P_o , at the pile top, base resistance, P_p , and side resistance P_f – displacement S_o at the pile top for A-4, in which dotted lines mean yield points of the P_o-S_o curves and chain lines mean peak values of side resistances. Figure 3 also shows P_o , P_p and P_f-S_o relations for A-1, which are typical piles with displacements of up to around 2 to 5% of the pile diameter. In Figure 3, no peak values (chain lines) but only yield points (dotted lines) are shown because the former was not observed due to the small magnitude of the maximum loads.

Figures 2 and 3 reveal the following: (1) peak side resistances are mobilized at the displacement of around 2 to 5% of the pile diameter, (2) base and total resistances increase in proportion to the increased load at the pile top with displacement of more than 10% of the pile diameter, and (3) total resistances

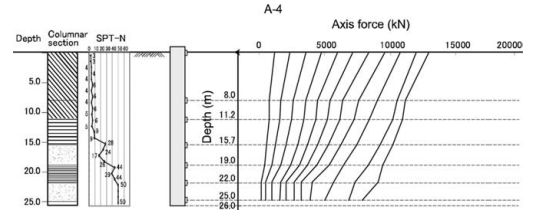


Figure 1. Distribution of pile axial forces (A-4).

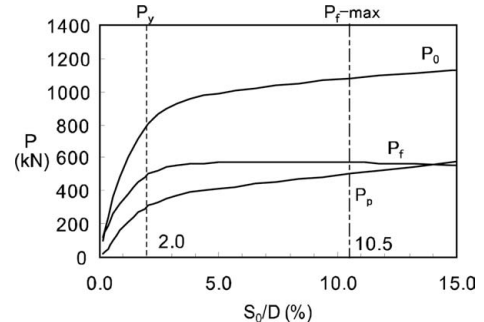


Figure 2. Total, base and side resistances of pile (A-4).

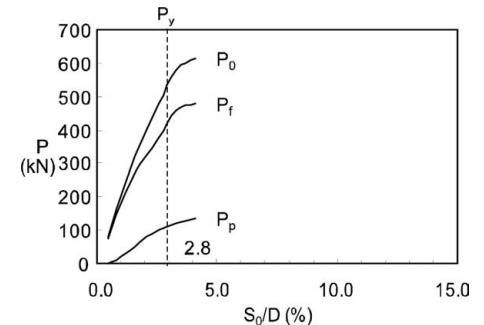


Figure 3. Total, base and side resistances of pile (A-1).

tend to yield at around the points where the peak side resistances are fully mobilized.

Figures 4 and 5 show the relations of unit side resistance by normalized by SPT- N value (f/N) – pile top displacement normalized by pile diameter (S_o/D) in each layer for piles A-4 and A-1, respectively, in which yield points (dotted lines) of P_o-S_o curves and peak values of side resistances (chain lines) are also shown. In these figures, the symbols As, Ac, Ds, and Dc mean alluvium sand, alluvium clay, diluvium sand and diluvium clay, respectively. As shown in these figures, we can obtain the yield point (f_y/N) but it is hard to find the peak value (f_p/N) of the side resistances compared to f_y/N .

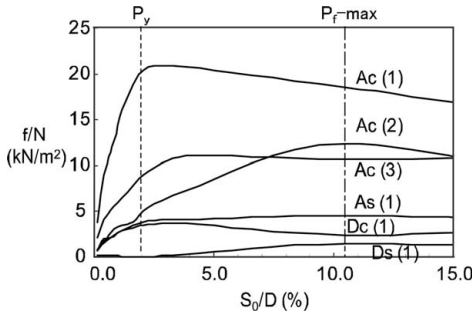


Figure 4. Unit side resistances of pile (A-4).

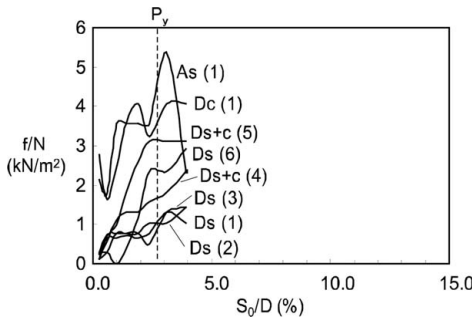


Figure 5. Unit side resistances of pile (A-1).

3 CHARACTERISTIC VALUES AND THEIR RELIABILITY INDICES

In this section, we examine the reliability of two SPT- N value normalized unit side resistances in each layer, f_y/N and f_p/N , by using the reliability index, β . Our research goal is to clarify which definition (f_y or f_p) is more reliable. Of course SPT- N values have large variability, but this fact is applicable to both f_y and f_p . Thus the effect of variability of SPT- N values can be incorporated into unit side resistances. Accordingly, we may only consider the variability of f_y and f_p as observed parameters even when we discuss the variability of f_y/N and f_p/N . The result shows that f_y/N has higher reliability than f_p/N .

Statistical values of f_y/N and f_p/N for each pile type and ground condition are shown in Table 1, in which 95% reliability lower levels of mean values (hereafter, characteristic values) from the mean values are also provided. The characteristic values are estimated by the following equation:

$$\hat{\mu}_{f/N} = \bar{x} - s \frac{t_{n-1}(1-\alpha)}{\sqrt{n}} \quad (1)$$

where, \bar{x} : sample mean, s : sample standard deviation, n : number of data, and t : t -distribution of confidence level $(1 - \alpha)$.

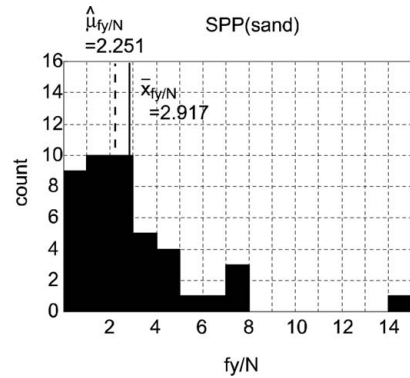


Figure 6(a). f_y/N histograms of pile type SPP.

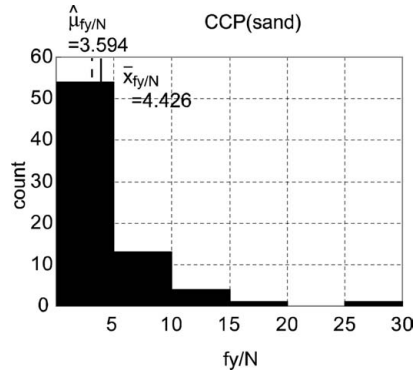


Figure 6(b). f_y/N histograms of pile type CCP.

Figures 6 and 7 show f_y/N and f_p/N histograms of pile types SPP and CCP for sand based on the values provided in Table 1. In these figures, sample mean values of $\bar{x}_{f_y/N}$ and $\bar{x}_{f_p/N}$ with full lines and characteristic values of $\hat{\mu}_{f_y/N}$ and $\hat{\mu}_{f_p/N}$ with dotted lines are also marked. With regard to the reduction ratio of the characteristic to mean values, those of f_p/N are greater than those of f_y/N because the number of the former is remarkably smaller than that of the latter.

In order to estimate the reliability of the resistances f_y/N and f_p/N , we first set up $(f_d/N)_d = 0.667$ by using current design values $f_d/N = 2$ and a safety factor (=3 for the persistent situation) in the case of SPP sand, for example. The safety margin can be estimated with the reliability index, β , considering the characteristic values and variation of f_y/N , f_p/N and $(f_d/N)_d$ as following:

$$\beta = \frac{\hat{\mu}_{f/N} - (f_d/N)_d}{\sigma_{f/N}} \quad (2)$$

where $\sigma_{f/N}$ is standard deviation of f_d/N . Here β means reliability in a component of pile segments.

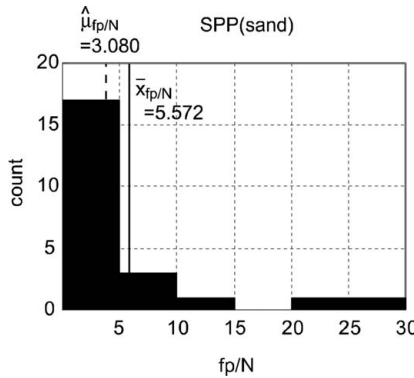


Figure 7(a). f_p/N histograms of pile type SPP.

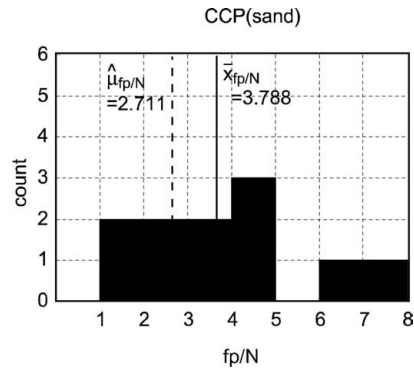


Figure 7(b). f_p/N histograms of pile type CCP.

Table 1. Statistics and reliability index of f/N .

pile	soil	No.	Ave.	St. dev.	COV	Characteristic value (95%)	β
f_y/N							
SPP	sand	44	2.917	2.629	0.901	2.251	0.603
	clay	41	10.084	9.861	0.978	7.524	0.425
CCP	sand	73	4.426	4.266	0.694	3.594	0.452
	clay	53	20.370	23.535	1.155	14.956	0.494
f_p/N							
SPP	sand	23	5.572	6.962	1.249	3.080	0.347
	clay	14	19.187	19.115	0.996	10.140	0.356
CCP	sand	11	3.788	1.470	0.520	2.711	0.530
	clay	5	13.707	4.276	0.312	9.630	1.472

In the case of SPP sand, f_p/N has a large β value derived from the small mean value and small variation whereas f_p/N has a small β value derived from the large mean value and large variation. The results of all

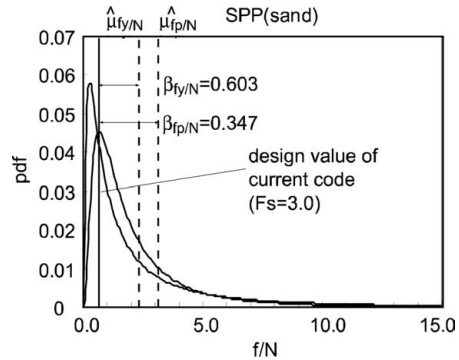


Figure 8. Reliability index of f_y/N and f_p/N of pile type SPP.

pile types (SPP and CCP) and soil types (sand and clay) are tabulated in Table 1 as follows:

1. f_y/N has a more stable safety margin than f_p/N because the β values of f_y/N are almost constant at 0.4 to 0.6 for every pile type and soil type, whereas the β values of f_p/N are small in the case of SPPs shown in Figure 8.
2. These f_y/N values correspond to 0.7 to 1.5 times the current design values in the Specifications.
3. High COVs are due to data of different population grouped together throughout Japan. These data were collected in the past for the setting up pile resistance formulae in the old-version Specifications.
4. When evaluating variation, CCP's f_p/N for sand and clay grounds is smaller than that of f_y/N .
5. In principle, it is desirable to select f_p/N rather than f_y/N as an index for estimating the side resistance of a pile. However, its statistical uncertainty becomes larger due to few test results with the peak value of the side resistance.
6. Most β values are so small. The following two reasons are considered: (1) The yield point of a P_o-S_o curve will be for use in the serviceability limit states, (2) Some of the COV are very high. The target β values of the serviceability limit states may be smaller than the β values of the ultimate limit states.

4 CONCLUSIONS

We examined the reliability of two SPT- N value normalized unit side resistances in each layer, f_y/N at the yield point of a P_o-S_o curve and f_p/N at the peak side resistance.

The main findings were as follows:

1. In the case of SPP, the mean value of f_p/N is larger than that of f_y/N by 90% whereas the characteristic

value (reduced from the mean value by considering the number of data) of f_p/N is larger than that of f_y/N by only 35%. In the case of CCP, on the contrary, reductions were 20 to 30% and 25 to 35% respectively.

2. With regard to the coefficient of variation, $V_{f_y}/N (= 0.7 \text{ to } 1.1)$ was smaller than $V_{f_p}/N (= 0.3 \text{ to } 1.2)$.
3. When comparing the reliability of f_y/N to f_p/N by using reliability index β , the former has a more stable safety margin than the latter because the β values of f_y/N are almost constant at 0.4 to 0.6 for every pile type (SPP and CCP) and soiltype (sand and clay), whereas the β values of f_p/N are small in the case of SPP but large in the case of CCP.
4. In principle, it is desirable to select f_p/N rather than f_y/N as an index for estimating the side resistance of a pile, unless it is generally hard to obtain information on f_p/N in the pile loading tests. Thus, overall it is practical to use f_y/N instead of f_p/N .

We emphasize that this result should be reviewed based on information obtained by loading test results with the displacement of 10% of the pile diameter.

REFERENCES

- Japan Road Association. 2002. *Specifications for Highway Bridges. Part IV Substructures*. Tokyo: Maruzen. (in Japanese, but the translated into English and edited one was published in 2003 as a technical memorandum of Foundation Engineering Research Team, PWRI).
- Okahara, M., Takagi, S., Nakatani, S. & Kimura, Y. 1991. A study on bearing capacity of single pile and design method of column shaped foundations, *Technical Memorandum of PWRI*. No.2919. (in Japanese).
- Shirato, M., Suzuki, M., Matsui, K. & Fukui, J. 2003. Design formula for the shaft resistance of a pile considering both the number and variability of load test data, Applications of Statistics and Probability. Der Kiureghian, Madanat & Pestana (Eds). *Proceedings of the ICASP 9 Conference*: 1385–1392. Rotterdam: Millpress.

Evaluation of vertical and lateral bearing capacity mechanisms of pile foundations using X-ray CT

K. Morita, J. Otani & T. Mukunoki

GeoX CT Center, Graduate School of Science and Technology, Kumamoto University, Kumamoto, Japan

J. Hironaka

Mitsui Chemicals Industrial Products, LTD, Saitama, Japan

K.D. Pham

Faculty of Civil and Industrial Construction, National University of Civil Engineering, Hanoi, Vietnam

ABSTRACT There are several types of failure patterns for both laterally and vertically loaded piles such as those proposed by Terzaghi, Meyerhof and Vesic for the vertically loaded pile and by Reese et al. for the laterally loaded pile. However, those have been proposed for the purpose of design calculation and are not based on close observation of real behavior. The objective of this paper is to visualize and to characterize the failure patterns of the ground under vertically and laterally loaded pile foundations using X-ray CT scanner. Here, a series of model loading tests for both vertical and lateral loadings at pile head were conducted with CT scanning of the ground. The model ground was made by Toyoura sand with controlling the relative density. Not only cross sectional images for the ground but also those in 3-D were reconstructed. A proper image processing analysis was conducted in order to obtain effective CT images. Finally, the bearing capacity mechanisms due to not only vertically loaded pile but also lateral ones were visualized and evaluated in three dimensions without any destruction and it was convinced that X-ray CT is one of powerful tool in geotechnical engineering.

1 INTRODUCTION

There are different types of pile foundations such as steel pipe pile, cast-in-place pile, under-reamed pile and so on. And the loading types such as vertical, lateral and those combined are also an important factor for the design of pile foundations. It is considered that a search for the failure pattern of the ground due to vertical and lateral loadings are another key issues for the design of pile foundations especially for the limit state design. So far, there are many failure patterns such as those proposed by Terzaghi, Meyerhof and Vesic (Lambe and Whitman 1969) for vertically loaded piles and Reese et al.(1974) and Kishida and Nakai (1979) for laterally loaded pile. However, those have been proposed for the purpose of design calculation and are not based on close observation of real behavior. Besides, these behaviors appear at the certain depth in the ground so that it is difficult to check such behavior.

Recently, an industrial X-ray CT (Computed Tomography) scanner which is one of the nondestructive testing method has been developed and the inside

behavior of the material could investigate without any destructions. Although the name of X-ray CT scanner has been well known as a medical diagnosis, this for the industrial ones has much higher resolution because of high power of the x-rays. An industrial X-ray CT scanner (TOSCAN NER-23200 min: TOSHIBA Corp.) has been installed at the GeoX CT Center in Kumamoto University, Japan. Authors have conducted a series of studies on the application of industrial X-ray CT scanner to geotechnical engineering such as characterization of soil failure (Otani et al. 2000) and visualization of the failure in mixed soil with air foams (Otani et al. 2002) and others (Otani & Obara 2003, Otani et al. 2005).

The objective of this paper is to visualize and to characterize the failure patterns of the ground under vertically and laterally loaded pile foundations using X-ray CT scanner. Here, a series of model loading tests for both vertical and lateral loadings at pile head are conducted with CT scanning of the ground. Not only cross sectional images for the ground but also those in 3-D are reconstructed. A proper image processing analysis is conducted in order to obtain effective

CT images. Finally, the bearing capacity mechanisms due to not only vertically loaded pile but also lateral ones are visualized and evaluated in three dimensions without any destruction and it is convinced that X-ray CT is one of powerful tool in geotechnical engineering.

2 X-RAY CT

The detected data are assembled and the cross sectional images are constructed using an image data processing device by means of the filtered back-projection method. By using all these cross sectional images around the circumference of the specimen, three dimensional (3-D) image can also be reconstructed. CT images are constructed by the spatial distribution of so called “*CT-value*” and this is defined as:

$$CT\text{-}value = (\mu_t - \mu_w)\kappa/\mu_w \quad (1)$$

where μ_t : coefficient of absorption at scanning point; μ_w : coefficient of absorption for water; and κ : constant (Hounsfield value). Here, it is noted that this constant is fixed to a value of 1000. Thus, the *CT-value* of air should be -1000 because the coefficient of absorption for air is zero. Likewise, *CT-value* for water is 0 from the definition of Eq. (1). CT images are presented with shaded gray or black color for low *CT-value* and light gray or white color for high *CT-value* in all the subsequent black and white colors. The total number of levels on these colors is 256. It is well known that this *CT-value* is linearly related to the material density. It is noted that the precise contents of X-ray CT method can be obtained in the reference by Otani et al. (2000).

3 TEST PROCEDURE FOR VERTICAL LOADED PILE

A series of model loading tests for three different model piles was conducted using a conventional loading apparatus as shown in Fig.1. The model piles were made of aluminum under consideration of material absorption for X-ray. Here, normal pile (diameter of 20 mm), under-reamed pile (diameter of 30 mm) and pipe pile (diameter of 20 mm) were selected in order to investigate the effect of different tip shape on the failure patterns and those are shown in Fig.2. Soil used in this test was Toyoura sand with min. dry density = 1.35 t/m³, max. dry density = 1.61 t/m³ and relative density = 100%.

The vertical load was applied at pile head under displacement control and the test was stopped at the settlement of 10 mm. For the CT scanning, initial and the stage at after 10 mm settlement were scanned with

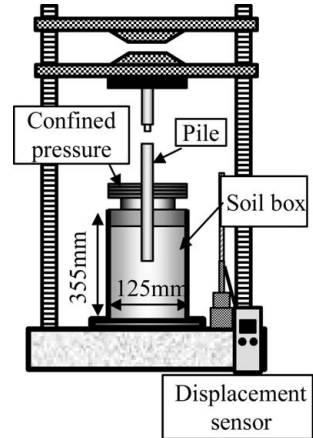


Figure 1. Model test apparatus.

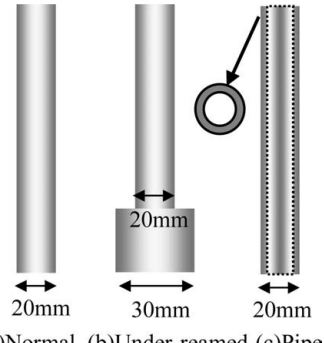


Figure 2. Model piles.

every 1 mm thickness for maximum depth of 60 mm below the pile tip. The reference by Otani et al.(2006a) shows more details of this test procedure.

4 TEST PROCEDURE FOR LATERALLY LOADED PILE

The details of this apparatus are shown in Fig.3 and its specification is denoted in Table 1. The model test apparatus is composed of soil box, loading machine, force transmission system, and control equipment. Confining air pressure can be also applied from the ground surface in the soil box in order to make experimental result to be more real. Photo. 1 shows the setup of this apparatus on the specimen table in the X-ray CT system. It is noted that during process of CT scanning, there should be no obstacles around the soil box that interfere with X-ray CT imaging.

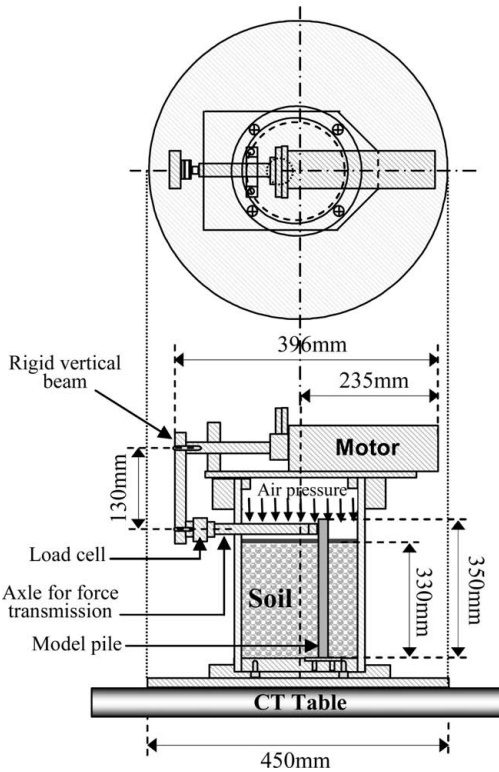


Figure 3. Details of model test apparatus.

Table 1. Specification of model test apparatus.

Maximum capacity of loading	(N)	1000
Maximum loading speed	(mm/s)	100
Minimum loading speed	(mm/s)	0.05
Maximum capacity of confining air pressure	(MPa)	0.2
Size of soil specimen		Diameter: 120 mm = Height: 330 mm

Soil used in this test was Toyoura Sand. A rectangular cross sectional shape of the pile made of aluminum was used in this test in order to discuss clear failure patterns in the ground although most of piles are circular shape in cross section. Total number of 20 strain gauges was installed on the model pile to obtain the distribution of lateral displacement along the pile shaft. All the measurements were operated using personal computer. Pile loading test and CT scanning were conducted as a consecutive test. The reference by Otani et al.(2006b) shows more details of this test procedure.

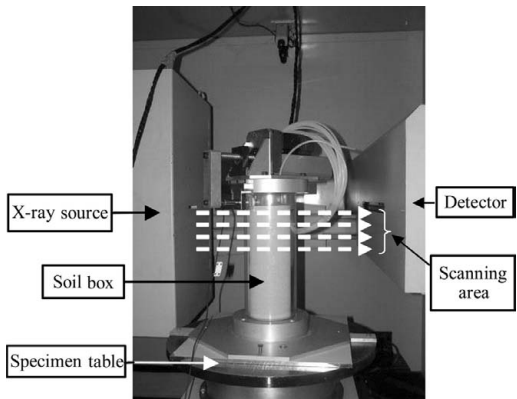


Photo 1. Setup of model test apparatus on specimen table in CT room.

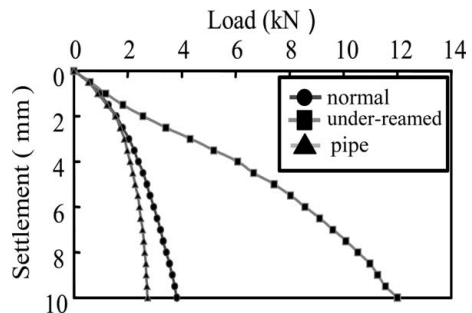


Figure 4. Load-settlement relationship.

5 RESULTS AND DISCUSSION

5.1 Vertically loaded piles

Figure 4 shows load-settlement relationships for all the cases. There are no peak loads for any of the cases, so that failure may be considered to be progressive failure rather than total failure. It is also realized that the case of under-reamed pile shows much higher capacity than the other cases. Figure 5 shows the cross sectional images for after 10 mm settlement at the depth of within 2 mm below the pile tip and the cross sectional image at the same location as before loading (initial condition) is also shown in this figure for three cases. As easily realized, the density around the circumference of the pile at the tip is decreased as the pile is penetrated, which is the appearance of the area of ring shape with black color in the image. Since the large number of cross sectional images are obtained for each case, a vertical cross sectional

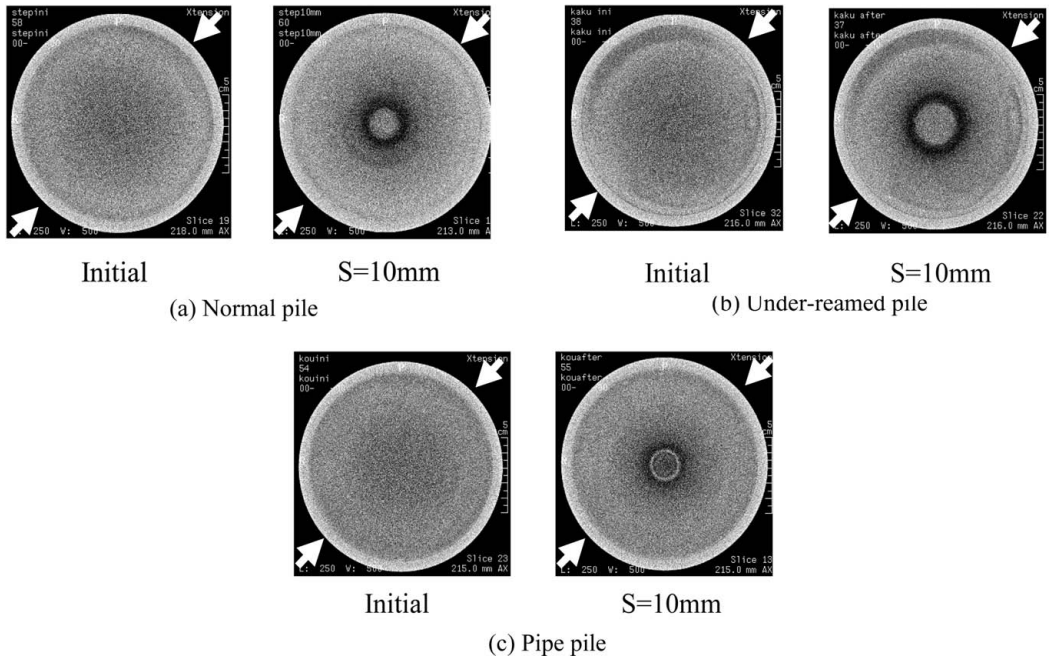


Figure 5. Horizontal cross sectional images.

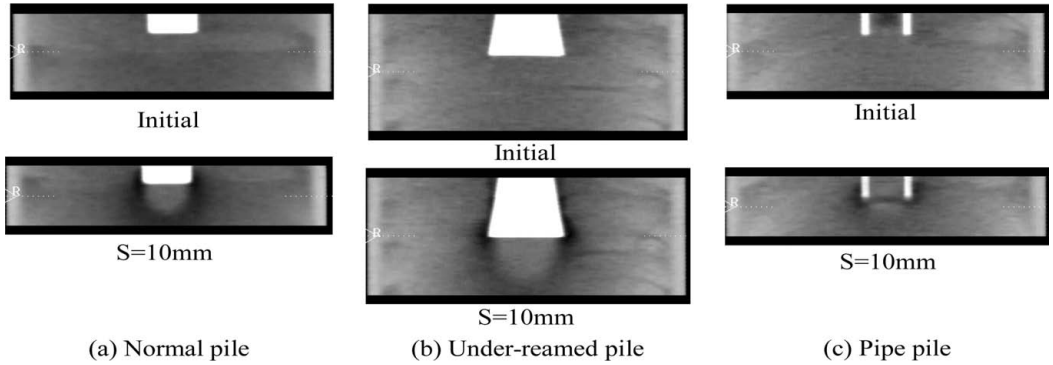


Figure 6. Vertical cross sectional images.

image or three dimensional image can be also reconstructed. Figure 6 shows vertical cross sectional images for three cases, in which the area of white color indicates the material of piles. Figure 7 shows reconstruction images in three dimensions for all the cases. These images are reconstructed by the change of the density using the colors of black and white gradation in the image. It is clearly shown that the area of high density right below the pile tip is surrounded

by the banded area of low density for both cases of normal and under-reamed piles. For the case of pipe pile, more complicated low density area is observed, especially at right under the pile tip. It may be considered that those banded areas of low density are the areas of strain localization. And it is also confirmed based on the results of 3-D images for all the cases that the shape of the failure pattern seems to be axi-symmetric.

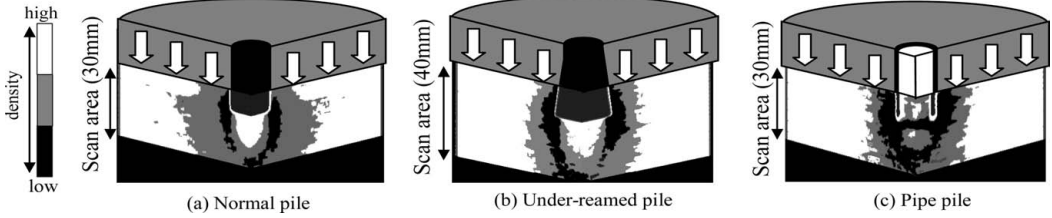


Figure 7. 3-D reconstruction images.

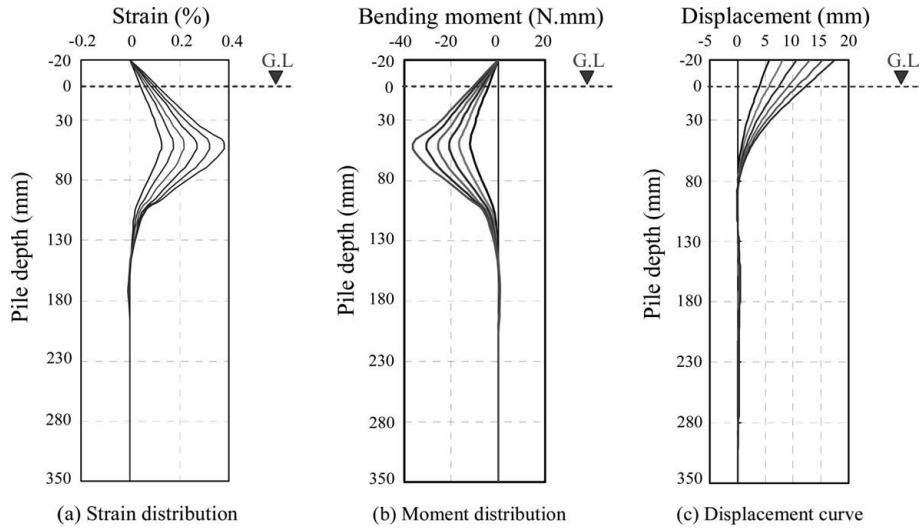


Figure 8. Results of measurement from strain.

Finally, it is concluded that the failure patterns for vertically loaded pile foundation could be well investigated using X-ray CT.

5.2 Laterally loaded piles

Figure 8 shows the results of measurements from strain gauges including distributions of strain, moment and lateral displacement along the pile shaft. From the distributions of the strain, moment and displacement distributions on the pile shaft were calculated. Figure 9 shows cross sectional CT images for six displacement cases of 5 mm, 7 mm, 9 mm, 11 mm, 13 mm, and 15 mm including images of initial condition at four different depths from the ground surface of 13 mm, 33 mm, 53 mm and 73 mm, respectively. It can be realized that the area of strain localization, which shows the banded area of black color in the image, appears in the ground towards the direction of

applied loading and these are extended as pile loading increases. It is also observed that the size of this localization becomes smaller as the depth of the ground increases in each loading step.

Figure 10 shows 3-D reconstruction images through soil box including pile at the area from the ground surface to the depth of 53 mm and 73 mm at both displacement cases of 13 mm and 15 mm, respectively. Each of these cases includes two images depicted in two different directions. Here, a smoothing technique in the image processing analysis on the CT image was employed. As realized easily, a large number of low density or strain localization zones appear, which are shown by relatively dark colors. It is considered that this strain localization seems to be the boundary of failure or the failure surface due to laterally loaded pile in three dimensions. As seen in those images, the size of this area tends to enlarge according to the increase of loading and becomes decreased along

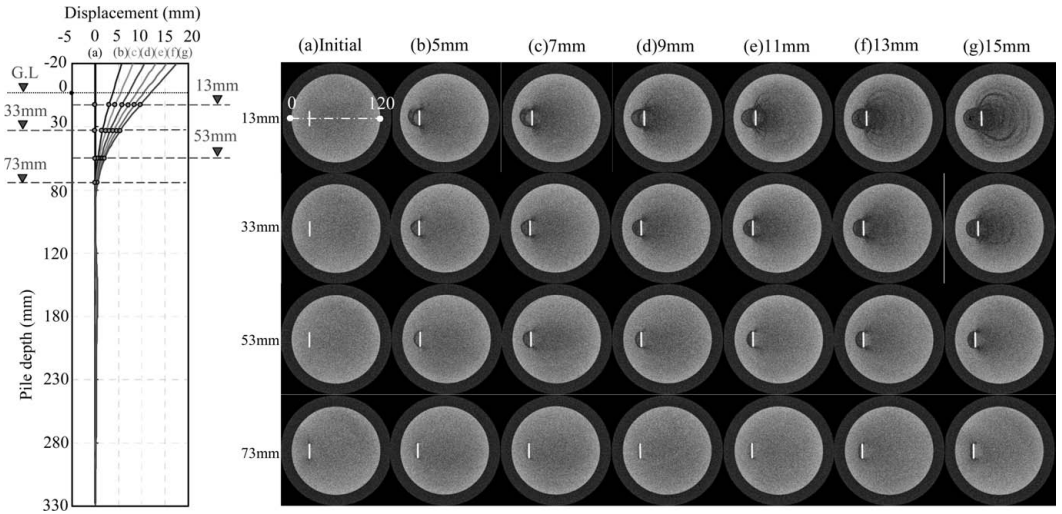


Figure 9. CT images of (a) initial condition and six displacement cases of (b) 5 mm, (c) 7 mm, (d) 9 mm, (e) 11 mm, (f) 13 mm and (g) 15 mm at four depths of 13 mm, 33 mm, 53 mm, and 73 mm.

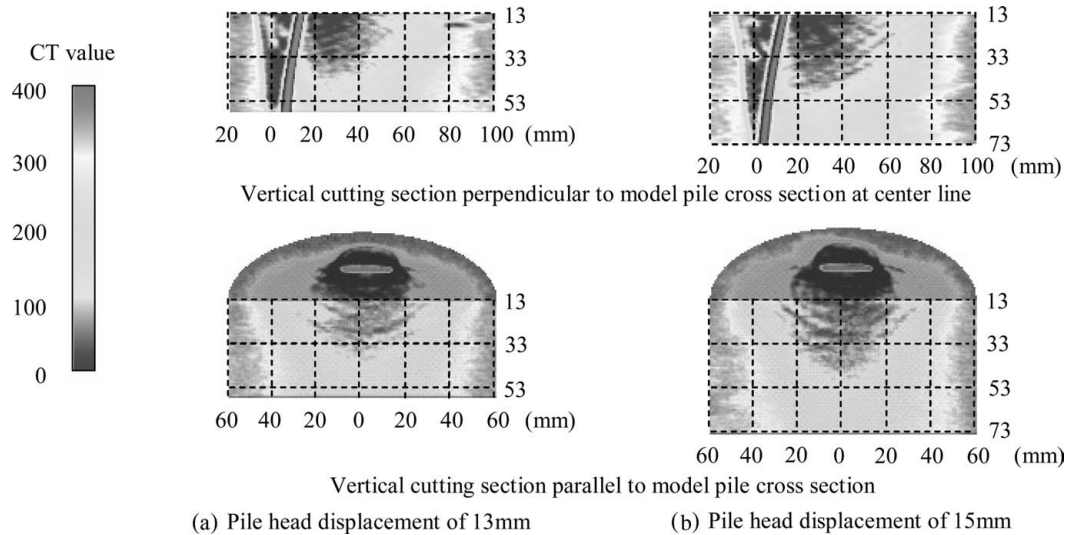


Figure 10. 3-D reconstruction image of soil box.

the pile depth in each loading case. Therefore, it can be said that the area within this boundary is the region of soil resistance against lateral pile loading and can be realized as a failure zone for the calculation of lateral bearing capacity such as on the use of limit equilibrium method or upper bound analysis in the limit analysis.

Although the failure patterns of the ground were not only visualized but also characterized based on

CT images in both 2-D and 3-D, more quantitative discussion is indispensable. Figure 11 shows the results of image processing analysis, which are depicted total failure zones at six different displacement levels of 5 mm, 7 mm, 9 mm, 11 mm, 13 mm, and 15 mm, respectively; and an assumed failure pattern of soil based on failure regions observed that emphasizes on conical shape of failure area and failure volume and failure angle. It is noted that the shape

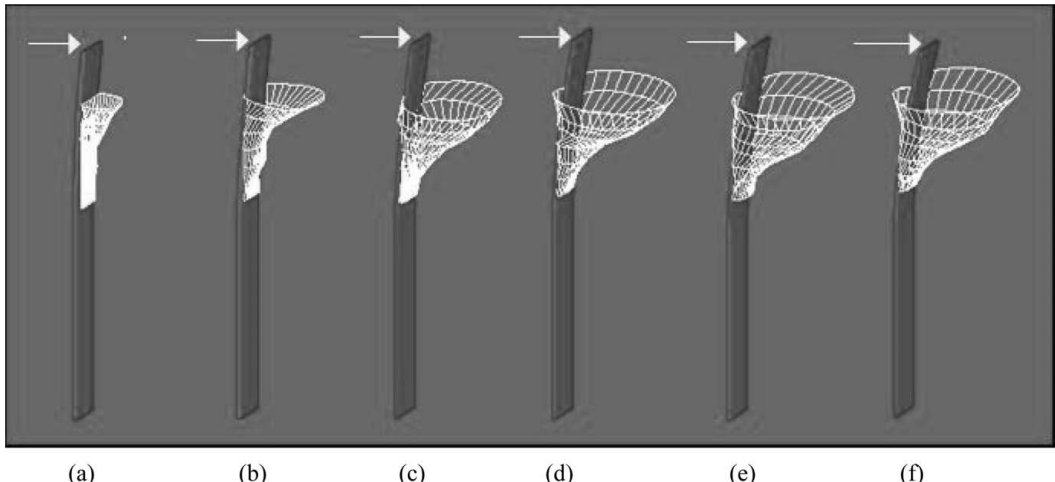


Figure 11. Failure zones at six displacement cases of (a) 5 mm, (b) 7 mm, (c) 9 mm, (d) 11 mm, (e) 13 mm and (f) 15 mm; and assumed failure patten of soil.

of the pile shaft in each loading step is also depicted in these figures and simulated in the assumed failure pattern. Here, the thinning technique, which is one of the techniques in the image processing analysis under assumption of ellipse shape in each cross sectional CT image, was utilized in order to reconstruct the failure surfaces. It is realized that when the lateral load is increased, this failure zone is enlarged and the angle of this failure zone becomes larger. But it seems that there is an ultimate size of this zone.

6 CONCLUSIONS

Failure patterns for different types of pile foundations were visualized using industrial X-ray CT scanner. It is confirmed that those results make the quantitative discussion of the failure patterns possible and as far as the limit equilibrium method has been used for the design of pile foundation in practice, those observations could be appreciated. Finally, it is evident from all the discussion here that the industrial X-ray CT scanner promises to be a powerful tool even for the geotechnical engineering field.

REFERENCES

- Kishida, H. and Nakai, S. 1979. Analysis of laterally loaded pile with non-linear subgrade reaction. *Transaction of Architecture Institute of Japan*: 281, 44–55 (in Japanese).
- Lambe, T.W. and Whitman, R.V. 1969. *Soil Mechanics*:502: John Wiley & Sons.
- Otani, J., Mukunoki, T. and Obara, Y. 2000. Application of X-ray CT method for characterization of failure in soils. *Soils and Foundations*. 40(2): 111–118.
- Otani, J., Mukunoki, T. and Kikuchi, Y. (2002). Visualization for engineering property of in-situ light weight soils with air foams. *Soils and Foundations*. 42(3): 93–105.
- Otani, J. and Obara, Y. 2003. *X-ray CT for geomaterials*. Netherland: Balkema.
- Otani, J., Mukunoki, T. and Sugawara K. 2005. Evaluation of particle crushing in soils using X-ray CT data. *Soil and Foundations*. 45(1): 99–108.
- Otani, J., Hironaka, J., Mukunoki, T. and Hirai, T. 2006a. 3-D bearing capacity of pile foundation under vertical loading. *Journal of Geotechnical Engineering, JSCE*. 62(2): 311–319 (in Japanese).
- Otani, J., Pham, D. K., Sano, J. 2006b. Investigation of failure patterns in sand due to laterally loaded pile using X-ray CT. *Soils and Foundations*. 46(4): 529–535.
- Reese, L. C., Cox, W.R., and Koop, F.D. 1974. Analysis of laterally loaded pile in sand. OTC2080. *Proc. Offshore Technology Conference*. Houston.

Dynamic and static horizontal load tests on steel pipe piles and their analyses

P. Kitiyodom & T. Matsumoto

Kanazawa University, Kanazawa, Japan

K. Tomisawa

Civil Engineering Research Institute for Cold Region, Japan

E. Kojima & H. Kumagai

Japan Pile Corporation, Japan

ABSTRACT: In this research, dynamic and static load tests were performed on permanent foundation piles for an abutment of a highway bridge, which had a pile length of 38 m, 800 mm in outer diameter and 9 or 12 mm in wall thickness. The static horizontal load versus horizontal displacement derived from the dynamic load test conformed well to that measured in the conventional static horizontal load test, encouraging the use of dynamic horizontal load testing as an alternative for the conventional static horizontal load testing.

1 INTRODUCTION

For axial compressive pile load test methods, the dynamic load testing or the rapid load testing is widely used in Japan because of the fact that these methods are unsusceptible to reaction piles, and require less time and cost compared with the conventional static load test where reaction piles are employed. Application of the dynamic or rapid pile load test to horizontal pile load test would be very useful in seismic design of the pile foundation.

In Kitayodom et al. (2006), the possibility of the use of dynamic horizontal pile load test as an alternative method for the conventional static horizontal load testing is presented and discussed. In order to estimate the deformation and load distribution of a single pile subjected to dynamic horizontal load as well as vertical load, a numerical program KWaveHybrid, has been proposed.

In this paper, the results of static and dynamic horizontal load tests on the actual piles are presented and compared. Static load displacement relation of the pile is estimated using the soil parameters obtained from the wave matching analysis of dynamic horizontal pile load test signals. Both static and dynamic analyses are performed using KWaveHybrid. It is shown that the estimated results match very well with the measured values.

2 TEST DESCRIPTION

A bridge was constructed at the Shinotsu site for the Central Hokkaido Connection Road in 2006. Pile group foundations were employed for abutments of the bridge. In order to assess the performance of the constructed piles, a static alternating cyclic horizontal load test and a dynamic horizontal load test were carried out on the constructed foundation piles. The test piles are located next to each other with pile spacing of 2 m. The specifications of the test piles are summarised in Table 1.

Table 1. Specifications of the test piles.

Property	Value
Length (m)	38.0
Embedment length (m)	37.2
Outer diameter (mm)	800
Inner diameter (mm)	
upper part ($z < 7.5$ m)	776
lower part ($z > 7.5$ m)	782
Young's modulus (kPa)	2.06×10^8
Moment of inertia (cm^4)	
upper part ($z < 7.5$ m)	2.31×10^5
lower part ($z > 7.5$ m)	1.75×10^5
Shear wave velocity (m/s)	3187
Density (ton/m^3)	7.8
Mass (ton)	7.06

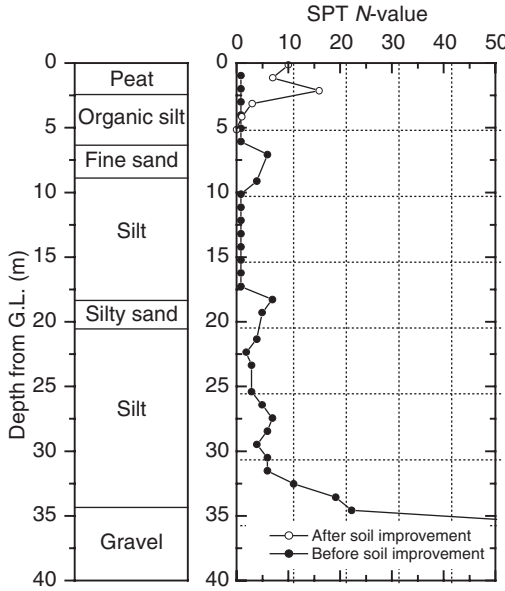


Figure 1. Profiles of soil layers and SPT N -values.

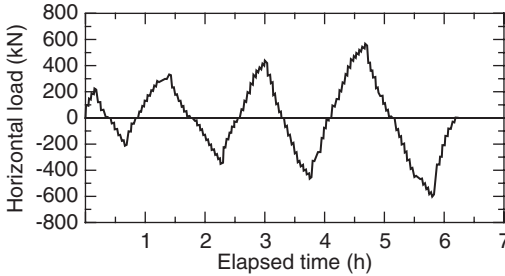


Figure 2. Loading history in static horizontal load test.

Figure 1 shows the profiles of soil layers and SPT N -values at Shinotsu site. The soil profile at this site is characterised by thick deposits of silt soils. SPT N -values are typically less than 7, except for gravel at depth from 35 m. At this site, soil improvement was carried out prior to the pile load tests. The SPT N -values after soil improvement are also shown in Figure 1.

Alternating cyclic horizontal loads shown in Figure 2 were applied to the pile in the static load test. Figure 3 shows the relationships between the horizontal load H and the horizontal displacement u . The residual displacement was measured at full recovery of horizontal load to 0 in each load step, and the elastic displacement was obtained by subtracting the residual displacement from the total displacement measured at the maximum load in each loading step. The residual displacement and the corresponding elastic

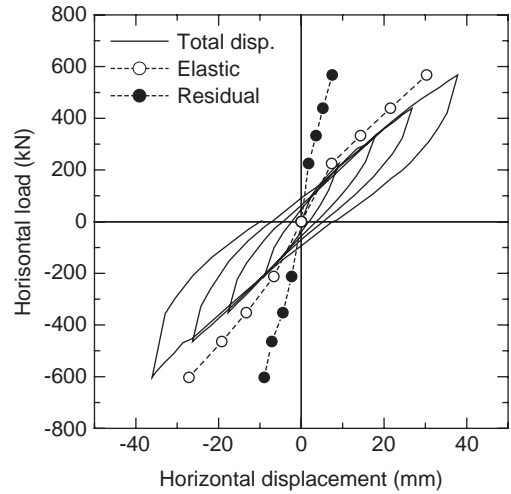


Figure 3. Static horizontal load vs horizontal displacement.

displacement at the maximum load in each load step are also shown in Figure 3.

In the dynamic horizontal load test, the pile was hit horizontally by a hammer of mass of 2.14 ton through a coil spring which was attached to the load cell at the point $z = 0.3$ m below the pile head as shown in Figure 4. Applied force, horizontal displacements and accelerations were measured at the same level of the hit point with a sampling interval of 15 μ s. The loading and measuring devices are shown in Figure 4. More details can be found in Kojima et al. (2006).

An example of the dynamic test signals is shown in Figure 5. The measured force increases and decreases smoothly with time, and has a peak of about 330 kN. The loading duration is about 55 ms. The measured displacement also increases and decreases with time having a peak of 20 mm at a time of 40 ms. The peak horizontal displacement delays 18 ms behind the peak horizontal load, showing dynamic effects.

During the dynamic horizontal load test, the axial strains at both sides of the pile were measured at different levels down the pile shaft. Figure 6 shows the profiles of bending moments along the pile obtained from the measured axial strains.

Figure 7 shows the relationship between the dynamic horizontal load and the horizontal displacement. It can be seen from comparison between Figure 3 and Figure 7 that the measured load displacement relation from the dynamic load test is totally different from the measured static load displacement relation. Therefore, in order to obtain the static load displacement relation of the pile from the measured signals of the dynamic load test, wave matching analysis of the measured signals is needed.

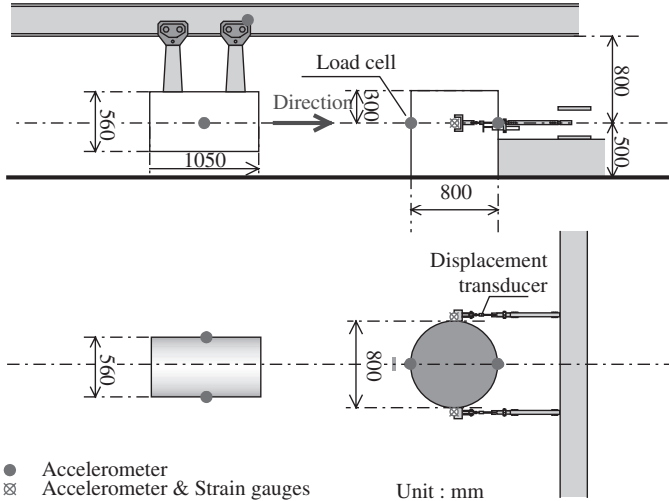


Figure 4. Loading and measuring devices for dynamic horizontal load test.

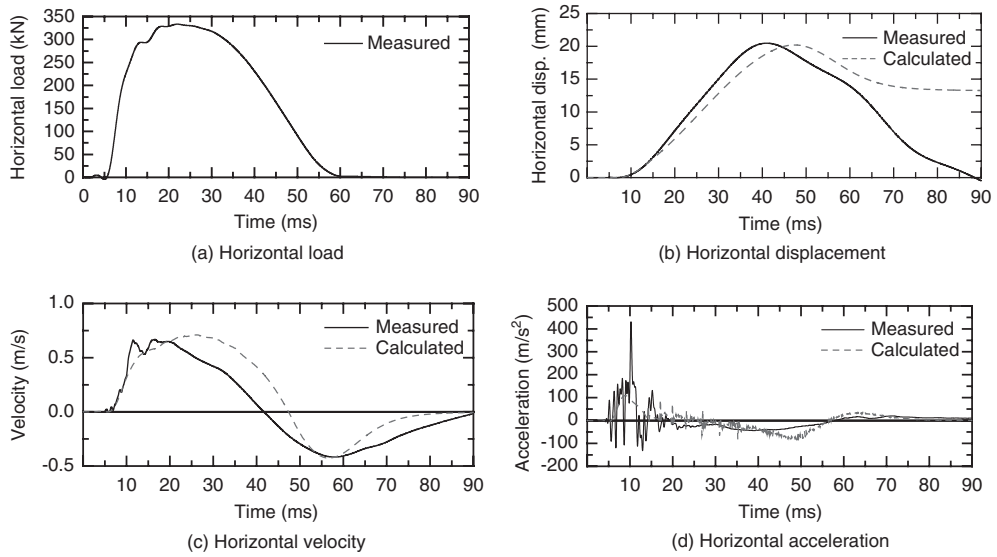


Figure 5. Measured and calculated pile load test signals.

3 ANALYSES OF TEST RESULTS

A computer program KWaveHybrid, developed by Kitiyodom et al. (2006), was used for the wave matching analysis of the dynamic horizontal load test. The program was also used to estimate the static load displacement relationship of the pile using the soil parameters obtained from wave matching analysis.

Figure 8 illustrates the hybrid modelling of the pile and the soil used in KWaveHybrid. The pile is modelled

as beam elements with masses and the soil is treated as springs and dashpots. More details of the analysis method can be found in Kitiyodom et al. (2006).

It should be noted here that the unloading and reloading curves measured in the static alternating cyclic load test (Figure 3) indicate that gapping between the pile and the surround soil occurs during unloading and reloading stages. Such gapping has not been incorporated in KWaveHybrid at present. Hence, monotonic horizontal loading of the pile is considered in the

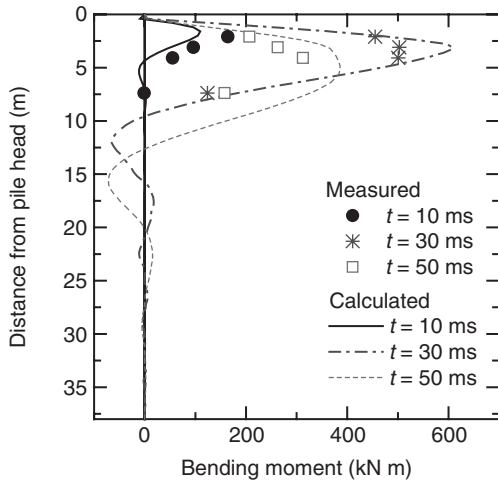


Figure 6. Measured and calculated bending moment.

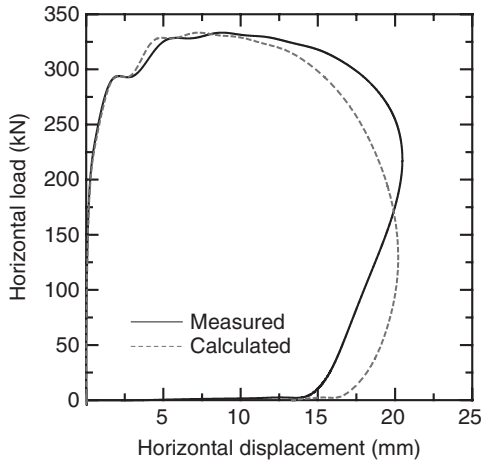


Figure 7. Measured and calculated load vs displacement in dynamic horizontal load test.

analysis. Note also that the interior of the pipe pile was almost filled with soil at the end of driving. It was assumed that the pipe pile was fulfilled by the soil with the density of 1.8 ton/m³, and the masses of the soil inside the pipe pile was taken into account in the analysis.

Matching analysis was repeated with assumed values for the maximum shaft horizontal pressure, q_h , and the soil shear modulus, G_s , using the measured dynamic load (Figure 5(a)) as the force boundary condition at the loading point, until a good matching between the calculated and the measured pile displacements was obtained. Soil parameters used in the final matching of the pile are listed in Table 2.

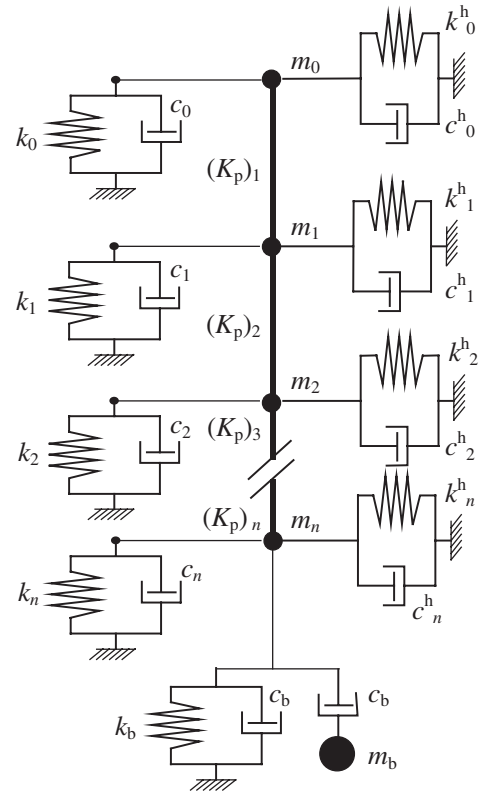


Figure 8. Hybrid modelling of the pile and the soil.

Table 2. Soil parameters identified in final matching.

Depth (m)	G_s (kPa)	q_h (kPa)
0 to 2.7	9615	116.0
2.7 to 18.4	836	Elastic range
18.4 to 31.8	1607	Elastic range
31.8 to 37.0	11587	Elastic range

Figure 5 and Figure 7 show the displacement, velocity, and acceleration versus time and load versus displacement of the test pile calculated in the final matching analysis, compared with the measured values. It can be seen that the calculated dynamic pile displacement overestimated the measured values after the peak displacement. This is thought to be due to the soil spring in KWaveHybrid. At the present, the values of the soil spring in KWaveHybrid during the loading and unloading states are the same. The values of the soil spring during the loading and unloading states should be different due to gapping between the pile and the surrounding soil as mentioned earlier. However, the calculated displacement matches well

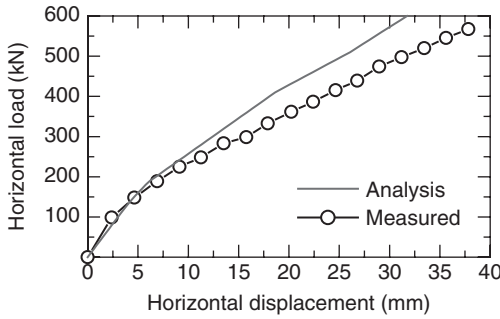


Figure 9. Measured and calculated static load vs displacement.

with the measured displacement until the peak displacement.

Figure 6 shows the comparison of the calculated profiles of bending moments along pile with the measured value. There are good agreements between two solutions. It can be seen from the figure that only the upper part of the pile deforms during the dynamic horizontal load test.

Using the same soil parameters as shown in Table 2, the static load displacement relation of the pile was estimated using KWaveHybrid. Figure 9 shows the comparison of the calculated static load displacement relation with the measured value. It can be seen that the calculated result matches well with the measured one.

4 CONCLUSIONS

In this paper, the results of alternating cyclic horizontal load tests and dynamic horizontal pile load tests on driven open-ended steel pipe piles constructed for foundations of a bridge abutment at Shinotsu site have been presented and discussed.

A good matching between the calculated and measured behaviours of the piles during dynamic loading as well as during static loading was obtained.

The possibility of the use of dynamic horizontal pile load test as an alternative method for the conventional static horizontal load testing was demonstrated.

REFERENCES

- Kitiyodom, P., Matsumoto, T., Kojima, E., Kumagai, H. & Tomisawa, K. 2006. Analysis of static and dynamic horizontal load tests on steel pipe piles. *Proceedings of 10th International Conference on Piling and Deep Foundations*: 690–699.
- Kojima E., Kumagai, H., Kitiyodom, P., Matsumoto, T. & Tomisawa, K. 2006. Dynamic horizontal load tests on steel pipe piles having different sizes in the same construction site and their analyses. *Proceedings of 10th International Conference on Piling and Deep Foundations*: 700–708.

New types of pile construction methods

Press-in piling technology: Development and current practice

M. Motoyama

Overseas Division, Giken Seisakusho Co., Ltd., Tokyo, Japan

T.L. Goh

Giken Seisakusho Asia Pte., Ltd., Singapore

ABSTRACT: Universally acceptable construction for sustainable society in 21st century must embody the “Five Construction Principles”, in conformity with the way the general public considers construction work ought to have been from the very beginning, i.e., Environmental Protection, Safety, Speed, Economy and Aesthetics should equally balanced for development of machine, design, planning and execution methods. The rapid development in robotics technology and machine automation have led to revolutionary change in design, function and capability of press-in piling machinery. Advanced machinery has been designed to improve the work safety with less human dependent and more environmental friendly. Using the latest press-in piling technology, high quality infrastructures can be constructed based on the new concept of “One-step Approach”. This construction concept eliminates the environmental impact and allows piling works to proceed efficiently and systematically on marginal site with the satisfaction of Five Construction principle. With systemized press-in piling machineries and associated equipments, implant structures are constructed with minimum reliance on temporary works. In this paper, the development concept of press-in piling technology will be presented with emphasis on the current start of art of this piling system being used in broader civil engineering applications.

1 INTRODUCTION

As aging civilizations continue their growth, there are needs to constantly expand the existing infrastructures such as road, bridge, rail, port and underground structures. Due to environmental concerns in urban construction, many typically simple infrastructure projects can become very complex or feasibly impossible. Physical disruption during construction works such as traffic obstruction, noise, ground vibrations and resulting air pollution are the common public discomforts, which could severely affect the business environment and quality of life. These are insoluble dilemma faced by planners and practicing engineers in constructing infrastructures to serve the general public better. Ironically, there are still lot of public complaints such as noise, ground vibrations and other physical disruptions during the execution of these construction works. Construction particularly for sustainable society should maintain the “Five Construction Principle”, in conformity with the way the general public considers construction work ought to have been from the very beginning.

Nevertheless, conventional dynamic pile driving methods is still used in many construction sites though it is well known for causing excessive noise, ground

vibrations and posing damage risk to critical structures. Design codes place limits on the noise and ground vibrations created by piling operations. Protection measures such as issuing fines and to a larger extend, imposing “stop work order” by local authorities have been directed to unmindful contractors. These limits and steps are intended to prevent disturbance to humans and damages to adjacent properties.

Besides stringent noise and vibration legislations, contractor also faces great difficulties in installing piles in a small confined area and uneven ground. The current conventional piling system requires a large construction corridor and relies on flat working platform to sit their machines. Often, the entire set up of these bulky machineries occupies a large working space which can easily cause major disruption to the existing daily activities.

The innovation of a relatively new concept to the machinery has redefined “doing the impossible” for construction works in the urban setting. By simply utilizing the earth itself as the base of reaction force, smaller machine can now be developed to perform similar quantum of works on site without occupying a large working space. The technique uses hydraulic rams to push piles into the ground.



Figure 1. Jack-in piling machine based on counter weight.

2 THE PRESS-IN METHOD

2.1 Historical background of the press-in method

The idea of pressing piles into the ground by static force is not a new concept, but it has taken sometime to develop a machine that is capable of consummating this idea. One of the earliest pile jacking machines was developed in China (Li et al., 2003). These machines rely on their self-weight to derive its reaction force (Figure 1), allowing square or circular pre-cast reinforced/pre-stressed concrete piles and H steel piles to be jacked into the ground to act as foundation piles. They are normally massive which will make difficult to move and to cause damages to the top of piles, and often require a large flat working space at site.

2.2 Development of the first press-in machine based on reaction principle

In 1967, Akio KITAMURA founded Giken Seisakusho Co., Ltd. (Kochi, Japan) to develop the first press-in machine (1975) based on the reaction principle. This press-in machine grips on previous installed piles to press-in subsequent piles (Figure 2) and allows the press-in machine to self-walk along the pile top. The press-in machine which is used in many construction sites over the world is better known as the “Silent Piler”. This method will have superiority in principle and satisfy the requirements of Five Construction Principle for construction work.

2.3 Self-walking mechanism of silent piler

Silent Piler consists of three distinct parts linked together by a sliding rail and mast (Figure 3). The upper and lower parts of the machine slide horizontally on the rail of the lower body. The lower body normally has three or four clamping claws to hold the body on the piles by gripping the previously installed piles tightly. The part attached to the upper body that grip the pile is

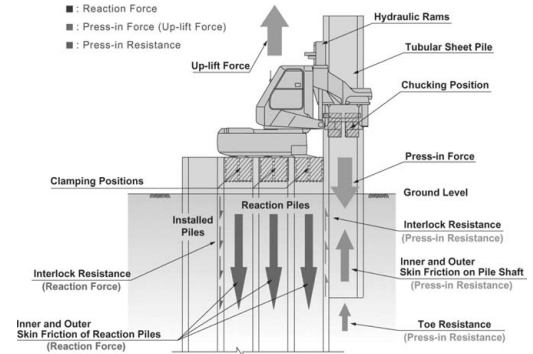


Figure 2. Press-in piling machine based on reaction principle.

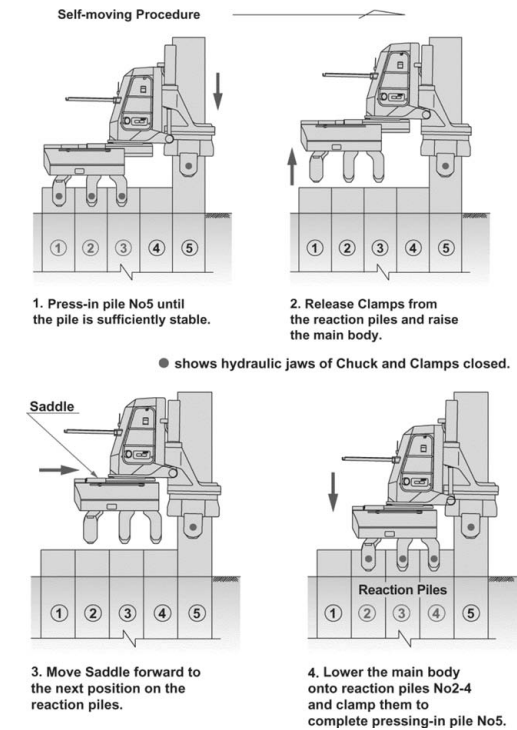


Figure 3. Self-walking of silent piler on reaction piles.

referred as the “chuck”. It moves vertically up and down along the mast of the upper body. This moving function allows the static pile driving to be carried out, which eliminate the noise and vibration. Half-way through the press-in operation, the clamping claws of the lower body release the piles. The body of the piler is lifted up by the hydraulic jack. The whole body is then held by the chuck on the pile. The lower body finally moves forward along the rail and sits on the piles back.

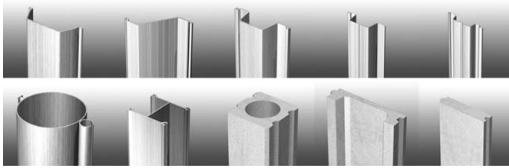


Figure 4. Typical sheet pile materials used in current practice.

2.4 Piling various types of sheet pile materials

Innovations in material usage have resulted in a whole series of new machines, allowing various piles in different shapes and materials to be pressed-in, such as U, Z, H, tubular steel sheet piles and concrete sheet piles (Figure 4). Most types of pile are already in practical use in Japan, Europe and United States while other types can also be found in other parts of Asia.

3 DEVELOPMENT OF PRESS-IN MACHINE

3.1 Non-staging press-in piling system

In 1982, the Giken Reaction Base (GRB) System has been developed to allow non-staging piling activities to proceed in sensitive areas, above water and on slope embankment. In the GRB System, piles are loaded onto the Pile Runner, which runs on top of the installed pile wall, to the Clamp Crane and subsequently, being pitched into the chuck of the Silent Piler (Figure 5).

3.2 Piling under constraint working space

Some cramped areas such as narrow streets between existing buildings are not able to be developed considering the difficulties of construction machine in gaining access. Nevertheless, the Silent Piler can infiltrate into such tight working space without causing disruption to the surroundings (Figure 6). This press-in piling machine is called the “Zero Piler”.

3.3 Piling under overhead restriction

Under overhead restriction such as under existing structure, bridge and high tension cables, piling works using the Clear Piler can still proceed smoothly (Figure 7). This is simply because the press-in point is located close to the ground level.

3.4 Piling into hard ground

Hard ground conditions usually create very difficult piling conditions. Often, the sheet pile is forced deliberately, causing the interlocks and pile toe to damage. Hence, there is a risk that the sheet pile has to be terminated at shallower depth. Since the major functions of sheet pile wall is to prevent water from seeping

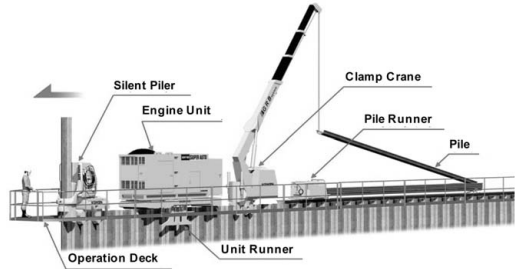


Figure 5. Systemized Giken Reaction Base (GRB) equipments.



Figure 6. Piling under tight working space using Zero Piler.



Figure 7. Piling under overhead obstruction using Clear Piler.

into the excavation side, insufficient penetration depth may cause considerable problems of water table drawdown during an excavation. To solve this difficulty for hard ground conditions, auxiliary techniques either by the water jetting (Figure 8) or the integral auguring (Figure 9) are used.

3.5 Piling with gyration at inclined angle

The press-in machine so called the “Gyro Piler” can install piles at an inclined angle with a set of rotational cutting bit (Figure 10) at the pile tip. It allows the raker and strut-free piles to be installed from the same position, allowing the construction of a robust structure through hard layer or obstacles.

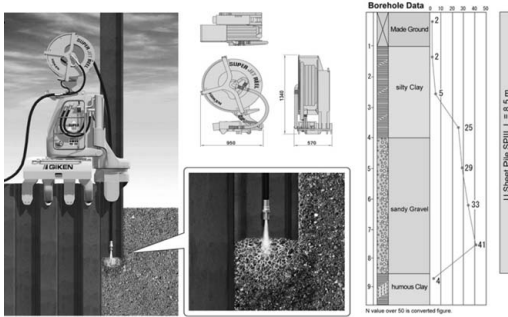


Figure 8. Hard ground penetration using piler jet system.

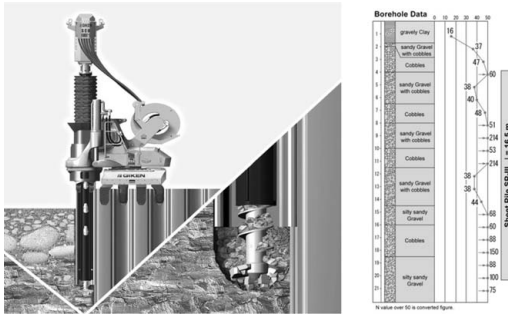


Figure 9. Hard ground penetration using super crush system.



Figure 10. Innovative Gyropress method using Gyro Piler.

4 INNOVATIVE CONSTRUCTION APPROACH

Conventional construction processes are no longer appropriate and must be replaced by new construction designs and methodologies in the way where the general public would consider the construction works ought to have been from the very beginning. New

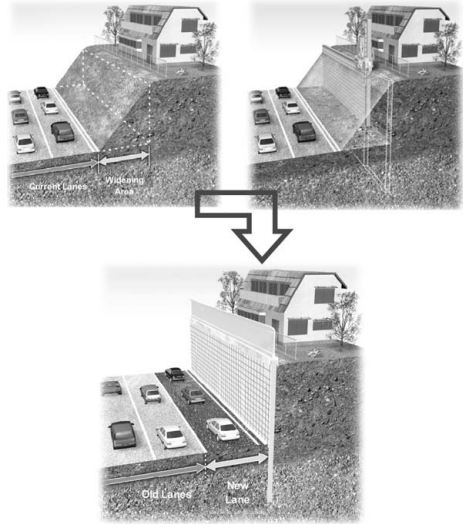


Figure 11. New construction concept of One-step Approach.

innovated construction methods have been practically feasible using the latest press-in piling system, allowing cost effective solutions to be implemented on site without causing damage to surroundings.

4.1 One-step Approach

The “One-step Approach” synchronizes the construction process into a single sequence of events in which the bulk of temporary works can be eliminated, allowing the construction works to proceed in a narrow construction corridor without encroaching onto nearby structures or services (Figure 11).

A subset of the “One-step Approach” would be the case of retaining structures, in which a conventional design would required an excavation, the installation of a footing and backfilling to be performed (“Footing-based Approach”, consisting of three steps) whereas the “One-step Approach” would involve only the construction of a cantilevered pile wall (Footing-less Approach), being installed systematically by the press-in piling method in a single process (Figure 12).

4.2 Implant Structure

The Implant Structure is made of modular prefabricated structural elements and installed into the ground using the press-in piling method. It functions both as a foundation pile and act ultimately as the body of a structure. During construction, no extensive temporary work is necessary. It is a structural revolution which changes the current footing-based approach into the footing-less structures (Figures 13 and 14).

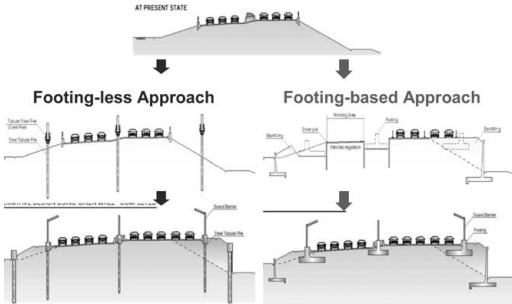


Figure 12. Benefit of using Footing-less Approach.

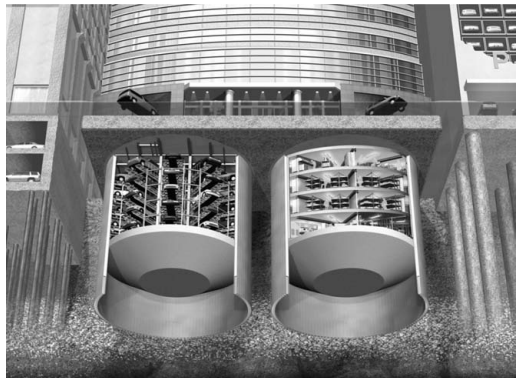


Figure 15. New foundation concept by implant shaft.

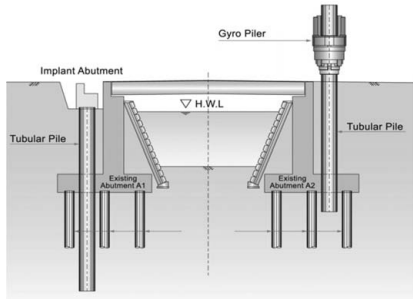


Figure 13. New construction concept of Implant Structure.

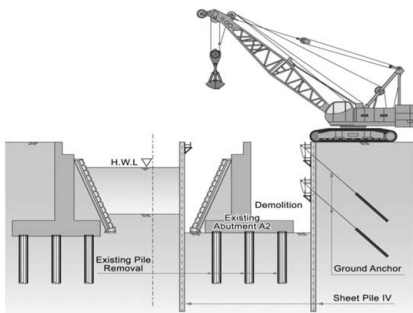


Figure 14. Ineffective conventional construction concept.

4.3 Versatile foundation

Underground space will not be effectively used if its function is only used to support the structure above it. Shaft has been constructed to provide the necessary underground space for functional facilities and doubles up as a foundation pile for the building (Figure 15). The underground space can be used as a parking facility, storage area for computer server or simply act as a shelter to protect properties or human lives from natural disaster or terrorist attack while the foundation piles

can also provide the resistance against wind and earthquake forces.

5 TYPICAL APPLICATIONS AND SOLUTIONS

5.1 Road construction works

In conventional road construction, slopes are being cut and filled to form flat ground for road paving. However, soil or rock mass on sloping ground has tendency to move downwards under the influence of gravity, causing tragedy of massive landslide onto the road with live traffic. Introducing a retaining wall on slope prevents the soil from caving in because the insertion of a new wall element into the ground will intercept the potential slip circle. The area occupied by the slope can now be excavated to form a new additional lane for the traffic to flow. This concept has been increasingly adopted for road widening projects in urban environment as an effective method to optimize the land usage.

Nevertheless, constructing a retaining wall on slope is a tedious process. Besides the sloping characteristic of ground, the working space is usually limited as there are continuous traffic flows on the adjacent side. Conventional piling methods will require massive temporary staging to be fabricated and removed during construction. Consequently, the use of implanted retaining wall on sloping ground for road construction becomes extremely difficult. Nowadays, this type of construction problem can be solved using the GRB non-staging piling system offered by the press-in piling technology (Figures 16 and 17).

This innovative GRB non-staging press-in piling system has been adopted for a major road widening project in Yokohama, Japan (Figure 17). Since the project is surrounded by residential housing, the construction

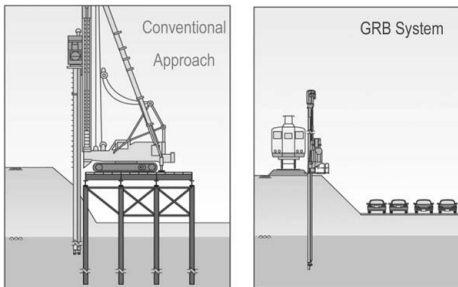


Figure 16. Retaining wall construction for road widening.



Figure 17. Hodogaya bypass (Japan) road widening works.

works to be carried out in an environment sensitive to noise and vibration restrictions.

5.2 Bridge foundation works

Replacing old bridges with new ones can often take place in rural environment where traffic flow is light and the land is inexpensive. However in densely populated urban area, re-development of old and narrow bridge becomes necessary considering the scarcity of land and unacceptable economical influence for the road closure during the construction stage (Figure 18).

New enlarged bridge piers and its foundation are to be constructed in strict overhead working condition above water. It is tedious and almost impossible if conventional piling system is adopted. However using the press-in piling technology, the equipment can allow piling works to be performed below the bridge without any disturbance to the traffic above. This will maintain the original functionality of the bridge during construction (Figure 19).

5.3 Rail renovation works

Construction of cut-and-cover tunnels for railway lines in urban area has always posed great challenges to contractors due to the constraint of working space.



Figure 18. Re-development works for aging bridge.



Figure 19. Press-in piling works for bridge foundation.



Figure 20. Press-in piling works for bridge foundation.

Often, the construction works has to be carried out in a tight corridor where the area is inadequate to house even a crane.

Hence, press-in piling technology will ease this concern with small, compact and lightweight machines (Figure 20).

5.4 Coastal infrastructure works

Due to ever increasing number of ships calling at the ports all over the world, it became necessary to expand the berth facility. The expansion of port will ensure fast, continuous and simultaneous loading and



Figure 21. Press-in piling works on marine condition.



Figure 22. Rescue method for flood defense works.

unloading of passengers and cargos. However, due to cramp space at the harbor vicinity area during construction, it would be very difficult to adopt the conventional off-shore piling system which has to rely on temporary staging. Alternatively, press-in piling technique can be used considering that it has the ability to self-walk efficiently over previous installed piles, allowing subsequent piles to be hydraulically jacked-in accurately into the ground above the water (Figure 21).

Without such innovation, in this case the ability to eliminate the time consuming temporary works (i.e. staging), it will have been difficult to materialize the function of the port and harbor as soon as possible.

5.5 Rescue and restoration works

During unpredictable natural disasters such as floods, landslides, typhoons, earthquakes, sinkholes and volcanic eruptions, immediate rescue and restoration

works shall be taken to protect human lives and properties. The press-in technique enables restoration works to be carried out immediately on site (e.g. flood defense works as shown in Figure 22).

6 CONCLUSIONS

Conventional dynamic pile driving such as percussive or vibratory methods causes excessive noise and ground vibrations to neighbors and poses damage risk to critical structures. Drilled shafts, slurry walls and other cast-in-place retaining wall systems alleviate some of these problems but add additional problems of their own with large bulky machines, reliance on dusty concrete plants and urban trucking grief. Due to these environmental concerns, many typically simple underground constructions in densely populated areas become very complex and feasibly impossible.

The innovation of a relatively new concept to the machinery has redefined “doing the impossible” for construction works in the urban setting. By simply utilizing the earth itself as the base of reaction force, smaller machine can now be developed to perform similar quantum of works on site without occupying a large working space. The current Silent Piler uses the most up-to-date technologies in ensuring the best performance on site.

From a simple hydraulic pile jacking system that relies on the reaction principle, the press-in piling technology has provided the construction solutions to the problems encountered during the installation of embedded retaining walls for urban deep excavation works. Continuous research and development has allowed more capable press-in machines to be released into the construction industry.

REFERENCES

- Goh, T. L. & Li, K. S. 2004. Installation of Embedded Retaining Wall by Press-in Piling. *Proc. of Symposium on Deep Excavation*. HK.
- Goh, T. L., Carter, M. W. T., Richardson, R., Ikeda, T. & Motoyama, M. 2004. Press-in Piling: A Construction Solution for Cut & Cover Tunnels. *ITA2004*. World Tunnel Congress. Singapore.
- Goh, T. L., Shiomi, T., Yamamoto, M., Ikeda, T. & Motoyama, M. 2004. Press-in Piling: A Solution for Road Construction. *6th Malaysian Road Conference*. KL.
- Goh, T. L., Shinoda, Y., Hino, I. & Carlito, M. C. 2004. Press-in Piling: A Solution for General Batangas Cargo Berth Construction. *Int. Conf. on Coastal Infrastructure Development*. HK.

Centrifuge modelling of the base response of closed-ended jacked piles

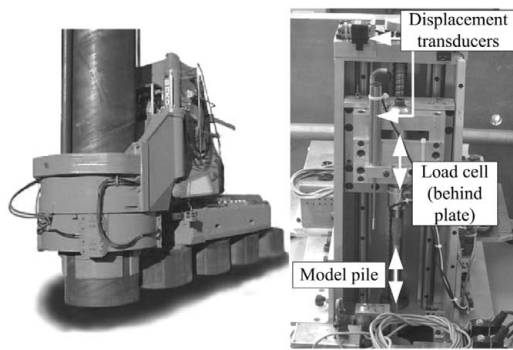
A.D. Deeks & D.J. White

Cambridge University Engineering Department, Cambridge, UK

ABSTRACT: Pile jacking techniques use static load to install pre-formed displacement piles without the noise and vibration associated with dynamic methods. To quantify the axial base response of displacement piles jacked into sand, the pile jacking process has been faithfully replicated in a geotechnical centrifuge. Six pile installations and companion load tests are reported. The tests are shown to be highly repeatable, with a lateral COV of penetration resistance an order of magnitude less than that for typical field test sites. The non-linear base response of jacked piles is shown to be well modelled by a parabola, for use in ‘t-z’ type analysis of pile response. The elastic solution for a rigid punch is used to link the base response to the operative soil shear modulus during loading. This parabolic model combined with the seismic CPT parameters G_0 and q_c , allows the initial stiffness, stiffness degradation and capacity at failure of the base response to be predicted.

1 INTRODUCTION

Pile jacking technology is well suited to the urban environment. The noise and vibration associated with dynamic pile installation methods is avoided by using static hydraulic force to install pre-formed displacement piles by jacking. A typical ‘press-in’ pile jacking machine is shown in Figure 1a. The ‘press-in’ technique uses the negative shaft resistance of previously-installed piles to provide reaction force. Kentledge is used to install the first piles of a group.



Typical pile jacking machine
(3MN vertical load capacity, piles up to 1200mm in diameter)

Figure 1. Pile jacking machines.

High capacity pile jacking rigs are in operation in Europe, Asia, North America and Australia, with jacking capacities of up to 7 MN (Lehane et al. 2003, Yang et al. 2006 and White et al. 2002). Installing piles using the jacking technique reduces ground-borne vibrations by an order of magnitude compared with typical percussive and vibratory techniques (Rockhill et al. 2003).

Displacement piles are stiffer than non-displacement bored piles (De Beer 1988, Ghionna et al. 1993 and Lee et al. 2003). Furthermore, Deeks et al. (2005) and Yetginer et al. (2006) present field data indicating that displacement piles installed by jacking are stiffer than dynamically-driven displacement piles. This relative performance can be attributed to the differing stress histories applied to the soil surrounding the pile by each installation procedure. Pile jacking pre-loads the soil beneath the pile tip during installation, and can trap residual base load. These effects stiffen the base response, and reduce the settlement required to mobilize the full base resistance.

This combination of high capacity, high stiffness and low induced ground vibration makes pile jacking technology suited to the construction of deep foundations in the modern urban environment.

If the high axial stiffness and capacity can be reliably predicted and utilised in design there is scope for improved design efficiency. Such improvements could lead to economies of cost and diminished environmental impact through reduced material use and installation time.

This paper describes an investigation into the base stiffness of piles jacked into sand. The process of pile jacking has been faithfully replicated in a geotechnical centrifuge, and the load-settlement response of an instrumented pile has been measured. Six installations are reported. A simple model to reliably predict the observed pile base response based on routinely measured in-situ test parameters is described.

2 METHODOLOGY

2.1 Apparatus

2.1.1 Geotechnical centrifuge

The 10 m diameter Turner beam centrifuge at the Schofield Centre, Cambridge University was used to conduct the tests described in this paper. The design and general operation of the centrifuge is described by Schofield (1980). Relevant scaling laws are discussed by Schofield (1980) and Wood (2004).

2.1.2 Model container and actuator

Tests were conducted using an in-flight piling actuator that bridged across a sand-filled model container. The model container is 850 mm in diameter and 400 mm in depth (Fig. 2). The actuator used to install the piles is described in detail by Silva (2005) and is shown schematically in Figure 2. It has a single, vertical, degree of freedom and can apply a maximum load of $+/-10\text{ kN}$ and travel at up to 10 mm/s.

An Aerotech BL-10-40 motor controller, providing a linearly-varying output, is mounted on the main beam of the centrifuge in an acceleration field of $\sim 15\text{ g}$. This motor controller drives a McLennan ME642TE 150 W brushed DC motor. The model pile, and two displacement transducers (long and short-range), are attached to the face plate of the actuator carriage. The actuator is manually rotated to a new test location when the centrifuge is stationary between tests (Fig. 2a).

Pile head load, base load and head displacement were sampled at a rate of 100 Hz throughout testing. Further details on the data acquisition and instrumentation systems used with this actuator are described by Deeks & White (2006).

2.1.3 Test pile

For this study a cylindrical, closed-ended model pile of 12.7 mm outside diameter, D, and 6.7 mm internal diameter was used. The maximum embedded depth of the model pile was $\sim 250\text{ mm}$. The axial stiffness of a field-scale pile was not modelled as prevention of pile buckling during installation was the dominant design criteria.

The model pile was manufactured from stainless steel. This material was chosen instead of aluminium in order to minimise the effect of surface abrasion

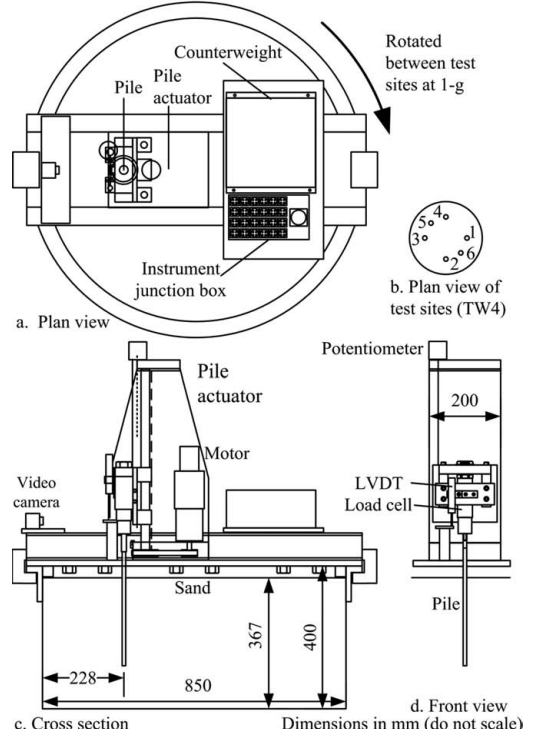


Figure 2. Centrifuge box and actuator.

during testing on the pile-soil interface friction angle, δ . Data from earlier centrifuge tests reported by Deeks & White (2006) showed that the average centreline surface roughness (R_a) of an aluminium pile can degrade during testing. Values of $2.7\text{ }\mu\text{m}$ and $0.3\text{ }\mu\text{m}$ were measured before and after testing. This degradation is due to mechanical surface abrasion during pile installation, and can influence the pile-soil interface friction angle.

By normalising R_a by the mean particle size of the test sand, $d_{50} = 119\text{ }\mu\text{m}$, (Fig. 3) the ratio R_a/d_{50} can be compared with the measurements of interface friction angle presented by Dietz (2000). This comparison shows that the degradation of R_a of the aluminium pile equates to a twofold reduction in peak interface friction angle δ_{peak} from $\sim 38^\circ$ to $\sim 21^\circ$.

Significant particle crushing occurs at the pile tip during deep penetration (White & Bolton 2004). As the pile penetrates deeper some of these fine particles remain at the pile-shaft interface. Consequently the actual value of d_{50} at the pile shaft-sand interface might be lower than for the virgin soil, and the normalised roughness and δ_{peak} consequently higher.

Using a Ferranti Surfcom 20C/30C the average centreline surface roughness (R_a) of the stainless steel

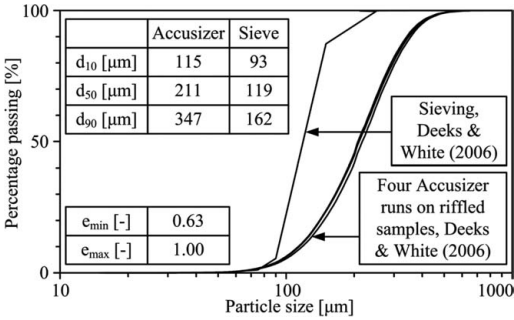


Figure 3. Particle size distributions of Fraction E silica sand.

model pile was measured as $3\text{ }\mu\text{m}$ both prior to and subsequent to testing. An internal load cell at the pile base (aluminium 6082-T6) allowed the base load to be separated from the shaft load.

2.1.4 Test sand

Gui et al. (1998) show that the ratio D/d_{50} of pile diameter to mean particle size d_{50} should exceed 20 in order for particle size effects to be negligible. The selected test sand, Fraction E silica sand, has a d_{50} particle size of $119\text{ }\mu\text{m}$ based on sieving analysis, which is 107 times smaller than the pile diameter (Fig. 3). An alternative particle size analysis was conducted using an optical laser method. This method provides a more detailed assessment of the particle size distribution by measuring the ‘shadow’ created by individual particles passing a laser, and idealising each particle as a sphere. This approach tends to oversize particles compared to sieving (White 2003).

A two-axis automatic sand pourer (Madabhushi et al. 2006) was used to air pluviate the sand in a dry state at 1-g. Sand was pluviated to a depth of 367 mm. Operation of the sand pourer is described by Zhao et al. (2006).

2.2 Control

Faithful replication of the pile jacking process requires a combination of displacement-controlled and load-controlled stages. Each jacking stroke involves displacement of the pile by a distance equal to the length of the hydraulic rams. After each jacking stroke the pile head is released to a condition of zero load.

The data acquisition card was used to output an analogue control signal indicating the target actuator velocity (updated at 100 Hz) to the motor controller which controls motion of the piling actuator. A proportional, integral, derivative (PID) control algorithm was implemented in the DasyLab (2004) software environment to provide mixed displacement and load

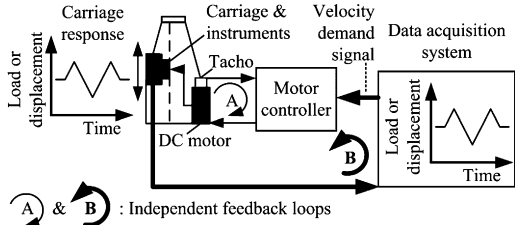


Figure 4. Schematic outline of the pile jacking control system.

control. This approach is described in detail by Deeks & White (2006). A schematic of the complete control system is shown in Figure 4.

3 RESULTS

3.1 Selected results

Test results from a single test week (denoted TW4) comprising 6 installations of the pile in the same soil sample are presented in this paper. A typical load-displacement history for a single test, comprising of installation, load testing and extraction is shown in Figure 5. Two of the six installations (TW4-01 & TW4-06) were monotonic: the pile was jacked to a depth of 190 mm in a single jacking stroke in stage (a). Tests -02 to -05 simulated the pile jacking process with stroke lengths equal to 1/10th, 1/10th, 1/50th and 1/5th of the embedded depth at the end of stage (a) respectively.

The centrifuge acceleration was 50 g at the sample base for all installations and tests. The results presented in this paper focus on (i) assessing the repeatability of the tests, (ii) assessing the sample density and stiffness based on the penetration resistance and (iii) identifying a simple model for the axial load-settlement response of the pile base.

The homogeneity of the sample and the repeatability of the tests is assessed from the base resistance recorded during each installation. Existing correlations are used to link the penetration resistance to the small strain stiffness of the soil.

Constant rate of penetration (CRP) load tests were conducted to quantify the stiffness of the axial load response (stages (b) & (e) shown on Fig. 5). Furthermore, since each jacking stroke starts from an initial state of zero head load and then proceeds at constant velocity, each installation stroke during stage (a) can also be analysed as a CRP load test. The sequence of installation strokes therefore provides a set of load tests conducted in the same sample but at different depths, and therefore different values of in situ stress. In some cases, axial load tests were performed after

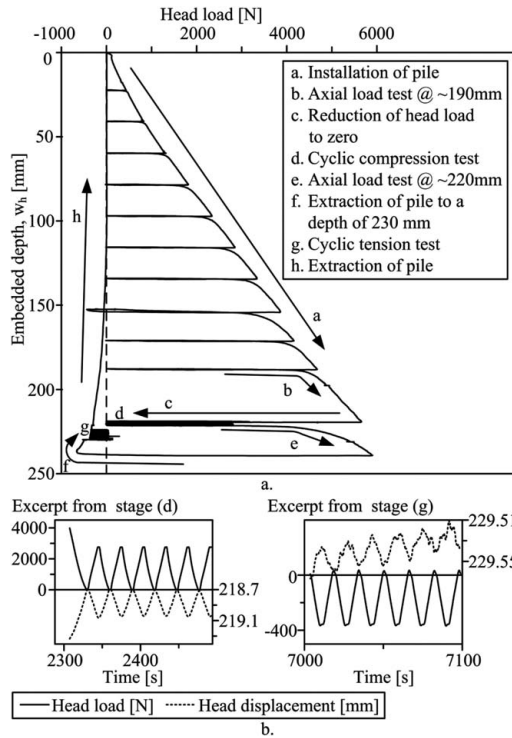


Figure 5. A typical test sequence (TW4-03).

cyclic loading of the pile head (stage (d)), but these results are not discussed in this paper.

3.2 Pile installation

3.2.1 Repeatability

Pile base resistance measured during installation, $q_{bf,install}$, was highly repeatable (Fig. 6). A ‘maximum path’ rule has been used in this figure to ignore unload-reload stages after each jacking stroke. The low ($\sim 5\%$) coefficient of variation (COV) of the base resistance recorded at a given penetration depth is in good agreement with Deeks & White (2006) and is an order of magnitude lower than found in the field (Phoon & Kulhawy 1999). High repeatability is also observed in the load tests performed subsequent to installation in stage (b) (Fig. 7).

There is a trend of increasing base resistance during the sequence of six tests (Figs. 6 & 7). The load test after the sixth installation recorded a 10% higher plunging base capacity than that of the first installation. This trend does not correlate with the number of cycles applied during installation. Similar behaviour was observed by Deeks & White (2006) for six monotonic pile installations. This trend can be attributed to

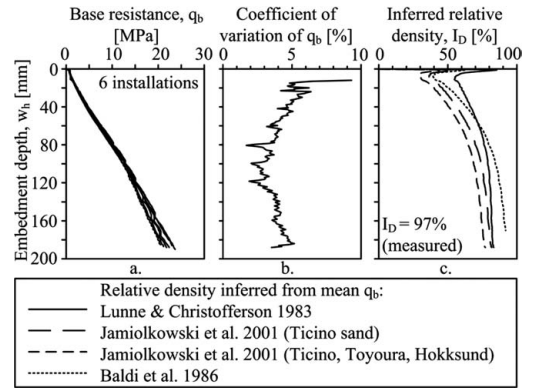


Figure 6. Base response during installation and inferred I_D .

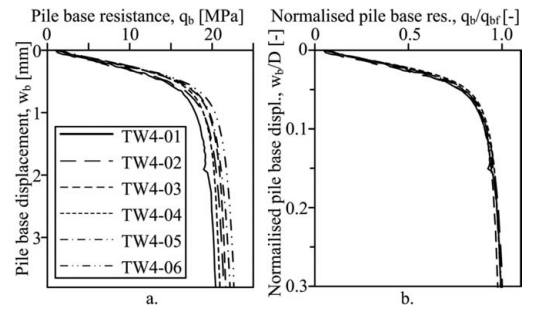


Figure 7. Load tests after installation (stage (b)).

densification of the soil sample as the g-level is cycled between tests. Alternatively, horizontal stresses are locked into the soil sample during installation, leading to higher penetration resistance when the pile is reinstalled nearby.

3.2.2 Correlations for relative density

The relative density, I_D , can be inferred from the base resistance during penetration using existing correlations for interpretation of cone penetration test (CPT) data in normally consolidated sands: $q_{bf,install}$ is effectively the cone tip resistance, q_c . The I_D profiles inferred using four popular correlations, which share the same functional form but have differing calibration coefficients, are shown in Figure 6.

The I_D profiles are approximately constant with depth after a penetration depth of 110 mm. This is consistent with data from Gui et al. (1998) who suggest that the deep penetration mechanism is fully activated at depths greater than 10 times the pile diameter (i.e. depths > 127 mm). I_D correlations based on q_c are unlikely to be reliable for shallower penetrations

than this critical depth. However, it is interesting to note that on either side of this critical depth the slope of the $q_{bf,install}$ profile is continuous and shows no obvious influence of this hypothesised change in penetration mechanism.

The mean inferred I_D for depths >130 mm is 15% less than that measured directly. The COV of these predictions – due to the differing calibration coefficients – is 9%. A unique $q_c - \sigma'_v - I_D$ relationship is not applicable to all sands. The difference between the relative density predicted by the correlations and the measured value for this test sand can be attributed to differences in the horizontal confining stress σ'_h (Houlsby & Hitchman 1988) and the sand compressibility (Robertson & Campanella 1983) between this test sand and the sands used to calibrate the correlations.

3.3 Base load-settlement response

3.3.1 Axial load tests during stage (b)

The six load tests conducted at an embedment of ~ 190 mm (stage (b), Fig. 5.) are compared in Figure 7. Axial compressive strain in the pile has been accounted for by dividing the axial load in the pile – at each instant in the load test – by the axial stiffness of the pile. Although these load tests take place at a constant rate of penetration, it has been shown that for centrifuge tests in dry sand, this approach gives results that are comparable to a conventional maintained load test since creep is negligible (Deeks & White 2006).

The load-settlement response is stiff: a displacement of 4% of the pile diameter mobilises 70% of the pile base capacity. The mean residual load is 1.2 MPa, and is equal to $\sim 8\%$ of the pile shaft capacity.

Normalising q_b by the base resistance at failure q_{bf} reduces the variation in the data by eliminating the slight increase in penetration resistance over the sequence of six installations. The base resistance does not reach a constant value at the end of each test, so true ‘plunging’ failure is not observed. In Section 4 a rigorous definition of q_{bf} is given, tied to the base resistance profile during steady penetration.

3.3.2 Axial load tests during installation

Installation profiles of q_b vs. embedment depth w_h , are shown for tests TW4-03 and TW4-06 in Figure 8. By taking $q_{bf,install}$ – for each installation – as a proxy for q_c , the small strain shear modulus G_0 , can be calculated following Baldi et al. (1989). The CPT rigidity ratio $G_{0,Baldi}/q_{bf,install}$ reduces by a factor of 2 over the depth of installation (Fig. 8). This variation emerges since G_0 is approximately proportional to $(\sigma'_v)^{0.5}$ (Mitchell & Soga 2005) and the penetration resistance profile is roughly linear with depth (or σ'_v) during these tests.

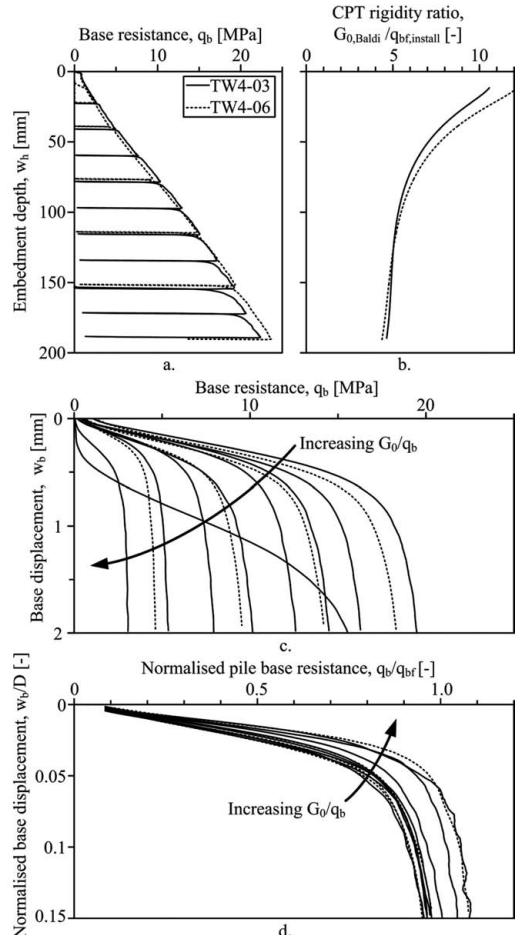


Figure 8. Load tests during installation (stage (a)).

During installation, the pile head displacement was recorded by a wire potentiometer with a range of 500 mm. This device had inadequate resolution or precision to measure the small displacements required to interpret the load test data. To increase the resolution of the displacement data, the velocity demand signal sent to the motor controller was integrated to give displacement. During subsequent load testing stages (i.e. (b), (d), (g) & (e)), a high quality LVDT transducer with a $+/-25$ mm range was suitably positioned to measure the displacement of the pile.

The initial stiffness of the $q_b - w_b$ response increases by a factor of ~ 5 from 7.4 to 34.1 MPa/mm as the initial embedment depth of the load test increases from 22 to 171 mm (Fig. 8). However, over the same depth range the base capacity increases by a factor of ~ 10 . As a result, the normalised initial stiffness on axes of

q_b/q_{bf} vs. w_b/D decreases by a factor of ~ 2 as the embedment depth increases.

This variation in base response matches with the trend of varying soil stiffness indicating that the initial base stiffness is proportional to the small strain shear modulus, G_0 . G_0 increases with depth, the response stiffness on $q_b - w_b$ axes follows the same trend. However the ratio G_0/q_b decreases with depth, so on normalised axes of $q_b/q_{bf} - w_b/D$ the initial normalised stiffness decreases in the same fashion. The decrease of initial stiffness with depth (on axes of $q_b/q_{bf} - w_b/D$) by a factor 2 matches the reduction in CPT rigidity ratio G_0/q_b .

The eighth load test – starting at a depth of 153 mm – is more compliant than the other tests. An error in the control system caused the pile to be pulled into tension prior to the load test (stage (a), Fig. 5). The response of this test is not shown on Figure 8d.

4 MODELLING THE BASE RESPONSE

4.1 A simple parabolic $q_b - w_b$ model

The aim of this research is to develop models – based on simple site investigation parameters – to predict the strength and stiffness of jacked piles. It is common to model the base and shaft response of a pile using the ‘t-z’ approach in which the response of the soil elements surrounding the pile is simplified into a single relationship linking the unit base or shaft resistance to the local displacement. Randolph & Wroth (1978) and Kraft et al. (1981) suggest appropriate relationships to link shaft and base resistance to local displacement, based on analytical solutions or calibrated against field data. Any non-linear response requires two input parameters. Deeks et al. (2005) & Yetginer et al. (2006) report field data indicating that a simple two-parameter parabola can be used to effectively model the base response of jacked piles in sand. A parabolic t-z response has been previously proposed by Randolph (1986), Aldridge & Schnaid (1992) and Randolph (1994).

A parabolic t-z curve provides a non-linear response until a constant ultimate capacity is mobilised, and is defined by only two parameters. If the load continues to increase with settlement beyond failure – so that the tangent stiffness never reaches zero – then an additional parameter is required, defining this gradient at plunging failure.

A parabolic model for base response in terms of normalised load, q_b/q_{bf} , and displacement, w_b/D is defined in Equation 1 and shown in Figure 9a, where K_I , K_P and w_{bf} are the initial gradient, plunging gradient and displacement to failure respectively. The gradients K_I and K_P are dimensionless. The response is parabolic up to failure ($q_b = q_{bf}$). Beyond failure

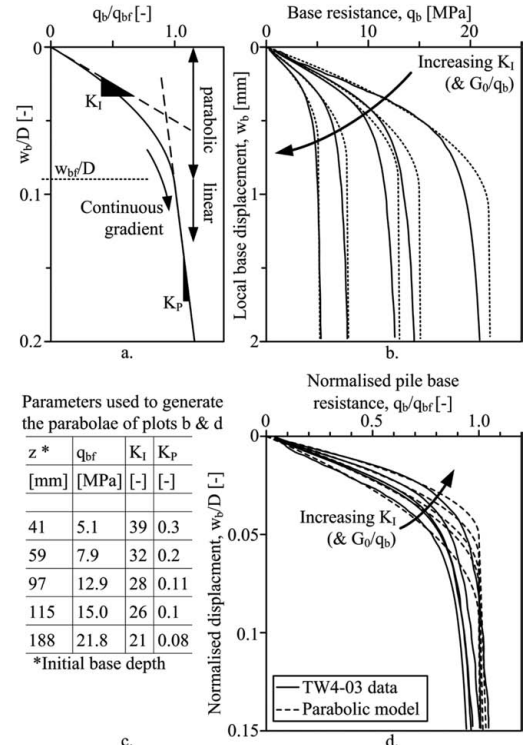


Figure 9. Parabolic modelling of base response during multiple load tests at different depths during a single test.

the parameter K_P allows the response during plunging failure to follow the gradient of the steady penetration ‘backbone’ curve.

The gradient of the curve is continuous in the transition from the parabolic to linear stage, which results in w_{bf} being equal to $2D/(K_I + K_P)$. Typically $K_I \gg K_P$ so $w_{bf} \sim 2D/K_I$.

For $w_b \leq w_{bf}$

$$\frac{q_b}{q_{bf}} = -\frac{1}{4} (K_P + K_I)^2 \left(\frac{K_I - K_P}{K_I + K_P} \right) \left(\frac{w}{D} \right)^2 + K_I \left(\frac{w}{D} \right) \quad (1)$$

For $w_b \geq w_{bf}$

$$\frac{q_b}{q_{bf}} = \frac{K_I - K_P}{K_I + K_P} + K_P \left(\frac{w}{D} \right)$$

4.1 Parabolic model: parameter derivation

4.2.1 Evaluating a load – settlement origin

In order to assess how well the load test results shown in Figure 8b can be fitted by a parabolic model it is necessary to derive the model parameters, q_{bf} , K_I and K_P from the measured data.

The presence of either residual base load or a soft initial response due to previous tensile loading affects the estimation of the initial gradient, K_I . A zero origin for the base settlement was assessed by linear extrapolation of the maximum tangent stiffness dq_b/dw_b present at low loads.

This method ensures that the settlement attributed to any residual load component is maximised, giving estimates of stiffness that are conservative. This approach also removes the soft initial response observed when a tensile load is initially applied to the pile.

4.2.2 Derivation of K_I

Data noise makes it difficult to evaluate the initial stiffness K_I directly from data about the $q_b = 0$, $w_b = 0$ origin. Consequently the maximum tangent stiffness of the $q_b - w_b$ response –taken over a running average of 5 data points– was used. The point at which this tangent value occurred is used to back-figure K_I such that its associated parabola has the same tangent stiffness at this point.

4.2.3 Derivation of K_p

K_p is evaluated from the gradient of the plunging portion of the load test data over the range $1 < w_b/D < 2$.

4.2.4 Derivation of q_{bf}

The final parameter to fit is q_{bf} , which varies with depth in these tests since K_p is non-zero. Consequently q_{bf} is evaluated using an extrapolation of the $q_b - w_b$ response during plunging failure. $w_{bf} \sim 2D/K_p$ so q_{bf} is evaluated as the value of q_b on this extrapolated response at the intersection with a line projected from the origin on modified $q_b - w_b$ axes that has a gradient equal to half K_I .

4.2.5 Comparison of the model with test data

In Figures 9b & 9d this model is compared to the load test data from Figure 8b (TW4). Good agreement is evident throughout typical working loads, and until $q_b/q_{bf} \sim 0.8$. The parameters used to generate these parabolae are shown in the table of Figure 9c. The parabolic model does not match the data well during the transition to plunging failure ($q_b/q_{bf} > 0.8$, Fig. 9d).

4.3 Properties of the parabolic model

For the case of $K_p = 0$ the parabolic model is unique on axes of q_b/q_{bf} vs. w_b/w_{bf} which eliminates the dependency on the CPT rigidity ratio G_0/q_{bf} . Figure 10 shows the load test data on these axes. The close alignment of the test data compared to Figures 9b & 9d demonstrates that normalisation using the CPT rigidity ratio G_0/q_{bf} is appropriate. Two parabolae are plotted on Figure 10, spanning the range of K_p present in the data. Despite K_p varying by an order of magnitude the parabolae are almost identical up to

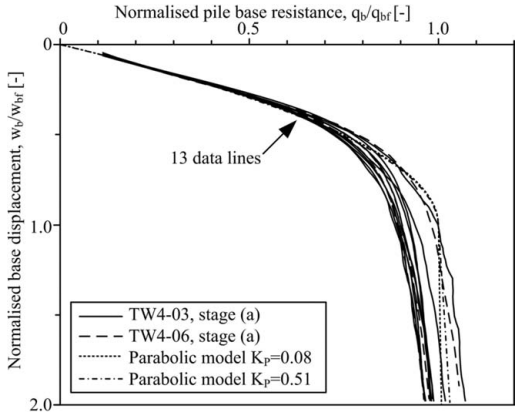


Figure 10. Normalised base load-settlement response for multiple load tests at different depths.

failure, due to the high ratio K_I/K_p . Furthermore, the simple parabolic model shows good agreement with the load test data throughout the load-settlement response.

4.4 Back-calculation of operative soil stiffness

The Boussinesq (1885) elastic solution for a point load in a half space can be integrated with appropriate boundary conditions, to give the solution for the indentation of a rigid punch on an elastic half-space (Timoshenko & Goodier 1970, Equation 2), where ν is Poisson's ratio.

$$w_b = \frac{\pi(1-\nu)}{8} \frac{q_b}{G} D \quad (2)$$

For the closed-ended piles reported in this paper, the response of the base can be back-analysed using Equation 2 to assess the operative soil stiffness when the pile base is loaded. The initial soil shear modulus $G_{b,init}$ is evaluated using the tangent value dq_b/dw_b evaluated at $w_b = 0$ (Equation 3a) and is linked to the initial stiffness K_I of the parabolic model by Equation 3b.

$$G_{b,init} = \frac{\pi(1-\nu)}{8} D \left. \frac{dq_b}{dw_b} \right|_{w_b=0} \quad (3a)$$

$$\frac{G_{b,init}}{q_{bf}} = \frac{\pi(1-\nu)}{8} K_I \quad (3b)$$

For design, the in situ small strain shear modulus G_0 , which can be assessed during seismic CPT testing, can be linked to $G_{b,init}$ by a modification factor χ_{Gb} , such that $G_{b,init} = \chi_{Gb} G_0$. This modification

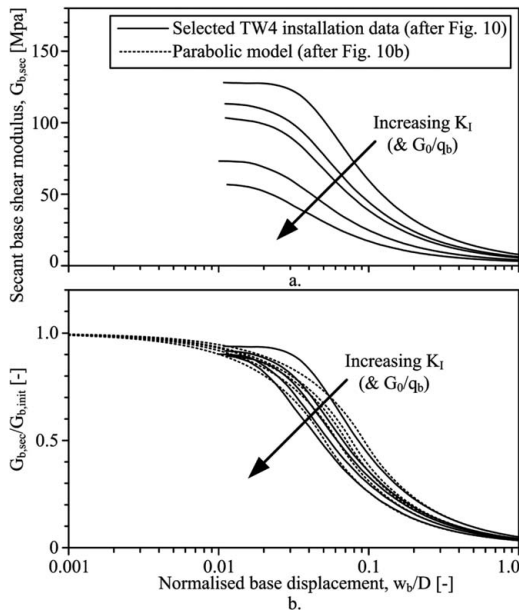


Figure 11. Selected shear modulus degradation curves.

factor captures any changes in soil stiffness around the pile base created by the installation process.

4.5 Degradation of operative soil stiffness

The rigid punch solution links the operative soil shear modulus at the pile base at any stage of the load test, $G_{b,sec}$ to the secant pile base stiffness, q_b/w_b (Equation 4).

$$G_{b,sec} = \frac{\pi(1-\nu)}{8} \frac{D}{w_b} q_b \quad (4)$$

Secant base shear modulus degradation curves for multiple load tests at different depths for the same pile installation (shown previously in Figure 9) are shown in Figure 11. Poisson's ratio has been assumed to equal 0.2 (following the suggestions of Bolton 1979 and Mitchell & Soga 2005 for typical sandy soils).

By normalising by the initial shear modulus $G_{b,init}$, (which is proportional to K_I) the data can be compared with the parabolic model (Fig. 11b). This mode of plotting the response highlights the degradation in operational stiffness more clearly than Figure 9 due to the logarithmic settlement axis.

Shear modulus degradation curves for the axial load tests of the six installations and tests of TW4 (i.e. stages (a), (b) & (e) shown in Fig. 5) are plotted in Figure 12. Data from the load test stages (b) & (e) is

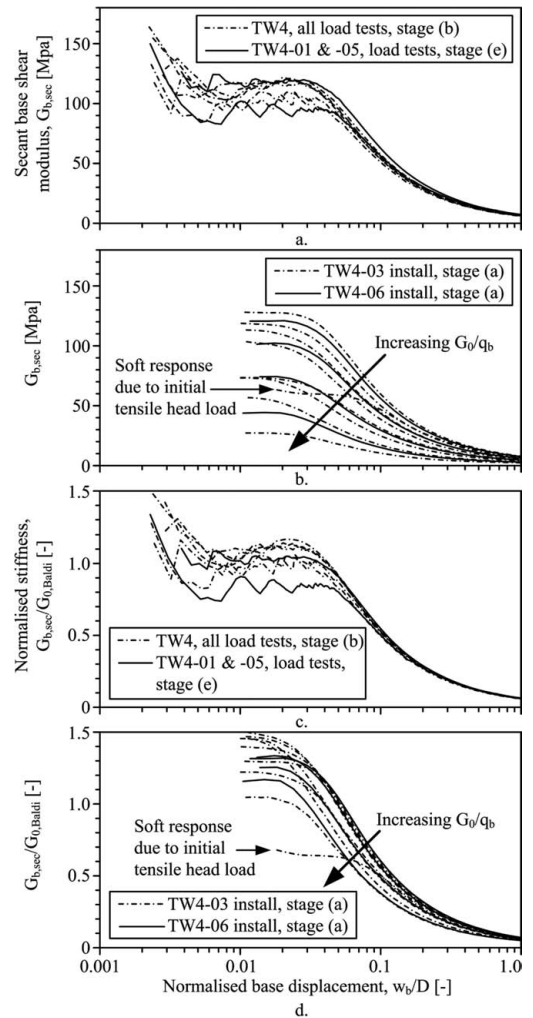


Figure 12. Secant shear modulus degradation curves.

presented to a higher resolution as higher quality displacement data was available for these tests.

These stiffness degradation curves can be normalised by the in situ small strain soil shear modulus estimated using Baldi's (1989) empirical correlation for G_0 (as described in Section 3.3.2) (Fig. 12b).

The parabolae for the load tests in this paper were on average best fitted with $\chi_{Gb} = 1.4$ (Figure 13). The stiffness ratio ($G_{b,sec}/G_{b,init}$) of the parabolae degrades to ~ 0.91 (for the relevant values of K_I & K_p) at a settlement of $w_b/D = 0.01$, corresponding to $G_{b,sec}/G_{0,Baldi} = 1.27$. This is in good agreement with the test data of this paper, which has a mean ratio of $G_{b,sec}/G_{0,Baldi}$ at a settlement of $w_b/D = 0.01$ is 1.23 (Figs. 12c & 12d).

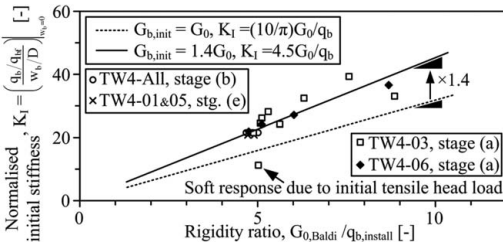


Figure 13. Rigidity ratio vs. normalised initial stiffness.

This ratio $\chi_{Gb} = 1.4$ indicates that the installation of the pile has the effect of increasing the local small strain soil stiffness by $\sim 40\%$, notwithstanding any error in the empirical estimate of G_0 .

5 DESIGN

The parabolic model combined with the seismic CPT parameters G_0 and q_c (from which q_{bf} is evaluated), allows the initial stiffness (Equation 5), stiffness degradation, capacity at failure (q_{bf}) and settlement to failure (Equation 6) of the base response of a closed-ended jacked pile to be estimated.

$$K_I = \frac{8}{\pi(1-\nu)} \frac{\chi_{Gb} G_0}{q_{bf}} \approx 3.2 \frac{\chi_{Gb} G_0}{q_{bf}} \quad (5)$$

$$\frac{w_{bf}}{D} = \frac{2}{K_I + K_p} \approx \frac{2}{K_I} \approx \frac{0.6}{\chi_{Gb} (G_0/q_{bf})} \quad (6)$$

During installation of a jacked pile the soil below the pile base is pre-loaded by the final installation stroke. The stiffness modification factor χ_{Gb} accounts for this effect. Data from these centrifuge tests (where G_0 has been inferred using Baldi's (1989) correlation) suggests $\chi_{Gb} = 1.4$ (Fig. 13). Alternatively, a conservative assessment, ignoring stiffness enhancement through preloading would be $\chi_{Gb} = 1.0$.

This pre-loading and additional stiffness leads to a high operative stiffness at typical working loads. The variation in normalised operative stiffness with load factor, $L_f = q_{bf}/q_b$, is illustrated on Figure 14. If $K_p = 0$, then the parabolic model is unique on these axes. If a load factor of 2 is applied to the base capacity (so $q_b/q_{bf} \sim 0.5$) then the operative shear modulus at the base is a high proportion of G_0 : greater than unity for the data presented in this paper.

Design curves for piles are commonly plotted as stiffness degradation curves on axes of $G_{b,sec}/G_0$ vs. w_b/D (Ghionna et al. 1993, Atkinson 2000 and Berardi & Bovolenta 2005). The parabolic models fitted to the data from the tests reported in this paper are

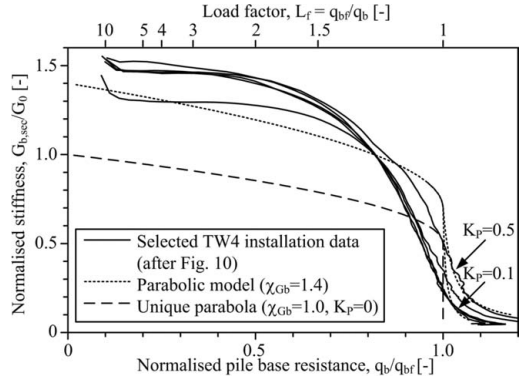
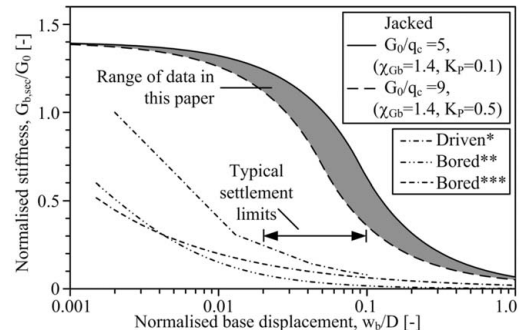


Figure 14. Degradation of stiffness with normalised load level.



*(API 2000), **(Berardi & Bovolenta 2005), ***(Ghionna et al. 1993)

Figure 15. A comparison with existing design guidance.

plotted against existing design guidance for bored piles (Ghionna et al. 1993 and Berardi & Bovolenta 2005) and driven piles (API 2000) on Figure 15.

At typical working settlements the back-analysed jacked pile response indicates a stiffness that is greater than that recommended for driven and bored piles by factors of approximately 5 and 10 respectively. Lower ratios would result if a conservative assessment of χ_{Gb} as unity is used.

The API (2000) guidance for driven piles is targeted at the design of large open-ended piles for use offshore. Due to the dynamic installation process these large driven piles typically install in a 'coring' fashion with the soil level inside the pile remaining near the ground surface throughout installation (Randolph et al. 1991). In contrast, the pile jacking process does not involve dynamic effects so a soil plug usually forms during installation (De Nicola & Randolph 1997). Jacked open-ended piles therefore penetrate in the same manner as closed-ended piles and are therefore likely to have a similarly stiff base response.

6 CONCLUSIONS

A series of centrifuge tests that faithfully model the installation and load test performance of jacked piles in dry sand has been conducted. The repeatability of the sample preparation method leads to a COV of penetration resistance that is an order of magnitude less than that of a CPT q_c profile at typical field sites. This high repeatability leads to less ambiguity in the interpretation of parametric studies compared to experiments conducted at field scale.

The axial load-settlement response for the pile base is captured by a parabola. Using the elastic solution for a rigid punch on a half space the initial base stiffness has been linked to G_0 . The ultimate capacity of the pile base is linked to the CPT parameter q_c , which is assessed as the base resistance during steady penetration in these tests.

The seismic CPT parameters G_0 and q_c , coupled with the parabolic model, provide a simple method for predicting the base response of a jacked pile. The CPT rigidity ratio G_0/q_c governs the initial stiffness of the response and the settlement at failure w_{bf} . The initial operative stiffness during loading is $\sim 40\%$ higher than G_0 , where this stiffness is assessed from q_c using the Baldi et al. (1989) empirical correlation.

The parabolic model is compared to existing design guidance proposed for bored piles (Ghionna et al. 1993 and Berardi & Bovolenta 2005) and driven piles (API 2000). At typical working settlements the proposed model for jacked piles is stiffer than driven and bored piles by factors of approximately 5 and 10 respectively. This observation supports previous research indicating that the base response of jacked piles is significantly stiffer than conventional bored or driven piles. Since pile design is usually governed by serviceability and stiffness, jacked piles offer the potential for improved design efficiency.

7 ACKNOWLEDGEMENTS

This research was funded by Giken Seisakusho Co. Ltd. The first author is supported by the George and Lillian Schiff Foundation. The technical support provided by Mr S. Chandler, and colleagues at the Schofield Centre is acknowledged.

REFERENCES

- Aldridge, T. R. & Schnaid, F. 1992. Degradation of skin friction for driven piles in clay. *Proceedings of the conference: Recent large-scale fully instrumented pile tests in clay*. London. Thomas Telford, 538–553.
- American Petroleum Institute 2000. *RP 2A-WSD: Planning, designing and constructing fixed offshore platforms – working stress design*, Washington DC.
- Atkinson, J. H. 2000. Non-linear soil stiffness in routine design. *Géotechnique*, 50 (5), 487–507.
- Baldi, G., Bellotti, R., Ghionna, V. N., Jamiolkowski, M. & Pasqualini, E. 1986. Interpretation of CPTs and CPTUs; 2nd part: drained penetration of sands. *Proc. of the 4th International Geotechnical Seminar*. Singapore. 1:143–156.
- Baldi, G., Belotti, R. & Ghionna, V. N. 1989. Modulus of sands from CPT's and DMT's. *Proc. 12th Int. Conf. on Soil Mech. & Fnd. Eng.* Rio de Janeiro. 1:165–170.
- Berardi, R. & Bovolenta, R. 2005. Pile-settlement evaluation using field stiffness non-linearity. *Proc. of the Inst. of Civil Engrs.: Geotechnical Engineering*, 158 (GE1), 1353–2618.
- Bolton, M. D. 1979. A guide to soil mechanics, Cambridge, UK, M D & K Bolton.
- Boussinesq, J. 1885. *Application des Potentiels a l'Etude de l'Equilibre et du Mouvement des Solides Elastiques*, Paris, Gauthier-Villars.
- Dasylab 2004. *Dasylab 8 user guide*. Moenchengladbach, Germany, measX GmbH & Co. KG
- De Beer, E. 1988. Different behaviour of bored and driven piles. *Proc. of the Int. Conf. on Bored & Augured Piles I*. Balkema, Rotterdam, 47–82.
- De Nicola, A. & Randolph, M. F. 1997. The plugging behaviour of driven and jacked piles in sand. *Géotechnique*, 47 (4), 841–856.
- Deeks, A. D. & White, D. J. 2006. Centrifuge modelling of jacked piles. *Proc. 6th Int. Conf. on Physical Modelling in Geot.* Hong Kong. Taylor & Francis. 2:821–826.
- Deeks, A. D., White, D. J. & Bolton, M. D. 2005. A comparison of jacked, driven and bored piles in sand. *Proc. 16th Int. Conf. on Soil Mech. & Geot. Eng.* Osaka. 3:2103–2106.
- Dietz, M. S. 2000. *Developing an holistic understanding of interface friction using sand within the direct shear apparatus*. PhD dissertation, University of Bristol, Bristol.
- Ghionna, V. N., Jamiolkowski, M. & Lancellotta, R. 1993. Base capacity of bored piles in sands from in situ tests. *Proc. of the Int. Conf. on Bored & Augured Piles II*. Balkema, 67–75.
- Gui, M. W., Bolton, M. D., Garnier, J., Corte, J. F., Bagge, G., Laue, J. & Renzi, R. 1998. Guidelines for cone penetration tests in sand. *Centrifuge '98*. Balkema. 155–160.
- Housley, G. T. & Hitchman, R. 1988. Calibration Chamber Tests of a Cone Penetrometer in Sand. *Géotechnique*, 38(1), 39–44.
- Jamiolkowski, M., Lo Presti, D. C. F. & Manassero, M. 2001. Evaluation of Relative Density and Shear Strength of Sands from CPT and DMT. *Soft Ground Construction 2001*. ASCE, GSP No.119. 201–238.
- Kraft, L. M., Ray, R. P. & Kagawa, T. 1981. Theoretical t-z curves. *ASCE J of Geot. Eng. Div.*, 107, 1543–1561.
- Lee, J., Salgado, R. & Paik, K. 2003. Estimation of load capacity of pipe piles in sand based on cone penetration test results. *ASCE J of Geot. & Geoenv. Eng.*, 391–403.
- Lehane, B. M., Pennington, D. & Clark, S. 2003. Jacked end-bearing piles in the soft alluvial sediments of Perth. *Australian Geomechanics*, 38 (3), 123–133.
- Lunne, T. & Christofferson, H. P. 1983. Interpretation of cone penetrometer data for offshore sands. *Offshore Technology Conference*. Houston. OTC4464. 181–192.
- Madabhushi, S. P. G., Houghton, N. E. & Haigh, S. K. 2006. A new automatic sand pourer for model preparation at

- the University of Cambridge. *Proc. 6th Int. Conf. on Physical Modelling in Geot.* Hong Kong. Taylor & Francis. 1:217–222.
- Mitchell, J. K. & Soga, K. 2005. *Fundamentals of Soil Behaviour*. New York, Wiley.
- Phoon, K. K. & Kulhawy, F. H. 1999. Characterization of geotechnical variability. *Canadian Geot. J.*, 36 (4), 612–624.
- Randolph, M. F. 1986. *RATZ – load transfer analysis of axially loaded piles*. UWA, Perth, Australia, GEO report 86033.
- Randolph, M. F. 1994. Design methods for pile groups and piled rafts. *Proc. 13th Int. Conf. on Soil Mech. & Fnd. Eng.* New Delhi. 5:61–82.
- Randolph, M. F., Leong, E. C. & Houlsby, G. T. 1991. One-dimensional analysis of soil plugs in pipe piles. *Géotechnique*, 41 (4), 587–598.
- Randolph, M. F. & Wroth, P. 1978. Analysis of deformation of vertically loaded piles. *ASCE J of Geot. & Geoenv. Eng.*, 104 (12), 1465–1488.
- Robertson, P. K. & Campanella, R. G. 1983. Interpretation of cone penetrometer tests: Part I: Sand. *Canadian Geot. J.*, 20 (4), 718–33.
- Rockhill, D. J., Bolton, M. D. & White, D. J. 2003. Ground-borne vibrations due to press-in piling operations. *Proc., BGA International Conference on Foundations*. 1:743–756.
- Schofield, A. N. 1980. Cambridge Geotechnical Centrifuge Operations. *Géotechnique*, 30 (3), 227–268.
- Silva, M. F. 2005. *Numerical and physical models of rate effects in soil penetration*. Ph.D, Cambridge University, UK.
- Timoshenko, S. P. & Goodier, J. N. 1970. *Theory of Elasticity*, New York, McGraw-Hill.
- White, D. J. 2003. PSD measurement using the single particle optical sizing (SPOS) method. *Géotechnique*, 53 (3), 317–326.
- White, D. J. & Bolton, M. D. 2004. Displacement and strain paths during pile installation in sand. *Géotechnique*, 54 (6), 375–398.
- White, D. J., Finlay, T. C. R., Bolton, M. D. & Bearss, G. 2002. Press-in piling: Ground vibration and noise during pile installation. *International Deep Foundations Congress*. Orlando, USA. ASCE. special publication 116:363–371.
- Wood, D. M. 2004. *Geotechnical Modelling*. London and New York, Spon Press.
- Yang, J., Tham, L. G., Lee, P. K. K., Chan, S. T. & Yu, F. 2006. Behaviour of jacked and driven piles in sandy soil. *Géotechnique*, 56 (4), 245–259.
- Yetginer, A. G., White, D. J. & Bolton, M. D. 2006. Field measurements of the stiffness of jacked piles and pile groups. *Géotechnique*, 56 (5), 349–354.
- Zhao, Y., Gafar, K., Elshafie, M. Z. E. B., Deeks, A. D., Knappett, J. A. & Madabhushi, S. P. G. 2006. Calibration and use of a new automatic sand pourer. *Proc. 6th Int. Conf. on Physical Modelling in Geot.* Hong Kong. Taylor & Francis. 1:265–270.

Development on battered pile with screw pile method (NS-ECO pile)

A. Komatsu

Nippon Steel Engineering Corporation, Tokyo, Japan

ABSTRACT: Installation tests and study for screw piles were executed, and the following results were obtained. 1. It is possible to drive into and through the dense sand with no discharge, low noise and low vibration. 2. Battered piling is available to keep an accurate inclination by using a casing driver.

1 INTRODUCTION

1.1 General

A battered pile foundation has excellent sustaining capacity for horizontal loads, especially for a bridge foundation on soft ground. In addition, in case of the lateral movement of the foundation, a battered pile foundation is evaluated as a more rigid foundation than the vertical pile foundation. A battered pile used to be installed with a driving hammer, but the driving hammer has been prohibited to prevent noise and vibration since the 1980s in Japan. So the battered pile has not been applied to bridge foundations. Recently, new pile installation methods such as the screw pile (NS-ECO pile) that can be installed with low noise and low vibration have been developed.

2 INSTALLATION AND FEATURES OF THE SCREWED PILE

The screw pile was developed to have a screwed-shaped steel blade attached to the open end as illustrated in Figure 1, 2. Using a pile driver or the like, the screwed pile is given a rotating torque, and is twisted into the ground with the wedge effect of the blade utilized the driving force. The screw pile feature the following:

1. It produces no surplus soil, muddy water, and other waste materials at all.
2. No soil is excavated and, because no mud water and cement is used, environmental contamination of water sources is can be avoided.
3. Low-noise, low-vibration work is available.
4. It is classified as displacement pile. A large bearing capacity can be expected due to the base enlargement effect of the blade.



Figure 1. Screw pile (NS-ECO pile).

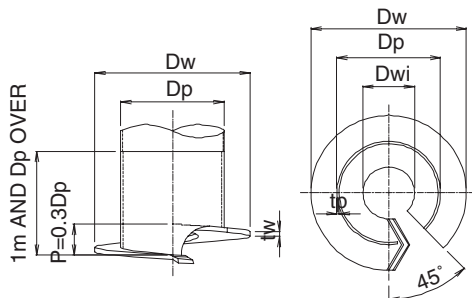


Figure 2. Details of NS-ECO pile.

5. A large uplift bearing capacity is expected due to the anchor effect of the blade.
6. The arrival of piles at the bearing stratum can be confirmed by means of rotation torque, and excellent deformation capacity can be provided.
7. Piling work in narrow yards and limited space is available by using casing drivers.

3 DEVELOPMENT OF NS-ECO PILE

3.1 Shape of blade

This study has the following purposes:

1. Check whether or not large diameter piles in the diameter range of over 500 mm, can be screwed in ordinary Japanese ground.
2. Extract and analyze blade shape parameters that affect the installation of screw piles.

The test sites were situated in Futtsu City, Chiba Prefecture. The subsurface investigation results are shown in Figure 3.

In the screw piling method, the end shape of screw piles has a large influence on the installability of the screw piles. The following can be considered as parameters:

1. Diameter of steel pipe body
2. Shape of blade (Figure 4)
3. Outside diameter of blade
4. Pitch of blade (elevation change per rotation)
5. Open-end ratio of bottom plate portion of steel pipe body

Full-size screw piles were installation tested to determine the effects of these five items on the installability of the screw piles.

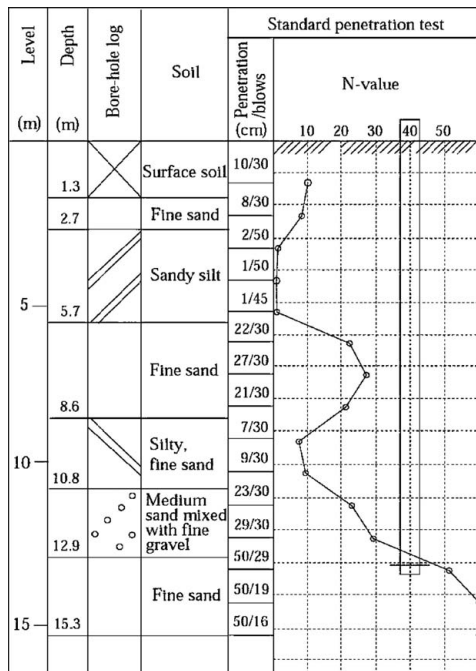


Figure 3. Boring data.

Table 1 lists the test specimens. The effect of each parameter was evaluated by the test results of the 24 specimens.

3.2 Results of installation test

The measurement items are a penetration per rotation (mm/rotation), applied load (kN), and in-pipe soil elevation (m). The penetration characteristics of the screw piles greatly depend on the blade shape parameters. Particularly where the N-value suddenly increased, the screw piles greatly differed in their penetration, and some screw piles were not driven any further. In each case, the penetration torque exhibited a good correlation with the N-value. The screw pile penetrated through a soft soil with relatively small torque. In the intermediate strata and the bearing stratum, the torque changed with the hardness of the soil encountered. The torque increased with increasing pipe diameter (blade diameter), indicating the effect of the pile area or volume. As the effect of the end shape, a single blade required a larger torque than two blades, but provided a larger penetration per rotation. The torque increased with increasing blade diameter and angle, and decreased with decreasing blade diameter and angle. The slip phenomenon that the penetration became practically zero was found to occur ahead of an intermediate stratum when the blade diameter ratio was 1.2 and ahead of the bearing stratum when the blade angle was 2.5 degree. The penetration per rotation can be controlled by changing the applied load. The screw pile can penetrate through soft soil by an amount approximately equal to the blade pitch, but cannot penetrate through hard soil by such a large amount. When the end resistance increases during a change from soft to hard soils, the slip phenomenon sometimes occurs. Application of load increases the pressure imposed on the bottom plate portion and facilitates the penetration of the pile into hard soil. The applied load-depth curve indicates how the load was applied to the pile at each depth.

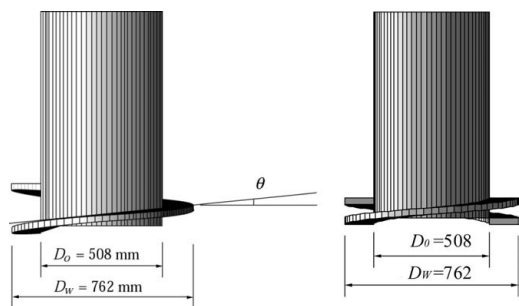


Figure 4. Shape of test pile (left side: single blade, right side: double blades).

The applied load includes the dead weight of the earth auger (151.9 kN).

3.3 Shape of blade and etc.

According to the installation tests and further study, the following results are obtained.

1. Open end

In order to penetrate more larger diameter piles over 500 mm, open end type blade was recommended. Now 1600 mm diameter pile (blade diameter/2400 mm) can be penetrated by using open end type blade.

2. Single spiral blade

Single blade and double blades was compared to evaluate the penetration efficiency of screw piles by installation tests. As a results, it is obtained that single blade is more efficient to penetration of piles than double blades because of the blade edge efficiency.

3. Casing driver

It is found that rotation torque more than 1000 kN·m is required in order to penetrate piles over 500 mm in diameter. Casing driver was used instead of auger driver.

3.4 Condition of penetration into the ground

By model tests for both sand and clay, condition of penetration of screw piles was observed. A cylindrical testing vessel has internal dimension of 1200 mm in diameter, 1200 mm in height. Model pile was 40 mm in diameter and its blade was 80 mm in diameter. The results of tests are shown in Figure 5, Figure 6. From these figures, it is found as follows:

1. Soil above the blade of screw pile is rising upwards.
2. Soil attached to the pile shaft is pulled down due to the shaft friction.
3. Soil beneath the blade is compressed bellow. It shows that soil around the blade is not loose.

Table 1. List of test piles.

Test pile	Steel pipe diameter D ₀ (mm)	Blade shape	Blade diameter ratio D _w /D ₀	Open-end ratio (%)	Blade angle depth θ(deg)	Embedment GL-(m)	Remarks
1 5W15M09	508	2 blades	1.5	90	5	13.7	11.6 Standard pile
2 5S15M09		1 blade				13.7	13.7
3 5W12M09			1.2			7.6	
4 5W20M09			2.0			13.5	13.5
5 5W15M07				70		11.5	14.0
6 5W15M00				0		13.3	12.0
7 5W15S09					2.5	11.7	13.7
8 5W15D09					10	13.0	13.7
9 5S15M00		1 blade		0		13.4	13.4
10 5S15M10		1 blade		100		13.7	13.4
11 5W15D10				100	10	13.1	
12 5W15D10-B				100	10	13.0	13.0 With excavation bit
13 5W17M09			1.75			13.8	13.7
14 5S15MBL		1 blade				13.6	Bottomless
15 6W15M09	609.6	2 blades	1.5	90	5	16.4	14.2
16 6W15S09	609.6				2.5	16.4	14.0
17 6W15D09	609.6				10	16.4	14.0
18 6S15M00	609.6	1 blade		0		16.4	
19 6S15M10	609.6	1 blade		100		16.4	13.5
20 6S15D09	609.6	1 blade			10	16.4	
21 3W15M09	318.5	2 blades	1.5	90	5	15.0	15.0
22 3W15M07	318.5			70		17.5	15.5
23 3S15M00	318.5	1 blade		0		16.2	
24 3S15M10	318.5	1 blade		100		16.8	

Data in blank space are same as those of standard pile(5W15M09).

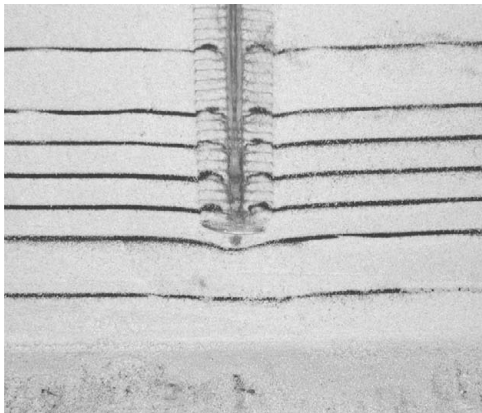


Figure 5. Sand model test.

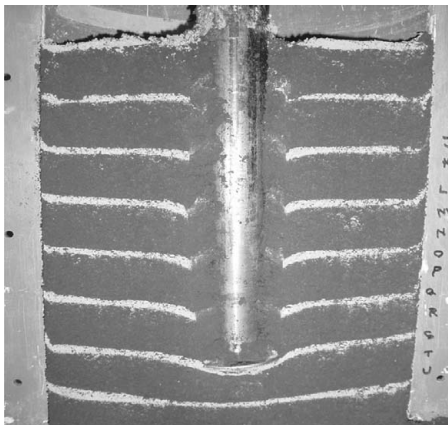


Figure 6. Clay model test.

4 INSTALLATION OF BATTERED PILES

4.1 Outline of installation condition

Battered screw piles were used for the foundation of the windmill at KITAKYUSU City, FUKUOKA Prefecture. The subsurface investigation results are shown in Figure 7. Comparison between vertical piles and battered piles is shown in Table 2.

4.2 Method of installation

The casing driver (RT200H) was used as the driving machine, and the crawler crane for 90tf lift was used. The arrangement of machines was shown in Figure 8, Figure 9.

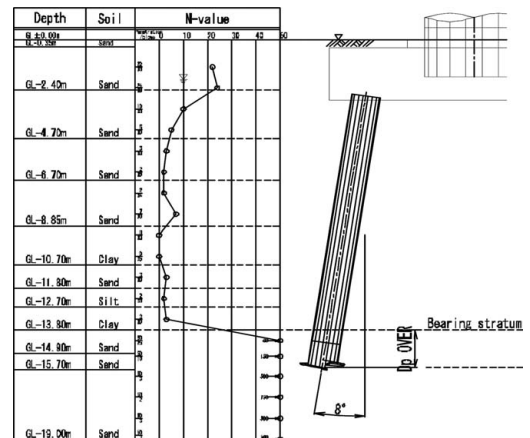


Figure 7. Boring data.

Table 2. Comparison results (screw piles).

	Vertical piles	Battered piles
Foundation arrangement		
Footing	Octagon shape	Square shape
Piles	$\varphi 1200\text{mm}/\text{blade}$ $\varphi 1500\text{mm}, 13\text{mL}, 9 \text{ nos.}$	$\varphi 1200\text{mm}/\text{blade}$ $\varphi 1500\text{mm}, 13\text{mL}, 6 \text{ nos.}$
Calculation result*	Compression: 4230kN Tension: -1619kN $\Delta h : 47.7\text{mm}$	Compression: 5504kN Tension: -1824kN $\Delta h : 13.2\text{mm}$
Construction cost	1.0	0.8

Note: Results * = acting loads on a pile top and a pile top deflection.

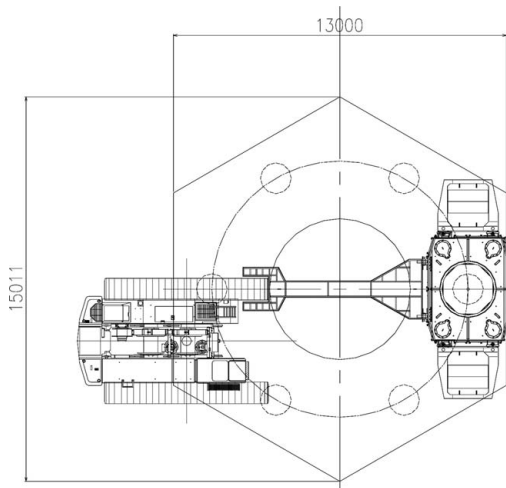


Figure 8. Plan of machine arrangement.

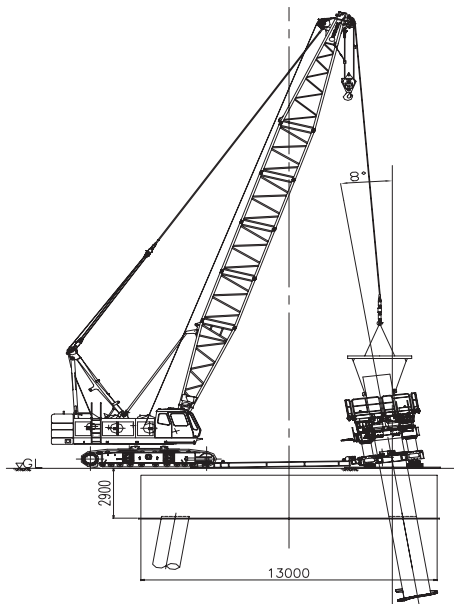
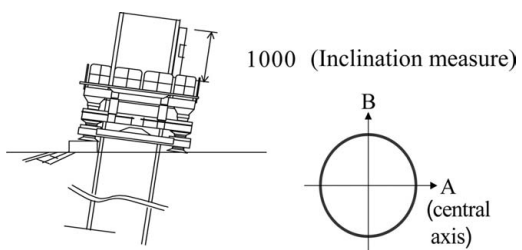


Figure 9. Elevation of machine arrangement.

The level jacks of casing driver are set on the stand in order to incline 8 degrees. The inclination angle was conformed every 750 mm lift by an inclination gauge and was adjusted by using the level jacks. In case of

Table 3. The pile inclination angle.

Pile no.	A	B	
1	7.9°	90.0°	OK
2	7.9°	90.0°	OK
3	8.2°	89.9°	OK
4	8.0°	90.1°	OK
5	8.2°	89.9°	OK
6	8.0°	90.0°	OK



welding an upper pile, it was lifted to keep the inclination angle of 8 degree.

4.3 Results of installation

The pile inclination angle after installation is shown in Table 3.

5 CONCLUSION

In this study, installation test and study for screw piles were executed, and following results were obtained:
 1. Regarding the efficiency of penetration, an open end blade and a single spiral blade were recommended.
 2. Battered piles can be installed by using the screw pile method to keep an accurate inclination.

REFERENCE

Saeki, E., Ohki, H. 1999. A Study of the Screwed Pile, *Architectural Institute of Japan*. 45(B): 453–462.

BCH method applicable to the construction under overhead restrictions

S. Tajima, T. Yoshikawa, S. Saito & H. Kotaki

Kajima Corporation, Tokyo, Japan

M. Koda

Railway Technical Research Institute, Tokyo, Japan

ABSTRACT: Bottom Circulation Hole method (BCH) has been developed, for the foundation piles constructed under the overhead restrictions and other site access restrictions, such as under the existing structures and the existing bridges. BCH is superior to the conventional BH method (normal circulation method), as the decrease of the bearing capacity due to high-density stabilizing slurry can be improved. The bearing capacity characteristics of the piles constructed by using BCH method was quantitatively confirmed by the static load tests conducted according to the Japanese Geotechnical Society Standard, JGS 1811. Furthermore, for large-diameter piles (up to 2.0 m), the experimental constructions were done with construction machinery, which is the same size as conventional machinery and designed for good performance in the excavation and the sludge unloading. In this paper, these experimental constructions and the pile loading tests are explained.

1 CONVENTIONAL CAST-IN-PLACE PILE METHOD FOR THE CONSTRUCTION UNDER OVERHEAD RESTRICTIONS AND OTHER SITE ACCESS RESTRICTIONS

Currently, the circulation method and the reverse circulation method are applied to the construction of the cast-in-place piles under the overhead restrictions and other site access restrictions. BH method and TBH method are the representative methods of the circulation and the reverse circulation method, respectively. In the circulation method, from its excavation mechanism, the construction machinery can be downsized. However, mud cakes can be easily formed in the excavation holes, and slime can settle around the pile end because of the circulation of the high-density stabilizing slurry with flowing excavated materials in the excavation hole. Therefore, it is considered that the piles constructed by this method are not reliable and of low quality from the point of view of the bearing capacity, when it is applied to permanent structures.

To the contrary, the piles constructed by the reverse circulation method are highly reliable and of high quality, because the excavation holes can be filled with low-density stabilizing slurry that has better quality. Thus, the method is widely applied to the construction of the piles as the permanent structures. However, as the large-sized construction machineries are necessary, the reverse circulation method is more

disadvantageous than the circulation method, from the point of view of the applicability to the pile constructions under the severe overhead restrictions and other site access restrictions.

Thus, Bottom Circulation Hole method (BCH) was established based on BH method (circulation method). By improving the quality of stabilizing slurry, the construction of foundation piles with the same bearing capacity characteristics as those constructed by TBH method can be realized.

2 MECHANISM OF BCH METHOD

The comparison of the excavation mechanism between BH and BCH method is shown in Figure 1. In BH method, the mud water, which is the mixture of excavated material and stabilizing slurry jetting from the end of the excavation bit, is lifted up and discharged to the ground surface. Therefore, it is difficult to keep the stabilizing slurry in good quality, while the required bearing capacity cannot be obtained unless stabilizing slurry is well controlled. To overcome this disadvantage, the following techniques are employed: (1) To avoid the circulation of mud water in the excavation hole, the mud water including excavated material is discharged through the unloading pipe located immediately above the excavation bit. (2) The excavation hole is constantly

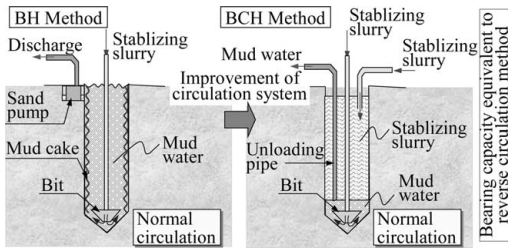


Figure 1. Comparison of BH method and BCH method.

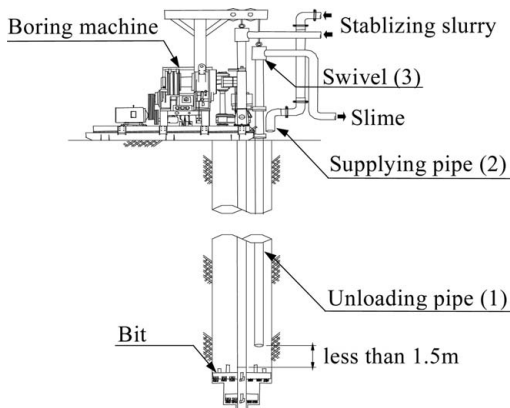


Figure 2. Conceptual drawing of BCH method.

filled with stabilizing slurry in good quality supplied from the ground surface. Thus, the cast-in-place pile with sufficient bearing capacity as a permanent structure can be constructed, under the severe overhead restrictions and other site access restrictions, by using the small-sized construction machineries.

The outline of BCH method is shown in Figure 2. Major features of the method are summarized as below.

- (1) The unloading pipe is installed within 1.5 m above the excavation bit. Excavated material is carried upward immediately after the excavation and discharged. The slime collected at the bottom of the hole is removed by the rotation of the bit after drilling.
- (2) For effective discharge of excavated material, the diameter of the unloading pipe and the pump capacity are enlarged. The stabilizing slurry in good quality and quantity is supplied from the ground surface.
- (3) For easier construction under site access restrictions, installations and de-installations of the unloading pipe are simplified by means of a swivel.

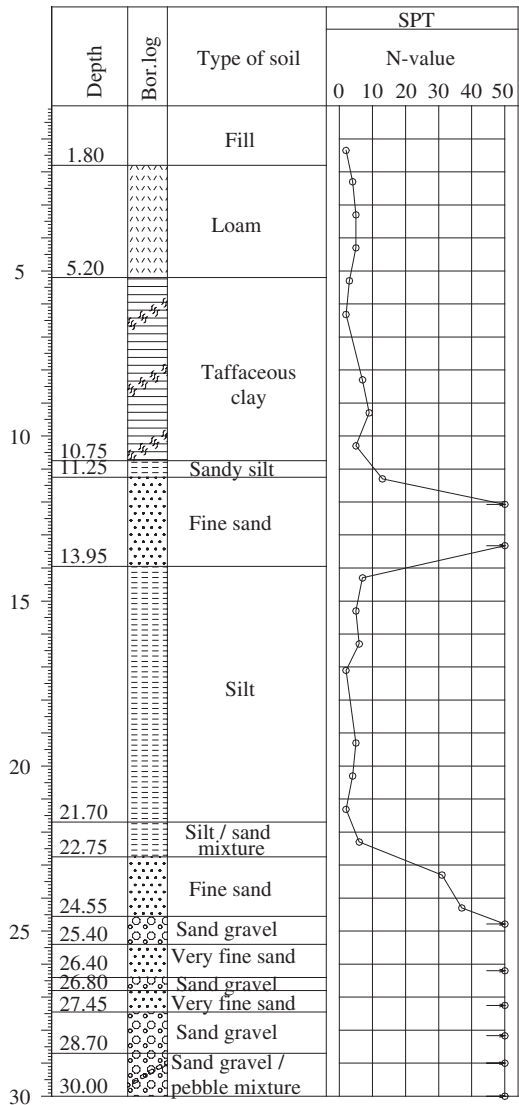


Figure 3. Boring Log.

3 CORROBORATION TEST AND LOADING TEST

The corroboration test and the static loading test were performed to confirm the function and quality of BCH method. The diameter of test pile is 800 mm, and the pile length is 26.5 m. As shown in Figure 3, the soil profile is, from the top to the bottom, loam, clay and silt. Bearing stratum is alternation of sand and gravel ($N > 50$).

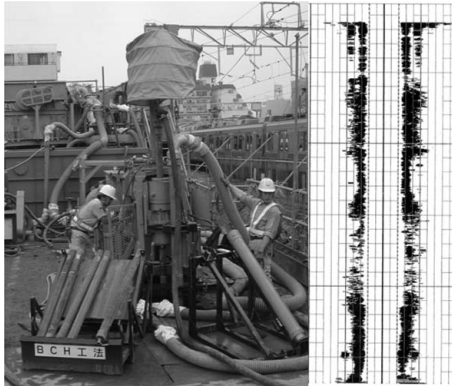


Figure 4. Result of supersonic measurement.

Table 1. Cycle time for experimental construction.

Description	Time (hour)
Preparation	0.25
Excavation	6.75
Primary slime treatment / Withdrawal of rods and unloading pipe	1.0
Measurement	0.5
Installation of reinforcement cage	1.0
Installation of tremie pipe / Secondary slime treatment	0.5
Concrete placement	2.5
Cleanup	0.25

3.1 Experimental construction

During the excavation, the specific gravity of the stabilizing slurry was measured at three points; GL-20 m (immediately above the bit), the ground surface, and GL-10 m (the midpoint of ground surface and GL-20 m). The result of measurement was satisfiable; at GL-20 m, the specific gravity was measured as 1.10, and at other two points it was approximately 1.08, while it was 1.03 (5% bentonite) before the excavation. In addition, from the result of the supersonic measurement, stabilizing slurry is kept in good quality (refer to Figure 4). Thus, sufficient bearing capacity for a railway structure foundation can be ensured. The cycle time for the experimental construction is summarized in Table 1.

3.2 Static loading test

Static loading test was carried out by using multi-phase loading / multi-cycle system. 4 reaction piles of diameter 800 mm are constructed by BCH method in the same way as the test piles (Refer to Figure 5). H section steel (H-400 × 400) was installed as a core, to the bottom.



Figure 5. Static loading test.

Bentonite density of the stabilizing slurry for the test piles is determined as 5%, as it is usually determined as 3 to 10% in actual constructions. However, the maximum frictional resistance and the standard bearing capacity of the pile end might exceed the design forces. Thus, the maximum design load is determined by multiplying R_{vd} by 1.5.

$$R_{vd} = R_p + R_f = 1,716 + 7,703 = 9,464 \text{ kN}$$

where,

R_{vd} : Design vertical bearing capacity (ULS with earthquake). Assumed bentonite density is less than 3%.

R_p : Standard bearing capacity of the pile end

R_f : Maximum frictional resistance

Therefore, the maximum design load is obtained as 15,000 kN.

In the static loading test, following items were measured: Settlements of the pile head, the pile end and the pile midpoint at one depth, displacement at the head and strain at 7 depths for the test piles. Strains at the pile head and uplift of the core (H-400 × 400) for reaction piles. The strain gauge was installed in the reinforcement cage, and the obtained strain was converted into axial force by using the modulus of elasticity of concrete. The layout of measurement instruments is shown in Figure 6. The static loading test was finished when the pile end displacement exceeded 100 mm (12.5% of the pile diameter) and the pile head reaction force was reached 13,500 kN.

3.3 Design bearing capacity and the maximum design load for static loading test

In accordance with the Design Standard for Railway Structures (Railway Technical Research Institute, 2000), design bearing capacity and the maximum

design load for static loading test were calculated as follows:

Design vertical bearing capacity at the pile head of a single pile is calculated by using the following equation.

$$R_{vd} = f_{rf} R_f + f_{rp} R_p$$

where,

- R_{vd} : Design vertical bearing capacity of a single pile (kN)
- R_f : Maximum frictional resistance of a single pile (kN) ($= U \sum \tau_i L_i$)
- $\sum \tau_i L_i$: Frictional resistance of a single pile per perimeter (kN/m)
- Cast-in-situ pile, bentonite density 0–3%, sandy soil : $\tau = 5N < 200\text{ kN/m}^2$
- Cast-in-situ pile, bentonite density 3–10%, sandy soil : $\tau = 2N < 100\text{ kN/m}^2$
- cohesive soil : $\tau = q_u/2$ or $10N < 80\text{ kN/m}^2$
- L : Length for skin friction (m)
- U : Pile perimeter (m)
- R_p : Standard bearing capacity of the pile end of a single pile (kN) ($= q_d \times A_p$)
- q_d : Standard bearing capacity of the pile end of a single pile per unit area (kN/m^2)
- A_p : Area of the pile end of a single pile (m^2)
- f_{rf} : Resistance factor of subgrade reaction to the frictional resistance of pile
- f_{rp} : Resistance factor of subgrade reaction to the bearing capacity of the pile end.

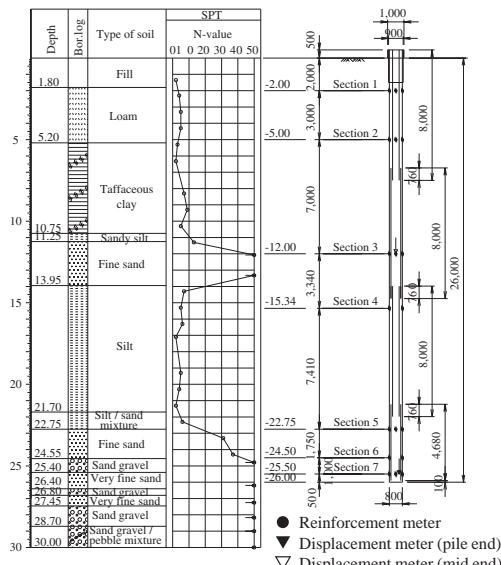


Figure 6. Layout of measurement instrument.

Limit state	f_{rf}	f_{rp}
Serviceability limit state (long-term)	0.30	0.60
Serviceability limit state	0.50	0.80
Ultimate limit state	0.70	1.00
Serviceability limit state with earthquakes	0.80	1.00
Ultimate limit state with earthquakes	1.00	1.00

Design bearing capacity was calculated from the above equation, and the maximum design load for the loading test facilities was determined as 1.5 times of the design bearing capacity for the ultimate limit state with earthquakes.

3.4 Results of static loading test

The results of the static loading test are summarized in Figure 7. Test value of the maximum frictional resistance and the standard bearing capacity of the pile end is determined as the value when the displacement is equal to 10% of the pile diameter and the peak value, whichever is greater. As for the coefficient of the shear subgrade reaction and the coefficient of the vertical subgrade reaction of the pile end, the cleavage gradient of the frictional resistance and the pile end-bearing capacity when the standard displacement is 10 mm.

3.4.1 Estimation of the characteristics of frictional resistance of pile

The greater the changes in the axial force distribution, the greater the frictional resistance, as shown in Figure 8. The frictional resistance is high in the clayey and silt layer. In the sand layer, both the frictional resistance and the pile end-bearing capacity are high. As for the maximum frictional resistance and the coefficient of the shear subgrade reaction, the test values are greater than the design values, as shown in Table 2.

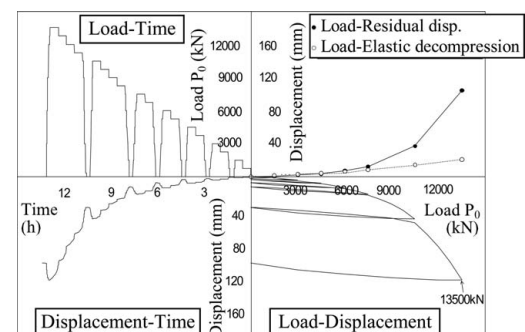


Figure 7. Results of static loading test.

3.4.2 Evaluation of the characteristics of pile end-bearing capacity

The test values are much greater than the design value, as shown in Table 3. The standard bearing capacity of the pile end is obtained as 2.8 times of the design value. The vertical coefficient of subgrade reaction is approximately 17 times of the design value.

3.4.3 Evaluation of the vertical bearing capacity

As the maximum loading on the pile head is 12,750 kN when the displacement of the pile head is equal to 10% of the pile diameter ($=80 \text{ mm}$), the secondary limit resistance force P_{ou} is regarded as 12,750 kN. The comparisons of the test values and the design values (when bentonite density is 3 to 10%)

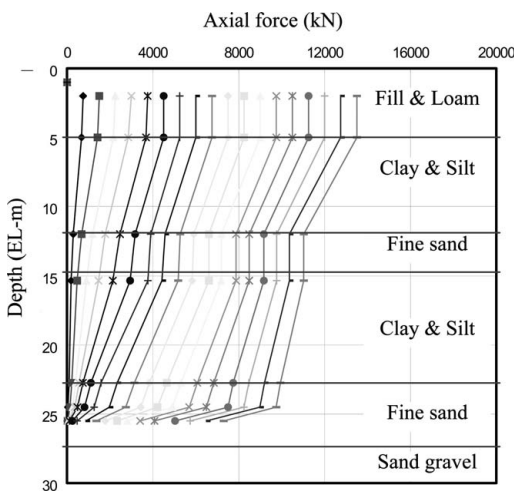


Figure 8. Distribution of axial force – depth.

for the vertical bearing capacity of the pile (the sum of the maximum frictional resistance and the standard bearing capacity of the pile end) are summarized in Table 4. The maximum frictional resistance is approx. 1.6 times, and the standard bearing capacity of the pile end is 2.8 times of the design value, respectively. Thus, the vertical bearing capacity is much greater than the design value.

The relationship between loads and displacements at the pile head and the pile end is shown in Figure 9.

Table 3. Standard bearing capacity of the pile end and vertical coefficient of subgrade reaction.

Soil	Standard bearing capacity of the pile end ($\phi 800$)		Vertical coefficient of subgrade reaction at the pile end	
	Design value q_{ptest} (kN/m^2)	Test value q_{pdesign} (kN/m^2)	Design value k_{vtest} (kN/m^3)	Test value k_{vdesign} (kN/m^3)
Sandy soil	9,630	3,500	1,470,000	88,700

Table 4. Standard bearing capacity of the pile end and vertical coefficient of subgrade reaction of the pile end.

Description	Maximum frictional resistance	Standard bearing capacity of the pile end	Total
Test value	7,907 kN	4,843 kN	12,750 kN
Design value*	4,840 kN*	1,761 kN	6,601 kN*

*Density of bentonite: 3–10%.

Table 2. Maximum frictional resistance and the coefficient of the shear subgrade reaction.

Section	Type of soil	Maximum frictional resistance		Coefficient of shear subgrade reaction		
		Test value r_{test} (kN/m^2)	Design value* r_{design} (kN/m^2)	Test value k (kN/m^3)	$k_{\text{svtest}} = k/1.5$ (kN/m^3)	Design value* k_{svdesign} (kN/m^3)
2–3	Tuffaceous clay	188	77	16,309	10,900	1,330
4–5	Silt	156	80	21,948	14,600	1,060
5–6	Fine sand	129	68	18,388	12,300	9,040
6–7	Sand gravel	1,330	100	122,077	81,400	13,300

*Density of bentonite: 3–10%.

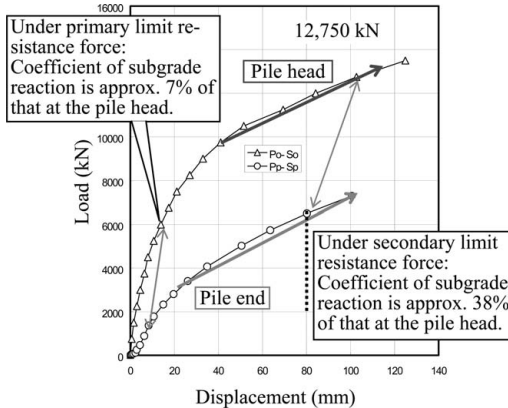


Figure 9. Load-displacement relationship at the pile head and the pile end.

If they are represented by using a double logarithmic plot, the primary limit is defined as the pile head load at the breakpoint. When the resistance force reaches the primary limit, the subgrade reaction at the pile end is approx. 7% of that at the pile head. When it reaches the secondary limit, the subgrade reaction at the pile end is 38% of that at pile head, and the displacement at the pile end is 80% of that at the pile head. Therefore, the resistance by skin friction is transiting to bearing by the pile end, as the settlement increases.

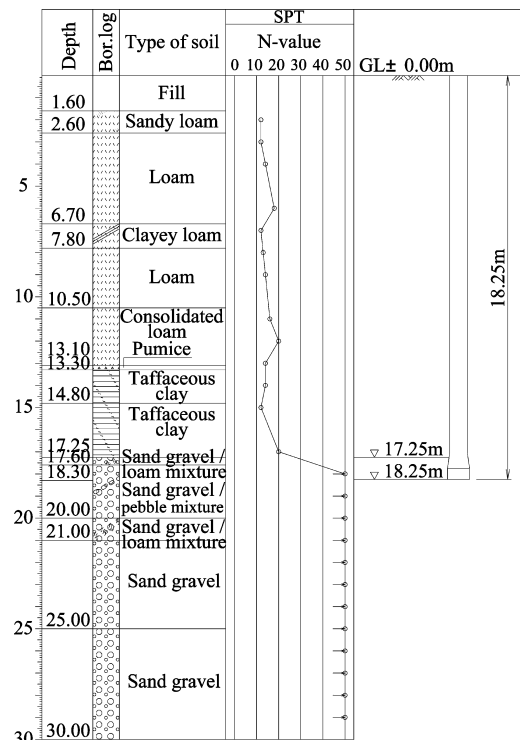
4 EXPERIMENTAL CONSTRUCTION

For the application of BCH method to the cast-in-situ piles of diameter 1.3–2.0 m, which is usually used in the railway constructions, the experimental excavation with the diameter of 1.8 m was done by using the construction machineries for the large-diameter construction (refer to Table 5). Considering the difficulties often involved in excavating gravel by BCH method, the ground mainly composed of gravel was selected as the construction site (refer to Figure 10). The comparison of construction machineries for BCH method is shown in Table 5. Besides the enhancement of the horsepower, the following improvements were made, to accommodate the large-diameter construction. (1) The diameter of unloading pipe was enlarged from 5 inches to 6 inches. (2) The capacity of suction pump was enlarged. (3) The discharge volume from the rod end was increased from 0.3–0.5 m³/min to 0.8–1.0 m³/min.

The diameter of the unloading pipe had been limited to 5 inches because of the space inside the excavation hole. However, the large-diameter excavation enabled the enlargement to 6 inches. From the improvements described in (1) and (3) above, gravels

Table 5. Comparison of usual construction machineries for BCH method.

Description	BCH Method	
	Standard piles	Large-diameter piles
Excavation machinery	TBM-88LH	TBM-150LH
Excavation diameter	φ0.7–1.5 m	φ1.3–2.0 m
Rotating speed (rpm)	14,27,50,70	25,50,85,120
Drilling rod	T90 (inner diameter 43 mm)	T150 (inner diameter 80 mm)
Required horsepower (kW)	18.5	22
Dimension (L × B × H)	2.84 × 1.1 × 1.76	3.15 × 1.1 × 1.89
Weight (t)	3.15	4.2
Uploading pipe (inch)	3–6	6–8
Upload mechanism	Suction pump (S80-1520)	Suction pump (S80-2520)



Loam was observed down to 17.3 m from the ground level. Sagamino Sand Gravel was observed underneath the loam (GL-17.3 m to -45.0 m). Groundwater level is at around GL-18.0 m.

Figure 10. Soil conditions for the experimental construction.



Figure 11. Excavated big coarse gravel.

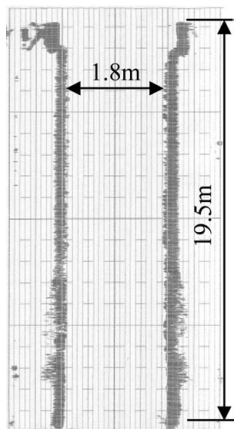


Figure 12. Measurement result of the wall inside the excavation hole.

can be carried upward more powerfully and the excavation can be done without any blockage. For reference, excavated gravel is shown in Figure 11.

The excavation speed was recorded as 80 min/m in the gravel layer (GL-17 m to -20 m) shown in Figure 10. The diameter of the gravels are from 50 to 100 mm as shown in Figure 11. As the excavation diameter is 1.8 m, the excavation speed calculated in accordance with the cost estimation standard is 78 min/m, which is almost the same as stated in the standard. The excavation efficiency is improved, because, from the improvement (1), the frictional resistance inside the unloading pipe is decreased, and the discharge volume was increased from 1.5–2.0 m³/min to 3.5–4.0 m³/min.

After the excavation, dimensions of the wall of the hole was measured (refer to Figure 12). Both the design diameter of the pile and the vertical accuracy

were satisfied throughout the depth. No slime was found at the bottom of the hole, which shows the effectiveness of the improved method.

As a result, the large-diameter cast-in-place piles approx. 2.0 m can be constructed by BCH method and these piles have the same or more bearing capacity comparing to the standard piles.

5 CONCLUSION

BCH method has been developed by improving BH method, for the construction of the cast-in-situ piles as a permanent structure foundation under the severe overhead / site access restrictions by using a circulation method. Effectiveness of the method was confirmed by the result of density measurement of bentonite in the excavation hole during construction, and the supersonic measurement of the wall inside the hole after construction.

In addition, from the result of the static loading test, the bearing capacity is quantitatively sufficient for a railway structure foundation. By using BCH method, the cast-in-situ piles can be constructed with overhead spacing of 2.7 m, and minimum spacing of 40 mm between the vicinal structure. Currently, BCH method is used more and more as a standard method mainly applied to the railway constructions. In the future, application to other constructions shall be studied, and static loading test data shall be collected as well, for further development of BCH as a more standard construction method.

REFERENCES

- Railway Technical Research Institute. 1997. *Design standard for railway structures*.
- Murata, Yoshikawa, Tanamura, Koda, Saito & Kotaki. 2004. Outline and major features of BCH method. *Proceedings of the 59th Annual Conference of the Japan Civil Engineering Society* 3: 929–930.
- Shimada, Kitamoto, Tanamura, Nishioka, Oka & Yamamoto. 2004. Bearing capacity characteristics of cast-in-situ pile constructed by BCH method. *Proceedings of the 59th Annual Conference of the Japan Civil Engineering Society* 3: 931–932.
- Japanese Geotechnical Society. 2004. *Japanese Geotechnical Society Standard “Vertical loading test for piles”*.
- Koda, Hiyoshi, Nogawa, Yoshikawa, Saito & Kotaki. 2005. Development and of BCH method. *The Foundation Engineering & Equipment* 33(2): 36–41.
- Koda, Nishioka, Shimada, Yoshikawa, Saito & Kotaki. 2005. Outline of BCH method. *Proceedings of the 40th Japan National Conference on Geotechnical Engineering*.
- Koda, Yoshikawa, Saito & Kotaki. 2005. Development of construction method for cast-in-situ pile under site access restrictions. *Construction Machinery & Equipment* 41(8): 35–40.

Mechanical joint “KASHEEN” for large-diameter steel pipe piles

G. Mori

JFE Steel Corporation, Tokyo, Japan

H. Tajika

JFE R&D Corporation, Kawasaki, Japan

ABSTRACT: JFE Group has developed a mechanical joint, “KASHEEN,” for large-diameter steel pipe piles. Through a series of bending tests and FEM analysis on the steel pipe piles with the mechanical joint, it is confirmed that the joint has larger strength than the body of a pile. A full-scale construction test of the joint part proved the reduction of construction time. And pile driving test proved good field performance, such as no remarkable deformation of the pipe, no loosening of bolts and no affection on construction efficiency.

1 INTRODUCTION

Formerly, field welding generally performed the joining works of steel pipe piles. However, since such welding has the problems (1) that the execution time is comparatively long and this tendency increases as the external diameter or wall thickness of the steel pipe increases, (2) that the work cannot be executed under bad weather conditions; such as rain, strong wind, etc., (3) that careful control and highly skilled welders are required to ensure the quality, and other problems.

These problems have been major causes of lengthened construction periods and increased construction costs, due to the recent tendency to use larger diameter and thicker walled steel pipe piles, the increasing frequency of construction works in narrow sites, and of others problems.

Considering the above-mentioned background, the JFE Group has developed “KASHEEN,” non-welded mechanical joints applicable to large diameter, thick steel pipe piles and its practical use has been realized.

This paper describes the introduction of the joint shapes and load transfer mechanisms, the results of strength tests and finite element method (FEM) analysis, and the conditions of the construction tests and actual operations.

2 OUTLINE OF KASHEEN

The structural outline of the KASHEEN system is shown in Figure 1. KASHEEN is produced by forging

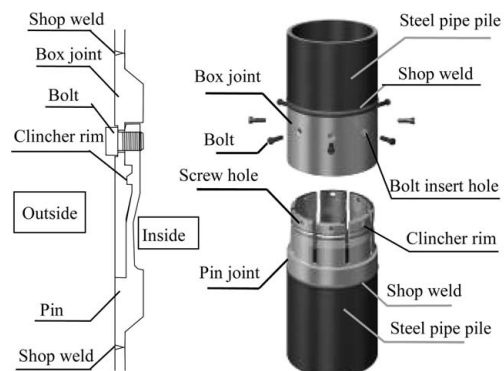


Figure 1. Outline of mechanical joint “KASHEEN” (Right side: Cross-section of jointed KASHEEN, Left side: Bird view).

and machining high-tension 780 MPa class, JFE-HITEN780 steel. The joint portion consists of a pin and a box joint, and each of these joints is pre-welded to the ends of steel pipe piles in the shop.

The details of the structure of the pin and box joints are as follows:

Pin Joint: This joint has a clincher rim and is circumferentially divided into 8 parts with slits provided. Bolt screw holes are provided in the uppermost portion of the joint.

Box Joint: This joint has a concave portion inside the joint, which corresponds to the clincher rim of the

pin joint, and the bolt insert holes are provided for the penetration of bolts corresponding to the locations of the bolt screw holes of the pin joint.

The joining procedure of KASHEEN is as follows.

- (1) Put the box joint end of a steel pipe (upper pile) onto the pin joint end of another steel pipe (lower pile).
- (2) The uppermost portion of the pin joint is inserted into the center side of the joint with deformation, by the own weight of the upper pile or by introducing a tensile force between the upper and lower piles.
- (3) The insertion is completed, when the lower end of the box joint strikes the pin joint.
- (4) Pull the pin joint to the side of the box joint, by inserting the bolts into the bolt insert holes of the box joint and into the bolt screw holes of the pin joint and tightening these bolts.
- (5) The joint is completed, by giving sufficient bolt tightening torque and engaging the clincher concave and convex portions of the box joint.

Furthermore, the qualification scope by the Construction Technology Review and Certification⁽¹⁾ of Public Works Research Center and by the Examination and Evaluation of Coast-related Technologies in the Private Sector⁽²⁾ of Coastal Development Institute of Technology is 400–1600 mm outside diameter (O.D.) steel pipe piles and steel pipe sheet piles of 6–30 mm in pipe thickness, and the applicable construction techniques of the pile is pile installation by the inner excavation method, the hybrid-steel pile and soil cement-pile method, the press-in piling method and the pile-driving method.

3 STRENGTH CONFIRMATION TEST

3.1 Outline

It was confirmed, by carrying out the experiments and analysis that the KASHEEN system possesses the expected strength.

Table 1 shows the experiments and analysis that were carried out. At this time, the tests carried out were the compression test, tensile test, bending-shear test and bending tests for the KASHEEN joint itself, and bending test for steel pipe with a KASHEEN joint. This paper reports on the bending test results of KASHEEN steel pipes of O.D. 1600 t25 mm which is the largest diameter of the above mentioned tests. In addition, the analysis of various diameters and wall thicknesses of steel pipes were carried out, by simulating the bending test for steel pipes with KASHEEN joints. This paper shows the results on the largest diameter and the largest wall thickness (O.D. 1600 t30 mm) in the applicable scope, out of the various above-mentioned analyses.

Table 1. Types and dimensions of experiments and analyses.

Type of experiment	Dimensions of specimen	
	Diameter (mm)	Thickness (mm)
Compression test	O.D. 600	12
Tensile test	O.D. 267.4	9
Bending-shear test	O.D. 267.4	9
	O.D. 1600	25
Bending test	O.D. 1200	25
	O.D. 600	12
	O.D. 1600	30
Bending analysis (FEA)	O.D. 1600	25
	O.D. 1200	25
	O.D. 800	25

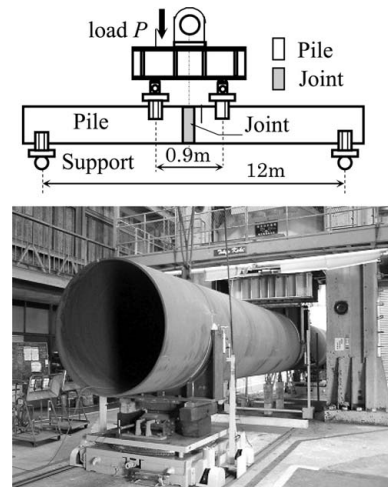


Figure 2. Outline of jointed pile bending test (O.D. 1600 t25).

3.2 Bending test for steel pipes with KASHEEN joints

It was confirmed by the bending test using full-scale specimens that the steel pipes with KASHEEN joints possess the required bending strength.

The test method is the four-point bending test shown in Figure 2, and the KASHEEN joint was located at the center of the loaded width, where the maximum bending moment is generated. Table 2 shows the materials used and their dimensions. The earthquake allowable load of steel pipes of (O.D. 1600 t25 mm) is 4848 kN if converted into an applied load, the load at which the steel pipe yields due to bending (yield load), P_y is 5493 kN, and the load at which the steel pipe cross section becomes fully plastic (full plastic load), P_p is 7104 kN. During the bending test, these loads are unloaded once and then they are loaded with the target

Table 2. Physical characteristics of steel pile and joint.

Part	Pile	Joint
Material	SKK490	JFEHITEN780
Young's ratio	N/mm ²	2.0×10^5
Poisson's ratio	—	0.3
Yield stress	N/mm ²	315
Tensile stress	N/mm ²	490
		685
		780

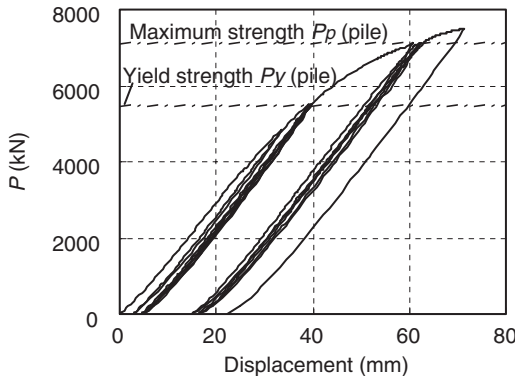


Figure 3. Load-deformation curve obtained from the bending test of jointed steel pipe piles.

load, to understand the influence on the behavior of the applied load. Furthermore, the yield load and the full plastic load were loaded 3 times each.

Figure 3 shows the test result (load-deformation curve). For the steel pipes with KASHEEN joints, the residual deformation due to loading of the earthquake allowable load and yield load is small and the steel pipe is still sound within the range of these loads. In addition, though the residual deformation amount due to full plastic load loading increases slightly, the progress of residual deformation is small even if the loading is repeated.

From the above, it could be confirmed that a KASHEEN joint has sufficient strength under bending loads.

3.3 Analysis of steel pipe with KASHEEN joints

To verify the bending strength of steel pipes with KASHEEN joints, the strength was analytically confirmed for the largest and thickest steel pipe (O.D. 1 600 t30 mm) applicable to the KASHEEN system, as well as being experimentally verified. The conditions of the materials (Table 2), shapes, boundary conditions, etc. were modeled in the same manner as the experiment (Figure 2). As for the element division (Figure 4), detailed modeling was carried out near mechanical elements, bolts, etc. exist in the joint portion

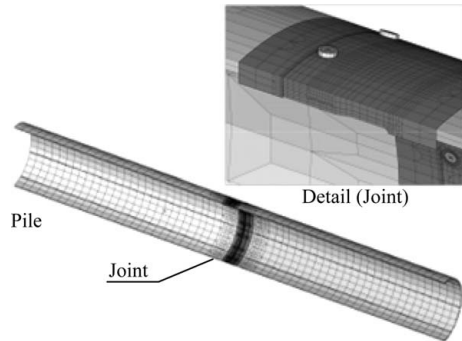


Figure 4. FEM model (O.D. 1600 t30).

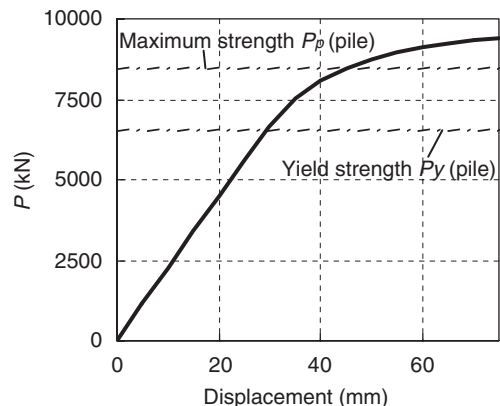


Figure 5. Load-deformation curve obtained from finite element analysis.

(KASHEEN), and the modeling for the steel pipe portion was carried out with rough element division.

The load P_y when steel pipe of O.D. 1600 t30 mm yields due to bending is 6519 kN if converted into an applied load, and the load P_p when the cross section of the steel pipe becomes fully plastic is 8472 kN. The analysis was executed with these loads considered as the target loads.

The analysis result (load-deformation curve) is shown in Figure 5. It is clear that the steel pipe with KASHEEN joints is sound even if the yield load of the steel pipe is exceeded. From the above, it has been confirmed that the strength of KASHEEN exceeds that of the body of the steel pipe. In addition, a reduction of the bending moment was not observed even when the full plastic load is exceeded and the maximum load is reached, and it has been confirmed that a reduction of strength of KASHEEN did not occur.

Furthermore, Figure 6 shows the distribution diagram of stress generated in the KASHEEN joint during loading of the yield load of the steel pipe. Due to bending, tensile stress is generated on the side of the

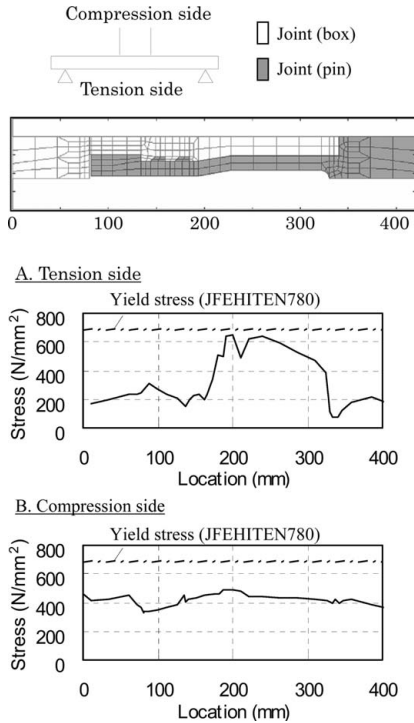


Figure 6. Cross-section of the joint and stresses in joint elements obtained from FEA.

support, and compressive stress on the side of the loading point. As the tensile stress is prominent at the thinnest portion of the pin joint, the distribution inside the joint is shown for the tension side, while the distribution outside the joint is shown for the compression side because the compressive force is transmitted owing to the striking contact between the tip of the box joint and the shoulder portion of the pin joint.

On the tension side, a big tensile stress is generated along the portion from the coordinates 200 mm to 300 mm. This portion is assumed as the critical cross section during tension in the design, and it shows that the setting of the critical cross section in the design is appropriate. Furthermore, when the yield load of the steel pipe was applied, a stress exceeding the material yield stress of JFE-HITEN780 was not generated. On the other hand, as for the compressive stress, this type of stress was generated uniformly in the box joint. Also as for the compressive stress, a stress exceeding the material yield stress of JFE-HITEN780 was not generated, when the yield load of the steel pipe was loaded. From the above, it could be confirmed that the steel pipe with KASHEEN possesses the expected bending strength, also for the case where the yield load of the body of the steel pipe was applied.

Table 3. Process time for jointing KASHEEN.

Case	Pipe specification (mm)		Number of bolts	Process time (jointing)	Process time (welding*)
	O.D.	Thickness			
1	1600	25	16	11.5 min	188 min
2	1200	14	32	15.5 min	61 min
3	400	8	8	11.5 min	13 min

* Calculated from estimation standard.

3.4 Summary

It was confirmed by these experiments and analysis that the strength of KASHEEN equals or exceeds that of the body of the steel pipe and exceeds the required strength. Accordingly, steel pipe piles with KASHEEN joints can be used without any problem under the design conditions.

4 FIELD TEST

4.1 Actual jointing test

In order to confirm the contractibility of KASHEEN joints, the joint test was carried out with full size steel pipes. Table 3 shows the joint test cases and the test results. The test was executed, by using KASHEEN joints for steel pipe of O.D. 1600 t25 mm in Case 1, that for O.D. 1200 t14 mm in Case 2, and that for O.D. 400 t8 mm as an example of a small diameter pile in Case 3.

During the test, the box joint was inserted, by gradually applying the own weight of the upper pile lifted by the crane onto the lower pile (box joint side) as shown in Photo 1. As the insertion can be completed in a short time and the joint is completed only by tightening the joint bolts after insertion, very excellent contractibility results could be obtained in all cases.

The measured times required for the individual joining works during the outdoor joint test were: time from the alignment of joints to the insertion was approximately 3 min regardless of the diameters of steel pipes and then the total joining work was completed within approximately 10–15 min as a result, though there was a difference of the time for the joint work varying according to the number of joint bolts. Table 3 shows the measured times, which were calculated based on the estimation standard, as a reference for comparison with the times to join the joints. When comparing both process times, for the steel joint by field welding, the process time increased rapidly as the steel pipe diameter and the wall thickness increased, while, the results of the joint test by KASHEEN executed at this time, an almost constant joint time was maintained for all diameters and a significant result

showing the reduction of construction time of the KASHEEN system was obtained.

4.2 Applicability of impact hammer and vibratory hammer

In order to confirm the applicability and the behavior during construction for the impact method and the vibratory hammer method of KASHEEN, the construction test was carried out by using KASHEEN for a steel pipe of O.D. 1200 t14 mm. Table 4 shows the specifications of the hammers used, Table 5 the construction conditions, and Photos 2 and 3 the test situations.



Photo 1. Insertion of KASHEEN.

Table 4. Specifications of hammers used in construction test.

Method	Equipment	Specifications
Vibratory hammer	Motorized vibratory hammer	120 kW class Force: 748.2 kN Freq. 16.3 Hz
Impact hammer	Hydraulic impact hammer	Ram weight: 10t Potential Energy: 141 kNm



Photo 2. Vibratory hammering using protection cap.

KASHEEN might be deformed and the joint may be damaged due to directly impacting KASHEEN with hammers in construction, so standard construction method is with a protective cap attached on pinned joint. Accordingly, when studying the applicability of KASHEEN to the vibratory and impact hammer methods, it was determined to verify the generated stress intensities of KASHEEN and the occurrence of loosening of joint bolts, paying attention to the case where protective caps are used and the condition of joined piles. The following explains the test results.

(1) Protective cap

As a result of construction with protective caps attached to KASHEEN, deformation at the joint portion was not

Table 5. Specifications of pile-driving tests.

Case	O.D.	Condition of pile	Method	Specifications
1	1200	Piling the lower pile using protection cap on pinned joint	Vibratory hammer	Time: 1000 seconds (about 20 min.) Number of vibrations: 16300 times
			Impact hammer	Ram height: Level 1–8 (max 1.44 m) Number of blows: 800 times (30 min.)
2	1200	Piling the whole piles (KASHEEN was jointed)	Vibratory hammer	Time: 1000 seconds (about 40 min.) Number of vibrations: 39120 times
			Impact hammer	Ram height: h = 1.44 m Number of blows: 900 times (60 min)



Photo 3. Impact hammering using protection cap.

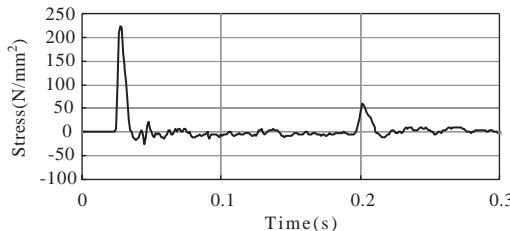


Figure 7. Stress obtained in impact hammer test.

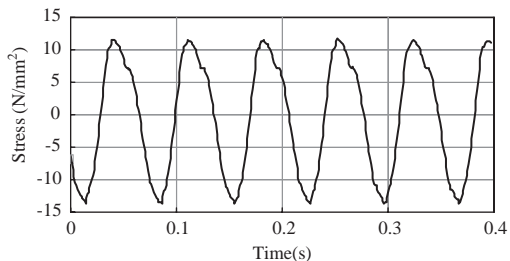


Figure 8. Stress obtained in vibratory hammer test.

recognized in either the impact or vibratory hammer methods, and the joining could be smoothly carried out after removal of the protective caps. Therefore, it could be confirmed that KASHEEN can be applied to steel pipe piles constructed by both the vibratory and impact hammer methods by adopting protective caps.

(2) Joined piles

After jointing piles using KASHEEN joint and after verifying the pile reaches the bearing stratum, the authors checked the stresses at joint during construction. Figures 7 and 8 show the stresses respectively by

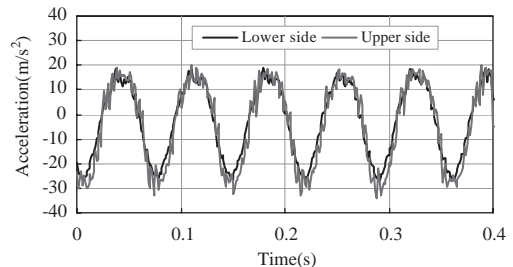


Figure 9. Accelerations obtained in vibratory hammer test.

vibratory hammer (120 kW class: approximately 40 min) and impact hammer (100 kW class hydraulic hammer: approximately 60 min). Generated stress by vibratory hammering was 15 N/mm², and that is 3% of the yield stress of KASHEEN (S_{yj} : 685 N/mm²). And generated stress by impact hammering was 223 N/mm² at the maximum, and this result is 33% of the yield stress of KASHEEN. From these results, it was confirmed that the stresses were within the material's elastic range.

In addition, when joint bolts were found to have loosened due to impact and vibration, the occurrence of large loosening was not observed, at the bolts which had been tightened with sufficient torque (torque value 150 kNm) and at the locations where locking bolts had been used.

Furthermore, Figure 9 shows the change of acceleration measured during construction by the vibratory hammer method on the upper and lower sides of the joint. As the change of acceleration does not change significantly on the upper and lower sides of the joint and the vibration is transmitted sufficiently even through the joint, it is understood that KASHEEN has no negative effect on construction efficiency. In addition, as for the specimens used for the impact and vibratory hammer tests at this time, the steel pipes with KASHEEN were subjected to bending tests after the withdrawal of the steel pipe piles and it was confirmed that the specified strength of KASHEEN can be obtained even after having been subjected to the hysteresis of impact and vibration. From the above-mentioned results, it has been confirmed that the piles joined with KASHEEN possess sufficient applicability to the impact and vibratory hammer method.

5 CONCLUSION

This paper introduced the results of strength confirmation tests and analysis, and the results of joint test for the non-welded mechanical joint, KASHEEN, for steel pipe piles and steel pipe sheet piles. KASHEEN has already obtained the qualifications of the Construction

Technology Review and Certification of Public Works Research Center (Mar. 2004) and of the Examination and Evaluation of Coast-related Technologies the in Private Sector of the Coastal Development Institute of Technology (Nov. 2004).

While the diameter of the steel pipe piles continues to increase, and the construction sites narrow greatly in the future, we are sure that the needs to use KASHEEN, which enables very convenient work to complete the joint works of steel pipe piles and assures the strength of the joint portion, will grow as a product to develop new possibilities to the construction sites of steel pipe piles.

REFERENCES

Public Works Research Center. 2004. *Construction Technical Review and Certification for "KASHEEN", Mechanical Joint for Steel Pipe Piles and Steel Pile Sheet Piles*. No. 0325.

Coastal Development Institute of Technology. 2004. *Examination and Evaluation of Coast-related Technologies in the Private Sector for "KASHEEN" Mechanical Joint for Steel Pipe Piles and Steel Pile Sheet Piles*. No. 04001.

New types of deep foundations

Vertical bearing capacity of bored pre-cast pile with enlarged base considering diameter of the enlarged excavation around pile toe

K. Kobayashi & H. Ogura

Engineering Development Division, Japanpile Corporation, Tokyo, Japan

ABSTRACT: In Japan, most pile foundations using pre-cast concrete piles are installed by the bored pre-cast piling method. In this method, the pre-cast piles are placed in holes that have been excavated beforehand and filled with cement milk. The bored pre-cast piling method with enlarged base, in which a portion near the pile toe is enlarged during boring operation, is widely used because of the cost benefits and the increased vertical bearing capacity that this method offers. The Hyper-MEGA method, further developed as an improved bored pre-cast piling method with enlarged base, is reported here. This report gives an overview of the Hyper-MEGA method and the evaluation of vertical bearing capacity based on examples of application of the method. As a result, this method can give a vertical bearing capacity coefficient at the toe of $\alpha = 423$ (for base enlargement ratio $\omega = 1.2$, where ω is defined as the ratio of enlarged base diameter to the pile nodule diameter). This is more than twice the corresponding value of $\alpha = 200$ for a conventional bored pre-cast pile.

1 INTRODUCTION

In Japan, most pile foundations using pre-cast concrete piles are installed by the bored pre-cast piling method, wherein pre-cast piles are inserted in holes that have been excavated beforehand and filled with cement milk (term used for cement water slurry in Japan). The bored pre-cast piling method with enlarged base, in which a portion near the toe is enlarged during boring operation, is widely used because of the cost benefits owing to the increased vertical bearing capacity that this method offers. Conventionally, the diameter of the grouted base was enlarged to 1.1 to 1.15 times.

The Hyper-MEGA method (hereafter referred to as “the HM method”) is a type of the bored pre-cast piling method with enlarged base. Its features include the use of nodular piles, the option of setting the enlargement excavation for the grouted base in the range of 1 to 2 times, and a longer enlarged excavation.

This report gives an overview of the HM method and the study on its vertical bearing capacity. Since the HM method makes use of various enlarged excavation diameters, the relationship between the end bearing capacity and the enlarged excavation diameter based on the results of loading tests is the focus of this report.

2 OVERVIEW OF THE HM METHOD

2.1 Nodular pile installation method

Nodular pile is a pre-cast concrete pile having protrusions in the form of nodes at fixed intervals over the pile shaft. Since its first appearance in the 1920s, the material has changed from reinforced concrete (RC) to pre-stressed spun concrete (PC) to pre-stressed spun high-strength concrete (PHC). The cross sections have changed from square/octagonal to triangular/hexagonal to cylindrical (spun pre-cast pile). In spite of the above, the pile diameter at the node had remained 440 mm (shaft diameter 300 mm) for a long period. The method used to install this pile until 1970 was generally the “sealing method” in which the pile was driven into the ground while filling gravel around it.

From the 1970s, nodular piles could not be installed in urban areas by the “sealing method” because of the noise and vibration problems and the bored pre-cast piling method began to be used instead. The GMTOP method was developed in the year 2000. It is a method for installing nodular pile in a hole formed by stirring and mixing excavated earth with cement milk. It uses a rotating blade with a slit in the helical part of the blade for excavation.

The HM method is an improved version of the GMTOP method. It was developed in 2006 in response

to the demand for high bearing capacity piles in recent years. The maximum diameter of the pile at the node has been increased to 1200 mm. A straight shaft pile with diameter equal to the diameter at the node can also be joined above the nodular pile (enlarged head nodular pile). This arrangement enables full utilization of all the advantages of the GMTOP method while also making its application as bearing piles possible. The end bearing capacity of the “bored pre-cast piling method with enlarged base” has been increased by enlargement excavation around the toe of 1 to 2 times. Furthermore, by enlarging the excavation over a range of up to 50% of the pile length, the skin friction resistance can also be increased significantly to realize high bearing capacity.

2.2 Applicable piles

Piles to which the HM method can be applied include nodular piles (including enlarged head nodular piles) with maximum diameter at the node of 1200 mm (shaft diameter 1000 mm), and straight piles (including enlarged head piles) such as PHC piles, PRC (pre-stressed and reinforced spun high strength concrete) piles, SC (steel encased spun high strength concrete) piles, and steel piles of maximum diameter 1200 mm that can be joined to nodular piles. Combinations of these piles can be freely used as long as a solid contact with the grouted base is achieved with nodular pile (including enlarged head nodular pile) at lower section. Figure 1 shows the form of nodular piles with diameter 800–1000.

Large horizontal resistance corresponding to the vertical bearing capacity can be obtained by using enlarged head nodular pile or enlarged head pile and by joining straight piles of diameter larger than that of the lower nodular pile at the top. Three kinds of piles

with concrete strength F_c of 85 N/mm² (long-term permissible compressive stress level of 24 N/mm²), 105 N/mm² (long-term permissible compressive stress level of 30 N/mm²), and 123 N/mm² (long-term permissible compressive stress level of 35 N/mm²) have been utilized.

2.3 Ground conditions and installation depth

The ground conditions and the maximum installation depth applicable to the HM method are given below.

- (1) Soil around pile toe: Sandy soil, gravelly soil, clayey soil (including silty soil)
- (2) Soil around the pile shaft: Sandy soil (including gravelly soil) or clayey soil (including silty soil)

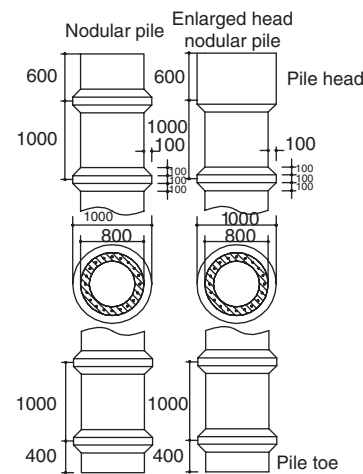


Figure 1. Shape of HC-TOP pile (φ1000–800).

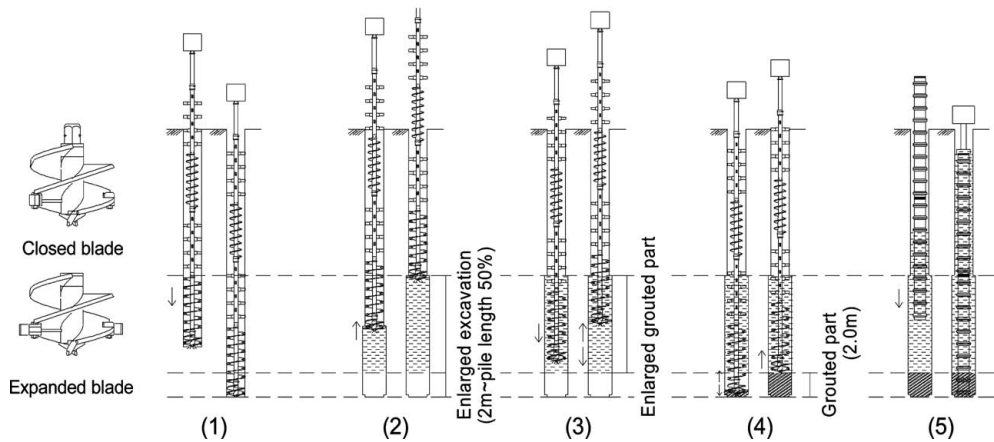


Figure 2. Installation sequence.

- (3) Maximum installation depth: 68.5 m when the soil around the pile toe is sandy soil or gravelly soil, and 60.0 m when it is clayey soil.

2.4 Installation method

An overview of the installation procedure for the HM method is shown in Figure 2. Stages (1) to (5) in the Figure are briefly explained below.

- (1) Centering of pile – normal excavation
- (2) Expand blade – enlarged excavation; pumping grout (cement milk)
- (3) Re-excavation as mixing and stirring continues
- (4) Forming the grouted base- withdrawing the auger
- (5) Pile placement and setting

The grout(cement milk) pumped before stirring and mixing may include expansive admixture in addition to the usual cement milk with the aim of increasing the shaft friction resistance. Use of grout without expansive admixture is referred to as “standard type,” while the latter is referred to as “expansion type.”

The enlargement head for boring may also be of two types – the mechanical type in which the blade is expanded by reverse rotation and the hydraulic type in which oil is pumped from the appropriate facility to expand the blade. Figure 2 shows the mechanical type of head. If the standard excavation diameter (diameter at the node + 50 mm) is D_s , and the enlarged excavation diameter is D_e , then the enlargement factor ω is defined as $\omega = D_e/D_s$.

Work monitoring is extremely important to ensure quality of the pile at the base in enlarged pre-boring and grouting method. The key points especially are checks to confirm that the expanded blade has correctly expanded and the grout has been properly pumped.

3 LOADING TEST AND INSTALLATION CONFIRMATION

Conventional static loading and pile toe loading test (Ogura et al. 2005) were carried out at 53 locations in various parts of the country from Hokkaido to Kagoshima in Japan. The pile diameter varied widely from 300 mm to 1200 mm, the pile length from 4 m to 68.5 m, the average N -value of the soil around the pile toe from 0 to 64.6 and the enlargement ratio ω from 1 to 2.

The load-displacement curve from the loading test (nodular pile with nodule diameter 500 mm and shaft diameter 400 mm, $\omega = 2.0$, overall pile length = 30 m, embedment depth = 29.2 m, standard type, Saitama Prefecture) in which the pile toe is positioned in gravelly soil is shown in Figure 3, as an example. In

principle, staged loading system (maintained load duration of new load cycle is 30 minutes) in which creep deformations occur until the first limit resistance was utilized. Subsequently, a continuous loading method in which the behavior during large displacement can be accurately tracked was utilized. The principle assumed was that loading continues until the pile toe settlement became greater than 10% of the enlarged excavation diameter. The toe resistance and the skin friction resistance were obtained from the measurement of strain gauges fitted along the shaft of test pile.

Furthermore, to confirm the condition of the grouted base of the pile as far as possible, the ground was excavated at a few locations on site where the pile was installed, and dimensions and strength of soil cement of the grouted base were investigated. Photo 1 shows a section of the grouted base when a pile of embedment depth 5 m, diameter at node of 440 mm, shaft diameter of 300 mm and $\omega = 2$ was excavated. A cross section (outside diameter 300 mm, inside diameter 180 mm) of the nodular pile shaft can be seen at the center. The core strength and measured dimensions of piles excavated at this and other sites were found to satisfy the requirement for soil cement shaft strength and dimensions.

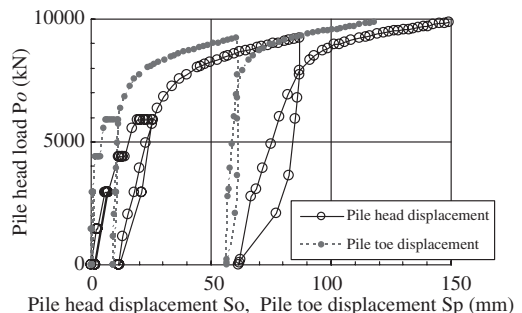


Figure 3. Load-displacement curve.



Photo 1. Building the grouted base.

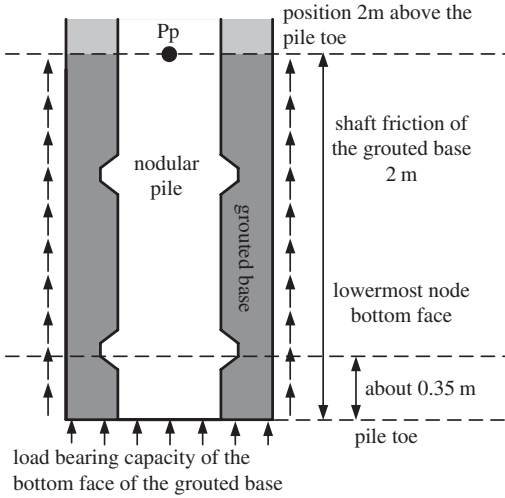


Figure 4. Evaluation position of pile end bearing capacity P_p .

4 STUDY ON VERTICAL BEARING CAPACITY

4.1 Study on end bearing capacity

As shown in Figure 4 and similar to other base enlarged pre-boring and grouting methods, the end bearing capacity P_p is evaluated by the axial force near the upper end of grouted base (at a position 2 m above the pile toe in this HM method). For this reason, the “end bearing capacity” includes the skin friction of the grouted base in addition to the load bearing capacity of the bottom face of the grouted base. As the two components are not evaluated separately in the conventional methods, relative contribution of these components in terms of bearing capacity mechanism has remained unclear.

The end bearing capacity P_p in the HM method is regarded as constituted by the combination of resistance P_{pp} of the pile toe bottom face and the shaft friction of the grouted base P_{pf} and evaluated accordingly. Actually, the axial force at the lowermost node position (about 0.35 m above the pile toe face) is used for P_{pp} .

The value obtained by dividing P_p and P_{pp} by the closed section area of the node A_p is taken as the end bearing pressure q_p and the bearing pressure of the lowermost node bottom face q_{pp} respectively.

To derive the equations for end bearing capacity in the HM method, the diameter of the grout base should be considered to vary in the range of 1 to 2 times corresponding to the standard excavation diameter. The conventional α is expressed by equation (1), where the coefficients a , b , c are determined from the data of loading tests.

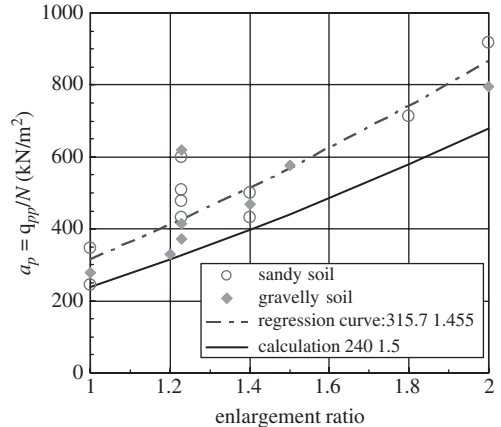


Figure 5. Relationship between α_p and ω .

$$a = \alpha_p + \alpha_f = a\omega^b + c\omega \quad (1)$$

here α_p = bearing capacity coefficient due to load bearing capacity at the pile toe face (lowermost node bottom face); α_f = bearing capacity coefficient due to skin friction resistance of grouted base; ω = enlargement ratio = $D_e / (D_o + 0.05)$; D_e = enlarged excavation diameter (grouted base diameter) (m); D_o = nodal diameter at node at the grouted base position (m).

Figure 5 shows the relationship between α_p and ω . The soil around the pile toe is taken as sandy soil and gravelly soil, and α_p plotted along vertical axis is the value obtained by dividing q_{pp} by average N-value of pile toe region (Ogura & Kobayashi 2005). The chained line in the figure is a regression curve approximated by applying the least squares method assuming exponential function. The regression equation in case of sandy/gravelly soil is given by $\alpha_p = 315.7\omega^{1.455}$. The value of b in equation (1) is taken as 1.5.

If the load-bearing capacity of the bottom face of the grouted base is considered proportional to the bottom area, then b is likely to be 2. However, the regression values of 1.455 for sandy/gravelly soil and 1.259 for clayey soil are smaller. Three possible reasons given below may be considered for the small values.

- (1) Skin friction resistance between the bottom face of the grouted base and the lowermost node bottom face (about 0.35 m) is included in P_{pp} .
- (2) The ultimate load-bearing capacity is being evaluated as the load bearing capacity when S_p has reached 10% of the pile diameter (diameter at the node) D_o and not 10% of the grouted base diameter D_e . For this reason, the increase in the toe resistance until S_p becomes $D_e/10$ from $D_o/10$ has not been reflected in q_{pp} .

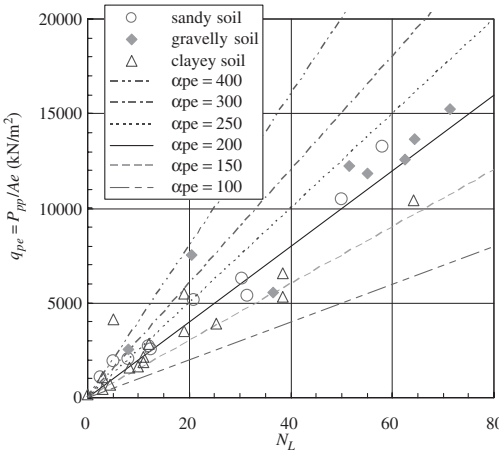


Figure 6. Relationship between q_{pe} and N_L .

- 3) A phenomenon by which the load bearing capacity is not proportional to the contact area (the so-called “dimensional effect”) may also have its effect.

If a value of a that does not exceed data is determined, then it becomes 245.5 in sandy/ gravelly soil, and 219.2 in clayey soil. The a values for bearing capacity evaluation are taken as 240 and 210 respectively. As a result, the equations are determined as $a_p = 240\omega^{1.5}$ and $\alpha_p = 210\omega^{1.25}$. The curve obtained from the equations above is also plotted in Figure 5. The physical significance of α_p may be studied here. For $\omega = 1$ when the bottom area of the grouted base is almost equivalent to A_p , the values of α_p are 240 kN/m² and 210 kN/m² respectively. Figure 6 shows the relationship between the value q_{pe} (obtained by dividing P_{pp} not by A_p but by the bottom area of the grouted base A_e) and the mean N-value N_L (obtained for N-value from the pile toe to the depth of $D_o + D_e$). It can be observed that most of the values of $q_{pe}/N_L = \alpha_{pe}$ lie between 200 to 300 for sandy soil/gravelly soil, and between 150 to 250 for clayey soil. That is, even in the base enlarged pre-boring and grouting method wherein α is apparently large, when evaluated by the bottom area of the grouted base, this value is the same as 200 kN/m² or 250 kN/m², which is the value of α in the conventional pre-boring method, which corresponds to values of α_p when $\omega = 1$.

Since the grouted base behaves as an integral part of the pile until the soil around the pile toe of the enlarged grouted base reaches ultimate load-bearing capacity, the settings for the strength of the grouted base were studied using the results of FEM analysis (Ogura & Yamazaki 2006).

The shaft friction resistance of the grouted base is considered to be proportional to the shaft area of the

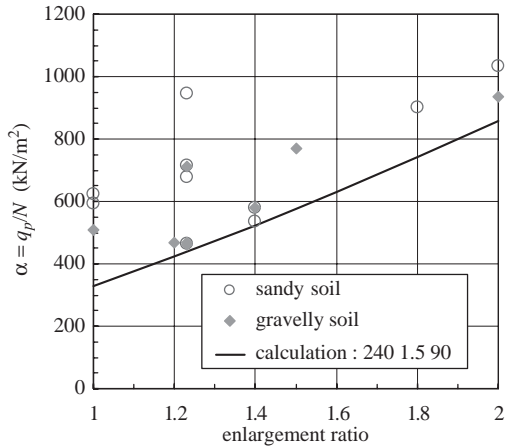


Figure 7. $\alpha-\omega$ relationship.

grouted base. The result of plotting the values of the shaft friction resistance divided by ω with respect to the average N-value in pile toe region shows that the slope of this relationship is c in equation (1). Its lower limit is 98.2 for sandy/ gravelly soil, and is 99.8 for clayey soil. Thus, the value of c for both kinds of soil is taken as 90 from here onwards.

Based on the above, the equations of α for the different soils are as given in (2) and (3) below.

$$\text{Sandy/ gravelly soil} \quad \alpha = 240\omega^{1.5} + 90\omega \quad (2)$$

$$\text{Clayey soil} \quad \alpha = 210\omega^{1.25} + 90\omega \quad (3)$$

When $\omega = 2$, the value of α for sandy/gravelly soil becomes 858, and for clayey soil it becomes 679. Figure 7 shows the $\alpha-\omega$ relationship based on the loading test data for sandy/ gravelly soil. The values in the data for both kinds of soil exceed the values obtained by the equations.

5 SHAFT FRICTION RESISTANCE OF PILE

Equations for calculating the shaft friction resistance are derived using the friction resistance in pile f_i , determined from the results of loading tests. The calculation equations are as shown in (4) and (5).

Sandy soil

$$P_{fs} = f_s L_s D \pi \quad (\text{kN}) \quad (4)$$

$$f_s = \beta N_s \quad (\text{kN/m}^2)$$

Clayey soil

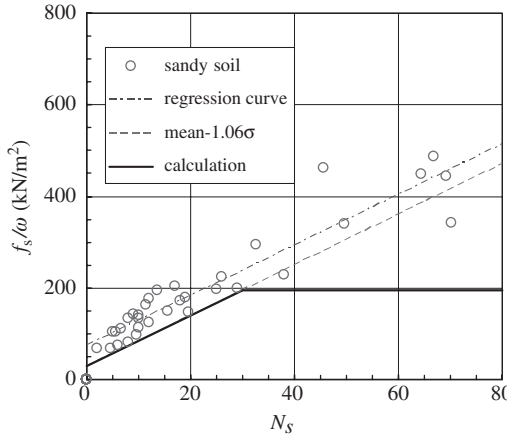


Figure 8. f_s - N_s relationship. (nodular pile; standard; sandy soil)

$$P_{fc} = f_c L_c D \pi \quad (\text{kN}) \quad (5)$$

$$f_c = \gamma q_u \quad (\text{kN}/\text{m}^2)$$

where P_{fc} = shaft friction resistance of sandy soil (kN); f_s = shaft friction in sandy soil (kN/m^2); L_s = total length of pile in contact with sandy soil (m); D = pile diameter (diameter at node in case of nodular pile) (m); β = shaft friction resistance coefficient of sandy soil; N_s = average N -value of sandy soil; P_{fc} = shaft friction resistance of clayey soil (kN); f_c = shaft friction in clayey soil (kN/m^2); L_c = total length of pile in contact with clayey soil (m); γ = skin friction resistance coefficient of clayey soil (kN); q_u = mean value of axial compressive strength (kN/m^2)

Load bearing mechanism has been studied based on the loading test data and values of shaft friction at ultimate load-bearing capacity. In case of nodular piles, the occurrence of slip between pile shaft and cement slurry due to bearing pressure of the node cannot be considered. Moreover, slip occurred between the cement slurry and the soil in the observations during loading tests. Accordingly, the skin friction resistance of nodular pile is decided by the frictional resistance between the cement slurry and the soil, and is considered to be proportional to the outer diameter (excavation diameter) of the cement slurry. Thus, the skin friction stress of nodular pile was estimated using the excavation diameter (taken as ωD_o) here and not the nodal diameter D_o .

Figure 8 shows the f_s - N_s relationship of sandy soil when standard type (no expansive admixture) slurry is used around the pile. The number of data points is 33. Since the equation for (mean - 1.06σ) is $f_s/\omega = 30.3 + 5.50 N_s$, the calculation equation for β becomes (6).

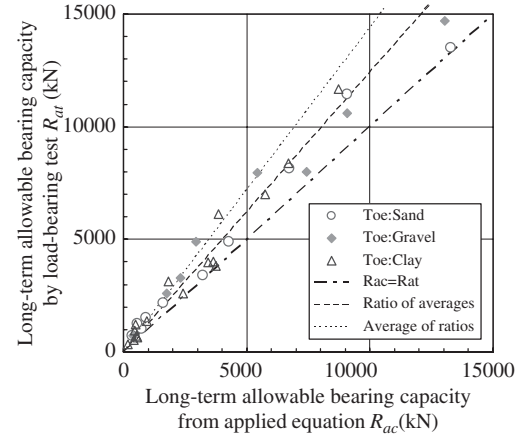


Figure 9. Correlation diagram for long-term permissible load-bearing capacity.

$$\beta N_s = (30 + 5.5N_s\omega) \quad (6)$$

Studies were carried out similarly for calculation equations for shaft friction resistance of other piles according to pile type, soil, and cement slurry around pile shaft (Ogura et al. 2007).

6 LONG-TERM PERMISSIBLE CAPACITY

P_p and P_f are determined from the calculation equations derived in the studies in Sections 4 and 5, and the long-term permissible vertical bearing capacity R_a was calculated taking a safety factor of 3.

Figure 9 shows the correlation between the long-term permissible load-bearing capacity R_{ac} from calculation, and the long-term permissible load-bearing capacity R_{at} obtained from loading tests (one-third the ultimate load-bearing capacity). In all the loading tests, R_{at} exceeds R_{ac} . The mean value of the ratio between the two parameters was 1.44, while the ratio of the mean values of the two parameters was 1.24. From the above, it is concluded that the proposed equation offers safe long-term permissible load-bearing capacity.

7 CONCLUSION

In the last few years, a new pre-cast pile installation method for high load-bearing capacity is being actively developed in Japan. This development is in response to the demand for an installation method that enables the design of one-column one-pile system by designers in order to reduce pile installation costs.

The Hyper-Mega method has the advantage that a pile diameter of 1 to 2 times can be arbitrarily selected without keeping the base enlargement factor at a fixed value. For this reason, the authors have collected valuable data during the development stage related to the effects of the excavation diameter on the end bearing capacity and shaft friction resistance. These characteristics of vertical bearing capacity have been explained and discussed in this report.

REFERENCES

- Ogura,H., Kuwayama, S., Suzuki, Y. & Yamamori, S. 2005. Pile Toe Load Test on Large Diameter Long Pre-cast-Test-Test result and Problems-. *Proceedings of the 41st Japan National Conference on Geotechnical Engineering*. Vol. 2: 1613–1614. (in Japanese).
- Ogura,H. & Kobayashi, K. 2005. Calculation Method of Pile Toe Average SPT N-Value for Bored Pile by Base Enlarged Pre-boring and Grouting Method. *Summaries of Technical papers of Annual Meeting Architecture Institute of Japan*. Vol. B-1: 567–568. (in Japanese).
- Ogura, H. & Yamazaki, M. 2006. Nodular Pile Toe Position in Enlarged Base of Pre-boring and Grouting Method (Study by FEM Analysis Considering Fracture of Enlarged Base). *Summaries of Technical papers of Annual Meeting Architecture Institute of Japan*. Vol. B-1: 509–510. (in Japanese).
- Ogura, H. Komatsu, G. Manabe, M. Oshima, A. Chikusa, N. Hosoda, Y. Sumi, M. & Mimura, T. 2007. Enlarged Boring Diameter and Vertical bearing Capacity Installed by Root Enlarged and Solidified Prebored Piling Method of Precast Pile. *G.B.R.C.* 32(1): 10–21 (in Japanese).

Seismic performance of a group-pile foundation with inclined steel piles

K. Okawa & H. Kamei

Mitsubishi Heavy Industries, Ltd., Japan

F. Zhang

Nagoya Institute Technology, Socio-Engineering, Japan

M. Kimura

Kyoto University, International Innovation Center, Japan

ABSTRACT: Static and dynamic characteristics of group-pile foundation with inclined piles are carefully investigated by centrifuge model tests and dynamic analyses on a full system to develop a newly proposed jacket-type steel-pile foundation. Moreover seismic performance of a real-scale group-pile foundation with inclined steel piles is evaluated using dynamic analyses in comparison with the caisson foundation.

1 INTRODUCTION

A jacket-type steel-pile foundation is proposed as a low-cost construction method for marine bridge foundation (Sekimoto et al., 2000). It can reduce the load acting on the piles drastically because the foundation and the superstructure are connected together by the jacket that is much lighter than a conventional top-heavy foundation. If inclined piles are properly used as a pile foundation, it is possible to increase efficiently the lateral resistance and the rigidity of the foundation. Moreover, the soil improvement is not needed even if the upper strata of the ground are very weak.

When a pile foundation with inclined piles is constructed in a soft ground, however, it is important to evaluate not only the inertial force from the mass of a superstructure but also the kinematic interaction between piles and ground due to the deformation of ground.

In this paper, an outline of jacket-type steel-pile foundation is described at first, then the static and dynamic characteristics of a group-pile foundation with inclined piles are carefully investigated conducting centrifuge model tests and numerical analyses. Moreover the seismic performance of a real-scale steel-pile foundation with inclined piles is investigated using dynamic analyses in comparison with a caisson foundation, which is originally designed with the same level of anti-earthquake as the steel-pile foundation with inclined piles.

2 OUTLINE OF JACKET-TYPE STEEL-PILE FOUNDATION

Figure 1 shows a jacket-type steel-pile foundation, whose features are given below:

- (1) The foundation is composed of a truss made of steel piles with a jacket structure and transmits load to the ground through the pile.
- (2) The superstructure and the jacket structure are of integral structure without any footing.

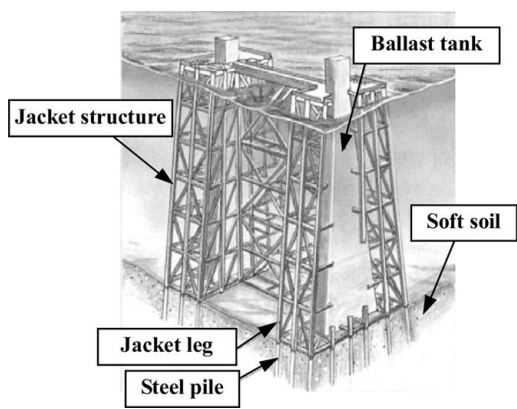


Figure 1. Jacket-type steel-pile foundation.

- (3) The ballast tank is installed to carry out buoyancy adjustment and to reduce the number of piles as well.
- (4) Pile group with inclined piles ensures high bearing capacity under lateral load.

The outline of construction procedure is as follows: the whole assembling of the jacket-type foundation is completed in the factory before launching. After the launching, the draught adjustment is made at the ballast tank before being towed to the marine site. When the jacket arrives at the site, water is injected into the ballast tank to sink at the position where the pilot pile had previously been driven. Then the steel-piles are driven through the jacket leg that acts as a guide and connect the pile head and the end of the leg. In erecting the superstructure, the ballast adjustment is carried out depending on the construction stage in order to reduce the load to the piles. Since this type of foundation is totally built in factory, field works can be drastically reduced, if compared with conventional gravitational type of foundation.

3 STATIC CHARACTERISTICS OF PILE GROUP WITH INCLINED PILES

The lateral resistance and failure mechanism of a group-pile foundation with inclined piles are investigated by centrifuge model tests as shown in Figure 2 (Kimura et al. 2002). The tested conditions are shown in Table 1.

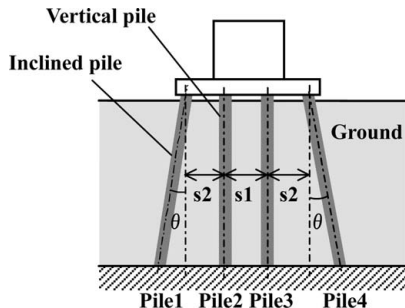


Figure 2. Pile group with inclined piles.

Table 1. Tested conditions.

Inclination angle (degs.)	Pile spacing		
	s1	s2	
Case1	0	2.5D	2.5D
Case2	10	2.5D	2.5D
Case3	0	3.75D	3.75D
Case4	10	3.75D	3.75D

Figure 3 shows the relation between lateral load and lateral displacement of pile group under lateral loading. The lateral resistance of pile group with inclined piles is larger than that of pile group consisted of vertical piles only. Increase of lateral resistance in Case2 compared to Case1 is much larger than those of Case3 compared to Case1. Therefore, using inclined piles is more effective to increase the bearing capacity of pile group under lateral loading than widening pile spacing.

Figure 4 shows sharing ratio of lateral load acting on each pile. The pile arranged at the first row along the loading direction has the biggest sharing ratio. The smaller the pile spacing is, the bigger the sharing

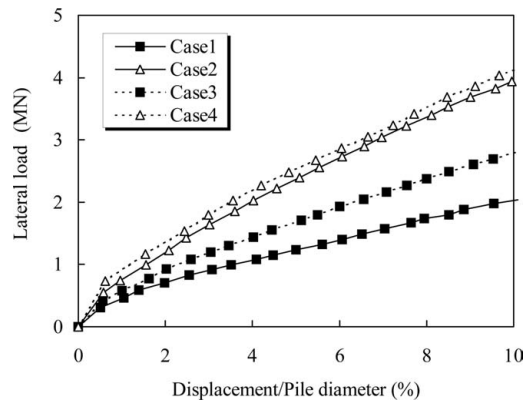


Figure 3. Relation between lateral load and displacement obtained from tests.

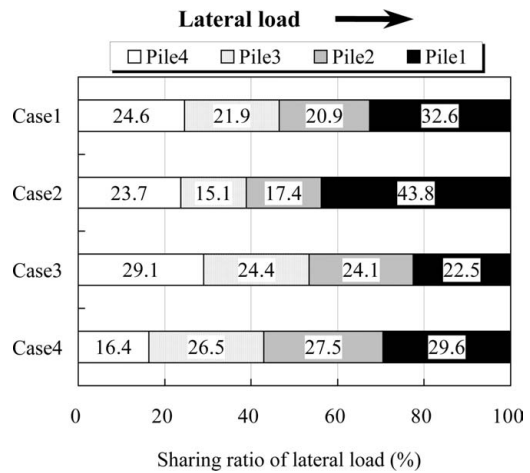


Figure 4. Sharing ratio of lateral load under lateral loading obtained from tests.

ratio is. Figure 5 shows the axial force of each pile. The piles arranged at the first and last row of pile group along the loading direction have the biggest forces in compression and tension respectively.

Figure 6 shows the enveloped curve of relation between lateral load and displacement of pile group under cyclic loading. The resistance of Case 2 is bigger than those of other cases when the lateral displacement is small. However it doesn't increase when the lateral displacement reached about 15 % of the pile diameter due to buckling of pile head occurred in inclined piles. Pile spacing, however, is widened, the sharing ratio of lateral load gets more uniform in each pile, and then the buckling of inclined pile doesn't occur at the same displacement.

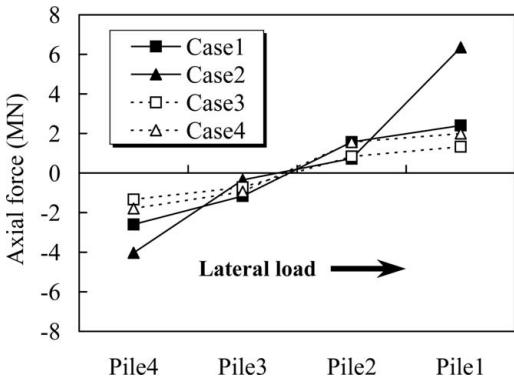


Figure 5. Axial forces acting on each pile under lateral loading obtained from tests.

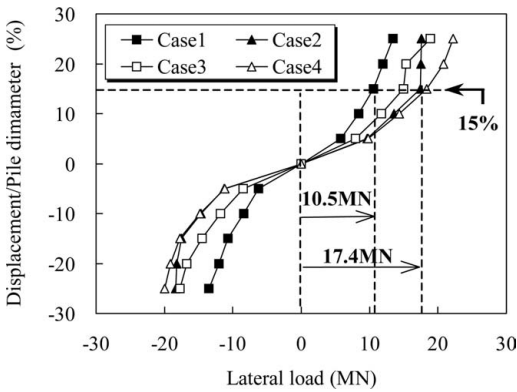


Figure 6. Enveloped curve of relation between lateral load and displacement of pile group under cyclic loading obtained from tests.

4 DYNAMIC CHARACTERISTICS OF PILE GROUP WITH INCLINED PILES

It is important to evaluate not only the inertial force from the mass of a superstructure but also the kinematic interaction between piles and ground due to the deformation of soils in seismic design of pile foundation in soft ground. The dynamic behavior of a pile group foundation with inclined piles is carefully investigated by dynamic centrifuge model tests and dynamic analyses on a ground-pile-structure system. Two types of 8-pile foundation, which is Type A composed of vertical piles only and Type B composed of 4 inclined piles outside foundation and 4 vertical piles inside, is used in the tests (Okawa et al. 2002). Dynamic analyses are conducted to simulate the dynamic centrifuge model tests of pile group with inclined piles in loose sand using a 3-D finite analytical code DGPILE-3D (Okawa et al. 2004). A hybrid element (Kimura & Zhang 2000) is introduced to simulate the pile because the pile-volume influence cannot be ignored in a group-pile foundation. The ground is simulated with t_{ij} -sand model (Nakai 1989). The determination of the parameters of the soil has already been checked through the dynamic centrifuge model tests on a ground only and a ground-single pile-pier system (Lu et al. 2001).

Figure 7 shows a comparison of the responded accelerations observed at the foundation and the ground surface. The difference of the accelerations of the ground in both types of foundation is not so big. The acceleration of the foundation in Type B, however, is much smaller than those of Type A.

Figure 8 shows comparisons of bending moment and axial force of piles obtained from centrifuge model tests, at the time when the maximum bending moment occurs in the piles. The maximum bending moment in Type B is smaller than that of Type A, which shows the same tendency as the responded acceleration of foundation which is dominant to sectional forces of piles. The axial forces of Pile 2 and Pile3 set inside

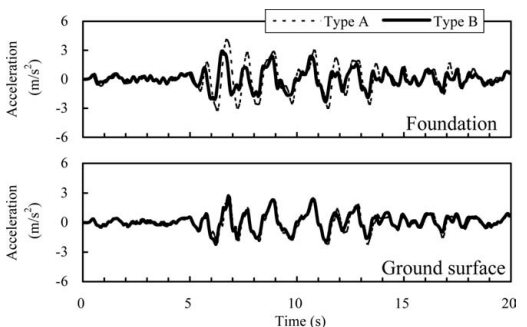


Figure 7. Responded accelerations of foundation and ground surface obtained from tests.

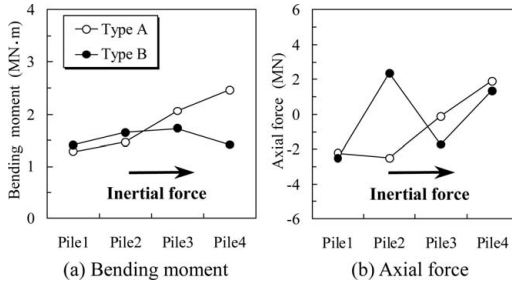


Figure 8. Comparison of bending moment and axial force of piles obtained from tests.

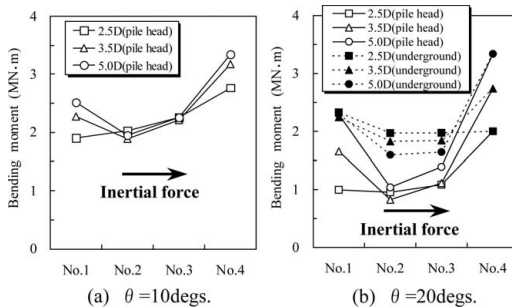


Figure 9. Comparison of bending moment of piles obtained from dynamic analyses.

of the pile group, however, are larger than those of Type A. The axial forces of Type B shown in Figure 8 is just because the reason that the pile group with inclined piles are rotated upward along the direction of the horizontal displacement of foundation. It is a typical pattern that can be found in pile group with inclined piles.

Figure 9 shows a comparison of the maximum bending moment of pile group obtained from dynamic analyses. With a wide pile spacing, the bending moment of inclined pile increases. The tendency is different from that of static characteristic as shown in Figure 4. Because not only the inertial force from the mass of a superstructure but also the kinematic interaction between piles and ground due to the deformation of soils are considered in dynamic analyses.

5 SEISMIC PERFORMANCE OF PILE GROUP WITH INCLINED PILES

The seismic performance of a real-scale steel-pile foundation with inclined piles is analyzed using DGILE-3D and evaluated in comparison with the performance of the caisson foundation, whose stability against earthquake is commonly known as good and

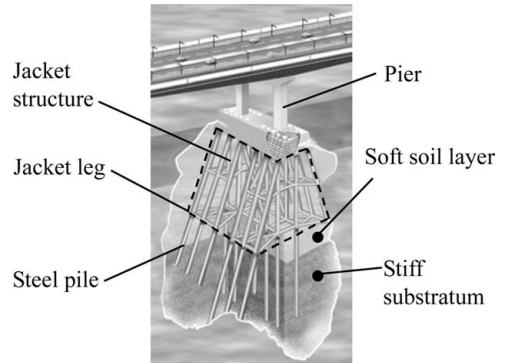


Figure 10. Real-scale steel-pile foundation with inclined piles.

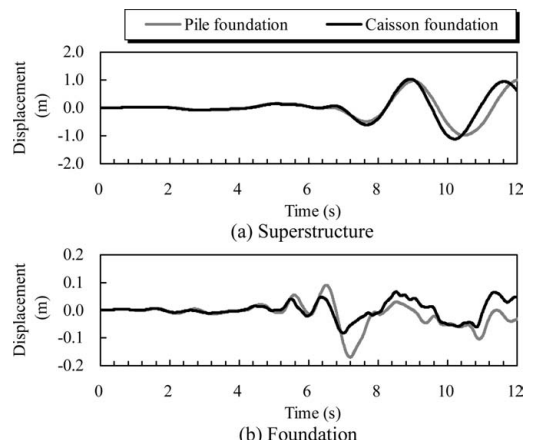


Figure 11. Comparison of responded displacements of different type of foundations obtained from dynamic analyses.

is often used for offshore foundation (Okawa et al., 2005). It is assumed that the caisson foundation has the same magnitude as the steel-pile foundation. The real-scale steel-pile foundation shown in Figure 10 has two sets of pile group. One pile group is composed of 6 inclined piles with 20 degrees in inclination angle and 4 vertical piles. The geologic profile is a typical soft ground covered with alluvial clay in Japan. Each pile is embedded into a bearing layer so that the depth of embedment is three times of the diameter of pile. The sand and the clay are described by t_{ij} -sand model (Nakai 1989) and t_{ij} -subloading clay model (Chowdhury 1999) respectively. According to the previous studies (Kimura et al. 2002), the piles are arranged in larger pile spacing than the normal pile spacing applied for highway bridges in Japan, and the head of hollow-cylindrical steel pile is filled with concrete to prevent buckling.

Figure 11 shows a comparison of the responded displacement between the pile foundation with inclined piles and the caisson foundation. Although the horizontal displacement of the caisson foundation is smaller than those of pile foundation, the responded displacements of both foundations for the superstructure are nearly the same. Therefore, it is reasonable to say that if the pile arrangement and the inclination angle of pile are designed adequately, the displacement of the superstructure supported by the pile foundation with inclined piles in soft ground can be repressed and the pile foundation may behave as stably as a stable caisson foundation.

6 CONCLUSIONS

Static and dynamic characteristics of group-pile foundation with inclined piles are carefully investigated by centrifuge model tests and dynamic analyses using a full system containing pile foundation, ground and superstructure, to develop a newly proposed jacket-type steel-pile foundation. Moreover the seismic performance of a real-scale steel-pile foundation with inclined piles is evaluated using dynamic analyses in comparison with the caisson foundation. If vertical piles and inclined piles are arranged properly, the seismic performance for a superstructure of a real-scale steel-pile foundation with inclined piles may be almost the same as those of a caisson foundation, which has the same magnitude as the steel-pile foundation.

REFERENCES

- Chowdhury, E. Q., et al. 1999. A Model for Clay Using Modified Stress under Various Loading Conditions with the Application of Subloading Concept. *Soils and Foundations*. 39(6): 103–116.
- Kimura, M. & Zhang, F. 2000. Seismic Evaluations of Pile Foundations with Three Different Methods Based on Three-Dimensional Elastic-Plastic Finite Element Analysis. *Soils and Foundations*. 40(1): 113–132.
- Kimura, M., et al. 2002. The Bearing Capacity of a Group-pile Foundation with Inclined Piles under Lateral Loading. *JSCE Journal*. No.722/III-61: 97–107. (in Japanese)
- Okawa, K., et al. 2002. Dynamic Behavior of a Group-pile Foundation with Inclined Piles in Loose Sand. *Physical Modelling in Geotechnics*: 729–734.
- Okawa, K., et al. 2004. Numerical Simulation on Dynamic Behavior of a Pile Foundation With Inclined Piles by Dynamic Analysis on a Full System. *JSCE Journal*. No.771/III-68: 33–49. (in Japanese)
- Okawa, K., et al. 2005. The Seismic Performance of a Steel-Pile Foundation with Inclined Piles. *JSCE Journal*. No.806/III-73: 1–12. (in Japanese)
- Lu, W., et al. 2001. The Behavior of The Jacket-Type Pile Foundation, -Numerical Simulation about Dynamic Centrifuge Model Tests for a Single Pile. *Proc. of 26th Annual Earthquake Engineering Symp.* 29(1): 119–137.
- Nakai, T. 1989. An Isotropic Hardening Elasto-plastic Model for Sand Considering the Stress Path Dependency in Three-Dimensional Stresses. *Soils and Foundations*. 29(1): 119–137.
- Sekimoto, H., et al. 2000. New Construction Method for Main Tower and Substructure of Marine Bridge at Great Water Depth. *Mitsubishi Heavy Industries Ltd. Technical Review*. 37(2): 35–38.

Development of design method for a soft landing breakwater with piles

Y. Kikuchi

Foundations Division, Port & Airport Research Institute, Yokosuka, Japan

ABSTRACT: The soft landing breakwater is composed of a lightweight wall, base plate, and piles inserted into the ground through the base plate. This type of breakwater was proposed for development of Kumamoto Port, which is located in an area with mild sea conditions and on thick, weak clayey ground. The former proposed design method was greatly simplified and suited only for limited conditions. A new design method was required for extension of the breakwater at Kumamoto Port. A new and more rational design method for the structure was proposed by reexamining the field loading test results and conducting laboratory model tests. Finally, a large-scale field loading test was conducted at the construction site in 2002 in order to evaluate the new design method. The test results confirmed the validity of the new design method. Soft landing breakwaters can be constructed inexpensively by applying the new design method.

1 INTRODUCTION

A soft landing breakwater was originally proposed for sites where the ground conditions are not good but wave conditions are rather mild (Kuchida et al. 1986). A key feature of the soft landing breakwater is its light self weight. As originally conceived, the horizontal resistance of this breakwater depends on the cohesion between the base plate and clay surface (Figure 1 a)) (MOT 1991). Usually, however, the horizontal resistance of this type is inadequate for wave forces, and piles are therefore used to improve its resistance capacity. This modification is called the piled type (Figure 1 b)) (MOT 1991). The mechanism of horizontal resistance in this type is rather complex because horizontal loads are borne not only by the base plate but also by the piles, and furthermore, the presence of piles may change the resistance mechanism of the cohesion between the base plate and the ground surface.

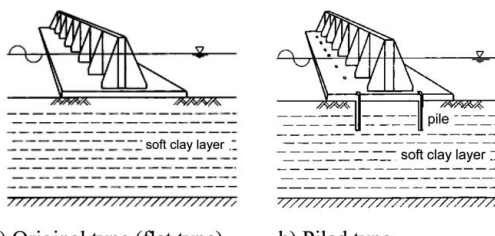


Figure 1. Image of soft landing breakwater.

A design method for the piled type was proposed in 1991 (MOT 1991), but was highly simplified and suited only for limited conditions. In this simplification, the lengths of the piles were limited to the category of short piles in the design method. Due to this limitation, the applicability of the structure was confined to sites where wave conditions are very mild and the sea depth is very shallow. An improved design method was therefore needed to overcome these limitations.

After proposal of the existing design method in 1991, the field loading test results were reexamined and laboratory model tests were conducted. A new and more rational design method for the structure was proposed based on this research (Kikuchi 2003). In the new design method, the equilibrium of the vertical and horizontal forces and moments are fully considered, the limitation on pile length is eliminated, the fixity of the pile heads is taken into consideration, and the effect of repeated loads is considered. Finally, a large-scale field loading test was conducted at the construction site in 2002 in order to evaluate the new design method.

This paper presents an outline of the proposed new design method and the results of the field loading test in 2002, and discusses the characteristics of the horizontal resistance of soft landing breakwaters with piles.

2 HORIZONTAL RESISTANCE OF FLAT TYPE

Before discussing the piled-type soft landing breakwater, the lateral resistance of the flat type will be discussed.

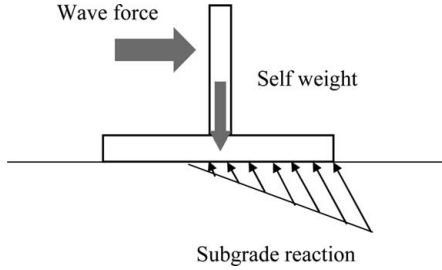


Figure 2. Image of forces acting on flat type.

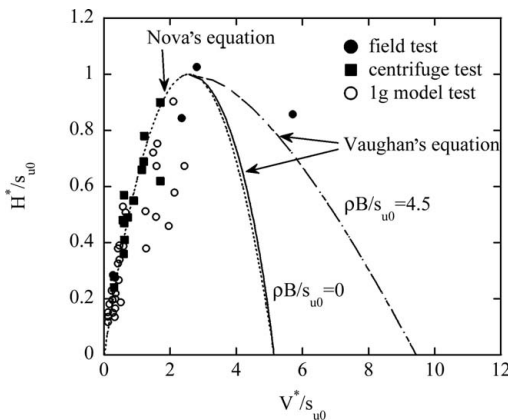


Figure 3. Failure of flat-type soft landing breakwater.

Figure 2 shows an image of the forces acting on the flat type. Lateral resistance can be considered to be a bearing capacity problem of a strip footing with inclined eccentric loads.

Figure 3 shows the experimental results of the resistance of rigid strip footings (Kikuchi 2003). The horizontal axis is V^*/s_{u0} . Here, $V^* = V/A_{ef}$; V is vertical load; A_{ef} is effective area of base for eccentric load, and s_{u0} is shear resistance of ground surface. The vertical axis is H^*/s_{u0} , where $H^* = H/A_{ef}$ and H is horizontal load. The figure shows the experimental results of the field tests, 1 g laboratory model tests, and centrifuge model tests.

Theoretically, the horizontal resistance of a rigid strip footing on clayey ground for $V^*/s_{u0} < (2 + \pi)/2$ is $H^*/s_{u0} = 1$, but the test results show that the horizontal resistance for $V^*/s_{u0} < (2 + \pi)/2$ is smaller than $H^*/s_{u0} = 1$ and coincides with Nova's equation (Nova et al. 1991). This means that, if the vertical load intensity is less than $V^*/s_{u0} < (2 + \pi)/2$, the base plate surface will not cohere sufficiently with the ground surface, and failure will be a kind of frictional mode similar to that of the strip footing on a sandy layer.

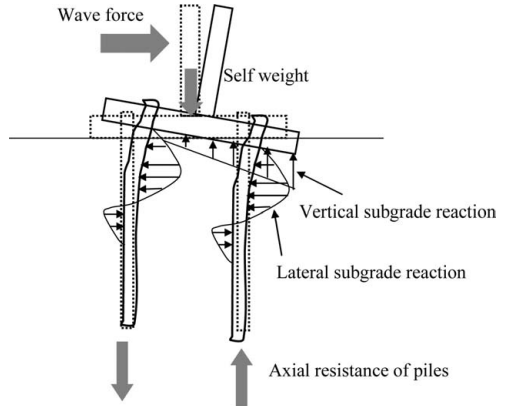


Figure 4. Image of forces acting on piled type.

3 HORIZONTAL RESISTANCE OF PILED TYPE

3.1 Forces acting on piled type

When piles are used to improve the horizontal resistance of the structure, the failure mechanism changes completely. Figure 4 shows an image of the forces acting on the piled type. As shown here, the structure will rotate, and when rotation occurs, surface friction will not work at failure.

In developing a design method for the piled type, it is necessary to examine the effects of the horizontal and axial resistance of piles and the fixity of the pile heads with respect to the horizontal resistance of the structure. Because the resistance of the piles becomes effective after some displacement of the structure, disturbance of the surrounding ground cannot be ignored. In this case, reduction of the resistance of the structure against cyclic loading must also be considered.

3.2 Experimental program

A series of field loading tests was conducted to determine the resistance mechanism of the piled-type model with long piles against both static and repeated loads (Kikuchi 2003).

Three static loading tests were conducted to examine the effect of the embedded length of piles with the piled-type model. In the piled model, the length of the model base plate was one-sixth that of an actual structure with two piles. The length of the model was 1.5 m and its width was 10 m. Figure 5 shows a view of the piled model used in the test. The embedded lengths of the piles were 5 m, 15 m, and 25 m, whereas the depth of the first 0 point of the bending moment l_{m1} (OCDI 2002) was about 10 m. In these cases, the piles used were H-shaped piles with flexural rigidities of 23 MNm^2 and

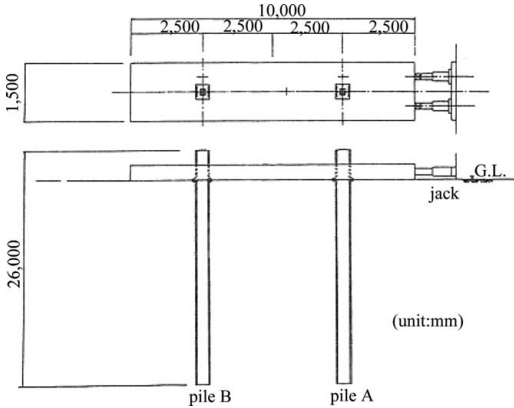


Figure 5. Model used in field test. This figure shows the piled model with the longest piles. The jacks on the right push the model statically to the left.

widths of 25 cm. For the repeated loading test, a stage repeated loading test was conducted with a model with 25 m piles. The subsoil was a normally-consolidated clay layer down to -40 m.

3.3 Subgrade reaction model for estimating lateral resistance of piles

Based on the single pile test results, it was found that the ground could be modeled as S-type ground by the PHRI method (OCDI 2002). The subgrade reaction model can be written as follows:

$$p = k_s \cdot x \cdot y^{0.5} \quad (1)$$

where p : subgrade reaction, k_s : coefficient of subgrade reaction in S-type model by PHRI method, x : depth, y : deflection.

The test results gave $k_s = 150 \text{ kN/m}^{3.5}$. Based on the test results, the subgrade reactions for the piles used in the soft landing structure were also modeled as S-type by the PHRI method.

3.4 Effect of embedded length of piles

Figure 6 shows the relationship between the displacement of the structure and horizontal load. Case 4 has smaller resistance than the other cases, whereas Cases 2 and 3 have similar resistance.

The relationship between the inclination of the base and horizontal load shows that inclination is small when the embedded length of the piles is long ($L = 25 \text{ m}$ and 15 m), but large when the embedded length is short ($L = 5 \text{ m}$).

In accordance with the shear strength of the ground, the maximum pull-out capacity of a pile is

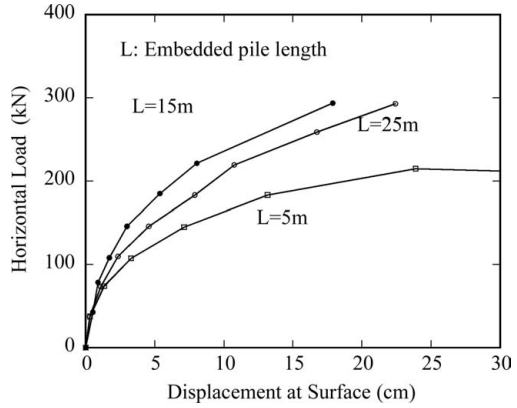


Figure 6. Relationship between displacement and horizontal load on models.

44, 350, and 850 kN for embedded pile lengths of 5 m, 15 m, and 25 m respectively. The measured results of the axial force of the piles show that piles embedded 5 m fully mobilized the pull-out resistance.

These results show that the axial resistance of piles functions effectively in securing the horizontal resistance of the structure. However, if the embedded pile length is insufficient, rotational failure of the soft landing structure will occur.

3.5 Fixity of pile head

Fixity between the pile heads and base plate plays an important role in the displacement and deformation mode of the structure. It also affects the bending moment distribution of the piles. In the test, the pile heads were connected to the base rigidly, but the test results were very far from those for a fixed pile head condition. Figure 7 shows the relationship between the ratio of fixity R_{fix} and the load applied to the model. These results show large variations, and R_{fix} changes depending on the loading level. Here R_{fix} is defined as shown in equation (2).

$$R_{fix} = M_{top} / M_{max-i} \quad (2)$$

where M_{top} : bending moment of pile head, M_{max-i} : M_{top} in fixed pile head condition.

3.6 Sharing of lateral resistance between piles and base plate

Figure 8 shows the relationship between horizontal load and the resistance of piles. The shear force applied to the pile heads is estimated from the distribution of the bending moment. The ratio of the resistance of the piles to horizontal loading is small at low

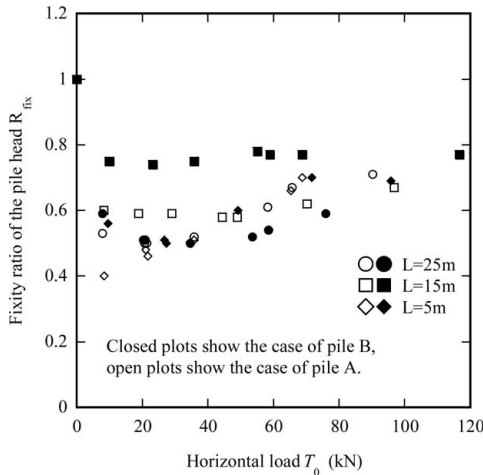


Figure 7. Relationship between fixity ratios and horizontal load.

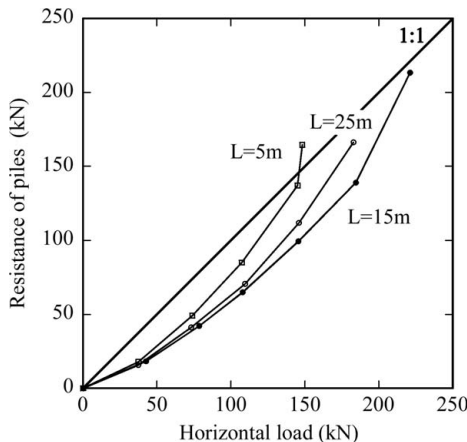


Figure 8. Relationship between resistance of piles and horizontal load.

loading levels and approaches unity at high loading levels. This result means that the horizontal resistance of the structure depends on the horizontal resistance of the piles when the structure is loaded to failure.

Earlier field test results from 1986 gave the opposite conclusion, namely, the horizontal resistance of the piles had an upper limit and the horizontal resistance of base plate functioned to some extent at failure. In this case, however, the shear forces acting on the pile heads were measured only for 4 piles among a total of 12 piles. In contrast, the results of a series of laboratory tests (Kikuchi 2003) agreed with the conclusion from Figure 9 that R_{fix} varies for each pile and the

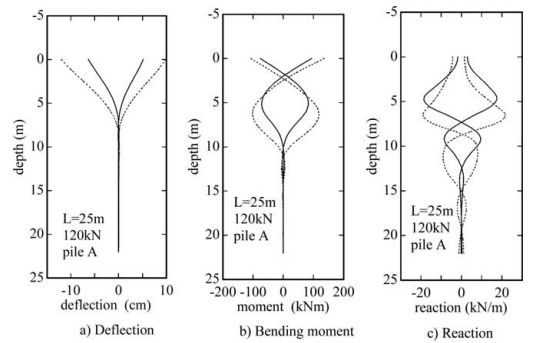


Figure 9. Effect of reduction of subgrade reaction by repeated loading (The solid lines show values of first maximum load in cyclic loading. The dotted lines show the values of the 100th maximum load in cyclic loading).

shear resistance of a pile is affected by R_{fix} . Thus, in order to estimate total pile resistance correctly, all the shear forces applied to the piles should have been measured. The failure to do so in the earlier field tests was the reason why the conclusion of the tests (Kuchida et al. 1991) was not correct and differs from the conclusion of other tests.

3.7 Change of lateral resistance of piles under repeated loading

A repeated loading test was conducted with a model of the same size using 25 m piles. Loading was applied reciprocally with a return period of 10 sec. First, a maximum load of 60kN was applied for 50 cycles, followed by 80kN loading for 30 cycles, and finally 120kN for approximately 100 cycles.

There are two reasons why displacement increases with cyclic loading: One is the weakening of the shallow part of the ground around the pile by repeated loading, which reduces the coefficient of subgrade reaction. The other is the reduction of the shear strength between the base plate and ground surface, which results in an increment in the shear force acting on the piles.

Reduction of the subgrade reaction of the shallow part with the increment of loading cycles causes an increment in the maximum bending moment and deflection, as shown in Figure 9.

The reduction of the subgrade reaction can be represented by the change of the coefficient of subgrade reaction. The coefficient of subgrade reaction reduction ratio R_k can be defined as follows:

$$R_k = k_m / k_{t1} \quad (3)$$

where k_m : coefficient of subgrade reaction when n th cycle maximum load is applied, k_{t1} : coefficient of subgrade reaction when first maximum load is applied.

The test results show that R_k decreases with the increment of loading cycles, and the final reduction of R_k depends on depth. The following can be concluded based on the test results: 1) Reduction of R_k reaches saturation when the number of cycles is exceeds approximately 25, 2) the final reduction of R_k differs according to the load intensity, and 3) the final reduction of R_k differs according to the depth. These effects can be modeled as follows:

$$R_k = 1 - \alpha\beta\gamma \quad (4)$$

where α : a parameter affected by load intensity, β : a parameter affected by the number of loading cycles, γ : a parameter affected by depth.

From the test results, parameters α , β , γ are defined as follows:

$$\alpha = 3.75y_0 / B$$

$$\beta = \begin{cases} \frac{n}{25} & (n \leq 25) \\ 1 & (n \geq 25) \end{cases} \quad (5)$$

$$\gamma = \begin{cases} 1 & (0.25l_{m1} \geq x) \\ \frac{0.5l_{m1} - x}{0.25l_{m1}} & (0.5l_{m1} \geq x \geq 0.25l_{m1}) \\ 0 & (x \geq 0.5l_{m1}) \end{cases}$$

where y_0 : deflection of pile at ground surface, B : pile width, n : number of loading cycles.

3.8 Feature of new design method

Construction of the breakwater at Kumamoto Port was completed quickly and safely with the former design method (MOT 1991). However, the former design method was a preliminary method, because (1) the piles were limited to short piles and the axial resistance of the piles was neglected and (2) only the rear row of piles was considered to resist horizontal forces.

The new breakwater is constructed in deeper water with severer wave conditions. Thus, a breakwater designed by the former method would become excessively large with deepening of the construction site.

The new proposed design method is more rational than the former method, as it gives proper consideration to the equilibrium of forces and effects of pile resistance. The following are the important points of difference from the former design method: (1) The model of the subgrade reaction is changed to the PHRI method. Both rows of piles display their full capacity in horizontal resistance. (2) The pull-out resistance and push-in resistance of the piles are taken into consideration. (3) Fixity of the pile head is taken into consideration. All the test results show that the pile heads are never fully fixed, but the average fixity of all piles is around 0.7. (4) A reduction model for the coefficient of subgrade reaction under repeated loading is introduced.

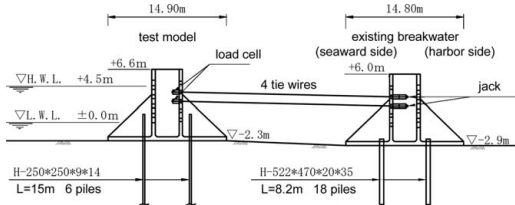


Figure 10. Field loading test.

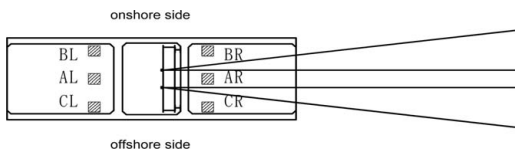


Figure 11. Plan view of test model and arrangement of piles.

4 FIELD LOADING TEST FOR EVALUATION OF NEW DESIGN METHOD

A field loading test was conducted to verify the validity of the newly-proposed design model. The site of the loading test was a marine area with a depth of C.D.L. –2.3 m adjacent to the actual breakwater construction site. The subsoil of the site is normally consolidated soft clay with a depth of more than 20 m. Tests including a geotechnical investigation, horizontal loading test with a single pile, and horizontal loading test with an actual size model were carried out.

4.1 Horizontal loading test

Figure 10 shows the elevation of the model. In this test, the actual breakwater was used for the reaction foundation. To investigate the failure mechanism of the structure, the test model was designed to fail. The length of the model was 1/3 that of the actual structure, and the piles used were of a smaller size. Figure 11 shows the plan view of the test model and arrangement of the piles. The bending moment distribution of each pile was measured in order to estimate the shear force applied to each pile.

Figure 12 shows the relationship between the horizontal load and horizontal displacement of the model. Horizontal displacement was negligible when loading was less than 300 kN and very small up to about 850 kN. The model began to move when the load exceeded 850 kN, and finally, when the maximum load was about 1100 kN, the model moved more than 40 cm.

The fixities of pile heads and shear resistances of piles were evaluated based on the measured bending moment distribution. The fixity of each pile head varies between 0 to 0.6. R_{fix} increases with the loading increment in some piles, but decreases in others.

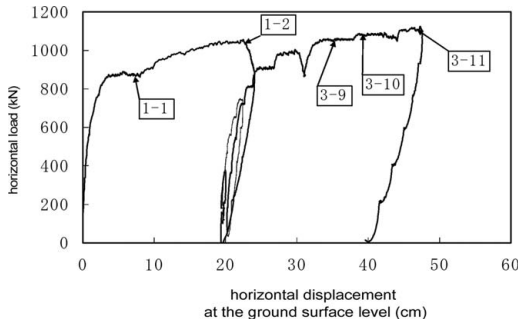


Figure 12. Horizontal displacement of test model.

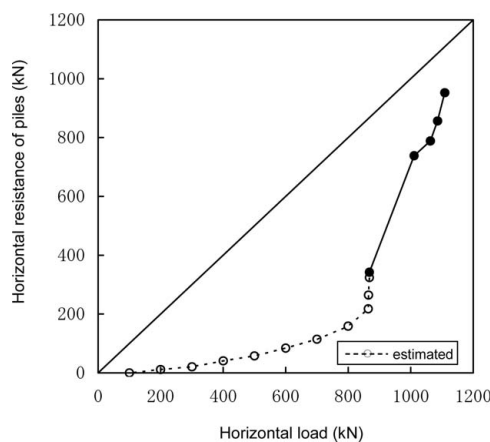


Figure 13. Relationship between horizontal loading and horizontal resistance of piles.

This means that, if piles are inserted in the base plate by the usual construction method, it will be difficult to control pile head fixity and fixity will vary from 0 to 0.6.

Figure 13 shows the relationship between the horizontal resistance of the piles and horizontal load. The lateral resistance of the piles is estimated by the bending moment distribution. The figure indicates that the horizontal resistance of the model is mainly due to cohesion between the base plate and ground surface in the early stage of loading, and the piles bear the resistance after the model moves horizontally. Finally, most of the horizontal resistance is borne by the piles themselves.

In this test, the effective weight of the model in the loading test was about 1800 kN, and load intensity was about 25 kN/m². The strength of the ground surface was about 12.4 kN/m². Under these conditions, the maximum cohesive resistance between the base plate and the ground surface was calculated at about 800 kN in accordance with Figure 3. The test results shown in Figure 13 support the conclusion that the

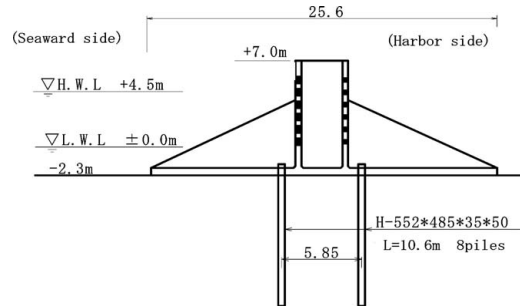


Figure 14. Breakwater design by existing design method.

cohesive resistance of the base plate was fully mobilized in the early stage of loading.

After full mobilization of base resistance, the model moved horizontally, and the horizontal resistance of the piles increased and base resistance decreased.

The model rotated 1.5° under maximum load. At this time, the maximum push-in force and pull-out force acting on the piles are about 300 kN. The ultimate axial resistance of each pile is estimated to be about 400 kN. As the total of push-in and pull-out resistance is 1200 kN, the axial resistance capacity is 4 times larger than the forces acting on the piles. For this reason, rotation of the model is very small.

This field loading test demonstrates the validity of the new design method with respect to the following points: (1) An S-type model by the PHRI method is suitable for estimating the horizontal resistance of piles. (2) The push-in and pull-out resistance of piles should be considered. (3) The fixity of the pile head is an important parameter for estimating the displacement of the structure and for designing the pile size. Fixity varies in a range from 0 to 0.6, and average fixity is about 0.3 at all the loading levels.

5 EFFECTS OF PROPOSED DESIGN METHOD

A trial design was prepared in order to compare the new and existing design methods. As assumptions, the breakwater is constructed at a depth of C.D.L. -2.3 m, C.D.L. +4.5 m of high water level, and C.D.L. +6.1 m of the required crown height level of the breakwater. The wave conditions of a return period of 50 years are $H_{max} = 4.5 \text{ m}$ ($H_{1/3} = 2.7 \text{ m}$); $T_{1/3} = 5.5 \text{ s}$, and the wave direction is rectangular with respect to the structure. A wave with a return period of 2 years is considered to take into account the effects of repeated loading. The wave conditions for this are $H_{max} = 2.0 \text{ m}$ and $T_{1/3} = 5.0 \text{ s}$.

Figures 14 and 15 show the results of design by the existing method and the new method, respectively.

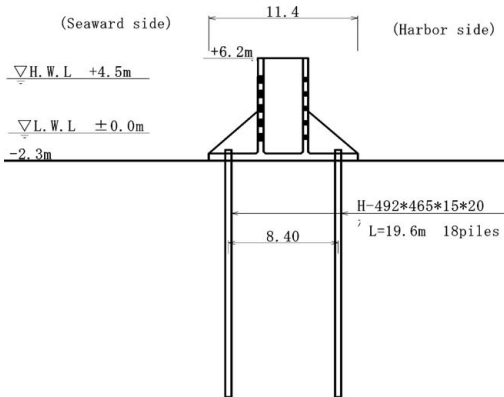


Figure 15. Breakwater design by new design method.

The structure designed by the existing method is 25.6 m in width and has an embedded pile length of 10.6 m, whereas the structure designed by the new method is only 11.4 m in width but has an embedded pile length of 19.6 m.

6 CONCLUSIONS

In this paper, the horizontal resistance of a soft landing breakwater with piles is examined and a new design method is proposed and compared with the

existing design method. The main conclusions of this paper are as follows: (1) The PHRI method gives an appropriate subgrade reaction model for the horizontal resistance of piles used in soft landing breakwaters. (2) The pull-out and push-in resistances of piles have a large effect on the horizontal resistance of the structure. (3) Structures designed by the proposed method, which is more rational than the existing method, were found to be more economical when the structure is constructed in deeper water.

REFERENCES

- Kikuchi, Y. (2003). Lateral resistance of soft landing moundless structure with piles, *Technical Note of the Port & Airport Research Institute*, No.1039, 192. (in Japanese)
- Kuchida, N., Ogura, K., Hosokawa, Y. & Nakano, T. 1986. Field tests on the development of soft landing breakwater – Horizontal loading tests and its results-. *Proc. of 41st Annual meeting of JSCE*, III: 137–138. (in Japanese)
- Ministry of Transport. 1991. *Design manual for soft landing breakwater*: 1–17. (in Japanese)
- Nova, R. & Montrasio, L. 1991. Settlements of shallow foundations on sand. *Geotechnique* 41(2): 230–253.
- Overseas Coastal Area Development Institute of Japan. 2002. *Technical Standards and Commentaries for Port and Harbour Facilities in Japan*: 284–309.
- Vaughan P.R., Davachi, M.M., El Ghamrawy, M.K., Hamza, M.M. & Hight, D.W. 1976. Stability analysis of large gravity structures. *BOSS '76*: 467–487.

Settlement and load-sharing of a piled raft foundation combined with grid-form soil-cement walls on soft ground

K. Yamashita & T. Yamada

R&D Institute, Takenaka Corporation, Chiba, Japan

ABSTRACT: This paper offers a case history of design and performance of a seven-story office building with a piled raft foundation on soft cohesive soil overlain by loose sand. It appeared from soil investigations that the loose sand has a potential of liquefaction during strong earthquakes. To cope with liquefaction a grid-form ground improvement was adopted to ensure adequate bearing capacity of the raft during and after earthquake. To confirm validity of the design of the piled raft, field measurements were performed on the foundation settlement, axial forces of the selected piles and contact earth pressure as well as pore-water pressure beneath the raft from the beginning of construction to about two years after completion of the building.

1 INTRODUCTION

Piled raft foundations have been frequently used in many countries because they are recognized to be able to offer a cost-effective alternative to conventional pile foundations (Randolph 1994, 2003; Poulos 2001; Poulos et al. 2001). For designing piled rafts, it is required to carefully consider interactions of raft-soil-pile system to predict settlement and load sharing between raft and piles. There exist, however, not so many case histories on monitoring load sharing between raft and piles as well as settlement (Kakurai et al. 1987; Yamashita & Kakurai 1991; Yamashita et al. 1994; Katzenbach et al. 2000). Thus accumulation of field evidences, especially on soil-structure interaction behaviour by monitoring full scale structures is required to develop more reliable design methods for piled rafts (Mandolini et al. 2005).

This paper offers a case history of design and performance of a seven-story office building with a piled raft foundation on soft cohesive soil overlain by loose sand. In this particular case, it appeared from soil investigations that the upper loose sand has a potential of liquefaction during strong earthquakes, and a grid-form ground improvement for the loose sand was adopted to ensure adequate bearing capacity of the raft during and after earthquake. The piled raft foundation was designed in order to ensure the consolidation settlement being not allowed and to ensure differential settlements being below a serviceability

limit. To confirm validity of the foundation design, field measurements were performed on the foundation settlement, axial forces of the selected piles and contact earth pressure as well as pore-water pressure beneath the raft from the beginning of construction to about two years after completion of the building.

2 BUILDING AND SOIL CONDITION

The seven-story office building with a flat dining hall is located in Minamisuna, Koto-ku in Tokyo (Photo 1). Figure 1 shows a schematic view of the building and foundation with soil profile. The building is a



Photo 1. Seven-story building in Minamisuna.

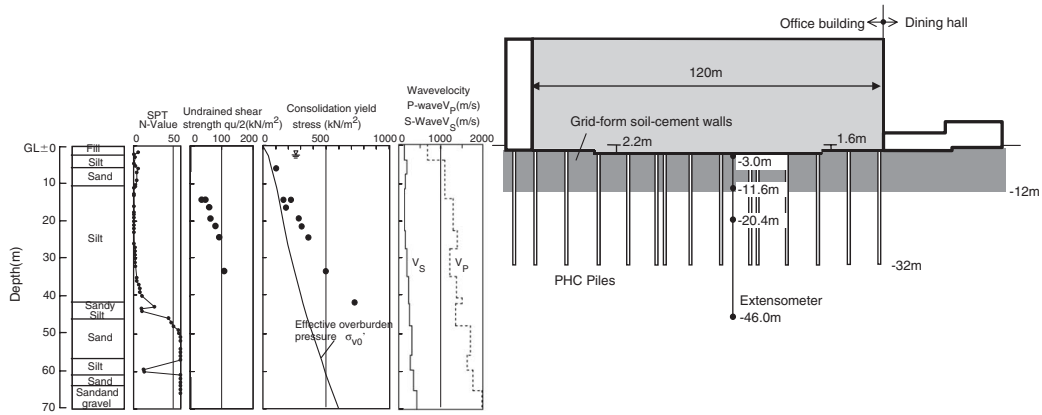


Figure 1. Schematic view of the building and foundation.

steel-frame structure and its plan measures 120 m by 33 m. The foundation level is at a depth of 2.2 m below the ground surface in the central part and at a depth of 1.6 m in both ends of the building. The subsoil consists of a soft alluvial stratum from the ground surface to about a depth of 46 m, underlain by a dense sandy layer of SPT N-values of 50 or more. The soil profile down to a depth of 11 m from the ground surface is made of soft silt and loose sand. From a depth of 11 m to 42 m below the ground surface, there lies a thick medium to hard silt layer. The upper medium silt layer at a depth of 11 m to 18 m from the ground surface is slightly overconsolidated with an overconsolidation ratio (OCR) of about 1.1. The lower hard silt layer at a depth of 18 m to 42 m from the ground surface is overconsolidated with an OCR of 1.8 or more. The shear wave velocity measured by a P-S logging varies 140 m/s² in the upper silt layer to 310 m/s² in the dense sand layer.

3 FOUNDATION DESIGN

3.1 Ground improvement

It appeared that the loose sand from a depth of 6 m to a depth of 11 m has a potential of liquefaction during an earthquake of the maximum horizontal ground-surface acceleration of 200 Gal, according to the simplified method of liquefaction potential evaluation recommended by Tokimatsu and Yoshimi (1983) or AIJ (2001). To cope with the liquefiable sand layer, a grid-form ground improvement (TOFT method) was introduced. In the method the grid-form soil-cement walls are constructed by deep mixing method as illustrated in Fig. 2. They confine a loose sand layer by the high-modulus walls with an unconfined compressive



Photo 2. Grid-form soil-cement walls.

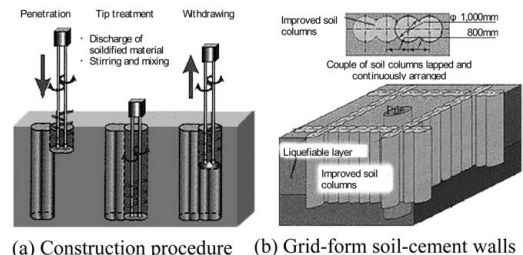


Figure 2. Grid-form ground improvement.

strength of 2000–4000 kPa, so as not to cause large shear deformation in the loose sand layer during a strong earthquake. The effectiveness of the grid-form ground improvement has become evident at the 1995 Kobe earthquake (Tokimatsu et al. 1996).

3.2 Pile specification

A total load in structural design is 378 MN which corresponds to the sum of dead load and live load of the building. The average contact pressure over the foundation is 100 kPa with the local maximum contact pressure of 142 kPa. When the foundation was designed as a raft foundation, more than 200 mm of consolidation settlement was predicted in the soft silt layer down to a depth of 6 m and the upper silt layer at a depth of 11 m to 18 m from the ground surface. In order to ensure the consolidation settlement being not allowed and to ensure differential settlements being below a serviceability limit, a piled raft foundation was proposed and designed based on a design philosophy of "creep piling" proposed by Hansbo (1984) and Jendeby (1986). According to the "creep piling", sufficient piles are included to reduce the net contact pressure between raft and soil to below the consolidation yield stress of the clay.

The consolidation yield stresses obtained from the oedometer tests are shown in Fig.1. For the upper medium silt layer the difference between the consolidation yield stresses and the effective overburden pressures, $(p_c - \sigma'_v)$, are proved to be more than 30 kPa. As to the soft silt layer an oedometer test result obtained in the neighboring site shows that the value of $(p_c - \sigma'_v)$ is not less than 30 kPa. The decrease in vertical effective stresses due to the excavation amount to 27 kPa and 37 kPa at the foundation levels, at a depth of 1.6 m and 2.2 m respectively, when the ground water table is assumed to be 2.2 m below the ground surface. So, assuming that the value of $(p_c - \sigma'_v)$ was equal to 30 kPa for the soft silt layers and the upper silt layer, maximum raft contact pressures were obtained as 57–67 kPa against the average contact pressure of 100 kPa, where the maximum raft contact pressure means the pressure above which consolidation settlement starts to occur. Then, the minimum load (per unit

area) which must be carried by piles could be roughly estimated to be the difference between the average contact pressure and the maximum raft contact pressure.

In designing piles of the piled raft the sum of a design pile load at a working condition was determined to be sufficiently larger than the estimated minimum load carried by piles. Furthermore, each pile was designed to operate below its design load at which significant creep starts to occur, at about 70% of its ultimate bearing capacity. To satisfy the above condition the piles were penetrated through the upper medium silt layer and embedded in the lower hard silt layer sufficiently to ensure their frictional resistance. Consequently a piled raft foundation with a total number of 70 piles of 30 m in length and 0.6 m to 0.9 m in diameter was adopted. Figure 3 shows a layout of the piles and the grid-form soil-cement walls. One or two piles are placed at each column position where the structure load is presumed to be concentrated. The piles are pre-stressed high-strength concrete (PHC) hollow piles. Each pile was constructed by inserting two 15 m-long PHC piles into a pre-augered borehole filled with mixed-in-place soil cement to avoid noise and vibration associated with pile driving.

4 INSTRUMENTATION

The settlement of the foundation, axial forces of the selected piles, earth pressures and pore-water pressure beneath the raft were monitored to confirm validity of the foundation design from the beginning of construction to about two years after completion of the building. The locations of the monitoring devices are shown in Fig. 3. Two piles at the locations of 7A and 7B were installed with a couple of LVDT-type strain gauges at pile head (at a depth of 4.3 m). Further, the pile 7B was installed with a couple of strain gauges at a depth of

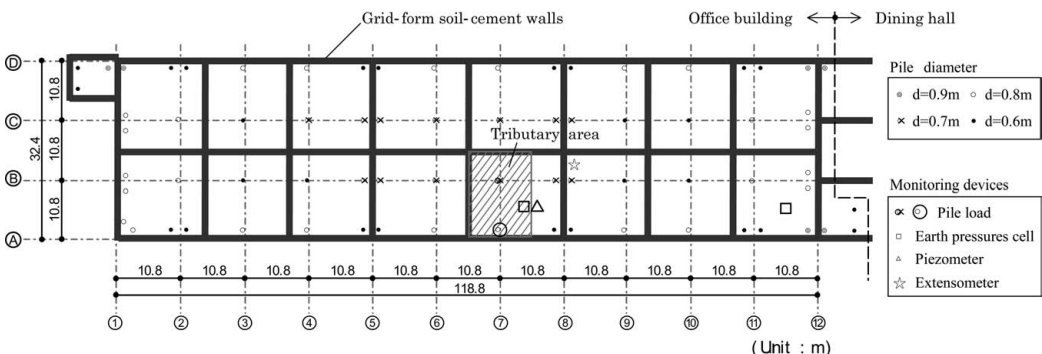


Figure 3. Layout of piles and grid-form soil-cement walls with locations of monitoring devices.

15.3 m and at a depth of 31.3 m from the ground surface to investigate the load distribution along the pile. A pair of earth pressure cell (E1) and piezometer was installed beneath the raft at a depth of 2.2 m. Another earth pressure cell (E2) has been installed beneath the raft at a depth of 1.6 m from the ground surface in the southern end of the foundation. The vertical ground displacement below the raft was measured by an extensometer at a location shown in Fig. 3. The extensometer in which LVDT-type transducers were installed at a depth of 3.0 m, 11.6 m and 20.4 m was reached down to a dense sand stratum at a depth of 46 m from the ground surface as shown in Fig. 1. The settlements of the foundation were measured at the selected column positions by an optical level where the bench mark was set to an existing nearby building supported by piles founded on a diluvial dense sand.

The measurement of axial forces of the piles, the earth pressures and pore-water pressure beneath the raft and the vertical ground displacement below the raft started early in December 2003 at the time just before constructing steel reinforcement for foundation slabs of 0.30 m in thickness. The measurement of the foundation settlement by an optical level began at the time just after casting the foundation slabs.

5 OBSERVATIONS

5.1 Settlement of the foundation

Figure 4 shows the measured vertical ground displacements below the raft at a depth of 3.0 m, 11.6 m and 20.4 m relative to a reference point at a depth of 46 m from the ground surface. The ground displacement at a depth of 3.0 m from the ground surface amounted to 15.6 mm at the time just after starting in building operation (early in December 2004). After that the settlement still slightly increased and reached 17.9 mm about one year after completion of the building. Thereafter the displacement increased at a very slow rate and reached about 18 mm, almost a state of equilibrium, early in 2006. The displacement amounted to 18.8 mm about two years after completion of the building. The vertical ground displacement at a depth of 11.6 m amounted to 10.1 mm at the time just after starting in building operation, thereafter the displacement increased in the same way as the settlement at a depth of 3.0 m, whereas the displacement at a depth of 20.4 m reached almost a state

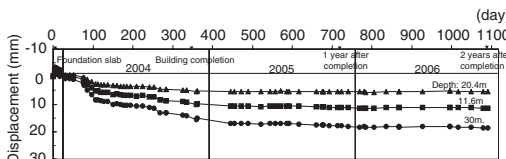


Figure 4. Measured vertical ground displacements.

of equilibrium at the time just after starting in building operation.

Figure 5 shows distributions of the measured vertical ground displacements with depth. At the time just before casting foundation slabs (late in December 2003), heaving of the ground due to the excavation amounted to 2.6 mm at a depth of 3.0 m. Considering the heaving of the ground the vertical ground displacement at a depth of 3.0 m amounted to 18.2 mm at the time just after starting in building operation and reached 21.4 mm about two years after completion of the building. During about two years after starting in building operation the increase in vertical displacement of the upper soil layers amounted to 3.0 mm, whereas the increase of the lower hard silt layer below a depth of 20.4 m was less than 0.5 mm.

Figure 6 shows the longitudinal settlement profile of the foundation measured by the optical level. The

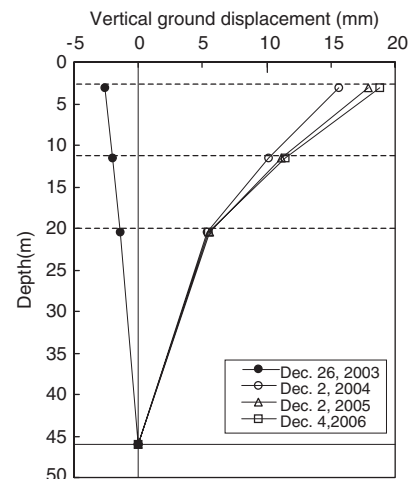


Figure 5. Measured distribution of vertical ground displacements with depth.

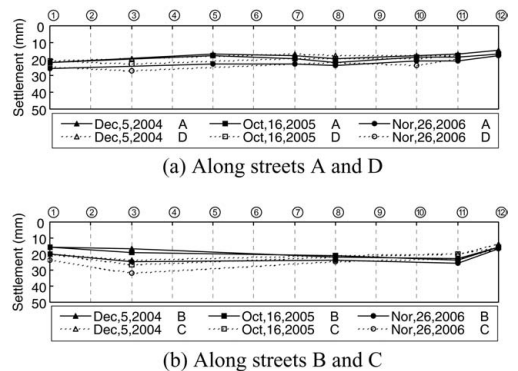


Figure 6. Measured longitudinal settlement profiles.

measured settlements were 14–24 mm at the time just after starting in building operation. Thereafter, the settlement slightly increased and reached 17–32 mm, about two years after completion of the building. At that time the maximum inclination angle obtained from the measured settlement profile was 1/1200 radian at the southern end of the foundation, which is less than the serviceability limit of 1/1000 radian.

5.2 Pile load, earth pressures and pore-water pressure beneath the raft

Figure 7 shows the measured axial forces of the piles 7A and 7B. For both piles the measured loads at pile-head increased after completion of the building and seemed to reach a state of equilibrium about one and half year after completion of the building.

Figure 8 shows the distributions of the measured axial forces on the pile 7B. At the time of starting in building operation, the average skin friction from a depth of 15.3 m to 31.3 m in medium to hard silt layer were 90 kPa whereas the average skin friction from a depth of 4.3 m to 15.3 m through the layers of the soft silt, the loose sand and the medium silt layer is 23 kPa. Thereafter, the average skin friction in the lower part of the pile increased and reached 115 kPa and that in the upper part of the pile slightly decreased and reached 20 kPa at the time about two years after completion of the building. The average skin friction mobilized in the lower part of the pile at the time just after starting in building operation is consistent with the average undrained shear strength of 81 kPa obtained from the unconfined compressive strength of the medium silt layer shown in Fig. 1. At the time about two years after completion of the building, the mobilized average skin friction became 40% larger than the average undrained shear strength. However, the mobilized skin friction of the pile shaft may still not reach its creep strength or

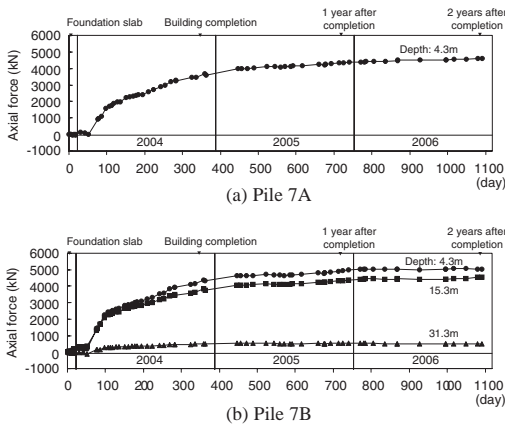


Figure 7. Measured axial forces of the piles 7A and 7B.

70–80% of the ultimate strength in the present because the settlement of the foundation has substantially ceased and/or decrease in the pile-head load is not observed.

Figure 9 shows development of the measured earth pressures and the pore-water pressure beneath the raft. The measured earth pressures increased in early stage of construction. However, they stopped to increase and seemed to reach a state of equilibrium at about half a year before completion of the building in spite of the increase in loading of construction. The measured earth pressures amount to 25–26 kPa in E1 located at the central part and 15–19 kPa in E2 located at the southern end of the foundation. The measured pore-water pressure increased in an early stage of the construction and a little fluctuated in the range of 6–9 kPa.

5.3 Load sharing between raft and piles

For piled rafts the equilibrium equation is expressed as follows:

$$W = W' + U_w = P_p + P'_r + U_w \quad (1)$$

where W is a total building load, W' is an effective building load, P_p is pile resistance, P'_r is an effective

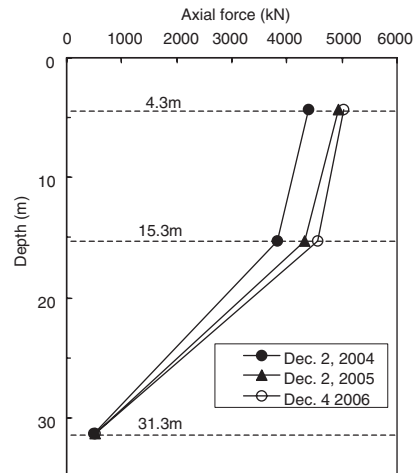


Figure 8. Measured axial force distribution along the pile 7B.

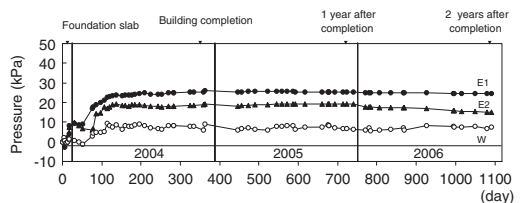


Figure 9. Measured earth pressures and pore-water pressure beneath the raft.

raft resistance, U_w is buoyancy. The load sharing between raft and piles for the building can be estimated by considering the measured results about the pile-head loads, the earth pressure and pore-water pressure beneath the raft on the tributary area shown in Fig. 3.

The effective raft resistance consists of the effective soil resistance and the effective resistance of the grid-form soil-cement walls i.e. a part of the load carried by the raft might be transmitted through the soil-cement walls to the upper silt layer. Then, Eq.(1) can be expressed as follows:

$$W_t = P_{pt} + p_s'(A_t - A_p - A_g) + p_g'A_g + u_w(A_t - A_p) \quad (2)$$

where W_t is a building load and P_{pt} is the sum of the pile-head load on the tributary area, p_s' is an effective earth pressure between the raft and soil, p_g' is an effective contact pressure between the raft and the grid-form soil-cement walls, u_w is a pore-water pressure beneath the raft, A_t is a tributary area, A_g is a plane-view area of the grid-form soil-cement walls and A_p is the sum of the cross-sectional area of the piles 7A and 7B. As the value of A_p/A_t is usually small, less than 0.5% and considered to be negligible in this case, Eq.(2) can be expressed as follows:

$$W_t = P_{pt} + p_s'(A_t - A_g) + p_g'A_g + u_w A_t \quad (3)$$

The building completed in mid-November 2004 and started in operation late in November 2004. Therefore the load acting on the foundation after December 2004 is considered to be approximately the design load which corresponds to the sum of dead load and live load of the building. So, assuming that W_t is equal to the design load of 16.1 MN, $A_t = 181.5 \text{ m}^2$ and $A_g/A_t = 0.10$ on the tributary area after December 2004, the load sharing between raft and piles can be estimated.

Figure 10 shows the time-dependent load-sharing among the piles, soil, grid-form soil-cement walls and the buoyancy on the tributary area. The ratio of the load carried by the piles to the total building load,

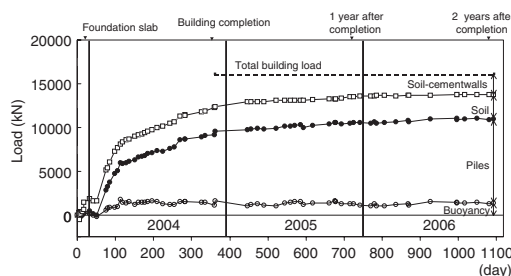


Figure 10. Time-dependent load sharing between raft and piles.

$\alpha_p = P_{pt}/W_t$, was 0.50 at the time just after starting in building operation. Thereafter, α_p increased to 0.60 about two years after completion of the building. Conversely the ratio of the load carried by the raft to the total building load, $\alpha_r = p_s'(W_t - P_p)/W_t$, was 0.50 at the time just after starting in building operation and α_r decreased to 0.40 at the time about two years after completion of the building. As to load sharing for the effective building load, the ratio of the load carried by the piles to the effective building load, $\alpha'_p = P_{pt}'/(W_t - u_w A_t)$, was 0.54 at the time just after starting in building operation and α'_p increased to 0.65 about two years after completion of the building. The ratio of the effective load carried by the soil to the effective building load, $\alpha'_s = p_s'(A_t - A_g)/(W_t - u_w A_t)$, was 0.21 at the time just after starting in building operation and α'_s slightly decreased to 0.19 at the time about two years after completion of the building. The ratio of the effective load carried by the grid-form soil-cement walls to the effective building load, $\alpha'_g = p_g'A_g/(W_t - u_w A_t)$, can be obtained from Eq.(3). The value of α'_g was 0.25 at the time just after starting in building operation and α'_g decreased to 0.16 at the time about two years after completion of the building.

As for the reason why the load carried by the piles slightly increased after building operation started, it is suggested that there exist some normally consolidated silt layers down to a depth of 6 m and consolidation settlement occurred in the soft silt layers by construction loading in excess of the decrease in the effective overburden pressure due to excavation.

6 CONCLUDING REMARKS

Field measurements were performed on the piled raft combined with grid-form soil-cement walls from the beginning of construction to about two years after completion of the building.

The measured settlements were 14–24 mm at the time just after starting in building operation. At the time about two years after completion of the building the settlements reached 17–32 mm and the maximum inclination angle amounted to 1/1200 radian which is less than the serviceability limit of 1/1000 radian.

As to load sharing between raft and piles, the ratio of the load carried by the piles to the effective building load was 0.54 at the time just after starting in building operation and increased to 0.65 at the time about two years after completion of the building. The ratio of the effective load carried by the soil α'_s and that of the effective load carried by the grid-form soil-cement walls α'_g to the effective building load were 0.21 and 0.25 respectively at the time just after starting in building operation. Thereafter, α'_s and α'_g slightly decreased to 0.19 and 0.16 respectively at the time about two years after completion of the building.

ACKNOWLEDGEMENTS

The authors are very grateful to Messrs. Nobuo Nakayama and Akihiro Miyashita of Takenaka Corporation for their contribution to the structural design for the piled raft foundation. The authors are also grateful to Messrs. Yasuyuki Shibata and Takashi Shibata of Takenaka Corporation for their assistance throughout the observation of the foundation behaviour.

REFERENCES

- Architectural Institute of Japan. 2001. *Recommendations for design of building foundations. Revised edition* (in Japanese).
- Hansbo, S. 1984. Foundations on friction creep piles in soft clays. *Proc. 1st Int. Conference on Case Histories in Geotechnical Engineering*. Vol.2 pp.914–915.
- Jendeby, L. 1986. Friction piled foundations in soft clay -A study of load transfer and settlements. Thesis. Chalmers University. Gothenburg. Sweden.
- Kakurai, M., Yamashita, K. & Tomono, M. 1987. Settlement behavior of piled raft foundation on soft ground. *Proc. 8th ARCSMFE*: 373–376.
- Katzenbach, R., Arslan, U. & Moermann, C. 2000. Piled raft foundations projects in Germany. In Hemsley J.A. (ed). *Design applications of raft foundations*: 323–392: Thomas Telford.
- Mandolini, A., Russo, G. & Viggiani, C. 2005. Pile foundations: Experimental investigations, analysis and design. *Proc. 16th ICSMGE*. Vol.1: 177–213.
- Poulos, H. G. 2001. Piled raft foundations: design and applications. *Geotechnique*. 51(2): 95–113.
- Poulos, H. G., Carter, J.P. & Small, J.C. 2001. Foundations and retaining structures. *Proc. 15th ICSMFE*. 4: 2527–2606.
- Randolph, M. F. 1994. Design methods for pile groups and piled rafts. *Proc. 13th ICSMFE*: 61–82.
- Randolph, M. F. 2003. Science and empiricism in pile foundation design. The 43rd Rankine Lecture. *Geotechnique*. 53(10): 847–875.
- Tokimatsu, K. & Yoshimi, Y. 1983. Empirical correlation of soil liquefaction based on SPT N-value fines content. *Soils & Foundations*. 23(4): 56–74.
- Tokimatsu, K., Mizuno, H. & Kakurai, M. 1996. Building damage associated with geotechnical problems. *Special Issue of Soils & Foundations*: 219–234.
- Yamashita, K. & Kakurai, M. 1991. Settlement behavior of the raft foundation with friction piles. *Proc. 4th Int. Conf. on Piling and Deep Foundations*: 461–466.
- Yamashita, K., Kakurai, M. & Yamada, T. 1994. Investigation of a piled raft foundation on stiff clay. *Proc. 13th ICSMFE*. Vol.2: 543–546.

Earthquake resistant reinforcement method for pile foundations using effect of confinement of ground solidification body

Y. Adachi & K. Urano

Hazama Corporation, Tsukuba, Ibaraki, Japan

T. Takenoshita

Toko Corporation, Minatoku, Tokyo, Japan

N. Tanzawa

Aoyama Kiko Corporation, Kotoku, Tokyo, Japan

M. Kawamura

Department of Architecture and Civil Engineering, Toyohashi University of Technology, Toyohashi, Aichi, Japan

ABSTRACT: In the past large earthquake, many pile foundations were suffered from destructed damage due to strong vibration and ground liquefaction. The necessity of earthquake resistant reinforcement to pile foundations has risen. However, applications of existing earthquake resistant reinforcement methods to pile foundations are limited because of various unfavorable construction conditions. The authors proposed a new method for the earthquake resistant reinforcement for pile foundations based on ground solidification techniques which is applicable to both new and existing pile foundations. The proposal method aims to increase the stiffness of the pile foundation by the effect of a two layered larmen structure by the reinforcement body made in the ground around piles, and was confirmed by model shaking table tests under 1.0 g gravitational field and numerical simulation analyses. This paper will show a full-scale model test of the proposed method that was conducted to examine the construction performance and the quality of reinforcement body in the pile foundation. The full-scale test includes horizontal load tests, vibration tests, and excavation of the reinforcement body for observation. Based on the test results, applicability of the proposed reinforcement method for a real pile foundation was confirmed.

1 INTRODUCTION

In recent years, re-evaluating the earthquake level and preparing existing structures and their foundations ready against the supposed coming large-scale earthquake have raised the necessity of earthquake-resistant reinforcement method. Actually, reinforcement methods for pile foundations are limited due to construction restrictions such as site and space. To deal with that problem, the authors proposed a new type of earthquake-resistant reinforcement method, applicable even for existing pile foundations. In this method, ground solidification technique is adopted in construction of a solidified body in the ground surrounding a portion of the pile group, which is in combination with the piles and footing resulting in a two-layer larmen structure strongly reinforcing the pile foundation against the earthquakes. The effectiveness of the method had previously been confirmed through 1 g-field shaking

table model test and numerical simulation (Adachi 2002). This paper reports about a full-scale experiment carried out for investigating the construction performance and quality of the proposed method at actual scale level of pile foundation.

2 EXPERIMENT OUTLINE

2.1 *Outline of the full-scale pile foundation model*

Outline of the pile foundation and ground used in the experiment are shown in Figure 1. This newly constructed pile foundation for experiment consists of four steel pipe piles, which are 406.4 mm in outer diameter, 9.5 mm in thickness and 10.0 m in length, being arranged at 2.0 m spacing. Pile installation was carried out by the method of inner pre-boring and tip

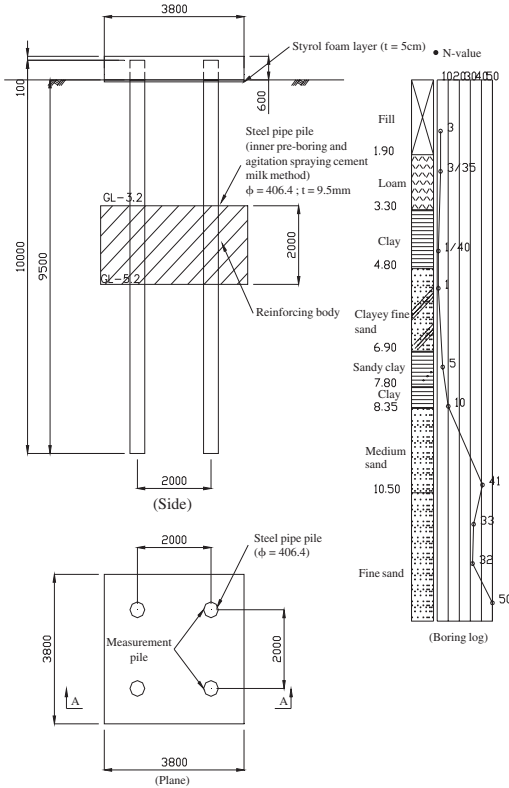


Figure 1. Full-scale model test outline.

grouting (cement milk spraying agitation technique). The pile heads were fixed with 0.5 m length embedded in a reinforced concrete (RC) footing of $3.8\text{ m} \times 3.8\text{ m} \times 0.6\text{ m}$ dimension. On the outer surface of two of the steel pipe piles, strain gauges and their protectors (L-type steel) were set up beforehand. Moreover, a 5 cm-thick styrene foam layer was layout at the bottom of the footing to eliminate the friction between the concrete and soil.

As for the ground conditions, beneath a 2 m thick surface fill layer, there exist a 5 m thick soft loam and clay layer with SPT N-value 1 followed by a 1.5 m thick clay of SPT N-value 5~10, which are underlain by a sand layer of SPT N-value 40. The pile tips were embedded for about 1 m inside the sand layer.

The reinforcement body is constructed by ground solidification treatment to bind the pile group at its middle length, so that together with the footing they form a 2-layer larmen structure, thank to its restraining effect the pile foundation rigidity is enhanced. The reinforcement body, being identical to the footing in horizontal dimension ($3.8\text{ m} \times 3.8\text{ m}$), is situated between the depths of $3.2\text{ m} \sim 5.2\text{ m}$ (2.0 m thick).

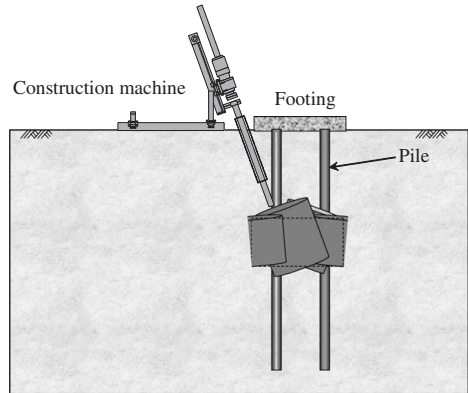


Figure 2. Situation of construction of reinforcement body.

Table 1. Material properties of steel pipe pile.

Steel pipe pile $\varphi 406.4\text{ mm}$, $t = 9.5\text{ mm}$, $L = 10.0\text{ m}$

Section area	$A (\text{m}^2)$	0.011846
Sectional 2-D moment	$I (\text{m}^4)$	0.000233
Sectional coefficient	$Z (\text{m}^3)$	0.001149
Young modulus	$E (\text{kN/m}^2)$	2.1×10^8
Bending rigidity	$EI (\text{kN/m}^2)$	4901.1

It is structured by spraying cement milk at 12 spots within a prescribed periphery using high-pressure jet-grouting method, which is capable for obliquely construction. The design strength of the reinforcement body is 1 MN/m^2 . The image of this ground formation is presented in Figure 2.

Three main subjects of the full-scale experiment to be carried out are:

1. Horizontal loading tests,
2. Vibration tests, and
3. Observation of excavated reinforcement body.

Outline of horizontal loading tests as well as the test results and observation of excavated reinforcement body are described hereafter.

3 HORIZONTAL LOADING TEST

3.1 Test outline

Horizontal loading tests were performed before and after construction of reinforcement body to compare the behaviors of the pile foundation. For horizontal loading, two oil pressure jacks were used to apply uniaxial load in multi-cycle loading style (JGS 1983).

Instrumentation with displacement transducer, inclinometer, load cell and strain gauges for measurements

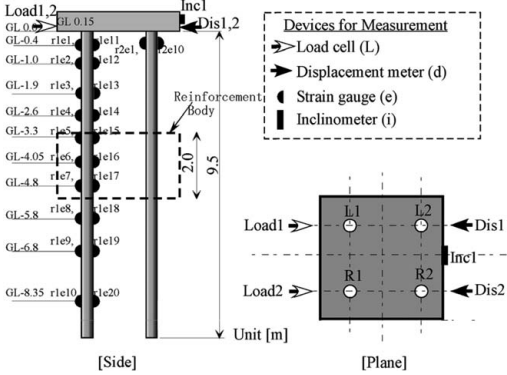


Figure 3. Horizontal loading test instrumentation.

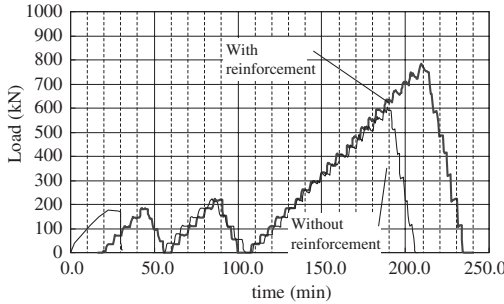


Figure 4. Load–Time curves.

in horizontal loading tests is shown in Figure 3. In this, 1 set of strain gauge is setup on one pile on the push-in side, while 10 sets are on another pile on the pull-out side.

3.2 Test results

(a) Load–Displacement relationship

Load–Time curves and Load–Horizontal displacement curves of the pile head from horizontal loading tests before and after reinforcement are presented together in Figures 4 & 5, respectively, for comparison. The maximal load before and after reinforcement was 600 kN and 787.5 kN, respectively. Compared to 17.2 mm of horizontal displacement of the footing at the moment of maximal loading in the test before reinforcement, the displacement after reinforcement was reduced to 4.8 mm only. Thus after reinforcement, even when approaching the maximal load of about 200 kN higher than before reinforcement, the load – displacement relationship still showed almost linear elastic behavior. Actually, according to the inclinometer equipped on the side surface of the

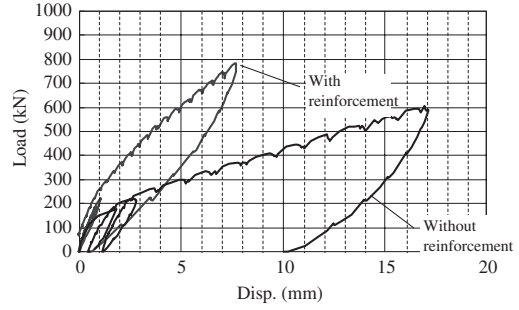


Figure 5. Load–Displacement curves.

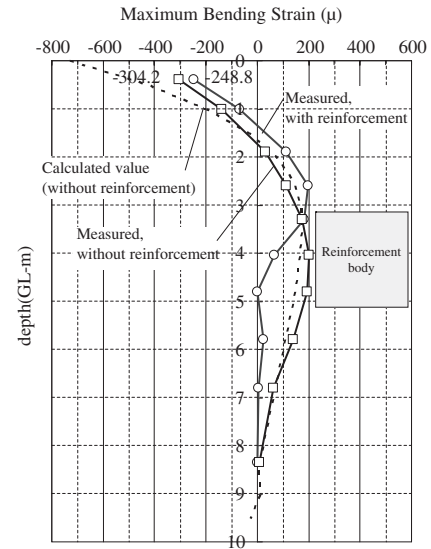


Figure 6. Bending strain distribution (under load intensity of 600 kN).

footing, the footing inclination angle at the moment of 600 kN load intensity was +0.0956 degree and +0.0608 degree in the tests before and after reinforcement, respectively (rotation in the direction of loading is signed as “+”).

(b) Bending strain distribution

Bending strain distribution before reinforcement under load intensity of 600 kN is shown in Figure 6. Also combined in the same figure is calculated bending distribution without reinforcement of an elastic beam above foundation level under pile head fixed condition (Chang method). The results of test without reinforcement showed a generally good agreement with calculated values. After reinforcement, due to confining effect of the reinforcement body set at the

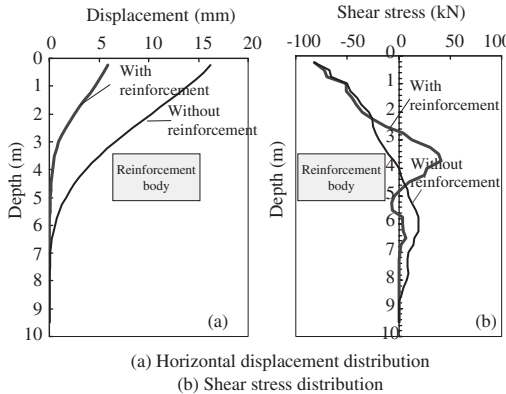


Figure 7. Distributions of horizontal displacement and shear stress in accordance to bending strain distribution (under load intensity of 600 kN).

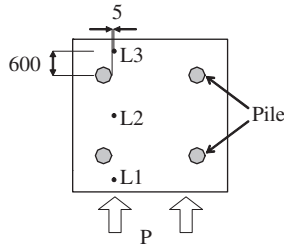


Figure 8. Core gathering positions.

middle part of the piles, bending strain was reduced near the pile head, but inversely increased near the end of reinforcement body. However, for the lower part of the pile (beneath the reinforcement body depth), bending strain was almost not occurred. Such behavior is considered due to the effect of two-layer larmen structure formed by setting the reinforcement body to relate the pile foundation and the footing.

Using elastic flexible curve from bending strain distribution shown in Fig.6, numerical integration and differentiation were performed, and calculated results of pile horizontal displacement distribution and shear force distribution are presented in Figure 7. In calculation, micro incremental interval of depth, $dx = 0.25$ m was adopted in pick up the values of the strain curve. As shown in Fig.7, by setting up reinforcement body, up to the depth of GL - 3.0 m the pile horizontal displacement largely decreased. Also in this case, the shear force near the top of the reinforcement body has been increased compared to that before reinforcement. Because of that, for actual design, thoroughly consider the shear stress in adjusting the thickness and position of the reinforcement body is necessary.



Photo 1. Situation of excavated reinforcement body.



Photo 2. Situation of excavated reinforcement body (pile surrounding status).

4 OBSERVATION OF REINFORCEMENT BODY FROM EXCAVATION

After completion of horizontal loading tests and vibration tests, the reinforcement body was excavated to observe its ready form as well as its quality.

To enable observation of the outer shape and side surface of the reinforcement body, excavation up to the ground level of GL - 3.5 m was performed. Excavation situations are shown in Photos 1 and 2. Observation indicated that the initially designed horizontal dimension of $3.8 \text{ m} \times 3.8 \text{ m}$ was satisfied, and the joining between the pile and the reinforcement body was in good adherence. Collection of continuous core along depth was carried out at 3 spots and the thickness of the reinforcement body was confirmed. It was understood that, a homogenous reinforcement body has been constructed within the depth from GL - 3.2 m to GL - 5.2 m. The status of the collected cores is illustrated in Photo 3.

Uniaxial compression tests were performed on specimens of collected cores to examine their strength characteristic. The loading was enforced by compression at constant strain of 1%/min. Results of compression tests on specimens of four weeks aging cores

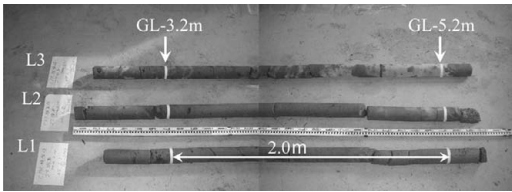


Photo 3. The collected cores.

Table 2. Mean value of axis compression examination result (four weeks).

Compression strength q_u	4.4 MN/m ²
Elastic coefficient E_{50}	1460 MN/m ²

are shown in Table 2. It was found that the obtained strength considerably surpassed the designed compressive strength of 1 MPa. Furthermore, mean value of moist density ρ_f was 1.48 g/cm³.

5 CONCLUSIONS

By conducting full-scale model test of earthquake-resistant reinforcement method on actual scale pile foundation using ground solidification technique, following points are made clear.

1. Comparing the behaviors of the pile foundation under horizontal loading (at load intensity of

600 kN), bending moment and displacement after reinforcement were reduced compared to those before reinforcement, which confirms the reinforcing effect of the proposed method.

2. According to measurement of the pile during construction of the reinforcement body, high-pressure jet-grouting work imposes only small influence to the piles.
3. By excavation of reinforcement body for observation, it was confirmed that the reinforcement body and the piles are well adhered as planned. Moreover, from the results of compression tests it is understood that the attained strength of the reinforcement body essentially satisfied the design value.

Therefore, it is concluded that this new reinforcement method is highly applicable to actual structures. Based on these data, following work would be conducting detailed investigation on influences of various specifications such as ground conditions, pile foundations and reinforcement body in order to establish a simple design method.

REFERENCES

- Adachi, Y., Urano, K. & Mihara, M. 2002: Investigation on pile foundation structure behaviors during liquefaction and related reinforcement method. *Proc. of 47th Symposium on Geotechnical Engineering*:187–192.
The Japanese Geotechnical Society. 1983: *Method of horizontal loading for piles*.

A design approach for composite ground pile and its verification

K. Tomisawa

Civil Engineering Research Institute for Cold Region, Hokkaido, Japan

S. Miura

Graduate School of Engineering, Hokkaido University, Hokkaido, Japan

ABSTRACT: This paper describes a practical foundation design method in which the ground is improved around the heads of pile foundations in soft ground or sandy ground subject to liquefaction. The shear strength increased due to ground improvement is reflected in the horizontal resistance of piles. The horizontal subgrade reaction of piles is determined by converting the shear strength S of improved ground to the modulus of deformation E . In this study, the increased earthquake resistance produced from ground improvements around pile heads was confirmed through a series of centrifuge shaking tests. The horizontal resistance of piles equivalent to the design value was also confirmed through an *in-situ* horizontal loading test of piles installed in the improved ground.

1 INTRODUCTION

When designing the foundations of piles to be constructed in improved ground, there is no rational and unified method for determining the subgrade reaction characteristics after ground improvement. Consequently, there is also no systematic seismic design method that considers the influence of the dynamic behavior of the improved ground on pile foundations during earthquakes.

Tomisawa and Nishikawa (2005a, 2005b) developed a reasonable design method in which, prior to constructing piles, the ground is improved around the heads of the pile foundations in soft ground and ground subject to liquefaction; in this method, the increased shear strength is reflected in the horizontal resistance. The construction method studied uses a combination of pile foundation construction together with common ground improvement methods (Civil Engineering Research Institute of Hokkaido, 2002; Public Works Research Center, 1999), including deep mixing, preloading, and sand compaction piling; the method is referred to as the composite ground pile method. This study presents a design procedure for the composite ground pile method for establishing the range of influence of the horizontal resistance of piles, or the necessary range of ground improvement, through engineering judgment and for determining the horizontal subgrade reaction of piles from the increased shear strength of improved ground. Earthquake resistance of the composite ground pile was

assessed through a series of dynamic centrifuge model tests. *In-situ* horizontal loading tests were also conducted on piles installed for a bridge foundation, and the validity of the design method was experimentally verified.

2 EVALUATION METHOD FOR HORIZONTAL RESISTANCE OF PILES INSTALLED IN IMPROVED GROUND

2.1 Consideration of the range of ground improvement

The range of influence of horizontal resistance in the ground when horizontal force is applied to a pile spreads gradually as load increases. As a result, when the failure limit state of the ground is reached following the horizontal displacement of the pile, a state of equilibrium is considered to be maintained between the maximum value of the horizontal subgrade reaction and the passive earth pressure.

In the composite ground pile method, therefore, the necessary range of ground improvement, i.e., the range of horizontal subgrade reaction to the pile, is proposed to be a three-dimensional domain formed with the gradient of the surface of passive failure $\theta = (45^\circ + \phi/2)$ (ϕ : angle of shear resistance of soil) from the depth of the characteristic length of piles, $1/\beta$ (\$\$), which is the depth of influence of the horizontal resistance of piles on the basis of the limit

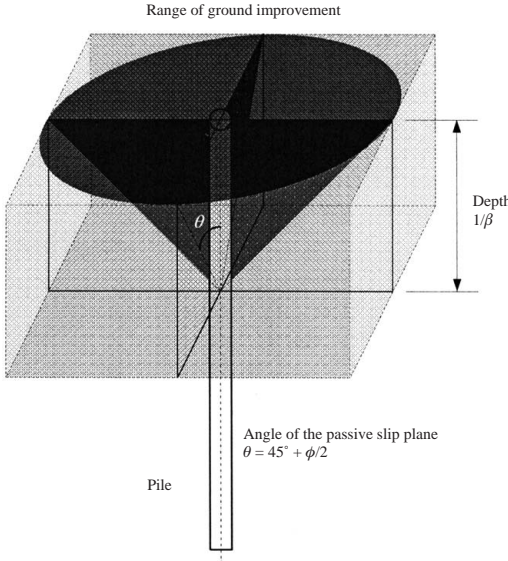


Figure 1. 3-D image of the lateral resistance of pile foundation and the setup for the range of ground improvement.

equilibrium and the Mohr-Coulomb failure criterion. Broms (1964a, 1964b) and Reese et al. (1974) indicated the similar failure patterns of ground around a pile horizontally loaded.

As a result, the necessary range of improvement is set as a three-dimensional inverted cone shape centered on the pile. However, since it is difficult to conduct ground improvement in a cone shape due to construction limitations, a cubic body covering the range of the invert cone shape shown in Figure 1 was proposed for the range of ground improvement. The method for setting the range of ground improvement for groups of piles is the same as that for a single pile.

2.2 Method for determining horizontal subgrade reaction

In determining the horizontal resistance of piles, the horizontal subgrade reaction p acting on a pile is considered to increase in proportion to the horizontal deflection y expressed by the equation $p = k \cdot y$, where the coefficient k is defined as the coefficient of horizontal subgrade reaction (k value), on the basis of the bending theory of beam on an elastic body (Chang 1937). The k value depends on pile specifications and ground properties (Terzaghi 1943; Vesic 1961); the formula for calculating k shown in Equation 1 is widely used for the design of pile foundations in Japan (Japan Road Association 2002). Accordingly, the horizontal resistance of piles constructed in improved ground can be calculated from the modulus

of deformation of improved ground E . The formula for calculating k is:

$$k = \frac{1}{0.3} \alpha E \cdot \left(\frac{\sqrt{D/\beta}}{0.3} \right)^{-3/4} \quad (1)$$

where E is the modulus of deformation of the improved ground (kN/m^2), α is a compensation coefficient for the k value, D is the pile diameter (m), and I is the second moment of area of the pile section (m^4).

When the deep mixing method is used for ground improvement with the composite ground pile method, composite ground is formed by placing improved columns with required strength around the piles. The shear strength of composite ground S is calculated by Equation 2 and 3 (Civil Engineering Research Institute of Hokkaido 2002), combining the shear strength of the improved column S_c and that of original ground S_0 according to the improvement rate a_p :

$$S = S_c \cdot a_p + S_0 (1 - a_p) \quad (2)$$

$$S_c = q_{up}/2, \quad S_0 = q_{u0}/2, \quad a_p = A_p/A \quad (3)$$

where S_c is the shear strength of the improved columns (kN/m^2), S_0 is the shear strength of the original ground, a_p is the ground improvement rate, q_{up} is the unconfined compression strength of improved columns (kN/m^2), q_{u0} is the unconfined compression strength of the original ground (kN/m^2), A_p is the area of the cross-section of the improved columns (m^2), and A is the distribution area per improved column (m^2). Greater strength can be expected for the composite ground when the deep mixing method is adopted for ground improvement; the shear strength of improved columns S_c in the composite ground pile method is usually 200 to 500 kN/m^2 , which is the range of commonly used design values. In this case, improved columns are installed one by one with an improvement rate of $a_p = 78.5\%$ or higher to ensure a certain level of the horizontal subgrade reaction of the piles.

Consequently, to properly select the horizontal subgrade reaction of piles in improved ground in a design for the composite ground pile, it is necessary to evaluate the increases in shear strength S and modulus of deformation E of the ground due to ground improvement. In the deep mixing method, the shear strength of improved columns S_c can be obtained from the relationship between unconfined compression strength q_{up} and shear strength of improved columns S_c ($= q_{up}/2$), as shown in Equation 3. It is also well established that the unconfined compression strength q_{up} is proportional to the modulus of deformation E_p of improved columns. For example, the design manual for the deep mixing method for onshore construction (Public Works Research Center, 1999) gives the

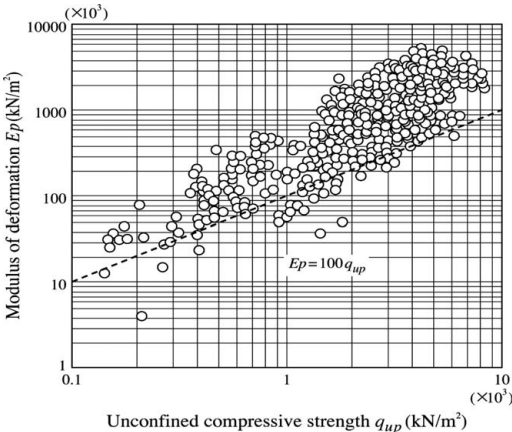


Figure 2. Relationship between the unconfined compressive strength q_{up} of improved columns and the modulus of deformation E (cohesive soil).

relationship $E_p = 100 q_{up}$ for improved cohesive ground (Figure 2). Therefore, it is said that the modulus of deformation of improved ground E can be treated equivalently to shear strength S . By regarding the increment in shear strength ΔS generated by consolidation as equivalent to the increment in the modulus of deformation ΔE achieved by ground improvement, the modulus of deformation E for the fully improved ground can be calculated in the same way.

3 EVALUATION OF EARTHQUAKE RESISTANCE FOR THE COMPOSITE GROUND PILE METHOD THROUGH DYNAMIC CENTRIFUGE MODEL TESTS

A series of dynamic centrifuge model tests was conducted to evaluate the earthquake resistance of the composite ground pile method. As mentioned above, a number of different ground improvement methods are suitable for use in the proposed composite ground pile method. To simplify the model for testing, the sand compaction pile method with a high improvement rate was adopted as the ground improvement method around the pile, and soft cohesive soil was assumed to be the original ground. The earthquake resistance of pile foundations was confirmed by using sandy soil as the improved ground and kaolin clay as the original soft ground.

For the dynamic centrifuge model test, a 1:50 model of ground and piles was prepared in a laminar model container with inner dimensions of $0.7\text{ m} \times 0.2\text{ m} \times 0.35\text{ m}$. A 50 g (g: gravitational acceleration) centrifugal acceleration field was adopted for the

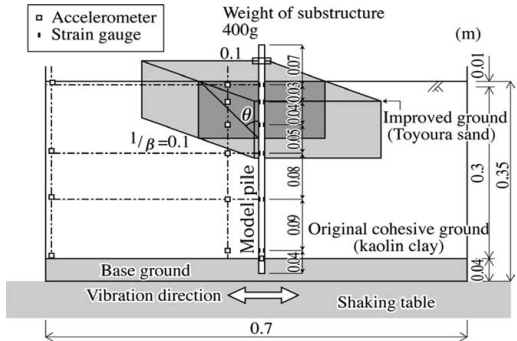


Figure 3. Model setup for the centrifuge shaking test (composite ground pile model).

test to satisfy the similarity law on the stress level. A model pile with an outer diameter $D = 0.01\text{ m}$, thickness $t = 0.002\text{ m}$, and pile length $L = 0.4\text{ m}$ was made from steel pipe and specially finished. A prototype scale steel pile with outer diameter $D = 0.5\text{ m}$ and thickness $t = 0.01\text{ m}$ was simulated in the centrifugal acceleration field for this model pile according to the similarity law. A steel block with a weight of $W = 3.92\text{ N}$ (equivalent to 490 kN at the prototype scale) was fixed to the pile head to simulate the substructure, and the lower end of the model pile was fixed in the model base ground with gypsum. Strain gauges were attached to the model pile to measure both axial and bending stress generated along the axis of the pile, and acceleration sensors were installed on the pile head and in the ground to measure the responses of both pile and ground during shaking. Figure 3 shows the setup of the test model. To form the model ground, a single layer of dry kaolin clay was prepared to simulate the uniform soft ground, and the improved ground was prepared by replacing kaolin clay with Toyoura sand in the area around the pile head to simulate ground improvement using SCP with a relatively high improvement rate. The improved ground using Toyoura sand was a cubic body with length and width of 0.2 m and height of 0.1 m centered around the pile to simulate the range of influence of the horizontal resistance of the pile, which was assumed to cover the inverted cone formed by the gradient of the surface of passive failure $\theta = (45^\circ + \phi/2)$ from the depth of the characteristic length of piles, $1/\beta$, based on the proposed setting method. The model grounds were prepared by pouring both kaolin clay and Toyoura sand from a certain height. Table 1 shows the physical properties of kaolin clay and Toyoura sand. The relative density of improved ground with Toyoura sand was set at 85%. In order to simplify the test conditions and clarify the changes of the k values with the difference in strength

Table 1. Physical properties of kaolin clay and Toyoura sand.

	Kaolin clay	Toyoura sand	
Unit weight	KN/m ³	10.101	15.574
Particle percentage			
Sand	%	—	97.3
Silt	%	50.3	0.8
Clay	%	49.7	1.9
Cone index q_c	MN/m ²	1.0	3.3

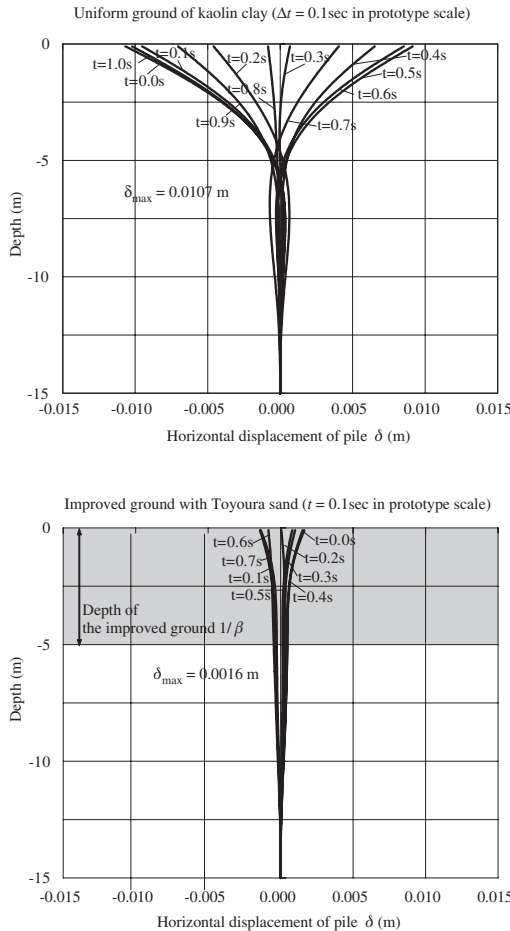


Figure 4. Distribution of horizontal displacement of pile during shaking.

or rigidity of the original and improved ground, the strength ratio expressed by the cone index q_c between kaolin clay and Toyoura sand, which represents the strength of the model grounds, was approximately set as 1:3 at 1 g field.

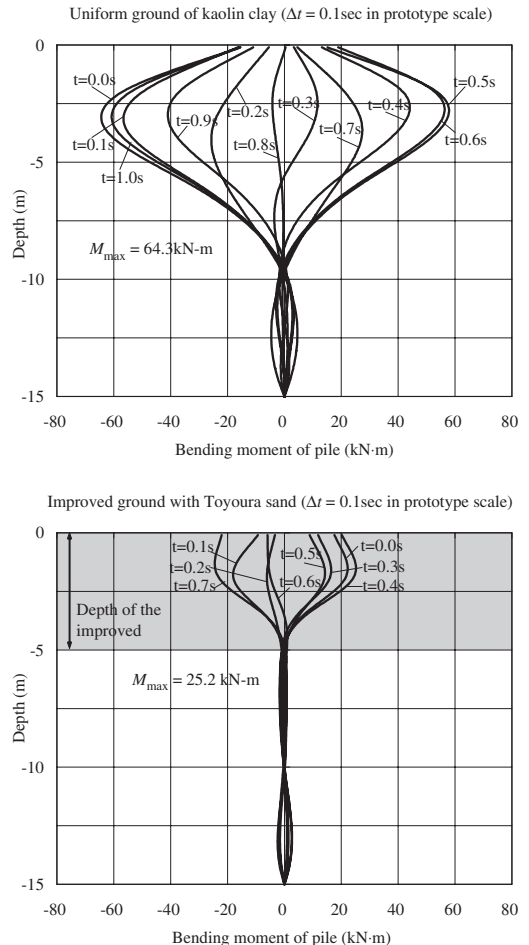


Figure 5. Distribution of bending moment of pile during shaking.

A sine-wave was used as input motion in the shaking tests. The acceleration level of the input motion in the model was set as 10 m/s^2 (equivalent to 20 gal at the prototype scale) to simulate the behavior of the pile and ground over a small range of deformation.

Figures 4 and 5 show the distributions of horizontal displacement and bending moment respectively along the axes of piles installed in the uniform ground of kaolin clay and improved ground using Toyoura sand at a time interval of $\Delta t = 0.1 \text{ sec}$. The data for these figures were obtained during shaking using the sine-waves with natural frequencies of piles as the input motions. The maximum displacement of the piles in the improved ground using Toyoura sand was only 1/6 of that of piles in uniform ground of kaolin clay (δ_{max} for the improved ground/ δ_{max} for the uniform ground $\approx 0.0016 \text{ m} / 0.0107 \text{ m}$). The maximum

bending moment occurred within the range of depth $1/\beta$ was 1/2.5 of that in uniform ground of kaolin clay (M_{max} for the improved ground/ M_{max} for the uniform ground $\approx 25.2 \text{ kN-m}/64.3 \text{ kN-m}$) and converged within the range of improved ground with Toyoura sand. This was considered to be due to the restriction on the pile head in improved ground and the decrease in displacement amplitude of the pile during shaking.

As a result, by using ground improvement around the pile head, a certain amount of earthquake resistance that restricts pile displacement and bending moment against earthquake motion was achieved, though careful attention should be paid to the shortening of the natural frequency of pile foundations in improved ground.

4 VERIFICATION OF THE PROPOSED DESIGN METHOD THROUGH *IN-SITU* HORIZONTAL PILE LOADING TESTS

This section presents a case study of *in-situ* horizontal loading tests on foundation piles of an abutment for the purpose of direct verification of the k value for the composite ground pile method. The site selected for the loading test was a cast-in-place pile foundation of a box-type abutment constructed in soft ground. In this site, the horizontal subgrade reaction of piles was small, and it was appropriate to use the deep mixing method for the composite ground pile method. The purpose of the *in-situ* horizontal loading test was to acquire common findings for the composite ground pile method, i.e., to verify the proposed design method.

The cast-in-place piles were 1.2 m in diameter and 17 m in length. In the area surrounding the cast-in-place piles of the abutment, the deep mixing method was adopted with a design unconfined compression strength of $q_{up} = 200 \text{ kN/m}^2$ and an improvement rate of $a_p = 78.5\%$ for the improved columns. The deep mixing method was applied in the same way as when it was employed for ensuring slip stability at the back of the abutment and as a countermeasure to prevent lateral spreading. The range of ground improvement was set as a three-dimensional cubic body around the piles to cover a space with the gradient of surface of passive failure $\theta = (45^\circ + \phi/2)$ from the depth $1/\beta = 3.65 \text{ m}$, i.e., the entire layer of soft ground subject to liquefaction. Figure 6 shows a general view of the bridge and the foundations.

The horizontal loading test was carried out using a multi-cycle load control system and was performed in accordance with the guideline for pile loading tests of the Japan Geotechnical Society (1983). A load cell, a hydraulic jack, and a loading tower were installed between the test and reaction piles, and a static load was applied in one direction until pile head displacement reached approximately 1% (0.012 m) of the pile

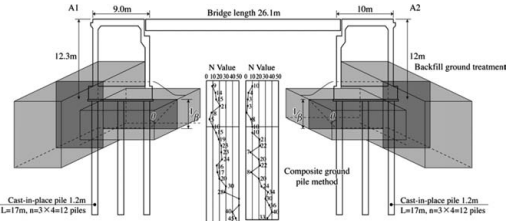


Figure 6. A bridge for which the composite ground pile method was adopted.

Table 2. Coefficients of horizontal subgrade reaction of piles.

	Coefficient of horizontal subgrade reaction (MN/m ³)	Ratio of coefficient of horizontal subgrade reaction to the design value
Design value for improved ground k	47.8	1.00
Original ground k_0	9.3	0.19
Value calculated from the unconfined compression strength k_U	107.0	2.24
Value estimated from the <i>in-situ</i> horizontal loading test k_H	100.0	2.09

diameter. To measure the bending stress of the test piles, reinforcing bar strain gauges were installed on two lines of the main reinforcing bars of the test piles at regular intervals along the depth.

Table 2 shows a comparison of the coefficients of horizontal subgrade reaction of piles, design value for composite ground piles k , the value for original ground k_0 , value calculated from the unconfined compression strength of improved columns k_U and the value measured in the horizontal loading test k_H together with the ratio to the design value of improved columns k . The value of the original ground k_0 was found to be $k_0 = 9.3 \text{ MN/m}^3$ from the modulus of deformation of the original ground E_0 where $N \approx 5$ or lower. The design value for composite ground piles k was calculated to be $k = 47.8 \text{ MN/m}^3$ by Equations. 1, 2 and 3 based on the design unconfined compression strength $q_{up} = 200 \text{ kN/m}^2$ and improvement rate $a_p = 78.5\%$ of improved columns. However, the average unconfined compression strength of the improved columns at the material age of 28 days after construction was $q_{up} = 408 \text{ kN/m}^2$ at the depth of $1/\beta$, and the

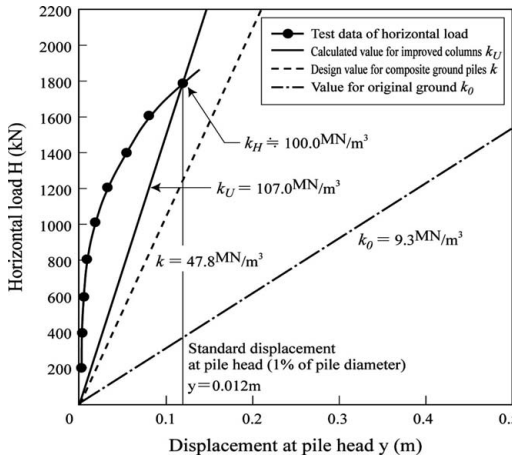


Figure 7. Relationship between horizontal load H and displacement at pile head y .

calculated value of k_U was 107.0 MN/m^3 , which was almost twice as high as the value of k . The value k_H was found to be around 100 MN/m^3 , from the secant gradient between the horizontal load H and the displacement of pile-head y , at which standard displacement of 1% of the pile diameter ($y = 0.012 \text{ m}$) was adopted. The displacement of pile-head y was determined according to Hayashi and Chang's method (Hayashi, 1921 and Chang, 1937) as:

$$y = [e^{\beta x}(C_1 \cos \beta x + C_2 \sin \beta x) + e^{-\beta x}(C_3 \cos \beta x + C_4 \sin \beta x)] / 2EI\beta^3 \quad (4)$$

where, C_1 , C_2 , C_3 and C_4 are integral constants and x is the depth of the pile (m).

Figure 7 shows (1) the relationship between the measured horizontal load H and pile head displacement y obtained from the *in-situ* horizontal loading tests of piles and (2) the relationship between H and y calculated by Equation 4. As a result, the value $k_H \approx 100 \text{ MN/m}^3$ measured in the horizontal loading test was equivalent to the standard displacement and coincided with the calculated value $k_U = 107.0 \text{ MN/m}^3$ from the proposed design method.

Therefore, it may be verified that the required horizontal subgrade reaction of the pile is generated from the shear strength of the ground in the range of passive earth pressure.

Figure 8 shows the pile bending stress calculated by the linear elastic subgrade reaction method compared with the pile bending stress measured from the *in-situ* horizontal loading test of piles at the horizontal load level of $H_{max} = 1800 \text{ kN}$. The bending stress calculated using k_U was close to the measured value, but was different from the value calculated from k_0 .

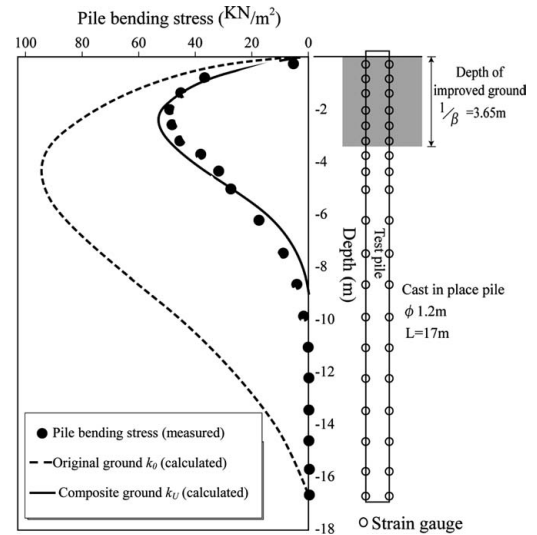


Figure 8. Distribution of pile bending stress obtained from the *in-situ* horizontal loading test together with the calculated values.

The validity of the proposed design method for the composite ground pile, i.e., setting the range of ground improvement as the shape of the gradient of the surface of passive failure $\theta = (45^\circ + \phi/2)$ from the depth of $1/\beta$, and calculating the horizontal subgrade reaction from the increased shear strength due to ground improvement, was also confirmed from the results of the *in-situ* horizontal pile loading test described above.

5 CONCLUSIONS

Through a series of experimental studies, a design procedure on the composite ground pile method was proposed. The possibility of design for the composite ground pile on the basis of the conventional design method of pile foundations was confirmed. Main findings drawn from this study are concluded as follows:

- The range of influence of the horizontal resistance of composite ground piles, or the necessary range of ground improvement, is a cubic body that covers the shape of the gradient of the surface of passive failure $\theta = (45^\circ + \phi/2)$ from the depth of the characteristic length of piles, $1/\beta$, based on engineering judgment.
- The coefficient of horizontal subgrade reaction k of composite ground piles is determined by converting the shear strength S of improved ground, which was increased by a variety of ground improvement methods, to the modulus of deformation E .

- A dynamic centrifuge model test for piles in composite ground revealed that earthquake resistance, such as the restriction of pile displacement and bending moment against earthquake motions, could be achieved by improving the ground around pile heads, and it was confirmed that there were no practical problems concerning the use of composite ground pile method.
- The validity of the design method was experimentally verified through an *in-situ* horizontal loading tests of piles for an actual bridge foundation.

REFERENCES

- Broms, B.B. 1964a. Lateral resistance of piles in cohesive soils. *Proc., ASCE*. Vol. 90, SM(3): 27–63.
- Broms, B.B. 1964b. Lateral resistance of piles in cohesionless soils. *Proc., ASCE*. Vol. 90, SM(3): 123–157.
- Chang, Y.L. 1937. Discussion on “lateral pile-loading tests” by L.B. Feagin. *Trans, ASCE*. Vol. 102: 272–278.
- Civil Engineering Research Institute of Hokkaido 2002. Manual for countermeasure against peat soft ground: 95–129 (in Japanese).
- Hayashi, K. 1921. Theorie des trägers auf elastischer unterlage und ihre anwendung auf den tiefbau. Springer Verlag.
- Japan Geotechnical Society 1983. Horizontal loading test method for pile foundations. *JGS standard* (in Japanese).
- Japan Road Association 2002. Specifications for highway bridges Vol. IV: Substructures (in Japanese).
- Public Works Research Center 1999. Deep mixing method for onshore construction -design and construction manual-: 48–148 (in Japanese).
- Reese, L.C., Cox, W.R. and Koop, F.D. 1974. Analysis of laterally loaded pile in sand. *Proc., Offshore Technology Conference*. Houston, TX, OTC2080.
- Terzaghi, K. 1943. Evaluation of coefficient of subgrade reaction. *Geotechnique*. Vol. 5, No. 4: 118–143.
- Tomisawa, K. and Nishikawa, J. 2005a. Pile design method in composite ground formed by deep mixing method. *Journal of Geotechnical Engineering*. Japan Society of Civil Engineers, No.799/III-72: 183–193 (in Japanese).
- Tomisawa, K. and Nishikawa, J. 2005b. A design method concerning horizontal resistance of piles constructed in improved ground. *Proc. of 16th International Conference on Soil Mechanics and Geotechnical Engineering*. September 12–16, 2h: 2187–2192.
- Vesic, A. 1961. Bending of beams resting on isotropic elastic solid. *Journal of Engineering Mechanics, ASCE*. 87(2): 35–53.

A study of reinforcing methods for existing bridges on soft ground with a solidification improvement

H. Fukada & K. Kato

Fudo Tetra Corporation, Tokyo, Japan

N. Segawa

Shiraishi Corporation, Tokyo, Japan

T. Ooya

Nittoc Construction Co., Ltd., Tokyo, Japan

Y. Shioi

Hachinohe Institute of Technology, Aomori, Japan

ABSTRACT: The foundations of many old bridges are insufficiently resistant to Level-2 earthquake motion. Therefore, we propose the anti-seismic reinforcement of existing foundations resting on soft ground. This construction method yields increased horizontal and vertical resistance by driving underground walls around the existing foundations and solidifying the ground inside. We performed static loading experiments in sandy ground with centrifugal modeling equipment at a scale of 1/50 under 50 G to examine the reinforcement effect quantitatively. Furthermore, a design model that tests a frame with the finite element method(FEM) was examined and simulations of the above experiment results were performed. The design model enabled us to simulate the load-displacement relationship with adequate accuracy.

1 INTRODUCTION

Disaster-prevention countermeasures for various kinds of civil structures are currently being reexamined, and development of an efficient anti-seismic reinforcing method for existing foundations is essential. However, these works have been undertaken only infrequently in the past along with other types of reinforcement due to the fact that foundation reinforcement work generally involves very significant construction costs and time requirements because of several factors such as the confined space under superstructures and because projects often tend to become large in scale.

Therefore, we propose an anti-seismic reinforcement method for existing foundations on soft ground that can reduce the costs and time necessary for completion of the foundations and that can be applied easily in a restricted space. This method can be expected to increase the resistance to damage from both horizontal and vertical motion by driving underground walls around the existing foundations and solidifying the ground inside as shown in Figure 1. By this process, we aim to have the improved area within the surrounding underground walls function as a foundation.

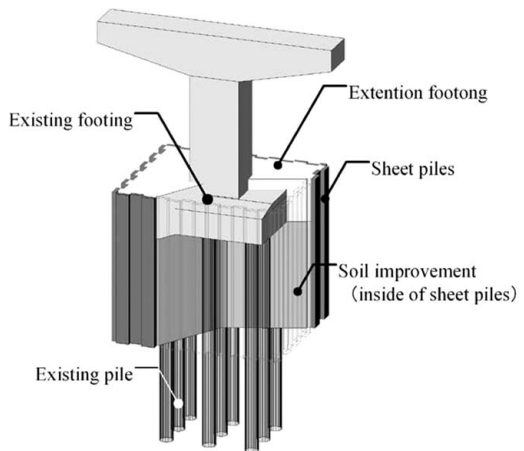


Figure 1. Outline of the proposed method.

Some researchers have carried out studies of newly constructed pile foundations surrounding solidified ground. Tomisawa and Nishikawa (2005) studied the increase in horizontal bearing capacity through

increasing the coefficient of the subgrade reaction of solidified ground. Maeda et al. (2001) proposed a composite soil-improved pile foundation. In this composite foundation, an increase in the horizontal bearing capacity is expected as a result of the cemented soil mass.

In the case of reinforcing the existing footing, several drilling holes created using the jet grout method are needed through the footing when the ground is entirely solidified inside the sheet pile. This means that the improved type that has partially solidified around the sheet pile is less affected by the rigidity of the footing concrete. However, as yet there have been few examined examples of partial improvements around foundations. Static loading experiments were thus performed to confirm the behavior of this reinforcing method.

This paper describes the results of static loading experiments in sandy ground determined through a centrifuge model equipment at a scale 1/50 under 50G. We also simulated these experiments using a design model that uses a frame with finite elements. Although some disagreement was expected, the design model enabled the simulation of the load-deformation relationship with sufficient accuracy.

2 OUTLINE OF THE PROPOSED METHOD

The mechanism of the reinforcement effect in this method is shown in Table 1. In this method, the increase of horizontal and vertical resistance by driving steel sheet piles to a given depth surrounding the existing foundation restrain the displacement and the rotation of the foundation.

A basic type of solidification is to improve entirely inside the sheet pile surrounding the existing footing. Considering the number of drilling holes, the method of solidifying the circumference region of existing footing can be considered realistic. In this case, it is thought that reinforcement effects differ according to the degree that the solidified soil restricts the piles. The types of solidification are shown in Figure 2. The partial solidification types are classified roughly into two types. The first is a circumference solidification type when there is no restriction of piles by the solidified soil and the other is a pile restriction type when

Table 1. Mechanism of resistance.

Mechanism of reinforcement	
Horizontal resistance	Originated in improved soil and sheet piles
Vertical resistance	Originated in friction of sheet piles
Rigid increase in base body	Originated in friction of between improved soil and piles

there is restriction of most circumference piles by the solidified soil. This reinforcing method can thus be characterized by the need to choose one particular type of improvement.

The features of this method are as follows.

- (1) The construction area can be reduced because the outer sheet piles can be used as earth retaining walls.
- (2) The size of the structure is small, so interference with traffic, etc., is minimal.
- (3) It is possible to implement the method within the limitations of a small workspace with small construction machines (sheet pile pressing machine, boring machine, etc.).

Here, this improvement method can be applied with the jet grout method using a threefold tube, with little influence on the existing structure.

3 STATIC LOADING TEST IN SANDY GROUND, CENTRIFUGAL MODEL

3.1 Abstract of experiment

The static loading experiments in sandy ground using the centrifugal equipment were performed to confirm the effects of reinforcement quantitatively. The structural model was based on a design example from "Reference Data on Reinforcement of Existing Highway Bridge Foundations, Japan Highway Association (2000)."

The pier model is shown in Figure 3. The pier and footing are modeled at the reduced scale of 1/50. This experimental setup is shown in Figure 4. The centrifugal acceleration is 50G and the size of the steel container is 600 mm in length × 500 mm in width × 530 mm in height.

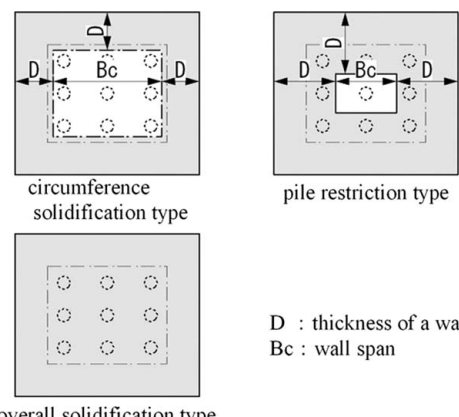


Figure 2. The types of solidification.

The horizontal displacement was transferred from the electric screw jack to the model of the existing footing with the reinforcement footing set up in the container. The displacement speed was kept below 0.3 mm/min and maximum horizontal displacement was 10 mm (in terms of the real structure, 500 mm). The distance from the loading point to the bottom of the footing is 80 mm (in terms of the real structure, 4.0 m).

The experiment cases are shown in Table 2. Case 1 is a model of the existing structure and Case 2 is a model of the circumference solidification type. Case 3 is a model of the pile restriction type. In the circumference solidification type, a thickness D of an improvement body is set to 1/2 of wall span B_c . In the pile restriction type, the distance with the existing pile center

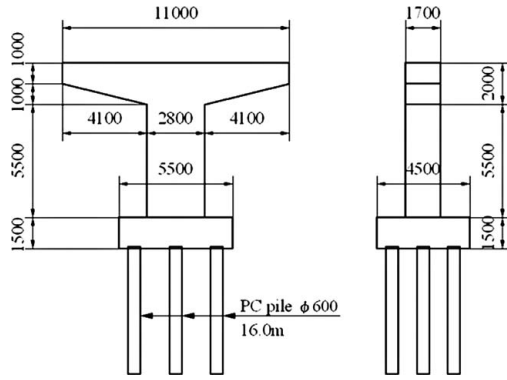
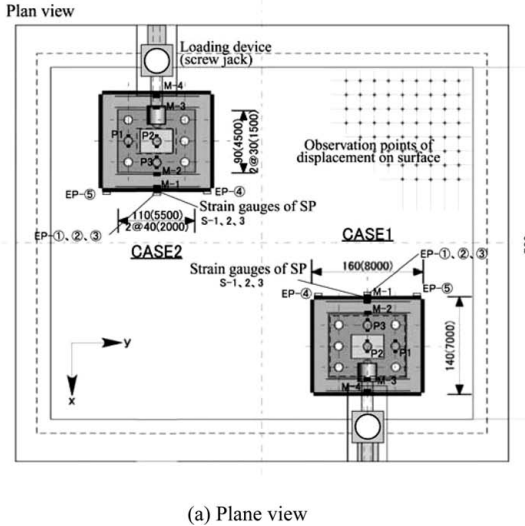


Figure 3. The pier model.



(a) Plane view

and the inner edge of the improvement body are set to the pile diameter, and a thickness D of the improvement body is set to more than 1/2 of wall span B_c .

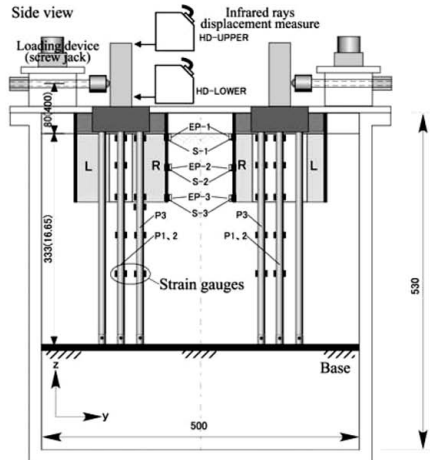
The model ground is the mixture of sand that has been shown in Table 3 for reproducibility in the experiment. The setup of the model structure is shown in Table 4. The measured variables were the horizontal load, the horizontal displacement at the loading point and footing, the axial and bending strain of piles, and the soil pressure at the top and bottom of the reinforced compartment. An observation mesh and reference point were set up at ground level, and measurement of the ground movement under load was made by measuring the reference point coordinates before and after loading through the gravitational field (1 G).

Table 2. The experimental cases.

Case 1	Model of the existing structure
Case 2	Model of the circumference solidification type
Case 3	Model of the pile restriction type

Table 3. The model ground.

Material	Toyoura sand 80%
Compaction factor	Caoline clay 20%
Relative density	$w_{opt} = 11.7\%$
	$\rho_{dmax} = 1.880 \text{ g/cm}^3$
	$D_r = 90\%$



(b) Side view

Figure 4. The experimental setup.

Table 4. The setup of the model structure.

	Experiment model	Real structure
Soil layer	Thickness 333 mm	16.65 m
Sheet pile	Thickness 4 mm Length 140 mm Depth 110 mm	Type IV, Coefficient of splice $\alpha = 0.8$ 7.0 m 5.5 m
Pile	Aluminium, diameter 12 mm	PC pile, diameter 600 mm
Improved area	Unconfined compressive strength q_u Addition rate of cement Thickness 110 mm	3000 kN/m ² 250 kg/m ³ 5.5 m
Footing	Width 160 mm, Thickness 140 mm	Width 8.0 m, Thickness 7.0 m

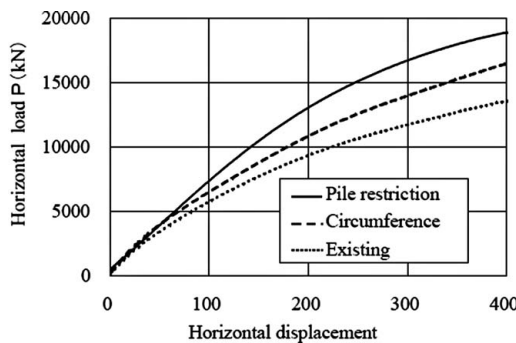


Figure 5. The relationship between load and displacement.

3.2 Results of the experiment

The relationship between the horizontal load and the horizontal displacement at the loading point of all cases are shown in Figure 5. At a displacement of 0.3 m (in terms of the real structure), the horizontal load of Case 2 is about 1.2 times compared with that of Case 1. The horizontal load of Case 3 is about 1.4 times compared with that of Case 1. In this result, a reinforcement effect for the existing structure of both the circumference solidification type and pile restriction type was confirmed. In this experiment, the bending strain of the piles was measured by the double gauge method. Figure 6 shows the measured points at P1, P2 and P3 piles. Here, P1 and P3 are arranged in the solidification improvement body in the pile restriction type. P2 is arranged in the inner ground of the improvement body in both the circumference solidification type and pile restriction type. Figure 7 shows the bending moment distribution of each pile at

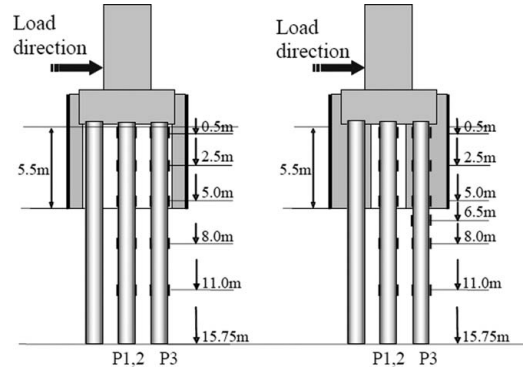


Figure 6. The measured points at P1, P2, P3.

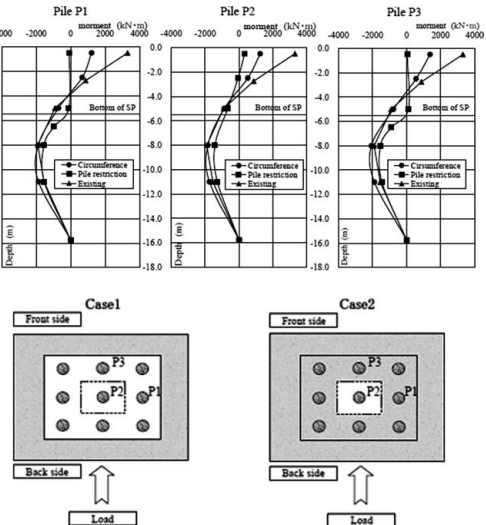


Figure 7. The bending moment distribution of piles.

load $P = 12,000$ kN. It is confirmed that the maximum bending moment of each pile in Case 2 is reduced compared with that of Case 1. The bending moment of pile P1 and P3 with solidification improvement in Case 3 is almost zero due to restraint by the solidification. The bending moment distribution of pile P2 without restraint by the solidification in Case 2 appears to be similar to that of pile P2 in Case 2.

4 OUTLINE OF THE ANALYTICAL MODEL

In the centrifuge model experiment, the reduction of the bending moment of piles and the increment of bearing

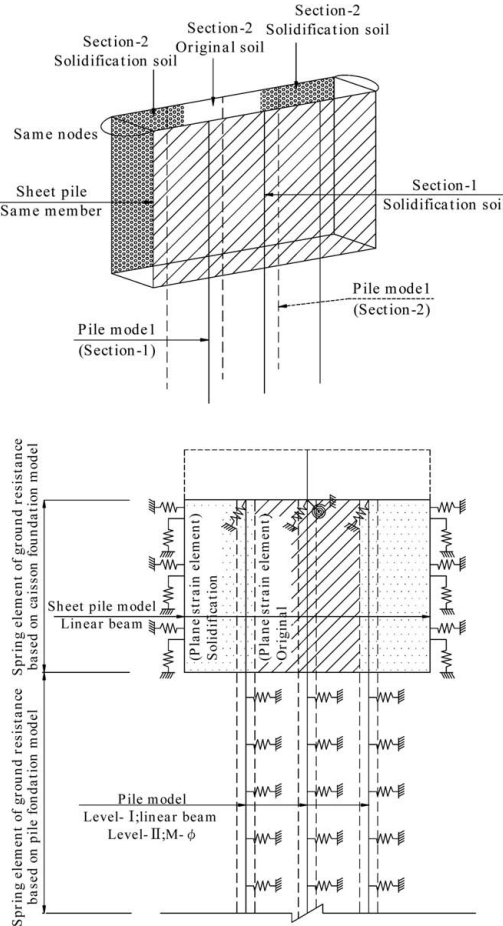


Figure 8. Outline of analytical model.

capacity are confirmed by the displacement restraint. Next, the analytical design model is built to evaluate reinforcement effects. The analytical model is a two-dimensional spring frame model added to the finite elements to express the reinforcement department. The outline of this model is shown in Figure 8. The degree of pile restraint as a result of the solidification improvement body is adequately evaluated to express the behavior of the pile. Therefore, two kinds of finite elements are added to the spring frame. One is the department of solidification improvement body and the other is the composite department of solidification body and ground. The rigidity of the improved area is evaluated considering the thickness of each of these departments.

In this model, the footing is modeled with the rigid body, and the sheet piles surrounding the footing are modeled with the linear beam member. Existing piles are modeled with the linear or non-linear beam member. The solidified improvement body is modeled with a

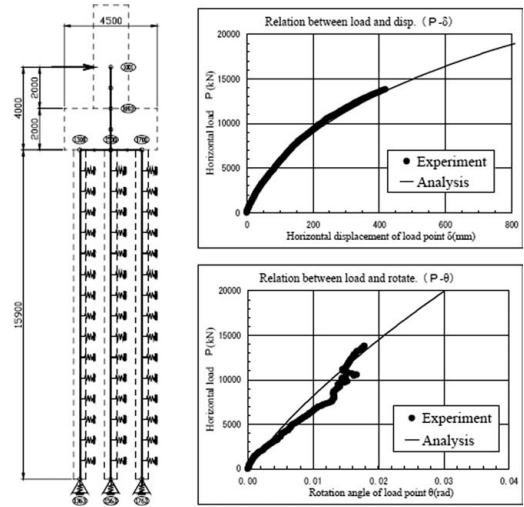


Figure 9. Load-displacement relationship and load-rotation angle relationship in existing foundation models.

plane strain finite element, and the node of each element is jointed with a node of the piles and the sheet piles.

The ground is expressed as a bilinear spring model in consideration of the non-linearity of soil. The rotation spring model is set to the lower part of existing footing in consideration of the vertical resistance of the side part of the reinforcement department.

5 EXAMINATION OF THE ANALYTICAL MODEL

5.1 Identification of conditions in existing foundation models

First, analysis conditions such as the experimental environment and ground conditions are set to reproduce the behavior of the centrifuge experiment in the existing footing. The existing foundation is based on design techniques of pile foundations that use a two-dimensional spring frame model.

In this analysis, a model pile is made using aluminum and is assumed for the elasticity model considering the axial direction rigidity that can reproduce the rotation behavior of the foundation. The angle of rotation of the footing, provided through an experiment, is used for adjustment of the boundary condition. Figure 9 shows both the load-displacement relationship and load-rotation angle relationship. The analytical result is almost the same as the result of the experiment.

5.2 Examination result for reinforcement models

Figure 10 shows the relationship between load and horizontal displacement of both the experiment result

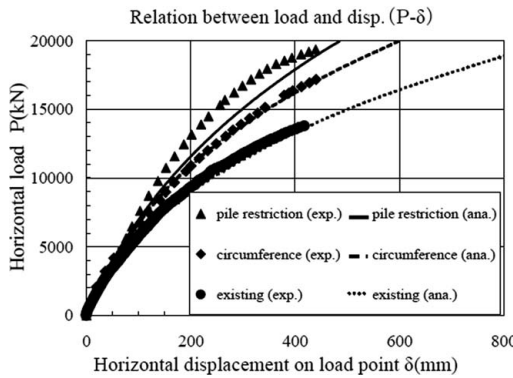


Figure 10. Load-displacement relationship in all cases.

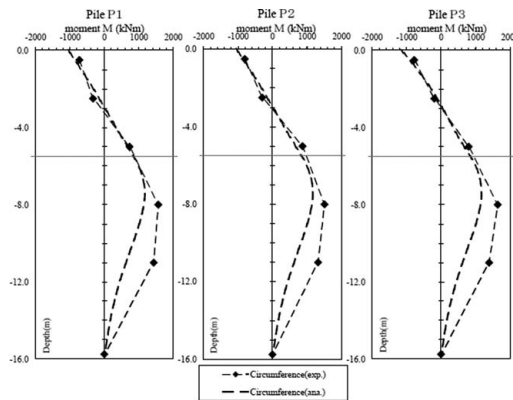


Figure 11. The bending moment distribution at Case 2.

and analysis result. In this figure, it is confirmed that the analysis result can reproduce the experiment result safely and express the reduction of horizontal displacement by reinforcement.

Figure 11 shows the bending moment distribution at load $P = 10,000$ kN in Case 2 (the circumference solidification type). In this case, as the piles are not restricted by an improvement body, the bending moment distribution is similar to that of Case 1 (existing foundations), but reduction of the bending moment at the pile head is expressed in the analytical result. Figure 12 shows the bending moment distribution at load $P = 10,000$ kN in Case 3 (the pile restriction type). In this case, it is confirmed that the analysis result almost reproduces the experiment result.

6 CONCLUSION

A reinforcement method by driving underground walls around the existing foundation and solidifying

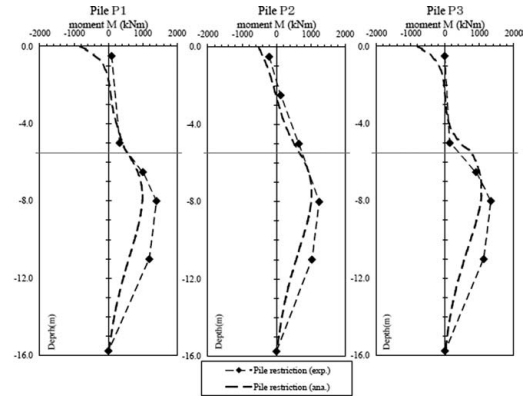


Figure 12. The bending moment distribution at Case 3.

the ground inside is proposed. Experiments and analyses were carried out to quantitatively evaluate the effect of reinforcement by the proposed method. The main conclusions are:

1. It is confirmed that the horizontal displacement can be reduced and bearing capacity can be increased in both the circumference solidification type and pile restriction type in the centrifuge model experiment.
2. It is confirmed that the maximum bending moment of the pile of the pile restriction type is small compared with that of the circumference solidification type.
3. The proposed analytical model is confirmed to reproduce the effect of this reinforcement method quantitatively.

ACKNOWLEDGEMENTS

The centrifugal experiment was conducted at the Research and Development Center of Nippon Koei Ltd. We wish to thank Dr. Lee, who provided significant guidance and advice in the planning and execution of this study.

REFERENCES

- Tomisawa, K. & Nishikawa, J. 2005. Pile design method in composite ground formed by deep mixing method, *Journal of J.S.C.E.* No.799/III-72: 183–193. (in Japanese)
- Maeda, Y., Ogata, T., Xu, G. L., & Hirai, T. 2001. A new composite foundation of steel piles with soil improved. *Journal of J.S.C.E.* No.686/VI-52: 91–107. (in Japanese)
- Japan Highway Association. 2000. *Reference Data on Reinforcement of Existing Highway Bridge Foundations*.
- Japan Highway Association. 2002. Chapter 12, Pile Foundation. *Design Codes for Japan Highway Bridges*. Vol. IV. Substructure.

Development of sheet-pile foundation combining footing with sheet-piles

H. Nishioka & M. Koda

Structure Technology Division, Railway Technical Research Institute, Kokubunji, Japan

J. Hirao & S. Higuchi

Obayashi Corporation, Tokyo, Japan

ABSTRACT: The authors have proposed a sheet-pile foundation as a new reasonable foundation structure. This foundation can be constructed at a lower cost than the pile foundation, and be used more widely than the shallow foundation. In this research, in order to evaluate the fundamental characteristics of the sheet-pile foundation, a series of static loading tests in laboratory and full-scale field tests were carried out. It was shown that the vertical bearing capacity and the horizontal resistance of the sheet-pile foundation were larger than those of the shallow foundation and the sheet-pile foundation was excellent in the performance against seismic force. Further, the field tests revealed that the sheet-pile foundation did not need the special construction workmanship and could reduce the construction cost of the foundation structure.

1 INTRODUCTION

Recently, construction work is increasing in densely populated urban areas in Japan. For example, in order to ease traffic congestion, railroads running through urban areas are re-laid on elevated bridges, which are constructed close to existing structures. Usually, the space allowable for construction work in urban areas is often very small. Further, in such construction work in urban areas, it is required to cut down costs and reduce noise and vibration. The disposal of surplus soil generated from construction work must be also taken into consideration.

To alleviate the above problems, “Sheet-pile Foundation” which combines the footing and sheet-piles has been proposed as a new foundation form (Koda et al. 2003, Nishioka et al. 2004). Since the sheet-pile foundation reinforces the ground with sheet-piles, the bearing capacity and horizontal seismic resistance are higher than those of the shallow foundation. Since the applicability is wider than that of the shallow foundation, it can be used, for example, on the loose sandy ground to which the pile foundation has been applied until now. The construction cost is almost the same as that of the shallow foundation and more inexpensive than that of the pile foundation. On the other hand, since pile excavation is not necessary, it can avoid various problems of pile foundation, for

example, the noise, the vibration and the disposal of surplus soil. Figure 1 shows an outline of the sheet-pile foundation compared with the shallow foundation and the pile foundation.

In this research, a series of static loading tests in laboratory and full-scale field tests were carried out for the purpose to evaluate the performance of the sheet-pile foundation.

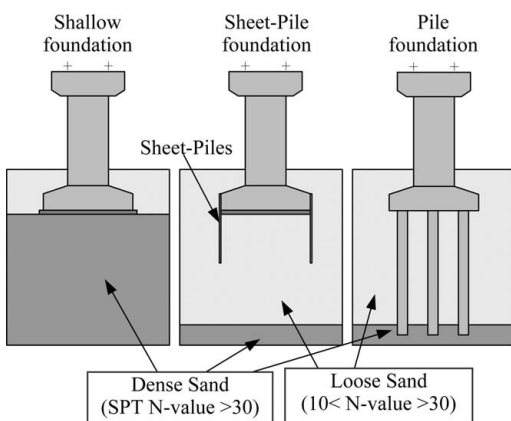


Figure 1. Outline of sheet-pile foundation.

2 MODEL TESTS IN LABORATORY

2.1 Outline of modeled ground and foundations

A modeled ground was made from dry Toyoura sand in a sand container. It was a two-dimensional model in plane strain condition. The sand container's planes of the front and backside were made of transparent acrylic plates to allow observation of the de-formation of the ground. In order to reduce friction between the acrylic plate and sand, rubber membranes were pasted on acrylic plate with grease. Moreover, target points were marked on the rubber membrane, and their displacements were measured from photographs taken with a digital camera through the acrylic plate by an Image Processing System (Watanabe & Tateyama, 2003). Table 1 summarizes the conditions of the modeled ground. The relative density D_r of the modeled ground was controlled by the height of the sand hopper to 90% or 60%.

The modeled footing was made of aluminum block of 100 mm in width B , and placed on the modeled ground's surface. Modeled sheet-pile was made of phosphor bronze plates of 0.2 mm in thickness, and they were pressed to concavo-convex form shown in Figure 2. The length L that was penetrating into the sand was 100 mm ($L/B = 1.0$) or 50 mm ($L/B = 0.5$). The value of βL shown in Equation 1 of modeled sheet-piles was the same grade as that of prototype.

$$\beta L = \sqrt[4]{k_h D / 4EI} \cdot L \quad (1)$$

where β : Characteristic value of pile (1/m), k_h : Coefficient of horizontal subgrade reaction (kN/m³),

Table 1. Conditions of modeled ground.

Ground size (W × H × D)	2000 mm × 580 mm × 600 mm
Material of ground	Dry Toyoura sand
Dry unit weight γ_d	$\gamma_d = 16.2 \text{ kN/m}^3$ ($D_r = 90\%$) $\gamma_d = 15.1 \text{ kN/m}^3$ ($D_r = 60\%$)
Lubricated layer	Rubber membrane ($t = 0.2 \text{ mm}$) with Grease (10 μm)

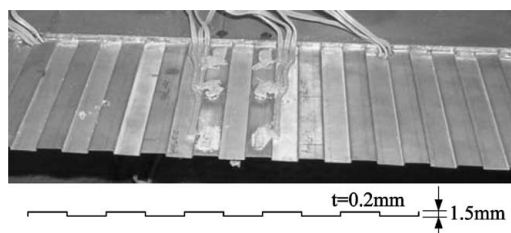


Figure 2. Picture of modeled sheet-pile.

D : Width of sheet-piles (m), EI : Flexural rigidity of sheet-pile (kNm²), L : length of sheet-pile (m). Table 2 summarizes specifications of modeled sheet-piles. In addition, the sheet-pile model was put into the model ground.

2.2 Vertical loading tests

The purpose of vertical loading tests was to check the ground conditions and the improvement effect of the bearing capacity of the sheet-pile foundation. Tests were carried out for three cases shown in Table 3, two cases were for shallow foundation without sheet-piles and the other case was for sheet-pile foundation.

An outline of vertical loading equipment is shown in Figure 3. A screw jack, which can apply the vertical load on the model foundation, was jointed to the center on the upper surface of the footing with a pin so that the moment could be removed. The vertical displacement of the screw jack was increased monotonically at a constant rate of 1 mm/min.

Table 2. Specifications of modeled sheet-piles.

	Prototype TYPE IV	Modeled sheet-pile
Thickness	15.5 mm	0.2 mm
Height of concavo-convex form	340 mm	1.5 mm
Width of Footing B	4.8 m	100 mm
Width of sheet-piles D	4.8 m	596 mm
Young's modulus E	200 kN/mm ² (Steel)	110 kN/mm ² (Phosphor bronze)
Geometrical moment of inertia I	$1.28 \times 10^{-3} \text{ m}^4$	42.9 mm^4
Coefficient of horizontal subgrade reaction k_h	$78,600 \text{ kN/m}^3$ (Sand N = 30)	$45,700 \text{ kN/m}^3$ ($D_r = 90\%$)
Length L	4.8 m ($L/B = 1.0$) 2.4 m ($L/B = 0.5$)	100 mm ($L/B = 1.0$) 50 mm ($L/B = 0.5$)
βL	3.74 ($L/B = 1.0$)	3.42 ($L/B = 1.0$)

Table 3. Cases of vertical loading tests.

Case	Density of ground	Foundation Form
VD1	$D_r = 90\%$ (Dense)	Shallow foundation
VL1	$D_r = 60\%$ (Loose)	Shallow foundation
VL2		Sheet-pile foundation $L/B = 1.0$

The relation between vertical load and displacement for all the cases is shown in Figure 4. In Figure 4, the displacement was set to zero, when the footing bottom contacts the sands. Therefore, in the case of sheet-pile foundation (case-VL2), the load corresponded to the bearing capacity of only sheet-piles, when the displacement was zero.

First, the relation between the density of ground and the bearing capacity of the shallow foundation was examined. Although it was natural, it was clear that the bearing capacity of the $D_r = 90\%$ case (case-VD1) was about three times higher than that of the $D_r = 60\%$ case (case-VL1). Moreover, the rigidity at early stages of the $D_r = 90\%$ case was larger than that of the $D_r = 60\%$ case. Further, in the $D_r = 90\%$ case (case-VD1), the load reached to the peak at 7 mm, and decreased afterwards greatly by 33% of the peak bearing capacity. On the other hand, in the $D_r = 60\%$

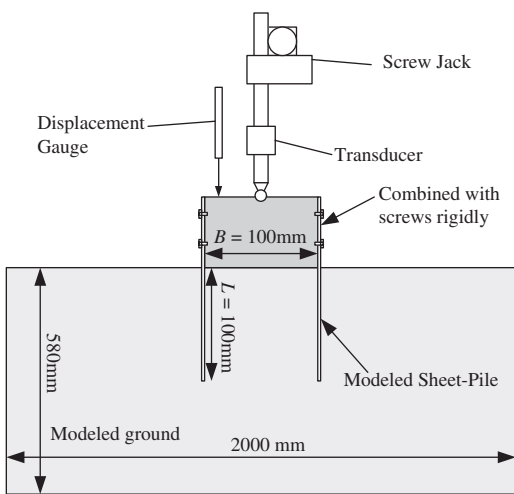


Figure 3. Equipment for vertical loading tests.

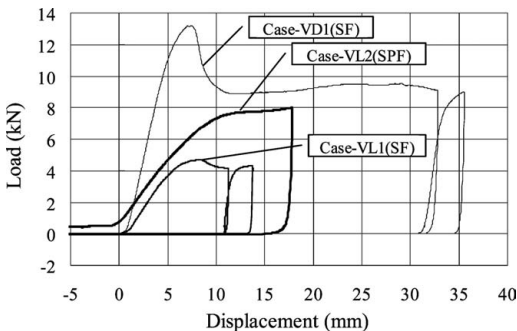


Figure 4. Relationship between vertical load and displacement.

case (case-VL1), the load decreased only no more than 10% of the peak value after it reached to the peak. It turned out that the $D_r = 90\%$ case corresponded to typical dense sands and the $D_r = 60\%$ case to loose sands.

Next, the effect of the improvement of the sheet-pile foundation on loose sand (case-VL2) was examined. Although the rigidity of the sheet-pile foundation was almost identical to the shallow foundation on the same ground density (case-VD1), the bearing capacity increased near to the residual bearing capacity of the shallow foundation on denser ground (case-VD1), and the load didn't decrease for larger displacement. Further, the residual plastic deformation of the sheet-pile model was negligible after the test.

Figure 5 shows the displacement measured by the Image Processing System. The line in the figure is the locus of each target point until the vertical displacement of the footing model reaches 10 mm.

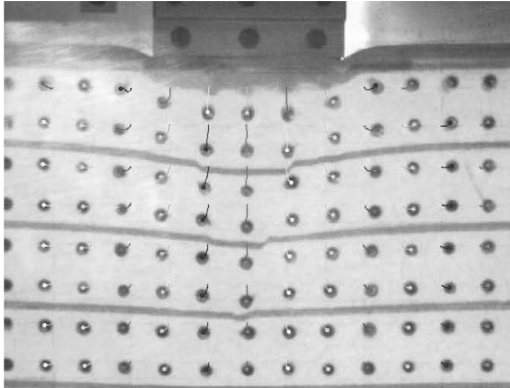
In all cases, the target points of the ground in a certain domain under the footing model were moved in the vertical downward direction, and the target points of the ground of outside that domain were moved in the horizontal outward direction. However, the sizes of that domain differed in different cases, and in the case of the sheet-pile foundation, that domain spread to a deeper area. This means that sheet-piles restricted the horizontal dilation toward the outside of the ground under the footing. Therefore, as a result of image processing, it became clear that the increase of the bearing capacity of sheet-pile foundation was due to its reinforcement effect of the ground.

2.3 Horizontal static reciprocal loading tests

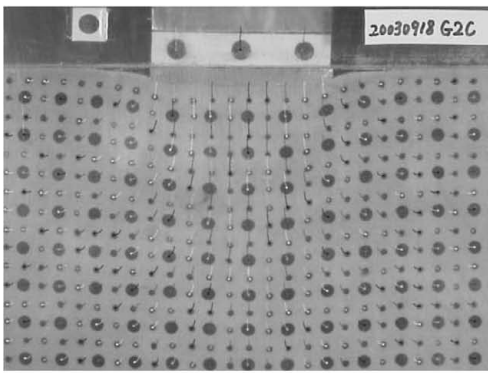
In the foundation structure design in Japan, the evaluation of resistance to earthquakes is very important. Then, in order to simulate the inertia force of the earthquake, the horizontal loading tests were conducted. The inertia force of the earthquake was modeled to the horizontal loads at the position corresponding to the bridge pier top.

An outline of the tests is shown in Figure 6. The horizontal displacement was applied with a screw jack statically and reciprocally at a height of 230 mm from the footing model bottom that was corresponding to the bridge pier top. The vertical load was kept at 1.2 kN by an air cylinder, which was about 10% of the bearing capacity of the shallow foundation on $D_r = 90\%$ (Case-VD1).

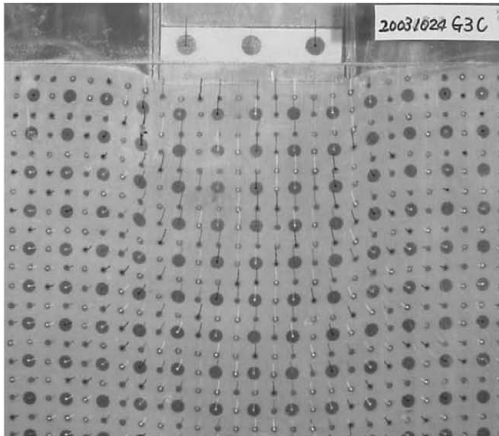
The relations between the horizontal load P and the horizontal displacement δ at the top of pier are shown in Figure 7 and Figure 8. Figure 7 shows historical curves, and Figure 8 shows skeleton curves, which connect the turning points on each reciprocal cycle. The sheet-pile foundation (Case-HL2, HL3) has higher horizontal resistance than that of shallow foundations



(a) Case-VD1: The shallow foundation on $D_r=90\%$



(b) Case-VL1: The shallow foundation on $D_r=60\%$



(c) Case-VL2: The sheet-pile foundation ($L/B=1.0$) on $D_r=60\%$

Figure 5. Displacement computed by an Image Processing System when vertical displacement is 10 mm.

(Case-HD1, HL1). Additionally, since the loop of the historical curve of the sheet-pile foundation was larger than that of the shallow foundation, it was clear that the historical damping of the sheet-pile foundation

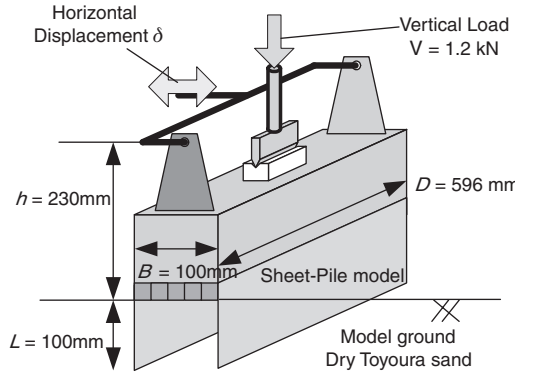


Figure 6. Outline of horizontal reciprocal loading test.

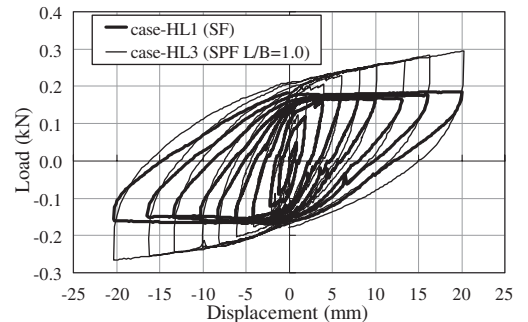


Figure 7. Historical curves of P - δ relationship.

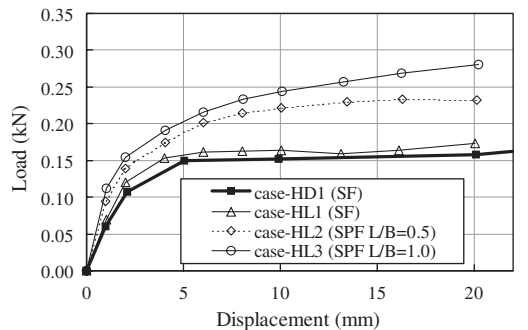


Figure 8. Skeleton curves of P - δ relationship.

was larger than shallow foundations. Moreover, the residual plasticity deformation of the sheet-pile model was unobservable after the experiment, the same as the vertical loading tests.

Table 4. Cases of horizontal loading tests.

Case	Density of ground	Foundation Form
HD1	$D_r = 90\%$ (Dense)	Shallow foundation
HL1	$D_r = 60\%$ (Loose)	Shallow foundation
HL2		Sheet-pile foundation $L/B = 0.5$
HL3		Sheet-pile foundation $L/B = 1.0$

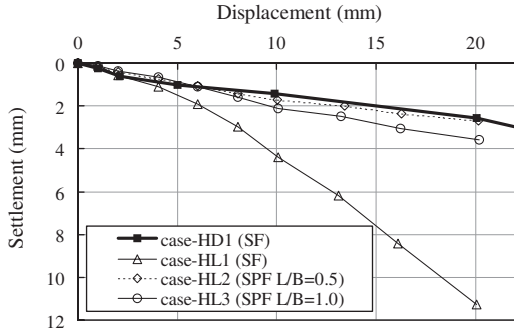
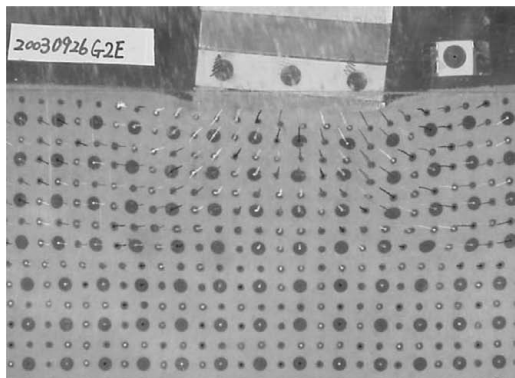


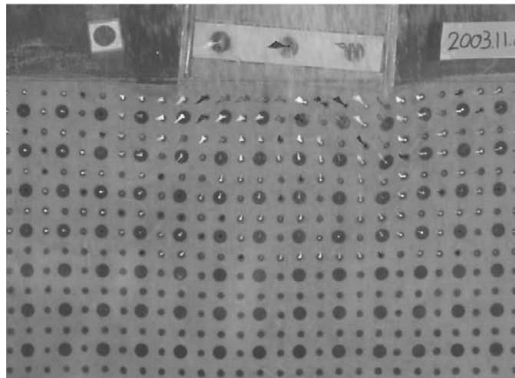
Figure 9. Skeleton curves of settlements.

The settlement characteristic is the important function of the railway structure. Figure 9 shows settlements of footing when the horizontal displacement reached to the peak in each reciprocal cycle. Settlement was increasing as the increase of horizontal displacement in all cases. Although, the shallow foundation on $D_r = 60\%$ (Case-HL1) had large settlement more than 10% of width of footing, the sheet-pile foundation on $D_r = 60\%$ (Case-HL2, HL3) had only small settlement of the same level as that of shallow foundation on $D_r = 90\%$ (Case-HD1). It was clear that the sheet-pile foundation restrained the settlement.

Figure 10 shows the displacement of two cases (Case-HL1 and HL2), computed by an Image Processing System. The line in the figure shows the locus of each target point until the horizontal displacement at the top of pier reaches 20 mm. The displacement of the ground was observed in a large area around the modeled footing. However, the measurement and direction of displacement differed from each other on the shallow foundation (Case-HL1) and the sheet-pile foundation (Case-HL2). In the case of shallow foundation, the ground had failure like a circular slip in the comparatively limited domain shallower than 50 mm on both sides. The displacement of the ground around the edges of the footing model turned in the outward horizontal direction. On the other hand, about the sheet-pile foundation, sheet-piles restrained the horizontal deformation of the ground. Since deeper areas of the ground were deformed, as a whole, local failure of the ground had not occurred.



(a) Case-HL1: Shallow foundation on $D_r = 60\%$



(b) Case-HL2: Sheet-pile foundation ($L/B = 1.0$) on $D_r = 60\%$

Figure 10. Displacement computed by an Image Processing System when horizontal displacement reaches 20 mm.

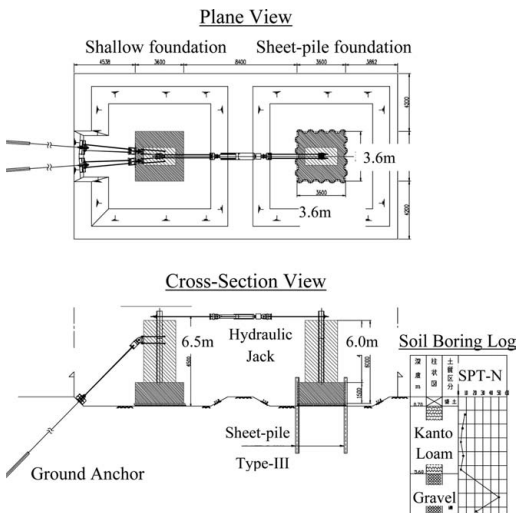


Figure 11. Outline of full-scale models.

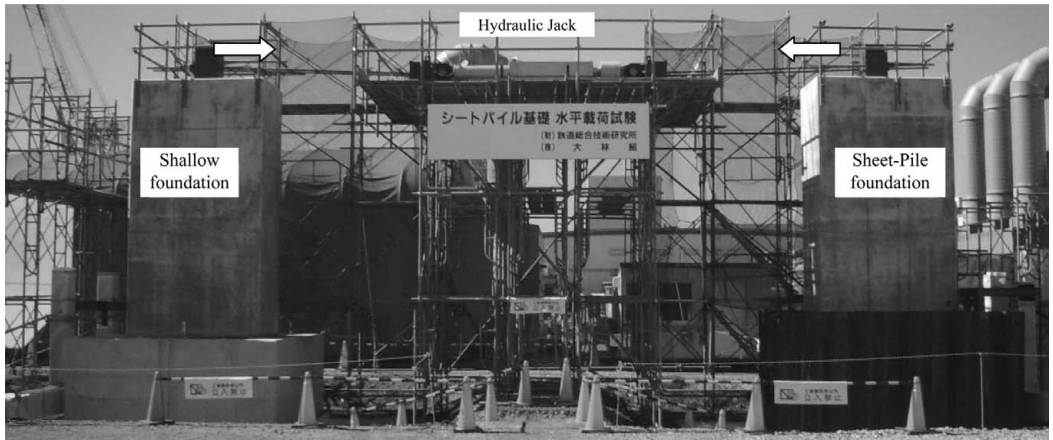


Figure 12. Picture of full-scale models.

3 FULL-SCALE FIELD TEST

3.1 Outline of full-scale models

Aiming at practical use, the full-scale field tests were conducted in Kawagoe-City, Japan.

The soil profile at the experiment site is shown in Figure 11. The surface diluvial clay (Kanto loam) with a thickness of 5 m is laid on the gravel layer. Each model of shallow foundation and sheet-pile foundation shown in Figure 11 and Figure 12 was constructed there. These footings were 3.6 m in width, and these piers were 6 m in height. The sheet-pile's length is 3.6 m, the same as the width of footing, therefore the tip didn't reach to the gravel.

3.2 Construction experiment

In practical use of sheet-pile foundation, the method to connect sheet-piles with footing concrete rigidly is very important. There is a simple method in which the reinforced bars are welded to sheet-piles, unifying sheet-piles with footing concrete. But this method has the disadvantage that the arrangement of reinforced bar of footing might be very difficult in case the working space is very narrow.

Therefore, the construction experiment by this method was conducted to confirm the possibility of arrangement of bar of footing. Figure 13 shows the photo of the work to weld reinforced bars to sheet-pile, and that of the finish state of arrangement of bar of footing. It was confirmed that this method was possible by this construction experiment.

3.3 Horizontal static loading test

The horizontal static loading test was conducted by pulling the tops of two models to each other by a



a) The work to weld reinforced bars to sheet-pile.



b) The finish state of arrangement of bar of footing.

Figure 13. Pictures of the construction experiment.

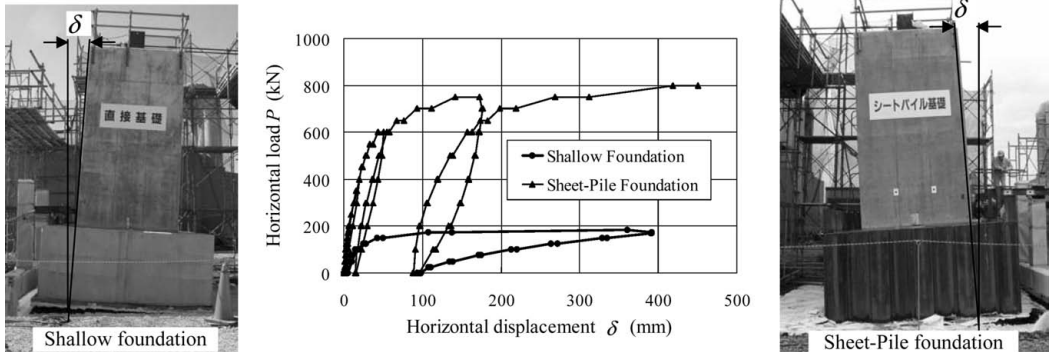


Figure 14. P - δ relationship and pictures of the models after loading.

hydraulic jack. At first, the shallow foundation was pulled by the sheet-pile foundation. Next the sheet-pile foundation was pulled by the shallow foundation rein-forced by ground anchor as shown in Figure 13.

The P - δ relation of each case is shown in Figure 14. Figure 14 shows the photo of the last deformation of each model. Figure 14 shows that the ratio of the horizontal resistance of the sheet-pile foundation against that of the shallow foundation was about four. This ratio was larger than that obtained by the laboratory test.

4 CONCLUSION

The following knowledge has been made in this research.

1. The vertical bearing capacity of the sheet-pile foundation is larger than that of the shallow foundation.
2. The horizontal resistance and settlement against earthquake of sheet-pile foundation are better than those of the shallow foundation.
3. The sheet-pile foundation does not need the special construction workmanship.

Based on the above, it was shown that the performance of the sheet-pile foundation was excellent against seismic force and could reduce the construction cost of the foundation structure. At present, a design method has been established, and some railway bridges with sheet-pile foundation have already been constructed actually in Japan. The sheet-pile foundation will be used more widely in the future.

REFERENCES

- Koda, M., Murata, O., Nishioka, H., Punrattanasin, P. & Kusakabe, O. 2003. The Proposal of Sheet-Pile Foundation Combining a Footing with Sheet-Piles. *TSUCHI-TO-KISO JGS* 51(11): 8–10. Tokyo: JGS. (in Japanese)
- Nishioka, H., Koda, M. & Murata, O. 2004. A Series of Static Loading Tests of Modeled Sheet-Pile Foundation Combining Footing with Sheet-Piles on Sand. *Proceeding of 15th Southeast Asian Geotechnical Society Conference*: 199–204. Bangkok.
- Watanabe, K. & Tateyama, M. 2003. Shaking Table tests on Seismic Behavior of Retaining Walls Using Image Processing System (in Japanese). *RTRI REPORT* 17(3): 19–24. Tokyo: Railway Technical Research Institute.

Recent technology development of steel pipe sheet pile foundation in Japan

Takeshi Katayama

Nippon Steel Corporation, Tokyo, Japan

ABSTRACT: This type of foundation was originally developed for large blast furnace foundation of Japanese steel maker. And then we were trying to apply this foundation for bridge pier with corporation of Ministry of Construction (Now, Ministry of Land, Infrastructure and Transport). Right now, we have had more than 2000 pier foundations in Japan. We use pipe-pipe type interlocking joints. This steel pipe wells are installed with circular, rectangular or oval shape. We can apply this foundation for large depth of water and soft ground. We could reduce the construction time and cost because we don't need temporary cofferdam. In this paper, I would like to show the development history of this foundation in Japan and recent development how to apply the large foundation with cost efficiency. So I would like to focus the type of inter-locking. Considering structural features of steel sheet pipe pile foundation, we needed to enlarge the shear capability of interlocking. After parametric study such as diameter, thickness and surface type of interlocking pipe and strength of mortar, we could reach the final specification. Final specification is pipe-pipe interlocking using 165.2 mm diameter and 11 mm thickness with projection. Case study using this new type of interlocking will be introduced compared to usual type. And real project using new type of inter-locking will be introduced.

1 INTRODUCTION

The text should fit exactly into the type area of 187 × In Steel Pipe Sheet Pile foundations(Fig.1), Sequentially driven steel pipe piles are integrated by connecting the top of each pile to a rigid footing to form a foundation that causes great bending moment and shear force in the footing, partition walls or intermediate piles are arranged inside the foundation section.

The shape of a foundation can be circular, rectangular, elliptic, etc.(Fig.2). The mechanical properties of these foundations are midway between those of steel pipe piles foundation and caisson foundation. Because of the rigidity and the elasticity, steel pipe sheet pile foundation has a decisive advantages over other types, especially when the foundation work is subjected to large horizontal loads and overturning moments.

As for the joints that interlock the steel pipe piles, the pipe-pipe or P-P type(Fig.3) is standard. The three tubular spaces divided by two joining pipes are thoroughly washed by jets of water etc. and are then filled with concrete mortar. This is done in anticipation of the transmission of shear forces among the steel pipe sheet piles and because of great water-sealing effect when the foundation functions as a cofferdam under construction.

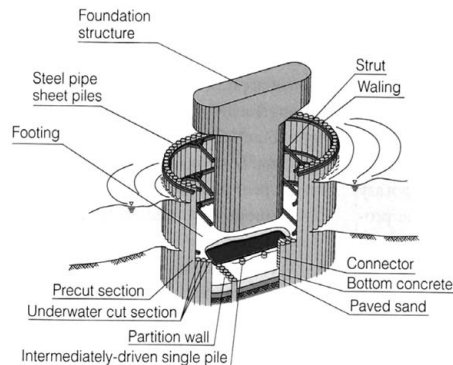


Figure 1. Schematic diagram for steel pipe sheet pile foundation.

2 MAJOR CHARACTERISTICS

It is true that compared to steel pipe pile foundations, steel pipe sheet pile foundations are not without disadvantages in terms of ordinary onshore work. But in many cases where the work is executed on water or on soft ground, they clearly demonstrate advantages over other foundations. On the water, in particular, the combination system for temporary cofferdam and foundation and the protruding foundation system

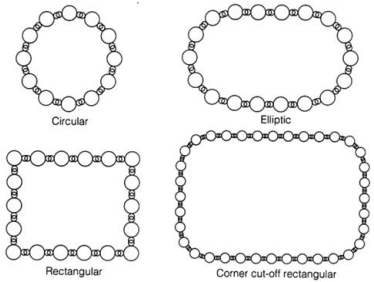


Figure 2. Plane shape of steel pipe sheet pile foundation.

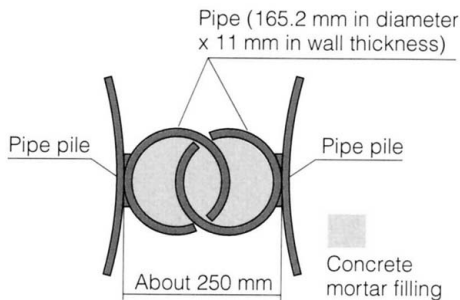


Figure 3. P-P type interlocking.

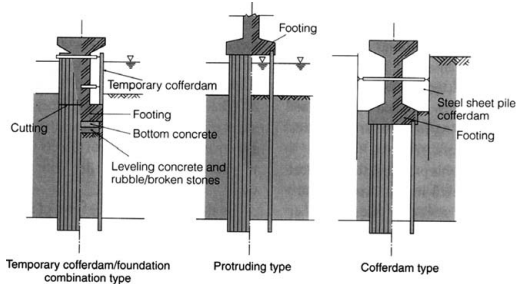


Figure 4. Type of steel pipe sheet pile foundation.

become more advantageous as water depth increases (Fig.4). There are few examples where types other than the combination system for temporary cofferdam and foundation are used.

The major characteristics of steel pipe sheet pile foundation can be summarized as follows.

- (1) The required dimensions of the foundation can be reduced to a minimum
- (2) These foundations can withstand major earthquakes.
- (3) These foundations are highly suited to construction on the water. In the case of the combined temporary cofferdam and foundation system,

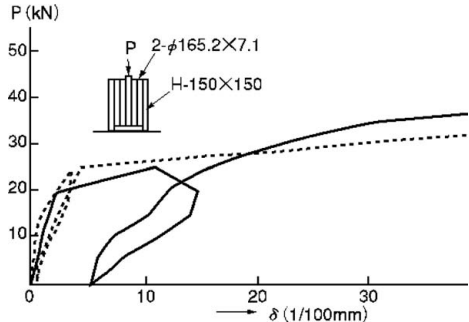


Figure 5. Shear test result of usual interlocking.

they show better safety when functioning as cofferdams and are thus extremely advantageous in terms of economy and construction time.

- (4) During execution, high technical capabilities are required with regard to driving, welding, mortar filling, the attachment of shear connectors and the underwater cutting of steel pipe sheet piles.
- (5) As steel pipe piles must be arranged in the form of a completely closed continuous wall as a well, the foundation not only requires a degree of high accuracy but is exposed to piling resistance each other. It is not suited for use among boulders or other strata that make pile driving difficult.

3 DEVELOPMENT OF INTERLOCKING

Ordinal interlocking of the steel pipe sheet pile foundations is P-P type with 165.2 mm diameters which connect both end steel pipe piles using 20 MPa filling mortar inside the interlocking. (Fig.3) As design stage of steel pipe sheet pile foundation, part of interlocking is modeled as shear springs. Shear rigidity and shear force capability are determined by shear tests which were done by PWRI (Public Works Research Center). (Fig. 4)

Before developing new interlocking, parametric study using large shear rigidity and shear capability were carried out. We founded that large shear force capability could reduce the number of steel pipe piles, so we could get small foundations. (Fig. 5)

4 HIGH SHEAR STRENGTH INTERLOCKING USING STEEL PIPE WITH PROJECTION

As the scale of a steel pipe sheet pile foundation becomes larger, the shear force that acts on the interlocking joints grows larger. Accordingly, if the shear strength of the joints were improved, foundations could be designed in a more rational manner. In recognition

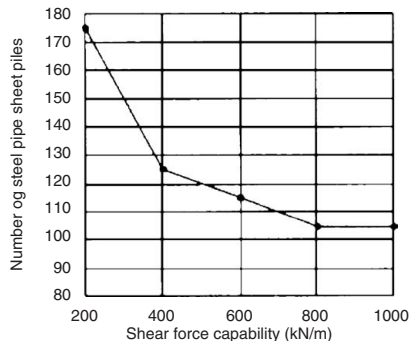


Figure 6. Parametric study based on the shear strength of interlocking between strength and required pile numbers.



Photo 1. Striped steel pipe interlocking.

of this, the Japanese Association for Steel Pipe Piles has developed a new interlocking joint that uses striped steel pipe, as shown in Fig.3 and Photo 1. This new interlocking joint has been confirmed by following experiments.

4.1 Shear test procedure

Frame of the loading test is shown in Fig. 7. Middle of the test specimen should be loaded with cyclic loading in order to certificate the effect of the earthquake. Loading pattern is control of the displacement of relative slip between interlocking. Up to the 5 mm slip, loading is 1 mm step, after 5 mm relative slip, in each 5 mm up to 20 mm, loading and unloading should be repeatedly on the test specimen.

4.2 Test specimen

Test specimen is shown in Fig. 8. Interlocking is welded to both end support of H beam-300 × 300. Within the interlocking, mortar is fulfilled. Both end support is welded to thick base plate, center of the specimen has some clearance in order to push down.

Specification of the interlocking is as follows.(Fig.3)

Diameter: 165.2 mm, Thickness: 11 mm

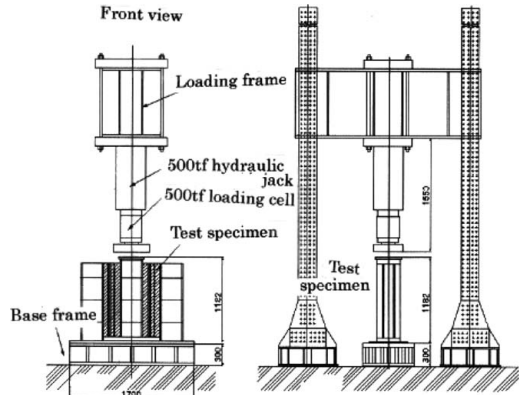


Figure 7. Frame of the loading test.

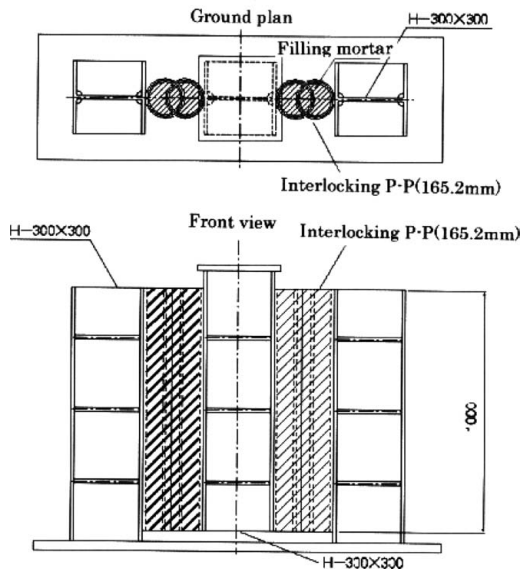


Figure 8. Test specimen.

Strength of mortar: 40 Mpa (2 times stronger than usual)

Height of the projection: average is 1.0 mm.

4.3 Test result

Relationship between shear strength and relative slip displacement in each three test specimen are shown in Figs. 8 to Fig.10. Ultimate shear strength is shown in the point of relative slip displacement 5 mm, then, shear strength decreases in accordance with relative slip displacement more increase. Average shear strength is about 1640 kN/m which is enough larger than usual one.

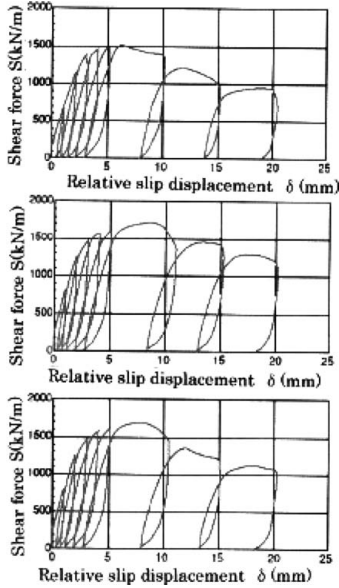


Figure 9. Relationship between shear strength and relative slip displacement.

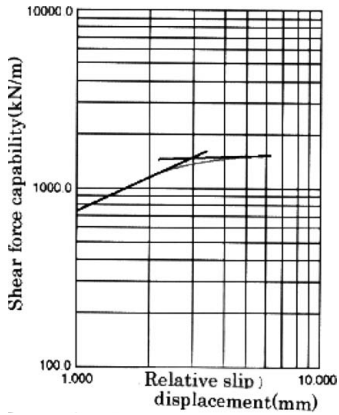


Figure 10. Example of the determination method for yield shear strength.

5 DESIGN CHARACTERISTIC OF NEW INTERLOCKING

5.1 Shear strength

In order to determine the shear strength design value, yield point was founded using relationship between shear strength and relative slip displacement. (Fig.10). Shear strength in time of level 2 earthquake was determined using safety factor 1.25 which is equivalent with usual interlocking. Shear strength of level 1

Table 1 Design value of striped steel pipe interlocking.

Case	Shear capability (kN/m)	Shear rigidity (kN/m ²)
Level 2 earthquake	1,150	
Level 1 earthquake	767	630,000
Ordinary situation	575	

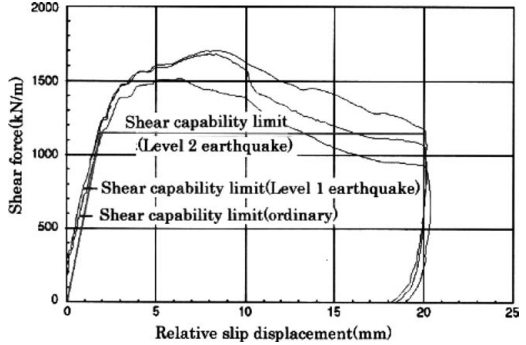


Figure 11. Shear performance of new striped steel pipe regarding design value.

earthquake and ordinal case was determined using safety factor 2.0 (level 1 earthquake) and 1.5 (Ordinal case).

In order to check the ultimate shear strength safety, real slip of interlocking using finite element method analysis was checked. Real slip displacement is about 8 mm. This new type interlocking has enough shear strength even considering the large slip displacement in more than 10 mm that is exceeding than 8 mm.

5.2 Shear rigidity

Shear rigidity is the line from origin and yield point which is already mentioned in 5.1. This method is good match with relationship between shear strength and slip displacement in design.

5.3 Design characteristic

Table 1 shows the shear strength and shear rigidity and Fig.11 shows the relationship between shear strength and rigidity and also show shear resistance model in each three level.

Table 1 Design value of striped steel pipe interlocking.

As already shown in previous section, design shear strength value is almost 5 times more than usual ones. As for spring model of interlocking, by-linear model is used as level 2 earthquake. And for level 1 earthquake and ordinary case, each case has upper limitation using as same as rigidity of level 2.

Table 2. Comparative study on big foundation in soft clay case.

Type of interlocking	Usual interlocking	New striped pipe interlocking
Plan of design result		
Number of steel pipe	175	106

It is very important that mortar must be fulfilled very carefully under water work. In this case, we need more than 40 MPa mortar, so mortar mix is carefully determined before real work.

6 CASE STUDY USING NEW STRIPED STEEL PIPE INTERLOCKING

Table 2 shows the comparative study result between new striped pipe interlocking and usual ones. This case is large scale foundation for big bridge such as Tokyo-Port Bridge (Temporary name). In this case, around 40% of steel pipe sheet piles could be reduced using new striped steel pipe interlocking.

7 CONCLUSIONS

Steel Pipe Sheet Pile Foundation is originally developed in Japan. In the time of high speed economic

development, this foundation was created for foundation of large blast furnace in Japanese Steel Maker aimed for very quick construction . So many efforts was done for applying this construction methods to bridge foundation in each field such public sector' engineer, academic people and construction people up to now. There are over 2000 foundations for bridge foundation up to now.

Japanese mill maker are now trying to apply this foundation to the projects outside Japan. Up to now, there are only three projects which were applied due to lack of technical transfer from Japan to outside countries. Design methodology and construction procedure are very unique but advantageous compared to another type of foundation in some cases. So we are now trying to transfer this technology to Asian countries such as Vietnam. In the success of technical transfer in near future, we will publish this experience how to transfer.

REFERENCES

- Katayama, T. et al. 2006. Steel Pipe Sheet Pile Foundation going outside Japan. *Civil Engineering Journal*. 47(2).
- Shioi, Y. 2003. Steel Pipe Sheet Pile Foundation-Structures and Major Characteristics. *Steel Construction Today & Tomorrow*. 3(4).
- Watanabe, et al. 2006. Steel Pipe Sheet Pile Foundation using striped steel pipe interlocking. Committee on road and bridge in Japanese Association for Steel Pipe Pile (ed). *Horizon* (74).

Development of three-dimensional frame analysis method for H-joint Steel Pipe Sheet Pile foundation system

M. Kimura

International Innovation Center, Kyoto University, Kyoto, Japan

K. Isobe

Department of Urban Management, Kyoto University, Kyoto, Japan

Y. Nishiyama

Data-Too Company, Tokyo, Japan

ABSTRACT: A new H-joint Steel Pipe Sheet Piles (SPSPs) in which two steel pipes are connected by H-steel section welded on them have been developed. To evaluate the mechanical characteristics of H-joint SPSPs appropriately, the three-dimensional frame analysis is extended and verified by comparing its results with the centrifuge model test results. The following observations were made from the studies: (1) A newly extended three-dimensional frame design method can express the mechanical behavior of the model tests accurately, (2) H-joint SPSPs have high rigidity hence large lateral bearing capacity making them suitable in ensuring the stability of SPSP foundation structures, and (3) H-joint SPSP contributes to the reduction of the number of piles based on the reduction in the dimension size of the SPSP foundations.

1 INSTRUCTION

1.1 Characteristics of H-joint Steel Pipe Sheet Piles

The authors have developed a new H-joint Steel Pipe Sheet Piles (SPSPs) technology from a simple idea in which two steel pipes are connected by welding H-steel section on them as shown in Fig. 1 in order to improve the performance and widen application areas of SPSP technology. The H-joint SPSP is expected to remediate problems of traditional joints in SPSPs. The main characteristics of H-joint SPSP are: (1) H-joint is completely waterproof, (2) H-joint SPSP is environmentally friendly since the number of grouted joints is reduced by about 50%, (3) Short construction periods and reduction in operation costs are achieved because two steel pipe piles can be driven at the same time, (4) H-joint SPSP have high bending rigidity because H-steel section is welded rigidly and continuously against two steel pipes.

1.2 Design analysis method of SPSP foundation

The designs for SPSP foundations are categorized into three methods. They are Method (1) referred to as beam analysis by finite length beam on an elastic bed,

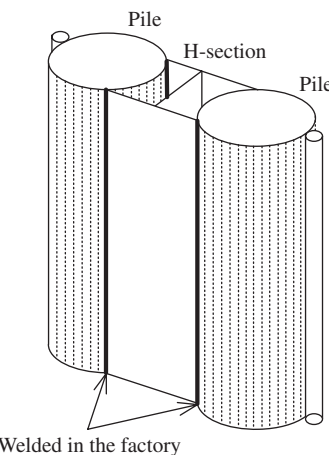


Figure 1. H-joint Steel Pipe Sheet Pile.

Method (2) referred to as beam analysis by virtual open caisson beam (Public Works Research Institute 1977) and Method (3) referred to as three-dimensional frame analysis. Generally, Method (1) is widely used by SPSP designers because it is relatively simple to use.

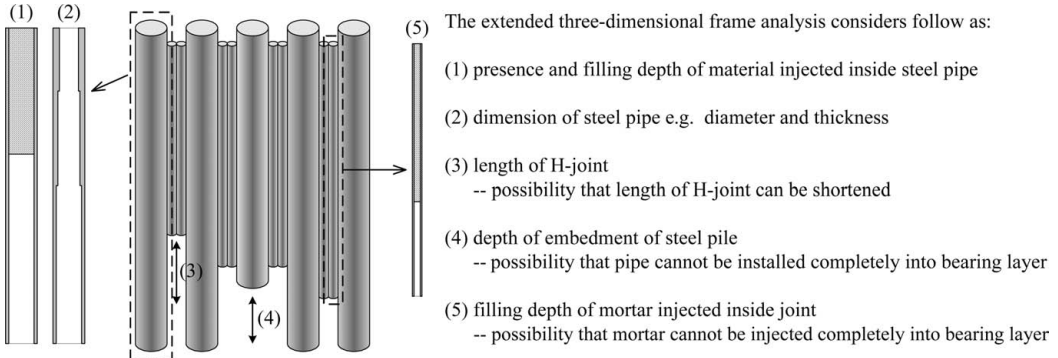


Figure 2. Flexible factors considered in the extended analysis method.

In the Method (1), the total rigidity of the overall SPSP foundation is estimated by reducing the moment of inertia using the joint efficiency (μ) (as in Equation (1)) to take into account joint movements which is the unique characteristics of SPSP foundation.

$$E_x I_z = E_s \left(\sum_{i=1}^{n_1} I_{oi} + \mu \sum_{i=1}^{n_1} A_{oi} y_i^2 \right) \quad (1)$$

where, I_{oi} = moment of inertia of each pile (pile i) about its own local axis; A_i = cross sectional area of pile i ; y_i = distance from the axis of an individual pile i to the global axis of the foundation; n_1 = number of piles.

Authors have estimated μ in applying H-joint SPSPs into SPSP foundation system and proposed a value of 0.85 for use as a joint efficiency for the design of H-joint SPSP foundation when a value of 0.75 is adopted as the joint efficiency for the design of P-P joint SPSP foundation (Kimura et al. 2006). However, to apply the H-joint SPSPs to SPSP foundation system, the analysis method which can investigate the mechanical behavior of H-joint SPSP foundation more appropriately needs to be developed. In this paper, the authors have expanded the versatility of three-dimensional frame analysis method to consider the mechanical characteristics of H-joint SPSP. The validity of the analysis method is verified in comparison with the centrifuge model tests results (Too et al. 2004).

2 DETAILS OF THREE-DIMENSIONAL FRAME ANALYSIS METHOD

2.1 Effectiveness of considering the mechanical characteristics of H-joint SPSPs

It is necessary to establish the design method for SPSP foundation system which can estimate the mechanical characteristics of H-joint SPSPs when they are applied to SPSP foundation system. The following problems

should be solved to overcome it: (1) modeling of H-joint SPSP in which two pipes welded by H-joint move together, (2) estimation of the rigidity of H-joint which should be considered. On the other hand, in the traditional three-dimensional frame analysis, users do not have the diversity on changing the length of pipes and joints. However, there is possibility that the length of H-joint can be shortened in applying the H-joint to SPSP foundation because H-joint SPSP foundation system has higher bearing capacity than the traditional SPSP foundation system. Therefore, it is also necessary that the design method which is flexible about setting the length of pipes and joints be established.

Besides, a more reasonable design is able to be conducted using the design method considering the presence and filling depth of material injected inside steel pipe, dimension of steel pipe e.g. diameter and thickness, depth of embedment of steel pipe and filling depth of mortar injected inside joint as shown in Fig. 2. In this paper, the three-dimensional frame analysis method considering these characteristics is developed based on the precedent three-dimensional frame analysis method.

2.2 Modeling of H-joint SPSP

Pile of usual SPSP is described by elastic beam elements with springs which model the vertical, tangential and normal resistance of joint as shown in Fig. 3, however, modeling of H-jointed SPSP piles should consider that two pipes welded by H-joint move together. In this paper, in order to model the mechanical behavior appropriately, the following model types have applied as shown in Fig. 4:

- (1) Model-1: one beam which has the total moment of inertia and the area of H-joint SPSP.
- (2) Model-2: two beams with rigid springs, in which each beam has half of the moment of inertia and the area of H-joint SPSP, and is connected by rigid spring.

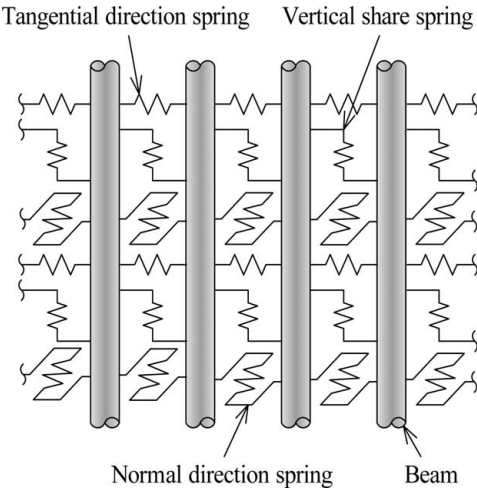


Figure 3. Model of joint of SPSPs.

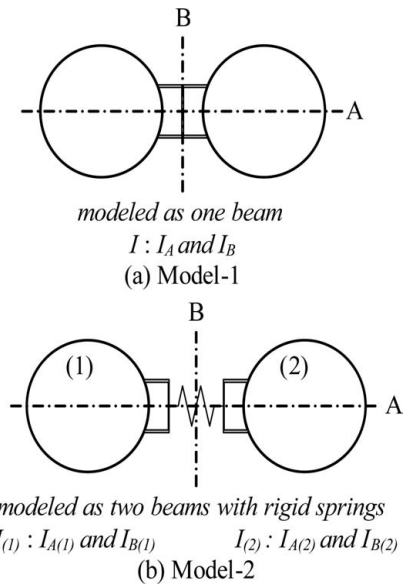


Figure 4. Tested analysis model of H-joint SPSP.

The elastic calculations are conducted to verify models. The analysis object is shown in Fig. 5. Load-displacement relation and lateral displacement distribution of piles are shown in Figs. 6 and 7. From these results, the results of Model-1 and Model-2 are almost corresponding. Although it is thought that Model-1 is one of the best for modeling H-joint SPSP in which two piles welded by H-section move

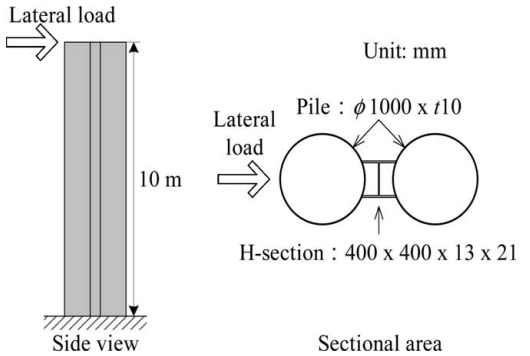


Figure 5. Analysis object of H-joint SPSP.

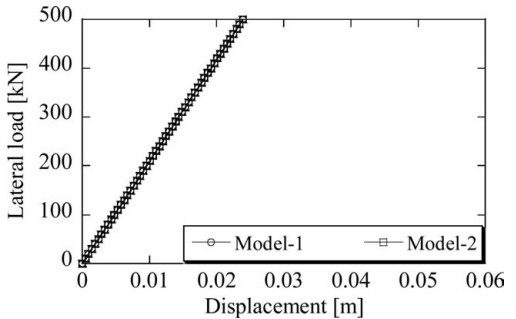


Figure 6. Load-displacement relationship.

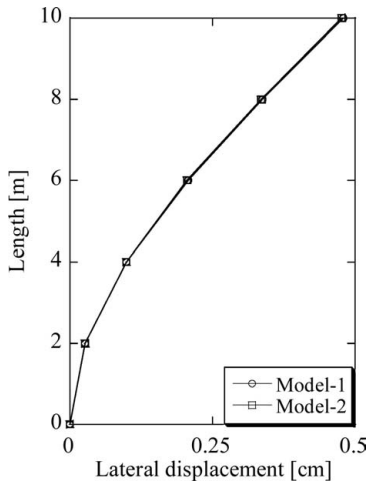


Figure 7. Lateral displacement distribution.

together under lateral load, Model-1 is not suitable to apply to SPSP foundation system which have various shapes e.g. circle, rectangle and oval. In addition, Model-1 cannot consider the diversity on changing

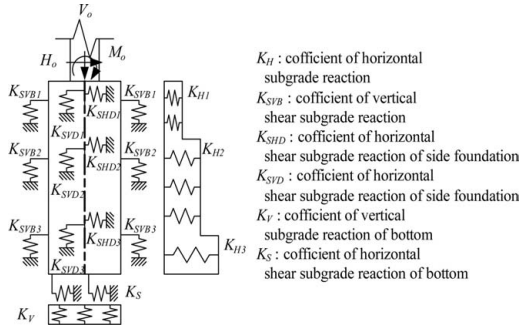


Figure 8. Soil springs in this analysis method based on reference for Highway Bridge Design Specifications for Highway Bridges (2002).

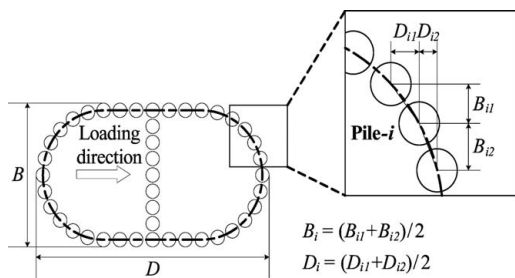


Figure 9. Width of pile perpendicular and parallel to horizontal loading direction.

the length of pipes and joints. Model-2 is, therefore, applied in this analysis.

2.3 Nonlinearity of ground and joints

The nonlinearity of ground resistance; (1) horizontal subgrade reaction, (2) vertical shear subgrade reaction, (3) horizontal shear subgrade reaction, (4) vertical subgrade reaction of bottom, (5) horizontal shear subgrade reaction of bottom is modeled by elasto-plastic springs as shown in Fig. 8. The parameters of the springs are determined by Reference for Highway Bridge Design Specifications for Highway Bridges (2002). The width of ground resisting perpendicular and parallel to horizontal loading direction which each pile shears is determined as shown in Fig. 9.

The nonlinearity of joints is also described, and determined by some compression, tension and shear tests of joints (Inazumi et al. 2005). The details of these tests and the results are shown in the reference.

2.4 Modeling of footing

Footing is modeled as shown in Fig. 10, in which the virtual nodes are set in the center of foundation system,

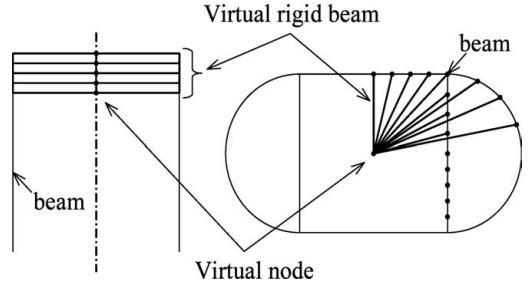


Figure 10. Modeling of footing.

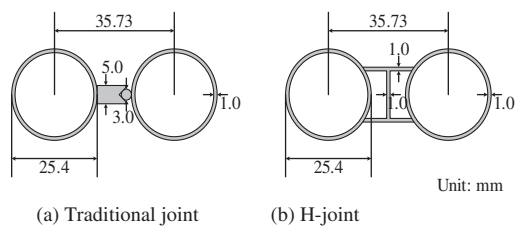


Figure 11. Modeling of traditional joint and H-joint SPSP in the centrifuge model test.

their nodes are connected to the beams which model SPSPs by the virtual rigid beams and the flexural rigidity of their beams set to be rigid.

3 VALIDITY OF THE ANALYSIS METHOD

3.1 Comparison with the centrifuge model test results

To investigate the mechanical behavior of SPSP foundation in which H-joint SPSPs are applied, two kinds of centrifuge model tests were conducted by Kimura et al. (2004). The analysis method extended in this paper is verified by comparing these results with the centrifuge model test results.

Figs. 11, 12 and Table 1 show the prototype dimension of rectangular SPSP foundation used in the centrifuge model tests which is named as Case-1. In Case-1, there are two types of SPSP foundation without footing: Case-1(a) referred to as the SPSP foundation in which traditional SPSP only are applied, Case-1(b) referred to as the SPSP foundation in which H-joint SPSP are applied. The parameter of soil spring is calculated back using the result of lateral load test of single pile conducted in the same ground condition and it is assumed that the coefficient of horizontal subgrade reaction is proportional to depth in this analysis as shown in Fig. 13. Joint parameter is

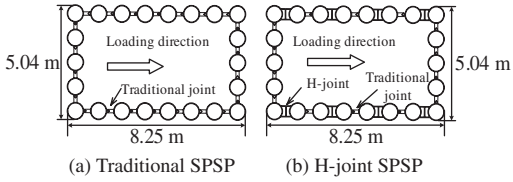


Figure 12. SPSP foundation used in the centrifuge model test of Case-1 (Prototype).

Table 1. SPSP foundation parameter of Case-1 (Prototype).

	Case-1(a)	Case-1(b)
Diameter	0.762 m	
Length	16.2 m	
Thickness	30.0 mm	
No. of piles	22	
Joint type	H-joint: 0 Traditional joint: 22	H-joint: 8 Traditional joint: 14
Footing		
Centrifuge acceleration	None	30 G

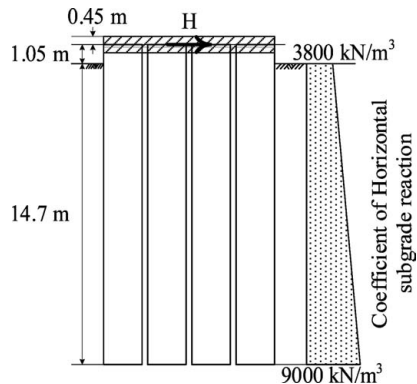


Figure 13. SPSP foundation dimension and coefficient of horizontal subgrade reaction assumed in the calculation of Case-1.

determined by shear test using model of SPSP (Too et al. 2004).

Fig. 14 shows load-displacement relation of Case-1. It is shown that the analysis results are in good agreement with the centrifuge model test results in each case: Case-1(a) and Case-1(b), besides, SPSP foundation using H-joint SPSPs has bigger horizontal bearing capacity than the traditional SPSP foundation.

Figs. 15, 16 and Table 2 show that the prototype dimension of square-shaped SPSP foundation used in the centrifuge model tests which is named as Case-2.

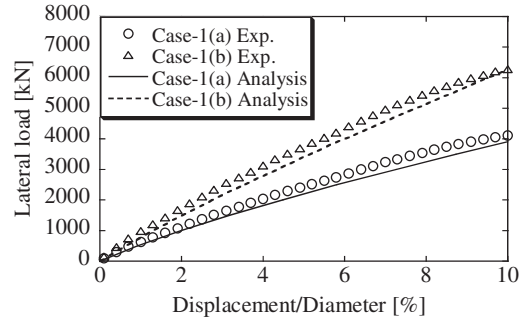


Figure 14. Load-displacement relationship of Case-1.

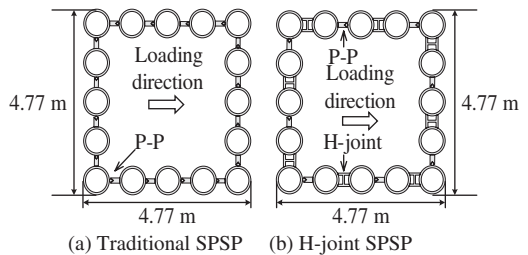


Figure 15. SPSP foundation used in the centrifuge model test of Case-2 (Prototype).

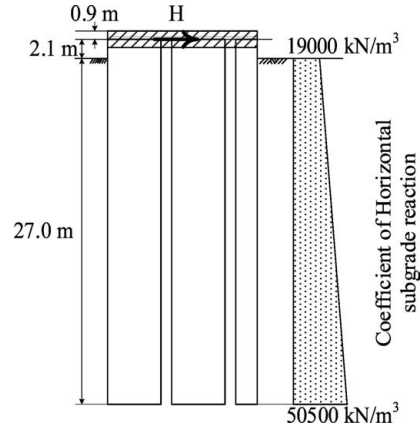


Figure 16. SPSP foundation dimension and coefficient of horizontal subgrade reaction assumed in the calculation of Case-2.

In Case-2, there are four types of SPSP foundation with and without footing: Case-2(a)-1 referred to as the SPSP foundation with footing in which traditional SPSP only are applied, Case-2(a)-2 referred to as the SPSP foundation without footing in which traditional

Table 2. SPSP foundation parameter of Case-2 (prototype).

	Case-2(a)-1	Case-2(b)-1	Case-2(a)-2	Case-2(b)-2
Diameter			0.762 m	
Length			30.0 m	
Thickness			60.0 mm	
No. of piles			16	
Joint type	H-joint: 0 Traditional joint: 16	H-joint: 8 Traditional joint: 8	H-joint: 0 Traditional joint: 16	H-joint: 8 Traditional joint: 8
Footing	None			Set
Centrifuge acceleration			60 G	

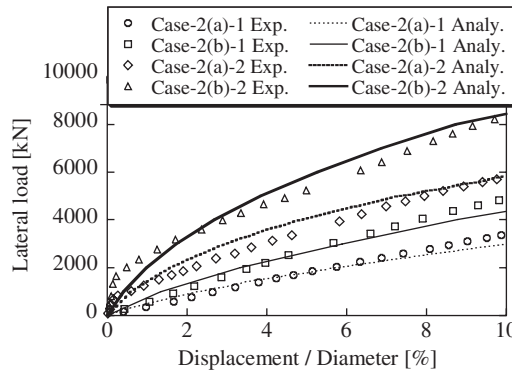


Figure 17. Load-Displacement relationship of Case-2.

SPSP only are applied, Case-2(b)-1 referred as the SPSP foundation with footing H-joint SPSP are applied, Case-2(b)-2 referred to as the SPSP foundation without footing H-joint SPSP are applied. The parameters of soil spring and joint spring are determined using the same method as Case-1.

Fig. 17 shows load-displacement relation of Case-2. It shows that the analysis results are in good agreement with the centrifuge model test results in each case: Case-2(a)-1, Case-2(a)-2, Case-2(b)-1 and Case-2(b)-2, furthermore, SPSP foundation using H-joint SPSPs has bigger horizontal bearing capacity than the traditional SPSP foundation just like the results of Case-1. Besides, SPSP foundation with footing has bigger horizontal bearing capacity than that without footing in each case.

These results show that the three-dimensional frame analysis extended in this research is verified, SPSP foundation in which H-joint SPSPs are applied have more lateral bearing capacity than the traditional SPSP foundation system in comparing with SPSP foundation which has same dimension, that is, the dimension of H-joint SPSP foundation is able to be reduced in designing SPSP foundation which has as same bearing capacity as the traditional SPPS foundation.

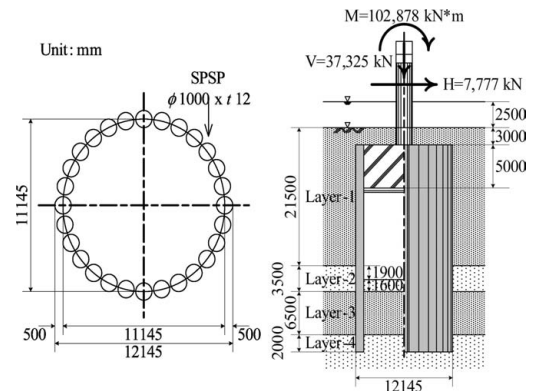


Figure 18. Dimension of SPSP foundation, ground condition and design load (Case-3).

Table 3. SPSP foundation parameter.

Diameter	1.0 m
Length	30.5 m
Thickness	12.0 mm
Pile number	28
Joint type	P-P: $\phi 165.2 \times t 11$ mm

3.2 Verification of applicability of the analysis method to real structure

The analysis object is the design example which is shown in the reference (JRA 1997). The dimension of circular-shaped SPSP foundation system, its ground condition and applied design load is shown in Fig. 18. The foundation parameter, the soil parameter and joint parameter are shown in Tables 3–5. The coefficient of subgrade reaction is determined by the reference in this simulation. Joint parameters of tangential tension and compression springs are determined based on the result conducted by Kimura et al. (2006). The other parameters are determined by the reference (JRA 1997).

Table 4. Soil parameter.

Soil	Thickness [m]	N-value	Cohesion [kN/m ²]	Internal friction angle ϕ [°]	Unit weight [kN/m ³]
Layer-1	Clay	21.5	2	30.0	16.0
Layer-2	Sand	3.5	14	0.0	18.0
Layer-3	Clay	6.5	10	80.0	17.0
Layer-4	Gravel	2.0	50	0.0	20.0

Table 5. Joint parameter.

	Tangential tension	Tangential compression	Normal	Vertical shear
Stiffness [kN/m ²]	12000	860000	50000	120000
Strength [kN/m]	144	1230	200	200

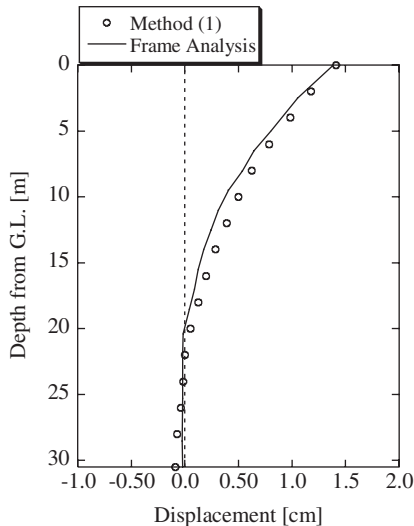


Figure 19. Displacement distribution (Case-3).

Fig. 19 shows displacement distribution of piles, which include the results of Method (1) and three-dimensional frame analysis. From this figure, the result of the new extended analysis is in good agreement with the design value calculated by Method (1) hence the verification of applicability of the analysis method to real structure is indicated.

4 CONCLUSION

The following observations were made from the studies: (1) A newly extended three-dimensional frame

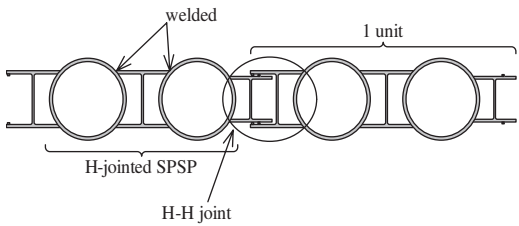


Figure 20. H-H joint developed as a new SPSP technology.

design method can express the mechanical behavior of the model tests accurately, (2) H-joint SPSPs have high rigidity hence large lateral bearing capacity making them suitable in ensuring the stability of SPSP foundation structures, and (3) H-joint SPSP contributes in the reduction of the number of piles based on the reduction of the dimension size of the SPSP foundations.

In our recent research, new joint for SPSP foundation which is called H-H joint is developed as shown in Fig. 20 (Inazumi et al. 2005). The H-H joint will have a number of merits over the traditional joints, they include: (1) high rigidity because existing H-steels are used, and (2) low hydraulic conductivity of the joint part. The H-H joint is designed to alternate in series with the H-jointed SPSP which improves the overall strength of the structure as discussed previously.

These mechanical characteristics about new H-H joint SPSP foundation wall can be considered in the analysis method extended in this paper hence these development about the new joint and the analysis method of SPSPs widens application areas of new SPSP technology.

REFERENCES

- Inazumi, S., Kimura, M., Too, A.J.K. & Kamon, M. 2005. Performance of H-jointed steel pipe sheet piles with H-H joint in vertical hydraulic cutoff walls. *Proceedings of the 16th International Conference on Soil Mechanics and Geotechnical Engineering*: 2269–2272. Osaka: Millpress.
 Japan Road Association (JRA) 2002. *Reference for Highway Bridge Design Specifications for Highway Bridges: Part IV; Substructures*. Japan Road Association.

- Japan Road Association (JRA) 1997. *Design and construction handbook for Steel Pipe Sheet Pile Foundation*. Japan Road Association, (in Japanese).
- Kimura, M., Inazumi, S., Too, A.J.K, Isobe, K., Mitsuda, Y. & Nishiyama, Y. 2006. Development and application of H-joint steel pipe sheet piles in construction of foundations for structures. *Soils and Foundations*, (in press).
- Public Works Research Institute 1977. *Design of Sheet Pile Foundation*. Public Works Research Institute, 1175 (1), (in Japanese).
- Too, A.J.K., Kimura, M., Inazumi, S., Isobe, K. & Nishiyama, Y. 2004. Improvement of stability of steel pipe sheet pile structures using H-joints. *Proceedings of the International Symposium on Engineering Practices and Performance of Soil Deposits (IS-Osaka 2004)*: 507–512. Osaka: Yodogawa Kogisya.

Development of a composite pile system consisting of soil cement columns and H-beams

O. Kaneko

TODA Corporation, Tokyo, Japan

ABSTRACT: A new composite pile system was developed based on the conversion of earth retaining walls into piles by inserting H-beams in individual soil cement columns with the aim of reducing cost and construction period. Quality and performance of the composite pile was evaluated by a series of field tests. Following standard installation procedure, soil cement columns readily meet the Deep Mixing Method standards in quality. The bearing capacity and the load-settlement response of the composite pile can be estimated by formulae proposed based on the static load test results in a manner similar to conventional pile foundations. The pile system was found to successfully contribute to reduction of cost and construction period in several applications.

1 INTRODUCTION

A new composite pile system was developed with the aim of reducing cost and construction period. It is common in Japan to utilize consecutive deep mixing (soil cement) columns for earth retaining walls referred to as Soil Mixing Wall (SMW). These soil cement columns can be converted into composite piles by inserting H-beams forming the core of the columns so that tentative earth retaining walls become composite piles forming part of the permanent structure. The conventional machines for SMW can be readily utilized for placement of composite piles with minimal additional time.

This paper presents the quality assessment of the soil cement through strength tests of specimens sampled from in-situ columns, and the load-settlement response of the composite pile based on the field test results. Some application examples of the pile are also described and compared with conventional piles. The test results show that quality of the soil cement column constructed by this method is acceptable as permanent foundations and the bearing capacity of the piles can be estimated by common bearing capacity formula. Analyzing load test results allows simulation of the load-settlement response of piles by load transfer functions.

2 OUTLINE OF THE COMPOSITE PILE SYSTEM

2.1 Load transfer mechanism

Figure 1 shows general assembly in cross section of the composite pile system. Load of the superstructure

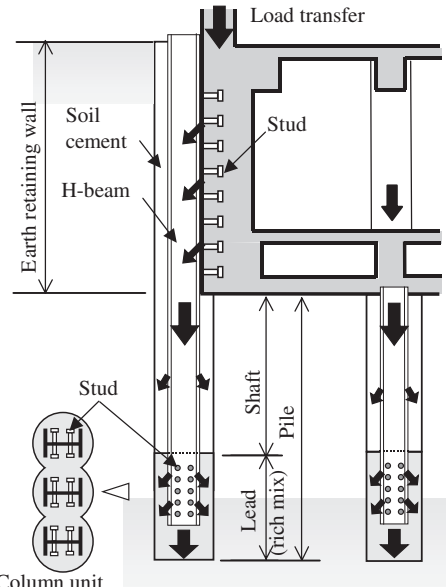


Figure 1. General concept of the pile system.

is transferred to the ground through the composite piles. Studs are placed on the lead section of the pile and above the pile head, which work as shear-pins for assuring load transfer.

2.2 Quality of soil cement

The target strength of the soil cement is set at 5 N/mm² for the lead section where a rich-mix of

binder is utilized, while it is 1 N/mm^2 for the shaft section. Besides, the quality of soil cement should conform to the standard deep mixing method in strength and uniformity.

2.3 Execution control

It is necessary for soil cement column to have a suitable consistency maintained at the time H-beam is inserted. In addition, soil cement columns should conform to design diameter and be vertical with accuracy of 1 in 100.

2.4 Applicability

The composite pile is installed by SMW machine (Photo 1), which is capable of installing soil cement columns 350 to 1,100 mm in diameter and 50 m in maximum depth with either three or five consecutive columns unit installed simultaneously. In some cases, the composite piles may be constructed as frictional piles that function as retaining walls as well.

3 QUALITY ASSESSMENT DURING INSTALLATION

Quality of the soil cement columns was verified through the in-situ tests to develop standard installation procedure. Four execution tests were conducted by setting mix proportions of binder and rotation number as shown in Table 1. Then, specimens sampled from various depths of each in-situ column were tested in unconfined compression. Table 2 shows the test results, where alphabets A to D refer to different cases of execution sequence. Case A involved three consecutive three columns unit installed on the same day. In case B, the



Photo 1. SMW machine.

Table 1. Summary of standard procedure.

Part	Target strength N/mm^2	Cement content kg/m^3	Water/Cement ratio %	Rotation number/ m rpm
Shaft	1	353	150	38
Lead	5	705	80	100

Table 2. Dimension and strength of piles for field tests.

PileNo.	Depth m	Diameter mm	Part	Number of sampling specimen	Average strength N/mm^2	Coefficient of variation	Design strength N/mm^2
A	17.5	650	shaft	39	6.9	0.43	3.0
				35	11.5	0.43	5.1
			lead	41	15.8	0.37	8.3
B	17.5	650	shaft	36	7.6	0.44	3.4
				36	12.9	0.43	5.8
			lead	44	14.7	0.35	7.9
C	17.5	900	shaft	39	3.9	0.31	2.3
				36	9.0	0.28	5.7
			lead	44	9.8	0.37	5.1
D	33.5	900	shaft	18	7.0	0.27	4.3
				15	3.6	0.35	1.9
			lead	13	18.4	0.24	12.6

third of the three units was installed the following day. In cases C and D, only single unit was executed. The required soil cement quality is satisfies in all cases. The compressive strength (q_u) from test results is larger than the target strength, and the coefficient of variation (COV) of q_u is well within the range of Deep Mixing Method standard. One element was dug out from the ground as shown in Photo 2. Verticality and external appearance were also confirmed to be good. It is known that the soil cement strength depends on the confining stress level. The COV in q_u can be expected to be even smaller had the overburden pressure of the ground been taken into account.

4 BEARING MECHANISM UNDER STATIC LOAD

4.1 Bearing capacity

Six static load tests were conducted in order to evaluate the bearing capacity and load-settlement behavior of the composite pile. Pile tip was embedded either in dense sand with SPT N-value >50 or in loose sandy silt with N-value from 4–10. The bearing capacity (R_u) of piles is commonly expressed by the following equations in Japan.

$$R_u = R_p + R_f \quad (1)$$

$$R_p = \alpha \cdot N \cdot A_s \text{ (sand)}, \text{ or } = \beta \cdot c_u \cdot A_s \text{ (cohesive soil)} \quad (2)$$



Photo 2. Dug-out three column unit.

$$R_f = \phi (10/3 \cdot N_s \cdot L_s + 1/2 \cdot q_{uc} \cdot L_c) \quad (3)$$

where, R_p = tip resistance, R_f = shaft friction, N = SPT N-value around pile tip, A_s = cross section of soil cement (m^2), c_u = cohesion of clayey soil (kN/m^2), ϕ = perimeter of soil cement (m), N_s = average SPT N-value of sand layers, q_{uc} = average unconfined compression strength of cohesive soil layers (kN/m^2), L_s or L_c = total length of sand layers or cohesive soil layers (m).

For the tip resistance (R_p) of the composite pile, coefficients α and β become 133–191 and 7.3–17.6 respectively, which are larger than those of the design values for deep mixing method ($\alpha = 75$, $\beta = 6$). Measured maximum shaft friction (R_f) is also larger than the values calculated by Equation 3. Thus, the bearing capacity of the composite pile can be safely assessed by Equations 1, 2 and 3.

4.2 Load-settlement response

Load-settlement behavior is to be modeled by means of equations 4 and 5, where regression curves are introduced for tip resistance and shaft friction. All of the coefficients in the equations are determined from the load test results analyzing tip resistance-settlement and shaft friction-settlement correlations in terms of soil type and SPT N-value.

$$\frac{S_p/d_p}{0.1} = a_p \frac{R_p/A_p}{(R_p/A_p)_u} + (1-a_p) \left[\frac{R_p/A_p}{(R_p/A_p)_u} \right]^n \quad (4)$$

$$\frac{\tau}{\tau_{max}} = \frac{0.1\delta}{a_f + b_f \cdot \delta} \quad (5)$$

In equations 4 and 5, S_p/d_p = tip settlement to diameter ratio, R_p/A_p = end resistance per unit area (suffix ‘u’ means ultimate), τ = shaft friction (kN/m^2), δ = settlement over various strain measurement intervals (m).

Derived coefficients are tabulated in Table 3. In Figure 2, the measured load-settlement behaviors in two cases are compared with the estimated curves by load transfer method using these coefficients. This evaluation approach seems to be effective in simulating the load-settlement response of the composite pile.

By taking axial stiffness of the composite pile in the following Equations 6 and 7, coefficient a_v is 0.01 and 0.60 in each example, which is closer to bored piles (0.01–0.013, 0.36–0.53) than other composite pile consisting steel pipe pile and soil cement (0.04, 0.15). This may reflect the high target strength ($5 N/mm^2$) at the leading section of the composite pile.

$$K_v = a_v \frac{A_h E_h + A_s E_s}{L} \quad (6)$$

Table 3. Coefficient in Equations 4,5.

In Equation 4

SPT N-value	a_p	n
>50	0.25	2.2
4	0.22	8.1

Soil layer	a_f	b_f	$\delta\tau_{max}$
Sandy soil	0.28	0.081	20 mm
Cohesive soil	0.19	0.086	10 mm

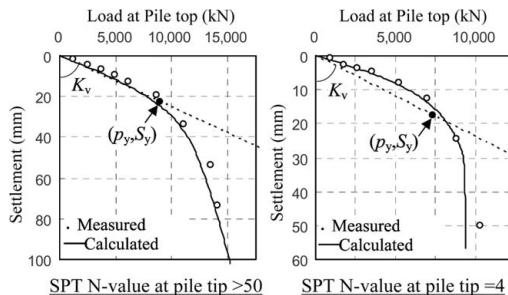


Figure 2. Load-settlement behavior of composite piles.

$$a_v = 0.01(L/D) + 0.60 \quad (7)$$

Here, A_h or A_s = cross section of H-beam or soil cement (mm^2), E_h or E_s = deformation modulus of H-beam or soil cement (kN/mm^2), L = length of soil cement (mm), D = diameter of soil cement (mm)

5 APPLICATION EXAMPLE

Basically, the composite piles are installed simultaneously along with earth retaining walls at the site. Closed earth retaining walls beneath the building foundation could confine inner soil mass featuring some advantages against shear deformation. Under such circumstances, the composite pile system could improve the resistance against pullout forces and soil deformation induced by liquefaction. In addition, the upper section above the pile head of H-beams can work as a composite wall together with reinforced concrete (RC) walls reducing the volume of foundation wall.

Table 4 shows the application examples of the composite pile so far. In the case **a**, internal columns are also supported by several single composite piles. In addition, higher liquefaction resistance was expected with this foundation system (Fig. 3). For a high-rise building in case **d**, tensile resistance was expected

Table 4. Application examples.

Case	Building's floors	Number of H-beam	Diameter of soil cement (mm)	Depth of soil cement (m)
a	6/1	94	550	12.0
b	7/1	24	600	15.8
c	9/2	182	600	25.5
d	28/2	91	550	16.2

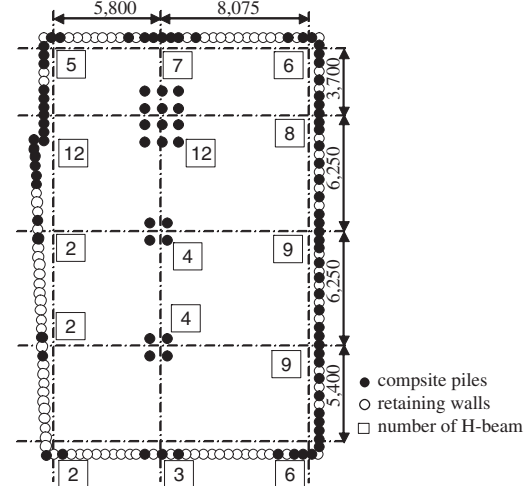


Figure 3. Arrangement of piles: Case a.

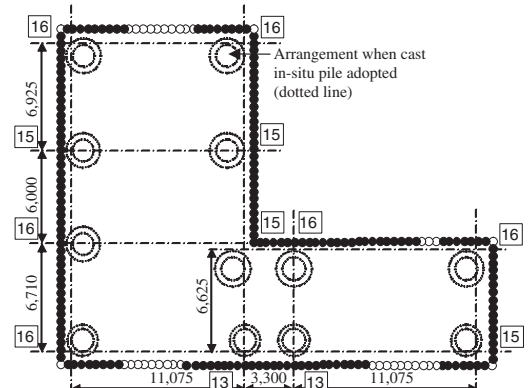


Figure 4. Arrangement of piles: Case c.

against earthquake loading. For case **c** shown in Figure 4, cast in-situ piles were replaced by composite piles, reducing the construction period and the RC wall volume.

Under comparable design situation, other piles are compared in Table 5 with cases **a** and **c**. All buildings

Table 5. Comparison of composite piles with design considering other alternatives.

Case	Design with conventional piles					Design with composite piles		
	Axial force kN	Type of pile	Number of piles	Diameter of pile tip mm	Bearing Capacity kN	Number of H-beams	Diameter of soil cement mm	Bearing Capacity kN
a	Max. 3,610 Min. 380	Precast concrete	3 1	700 600	4,810 1,216	12 2	550 550	4,224 704
c	Max. 7,200 Min. 5,090	cast in-situ concrete	1 1	2,200 2,000	7,800 6,500	16 13	600 600	7,928 6,482

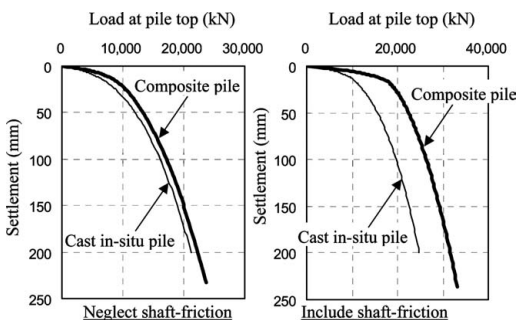


Figure 5. Estimated load-settlement behavior of composite piles: Case c.

were supported by piles bearing on soil stratum with N-value >50. The composite pile system can replace the conventional pile system in a rational manner. In Figure 5, estimated load-settlement response for the composite piles is compared with that for a single cast in-situ pile in case c of the previous table, over consolidated clay layer overlays the bearing stratum. Though shaft friction on this layer is neglected in the design, taking this friction into account makes the composite pile system advantageous in load-settlement performance.

6 CONCLUSIONS

A new composite pile system has been developed involving conversion of the soil-cement earth retaining wall into piles by inserting H-beams in consecutive soil cement columns. Quality and performance of the composite pile system has been investigated by a series of field tests.

Undertaking standard installation procedure, soil cement columns are known to provide good quality. The composite pile system exhibits suitable load-settlement response as a pile foundation. The bearing capacity and the load-settlement response of the pile can be estimated by formulae proposed based on the static load test results.

The pile system is verified to successfully contribute to reduction in construction period and cost through several applications.

REFERENCES

- Kaneko, O. 2004. Load-Displacement Characteristics of Soil cement and H-shaped Steel Composite Piles. *Proceeding of The 49th Geotechnical Symposium: 27-132*: he Japanese Geotechnical Society (in Japanese).
- Japan Road Association. 2002. *Specifications for highway bridges*. Part 4 Substructures.

Application of highcapacity micropiles for seismic retrofitting in Japan

Y. Otani

Hirose & Co., Ltd., Tokyo, Japan

M. Hoshiya

Musashi Institute Technology, Tokyo, Japan

ABSTRACT: The high-capacity micropile method was introduced into Japan from the USA in 1997 primarily to reinforce existing structures. Japan has already used this method in more than 20 actual examples of earthquake-resistant reinforcement for bridges. This paper reports its first application to the seismic retrofitting of a reinforced concrete water service tower in Japan.

1 INTRODUCTION

Micropile is a general term for cast-in-place or bored precast piles with a small end diameter (300 mm or smaller). They were developed primarily in Europe in the 1950's, and have been widely used, not only Europe, but also throughout the world. Being small diameter pile units, they have been mostly designed as friction piles from which no end bearing capacity is expected.

Micropiles are considered as promising measure for improving the bearing capacity of existing foundations of structures which are deteriorating. The advantage of the micro-piles is that they can be installed with minimum disturbance to both of the existing structures, subsoil and the environment.

The high-capacity micropile (below abbreviated as HMP)(JAHMP 1999, PWRI 2002) is a high-resistance pile unit consisting of high-strength steel pipe and reinforcing bars used as reinforcement members. It has been used in the United States since the Loma Prieta Earthquake in 1989 in earthquake-resistant reinforcement work for bridges, starting with damage to bridges from the San Fernando Valley Earthquake in 1971. It was introduced into Japan from America in 1997 to satisfy the requirements for seismic retrofitting for existing structures after the Hyogoken-Nanbu Earthquake in 1995.

2 REINFORCED STRUCTURE

The water service tower targeted for reinforcement (see Fig. 1) was built at the Rokku Water Purification Plant located on the eastern shore of the Yahagi River in

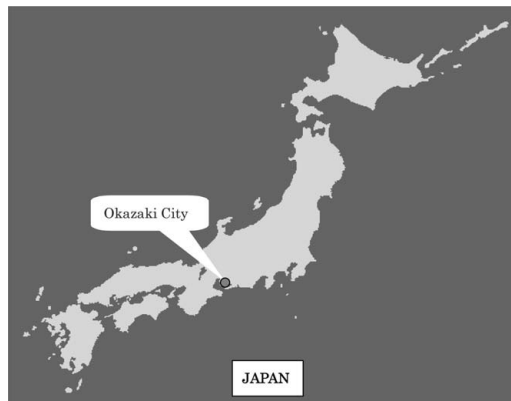


Figure 1. Location of the site.

midwestern Okazaki City, Aichi Prefecture, and is used to supply water from the plant. This tower is a building of historic significance constructed by Okazaki City in 1933, and is still functioning for water supply even after 70 years. As shown in Photo 1, its exterior, designed with inspection access stairs on the front ivy-covered wall, was awarded an urban landscape and environment prize by Okazaki City, and is listed in the Modern Architecture Guide (Kajima Publishing, Inc.) as a designated historic building. The front of the tower carries a plaque (Photo 2) inscribed with calligraphy by Baron Tatsuo Yamamoto, then Minister of Internal Affairs, who held successive positions as Governor of the Bank of Japan. Details of the design and construction at that time are unknown; however, it is said to have been designed by an Englishman.



Photo 1. View of the Water service tower.



Photo 2. Plaque on the ivy-covered wall.

After completion of the project at a total cost of US\$ 13,500 (at that time), underflow water from the Yahagi River has been collected from the Hina Source Water Supply Facility and supplied by natural flow after filtration and sterilization treatment at the purification plant from September 1, 1933 up to the present day.

3 SEISMIC DESIGN

The pile structure primarily consists of steel reinforcement such as steel pipes and reinforcing bars, and grout products (cement milk), classified according to the sectional configurations(Otani et al. 1998) in Table 1.

Taking advantage of their high workability under construction limitations, micropiles with a variety of resistances can be selected based on the acting load characteristics, load levels, and required deformation properties dictated by the targeted structures.

As a preliminary survey(OCWB 1996) on the water service tower, a secondary diagnosis was conducted to classify deterioration such as corrosion of the steel reinforcement bars, cracking, water leakage, and surface deterioration based on the primary diagnosis which investigated deterioration of the exterior/interior

Table 1. Classification of Micropiles.

	High capacity	↔	Low capacity
Reinforcement	Steel pipe + Steel bar	Steel pipe	Steel bar
Bearing capacity	$\geq 1000 \text{ kN}$	$1000 \text{ kN} >$	$420 \text{ kN} \geq$
Pile diameter	$300 \text{ mm} \geq D \geq 150 \text{ mm}$	$250 \text{ mm} \geq D \geq 100 \text{ mm}$	$150 \text{ mm} \geq D$

walls. Also, regarding the seismic retrofitting of existing structures, the maximum design horizontal seismic coefficient was set to take account of both inland direct strike type earthquakes caused by the Sanage/Sakaigawa Fault and marine plate boundary type earthquakes generated in Suruga Trough, in order to check the bearing capacity of the foundations.

The seismic design (OCWB 2001) for the water service tower was carried out, using the displacement response method during earthquakes at Level 1 and the ductility design method stipulated in Design Specifications for Highway Bridges (DSHB) during earthquakes at Level 2, in accordance with the Earthquake-resistant Construction Method Guidelines for Water Supply Facilities and Descriptions based on the preliminary survey.

The HMP design was carried out as shown in the design flow chart of seismic retrofitting in Fig. 2. When selecting a construction method (1), it was decided to use the micropile method with small boring machines because of construction limitations in reinforcing the existing structure. The HMP method with the relatively high resistance shown in Table 1 was used with micropiles capable of resisting Level 2 seismic vibrations for structures with tough allowable deformation.

Here, in sharing loads (2), the total weight of the building frame itself was borne by the existing foundations, while the weight of the internal water, new footings, soil over the footings, and the inertial force during an earthquake were borne by the existing foundations and the HMP spring rigidity. In sharing loads (3), all loads were borne by the existing foundations and the HMP spring rigidity. The HMP method enhances the earthquake-resistant capabilities of a flexible structure with relatively low rigidity by providing small diameter piles that are incorporated into the existing structure.

4 REINFORCEMENT WORK

4.1 Outline of the work

The water service tower is positioned inside the water purification plant located on the top of a hill, and

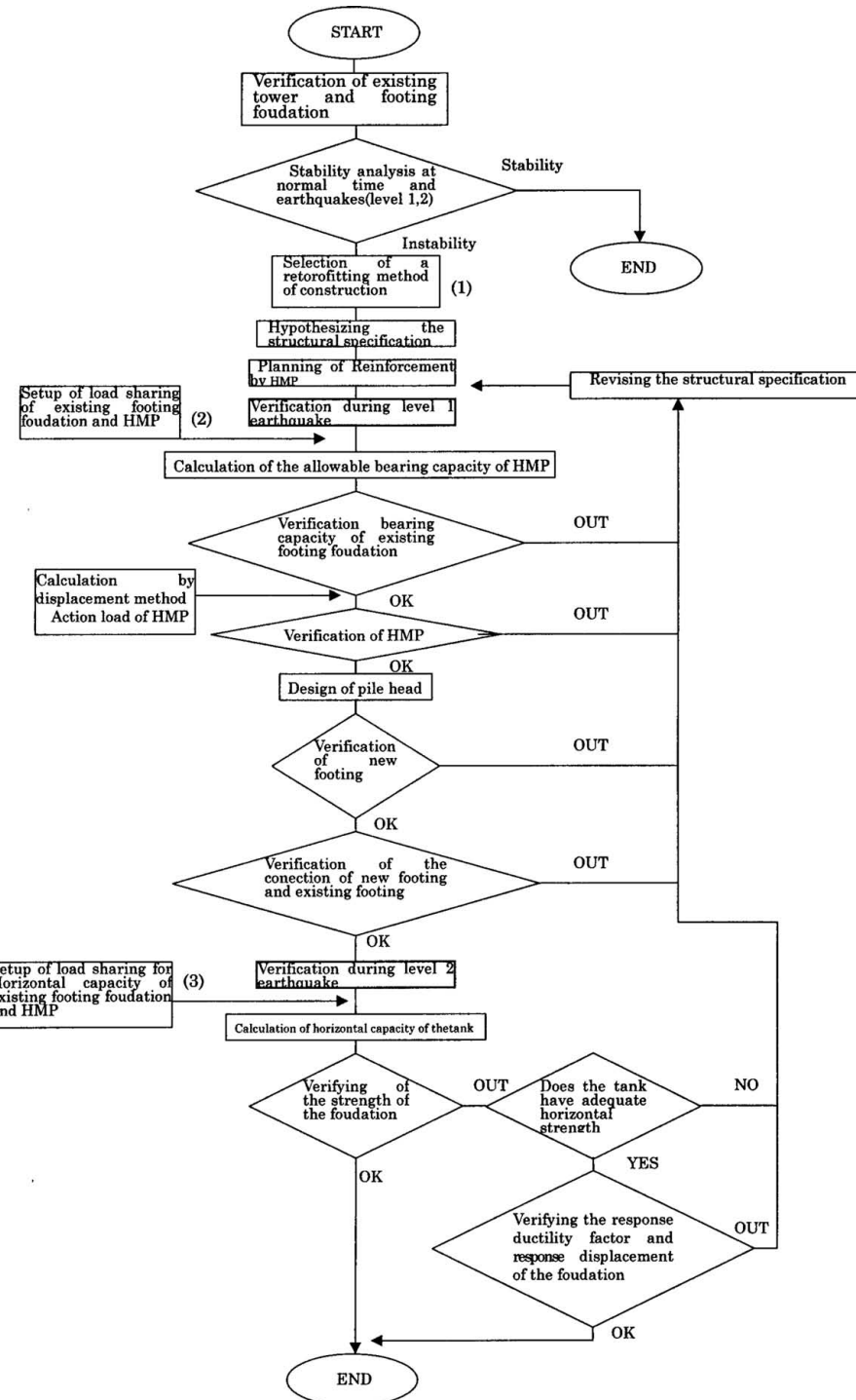


Figure 2. Design flow chart seismic.

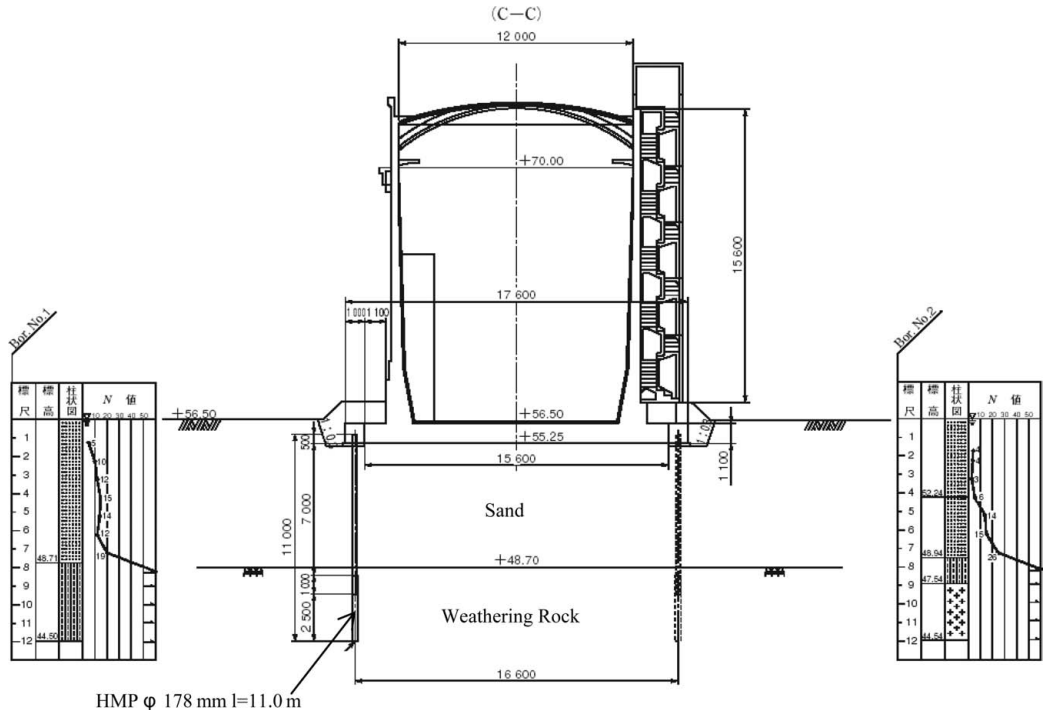


Figure 3. Cross section of planning.

Table 2. Outline of project.

Construction scale

HMP	Number of pile	32
	Pile length	352.0 m
	Length of boring	336.0 m
	Length of steel pipe	272.0 m
	Composition	Steel pipe(API-N50) ϕ 177.8 mm t 12.7 mm Deformed bar (SD490) D51 Grout (cement milk) $f_{ck} = 30 \text{ N/mm}^2$
New footing	V	56.04 m^3

Construction period Sep. 3.2002 ~ Mar.20.2003

constructed with a spread foundation on sandy soil layer (N-value: 4 ~ 26) with a surface thickness of 7.5 m~7.8 m on a weathered granite base. As shown in Table 2 and Fig. 3, the seismic retrofitting consisted of placing HMP piles around the tower foundation and new footings to connect the pile heads and the existing foundation.

The HMP shown in Fig. 4 is 11.0 m long in total, consisting of a 0.5 meter-long steel pipe head, an

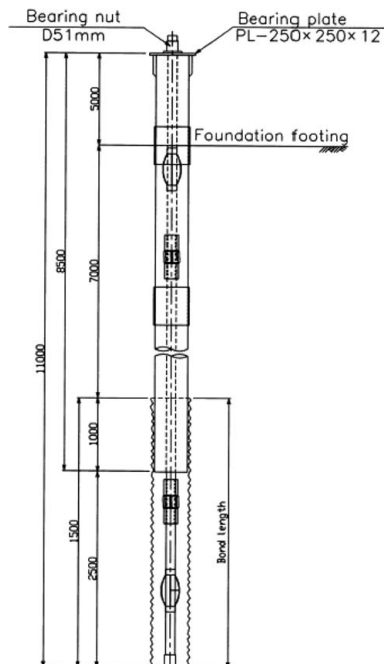


Figure 4. Structure of the pile.

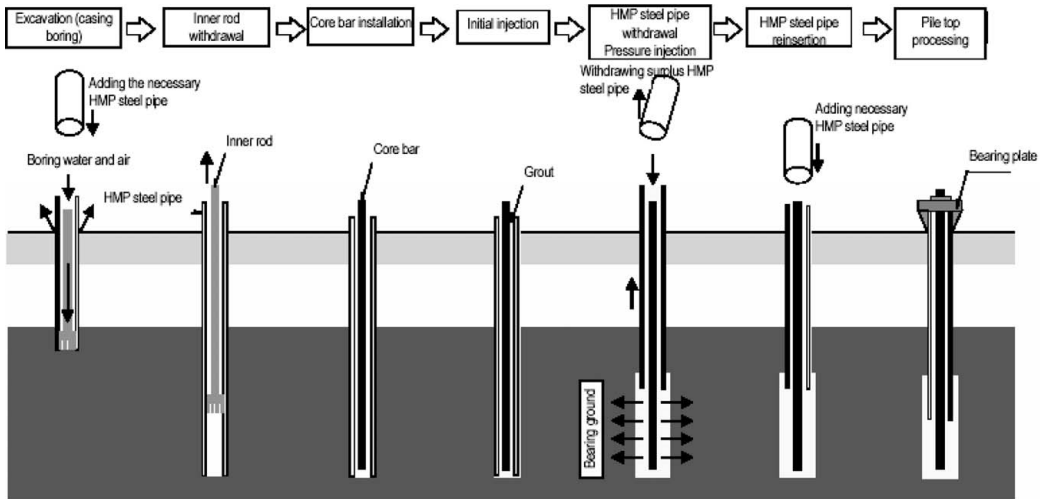


Figure 5. Execution procedure of HMP.



Photo 3. Boring for HMP placing.



Photo 5. Completion of the work.



Photo 4. Construction of new footing.

8.0 meter-long steel pipe, and a 2.5 meter non-steel pipe, with steel reinforcing bars laid along its full length. Therefore, it required a 10.5 m boring depth to place a pile unit in the ground. When extracting the steel pipe, after injecting the initial grout, pressurized grout was injected into a 3.5 m stretch of the anchor bond portion in the weathered granite layer that formed the bearing ground.

4.2 Construction process

Piles were emplaced after the perimeter of the circular tower foundation floor was dug to the height of the batholith of the new footing for connecting the pile heads and tower foundation. Before digging, the branches and roots of the ivy that covers the exterior wall were protected from any adverse effects from the construction work.

HMPs were placed following the procedure shown in Fig. 5. Boring was carried out with a boring machine that met the specifications for large diameter ground anchors, using steel pipes as the boring casings (see Photo 3). Finally, HMPs were placed, steel head pipes were attached to the placed steel pipes, and reinforcing bars were laid for the new footing cast in concrete, connecting the HMPs and the tower foundation (Photo 4).

Placing the piles did not interfere with maintaining the tower's function in supply water during the reinforcement work, which was completed without any problems in March 2003 (Photo 5).

5 CONCLUSIONS

The target for improvements to currently existing infrastructures is the construction of environmentally-sound structures that blend with the landscape for which long-term maintenance is accounted for in the life-cycle costs. The HMP method shown in these application examples is making this possible. This is because the method can respond to revisions in the standards for earthquake-resistant structures and to changes in the demands of society to maintain and reinforce existing structures in ways that are not detrimental to the landscape and cultural values.

We consider it our mission to provide further functionality, design, construction, and maintenance that embody quality and integrity, aiming to construct

public structures that will last for the benefit of future generations.

REFERENCES

- Japan Association of high-capacity Micro Piles. 1999. *Design and Construction Manual of High-capacity Micro Piles (draft)*.
- Public Works Research Institute and others.2002. Report on Joint Research on the Development of Seismic Retrofitting Technologies for Existing Foundation (Part 3). *Joint Research Report*. (282).
- Otani, Y., Mega, M., & Hamathuka, S. 1998. Case histories of Micro-piles, *The Foundation Engineering & Equipment*. 26(7).
- Okazaki City Waterworks Bureau. 1996. *Investigation Report of an earthquake disaster measure of Water Service Tower on Rokku (Water purification plant)*.
- Okazaki City Waterworks Bureau. 2001. *Report of Design Work for Seismic Retrofitting Water Service Tower on Rokku (Water purification plant)*.

Field experiment on installation of suction foundation

H. Yamazaki

Port and Airport Research Institute, Yokosuka, Japan

H. Yoshinaga

Ministry of Land, Infrastructure and Transport, Niigata, Japan

K. Kaneda

Port and Airport Research Institute, Yokosuka, Japan

ABSTRACT: A suction foundation is installed by penetration of a cylindrical caisson into the seabed by means of suction force. The penetration gives the foundation advantages such as increases in lateral resistance and bearing capacity. In addition, when a soft soil layer is present over a stiff soil layer, the suction foundation can be constructed without any soil improvement, because the caisson has penetrated the soft layer to the stiff layer. The paper describes a field experiment conducted to examine the installation process of the foundation.

1 INTRODUCTION

As shown in Figure 1, a suction foundation is installed by penetration of a bottom-open cylindrical caisson into the seabed by means of suction force. The penetration enhances the horizontal resistance of the foundation, due to the passive earth pressure. In the case where soft soil layers are present, the foundation can obtain sufficient bearing capacity, without any soil improvement, by penetration into the stiff soil layer. The foundation is anticipated to be applied to marine structures such as breakwaters and quay walls, or to situations where a soft layer overlies a stiff layer.

In this paper, the design method for installation of the suction foundation and its field experiment are described.

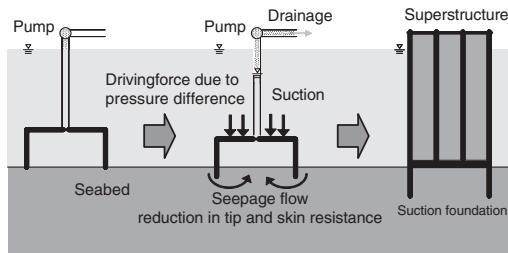


Figure 1. Penetration of the suction foundation.

2 INSTALLATION OF SUCTION FOUNDATION

2.1 Suction for penetration

The forces considered in the penetration of suction foundations are depicted in Figure 2 (after Zen et al. 1998). Suction is applied to the inside of the open-bottom caisson by pumping water out of the caisson. The reduction in water pressure inside the caisson

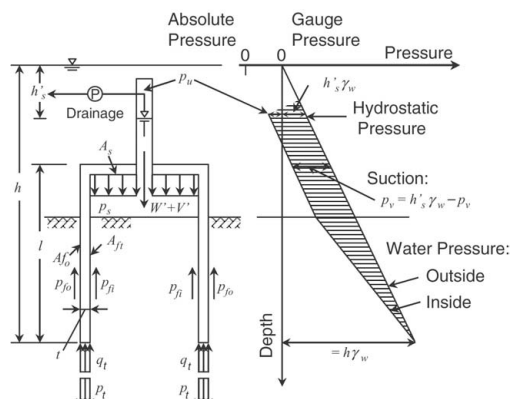


Figure 2. Forces acting on suction foundation in penetration.

produces the suction, and the suction p_s is given by the following equation.

$$p_s = h'_s \cdot \gamma_w - p_v \quad (1)$$

where h'_s = water head reduction, p_v = pressure inside the caisson, and γ_w = unit weight of sea water.

The penetration force F_D acting on the caisson is the sum of the suction force and the combined weight of the caisson and ballast placed on the caisson. The resistance F_R against the penetration is the sum of the skin friction and tip resistance of the caisson. F_D and F_R are expressed by the following equations.

$$F_D = p_s \cdot A_s + P_t \cdot A_t + W' + V' \quad (2)$$

$$F_R = p_{fo} \cdot A_{fo} + p_{fi} \cdot A_{fi} + q_t \cdot A_t \quad (3)$$

where A_s = sectional area inside the caisson, A_t = the tip area of the caisson wall, W' = effective weight of the caisson, V' = effective weight of the ballast p_{fo} and p_{fi} = outside skin resistance and inside skin resistance of the caisson, q_t = the tip resistance of the caisson wall, A_{fo} and A_{fi} = outside and inside surface area of the caisson wall, and p_t = suction at tip. (Hereafter, subscript “_o” or “_{out}” indicates the outside of the caisson, and “_i” or “_{in}” indicates the inside of the caisson.)

Suction necessary for the penetration, lower limit suction, is given by following equations.

$$F = \frac{F_D}{F_R} \quad (4)$$

$$p_s = \frac{F \cdot (p_{fo} \cdot A_{fo} + p_{fi} \cdot A_{fi} + q_t \cdot A_t) - (P_t \cdot A_t + W' + V')}{A_s} \quad (5)$$

where F = safety factor for the penetration.

In the case where suction becomes very large, the upward flow due to the suction causes boiling, heaving, or disturbance of the soil, and the penetration may become difficult. Therefore, there exists a critical suction to be applied, called upper limit suction. The upper limit suction that causes boiling is estimated by Terzaghi's method.

2.2 Penetration resistance

As shown in Figure 2, resistance against penetration is the sum of skin resistance and tip resistance of the caisson wall. The skin resistance and tip resistance of the caisson wall are given by following equations summing frictional resistances and cohesive resistances.

$$p_{fi} = \mu \cdot K_{in} \cdot \sigma_{vin} + c_h \quad (6)$$

$$p_{fo} = \mu \cdot K_{out} \cdot \sigma_{vout} + c_h \quad (7)$$

$$c_h = \alpha_c \cdot c_u \quad (8)$$

where μ = skin frictional coefficient of the caisson wall, K_{in} and K_{out} = earth pressure coefficients of the caisson, σ_{vin}' and σ_{vout}' = effective vertical pressures, c_h = adhesion, c_u = undrained shearing resistance, and α_c = adhesive coefficient considering soil disturbance by penetration. The upward seepage forces and closing effect due to the skin resistance should be taken into consideration in the estimate of the effective vertical pressures of the caisson.

The tip resistance of the caisson wall is estimated by the following equation under the assumption that the contact pressure of the caisson wall is equal to a strip load applied over a width and a length equal to the thickness of the caisson wall and the periphery of the caisson, respectively.

$$q_t = s_c \cdot c' \cdot N_c + s_r \cdot \gamma_1' \left(\frac{t}{2} \right) \cdot N_\gamma + s_q \cdot \sigma_v' \cdot N_q \quad (9)$$

where N_c , N_γ , N_q = bearing capacities, c' = cohesive coefficient in terms of effective stress, γ_1' = submerged unit weight of soil beneath the caisson bottom, and s_c , s_γ , s_q = shape factors. ($s_c = 1 + 0.3t/L$, $s_\gamma = 1 - 0.2t/L$, $s_q = 1.0$. t and L = thickness and periphery of the caisson wall.)

The bearing capacity factors are obtained by bearing capacity formulae.

3 FIELD EXPERIMENT

The Niigata port and airport construction office has carried out a field experiment on suction foundations. Design implementation was conducted in accordance with the method described above.

3.1 Outline of the field experiment

Figure 3 shows the plan of the breakwaters and the results of soil investigations at four points in the site. Composite-type breakwaters are constructed on both sides of the breakwaters, from suction foundations, and the total length of the breakwaters is 430 m. The investigations reveal that the site has inhomogeneous soil layer systems.

The seabed surface is located at DL-10 m and it slopes at 1/120. A dense sandy soil layer with N-values of 5 to 30 is located at +10 to -12 m, a stiff clayey soil layer with unconfined compressive strength greater than 100 kN/m² at +12 to -16 m, and a dense sandy soil layer with N-values of 10 to 40 below -16 m.

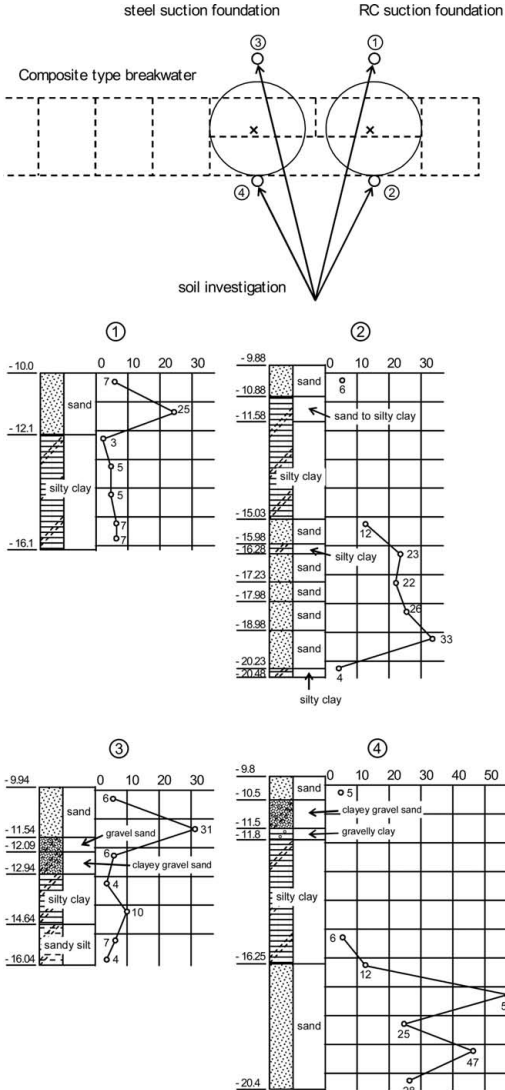


Figure 3. Plan and soil properties of the site.

Significant wave height is 5.7 m, maximum wave height is 8.3 m, and the design wave period is 12.1 s. The tide level is DL + 0.5 m for HWL and DL0 m for LWL. The design wave force acting on the breakwaters is about 1100 kN/m.

Figure 4 shows a breakwater using an RC suction foundation and a breakwater using a steel suction foundation. Hereafter, only the RC suction foundation is described. An open-bottom cylindrical caisson having a height of 8.0 m, a diameter of 21.9 m, a wall thickness of 0.55 m, and a weight of 14000 KN is used

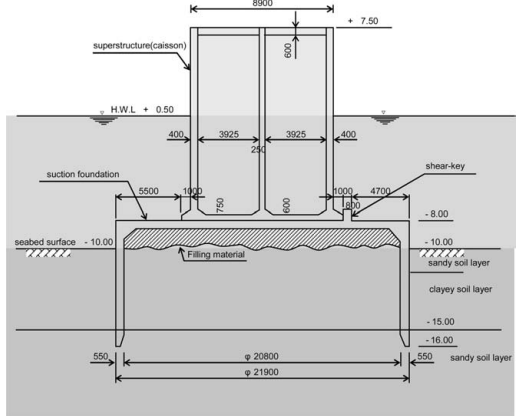


Figure 4. Breakwater with the RC suction foundation.

for the RC suction foundation. A shear key is formed on the upper plate of the cylinder, in order to prevent sliding of the superstructure. The superstructure is a rectangular caisson having a width of 10.9 m, a height of 15.5 m, and a length of 23.9 m.

3.2 Installation

The RC cylindrical caisson was carried by a floating crane having a lifting capacity of 30000 kN, and set on the seabed surface. Ballasts were loaded on the cylinder, because the tip resistance was predicted to be too large for the cylinder to penetrate to the prescribed depth under only suction.

The penetration was conducted by applying suction inside the cylinders with pumps on the floating crane. The pumps were connected to the cylinders through hoses, and pumped water out of the cylinders. Four wires of the crane were connected to the cylinder and controlled its position and inclination during the penetration process. Three open standpipes were equipped on the cylinder to measure water head inside the cylinder and to prevent application of excessive suction or excessive positive pressure.

Transducers for measurement of pore pressures, earth pressures, and wave pressures were provided on the cylinders and the rectangular caissons. Inclinometers and pore pressure transducers were also installed in the seabed to observe the behaviors of the surrounding soils. The uplift forces provided by the four wires of the crane during the penetration were measured with load cells.

3.3 Installation results

Figure 5 shows the time history of discharge by pumping, penetration depth, total uplift forces of the

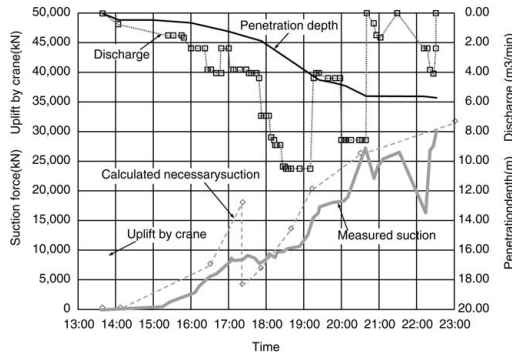


Figure 5. Time history during penetration.

four wires of the crane, design suction force necessary for the penetration, and measured suction force during the penetration. The discharge was not measured by any sensor, but estimated from the nominal values for the valve adjustments of pumps. Measured suction force is a net suction force not including the ballast weight and uplift by the crane, and is equal to the product of the inner area of the cylinder and the measured suction. The required suction force, which is theoretically necessary for the cylinder to penetrate the ground, is calculated by the method described in Chapter 2.

Figure 5 shows that the cylinder was placed on the seabed before 14:00, and the uplift force was gradually released, at which time penetration of the cylinder began due to its weight. The uplift force was not completely released, in consideration of control of the cylinder. Penetration due to the weight stopped around a penetration depth of 0.6 m past 14:00. At that point, penetration of the cylinder using suction force began, finishing at a penetration depth of 6 m past 22:00.

The maximum uplift force necessary for control of the cylinder during the penetration was about 4000 kN. Maximum nominal discharge was 11 m³/min. The required suction force corresponded to the measured suction force.

Table 1 shows parameters of penetration resistance. Skin frictional coefficient μ is defined as the ratio of the friction to the effective normal stress on the cylinder wall. The effective normal stress, which is the effective earth pressure, is obtained by subtracting the measured pore pressure from the measured earth pressure on the cylinder wall. The earth pressure coefficient K is defined as the ratio of the effective horizontal pressure to the effective vertical pressure. The effective horizontal pressure is the effective earth pressure, and the effective vertical pressure is obtained by subtracting the measured pore pressure from the initial effective overburden pressure calculated from the unit weight of the soil and the depth. The adhesive

Table 1. Parameters of penetration resistance.

Parameters	Depth (m)	Inside	Outside
μ	0–1.6	0.675	0.873
κ	0–1.6	0.870	0.954
α_c	2.0	0.08	0.27
α_c	3.0	0.10	0.27
α_c	4.0	0.23	0.35
α_c	5.0	0.28	0.41
Average of α_c	2.0–5.0	0.17	0.33

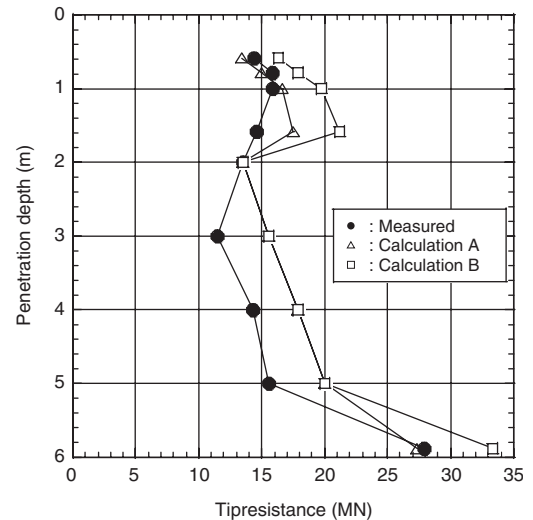


Figure 6. Tip resistance and penetration depth.

coefficient α_c is calculated by dividing the skin friction of the wall by the undrained shear strength c_u of the clayey soil.

From Table 1, the skin frictional coefficients of the cylinder are 0.68 for the inside and 0.87 for the outside, and the earth pressure coefficients are 0.87 for the inside and 0.95 for the outside. The adhesive coefficients are 0.17 for the inside and 0.33 for the outside. The differences in the respective parameters between the inside and the outside of the cylinder are due to the disturbance caused by the soil moving into the inside of the cylinder during the penetration. The earth pressure coefficient at rest, which is usually 0.5, because the horizontal pressure increases by the penetration.

The results of measurement of tip resistance and suction are presented in Figures 6 and 7, along with the tip resistances and necessary suction calculated by the method in Chapter 2. Two calculated results are obtained with respect to the parameters. Calculation

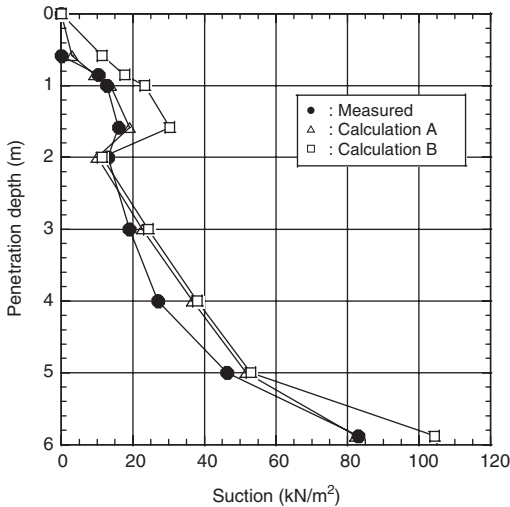


Figure 7. Suction and penetration depth.

A was conducted by correcting the earth pressure coefficients and frictional angles(ϕ) so that the calculated skin frictions and calculated tip resistances obtained the best fit with the measured values at penetration depths of 0 m to 1.6 m. Calculation B was conducted by using the earth pressure coefficients rounded to 1.0 and the measured frictional angles evaluated with the SPT-N values.

As shown in Figure 6, tip resistance rapidly increases at a penetration depth of 0.6 m and decreases at a penetration depth of 0.8 m. Tip resistance increases again at a penetration depth of 3.0 m and rapidly increases at 6.0 m. These changes in tip resistance are ascribed to the changes in soil properties from clayey soil to sandy soil, or from sandy soil to clayey soil. As

shown in Figure 7, suction increases at a penetration depth of 0.6 m. After reaching a maximum value of 16 kN/m² at a penetration depth of 1.6 m, the suction decreases discontinuously, because of the change of soil layers from the upper sandy soil layer to the clayey soil layer, and the suction increases to about 83 kN/m² at the final penetration depth of 6 m.

Comparison of the measured and calculated plots in Figures 6 and 7 shows that, on the whole, the measured plots fit the calculated plots. Therefore, the methods for evaluating tip resistance during penetration and the suction necessary for the penetration are effective if the parameters are appropriately determined.

3.4 Concluding remarks

A design method and a field experiment for the installation of the suction foundations are presented. The results verify that the design method is applicable if the parameters are appropriately determined. The suction foundations are anticipated to be widely applied for offshore structures as well as breakwaters.

REFERENCES

- Zen, K., Yamazaki, H. & Maeda, K. 1998. Case history on the penetration of caisson-type foundations into seabed by use of suction force. *Journal of JSCE*. No.603/III-44: 21–34. (in Japanese)
- Yamazaki, H. & Takahashi, K. 2000. Suction Foundation and case history of its application to breakwaters, *Foundation engineering & Equipment*. 28(1): 74–76. (in Japanese)
- Yamazaki, H., Morikawa, Y. & Koike, F. 2003. Study on design method of suction foundation using model tests. *Soft Ground Engineering in Coastal Areas*: 419–422: BALKEEMA.

Sample of proposal in consulting services using new technology/methods

M. Komatsu

Japan Bridge & Structure Institute, inc., Tokyo, Japan

ABSTRACT: The purpose of this document is to illustrate the present trend in preparing technical proposals for engineering consultancy services. Lately, cost structural reform in public works was implemented and new innovations in technology having proven originality combined with advanced construction methods were being incorporated in most technical proposals by various design and consultancy services firms as a way of gaining advantage over their competitors. As Consultants, the use of new technologies and construction methods in preparing technical proposals is imperative and there are various approaches in arriving to a viable proposal. As an example of those approaches, NETIS was used recently in the preparations and will be described later in this paper.

1 INTRODUCTION

In public work projects, the evolution in bidding systems and budgetary constraints in the design and construction of infrastructures were the primary factors in the conception and introduction of innovative technologies in the design and consultancy services.

Since the enactment and passing of Japanese Bidding Law of 1900 in Japan, a designated competitive bidding system was established and enforced by government authorities as the legal means of public works procurement. In the established a designed competitive bidding system, prospective bidders are pre-qualified to avoid the participation of unsatisfactory entities in the bidding process and to ensure that contracts will be awarded only to qualified or capable bidders.

In 1993 however, a corruption scandal in Japan was uncovered wherein certain general contractors favored by biddings officials in public work contracts through anomalous bidding practices. As a countermeasure, the government authorities in 1994 ensured that future biddings were fair and free of irregularities by introducing an open bidding system to public works projects having a certain minimum estimated amount and cost savings on the government were realized as a result. Some other problems surfaced afterwards however, such as dumping and the use of sub-standard quality of work and construction materials. As a countermeasure, the government in 1997 introduced a new policy of allowing private individuals to propose new alternative technologies and innovations for trials. By

1900	Imperial ordinance on procurement was introduced
	• Introduction of a competitive bidding system
1921	Amend of accountancy law
	• Revisions for a principal open bidding system
1949	Enactment of the construction law
	• Enforcement of the contractor's registration
	• Stipulation of construction contract
	• Appointment of engineers
1958	Practical use of the construction consultants was officially started
1971	Amendment of the construction law
	• From entry system to approval system
	• Adoption of approval system for special construction works
1994	Agreement reached during cabinet meeting
	• Introduction of an open bidding system (regard cost as important)
1996	VE, Design and Build procurement methods were tentatively adopted
1997	Method in utilizing private technology was tentatively adopted
2005	Bill for Ensuring the Quality of Public Works officially became law
	• Evaluation of every factors except the cost

Figure 1. Summary of transition of public works procurement in Japan.

this policy, new proposals having technological originality were evaluated except its cost and subsequently approved for use if its quality is found acceptable.

And as result, new innovations in technology having proven originality combined with advanced project management techniques were being used in most contract proposals lately by design and consultancy services firms as way of gaining advantage over its competitors.

2 COST SAVING POLICY FOR PUBLIC WORKS PROJECTS

As economic condition declined in recent decade in Japan, cost cutting measures in public works projects was implemented based on action plan drawn up in April 1997 and successfully achieved over 20% of cost savings from 1997 to 2000. As the financial condition had stagnated or worsened further during the past few years, a new cost cutting measure called "*cost structural reform in public works*" was implemented in 2003 to cope up with growing budgetary constraints.

Cost structural reform could be carried out in three (3) ways:

1. By optimization in all phases of work from planning / design to project management.
2. By shortening the project completion schedules.
3. By optimization of contract amount through efficient bidding and cost estimation.

As for design and project management Consultants, it would be important to take into consideration Item 1 above. It normally would cover various work actions such as: (a) Shifting to performance specifications of standard criterions. (b) Speed up writing of applicable standard considering the regional conditions. (c) Use of new technology and innovative methods. (d) Reduction of management cost by efficient management.

In foundation structural design, work actions a, b and c above could be used successfully if properly applied. These work actions by the Design Consultants will be discussed in the following chapter below.

3 COST STRUCTURAL REFORM IN PUBLIC WORKS BY THE CONSULTANTS

3.1 *Shifting to performance specifications of standard criterions*

At present, vigorous research works are conducted by several technical committees under Japan Society of Civil Engineers and Japanese Geotechnical Society to be able to draw up an upgraded performance specifications for foundation structural design. Using performance specifications however, has pitfalls such as complicated system of verifying performance and designer's responsibility in structural safety was not

clearly defined. Due to these reasons, using performance specification as standard method in the preparation of proposals for general design and consulting services may not be readily acceptable to the Clients at present.

3.2 *Speed up writing of applicable standard considering the regional conditions*

In structural design of foundations, designs are carried out after the determination of applicable earthquake scale to be used considering the seismic conditions prevailing in the particular region and upon evaluation of the earthquake hazard analysis using the hypo-central fault model. At present however, available data is insufficient and it appeared that more time and resources would be needed to gather sufficient ground information to improve the accuracy and reliability of data obtained due to the enormity of parameter analyses necessary. For that reason, this cost reduction method will not be readily acceptable to the Clients after considering the balance of reliability, safety, economy and rationality.

3.3 *Use of new technology and innovative methods*

New technology and innovative methods could be used in the design proposals by referring from New Technology Information System (NETIS). It is open to the general public on the Internet since the year 2001. Utilization of NETIS is recommended in the design specification of Ministry of Land Infrastructure and Transport and therefore, using it as a means in cost structural reform would be readily acceptable to the Clients. To be assured of the cost reduction and subsequent Client's acceptance, the Consultant should make appropriate verification first before using those new technologies and methods in the preparation of technical proposals.

4 GUIDE IN UTILIZATION OF NEW TECHNOLOGY INFORMATION SYSTEM (NETIS)

Described below is the abbreviated guideline in obtaining valuable technical data on new technology from the Internet using NETIS. (<http://www.kangi.ktr.mlit.go.jp/EvalNetis/NewIndex.asp>)

First, search the NETIS web site in the Internet and look for the particular subject of interest say "Foundation Works" and click the subject to open. Then, the list of new technologies / construction methods in foundation works would be indicated. In such case where a person wishes to have detailed information on any of the new construction methods, a summary of construction methods, originality, applied condition, cost and past experience are available after

selecting the name of the particular construction method. As an example, if someone is interested to know in new technologies on pile foundation, list up the most suitable one for the particular bridge location from all listed construction methods in NETIS. Then, verify the economy, workability and environmental impact, etc., the most suitable construction method could be proposed and adopted after discussion with the particular Client. As an example, the new construction method which is registered with NETIS is shown below Figure 2 to Figure 6.

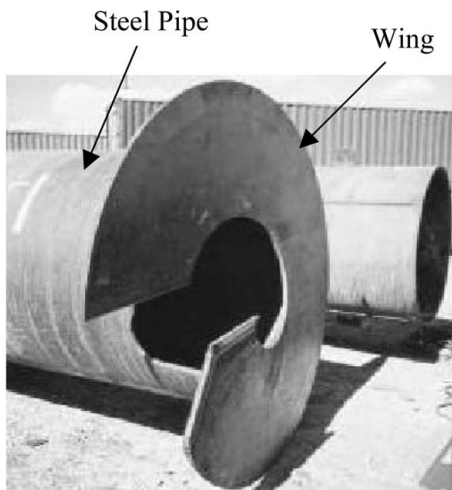


Figure 2. Example of New Technology. (Screwed Steel Pipe)

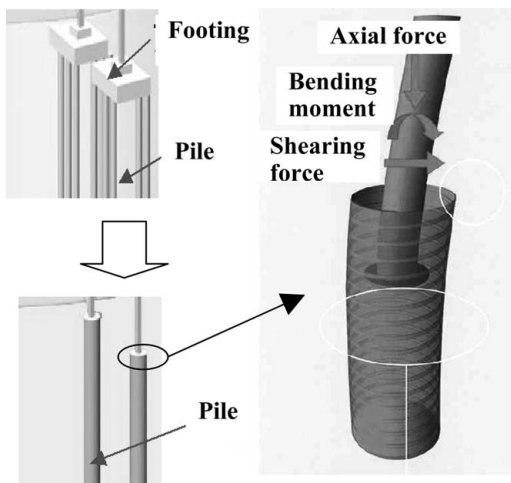


Figure 3. Example of New Technology. (Steel pole in steel pipe pile method)

5 CONCLUSION

In order to comply with the public works cost reduction program required by the authorities and help stabilize the economy at present, it would be necessary for the Consultants to obtain new technology and

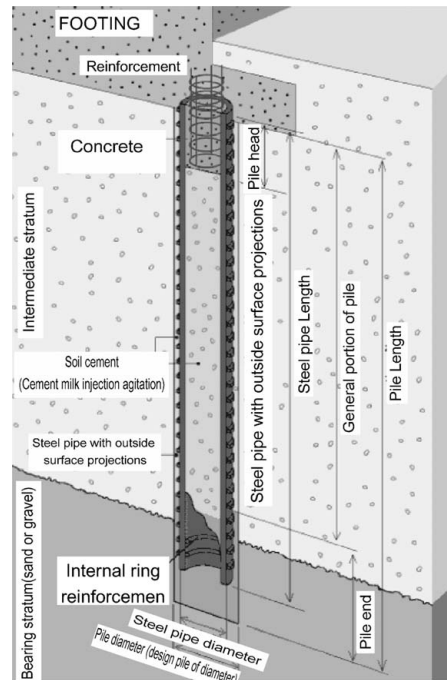


Figure 4. Example of New Technology. (Steel-pipe soil cement pile method)

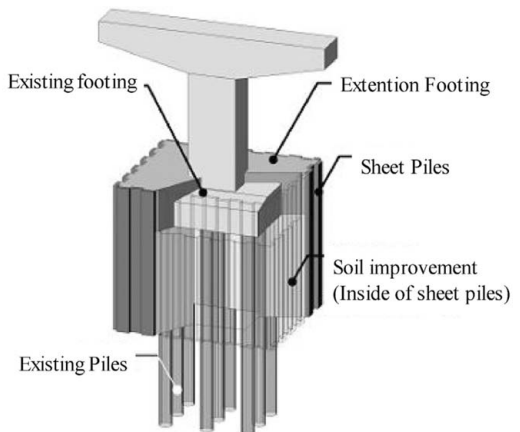


Figure 5. Example of New Technology. (In-Cap method)

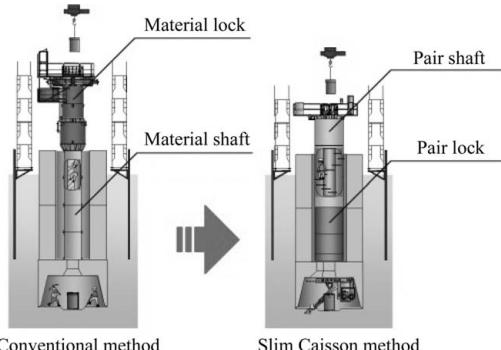


Figure 6. Example of New Technology. (Slim Caisson method)

innovative methods for use in future proposals. There are three(3) cost cutting approaches to be made proposing new technology and construction methods but due to reasons presented in foregoing paragraphs, it

would require a great deal of convincing before Client's approval could be obtained.

As a conclusion, the only cost cutting measure available to the Consultant and acceptable to Clients at present is the use of new technologies and construction methods to meet the limited budget but without sacrificing the quality, structural integrity and safety of public works structures.

REFERENCES

- National Institute for Land and Infrastructure Management. 2006. *NILIM Annual Report 2006*.
- Ministry of Land, and Transport Infrastructure Japan. 2005. *MLIT White Paper 2005*.

Ground improvement

Bearing capacity and settlement behavior of the spread foundation building on improved ground by non-vibratory sand compaction pile method

H. Yoshitomi & T. Ohnishi
Fudo Tetra Corporation, Tokyo, Japan

Y. Yoshinari & T. Umeno
Kumesekkei Corporation, Tokyo, Japan

ABSTRACT: As the sand compaction pile method which is one of the liquefaction prevention methods increases ground density, increases in both vertical bearing capacity and liquefaction strength can be expected as improvement effects. In order to prevent liquefaction and to increase the bearing capacity, a non-vibratory sand compaction pile method was adopted at the senior high school campus construction site, and spread foundation design for the school building was performed. This paper presents the foundation design outline of a building of five stories of reinforced concrete, the results of a plate loading test and rapid loading test and the settlement measurement results by the differential settlement gauge.

1 INTRODUCTION

As the sand compaction pile method which is one of the liquefaction prevention methods increases ground density, increases in both vertical bearing capacity and liquefaction strength can be expected as improvement effects. Therefore, spread foundations on the improved ground using the sand compaction pile can be seen as feasible and economic compared with pile foundations as a design condition. At the senior high school campus construction site, a non-vibratory sand compaction pile method was adopted in the spread foundations of five stories building of reinforced concrete as a liquefaction prevention method and to increase vertical bearing capacity (Yoshinari et al. 2004, Umeno et al. 2004). This paper gives an outline of the foundation design of this building and the confirmation of improved effect.

2 GROUND CONDITIONS AT THE SITE

Soil properties at the site are shown in Figure 1. The upper part is a loose sand layer and lower part is weathering granite. The lowest layer is granite. The loose sand layer liquefies easily as the N-value is

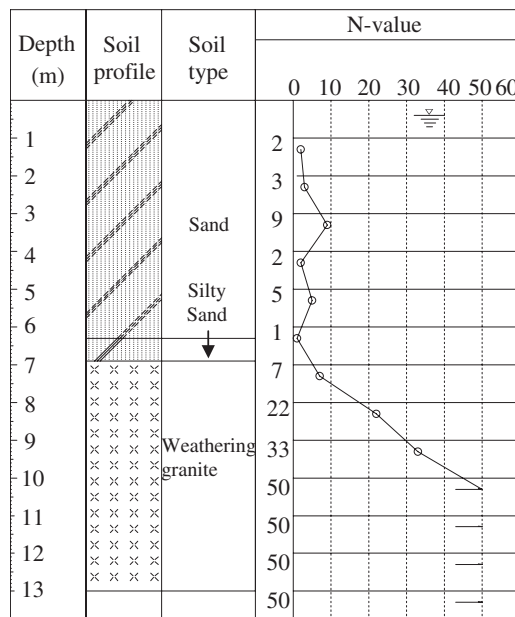


Figure 1. Soil properties.

between 2 and 9, and the fine content is from 8% to 23%. The weathering granite is called ‘Masado.’

3 OUTLINE OF FOUNDATION DESIGN

3.1 Outline of foundation design

The school building has five stories of reinforced concrete and is 23.1 m in height. The foundation arrangement is shown in Figure 2. The foundation type is raft foundation and depth is GL – 2.35 m. The maximum design load at the serviceability limit state is about 130 kN/m² and the maximum design load of the end of the foundations at the damage limit state is about 250 kN/m². The criteria of the foundations and improved ground are shown in Table 1.

3.2 Design of ground improvement

The design procedure of the sand compaction pile is followed as a method for using the “effective compaction rate R_c ”(Yamamoto et al. 2000) and the sand pile interval and increase in N-value is calculated. As a result of repetition, the following specifications are adopted: the arrangement is a square pattern, the pile diameter is 800 mm, the sand pile interval is 2.3 m and the replacement area ratio as is 9.5%. Improved depth is set to GL-8.6 m for the sand layer as the liquefaction layer. The extent of the improved area is adopted with 1/2 of the improvement depth than the side of the footing beam. Figure 3 shows the arrangement of the sand compaction pile and Figure 4 shows

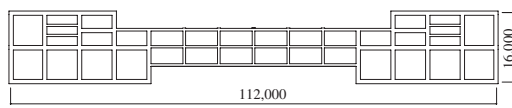


Figure 2. Foundation arrangement.

Table 1. Criteria of the foundations and improved ground.

Limit state	Bearing capacity	Settlement of foundation	Evaluation of liquefaction
Serviceability limit state (Always load)	$q_L \geq 150 \text{ kN/m}^2$	Member rotation angle $\theta \leq 1/1000$	–
Damage limit state (Middle earthquake)	$q_s \geq 300 \text{ kN/m}^2$	–	<ul style="list-style-type: none"> Liquefaction does not occur in a condition of $\alpha_{\max}^{*1} = 160(\text{cm/s}^2)$ Safety factor against liquefaction $F_l > 1.0$ at all depth. Degree of liquefaction is slight in a condition of $\alpha_{\max} = 320(\text{cm/s}^2)$ Earth surface displacement due to dynamic loading $D_{cy}^{*2} \leq 5.0 \text{ cm}$.
Ultimate limit state (Large earthquake)	–	–	

*1 α_{\max} : Design acceleration in the horizontal direction at the ground surface.

*2 D_{cy} : Specified in “Recommendation for Design of Building Foundations”.

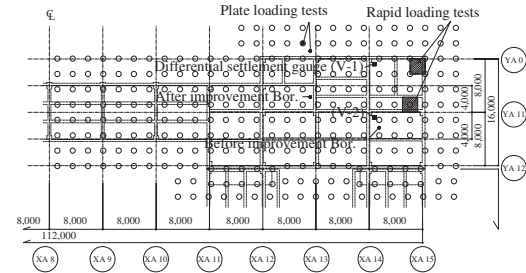


Figure 3. Arrangement of sand compaction pile method.

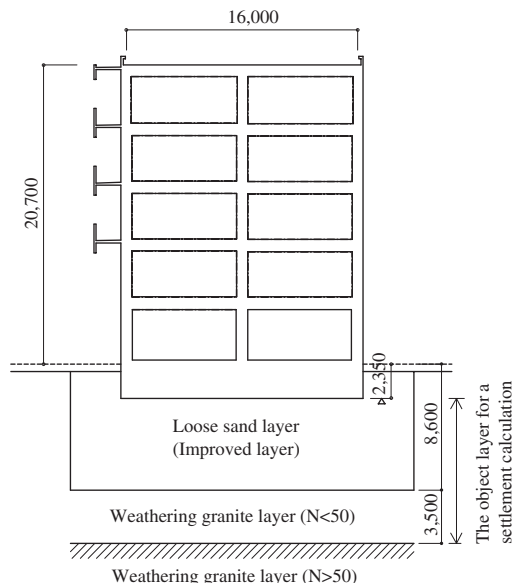


Figure 4. Cross section.

the cross section. In addition, granulated-blast-furnace-slag is used as the supplied material.

3.3 Prediction of immediate settlement after improvements

Immediate settlement is calculated with a lattice beam model considering the rigidity of beam, and the ground spring is calculated with a Steinbrenner approximation solution. The ground model is a two-layered model consisting of both a loose sand layer and a weathering granite layer. The modulus of deformation E of each layer is calculated as $E = 1400 \text{ N} (\text{kN}/\text{m}^2)$. Here, the adopted N-value of the loose sand layer is the average N-value after improvements and that of the weathering granite is the average N-value. Figure 5 shows the contour of immediate settlement considering the rigidity of the beam. The member rotation angle is less than $1/1,000$ at the maximum and satisfies the criteria. In addition, the foundation section is set to $B = 1 \text{ m}$, $D = 2.15 \text{ m}$ considering the differential settlement.

4 CONFIRMATION OF IMPROVED EFFECT

A standard penetration test was performed after the improvements by the non-vibratory sand compaction pile method to evaluate the vertical bearing capacity of the improved ground. The investigation position is shown in Figure 3. The N-value of the improved ground between the sand piles is shown in Figure 6. The average N-value of the improved ground needed to satisfy the bearing capacity is 9 or more.

5 PLATE LOADING TEST

A plate loading test using a 30 cm diameter plate was carried out between sand piles and at the center of the sand piles after the improvement. The level of the plate is the bottom of the raft foundation. The plate

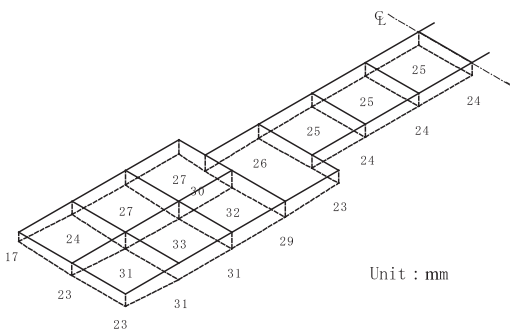


Figure 5. Contour of immediate settlement.

loading test was also performed at the unimproved ground. Figure 7 shows the relationship between the load and settlement. In this figure, it is confirmed that the modulus of deformation and bearing capacity of the improved ground increase together compared to the unimproved ground. On the other hand, the modulus of deformation of the test at the center of the sand pile is similar to that between the sand piles. However, the bearing capacity of the test at the center of the sand pile is larger than that between the sand piles. As the settlement of improved ground both at the center of the sand pile and between the sand piles did not increase at load level $800 \text{ kN}/\text{m}^2$, the ultimate bearing capacity is assumed to be greater than $800 \text{ kN}/\text{m}^2$. So it is

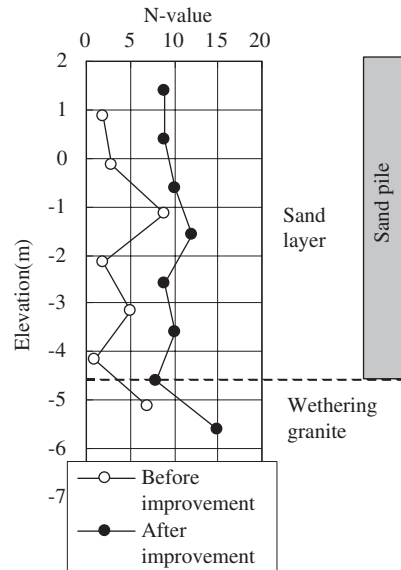


Figure 6. N-value of before and after improvement.

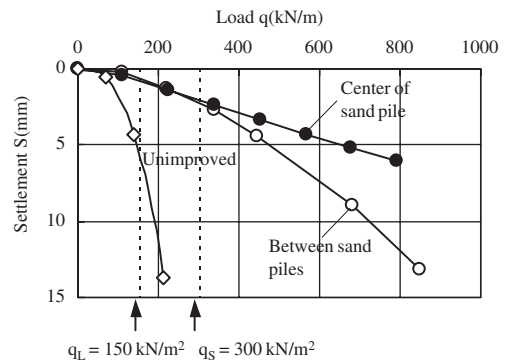


Figure 7. Relationship between the load and settlement of plate loading tests.

confirmed that the bearing capacity of the improved ground satisfies the criteria.

6 RAPID LOADING TEST USING THE LARGE SCALE PLATE

A rapid loading test was carried out to confirm the bearing capacity and rigidity of improved ground at the serviceability limit state level. The loading plate is a steel plate square of 2.3 m, the same size as the interval between the sand piles, and the thickness of the plate is 24 cm. Two kinds of test were performed. One was the case in which the center of the plate is placed at the center of the sand piles (Case 1), and the other is the case in which the four corners of the plate are placed on four sand piles (Case 2). In this test, a weight of 50 kN was dropped from a height of 10 cm to 100 cm step by step through cushioning on a plate and the settlement was measured by an optical displacement gauge every 1/1,000 seconds. The proce-

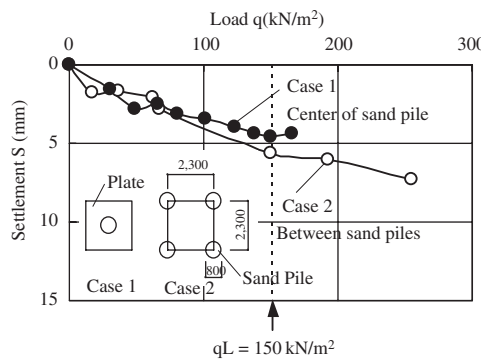


Figure 8. Relationship between the load and settlement of rapid loading tests.

dure of calculating the static load-displacement relationship follows Kubo et al. (2003). Figure 8 shows the relationship between load and settlement for this test. There were no differences in the test between Case 1 and Case 2. The behavior of the improved ground appears elastic at the serviceability limit level 150 kN/m².

7 DIFFERENTIAL SETTLEMENT

Figure 9 shows the depth of the differential settlement gauge. The differential settlement gauge is set at two points. One is the circumference of the building(V-1) and the other is the center of the building(V-2). Differential settlement was measured from the start to completion of the building. The depth of the differential settlement gauge is DL-6.25 m and standard point is DL-11.05 m. Here, the bottom level of the raft

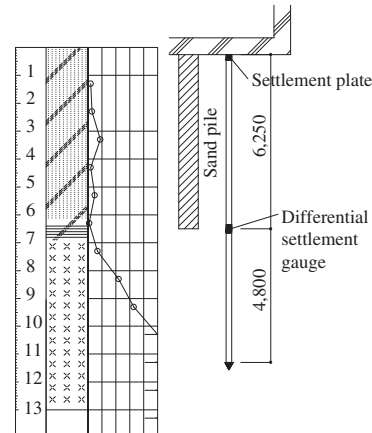


Figure 9. Depth of the differential settlement gauge.

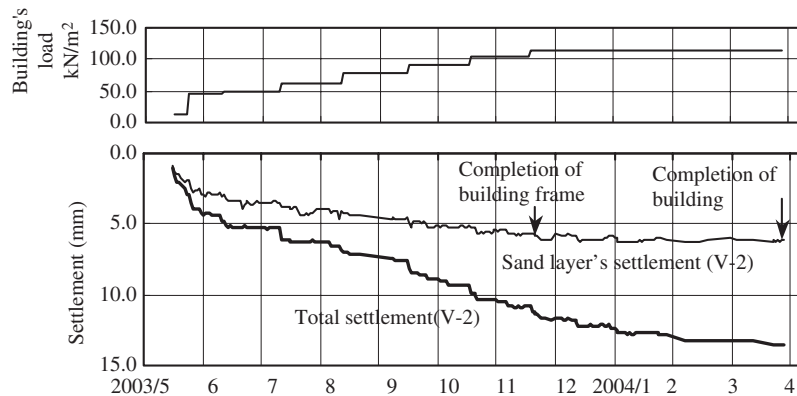


Figure 10. Measurement result at V-2.

foundations is DL 0.0 m. It was confirmed from the settlement measurement results that settlement at the circumference of the building is about 11 mm, settlement at the center of the building is about 14 mm, relative settlement is about 3 mm and the member rotation angle is 1/2, 667. This result has no effect on the use of the building. Figure 10 shows the measurement result at V-2.

After February, settlement almost converges. In addition, the increase of settlement occurring after the building frame is completed depends mainly on the mechanic foundations of the roof and other areas. Because the rigidity of the raft foundations was ignored, evaluating the modulus of deformation of the improved ground into small values, the measured settlement was considered to be less than the predicted value.

8 CONCLUSION

Spread foundations were built on sandy ground improved by a non-vibratory sand compaction pile method. As a result of carrying out the plate loading test and measuring the settlement, it was confirmed that the improvement ground satisfies the criteria.

The authors are grateful to both the client and to the working members.

REFERENCES

- Yoshinari, Y., Umeno, T., Yoshitomi, H. & Ohnishi, T. 2004. Bearing Capacity and Settlement Behavior of Building on Spread Foundation of Ground Improved by Non-vibratory Sand Compaction Pile Method (Part 1,Part 2). *Summaries of Technical papers of Annual Meeting Architectural Institute of Japan*: 389–392. (in Japanese)
- Umeno, T. & Yoshinari, Y. 2004. The school plant supported directly on the improved ground by compaction pile method. *The Kenchiku Gijutsu* 656: 144–145. (in Japanese)
- Architectural Institute of Japan 2001. *Recommendation for Design of Building Foundations*.
- Yamamoto, M., Harada, K. & Nodu, M. 2000. New Design of Sand Compaction Pile for Preventing Liquefaction in Loose Sandy Ground, *Tsuchi-to Kiso* 48(11): 17–20. (in Japanese)
- Kubo, Y., Minagawa, K., Fujisawa, H., Sakagami, E., Kuwabara, F., Abe, A., Wakame, Y., Sato, T. & Tashiro, I. 2003. Applicability of Simple Simulation Method for Rapid Load Test for Pile. *Proceedings of 39th Japanese Conference on Geotechnical Engineering*: 1391–1392. (in Japanese)

Centrifuge model tests on deep mixing column failure under embankment loading

M. Kitazume

Port and Airport Research Institute, Yokosuka, Japan

K. Maruyama

Geo-design Co. Ltd., Tokyo, Japan

ABSTRACT: The Deep Mixing Method, an in-situ soil stabilization technique using cement and/or lime, is often applied to improve soft soils. The group column type improvement is extensively applied to stabilize foundations of embankment or lightweight structures. The improved ground design procedure in Japan assumes two failure patterns related to external and internal stabilities. External stability is evaluated for the possibility of sliding failure, in which DM columns and clay between show horizontal displacement on a stiff layer without any rearrangement of columns. For internal stability, the possibility of rupture breaking failure is evaluated by slip circle analysis, assuming the shear failure mode of DM columns. In this study, a series of centrifuge model tests was carried out to investigate the internal stability of improved ground under embankment loading.

1 INTRODUCTION

The Deep Mixing Method, an in-situ soil stabilization technique using cement and/or lime, is often applied to improve soft soils (CDIT 2002). The group column type improvement is extensively applied to stabilize foundations of embankment or lightweight structures. The Japanese current design method, established for reinforcing embankment (PWRC 2004), assumes two failure patterns related to external and internal stabilities. For internal stability, the possibility of rupture breaking failure is evaluated by slip circle analysis, assuming the shear failure mode of DM columns.

Recent research results revealed that the failure pattern is not same as the practical behavior and the current design method overestimates the stabilities. The authors conducted a research project on the failure mechanism and stability of group column type improved ground subjected to embankment loading. The project involved investigating the failure criteria of two stability analyses and the failure pattern related to external and internal stabilities. The research results on external stability have been presented (Kitazume and Maruyama 2005, 2006 and 2007). This study targets the internal stability in which a series of centrifuge model tests was carried out to investigate the effect of DM column strength and improved ground width. In the model tests, the column failure were measured in detail to address the failure mechanism.

This paper describes the failure modes of DM columns and a proposed simple calculation.

2 CENTRIFUGE MODEL TESTS

Figure 1 schematically shows a typical example of model ground setup, in which a normally consolidated clay ground with 20 cm thick and five rows of DM columns are modeled. An embankment is constructed on the model ground by means of an in-flight sand raining device in a 50 g acceleration field. The model ground material and preparation, and the loading procedure were described in detail by Kitazume and Maruyama (2005, 2006 and 2007).

The six model tests of 11 tests were carried out for the internal stability as well as unimproved ground, as summarized in Table 1. In the test series, two cement treated model column, 2cm in diameter and 20cm in length, were used as a DM column (named as Tl-column with q_u of about 400 kN/m² and Th-column with q_u of about 1300 kN/m²). The Tl- and Th-columns were manufactured using a mixture of Kawasaki clay and normal Portland cement. In order to detect the model column failure during embankment loading, a carbon rod was embedded into each column before hardening, as shown in Figure 2. Both ends of the carbon rod were connected to a thin cable to measure electric resistance during the test.

As the carbon has high electrical transfer, its electric resistance is quite low; however, when the carbon rod is broken due to the rupture breaking failure of the column, the electric resistance jumps to infinity. Accordingly, the measurement of electric resistance can be an indicator for detecting the point in time of column failure, although the location of the failure point would not be detected until after the test. In Cases 6 to 11, all the columns embedded in the model ground had a carbon rod, while the electric measurements were conducted in the b, c and d column lines (see Figure 1).

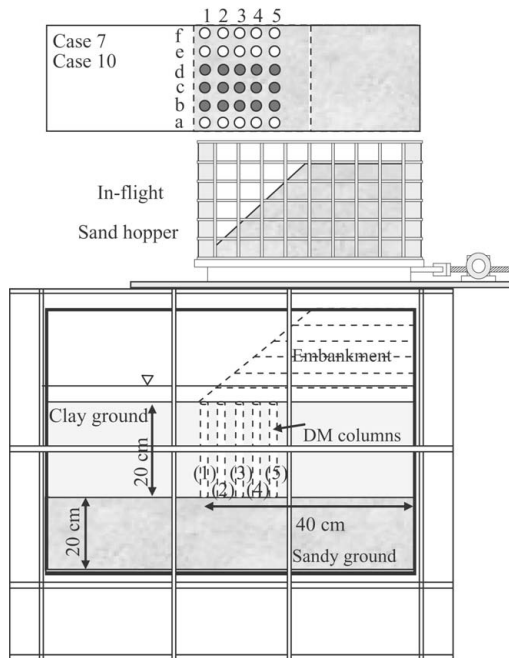


Figure 1. Model ground setup (Cases 7 and 10).

Table 1. Test conditions and major test results.

	Width (cm)	No. of rows	Improvement condition			q_u (kN/m ²)	σ_b (kN/m ²)	Test result
			Improvement area ratio, a_s	Column material	σ_b/q_u			
Case 1	—	—	—	—	—	—	—	10.8
Case 6	8.6	3	0.28	Tl	425	122	16.9–23.7	
Case 7	15.2	5	0.28	Tl	411	131	26.2–35.3	
Case 8	21.8	7	0.28	Tl	391	142	25.4–32.6	
Case 9	8.6	3	0.28	Th	1271	312	33.3–49.7	
Case 10	15.2	5	0.28	Th	1290	367	34.2–50.2	
Case 11	21.8	7	0.28	Th	1434	316	47.9–68.5	

Figure 3 shows the relationship between unconfined compressive strength, q_u , and bending strength, σ_b , measured on the reference columns trimmed to 4 cm in length for the q_u test and 20 cm for the σ_b test. Although there is a lot of scatter in the measured data for Th-column, an average strength ratio of 0.28 was

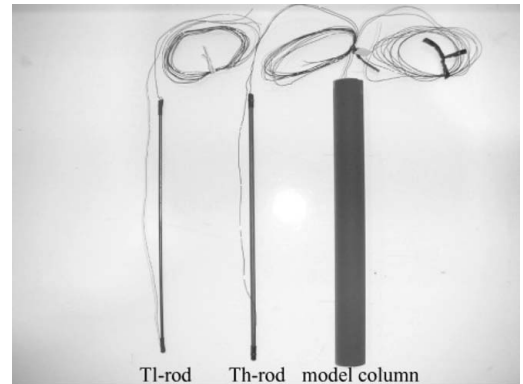


Figure 2. Model column and carbon rods.

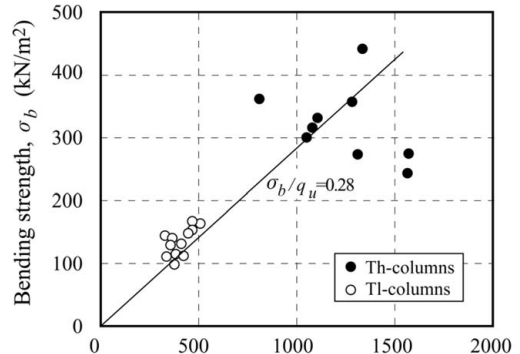


Figure 3. Strength ratio of model columns.

obtained, which is within the range of previous research (Terashi et al. 1980).

3 TEST RESULTS

3.1 Embankment pressure and displacement

The embankment pressure, p_e , and displacement, δ_h , curves of Cases 7 and 10 are plotted in Figure 4. In the figure, the letters beside the curves indicate the point in time and the ID number of the column that shows rupture breaking failure. The column ID is numbered from the forefront column, and the window, as shown in Figure 1.

In Case 7, Tl-1b column failed first at p_e of 26.2 kN/m², and Tl-2b, Tl-2d and Tl-3c failed at the same time. As p_e increased, the columns failed one by one in sequence from the forefront to the rearmost column. A similar phenomenon was observed in Cases 6 and 9. In Case 10, the forefront columns failed one by one at p_e of 34.2 to 50.2 kN/m². When p_e increased to 79.6 kN/m², Th-5b, Th-5c and Th-5d failed instead of the second, third and fourth row columns. After that, Th-4 and Th-3 failed in reverse sequence from the rearmost to the forefront column.

It is of interest to note that p_e continually increases even after many columns fail although the residual strength of cement treated soil is quite low in no confining pressure.

3.2 Column failure

Figures 5(a) and 5(b) show the failure pattern of columns observed after the embankment loading in Cases 7 and 10, respectively. In Case 7, all the columns tilted counterclockwise. As the embankment

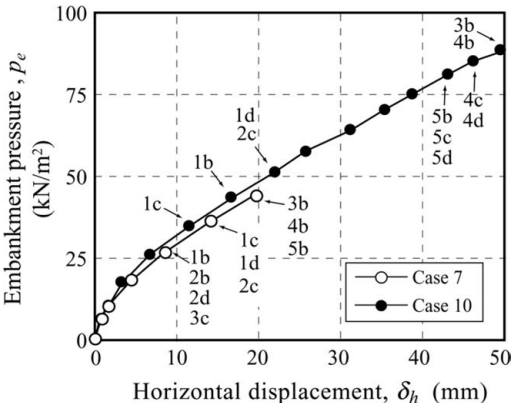


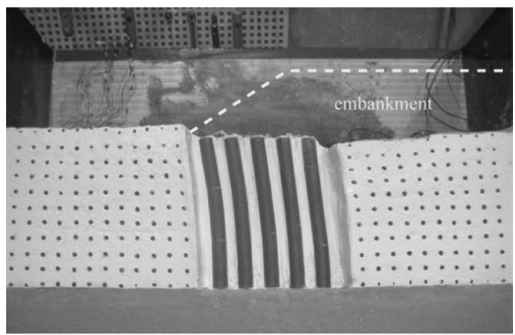
Figure 4. Embankment pressure and horizontal displacement curves together with indication of column failure.

loading was terminated at a relatively small embankment pressure to prevent heavy column failure, the tensile cracks can not be observed clearly in the figure. According to Figure 4, Tl-1b and Tl-2b failed first and then the other three columns, Tl-3b, Tl-4b and Tl-5b, failed at the same p_e of 43.9 kN/m². In Case 10, all the columns tilted counterclockwise at two depths. The figure clearly shows that the column did not fail by shear failure mode but rather by bending failure mode. According to the detailed observation after the test, bending failure took place at a shallow depth first and then at a deep depth.

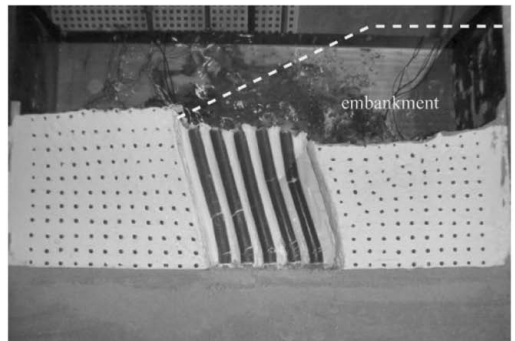
According to the observation, it is found that the DM columns do not fail simultaneously but fail one by one by bending failure mode, and the depth of the bending failure is shallower in the low strength column (Case 7) compared to the high strength column (Case 10), and shallower in the rear side columns compared to the front side columns.

3.3 Ground deformation

The ground deformation obtained after the ground failure is shown in Figure 6 for the unimproved

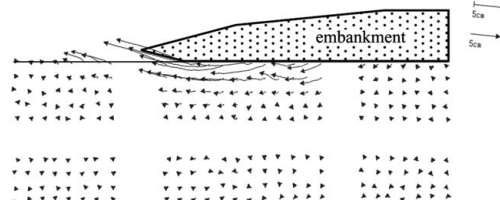


(a) Case 7 (b-line)

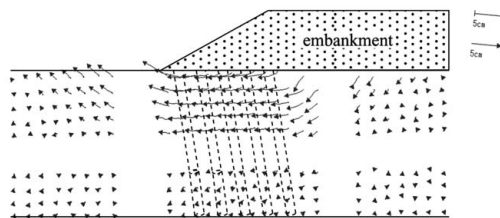


(b) Case 10 (c-line)

Figure 5. Columns' failure.



(a) Unimproved ground (Case 1), $p_e = 47.5 \text{ kN/m}^2$



(b) Improved ground (Case 10), $p_e = 56.5 \text{ kN/m}^2$

Figure 6. Ground deformation.

ground (Case 1) and the improved ground with Th-column (Case 10). The data was obtained by digitizing the coordinates of the target markers placed on the side surface of the model ground. In the case of the unimproved ground (Case 1), a sort of slip circle deformation can be clearly seen at a shallow depth close to the embankment slope. After the ground failure, a large horizontal ground displacement is typically observed with further embankment loading.

In Case 10, a relatively large ground deformation can be seen at a shallow and mid depth. As further embankment loading, the ground displacement increased but no slip circle failure took place. The ground deformation in the other improved ground is very similar to that of Case 10, where no slip circle failure was observed.

It can be concluded that the DM column has the effect of changing the ground failure mode from slip circle failure to collapse failure. The collapse failure pattern rather than the sliding failure pattern is observed in the improved ground.

4 DISCUSSION

A simple calculation based on the bending failure mode is proposed. In the calculation, all the DM columns are assumed to fail simultaneously in bending failure mode and the improved area above a failure plane is assumed to deform as a simple shear.

The relationship between the depth of failure plane, $z_{f,bending}$, and improvement width, D , is shown in Figure 7 for various q_u values. The z_f value increases monotonically with increasing D , and with

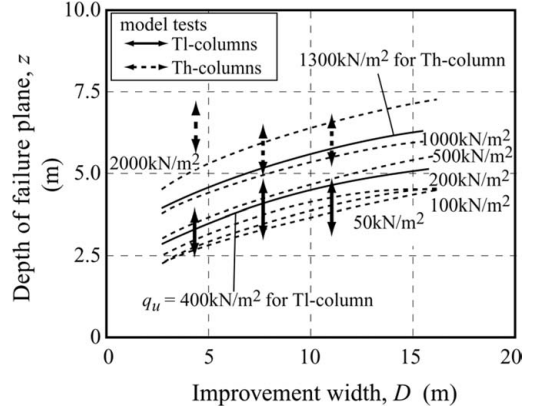


Figure 7. Depth of failure plane and improvement width for bending failure mode.

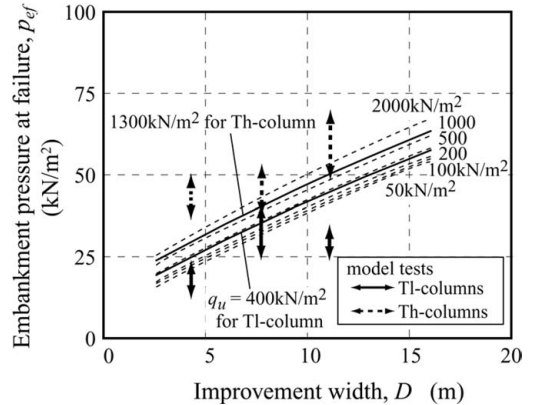


Figure 8. Embankment pressure at ground failure and improvement width for bending failure mode.

increasing q_u . Compared with the tests, the calculation gives a reasonable estimation.

The embankment pressure at ground failure, p_{ef} value increases with increasing D and q_u (Figure 8). The model test results are also plotted in the figure. The measured $p_{ef,bending}$ increases with increasing D and q_u . The calculation gives a reasonable estimation of the $p_{ef,bending}$ value, overestimated in the case of low column strength, but underestimated in the case of high column strength.

Although the proposed calculation is based on simple assumptions, it has high applicability for evaluating the internal stability of group column type improved ground. This demonstrates the importance of simulating an appropriate failure pattern to evaluate the stability accurately.

5 CONCLUSIONS

The failure pattern of group column type DM improved ground under embankment was investigated. The major conclusions derived in this study are as follows:

- (1) The embankment pressure monotonically increases with increasing ground displacement even after many DM columns fail. The embankment pressure at ground failure increases gradually with increasing improvement width and column strength.
- (2) The DM columns fail one by one in the bending failure mode instead of shear failure mode.
- (3) The DM column has the effect of changing the ground failure mode from slip circle failure to collapse failure. The collapse failure pattern rather than the sliding failure pattern is observed in the improved ground.
- (4) A simple calculation based on the bending failure mode of the columns has relatively high applicability for evaluating the internal stability of the ground.
- (5) The importance of simulating an appropriate failure pattern of the DM columns is demonstrated for evaluating the internal stability accurately.

REFERENCES

- Coastal Development Institute of Technology. 2002. *The Deep Mixing Method – Principle, Design and Construction*: A.A. Balkema.
- Kitazume, M. & Maruyama, K. 2005. Collapse failure of group column type deep mixing improved ground under embankment. *Proc. of the International Conference on Deep Mixing – Best Practice and Recent Advances* 1.2: 245–254.
- Kitazume, M. & Maruyama, K. 2006. External stability of group column type deep mixing improved ground under embankment. *Soils and Foundations* 16(3): 323–340.
- Kitazume, M. & Maruyama, K. 2007. Internal stability of group column type deep mixing improved ground under embankment. *Soils and Foundations* (in print).
- Public Work Research Center. 2004. *Design and construction manual on deep mixing method for inland construction* (in Japanese).
- Terashi, M., Tanaka, H., Mitsumoto, T., Niidome, Y. & Honma, S. 1980. Fundamental Properties of Lime and cement treated Soils (2nd Report). *Report of the Port and Harbour Research Institute* 19(1): 33–62 (in Japanese).

Load transfer and failure mechanisms in the reinforced ground beyond vertically loaded pile

J. Hironaka & T. Hirai

Mitsui Chemicals Industrial Products, LTD, Saitama, Japan

Y. Watanabe & J. Otani

GeoX CT Center, Graduate School of Science and Technology, Kumamoto University, Kumamoto, Japan

ABSTRACT: When the embankment is constructed on soft ground, any kinds of geotechnical solutions, for example, pile foundation and deep mixing method, have been used for the purpose of reducing differential settlement. This paper deals with a combined method of pile foundations with earth reinforcement technology using geogrids. This type of the combined method offers decrease of load concentration on soft ground due to the reinforcing effect by geogrids. And it is considered that a search for the load transfer mechanism in three dimensions is important for the performance-based design of this method. Recently, an industrial X-ray CT (Computed Tomography) scanner has been developed and the behavior in the soils could be investigated without any destruction in three dimensions. The objective of this paper is to visualize load transfer mechanism in the system of reinforced soil beyond vertically loaded piles using industrial X-ray CT scanner. A series of model test were conducted. Then, the behavior in the soil was scanned during the settlement of the ground using X-ray CT scanner. Based on these results, the reinforcing effect by the geogrids and the soil arching effect over the pile heads were discussed precisely. And finally, the evaluation of failure mechanism of this system was examined, quantitatively.

1 INTRODUCTION

Construction of embankment on soft ground often causes the differential settlement. Pile foundations with earth reinforcement technology are used in order to reduce this settlement as shown in Figure. 1. This combined method offers the reduction of the loading at soft ground by using geogrids, because the embankment load is transferred to both geogrids and piles in the ground. It is usually considered that the embankment load can be transferred with arching effect in the reinforced soil above the pile heads and membrane effect of geogrids. And it is considered that a search on the load transfer mechanism under this system is important for the performance-based design of this method.

Recently, an industrial X-ray CT (Computed Tomography) scanner which is one of the nondestructive testing method has been used in geotechnical engineering field and the inside behavior of soils can be investigated without any destructions. Authors have conducted a series of studies on the application of industrial X-ray CT scanner to geotechnical engineering such as characterization of soil failure (Otani et al.,

2000) and visualization of the failure in mixed soil with air foams (Otani et al., 2002) and others (Otani & Obara 2003, Otani et al., 2005).

The objective of this paper is to visualize the load transfer and failure mechanisms over the system of earth reinforcement method with pile foundation using industrial X-ray CT scanner. A series of model test are conducted. Then, the behavior in the soil is scanned after the settlement using X-ray CT. Based on these results, the reinforcing effect by geogrid and the soil arching effect over the pile heads are discussed

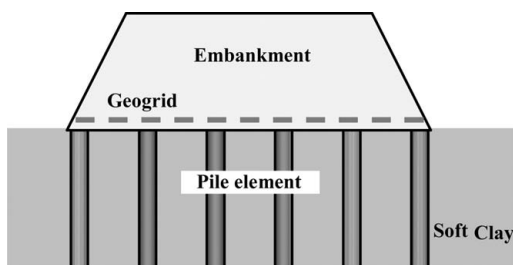


Figure 1. The outline of combined method.

precisely. And finally, the evaluation of failure mechanism of this system is examined, quantitatively.

2 X-RAY CT

The detected data are assembled and the cross sectional images are reconstructed using an image data processing device by means of the filtered back-projection method. By using all these cross sectional images around the circumference of the specimen, three dimensional (3-D) image can also be reconstructed. CT images are constructed by the spatial distribution of so called “*CT-value*” and this is defined as:

$$CT\text{-}value = (\mu_i - \mu_w)\kappa / \mu_w \quad (1)$$

where μ_i : coefficient of absorption at scanning point; μ_w : coefficient of absorption for water; and κ : constant (Hounsfield value). Here, it is noted that this constant is fixed to a value of 1000. Thus, the *CT-value* of air should be –1000 because the coefficient of absorption for air is zero. Likewise, *CT-value* for water is 0 from the definition of Eq. (1). CT images are presented with shaded gray or black color for low *CT-value* and light gray or white color for high *CT-value* in all the subsequent black and white colors. The total number of levels on these colors is 256. It is well known that this *CT-value* is linearly related to the material density. It is noted that the precise contents of X-ray CT method can be obtained in the reference by Otani et al. (2000).

3 TEST PROCEDURE

A series of model tests for different types of geogrids were conducted using newly developed test apparatus as shown in Figure. 2. The case without reinforcement was also conducted in order to discuss the load transfer mechanism with pile foundations. The soil box in the apparatus made by an acrylic mold, which is the size of 200 mm with the height of 126 mm diameter, was set in the CT room. Photo.1 shows the setup of this apparatus on the specimen table in the CT room. A model pile, which was the size of 15 mm diameter, was set on the bottom of the soil box. And, total of four piles were installed at intervals of 45 mm between every adjacent two piles. The settlement plate, which can penetrate through the piles using automatic settlement plate apparatus, was set at the bottom of the ground. The method of pulling down this settlement plate at constant speed was assumed to be the consolidation settlement of the ground due to embankment load. In order to discuss the effect of different soils on the load transfer mechanism, Toyoura sand, Silica sands (No. 7 and No. 8) and Dry clay powder were used. In the case with reinforcements, Toyoura sand was used. The material properties of all

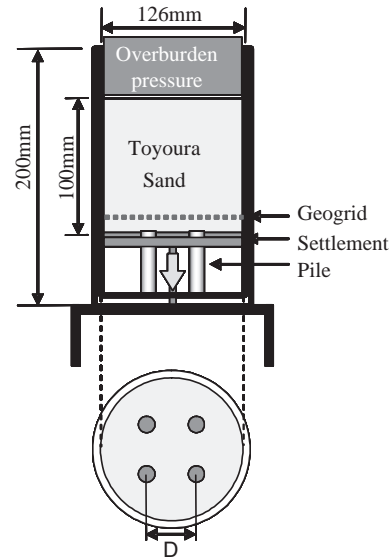


Figure 2. Settlement apparatus.

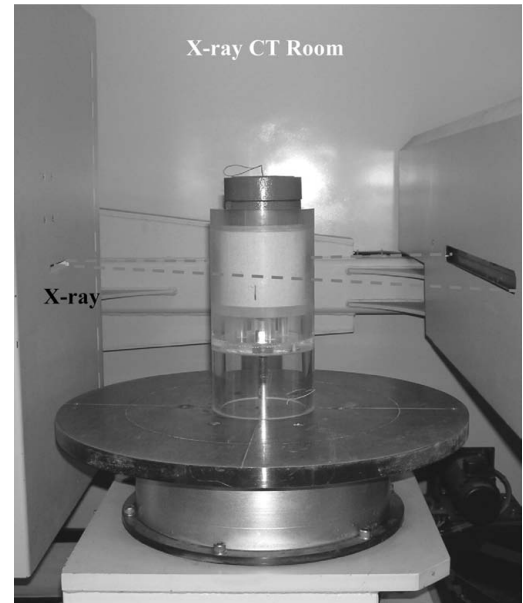


Photo 1. Setup of test apparatus.

the soils are shown in Table 1. In this test, the density was fixed to be the relative density of 80% for all the soils and the overburden pressure of 3.2 kPa was applied by dead-load in order to apply relatively large confining pressure. The settlement plate was pulled down with the loading speed of 1 mm/min under

Table 1. Material properties.

	Effective particle size D_{50} (mm)	Uniformity coefficient U_C	Internal frictional angle φ (deg)
Toyoura sand	0.19	1.56	39.4
Silica sand No.7	0.15	1.63	36.0
Silica sand No.8	0.12	1.86	33.9
Dry clay powder	0.0026	10	25.9

Table 2. Test cases.

	Ground materials	Reinforcement
CASE 1	Toyoura sand	Without
CASE 2	Silica sand No.7	Without
CASE 3	Silica sand No.8	Without
CASE 4	Dry clay powder	Without
CASE 5	Toyoura sand	Grid-A
CASE 6	Toyoura sand	Grid-B

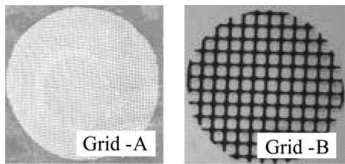


Figure 3. Geogrids.

displacement control and the loading was stopped at the settlement of 5 mm. For the CT scanning, the model grounds at initial and after 5 mm settlement were scanned with 1 mm thickness until the height of 40 mm above the settlement plate. The test cases are listed in Table 2, in which CASE1, CASE2, CASE3, and CASE4 are the cases without reinforcement and CASE5 and CASE6 are the cases with different types of the reinforcements. The load transfer mechanism is examined with CASE1 to CASE4 and the reinforcing effect is discussed with the results of CASE5 and CASE6. Figure.3 shows the materials of geogrid as the reinforcing materials used in this test. Figure.4 shows tensile force – strain relationship for these geogrids, in which Grid-A is a geogrid with its spacing of 2 mm while Grid-B is a geogrid with that of 9 mm. These geogrids were installed at 5 mm height above the pile head in the soil for CASE5 and CASE6.

4 RESULTS AND DISCUSSION

4.1 Load transfer mechanism

Figure.5 shows the results of CT scanning which is the vertical cross sectional images for CASE1, CASE2,

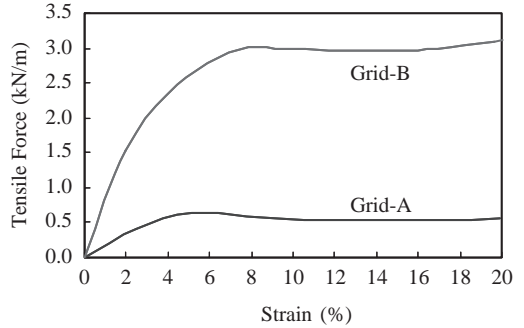


Figure 4. Tensile force – Strain relationship.

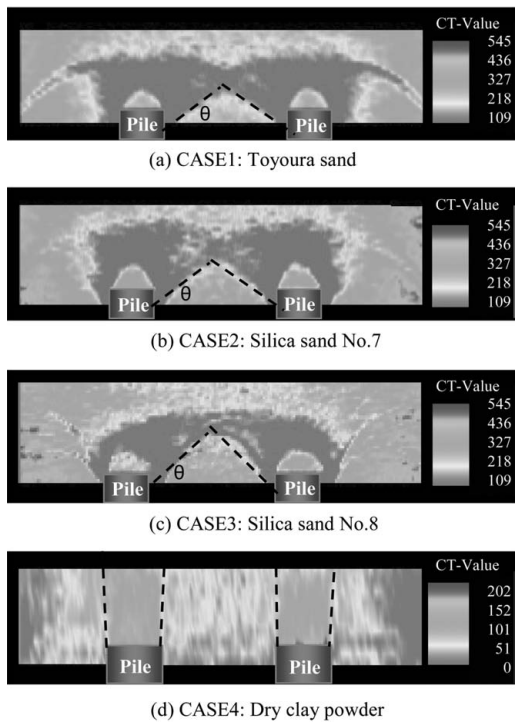
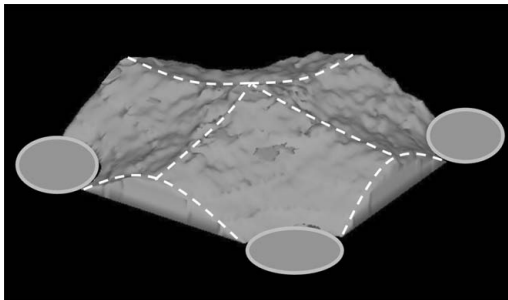
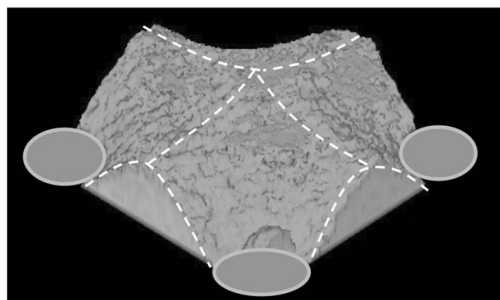


Figure 5. Vertical cross sectional images.

CASE3 and CASE4 at the end of the test. It is observed that there is the area of high density with cone shape at the pile head. And as easily realized, the density around the circumference of the pile head is decreased due to the settlement, which is the appearance of the area of ring shape in CASE1. These low density areas are interrupted in each other for the adjacent two piles at the area of within 10 mm height above the settlement plate. The angle, θ between these interrupted areas which is shown with dotted line in the image was about



(a) CASE1: Toyoura sand



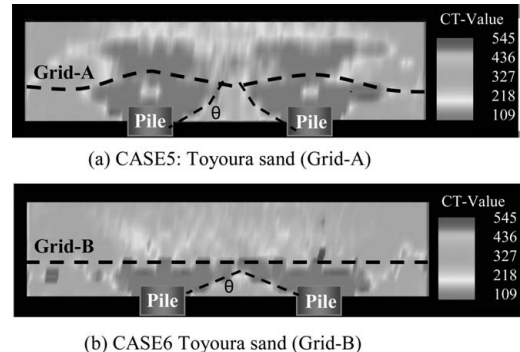
(b) CASE2: Silica sand No.7

Figure 6. 3-D extraction images.

38 degree for the CASE1. Although the behaviour of the density changes for CASE2 and CASE3 were almost the same as CASE1, the angle, θ was 48 degree and 55 degree, respectively. For CASE4, it is totally different from all other results and this angle was almost 90 degree. Based on these results, it is concluded that the smaller the angle, θ is, the wider the load transfer is and this angle becomes larger when the soil strength is smaller. Figure 6 shows some of the examples of 3-D extraction images of the interrupted areas for CASE1 and CASE 2. This 3-D area is considered to be the area where some part of embankment load is applied except that applied on the pile heads. And this model could be used for the design of the reinforced embankment with pile foundations.

4.2 Effect of reinforcement

Figure 7 shows the vertical reconstruction images for the cases with geogrids. These images were reconstructed by the density change using different colours. For CASE5, the area of density change extends to horizontally due to the existence of geogrid. Thus, the angle of density change for CASE5 is decreased due to the effect of Grid-A. For CASE6, the area of changing density was not as large as that of CASE5 and it seems



(a) CASE5: Toyoura sand (Grid-A)

(b) CASE6 Toyoura sand (Grid-B)

Figure 7. Vertical cross sectional images.

that the stress concentration is rather smooth. And the area of density change was observed between the piles and the geogrid. Here, if it is assumed that the transmission of the overburden pressure due to the settlement influences the density change over the pile head, it can be considered that the smaller the angle of this density change is, the wider the load distribution in the ground is. And this can be also considered to be the effect of soil arching and at the same time, the membrane effect due to existing of geogrid.

5 CONCLUSIONS

The following conclusions are drawn from this study:

- (1) The load transfer mechanism in embankment beyond pile foundations due to the settlement was observed using X-ray CT scanner; and
- (2) It may be said that earth reinforcement is effective with the use of pile foundations for the purpose of stress re-distribution in the soil.

Finally, it is evident from all the discussion here that the industrial X-ray CT scanner promises to be a powerful tool even for the geotechnical engineering field.

REFERENCES

- Otani, J., Mukunoki, T. & Obara, Y. 2000. Application of X-ray CT method for characterization of failure in soils. *Soils and Foundations* 40(2): 111–118.
- Otani, J., Mukunoki, T. & Obara, Y. 2002. Visualization for engineering property of in-situ light weight soils with air foams. *Soils and Foundations* 42(3): 93–105.
- Otani, J. 2003. State of the art report on geotechnical X-ray CT research at Kumamoto University. *X-ray CT for Geomaterials* : 43–77. Netherlands: Balkema.
- Otani, J., Mukunoki, T. & Sugawara K. 2005. Evaluation of particle crushing in soils using X-ray CT data. *Soils and Foundations* 45(1): 99–108.

Ground improvement for the second phase construction of Kansai International Airport

Y. Morikawa

Port and Airport Research Institute, Foundations Division, Yokosuka, Japan

T. Tabata

Kansai International Airport Land Development Co., Ltd., Izumisano, Japan

T. Emura

Kansai International Airport Co., Ltd., Construction Office, Izumisano, Japan

ABSTRACT: Kansai International Airport was planned as a fundamental solution to the problems of aircraft noise pollution in the area surrounding the existing Osaka International Airport and increasing aviation demand. The new airport was constructed 5 km offshore in Osaka Bay as a manmade island to minimize noise pollution in residential areas and began operation in 1994. A second island, which is being built as a second phase expansion of the airport, is now under construction further offshore than the first island. Since the ground below the construction site consists of many compressible clay layers, the construction of the airport islands was expected to induce large and long-term settlement. This settlement was predicted and reflected in the design of the airport islands. Furthermore, the Holocene clay layer (immediately below the seabed) was improved to complete its settlement during the construction and achieve an early increase in seabed strength. This report describes the ground improvement carried out in the second phase construction of the Kansai International Airport.

1 INTRODUCTION

Kansai International Airport is situated in the southern part of the huge Osaka Bay in the Kansai region of western Japan. The Kansai region accounts for about 20% of Japan's total population, gross domestic product, and value of shipments of industrial products. Despite its prosperity, aviation service had long been limited to the inland Osaka International Airport (Itami Airport). The proximity of Itami Airport to residential areas made it impossible to expand the airport to meet increasing aviation demand. Furthermore, aircraft noise and other environmental problems around the airport had become increasingly serious. Kansai International Airport was planned as a fundamental solution to these problems. The new airport was constructed 5 km offshore in Osaka Bay as a manmade island in order to avoid the impact of aircraft noise on residential areas (Fig. 1). The airport began operation in 1994 as Japan's first 24-hour airport and is playing an important role as an international hub in the global aviation network.

At Kansai International Airport, the number of aircraft take-offs and landings during peak hours is

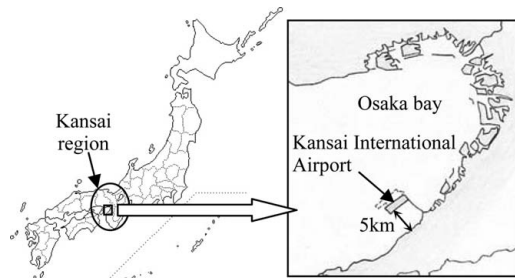


Figure 1. Location of Kansai International Airport.

already close to the airport's handling capacity (30 per hour). In response to requests from both home and abroad to expand its capacity as an international hub airport, the second phase project was started in 1999. Figure 2 shows an image of the airport after completion of the second phase project (Furudoi 2005, Tabata & Morikawa 2005).

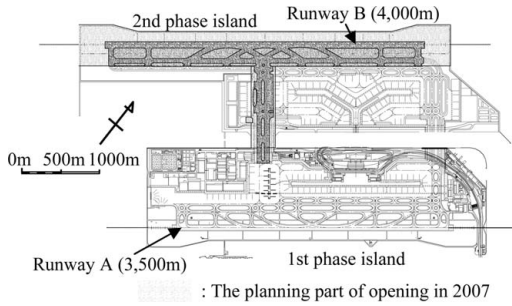


Figure 2. Image of Kansai International Airport after completion of second phase project.

2 SCALE AND NATURAL CONDITION

In the first phase project of Kansai International Airport, an airport island with an area of about 510 ha was reclaimed, on which a 3500 m runway and related facilities were built. This first island was surrounded by an 11 km seawall. About 180 million m^3 of soil was used in the construction of this island.

The second phase project involves development of another manmade island of 545 ha located 200 m offshore from the existing island. Thus, the second phase construction is being conducted under severer conditions than those encountered in the first phase. The thickness of the compressible clay layers and water depth at the second phase construction site are greater than those in the first phase. The second phase island is also expected to settle more than the first phase island, settlement of the second phase island being estimated at about 18 m. The deeper water and greater expected settlement required a thicker layer of reclamation soil. The reclamation layer will have an average thickness of more than 40 m, and is expected to require around 250 million m^3 of soil. A comparison of the scale and natural conditions in the first and second phases is shown in Table 1. In order to complete this larger project under these severe conditions within a limited period (Table 2), the most advanced technologies were employed in combination with the experience accumulated during the first phase construction.

3 GEOTECHNICAL CONDITIONS

3.1 Soil investigations

Detailed investigations of geotechnical properties were conducted prior to commencing the first phase project, which provided information about soil properties and layer configurations. A total of 65 boring explorations were conducted. Two boring excavations were at the -400 m level, and the others were at the -100

Table 1. Comparison of scale and natural conditions between the first and the second phase construction.

	Scale		Natural conditions		
	Reclamation Area	Volume	Seawall length	Water depth	Thickness of compressible clay
1st phase	510 ha	180 Mm^3	11 km	16–19 m	150–200 m
2nd phase	545 ha	250 Mm^3	13 km	18–20 m	250–300 m

(M: million)

Table 2. Construction schedule of the project.

year	1999	2000	2001	2002	2003	2004	2005	2006	2007	
	2nd phase		1st phase							
	Ground improvement	Seawall construction	Rough completion of the seawalls	Completion of reclamation for major airport facilities	Opening of new runway					
year	1987	1988	1989	1990	1991	1992	1993	1994		
	Ground improvement	Seawall construction	Rough completion of the seawalls	Reclamation	Airport facilities				Opening of the airport	

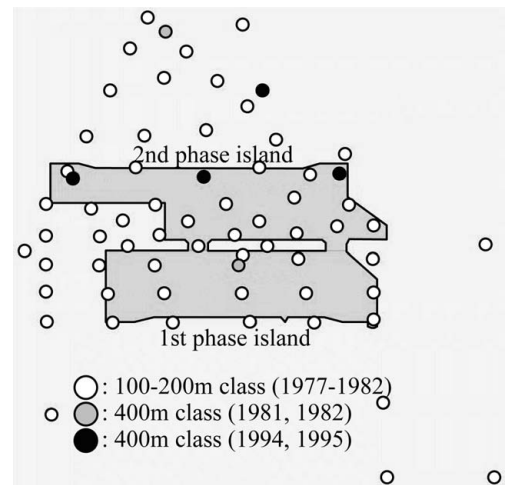


Figure 3. Exploratory boring map of Kansai International Airport site (after Furudoi 2005).

to -200 m level. In addition, four -400 m level boring explorations were conducted before the second phase construction. Figure 3 shows the locations of the boring explorations. The wire line drilling method

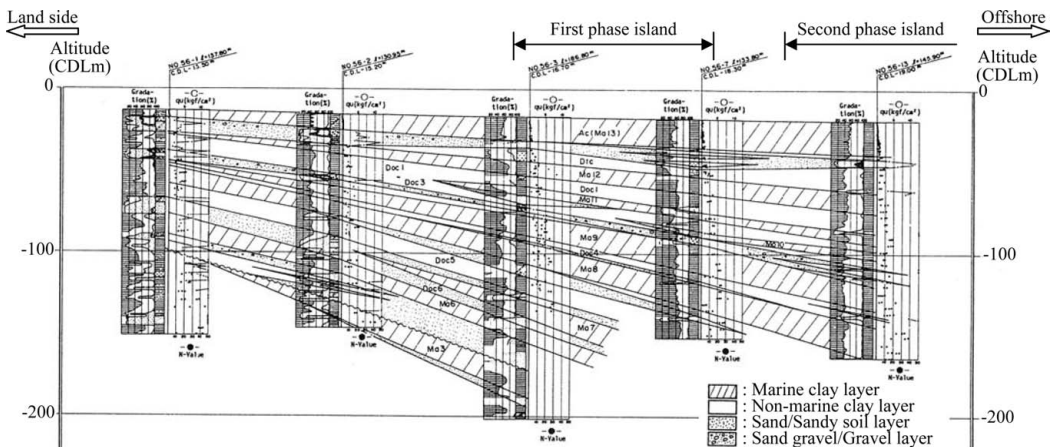


Figure 4. Geotechnical profiles at airport island northern edge line (after Kanda et al. 1991).

developed by the Port and Airport Research Institute (former Port and Harbour Research Institute) was used to ensure high quality and efficiency in boring explorations.

Figure 4 shows the geographical profile estimated using results along the line perpendicular to the airport islands' coastal line, passing through the islands' northern edge. The ground under the seabed of the airport islands consists of a soft layer of Holocene clay and alternative layers of Pleistocene clay and sand. At the second phase construction site, the average thickness of the Holocene clay layer is 25 m, while the total thickness of compressible Pleistocene clay and sand layers amounts to 250–300 m. Pleistocene clay was deposited from 2 million to 10 thousand years ago during repeated glacial and interglacial periods. The "Ma numbers" in Figure 4 are given to marine clay layers in order of decreasing depth. Ma 13 is the Holocene clay layer. Other numbers refer to the Pleistocene clay layers. Because the Osaka Bay seabed slopes and settles toward its center, the strata slope offshore from the coastal line.

The Holocene clay layer was considered to be normally consolidated since its consolidation yield stress is almost equivalent to the effective overburden pressure. Pleistocene clays were considered to be normally consolidated aged clay since they exhibit apparent overconsolidation without a definite mechanical overconsolidation history (Kanda et al. 1991).

The coefficient of volume compressibility m_v and coefficient of consolidation c_v of the Holocene clay obtained from consolidation tests are shown in Figures 5 and 6. These values are similar to those of clays in other regions in Japan. In construction management of the second phase construction, the " m_v method" was employed, and $m_v = 0.13 \bar{p}^{-1}$ (cm^2/kgt) and $c_v = 90$ (cm^2/day) were used (Shinohara 2003). (On the other hand, one-dimensional consolidation

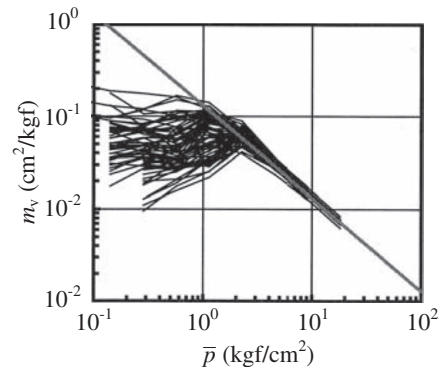


Figure 5. Coefficient of volume compressibility of Holocene clay (after Shinohara 2003).

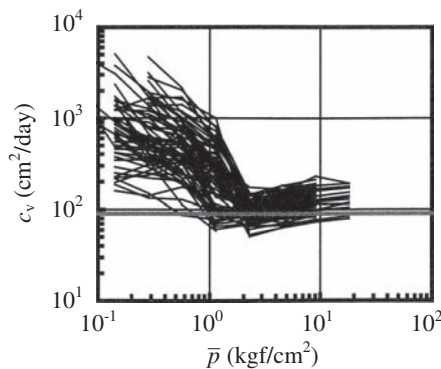


Figure 6. Coefficient of consolidation of Holocene clay (after Shinohara 2003).

analysis and a bilinear elasto-viscoplastic constitutive model were employed in prediction of long-term settlement (Shinohara 2003, Furudoi 2005).)

3.2 Measures against large and long-term settlement in second phase construction

Since thick clay layers exist under the seabed of the second phase construction site, as mentioned earlier, sizable settlement is expected to take place under the large load of reclamation soils. According to the current estimate, settlement of about 12 m will take place in the period from the beginning of construction to the opening of the runway. Residual settlement, which will take place over a 50-year period after the opening of the runway, is expected to be about 6 m (Tabata & Morikawa 2005).

The Holocene clay layer is very thick and compressive, and a large settlement of 8 m is estimated. Therefore, sizable residual settlement will continue over an extended period unless this subsoil layer is improved prior to construction of the island. Moreover, it is very difficult to stabilize the seabed for reclaimed soils during the construction work. Because the Holocene clay layer sits immediately below the dumped and heaped soils, uneven settlement of the Holocene clay layer is expected to have an almost direct effect on the ground surface. Without improvement of this Holocene clay layer, it would have been impossible to complete airport construction within the given period of time, as the reclamation work would have required longer intervals to allow the soil to consolidate. Therefore, a decision was made to improve the Holocene clay layer within the entire construction site by the sand drain method so as to complete its settlement and stabilize the seabed during the construction period.

Pleistocene clay layers exist deeper under the seabed, and from a technical perspective, it is difficult to improve these layers. Therefore, settlement of these Pleistocene clay layers is expected to continue even after the opening of the runway. To maintain the operability of the airport island, it is necessary to take into account the long-term settlement of the Pleistocene clay layers and the associated problems of uneven settlement. Long-term settlement has been predicted carefully, and the airport island was designed to maintain airport functions for over 50 years after opening. Reclamation is being carried out carefully so as to minimize uneven settlement and ensure the thickness of reclaimed soils by properly managing the reclamation work.

4 GROUND IMPROVEMENT OF HOLOCENE CLAY LAYER

4.1 Outline of second phase construction

The second phase construction commenced in July 1999. First, ground improvement works for the

Holocene clay layer were carried out, mainly using the sand drain method. Next, a seawall was built completely surrounding the second phase island site in order to start reclamation. The reclamation work consists of three stages: direct soil-dumping by sand carriers, direct soil-heaping by reclamation barges, and indirect soil-heaping by reclamation barges, followed by soil-spreading by bulldozers and compaction by vibration rollers. Figure 7 shows procedure used in the second phase construction.

4.2 Ground improvement work

The subsoil immediately below the seabed surface consists of a thick, compressible Holocene clay layer, as mentioned above. To ensure stability during seawall construction and reclamation works and minimize residual or uneven settlement after the opening of the airport, ground improvement work was carried out throughout the entire seawall and reclamation areas.

In the second phase construction, as in the first phase, ground improvement by the sand drain method was applied to most parts of the seawall construction area and all of the reclamation area (Fig. 8). In the beginning, an approximately 1.5 m thick sand layer was spread evenly over the seabed, blanketing the entire construction site, as a permeable layer for drained water. Once the sand blanket had been laid, sand piles were driven into the seabed. Sea sands with a fine-grain fraction content of less than 10% were used for both the sand blanket and sand piles to facilitate drainage.

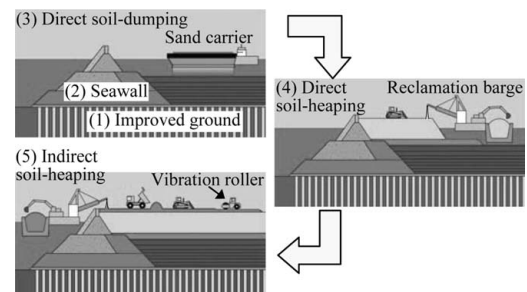


Figure 7. Procedure of second phase construction.

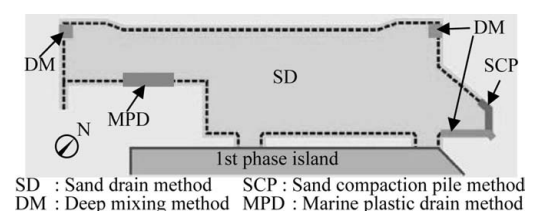


Figure 8. Ground improvement applied in second phase construction.

Using eight large sand-piling barges, each capable of driving 12 sand piles at a time (Fig. 9), about 1.2 million sand piles of 40 cm diameter were driven into the Holocene clay layer, which had an average thickness of approximately 25 m. The spacing of the sand piles was in $2.5\text{ m} \times 2.5\text{ m}$ square grids, with which the settlement of the Holocene clay layer will be completed during the construction period. In the area beneath the seawall, the spacing was set in $1.6\text{ m} \times 2.5\text{ m}$ rectangular grids to achieve early strengthening of the Holocene clay with accelerated consolidation, in consideration of the seawall construction procedure.

Based on the experience from the first phase, a decision was made to drive the sand piles until they reached a sand layer below the Holocene layer so as to ensure effective drainage through the Holocene layer. The sand pile driving operation was carefully controlled to ensure that the pile driver shafts reached the sand layer. This was confirmed by monitoring the penetration resistance, which was estimated from the penetration speed or load (Fig. 10). The criterion of



Figure 9. Sand-piling barge.

penetration resistance used by each sand-piling barge was determined by penetration tests carried out at sites where the Holocene clay layer thickness had been obtained by boring (Tabata & Morikawa 2005). Since each sand pile was very long and thin, extending for a length of 20 m or more, the casing pipe was vibrated with a vibro-hammer to prevent discontinuity. Sand piles were driven at the prescribed points by linking the position control systems of the sand-piling barges with the RTK-GPS.

About 1.2 million sand piles were driven by 8 sand-piling barges over a period of 16 months beginning in August 1999. As a result of the scrupulous management of penetration mentioned above, only 0.01% of the sand piles failed to satisfy the penetration criterion. In almost all cases, failure to satisfy the criterion was caused by unsuccessful data collection.

5 RESULT OF GROUND IMPROVEMENT

At several points in the second phase construction site, the total settlement of the Pleistocene clay layers is being measured in addition to total settlement. An example of the results is shown in Figure 11. The settlement (compression) of the Holocene clay layer can be obtained from the total settlement by subtracting the total settlement of the Pleistocene clay layers, and is also shown in Figure 11. Figure 11 shows that the settlement of the Holocene layer was substantially completed after 2005 when reclamation had been finished at this point. The settlement data for the Holocene layer at other points show the same tendency as in Figure 11. This result suggests that the ground improvement was successful.

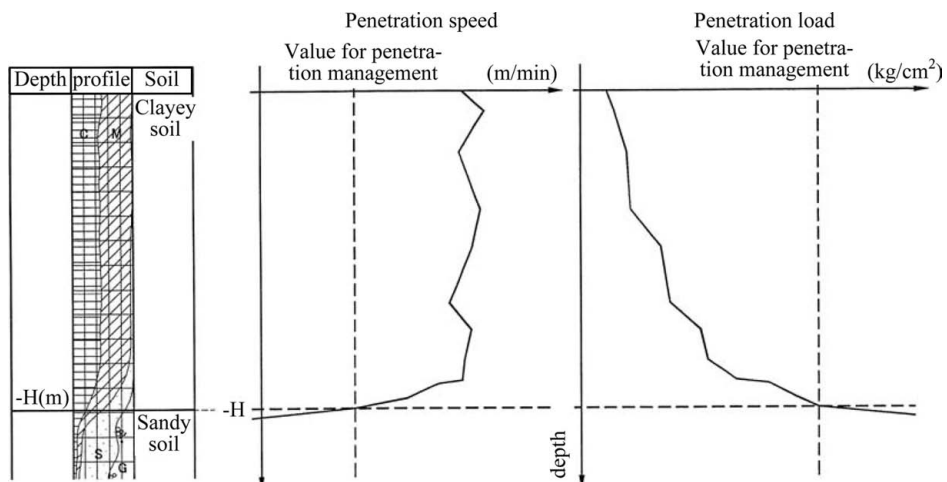


Figure 10. Criterion of the penetration resistance (after Furudoji 2004).

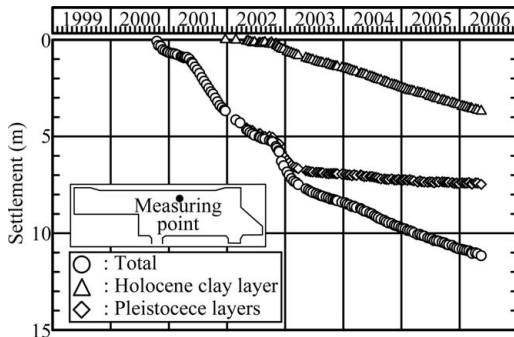


Figure 11. Settlements observed at Holocene and Pleistocene clay layers.

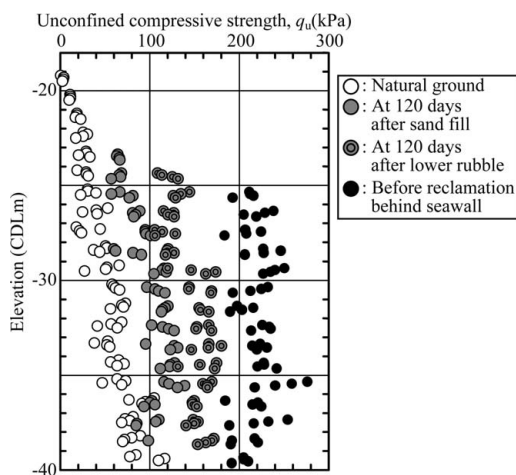


Figure 12. Change of strength of ground improved by sand drain (after Tabata & Morikawa 2005).

Check borings were drilled at the end of each consolidation period, and unconfined compression tests were conducted using specimens from the boreholes (Fig. 12). The next stage was commenced only after verifying that the strength of the Holocene clay layer had increased sufficiently for the next stage. Depending on the check boring results, measures such as modification of the work procedure and/or loading configuration were taken as required. Check borings were carried out for 19 sections of the seawalls and 15 points in the reclamation area.

6 CONCLUSION

In construction of the second phase island at Kansai International Airport, ground improvement work was carried out in the entire construction area in order to ensure the stability of the seabed during construction



Figure 13. Overview of first and second airport islands.

and minimize residual and uneven settlement after the opening of the airport. In the second phase construction, the sand drain method was applied to the Holocene clay layer in most parts of the seawall construction area and all of the reclamation area. About 1.2 million sand piles were driven in a short period. As a result of scrupulous management of penetration, almost all sand piles satisfied the penetration criterion. Settlement of the Holocene layer was seen to be completed after reclamation was finished. The strength of the seabed required for the construction work was obtained as a result of this ground improvement.

The second phase project is proceeding smoothly (Fig. 13). The new runway, the taxiway connecting the first and second islands, and related facilities are scheduled to open on August 2, 2007.

REFERENCES

- Furudo, T. 2004. Present condition and foundation improvement technology of Kansai International Airport Construction. *Proceedings of the sixth national symposium on ground improvement*: 1–10.
- Furudo, T. 2005. Second phase construction project of Kansai International Airport - Large-scale reclamation works on soft deposits-. *Proceedings of the 16th international conference on soil mechanics and geotechnical engineering* 1: 313–322.
- Kanda, K., Suzuki, S. & Yamagata, N. 1991. Offshore soil investigation at the Kansai International Airport. *Proceedings of the international conference on geotechnical engineering for coastal development* 1: 33–38.
- Shinohara, M. 2003. Settlement analysis and intelligent site management of the second-phase land reclamation works for Kansai International Airport. *Soft ground engineering in coastal areas, Proceedings of the Nakase memorial symposium*: 159–167.
- Tabata, T. & Morikawa, Y. 2006. The second phase construction of KIA considering the large and long-term settlement of the clay deposit. *Proceedings of the symposium on geotechnical aspects of Kansai International Airport*: 7–16.

Seismic design and seismic problems

Seismic design specifications for Japanese highway bridge deep foundations against large earthquakes

M. Shirato & S. Nakatani

Public Works Research Institute, Tsukuba, Japan

ABSTRACT: The 1996 Japanese Specifications for Highway Bridges introduced ductility design for seismic design of deep foundations against large earthquakes. Ductility design considers both the strength and ductility of a foundation system being comprised of structural members and vertical and horizontal soil resistances. This paper first describes the principles of seismic design, design seismic motion, and required seismic performance level for highway bridges. Then the limit states and typical seismic design procedures for grouped-pile foundations are summarized.

1 INTRODUCTION

Right after the 1995 Hyogo-ken Nanbu (Kobe) earthquake in Japan, the Japanese Specifications for Highway Bridges (referred to as “the Specifications” hereafter) were revised (Japan Road Association 1996). Ductility design for deep foundations of piers against large earthquakes has been adopted since then. This paper describes the summary of the ductility design for highway bridge foundations, especially for pile foundations of piers.

Before the 1995 Hyogo-ken Nanbu earthquake, only the elastic and working stress design methodology involving small-to-medium earthquakes was employed in foundation design, and the foundation performance during large earthquakes was not directly checked. When it comes to pile foundations, the verification is conducted for each pile in the foundation.

As a result of the disastrous consequences of the 1995 Hyogo-ken Nanbu (Kobe) earthquake, structural engineers are eager to develop a design methodology that can account for a realistic description of the ultimate behavior of structures. Although the damage was less serious than in the severely damaged piers, the earthquake caused significant cracking and yielding in many pile foundations. Therefore, a design calculation method to assess the seismic performance of a foundation subjected to a severe earthquake had to be developed.

The ductility design method takes into account both the strength and ductility of foundations against large earthquakes. Although it is widely recognized that a seismic design philosophy considering the ductility of structures is important, its application to

foundation design is rare. From this viewpoint, the Japanese Specifications for Highway Bridges are one of the leading design codes with respect to the application of ductility design to foundation systems.

2 REQUIRED PERFORMANCE FOR TOTAL BRIDGE SYSTEMS

2.1 Performance matrix for highway bridges

A two-level design method is employed. The first level is the seismic design against small-to-medium earthquakes, which has been traditionally implemented. The second level is the seismic design against large earthquakes such as the 1923 Kanto and 1995 Hyogo-ken Nanbu (Kobe) earthquakes.

Table 1 shows the basic principles in seismic design in the Specifications through a performance matrix of design earthquake ground motion and Seismic Performance Level (SPL). This performance matrix illustrates the combinations of the two levels of earthquake motions and the corresponding requirements of structural performance level required by the Specifications.

2.2 Typical design ground motions

Level 1 earthquakes are of small to medium magnitude, and their acceleration response spectrum (ARS) amplitudes are around 0.2 G to 0.3 G for the usual characteristic periods of highway bridges. Level 2 earthquakes are extremely strong, but they are very unlikely to strike a structure during its service period.

Table 1. Seismic performance matrix.

Type of design ground motion		Standard bridges (Type-A)	Important bridges (Type-B)
Level 1 earthquake: high-probability ground motion		SPL 1: Prevent damage	
Level 2 earthquake: low-probability ground motions	Interplate earthquakes (Type I) Inland earthquakes (Type II)	SPL 3: Prevent critical damage	SPL2: Limited damage for function recovery

The characteristics of inelastic behavior of both soils and structural members during an earthquake are greatly affected by the intensity and the duration of the earthquake; examples are the liquefaction resistance of sandy soils and the ultimate compressive strain of concrete. Accordingly, the Level 2 earthquakes involve two types of ground motion, i.e., Type I and Type II Earthquake motions.

The ground motion in Tokyo during the 1923 Kanto earthquake is typical of Type I Earthquake motions. This ground motion is associated with the interplate-type earthquake having a magnitude of approximately 8 and is generated at plate boundaries in the ocean. The peak amplitudes associated with Type I Earthquake motion are smaller than those of Type II Earthquake motion, but Type I Earthquake motions have longer durations. The ARS amplitudes of Type I Earthquake motion are approximately 0.7 G to 1.0 G for the usual characteristic periods of highway bridges.

The ground motion in Kobe during the 1995 Hyogoken Nanbu earthquake is typical of Type II Earthquake motions, which are inland-strike-type earthquakes having magnitudes of approximately 7 and are caused by faults located at short distances from bridge sites. Type II Earthquake motions have high intensities but short durations. The ARS amplitudes of Type II Earthquake motion are approximately 1.5 G to 2.0 G for the usual characteristic periods of highway bridges. The return period of Type II Earthquake motion may be longer than that of the Type I Earthquake motion.

2.3 Performance level of bridges

The Seismic Performance Level (SPL) depends on the importance of the bridge. Bridge importance is classified into two groups: standard bridges (Type-A bridges) and important bridges (Type-B bridges). Both Type-A and Type-B bridges must resist Level 1 earthquakes to achieve SPL 1, where SPL 1 prescribes that the bridge performs elastically during an earthquake with minimal or no damage. While minor damage may occur, the function level of the bridge is maintained following the earthquake and repair work is easily completed. Type-A bridges must resist Level 2 earthquakes to achieve SPL 3, where SPL 3 prescribes that the bridge resists critical failure that would lead to the collapse of the bridge during an earthquake. Type-B bridges

must resist Level 2 earthquakes to satisfy SPL 2, where SPL 2 prescribes that the bridge is functional especially for rescue operation even after sustaining a limited degree of damage.

3 LIMIT STATES OF PILE FOUNDATIONS

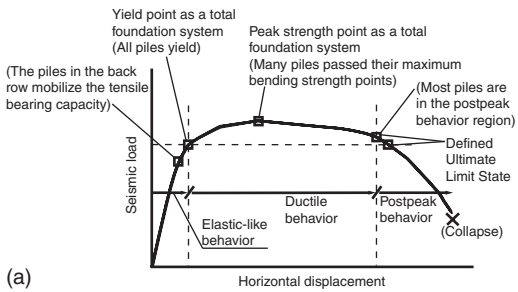
A bridge is comprised of structural components like girders, piers, bearings, foundations etc., and serves as a system. For achieving the required total bridge system performances, the Specifications also request the limit states of individual structural components. The idea is that integrating the components that are verified for their limit state criteria can achieve the required total bridge system performance. Accordingly, the Specifications conceive limit state design as a concept for design of individual structural components, not for design of bridge structure as a system.

As for pile foundations, SPL 1 of total bridge system performance is achieved, when the region of elastic like behavior is not exceeded for each pile. Accordingly, the two items are checked for each pile in design. The sectional forces are checked from the structural viewpoint and, moreover, the properties of the vertical and horizontal soil resistances to the pile are checked from the geotechnical viewpoint.

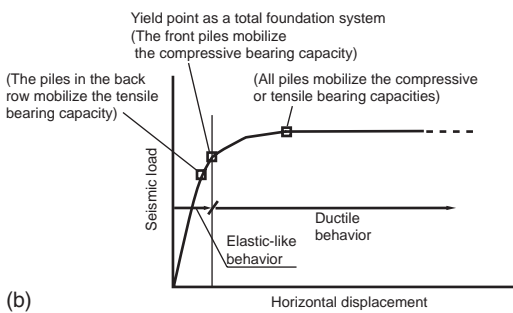
The limit states of pile foundations to achieve SPL2 and SPL3 of total bridge system agree with each other. The pile foundation has to remain as a system in the region in which the foundation retains sufficient strength and a safety margin for the deformation capacity, so that damage to piles in grouped-piles will not go over the state at which it becomes impossible to restart the service of the bridge early. In addition, any damage can be managed after the earthquake. The salient point in the ductility design is to consider the relationship between possible damage states and the stability of the foundation system, not individual piles, from the viewpoint of deformation capacity.

4 TYPICAL COLLAPSE PROCESS OF PILE FOUNDATION AS A SYSTEM

The relationship between a typical collapse process of grouped-pile foundations and the limit states can be associated as illustrated in Figure 1.



(a)



(b)

Figure 1. Idealized collapse processes of grouped-pile foundations. (a) Structural damage to piles dominates the nonlinear foundation behavior (b) Pile bearing capacities dominate the nonlinear foundation behavior

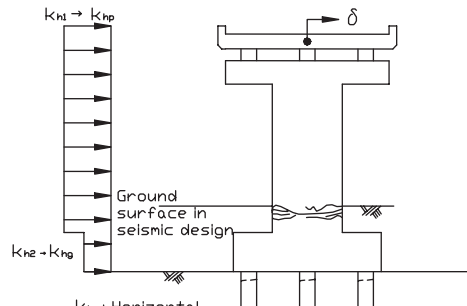
As the seismic loads increase, some parts of lateral soil resistance elements mobilize the maximum resistances, some piles reach the tensile bearing capacity, and the materials in some piles yield. However, the foundation as an overall system, not each pile, still behaves in the elastic manner. The sudden increase in the horizontal displacement in the overall system behavior typically occurs at which

- a compressive reaction force at the pile top of the front piles reaches the bearing capacity of the pile, or
- all piles yield.

These are conceived to usually characterize the yield point of the overall foundation system.

Then the foundation reaches the peak strength point, where many piles passed their maximum strength points, when structural damage to piles dominates the nonlinear foundation behavior. After that, most piles are in the postpeak behavior region, and the foundation system reaches the postpeak behavior region from the ductile behavior region.

As a result, the yield point or somewhere around the peak strength point may be associated with the defined limit states to be verified in the ductility design.



K_{Hp} : Horizontal seismic coefficient on the ground surface

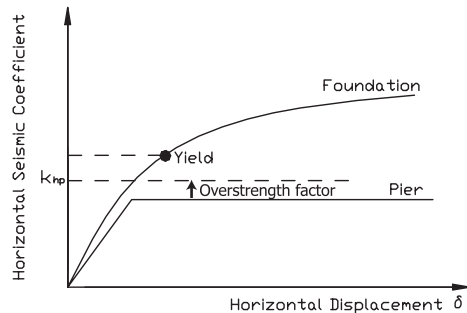


Figure 2. Ductility design of pier foundations for verification in usual cases.

5 DUCTILITY DESIGN OF PILE FOUNDATIONS — A STANDARD VERIFICATION METHOD AGAINST LEVEL 2 EARTHQUAKES

Since foundations are placed underground, it is time-consuming to examine and repair damaged portions before restarting the service of a bridge after an earthquake. Therefore, the Specifications specify that the clear inelastic behavior of foundations as systems is not expected in principle, and that seismic energy dissipation should be expected at other structural components, such as the bottoms of piers or seismic energy absorption bearings. The behavior of the foundation is checked by pushover analysis as shown in Figure 2.

First the pushover analysis is conducted for the pier with the fixed-end boundary condition to obtain the seismic coefficient at which the pier mobilizes the design maximum strength. Then the pushover analysis is repeated for the foundation to capture the collapse process of the overall foundation system in a step-by-step manner with respect to the increasing lateral seismic coefficient, k_h . The summary of the design calculation model of pile foundation will be described later. Finally, it is verified that the foundation does

not reach the range in which the behavior of the foundation system is clearly nonlinear when the increasing lateral seismic coefficient reaches the seismic coefficient corresponding to a factored maximum strength of the pier, k_{hp} .

The factored maximum strength of the pier is given by multiplying the design maximum strength considered in the pier design by an overstrength factor which is larger than one. An overstrength factor value of 1.1 is adopted based on engineering judgment. It considers the material strength variation of piers, foundation members, and soils, the fact that the contribution of covering concrete is neglected when obtaining pier strengths, and so on.

The initiation of yield on the overall system behavior of foundation can be derived by, for example, the so-called ‘ $\log k - \log \delta$ analysis’ with the relationship between seismic coefficient, k_h , and horizontal displacement at the point of seismic lateral load in the superstructure, δ . The point of seismic lateral load in the superstructure is basically defined as the gravity point of the superstructure. As mentioned above, the initiation of yield of the overall system behavior of pile foundations having usual dimensions is generally characterized by a point:

- when a compressive reaction force at the pile top of the front piles reaches the bearing capacity of the pile, or
- when all piles yield.

However, it is unavoidable to consider inelastic behavior in Level 2 earthquakes, especially, when liquefaction of subsoil layers occurs or when a pier ends up possessing a large capacity due to factors outside the seismic design process. Accordingly, the foundation will be designed to have sufficient ductility to work as the energy dissipation part and possess a strength so that the inelastic foundation system response will not exceed the ductility capacity. Plus, it is essential to restrict the damage to foundations such that it is easy to reuse foundations immediately after an earthquake without any repair work.

When checking the ductility of foundations, it is verified that the foundation does not reach a threshold displacement level described with ductility, with a safety margin, as shown in Figure 3. The nonlinear response is estimated by the energy conservation method, and the verification is conducted with response and allowable ductility factors, μ_{FR} and μ_{FL} , respectively, where the ductility factor, μ , is defined below by dividing the displacement at the superstructure, δ , by the yield displacement, δ_y :

$$\mu = \frac{\delta}{\delta_y} \quad (1)$$

The allowable ductility factor, μ_{FL} was assessed basically based on experimental results of model

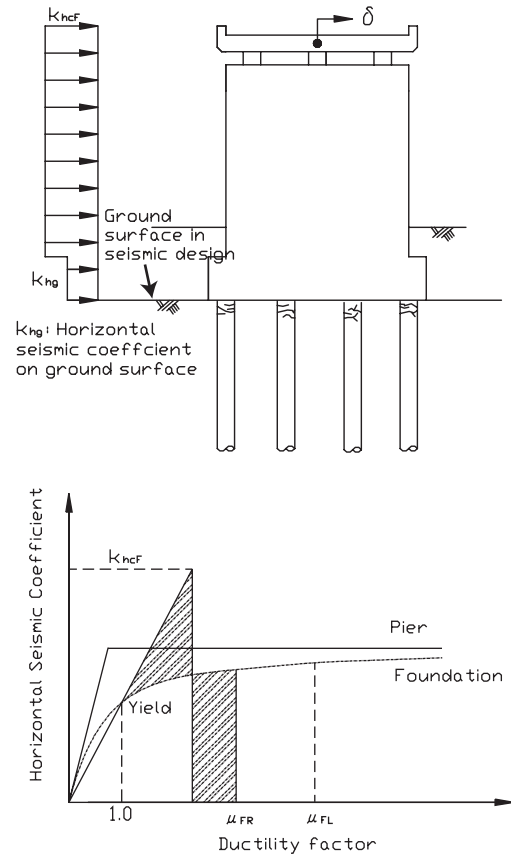
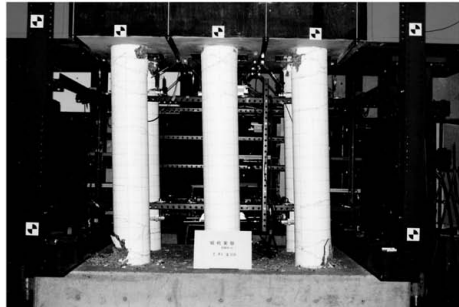
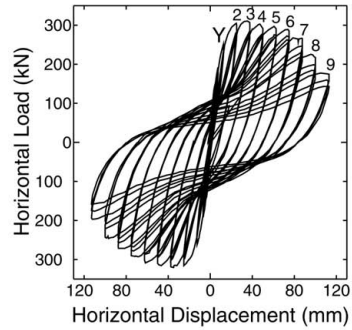
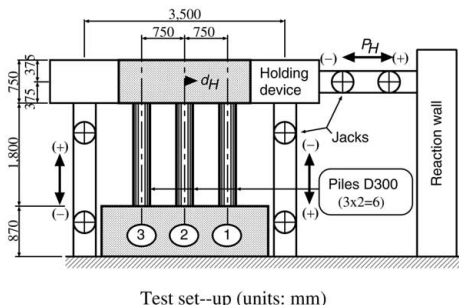


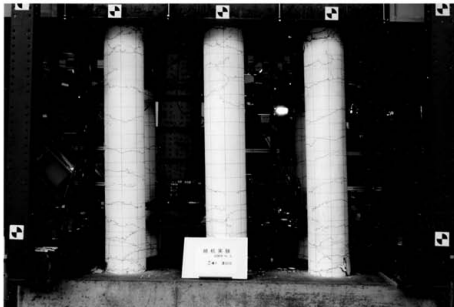
Figure 3. Ductility design of pier foundations for verifying that foundation has sufficient ductility capacity (Japan Road Association 2002).

grouped-piles subjected to coupled lateral and overturning moment cyclic loads (Kimura et al. 1998; Nakano et al. 1997; Matsuda et al. 1997), as shown in Figure 4. The model grouped-piles are comprised of steel pipe piles, PHC (Prestressed High-strength Concrete) piles, and drilled shafts (or RC piles) with several numbers of pile rows. Regarding grouped-pile foundations, the allowable ductility factor, μ_{FL} , is specified deterministically to be four. It is considered that an allowable ductility factor of 4 plans to confirm the following items:

- The foundation mobilizes the maximum strength level. Even though no repair work is done, the foundation will be able to have the equivalent load carrying capacity to that before the earthquake.
- The overall foundation systems still have a safety margin. Compared to the energy absorbed until the foundation reaches the allowable ductility factor, the foundation will be able to have a sufficient remaining



Side view of the model group pile at $4\delta_y$ cycles



Side view of the model group pile at $7\delta_y$ cycles

(A horizontal jack and two vertical side jacks were simultaneously controlled to maintain the ratio of the horizontal and overturning moment loads during the experiment. $7\delta_y$ (Y) is defined as the displacement when all the poles yield.)

Figure 4. A large scale experiment of a 3×2 model group-drilled shaft (cast-in-place RC group-pile) subjected to cyclic horizontal and overturning moment loads at the top of the foundation (Kimura et al. 1998).

energy absorption capacity against another large earthquake, even though no repair work is done.

- Severe damage to piles will not occur, so that the foundation can be re-used.

This recommended allowable ductility factor is assumed to be independent of the number of rows of piles and the type of piles, as long as the piles satisfy the recommended structural details in the Specifications, although it should be true that the limit ductility factor depends on those elements. The reasons for the recommended allowable ductility factor being made constant are as follows. First is that the proposal is based only on a small number of experimental studies. Second is that conventional numerical models are not sufficiently developed, especially in postpeak behavior, to allow reliable estimates of the relationship between pile foundation stability and the damage sustained by each pile.

Note that the value of four for the allowable ductility factor is also applied in practice when the initiation of yield of the foundation results from mobilizing the ultimate compression bearing capacity of the leading piles.

6 CALCULATION MODEL

The calculation model for the ductility design of pile foundations is summarized in Figure 5. Note that the background of the calculation models for pile foundations and caisson foundations in the Specifications is shown in, for example, Fukui et al. (1997a, 1997b).

The piles are modeled with beam elements. Nonlinearity in the bending resistance of piles is considered in their bending moment-curvature ($M-\Phi$) relations. It has been confirmed that pushover analyses using the modeling shown in the Specifications can result in a good approximation up until the model grouped-pile yields or reaches the peak strength for the structural experiment shown in Figure 4.

The vertical soil resistance of a pile against axial forces at the pile top ($P-S$ relationship in Figure 5, in which P = load and S = displacement) is modeled as an elastic-perfectly plastic bilinear curve having its critical loads at the ultimate bearing capacity for compression and the ultimate pull-out capacity for extension.

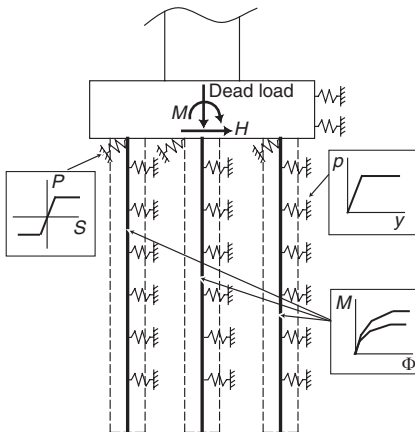


Figure 5. Calculation model of pile foundations in ductility design.

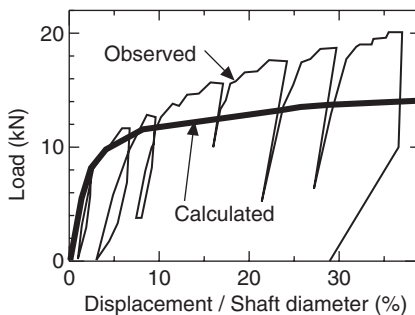


Figure 6. Comparison between the observed and calculated results of load-displacement relationship of a 3 by 3 grouped-drilled shaft foundation subjected to a lateral load at the pile cap.

The piles are horizontally supported by distributed springs with p - y curves, where p is the horizontal sub-grade reaction and y is the pile displacement. The p - y curve is modeled by an elastic-perfectly plastic bilinear property. The maximum horizontal subgrade reaction to a single pile is assumed to be three times the passive earth pressure intensity for cohesionless soil and 1.5 times the passive earth pressure intensity for cohesive soil. Finally, group efficiencies are applied to the p - y curves.

These modeling of soil resistances are based on past in-situ and laboratory load test results in Japan. For example, the horizontal load-displacement relationship observed in the in-situ lateral load experiment of a 3 by 3 grouped-drilled shaft foundation (Kimura et al. 1994) and the calculation result are compared in Figure 6 (Fukui et al. 1997a; Fukui et al. 1997b). The shaft diameter was 1.2 m and the nominal distance between piles was 2.5 times the shaft diameter.

When there are the subsoil layers that have liquefaction potentials, reduction factors with respect to soil liquefaction are applied to the axial and horizontal soil resistances to piles.

7 CONCLUDING REMARKS

Recent large earthquakes such as the 1995 Hyogo-ken Nanbu (Kobe) earthquake have increased the public's awareness of the seismic performance of structures. In response to the increased demand, a design method that can account for a realistic description of the ultimate behavior of a foundation as a system is required. The ductility design is one of the solutions that we have shown the public. It simultaneously takes account of the strength and ductility of the foundations as a system. We strongly hope that this report contributes to progress in the design of deep foundations.

Note that the ductility design for foundations of abutments also has been introduced in the 2002 Specifications and the summary of the ductility design of abutment foundations is available elsewhere (Shirato et al. 2006).

REFERENCES

- Fukui, J., Kimura, Y., Ishida, M. & Nanazawa, T. 1997a. Strength and ductility characteristics of highway bridge foundations. In *Proc. of the 29th joint meeting of U.S.-Japan panel on wind and seismic effects, UJNR*: 567–582. Published as Technical memorandum of PWRI (3524): PWRI.
- Fukui, J., Kimura, Y. & Okoshi, M. 1997b. Strength and ductility characteristics of pile foundations. In *Proc. of the second Italy-Japan workshop on seismic design and retrofit of bridges*: 255–274. Published as Technical memorandum of PWRI (3503): PWRI.
- Japan Road Association 1996. *Specifications for Highway Bridges, Part V. Seismic Design*. Tokyo: Maruzen.
- Japan Road Association. 2002. *Specifications for Highway Bridges, Part V. Seismic Design*. Tokyo: Maruzen.
- Kimura, M., Kosa, K. & Morita, Y. 1994. Full-scale failure tests on lateral loading cast-in-place concrete piles. In *Proc. of 5th Int. Conf. and Exhibition on Piling and Deep Foundation*, Bruges: 5.15.1–5.15.10.
- Kimura, Y., Okoshi, M., Nakano, M., Fukui, J. & Yokoyama, K. 1998. An experimental study on the ductility of pile foundations. *J. of Struct. Eng., JSCE* 44A: 1597–1606. (in Japanese).
- Matsuda, H., Shioi, Y., Kimura, M. & Hasegawa, A. 1997. Improvement of ultimate behavior of steel pipe pile foundation. *J. of Struct. Eng., JSCE* 43: 1397–1402. (in Japanese).
- Nakano, M., Kimura, Y., Ishizawa, T., Shimazu, A. & Koyama, S. 1997. Experiments of grouped steel pipe piles subjected to horizontal loading, Part 1. In *Proc. of 32th Annual Conf. of JGS*: 1573–1574. (in Japanese).
- Shirato, M., Fukui, J. & Koseki, J. 2006. Current status of ductility design of abutment foundations against large earthquakes. *Soils and Foundations* 46(3): 377–396.

New seismic design concept for port facilities

T. Sugano & T. Tanaka

Structural Dynamics Division, Port and Airport Research Institute, Japan

ABSTRACT: In a modern society, it is very important to maintain the logistic system through port functioning even immediately after serious earthquakes. In the past, especially the experiences from the 1995 Hyogoken-Nambu Earthquake (the 1995 Kobe earthquake) resulted in a lot of ideas full of suggestions to the people concerned with all the departments of the port (management, administration, operation, shipping, shipper, contractor, etc.). The paper gives the information on the Japan's earthquake preparedness policy and the revision of seismic design for ports.

1 LESSONS LEARNED FROM THE 1995 KOBE EARTHQUAKE

1.1 *Damage to Kobe port (Inagaki et al. 1995)*

The 1995 Kobe earthquake occurred at 5:46 a.m. on January 17, 1995. The epicenter of this earthquake was about 20 km west-southwest from the Kobe Port and 16 km deep, very near from the Kobe Port. This earthquake destroyed most of the major facilities of the Kobe Port and seriously affected operation of the logistic system through and around the port. This resulted in long-term suspension of the port operation dealing serious blow to the regional economy, especially the Kobe city economy, for several years.

This experience raised our concerns for the preparation of port facilities against destructive earthquakes. From the investigation and analyzing results of the damages to container terminal facilities, we found that all the container terminal quays were seriously damaged and all the quayside container cranes (container crane) were collapsed or seriously damaged. However, three berths of earthquake resistant quay (not for container terminal) remained undamaged. In the Kobe Port, all the container terminal quays were constructed of concrete caissons. During strong ground motion, all concrete caissons inclined and moved toward sea few meters (about 5 m maximum). Therefore berthing container ships to the quays were impossible and collapsed or damaged cranes could not be functional any more.

1.2 *Promotion of renovation for earthquake-resistant port*

From the point of view of the social port function, this experience showed us the following two important concepts for port administration and management. Those are;

- (A) Starting special operation for transporting living necessities for sufferers' daily life immediately (within one day) after the earthquake.
- (B) Restarting commercial logistic operation within one week after the earthquake.

The concept (A) is the policy to support these sufferers' minimum standard of living. Just after the strong earthquake, many people lose their shelter, food and clothing. Almost all the land routes are cut off, and so the sea and air routes are the only alternative for transporting relief goods. Ports are the only entrance to the earthquake-stricken area. This concept leads to the key technology (A) stated below.

The concept (B) is the policy to support the activities of the enterprises located around the port. If the port cannot restart functioning its logistic operation within one week, the enterprises around the port lose their way for transportation to support their activity and have to develop the new route through other ports in order not to lose their competitive power. Eventually they don't come back to the port when the port restarts operation. This scenario is not ideal for the two sides: the port authority and the customers of the port. But

unfortunately, this scenario was realized in case of the Kobe Port after the devastating earthquake in 1995.

In order to realize these objectives stated above, the Ministry of Land, Infrastructure and Transport (MLIT) of Japan planned the Japan's Port Policy for Preparedness against Earthquake. This strategy policy includes the following 2 key technologies.

- (A) Constructing earthquake resistant quays for supporting citizen's life.
- (B) Constructing earthquake-proof container and car-ferry terminals for supporting BCP (Business Continuity Plan).

The MLIT has designated over 336 berths of earthquake resistant quays in Japan and 54% berths have been completed or are under construction as of 2005. As for the earthquake-proof container terminal, the MLIT designated over 30 berths all over Japan.

The Technical Standards and Commentaries of Port and Harbour Facilities in Japan (The Technical Standards) had been revised in 1999 with halfway measures considering the lessons learned from the 1995 Kobe earthquake. This paper reported that new concept of seismic design including the Technical Standards which will be published in 2007.

2 NEW SEISMIC DESIGN PHILOSOPHY

2.1 Performance-based methodology

Performance-based design is an emerging methodology, which was introduced based on the lessons learned from earthquake damages in the 1990's, especially, 1995 Kobe earthquake. In performance-based design, appropriate levels of design earthquake motions must be defined and corresponding acceptable levels of structural damage must be clearly identified. Two levels of earthquake motions are typically used as reference motions, defined as following.

Level 1 (L1): the level of earthquake motions that are likely to occur during the life-span of the structure.

Level 2 (L2): the level of earthquake motions associated with infrequent rare events that typically involve very strong ground shaking.

The acceptable extent of damage is specified according to the specific needs of the facilities' users/owners, and may be defined based on the acceptable extent of both structural and functional (operational) damages. For example, the case of an important container terminal, the required functions are, berthing a container ship, unloading and loading containers and transport conveyance by land and sea. To satisfy the requirements, both quay wall and container cranes can operate just after an earthquake with slight repair work or without repair work.

The principal steps taken in performance-based design are as follows

- (1) Select a performance grade of S, A, B, or C: This step is typically done by referring to Tables 1 and 2 and selecting the damage level consistent with the needs of the users/owners and the importance of the facility.
- (2) Define damage criteria: Specify the level of acceptable damage in engineering parameters such as displacements, limit stress states or ductility factors.
- (3) Evaluate seismic performance of a structure: Evaluation is typically done by comparing the response parameters from a seismic analysis of the structure with the damage criteria.

2.2 Reference levels of earthquake motion

Level 1 earthquake motion (L1) is typically defined as motion with a probability of exceedance of 50% during the life-span of a structure. Level 2 earthquake motion (L2) is typically defined as a motion with the largest motion of

- (a) historical earthquake record and/or paleoseismic date from trenching, or,
- (b) scenario earthquake based on empirical, semi-empirical, theoretical and hybrid methods.

Table 1. Acceptable level of damage.

Level of damage	Structural	Functional
Degree I: Serviceable	Minor or no damage	Little or no loss of serviceability
Degree II: Reparable	Controlled damage	Short-term loss of serviceability
Degree III: Near collapse	Extensive damage in near collapse	Long-term or complete loss of serviceability
Degree IV: Collapse	Complete loss of structure	Complete loss of serviceability

Table 2. Performance grade.

Performance grade	Design earthquake motion	
	Level 1	Level 2
Grade S	Degree I: Serviceable	Degree I: Serviceable
Grade A	Degree I: Serviceable	Degree II: repairable
Grade B	Degree I: Serviceable	Degree III: Near collapse
Grade C	Degree II: Repairable	Degree IV: Collapse

2.3 Performance evaluation

As a guide for evaluating performance criteria at a specific port, the relationship between degree of damage and the design earthquake motion is illustrated in Figure 1. The curves in this figure are configured by Tables 1 and 2, form the basis for the performance evaluation procedure.

The objective of performance evaluation is to evaluate the seismic response of the port structure with respect to allowable limits. (e.g. displacement, stress, ductility and strain, etc.) There are two way to evaluate such seismic response by (1) Numerical analysis and (2) Model test.

- (1) Numerical analysis (International Navigation Association 2001): Higher capability in analysis is required for a higher performance grade facility. A variety of analysis methods are available for evaluating the local soil deposit effects, liquefaction potential and the seismic response of port structures, which are categorized based on a level of sophistication and capability as follows,
 - (a) Simplified analysis: Appropriate for evaluating approximate threshold limit for displacements and /or elastic response limit and an order of magnitude estimate for permanent displacements due to seismic loading.
 - (b) Simplified dynamic analysis: Possible to evaluate extent of displacement/stress/ductility/strain based on assumed failure modes.
 - (c) Dynamic analysis: Possible to evaluate extent of displacement/stress/ductility/strain.

It is required to confirm the accuracy and applicability of methods for analysis of port structures by using suitable case histories or model test results before accomplishing the seismic performance evaluation.

- (2) Model test: The reconsideration of the earthquake-proof design method of the port facilities which contain a container wharf/terminal since the 1995 Kobe earthquake was rapidly carried out. The first stage of design procedure was using the pseudo

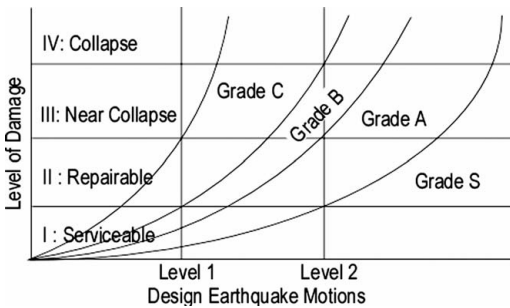


Figure 1. Schematic figure of performance grade.

static method. In addition, it was necessary to evaluate the dynamic performance of facilities during an earthquake. According to design code of port facilities dynamic analysis was required to evaluate the performance of port structures. On the other hand, in Japan, the conventional design technique for container cranes treated only the static response of structural member's stress level. The pseudo static horizontal force is obtained by applying a coefficient $k_h = 0.2$. During the 1995 Kobe Earthquake, the actual damage of container cranes were caused by the uplifting phenomenon of the legs. For this reason, the dynamic analysis technique and performance-based design methodology have been incorporated to the design practice.

In order to develop a high seismic performance of container terminal, the knowledge of dynamic interaction characteristics between pile supported wharf and container crane during earthquakes is needed. To understand the interaction characteristics/behaviors, model tests were conducted. Figures 2 and 3 show that the overview of the model and the underwater shake table. The principal dimension of the test model (Figure 3) was determined to be 1/30 of the actual structure because of the limitation of the shake table size. Because of the fact that the 1G gravity field plays an essential role in the legs uplifting phenomenon, scale ratio of acceleration must be unity. In this test, dimensions of the cross section of the members were appended to compensate the reduced weight. Because the elastic motion of this model is dominated by the bending deformation of the members, the axial stiffness does not play an important role. Principal scaling relations between the prototype structure and the model are shown in Table 3. The natural vibration period of the prototype crane is about 2.0 s in prototype scale.

In order to reduce the dynamic interaction between pile supported wharf and container crane, we introduced base-isolation system at the legs of crane. The

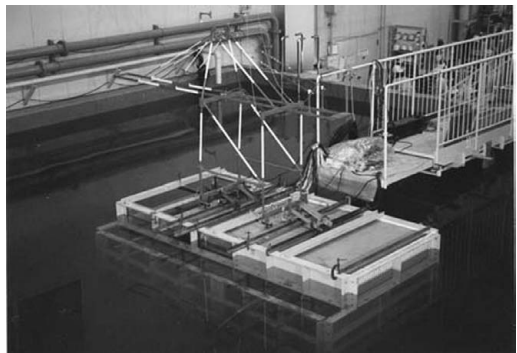


Figure 2. Model setup on the underwater shake table.

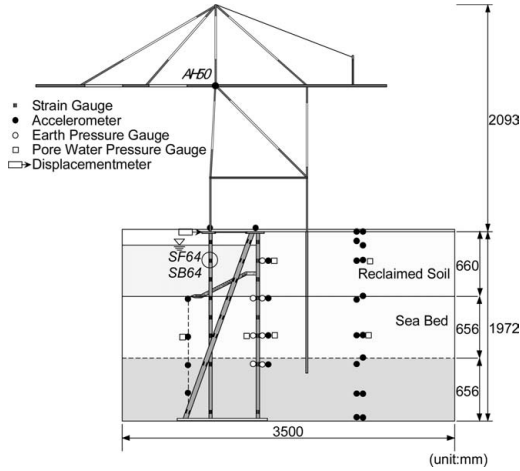


Figure 3. Cross section of 1/30 model.

Table 3. Scaling relationship between prototype and model.

Measure Quantity	Unit	Prototype	Model
Length	m	1	1/30
Time	s	1	$1/30^{1/2}$
Acceleration	m/s^2	1	1
Mass	kg	1	$1/30^3$
Moment of inertia	m^4	1	$1/30^4$
Elastic modulus	N/m^2	1	1
Bending rigidity	Nm^2	1	$1/30^5$

base-isolation system is often used for buildings and bridges, however, in case of container crane, the crane has to move by wheel during operation.

The response acceleration of both pile supported wharf and container crane are reduced around 1/2 when the base-isolation system is working. In addition the axial force during shaking is also reduced because of the base-isolation system suppressing uplift of legs and impact forces against the piles as shown in Figure 4.

3 EARTHQUAKE MOTIONS

As shown in Figure 5, earthquake motions from scenario earthquakes may be determined by empirical, semi-empirical, theoretical, and hybrid methods with consideration of

- (1) fault plane size of the scenario earthquake,
- (2) initiation of fault rupture,
- (3) fault rupture process,
- (4) seismic wave propagation,
- (5) firm ground at the site, and,
- (6) local soil deposit

The semi-empirical method computes time histories of earthquake motion caused by the large scenario earthquake by combining the recorded or simulated earthquake motions from smaller earthquakes with assumption of a small earthquake motion is generated from each small fault element.

The local soil deposit site effect can be determined by boring survey, in-situ sounding and laboratory soil tests.

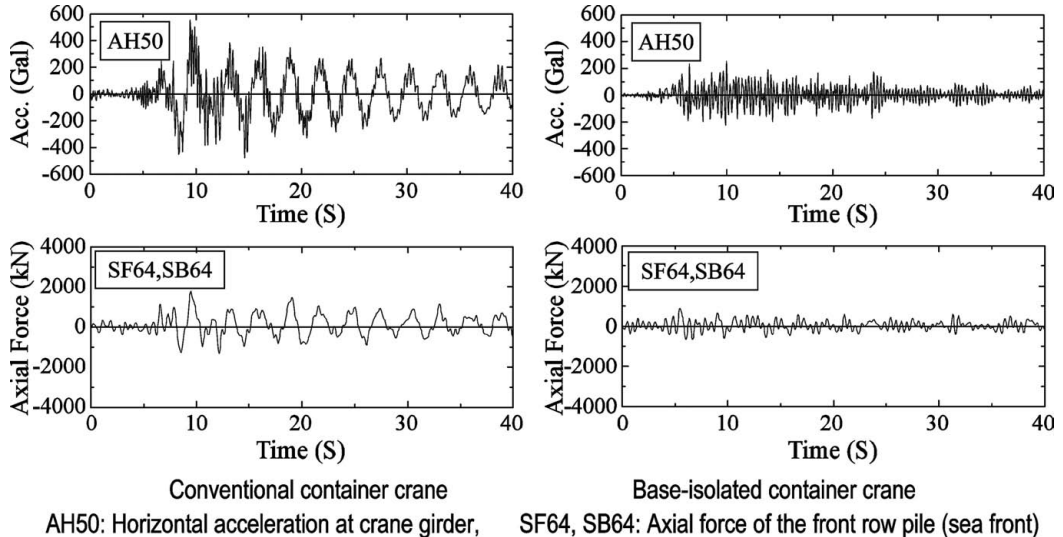


Figure 4. Responses of pile supported 1/30 model wharf with/without base-isolation system during 1995 Kobe Earthquake.

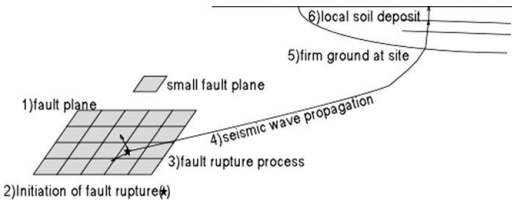


Figure 5. Semi-empirical earthquake motion determination.

The L1 earthquake motion is defined as the motion with a probability of exceedance of 50% during the life-span of a structure. If the life-span of a port structure is 50 years, the return period for L1 earthquake is 75 years. (Kameda & Nojima, 1988)

4 REMARKS

In order to mitigate hazards and losses due to earthquakes, an earthquake preparedness policy for port is

an important issue. This paper introduced the Japanese government's approach and development of seismic design concept from the port functional point of view.

REFERENCES

- Japan Port and Harbour Association. 1999. *Technical Standard for Port and Harbour Facilities and Commentaries*. (in Japanese)
- Inagaki, H., Iai, S., Sugano, T., Yamazaki, H. & Inatomi, T. 1996. Performance of caisson type quay walls at Kobe port. *Soils and Foundations. Special Issue on Geotechnical Aspects of the January 17 1995 Hyogoken-Nambu Earthquake*: 119–136.
- Kameda, H. and Nojima, N. 1988. Simulation of risk-consistent earthquake motion. *Earthquake Engineering and Structural Dynamics*. Vol.16: 1008–1019.
- International Navigation Association. 2001. Seismic design guidelines for port structures: 309–378. A.A. Balkema.

Centrifuge tests on pile foundation-structure systems affected by liquefaction-induced soil flow after quay wall failure

T. Tazoh

Institute of Technology, Shimizu Corporation, Japan

M. Sato

National Research Institute for Earth Science & Disaster Prevention, Japan

G. Gazetas

National Technical University of Athens, Greece

J. Jang

Institute of Technology, Shimizu Corporation, Japan

ABSTRACT: The paper investigates experimentally the behavior of a structure-footing-four piles system under the action of seismic shaking causing liquefaction of a critical soil layer and subsequent soil flow towards a laterally displacing quay-wall. A series of innovative centrifuge tests explore in parametric fashion the role of this pile foundation in the response of the system. The response is recorded in 38 channels providing time histories of acceleration, displacement, excess pore water pressure, pile axial and bending strains, and earth pressure. The results provide significant quantitative information and qualitative insight on the behavior of this realistically complex soil-foundation-structure system.

1 INTRODUCTION

Soil liquefaction may cause significant damage to structures, especially when lateral soil flow takes place. Such flow (which often takes the form of “lateral spreading”) was triggered along river banks and sea coasts behind quay-walls in Kobe during the 1995 Great Hanshin Earthquake. (Tazoh, et al., 2001, 2002)

Numerous studies have been published in the last decade on lateral flow failures induced by soil liquefaction. Numerical and experimental studies focused on the damage mechanism of structures and on the external forces induced by the soil flow on deep foundations. Many important structures exist along and near waterfronts in Japan, and their safety in the next major earthquake must be secured. Thus, the study of liquefaction-induced soil flow, together with remedial measures to mitigate the damage, is a crucial earthquake engineering issue. (Tazoh, et al., 1996)

In this study, a series of centrifuge tests was conducted to shed light on the seismic performance of pile-foundation-structure systems located behind quay-walls, arising from the large displacement or collapse of these walls and the ensuing soil flow.

Furthermore, remediation using batter piles is proposed, and the effectiveness of this measure is examined parametrically.

2 CENTRIFUGE TESTING

To investigate quantitatively the effect of quay-wall collapse on the seismic performance of pile-foundation-structure systems, we compare two cases: one in which the quay-wall collapses and triggers flow of the soil, and one in which the wall remains standing displacing almost elastically. We also investigate qualitatively the effectiveness of remedial measures by comparing the behavior of structures with and without remediation.

Each test for each model is carried out under nearly identical conditions with respect to input motions, soil liquefaction, and quay-wall collapse. Note, however, that it is impossible to achieve complete similarity between tests, due to the difficulty of reproducing failure events of soil and quay-walls.

Therefore, some innovative ideas must be adopted in the centrifuge testing. In this study, a partition is

placed at the center of the soil container, and two quay-walls with two models of the pile-foundation-structure behind each quay-wall are installed parallel to the partition. One quay-wall is fixed to the base of the soil container and the other is left “floating” (unattached to the base). The difference between the responses of the two pile-foundation-structures represents the effect of the amount of movement of the quay-wall on the seismic performance of the system. In these tests the loading is of a kinematic nature: quay-wall collapse induces soil flow failure, thereby loading the pile-foundation-structure system.

Batter piles are proposed as a remedial measure against damage caused by liquefaction-induced soil flow. Batter piles can be used with little or no additional expense, no special design, and hardly any difficulty in construction. In these centrifuge tests, a partition is placed at the center of a soil container with two models in each side: a vertical-pile-foundation-structure and a batter-pile-foundation-structure. These are installed parallel to the partition behind a quay-wall with free tip-end, which will be collapsed in the tests. All tests were conducted at centrifugal acceleration of 30 g on a 1/30-scale model.

3 EFFECT OF QUAY-WALL COLLAPSE ON THE SEISMIC PERFORMANCE OF THE PILE FOUNDATION

The experimental model used in the tests is shown in Figure 1. Both quay-walls consist of sheet piles, either fixed to the base of the soil container or terminated in the stiff base layer, i.e. unattached to the base. A laminar box is used as a soil container to allow shear deformation of the deposit as in the free field.

The soil in the container is divided into two parts: “A-side”, where the quay-wall is fixed to the base, and “B-side” where the quay-wall is unattached. Three tests are carried out by changing the distance from the quay-wall to the structure. Table 1 shows the distances of these cases.

The soil deposit consists of four soil layers: the first, third, and fourth soil layers are non-liquefiable; the second is liquefiable. The thickness and relative density of each soil layer are shown in Table 2.

Thirty-eight monitoring channels were installed, with the sensors comprising accelerometers, pore water pressure transducers, strain gauges, non-contact displacement meters, and earth pressure cells. Moreover, numerous colored beads were embedded in the soil layers to visually identify the soil deformation at the final stage.

Photograph 1 shows the condition after the test of Case 1. The recorded excess pore water pressure in the liquefied soil layer at the almost free field sensor PP2 (GL-90 mm, prototype: 2.7 m), is shown in Figure 2.

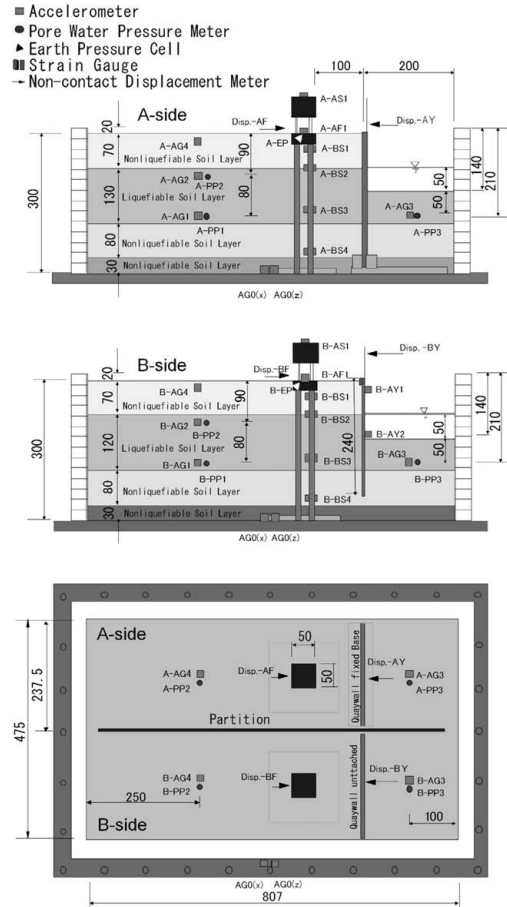


Figure 1. Longitudinal sections and plan of the 1/30-scale centrifuge model of Case 2 (scale unit: mm, for the prototype dimensions: multiply by 30).

Table 1. Three cases of the tests.

Case	Distance from the quay-wall to the pile-foundation-structure
Case 1	200 mm (prototype: 6.0 m)
Case 2	100 mm (prototype: 3.0 m)
Case 3	50 mm (prototype: 1.5 m)

The two time histories recorded in A-side and B-side, showing the accumulation and dissipation of excess pore water pressure, are very similar. Thus, there is no difference between the two sides with respect to the liquefaction occurrence and evolution. Liquefaction started at around 4 sec at the depths of GL-90 mm (prototype -2.7 m). The peak acceleration value of the

Table 2. Soil profiles of the soil layers.

Soil layer	Thickness	Soil profile	Liquefiable
1st soil layer	70 mm (2.1 m)	Silica sand No. 8, Dr = 50%	Non-liquefiable (above water table)
2nd soil layer	120 mm (3.6 m)	Silica sand No. 8, Dr = 50%	Liquefiable
3rd soil layer	80 mm (2.4 m)	Toyoura sand Dr = 90%	Non-liquefiable
4th soil layer	30 mm (0.9 m)	Silica sand No. 3	Non-liquefiable

(): prototype dimensions

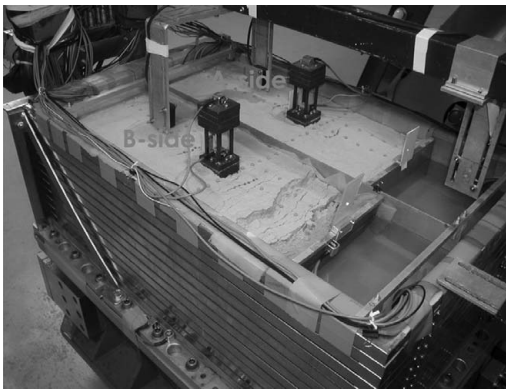


Photo 1. Condition after the test (Case 1).

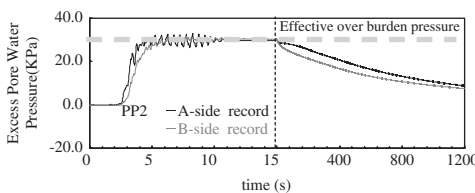


Figure 2. Excess pore water pressure records in the second soil layer (Case 2).

input motion (Case 2) is 258 gal and the significant duration is about 8 seconds (refer to Figure A-1 in the Appendix). The measurements were continued for sufficient time after the end of excitation, to fully capture the evolution of the liquefied-induced soil flow. Note in Figure 2 that the time axis from 15 to 1200 sec is at 1/8 of the scale from 0 to 15 sec.

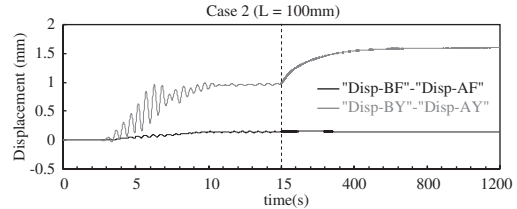


Figure 3. Relative horizontal displacements of quay-walls and footings in A-side and B-side (Case 2).

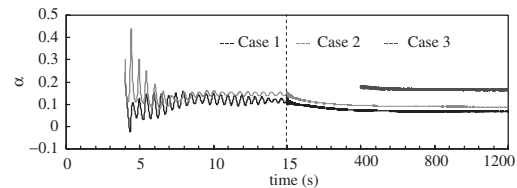


Figure 4. Influence factor α of Case 1 to 3. Effect on the horizontal displacement of the footing to unit horizontal displacement of the collapsed quay-wall.

The relative displacements between quay-wall and footing for A-side and B-side of Case 2 are plotted in Figure 3. Furthermore, for comparing among the three cases, the relative horizontal displacements of the footings [$\text{Disp(BF)} - \text{Disp(AF)}$] are divided by the relative horizontal displacements of the quay-walls [$\text{Disp(BY)} - \text{Disp(AY)}$] and the influence factor α is defined as follows:

$$\alpha = \frac{\text{Disp(BF)} - \text{Disp(AF)}}{\text{Disp(BY)} - \text{Disp(AY)}} = \frac{\text{r. h. displacement of footings}}{\text{r. h. displacement of quay-walls}}$$

(r. h.: relative horizontal)

The influence factor α represents the horizontal displacement of the footing to unit horizontal displacement of the collapsed quay-wall. It is plotted in Figure 4. In this figure, the time histories from 0 to 4 sec of Cases 1 and 2, and also from 0 to 400 sec of Case 3, have been omitted, because in these intervals the factor α becomes infinity (the denominators vanish).

It can be clearly seen that the influence factor α is largest in Case 3 (the distance from the quay-wall to the footing $L = 50$ mm, prototype $L = 1.5$ m), followed by Case 2 ($L = 100$ mm, prototype $L = 3$ m) and Case 1 ($L = 200$ mm, prototype $L = 6$ m). This implies that the shorter the distance from the quay-wall to the footing, the stronger the effect of the collapse of the quay-wall.

The influence factor α , at the final stage of the 1200 sec, is summarized in Table 3. The physical

Table 3. Influence factor α at the final stage of 1200 sec.

Case	Influence factor α
Case 1 ($L = 200$ mm, prototype = 6 m)	0.07
Case 2 ($L = 100$ mm, prototype = 3 m)	0.09
Case 3 ($L = 50$ mm, prototype = 1.5 m)	0.17

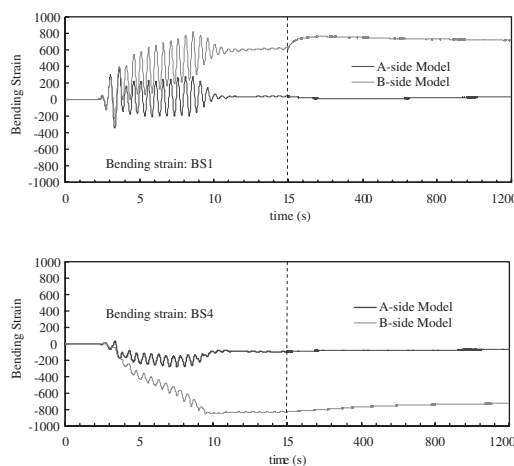


Figure 5. Comparison between the bending strains of the pile-heads and pile-tips at A-side and B-side (Case 2).

meaning of the influence factor α is that if the quay-wall displaces 1 m forward, the pile-foundation located at the distance 1.5 m from the quay-wall will move 0.17 m forward (residual displacement).

Figure 5 compares the time histories of the bending strains of the piles for Case 2. In addition, the differences between the strains at B-side and A-side at 1200 sec of the final stage are shown in Table 4. The influence factor β , which represents the effect on pile strains of the collapse of the quay-wall (at $t = 1200$ sec), is calculated as shown in Table 4. Incidentally, the influence factor β (absolute value) is obtained as follows:

$$\beta = \text{abs} \left| \frac{\text{pile strain (B-side)} - \text{pile strain (A-side)}}{\text{pile strain (A-side)}} \right|$$

Note that strains in the A-side piles are quite small compared with those in the B-side piles. It therefore appears that the influence of the displacement of the quay-wall on pile strains is extremely large. The influence factor β increases clearly in inverse proportion to the distance from the quay-wall to the footing.

Table 4. Influence factor β (Effect on pile strains of the collapse of the quay-wall at 1200 sec) (Case 2).

Case 2	B-side	A-side	B-side – A-side	β_{axial}
Axial Strain (μ)	BS1	-77.4	-20.7	-56.7
	BS4	-99.2	-16.8	-82.4
Bending Strain (μ)	BS1	716.0	35.9	680.1
	BS4	-724.0	-70.7	-653.3
β_{bending} at Pile-head: BS1 of Case 1, 2, 3		Case 1	Case 2	Case 3
β_{bending} at Pile-head: BS1		5.7	18.9	46.2

Table 5. Four tests of the remedial measure with batter piles.

Case	Distance from quay-wall to pile-foundation	Inclination angle of batter piles (degree)
Case 31	200 mm (prototype: 6 m)	10
Case 32	100 mm (prototype: 3 m)	10
Case 33	50 mm (prototype: 1.5 m)	10
Case 34	100 mm (prototype: 3 m)	5

Remedial measures against liquefaction-induced soil flow usually focus either on reinforcement of the pile-foundation-structures themselves, using additional piles, or soil improvement such as using vibro-flootation and other techniques. However, it is important to also strengthen the quay-walls to prevent their collapse during strong shaking, in addition to reinforcing the structures.

4 EFFECT OF THE REMEDIAL MEASURE AGAINST LIQUEFACTION-INDUCED SOIL FLOW

Several remedial techniques against liquefaction-induced soil flow have been proposed in the past. In this study, we proposed batter piles as a remedial measure, and examined its effectiveness by means of centrifuge tests.

Four tests are carried out as shown in Table 5, by changing the distance from the quay-wall to the pile-foundation-structures and the pile inclination angle.

The model for Case 32 is shown in Figure 6. A partition is placed at the center of the soil container, and a quay-wall with two models of the

- Accelerometer
- Pore Water Pressure Meter
- Earth Pressure Meter
- Strain Gauge
- Noncontact Displacement Meter

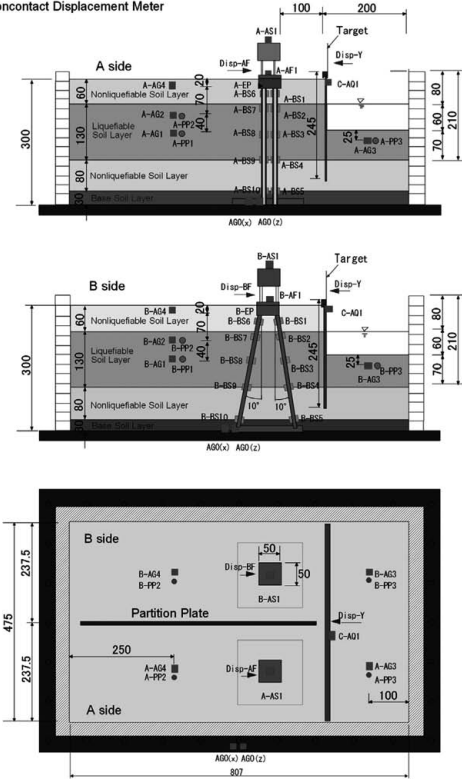


Figure 6. Longitudinal sections and plan of the 1/30-scale centrifuge model of Case 32 (scale unit: mm).

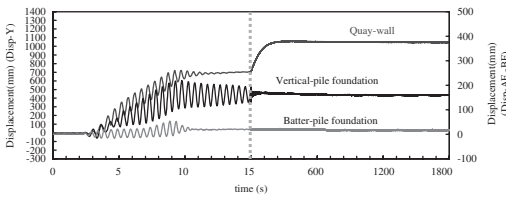


Figure 7. Time histories of the horizontal displacements of the quay-wall (Disp-Y), and the footings of the vertical piles in A-side (Disp-AF) and of batter piles in B-side (Disp-BF).

pile-foundation-structure behind the quay-wall is installed parallel to the partition. The tip-end of the quay-wall remains unattached to the base of the soil container. The soil container is divided into two parts: A-side and B-side where the vertical pile foundation and the batter pile foundation are installed, respectively.

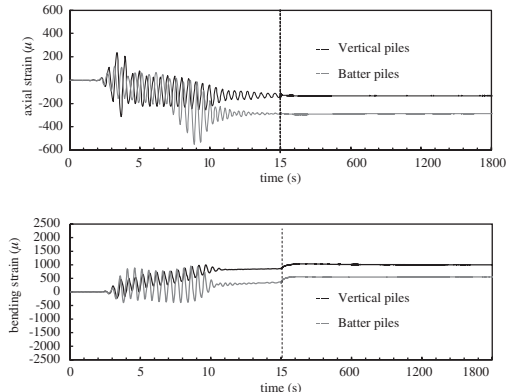


Figure 8. Comparisons between the time histories of the axial and bending strains of the vertical and batter piles at the pile-head: BS1 (Case 32).

Figure 7 shows the time histories of the horizontal displacements of the quay-wall (Disp-Y), and the footings in A-side (Disp-AF) and B-side (Disp-BF). The effectiveness of the batter piles in reducing the horizontal displacements of the foundation is clear.

Figure 8 compares the time histories of the axial bending strains in the vertical and batter piles for Case 32. The effectiveness of the batter piles is again quite clear.

5 EARTH PRESSURE CAUSED BY LIQUEFACTION-INDUCED SOIL FLOW

Our measurements allow the study of earth pressures generated by laterally flowing liquefied soil, on the back of the foundation. Many researchers have attempted to clarify the mechanics of soil pressure after liquefaction following the 1995 Kobe Earthquake. The Japanese Highway Bridge code was revised in 1996 based on substantially increased earth pressures.

On the contrary, other researchers have claimed that the damage was caused by the loss of the horizontal bearing capacity of the soil, after failure of quay-wall, rather than from the increased earth pressures.

Figure 9 compares the time histories of the horizontal displacement (Disp-EF, -FF) of the footings (pile caps) and the earth pressure (EP) acting on the back of the footings, for Case 32.

Apparently, earth pressures acting on the back of the footings (pile caps) increase during excitation. The increase is huge in the case of inclined piles – an expected outcome in view of the rigidity of this pile system and the consequent diminution of lateral displacements. With exclusively vertical piles, the lateral displacements are nearly 10 times larger and hence

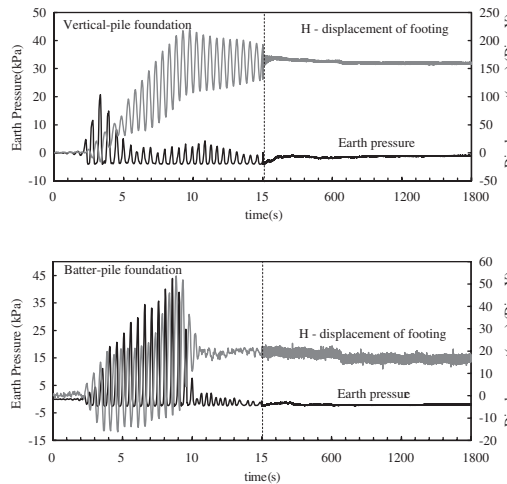


Figure 9. Comparison between the horizontal displacement of the footings and earth pressures acting on the side of the footings (Case 32).

the earth pressures are substantially smaller. Immediately after the end of excitation the earth pressures reduce and finally they completely disappear after 15 sec, for both batter and vertical piles.

6 CONCLUSIONS

The main conclusions of the study are:

- (1) The shorter the distance from the quay-wall, the stronger the effect of the collapse of the quay-wall on the pile foundation.
- (2) Pile distress is affected by the lateral displacement and failure of the quay-wall. To mitigate severe damage to pile-foundation-structures constructed in the vicinity of quay-walls, one must ensure that quay-wall displacements are kept to a minimum, even after the soil has liquefied.
- (3) The effect of the inertial force can be identified as appreciable during excitation; naturally, it disappears in the course of continued soil flow after shaking.
- (4) Batter piles are clearly effective in restricting horizontal displacement of the foundation in a liquefied soil flow environment. The disadvantages of such piles are the larger axial forces in the piles and the higher earth pressures in the back of the footing (pile cap).
- (5) The earth pressures acting on the back of the footings are insignificant when the piles are exclusively vertical and thereby their lateral displacements are huge (from the failing wall). Such pressures are very substantial only when batter piles “put a

break” on the lateral displacement and thereby invoke passive earth pressures. In both cases, after the shaking has ended, the earth pressures quickly reduced to their static values, without residuals.

- (6) The damage to pile-foundation-structures behind quay-walls is not directly caused by the force imposed by the flowing soil on the back of the footing.
- (7) It is very important to strengthen quay-walls to prevent large displacements in soil, in addition to other reinforcement measures of the structures themselves. In any case, batter piles deserve serious consideration as a means of defending against large soil displacements.

REFERENCES

- Tazoh, T., Ohtsuki, A., Fuchimoto, M., Nanjo, A., Yasuda, F., Fujii, Y., Nakahira, A. & Kuroda, C. 2002. Analysis of Seismic Damage to the Pile Foundation of a Road Bridge Caused by the Great Hanshin Earthquake. *Shimizu Technical Research Bulletin*. (18): 1–25: Shimizu Corp.
- Tazoh, T., Sato, M. & Mano, H. 2001. The Cause of Ground Fissures Radiating from the Footing of a Bridge Pier Generated by the 1995 Great Hanshin Earthquake. *Proceedings of Fourth International Conference on Recent Advances in Geotechnical Earthquake Engineering and Soil Dynamics*. Paper No. 4.57: 1–6.
- Tazoh, T. & Gazetas, G. 1996. Pile Foundations Subjected to Large Ground Deformations: Lessons from Kobe and Research Needs. *Proceedings of the Eleventh World Conference on Earthquake Engineering*, Paper 2081.

APPENDIX

Table A-1. Materials and dimensions of the test model.

	Material, Size
Laminar box	Length: 805 mm, Width: 475 mm, Height: 324 mm (Inner size)
Pore water	Silicon oil (30 cSt) with 30 times the viscosity of water
Pile	Material: Stainless steel Number of piles: 4 (2 by 2) Length: 270 mm (prototype: 8.1 m), Outer diameter: 10 mm (prototype: 30 cm), Thickness: 0.2 mm (prototype: 6 mm)
Footing	Material: Steel Thickness: 20 mm (prototype: 60 cm), Length and width: 50 mm by 50 mm (prototype: 1.5 m by 1.5 m)
Superstructure	Material: Steel Rigid part: Length: 50 mm, Width: 50 mm, Height: 30 mm (prototype: 1.5 m, 1.5 m, 0.9 m)

(Continued)

Table A-1. (Continued)

Material, Size	
Number of support columns: 4 columns, Thickness: 60 mm, Size: 6 mm by 2 mm (prototype: 18 cm, 1.8 cm by 0.6 cm)	
Sheet pile quay-wall	Material: Aluminum A-side quay-wall (fixed to the base): Height: 300 mm, Length: 235 mm, Thickness: 10 mm (prototype: 9 m, 7.05 m, 30 cm) B-side quay-wall (not fixed to the base): Height: 250 mm, Length: 235 mm, Thickness: 10 mm (prototype: 7.5 m, 7.05 m, 30 cm)
Partition	Material: Aluminum Height: 305 mm, Length: 750 mm, Thickness: 2 mm (prototype: 9.15 m, 22.5 m, 6 cm)

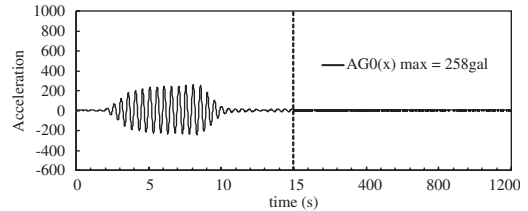


Figure A-1. Input motion (acceleration) of Case 2.

Table A-2. Installed sensors.

Sensor	Symbol	Installed locations	Sensor notation
Accelerometer	A	Shaking table	AG0
		Soil layer	AG1 to AG4 (both sides A and B)
		Superstructure	AS1 (both sides A and B)
		Footing	AF1 (both sides A and B)
		Quay-wall	Y1, Y2 (both sides A and B)
Pore water pressure meter	PP	Soil layer	PP1 to PP3 (both sides A and B)
Strain gauge	BS	Pile	BS1 to BS4 (both sides A and B)
Non-contact displacement meter	Disp	Footing	Disp-F (both sides A and B)
		Quay-wall	Disp-Y (both sides A and B)
Earth pressure cell	EP	Footing	EP (both sides A and B)

Mechanical behaviors of sandy ground during or after liquefaction

B. Ye & A. Yashima

Department of Civil Engineering, Gifu University, Gifu, Japan

G.L. Ye

Geo-Research Institute, Osaka, Japan

F. Zhang

Department of Civil Engineering, Nagoya Institute of Technology, Nagoya, Japan

ABSTRACT: Shaking-table tests and a numerical simulation on saturated sandy ground with repeated liquefaction-consolidation process are presented. Comparisons between the experiment and the numerical simulation show that the numerical simulation is capable of reproducing almost all main characteristics of the repeated liquefaction-consolidation of sandy grounds with different densities. It is found that once liquefied loose sandy ground will get denser in its consolidation process but is still possible to liquefy again in the next strong motion. With ground getting denser and denser, acceleration response of the ground will increase and the dissipation time of EPWP after liquefaction is getting shorter and shorter. Finally, the differences between finite deformation analysis and infinitesimal deformation analysis are clarified.

1 INTRODUCTION

Researchers have made great efforts to make clear the mechanism of liquefaction in sandy soil experimentally and numerically. In many cases, people have to deal with grounds under repeated liquefaction and consolidation condition. For example, during an earthquake, a ground maybe liquefies in the main-shock, and then consolidates as excess pore water pressure (EPWP) dissipates. When after-shocks come, the ground maybe liquefies again and causes further damage to structures. A liquefied ground will be denser than its original state because pore water flows out from ground. Other factors, such as soil structure, anisotropy, and stress distribution are also probably changed. Therefore, its mechanical behaviors are certainly different from the original ground when subjected to strong motion. Moreover, it is possible that people have to build new structures in a ground that has experienced liquefaction before. Certainly, the ground at this stage is much different from the virgin ground, because it has experienced densification, change in configuration, as well as stress histories. So, predicting the responses of a ground under repeated liquefaction and consolidation condition is important and necessary.

2 SHAKING-TABLE TESTS AND NUMERICAL SIMULATION

2.1 Brief description of the shaking-table tests

In order to investigate the mechanical behaviors of a sandy ground in the repeated liquefaction and consolidation process, shaking-table tests were conducted in Gifu University (Ye et al. 2006). The model ground is shown as Figure 1. It was made of Toyoura sand,

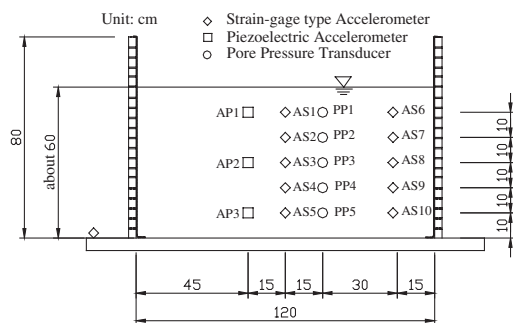


Figure 1. The model ground of shaking-table tests (Ye et al 2006).

Table 1. Cases of shaking-table tests.

Case	Average void ratio before shaking	Relative density	Input wave	Frequency
1	0.78	52%	sine	4 Hz
2	0.75	61%		
3	0.70	74%		

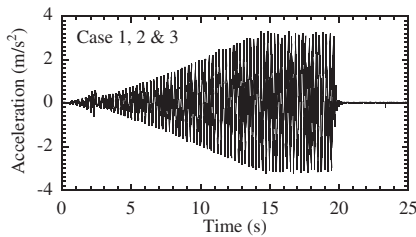


Figure 2. The input wave.

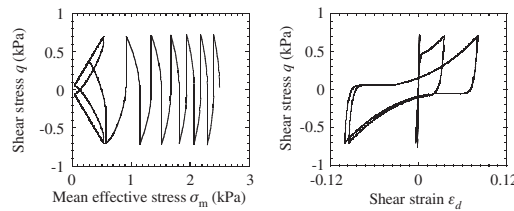


Figure 3. Element simulation.

which is widely used in geotechnical experiments in Japan. Accelerations and EPWP were measured at different depths of the model ground. The ground was shaken by three times in succession, marked by Case 1, 2 & 3, and the corresponding physical quantities are listed in Table 1. The shakings in Case 2 and Case 3 were applied to the model ground after the EPWP built up in the previous case had dissipated completely. The model ground became denser and denser after the repeated vibrations due to the dissipation of pore water in the model ground during and after each shaking. The input waves in all cases are the same, as shown in Figure 2. It is a sweep sine wave increasing from zero to about 300 Gal.

2.2 Numerical methods and simulation procedures

The numerical simulation was carried out with a 2D&3D FEM program called DBLEAVES. The program incorporates a newly proposed elasto-plastic constitutive model (Zhang et al. 2006) that can describe different liquefaction behaviors of sands with different densities with unique values of material parameters. The element simulation of cyclic mobility behavior is shown in Figure 3. It can be seen that

Table 2. Material parameters of Toyoura sand.

Compression index λ	0.05
Swelling index κ	0.0064
Critical state parameter M	1.30
Void ratio N ($p' = 98$ kPa on N.C.L.)	0.74
Poisson's ratio ν	0.30
Degradation parameter of overconsolidation m	0.10
Degradation parameter of structure a	2.2
Evolution parameter of anisotropy b_r	1.5

Table 3. Initial conditions of sands in numerical simulation.

Initial void ratio e_0	0.78
Initial mean effective stress p' (kPa)	2.50
Initial degree of structure R_0^*	0.80
Initial degree of overconsolidation $1/R_0$	25.0
Initial anisotropy ξ_0	0.00

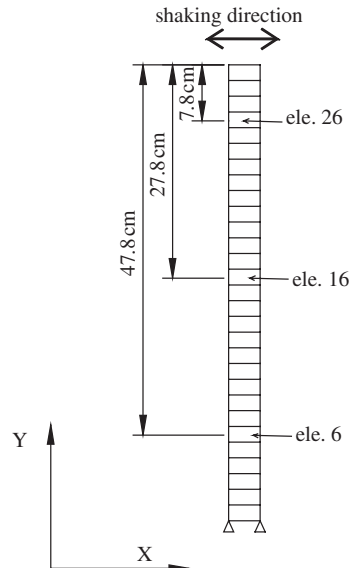


Figure 4. The simplified FEM mesh.

the behavior of cyclic mobility can be described well using the newly proposed constitutive model.

The liquefaction analysis by DBLEAVES is based on a soil-water coupled two-phase field theory that can properly take into account the interaction between soils and pore water. The adopted material parameters and initial state parameters are shown in Table 2 & 3.

Because the model ground is a level ground, the FEM model can be simplified to a one-dimensional column of soil elements, shown as Figure 4. Here we assume that the ground is uniform across any lateral plane. The input motion is the same as what was used in the experiment (Fig. 2). The numerical simulation

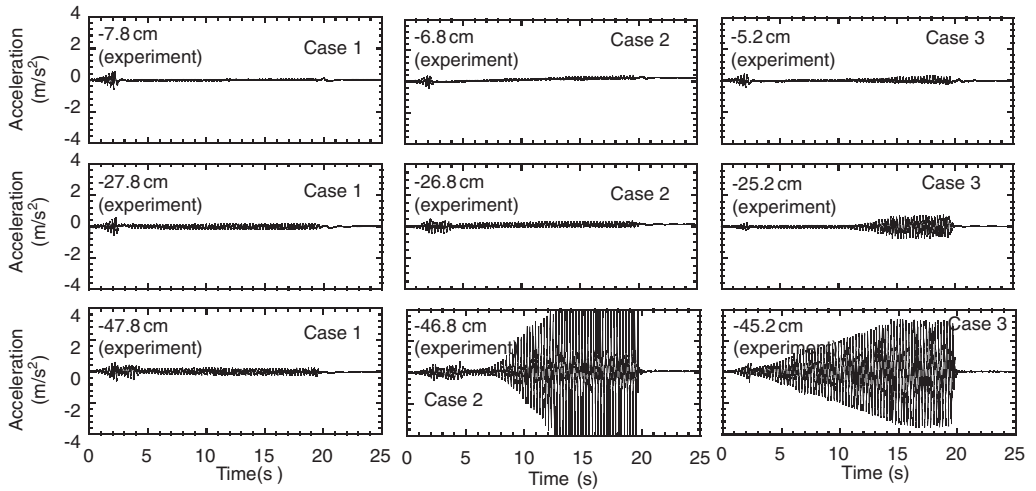


Figure 5. Lateral acceleration of experimental results.

aims to reproduce the three cases of shaking-table tests, in which the model ground was shaken three times in succession and became denser and denser after each shaking. In the numerical calculation, the process during shaking is simulated by a dynamic soil-water coupled analysis, while the process of dissipation of EPWP is simulated by a static consolidation analysis. The whole process of the model tests, which consists of three shakings and three consolidations, is a continuous one and therefore it should be simulated in sequential continuously. The simulation is therefore divided into six stages, i.e. three stages of dynamic analysis and three stages of consolidation analysis. The dynamic analysis lasts for 20 seconds until shaking stops, and the consolidation analysis lasts for 1000 seconds until EPWP dissipates completely. The values of material parameters, listed in Table 2, are the same in all 6 stages. Five initial state parameters before shaking are listed in Table 3. The state of soil elements evaluated by these five state parameters is only prescribed at the very beginning and the values of these parameters will be delivered automatically to the next stage of the analysis in the whole process, which is totally the same as what been done in the model test.

2.3 Comparison of the simulation and the experiment

Figure 5 shows the test results of acceleration responses at different depths in different cases. In Case 1, it can be seen that after liquefaction the acceleration responses became very small throughout the ground, implying that the loose ground liquefied completely. Strictly speaking, liquefaction means the

situation in which, the effective stress reduce to zero and the EPWP keeps the value of the initial effect stress during shaking. This can be verified with the time change of EPWP. It can also be predicted indirectly with the time change of the responding acceleration of surface ground because after liquefaction the responding acceleration of the ground above the liquefied soil layer became very small. In Case 2 and Case 3, the acceleration responses remained small in the ground near surface but keep large in deeper places, showing that after experiencing liquefaction, the densities of sands increased and the sands in deeper places may not liquefy in the next vibration.

Figure 6 shows the simulated results of acceleration responses at different depths in different cases. It can be seen that acceleration responses of ground increased with ground becoming denser and denser case by case, which shows the same tendency as the experimental results. In every case, acceleration was small near ground surface, and increased along with the increase of depth. Experimental results also show this trend.

Figure 7 shows the EPWP measured at different depths in different cases. It is noticeable that EPWP did not differ too much near ground surface in different cases, while quite different near the bottom of the model ground. With the ground becoming denser in Case 2 and Case 3, the EPWP near bottom of the model ground began to vibrate. This is the typical characteristic indicating cyclic mobility occurs.

Figure 8 shows the simulated result of EPWP at different depths in different cases. In Case 1, EPWP built up quickly to the highest value that is equal to the vertical effective stress. The value of EPWP kept almost constant until EPWP started to dissipate. In Case 2 and Case 3, however, when EPWP built up to

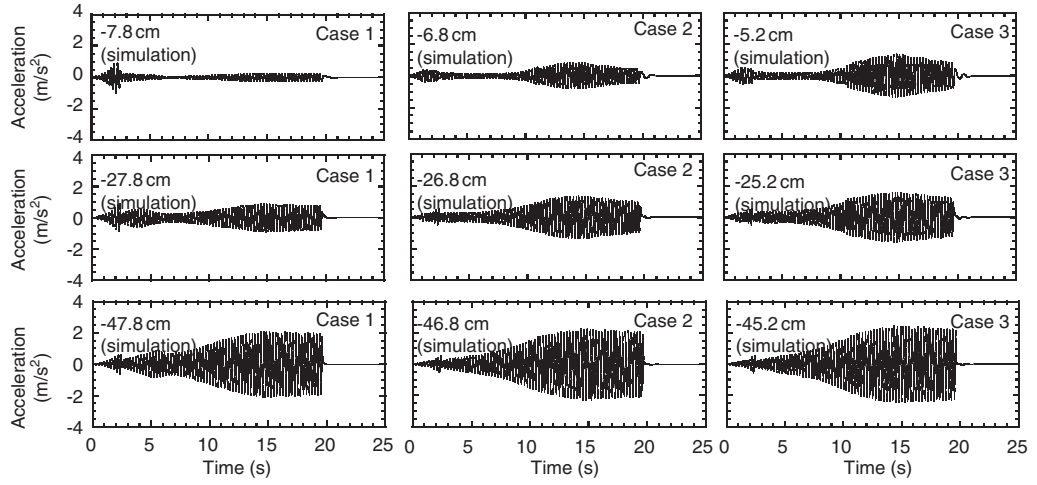


Figure 6. Lateral acceleration of simulation results.

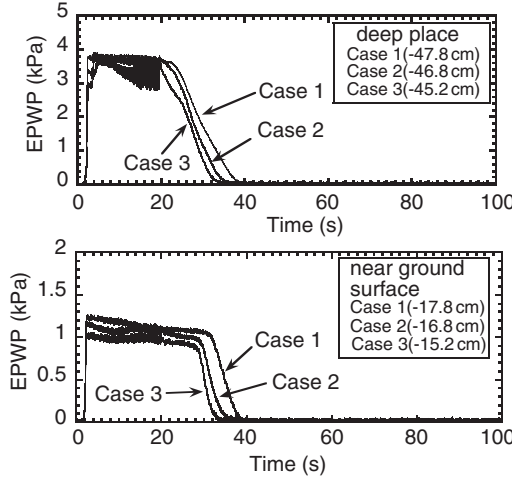


Figure 7. Comparison of experimental EPWP in different cases.

a value close to vertical effective stress, the curves of EPWP began to vibrate and drop a little especially at deep places, which indicated that cyclic mobility began to occur in the sands of Case 2 and Case 3 due to the densification of the sand experienced the first liquefaction and consolidation process in Case 1. The above phenomena are in agreement with experimental results shown in Figure 7. As to dissipation time for EPWP, however, simulated result was much longer than the corresponding experimental results. This disagreement of dissipation time will be discussed in next subsection. In spite of the disagreement of dissipation time, it can be seen from the simulated results that dissipation time depends on the density of sands, that

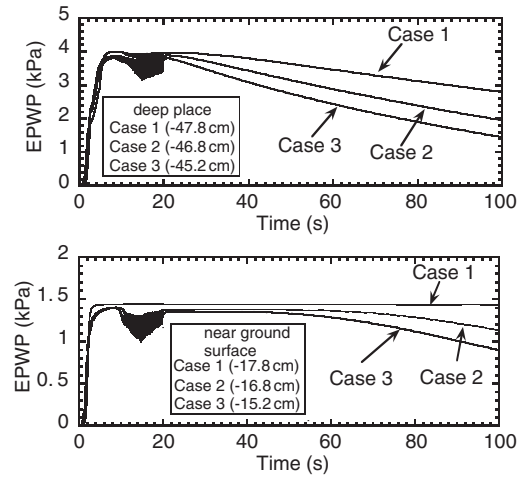


Figure 8. Comparison of experimental EPWP in different cases.

is, the denser the sand is, the faster the dissipation of EPWP will be. This simulated result is in agreement with the experimental one shown in Figure 7.

Figure 9 shows the calculated settlement of the ground surface. The small circles represent the measured settlements at the end of every case. The calculated settlement was larger than the measured settlement in Case 1, but agreed with the measured settlements in Cases 2 and 3. This disagreement is probably due to the inaccurate evaluation of the stress condition for loose sand at very low confining pressure that cannot be easily confirmed with conventional triaxial compression tests.

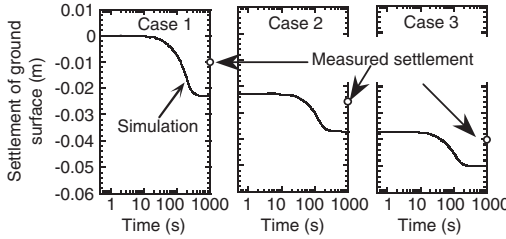


Figure 9. Settlement of ground surface.

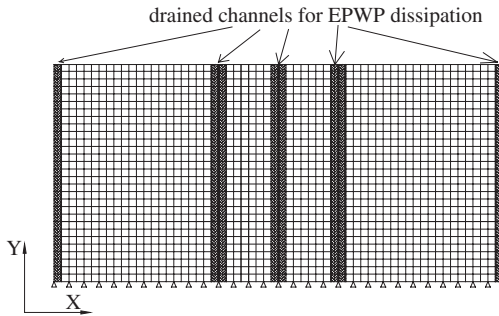


Figure 10. New FEM mesh considering the existence of drained channels for EPWP dissipation.

2.4 Some discussions on the dissipation time of EPWP

As mentioned in the previous subsection, the dissipation time of EPWP in present simulation is much longer than the experimental results. This disagreement is maybe caused by the evaluation of the permeability of sands. In the analysis, the permeability is assigned as 1.0^{-4} m/s, a commonly used value for Toyoura sand. It is assumed in the analysis that the ground keeps uniform throughout the whole process of repeated shaking and consolidation. But according to the observation of ground surface during experiment, some cracks (drainage piping) were observed in the ground surface, especially around the positions where measuring sensors were set and the side boundaries of shear box. Therefore, the ground will not be uniform after shaking and EPWP may dissipate more quickly from these cracks. In some places, even the phenomenon of sand boiling was observed. There also are some other experimental evidences of the increase of permeability during liquefaction, which can be found in literatures (Ishihara 1993, Coelho et al. 2005). In order to investigate the influences of these cracks in the ground, we conducted a numerical analysis with the same sands but a different finite element mesh, in which the existence of some channels for pore-water dissipation is considered. These channels exist in the positions where the measuring sensors were set and

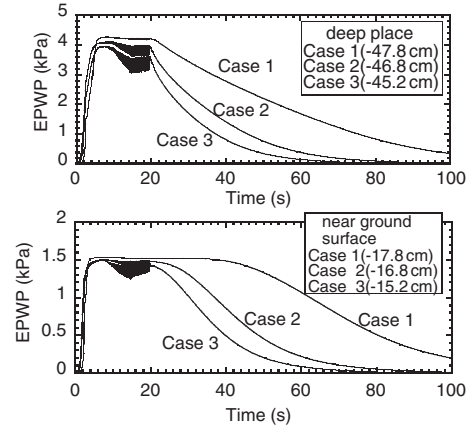


Figure 11. Simulated results of EPWP considering the existence of drained channels for EPWP dissipation.

the side boundaries of shear box, as shown in Figure 10. The material of these channels are the same as the other sands except that the permeability is set as 1.0^{-3} m/s, one order larger than the usual sand. Figure 11 shows the history of EPWP calculated with the new FEM mesh. By comparing Figure 11 with Figure 8, it is clear that the channels for pore-water dissipation can greatly shorten the dissipation time of EPWP.

3 COMPARISON OF FINITE DEFORMATION ANALYSIS AND INFINITESIMAL DEFORMATION ANALYSIS

The simulation results presented in the former sections are all calculated using finite deformation algorithm, which is considered more suitable for liquefaction analysis because large deformation may occur during liquefaction. In order to clarify the difference between finite deformation analysis and infinitesimal deformation analysis, we also did an infinitesimal analysis of the same boundary value problem and made a comparison between two kinds of analysis.

We pick up the element in the center of the ground (element 16 in Fig. 4) to investigate the differences between two kinds of analysis. Figure 12 shows calculated accelerations of two kinds of analysis. In order to see more details of the graphs, only the results of the first 5 seconds are displayed. In Case 1, the calculated accelerations of two kinds of analysis are very close to each other. However, in Case 2 and Case 3, there are some differences appearing in the results. In Case 1, two kinds of analysis both start from the initial mesh and the deformation is not large so that there are not remarkable differences between each other. However, the mesh size in the infinitesimal analysis is

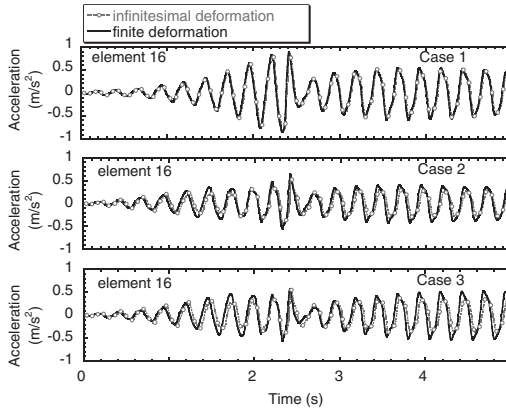


Figure 12. Acceleration of infinitesimal deformation analysis and finite deformation analysis.

invariable, while the mesh in the finite deformation analysis is refreshed all the time according to the ground deformation. So, in Case 2 and Case 3, the infinitesimal analysis is still based on the initial mesh, and the finite deformation analysis is always based on the deformed mesh. Considering that there are rather large residual deformation existed in the ground at the end of every case, the FEM mesh sizes of finite deformation analysis in Case 2 and Case 3 are much different from that of infinitesimal. So, the larger difference of acceleration can be found in Case 2 and Case 3.

The same trend can also be seen in the results of EPWP, shown as Figure 13. The EPWP of two kinds of analysis are very close to each other in Case 1, but show some differences in Case 2 and Case 3. The dissipation time of finite deformation analysis is shorter than that of the infinitesimal analysis because the deformed mesh can take into account the densification of ground more rightly.

Figure 14 displays the computed stress-strain relations and stress paths of infinitesimal deformation analysis and finite deformation analysis. In order to see more details of graphs, only the results of the first 5 seconds are displayed. From the stress-strain relationships, it is clear that there is residual deformation existed at the end of every case because the strain does not start from zero at the very beginning of Case 2 and Case 3. This residual deformation can be reflected in the FEM mesh sizes with the use of finite deformation analysis, but cannot be reflected in the infinitesimal deformation analysis.

The settlement of ground surface is presented in Figure 15. The settlement calculated by finite deformation analysis is smaller than that calculated by infinitesimal deformation analysis. It is also because that the

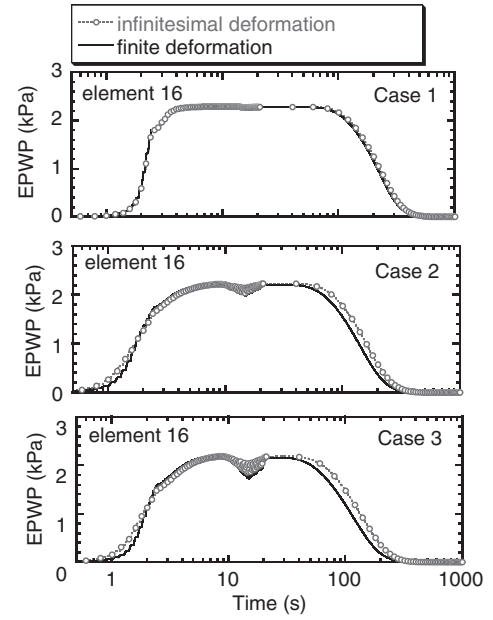


Figure 13. EPWP of infinitesimal deformation analysis and finite deformation analysis.

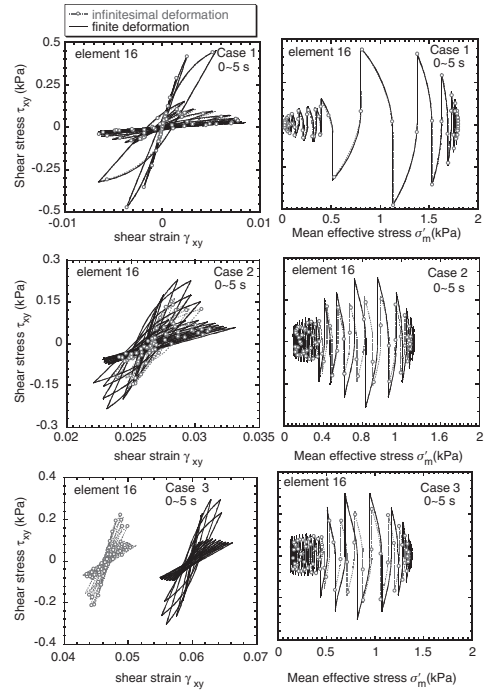


Figure 14. Computed stress-strain relations and stress paths of infinitesimal deformation analysis and finite deformation analysis.

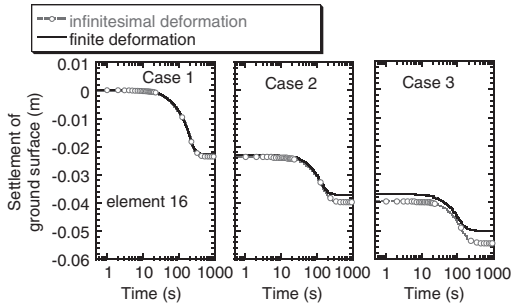


Figure 15. Settlement of ground surface of infinitesimal deformation analysis and finite deformation analysis.

mesh size of finite deformation analysis is changed with settlement of ground, so the stiffness of FEM elements becomes larger than that of infinitesimal deformation analysis.

4 CONCLUSIONS

By comparing the numerical results with the experimental results, it is known that the analysis conducted in this paper is capable of reproducing uniquely the different responses of liquefied grounds with different densities during repeated shaking and consolidation. But the simulated dissipation time of EPWP is much longer than the experimental result. It is understood by numerical simulations that the cracks within a liquefied play a very important role in estimating the dissipation time of EPWP in the process of post-liquefied consolidation.

From experimental and simulated results, it is found that once liquefied loose sandy ground will get denser

in its consolidation process but is still possible to liquefy again in the next strong motion. It is also found that a ground is getting denser and denser in the repeated liquefaction-consolidation process, acceleration response of the ground will increase and the dissipation time of EPWP after liquefaction is getting shorter and shorter.

Comparison between finite deformation analysis and infinitesimal deformation analysis shows that the calculation results of two kinds analysis are close in Case 1, but rather different in Case 2 and Case 3. The finite deformation analysis can take into account the densification of ground more rightly, and it is more suitable for the analysis of repeated liquefaction and consolidation of sand.

REFERENCES

- Coelho, P., Haigh, S. & Madabhushi, S. 2005. Development, effects and mitigation of earthquake-induced liquefaction: A comprehensive study based on dynamic centrifuge modeling. *Proc. 16th International Conference on Soil Mechanics and Geotechnical Engineering*, Vol. 4: 2635–2639.
- Ishihara, K. 1993. Review of the predictions for Model 1 in the VELACS program. Arulanandan & Scott (Eds). *Intern. Conf. on the Verification of Numerical Procedures for the Analysis of Soil Liquefaction Problems*, Rotterdam: Balkema.
- Ye, B., Yokawa, H., Kondo, T., Yashima, A., Zhang, F. & Yamada, H. 2006. Investigation on Stiffness Recovery of Liquefied Sandy Ground after Liquefaction using Shaking-Table Tests. *Soil and Rock Behavior and Modeling*. ASCE Geotechnical Special Publication 150: 482–489.
- Zhang, F., Ye, B., Noda, T., Nakano, M. & Nakai, K. 2006. Explanation of cyclic mobility of soils: approach by stress-induced anisotropy. *Soils and Foundations* (accepted).

Author index

- Adachi, Y. 307
Cho, C. 125
Danno, K. 203
Deeks, A.D. 3, 241
Emura, T. 389
Fukada, H. 321
Gazetas, G. 409
Goh, T.L. 233
Higuchi, S. 327
Hirai, T. 385
Hirao, J. 327
Hironaka, J. 217, 385
Hoshiya, M. 355
Huang, M. 115
Isobe, K. 203, 341
Jang, J. 409
Jeong, S. 125
Kamei, H. 285
Kaneda, K. 361
Kaneko, O. 349
Katayama, T. 335
Kato, K. 321
Kawamura, M. 307
Kikuchi, Y. 177, 183, 291
Kim, Y. 125
Kimura, M. 203, 285, 341
Kitazume, M. 379
Kitiyodom, P. 143, 225
Kobayashi, K. 277
Koda, M. 259, 327
Kojima, E. 225
Komatsu, A. 253
Komatsu, M. 367
Kotaki, H. 259
Kumagai, H. 225
Lee, J. 125, 125
Lehane, B.M. 69
Leung, C.F. 27
Li, Z. 115
Liang, F. 115
Maeda, Y. 195
Maruyama, K. 379
Matsui, K. 211
Matsumoto, T. 143, 225
Miura, S. 313
Mizutani, M. 177
Mori, G. 267
Morikawa, Y. 389
Morita, K. 217
Motoyama, M. 233
Mukunoki, T. 217
Nakatani, S. 211, 397
Nishioka, H. 327
Nishiyama, Y. 341
Ochiai, H. 195
Ogura, H. 277
Ohnishi, T. 373
Okawa, K. 285
Ooya, T. 321
Otani, J. 217, 385
Otani, Y. 355
Pham, K.D. 217
Prezzi, M. 49
Saito, S. 259
Salgado, R. 49
Sato, M. 409
Schneider, J.A. 69, 183
Segawa, N. 321
Seo, D. 125
Seo, H. 49
Seol, H. 125
Shintani, T. 143
Shioi, Y. 321
Shirato, M. 211, 397
Sugano, T. 403
Suzuki, M. 211
Tabata, T. 389
Tajika, H. 267
Tajima, S. 259
Takenoshita, T. 307
Tanaka, T. 403
Tanzawa, N. 307
Tazoh, T. 409
Tomisawa, K. 225, 313
Umeno, T. 373
Urano, K. 307
Vipulanandan, C. 87
Vrettos, C. 101
Watanabe, Y. 385
White, D.J. 3, 183, 241
Xu, X. 69
Yamada, T. 299
Yamashita, H. 177
Yamashita, K. 299
Yamazaki, H. 361
Yashima, A. 417
Yasuda, S. 195
Yasufuku, N. 195
Ye, B. 417
Ye, G.L. 417
Yoshikawa, T. 259
Yoshinaga, H. 361
Yoshinari, Y. 373
Yoshitomi, H. 373
Zhang, F. 285